
6
EPPC
European Conference
on Controlled Fusion
and Plasma Physics
Moscow 1973
July 30 - August 4
Vol. I

DV

Po(T) 30

SIXTH EUROPEAN CONFERENCE ON CONTROLLED FUSION AND PLASMA PHYSICS

Moscow, USSR

July 30 - August 4, 1973

Vol. I
CONTRIBUTED PAPERS

The Conference Proceedings are distributed free of charge to all registered participants

18023

Max-Planck-Institut für Plasmaphysik
14. AUG. 1973
Bibliothek

ORGANIZING COMMITTEE

B.B.Kadomtsev - president, Kurchatov Institute of Atomic Energy
M.S.Rabinovich - vice-president, Lebedev Physical Institute
E.P.Velikhov - vice-president, Kurchatov Institute of Atomic Energy
E.I.Kusnetsov - scientific secretary, USSR State Atomic Energy Committee
D.K.Akulina - Lebedev Physical Institute
N.V.Belousov - Academy of Sciences of the USSR
A.B.Beresin - Ioffe Physico-Technical Institute
N.S.Cheverev - USSR State Atomic Energy Committee
L.V.Dubovoi - D.V.Efremov Sci. Res. Institute of Electrophysical Apparatus
D.P.Filippov - USSR State Atomic Energy Committee
A.S.Fursov - Moscow State University
V.E.Golant - Ioffe Physico-Technical Institute
I.N.Golovin - Kurchatov Institute of Atomic Energy
S.G.Gusev - USSR State Atomic Energy Committee
A.A.Kusovnikov - Moscow State University
N.I.Leontjev - Sukhumi Physico-Technical Institute
V.V.Makarov-Zemljansky - USSR State Atomic Energy Committee
A.T.Matvejev - Moscow State University
S.V.Mirnov - Kurchatov Institute of Atomic Energy
M.I.Pergament - Kurchatov Institute of Atomic Energy
V.D.Pismenny - Moscow State University
M.K.Romanovsky - Kurchatov Institute of Atomic Energy
D.D.Ryutov - Siberian Institute of Nuclear Physics
R.Z.Sagdeev - High Temperature Institute, Moscow
V.D.Shafranov - Kurchatov Institute of Atomic Energy
I.S.Shpiegel - Lebedev Physical Institute
V.T.Tolok - Physico-Technical Institute, Ukr. SSR

P r e f a c e

This volume contains the Contributed Papers, which have been selected out of 214 available papers by Paper Selection and Programme Committee /PSPC/ of the "VI European Conference on Controlled Fusion and Plasma Physics".

The PSPC meeting took place in Moscow from May 10-th till May 12, 1973. The Papers which were received by the Organizing Committee after May 12-th were not taken into consideration. A number of Papers supplemented by new results obtained after the date will be printed in the second volume of the Proceeding together with the Invited Papers in accordance with the authors' desire or with the decision of PSPC. This volume does not contain the texts of those Contributed Papers which in the opinion of PSPC could be delivered at informal sessions or included in the Invited Papers.

For the sake of speeding the publication the present Proceedings have been printed by both typing and photo-offset lithography methods. No editorial work was carried out with the exception of 4 papers, the presentation of which was really not adequate. It means that the authors must bear responsibility for their texts.

In the Proceedings the Papers have been arranged in groups divided by coloured pages. Session and paper indexes in this volume and in the Programme of the Conference coincide.

For the sake of readers' convenience a print larger than that of the previous Proceedings is used and in this connection the size of the book has been changed. We sincerely thank the authors for carrying out the "Instruction for Preparing Papers". We wish to thank the members of the PSPC and the Scientific Institutions they represent for their co-operation.

The Organizing Committee

May 21 1973

Moscow

PAPER SELECTION AND PROGRAMME COMMITTEE

T.Consoli /France/
V.Copecky /CSSR/
B.Kadomtsev /USSR/
E.Kusnetsov /USSR/
D.Pfirsh /BRD/
M.Rabinovich /USSR/
P.Reynolds /UK/
V.Shafranov /USSR/

The Conference is under the auspices of the

EUROPEAN PHYSICAL SOCIETY

/Plasma Physics Division/

Organized

by LEBEDEV PHYSICAL INSTITUTE

KURCHATOV ATOMIC ENERGY INSTITUTE

LOMONOSOV MOSCOW STATE UNIVERSITY

Sponsored

by ACADEMY OF SCIENCES OF THE USSR

USSR STATE ATOMIC ENERGY COMMITTEE

USSR MINISTRY OF HIGHER AND SPECIAL SECONDARY EDUCATION

CONTENTS



1.1. TOKAMAKS: LARGE DEVICES

1.1.1. BEHAVIOUR OF IONS IN THE TOKAMAK-4 PLASMA. 1
E.P.Gorbunov, V.S.Zaverjaev, M.P.Petrov.

1.1.2. THE CLEO TOKAMAK EXPERIMENT. 5
J.W.M.Paul, A.Gibson, J.Hugill, J.Lang, P.Reynolds, P.E.Stott.

1.1.3. FIRST RESULTS ON T.F.R. 9
C.Breton, J.P.Bussac, J.P.Grenn, R.Dei-Cas, M.Delmas, P.Ginot, M.Huguet, D.Launois, P.Lecoustey, M.Mattioli, P.Moriette, P.Plinate, Z.Sledlewski, P.H.Rebut, A.Torossian, J.Tachon.

1.1.4. CONFINEMENT OF AN ANOMALOUSLY HEATED PLASMA IN A TOKAMAK (T.T.F.) 10
M.Martone

1.1.5. CURRENT AND PRESSURE DISTRIBUTIONS IN THE "HIGH β TOKAMAK" EXPERIMENT TEE 14
P.Noll, M.Korten, E.Kugler, F.Sand, F.Waelbroeck, G.Wiadmann.

1.1.6. STABILITY AND HEATING EXPERIMENTS ON THE ATC TOKAMAK 18
K.Bol, J.L.Cecchi, C.C.Daughney, R.A.Ellis, Jr., H.Eubank, H.P. Furth, R.J.Jakobsen, L.C.Johnson, E.Mazzucato and W.Stodiek.

1.2. TOKAMAKS: NEOCLASSICAL TRANSPORT

1.2.1. NEOCLASSICAL TRANSPORT PHENOMENA IN A TOKAMAK 25
V.Daybelge.

1.2.2. RADIAL TRANSPORT OF IONS IN TOKAMAKS INCLUDING DIFFUSING OXYGEN AND CARBON IMPURITIES 29
D.F.Duchs, H.P.Furth, P.H.Rutherford.

1.2.3. EFFECT OF MAGNETIC FIELDS IRREGULARITIES ON PLASMA DIFFUSION 33
G.Casati, M.Dobrowolny, E.Lazzaro, A.Orefice.

1.2.4. EFFECT OF NON-AXISYMMETRY ON THE TRANSPORT COEFFICIENTS OF A TOROIDALLY CONFINED PLASMA 37
R.K.Varma, A.Sen.

1.2.5. EQUILIBRIUM AND ENERGY BALANCE IN TOKAMAKS 41
Y.H.Dnestrovskii, D.P.Kostomarov, N.V.Karetkina, N.L.Pavlova, A.M.Popov.

1.2.6. MHD SIMULATION OF ANISOTROPIC TOROIDAL PLASMAS 45
W.Sharp, J.C.Taylor.

1.3. TOKAMAKS: NEWS AND VIEWS...

1.3.1. NEUTRAL INJECTION ON THE CLEO TOKAMAK 51
D.Aldcroft, J.Burcham, H.C.Cole, M.Cowlin, J.Sheffild, E.Speth, and P.E.Stott.

1.3.2. PLASMA COLUMN PERTURBATIONS PRECEDING TO DISTRUPTIVE INSTABILITY IN T-6 TOKAMAK 55
V.S.Vlasenkov, V.A.Krupin, V.M.Leonov, V.G.Merezhkin, V.S.Mukhovatov.

1.3.3. VACUUM BUBBLES IN TOKAMAK PLASMAS 59
B.B.Kadomtsev, O.P.Pogutse.

1.3.4. INVESTIGATION OF HF PLASMA HEATING AND OF PLASMA BEHAVIOUR IN THE TM-3 TOKAMAK 63
V.V.Alikaev, Yu.I.Arsen'ev, G.A.Bobrovskii, V.I.Poznyak, K.A.Razumova, Yu.A.Sokolov.

1.3.5. ORMAK AND NEUTRAL INJECTION 67
C.F.Barnett, L.A.Berry, C.E.Bush, J.D.Callen, J.F.Clarke, R.J.Colchin, R.A.Dory, A.C.England, J.T.Hogan, G.G.Kelley, J.R.McNally, Jr., M.Murakami, R.V.Neidigh, M.Roberts, J.A.Rome and W.R.Wing.

1.4. TOKAMAKS: STABILITY, STABILITY, STABILITY...

1.4.1. EQUILIBRIUM AND LOCALIZED CRITERIA ON MAGNETIC SURFACES WITH CROSS SECTIONS OF ARBITRARY SHAPE 75
C.Mercier.

1.4.2. EFFECT OF PARABOLIC CURRENT ON THE STABILITY OF M.H.D. EQUILIBRIUM IN TOKAMAK WITH NON CIRCULAR CROSS SECTION 79
P.Grelot, J.Weisse.

1.4.3. MHD MODAL ANALYSIS OF TOKAMAK LIKE PLASMA WITH VARIOUS CURRENT DENSITY PROFILES 83
W.Grossman, S.Ortolani.

1.4.5. KINK INSTABILITIES IN HIGH β TOKAMAKS AND BELT PINCHES 87
J.P.Freidberg,F.A.Haas, B.M.Marder.

1.4.6. STABILITY CRITERIA FOR GENERAL MHD EQUILIBRIA 91
D.Lortz.

1.4.7. STABILITY OF TRAPPED PARTICLE AND DRIFT WAVE NORMAL MODES WITH ESTIMATES OF ANOMALOUS TRANSPORT 95
W.Horton, D.W.Ross.

1.5. S T E L L A R A T O R S

1.5.1. ENERGY CONTAINEMENT IN THE WENDELSTEIN IIB STELLARATOR WITH OHMIC HEATING 101
G.Grieger, H.Hacher, G.Pacher, H.Renner, H.Ringler, E.Wuersching.

1.5.2. ENERGY CONFINEMENT DURING HF HEATING OF PLASMA IN "URAGAN" STELLARATOR 105
A.G.Diky,S.S.Kalinichenko, I.I.Konovalov, S.S.Ovchinnikov, O.S.Pavlichenko, V.K.Pashnev, A.S.Slavny, V.A.Suprunenko, V.F.Tarasenko, V.T.Tolok, O.M.Shvets.

1.5.3. RECENT RESULTS FROM THE GARCHING HIGH-BETA STELLARATOR TORUS ISAR T.1 109
E.Funfer, M.Kaufmann, W.Lotz, J.Neuhauser, G.Schramn.

1.5.4. LASER PLASMA CONTAINMENT IN TOR-1 STELLARATOR 113
E.D.Andrykhina, G.S.Voronov, U.V.Kholnov, I.S.Shpiegel.

1.5.5. A STELLARATOR FIELD PRODUCED BY TWISTED COILS 117
S.Rehker, H.Wobig.

1.5.6. FLUCTUATIONS AND CONTAINMENT OF PLASMA IN JIPP L = 3 STELLARATOR 121
T.Dodo, M.Fujiwara, K.Miyamoto, A.Ogata.

1.5.7. PLASMA CONFINEMENT BY HYBRID STELLARATOR FIELD OF l = 2 and l = 3 125
M.Fujiwara, K.Kawahata, A.Mohri and K.Miyamoto.

1.6. INTERNAL RINGS, TRANSPORT

1.6.1. NEUTRAL INJECTION AND OHMIC PLASMAS IN THE CULHAM LEVITRON 131
M.W.Alcock, R.E.Bradford, R.Freeman, D.P.Hammond, A.C.Riviere, D.R.Sweetman.

1.6.2. CRITICAL β FOR QUADRUPOLE CONFIGURATIONS 135
E.Rebhan, D.Lortz.

1.6.3. PLASMA CONFINEMENT PROPERTIES IN FM1-SPHERATOR 139
K.Chen, D.Meade, M.Okabayashi, J.Schmidt, S.Yoshikawa.

1.6.4. OBSERVATION OF DRIFT INSTABILITY DUE TO PARTICLE TRAPPING IN A CORRUGATED GEOMETRY 143
P.Deschamps, R.Gravier, C.Renaud, A.Samain.

1.6.5. INFLUENCE OF THE SLOW INHOMOGENEITIES ON TRANSPORT PHENOMENA IN THE HIGH TEMPERATURE PLASMA IN THE STRONG MAGNETIC FIELD 147
Yu.A.Dreizin, A.M.Dykhne.

1.7. TOKAMAKS: NEW TRENDS

1.7.1. EXPERIMENTS ON THE TO-1 TOKAMAK HAVING AN AUTOMATIC SYSTEM FOR CONTROLLING THE EQUILIBRIUM 153
L.I.Artemenkov, P.I.Koslov, P.I.Melikhov, V.S.Svishev.

1.7.2. PLASMA EQUILIBRIUM IN CLEO-TOKAMAK 157
J.Hugill, J.W.M.Paul, G.W.Reid and P.E.Stott.

1.7.3. EFFECT OF SHAPING FIELD ON DOUBLET DISCHARGES 161
T.Ohkawa, T.H.Jensen, M.S.Chu, R.K.Fisher and C.L.Hsieh.

1.7.4. THE FIRST EXPERIMENTAL RESULTS IN FINGER RING TOKAMAK 165
A.V.Bortnikov, Yu.T.Baiborodov, N.N.Brevnov, V.G.Zhukovskii, L.E.Zakharov, D.V.Orlinskii, V.I.Pergament, M.K.Romanovskii, N.I.Sokolov, A.M.Us.

1.7.5. DYNAMIC STABILIZATION OF A PLASMA IN STELLARATOR AND TOKAMAK MACHINES 169
R.A.Demirkhanov, A.G.Kirov, V.N.Zharikov, N.I.Malokh, L.F.Ruchko, G.I.Astapenko, V.A.Zhdanov.

1.7.6. AN AXISYMMETRIC DIVERTOR IN TOKAMAK WITH A TEAR DROP-LIKE CROSS SECTION (DIVA) 173
M.Yoshikawa, Y.Shimomura, H.Maeda, A.Kitsunezaki, and S.Mori.

1.7.7. STUDY OF DYNAMIC STABILIZATION CONDITIONS OF TOROIDAL DISCHARGE IN MODULATED LONGITUDINAL MAGNETIC FIELD 177
M.A.Vasilevsky, E.G.Komar, I.M.Roife, E.V.Seredenko.

1.8. TOKAMAKS: DIAGNOSTICS

1.8.1. NEUTRAL DENSITY DETERMINATION BY SCATTERING OF VACUUM-UV RADIATION 183
C.Breton, R.Papoular.

1.8.2. A KINETIC MODEL FOR THE NEUTRAL GAS BETWEEN PLASMA AND WALL 187
S.Rehker, H.Wobig.

1.8.3. MEASUREMENT OF THE MAGNETIC FIELD DIRECTION IN A TOKAMAK PLASMA USING THE POLARIZATION OF AN IMPURITY LINE 191
J.Fujita, K.McCormik.

1.8.4. POLOIDAL FIELD MEASUREMENTS IN THE ST TOKAMAK BY HARMONIC GENERATION AT THE UPPER HYBRID LAYER 195
R.Cano, I.Fidone, J.Hosea.

1.8.5. SPACE POTENTIAL MEASUREMENTS IN THE ST TOKAMAK 199
F.C.Jobes, J.C.Hosea.

1.9. TOKAMAKS: EQUILIBRIA (THEORY)

1.9.1. STATIONARY CONVECTION IN TOKAMAK PLASMAS 205
E.K.Maschke, R.B.Paris.

1.9.2. MULTIPOLE TOKAMAK EQUILIBRIA WITH FINITE β 209
W.Feneberg, K.Lackner.

1.9.3. EQUILIBRIUM ROTATION OF A TOKAMAK DURING NEUTRAL INJECTION 213
E.Canobbio, O. de Barbieri.

1.9.4. THE SIMULATION OF CLASSICAL TOROIDAL PLASMAS IN THE PLANE 217
D.E.Potter, G.H.Tuttle.

1.9.5. VARIATION OF A TOROIDAL EQUILIBRIUM 221
M.Bineau

1.9.6. ARBITRARY SHAPED RESISTIVE TOKAMAK EQUILIBRIA 225
B.E.Green, K.U.v.Hagenow, H.P.Zehrfeld.

1.9.7. THE EFFECT OF PLASMA FLOW ON THE TOROIDAL EQUILIBRIUM SHIFT 229
B.J.Green, H.P.Zehrfeld.

2.1. OPEN TRAPS

2.1.1. INVESTIGATION OF THE INSTABILITY OF COLLISIONAL PLASMA IN PR-6 MIRROR TRAP 235
B.I.Kanaev, E.E.Yushmanov.

2.1.2. A COMPUTATIONAL STUDY OF SPACE CHARGE LIMITATIONS IN DIRECT CONVERSION SYSTEMS 239
F.B.Marcus, C.J.H.Watson.

2.1.3. PLASMA CONFINEMENT IN THE PRESENCE OF FEEDBACK SYSTEM IN OGRA-3 DEVICE 243
V.A.Chuyanov, V.Kh.Likhtenshtein, D.A.Panov, V.A.Zhil'tsov, A.G.Scherbakov.

2.1.4. HOT ELECTRON PLASMA ACCUMULATION IN AN OPEN ENDED MINIMUM-B SYSTEM 247
R.Bardet, P.Briand, L.Dupas, C.Gormezano, G.Melin.

2.1.5. INVESTIGATION OF PLASMA CONFINEMENT BY ELECTRO-MAGNETIC TRAPS 251
O.A.Lavrent'ev, V.A.Sidorkin, V.P.Goncharenko, Yu.S.Asovsky, L.I.Ovcharenko, V.A.Potapenko, I.A.Stepanenko, Yu.I.Pankrat'ev, V.A.Naboka, S.A.Vdovin.

2.1.6. 200 KW NEUTRAL BEAM INJECTION INTO THE 2X II MIR-ROR DEVICE 255
F.H.Coensgen, W.F.Cummins, W.E.Nexsen Jr., A.W.Molvik, T.C.Simonen.

2.1.7. EXPERIMENTAL INVESTIGATION OF THE QUASI-ELASTIC REFLECTION OF A PLASMA BY A COMBINED HF-MAGNETO-STATIC MIRROR AT ECR 259
V.D.Dougar-Jabon, K.S.Golovanivsky, L.A.Pokhmelnykh.

2.2. TOROIDAL PINCHES

2.2.1. FURTHER STUDIES OF A HIGH-BETA REVERSED FIELD PINCH 265
C.W.Cowers, J.W.Long, A.A.Newton, D.C.Robinson, A.J.L.Verhage, H.A.B.Bodin.

2.2.2. RESISTIVE INSTABILITIES IN DIFFUSE PINCHES 269
J.E.Crow, J.Killeen, D.C.Robinson.

2.2.3. STABILITY, RADIATION LOSSES AND EQUILIBRIUM IN THE GARCHING BELT PINCH ISAR IV 273
H.Krause, R.Wilhelm, H.Zwicker.

2.2.4. PLASMA COOLING BY IMPURITY RADIATION 277
W.Engelhardt and Glen Bateman.

2.2.5. THE INFLUENCE OF A LONGITUDINAL HIGH FREQUENCY CURRENT ON PLASMA STABILITY IN A COMBINED PINCH 281
G.G.Zukakishvili, I.F.Kwartskhawa, E.K.Tikhanov.

2.2.6. ASPECTS OF DYNAMIC STABILIZATION OF A HIGH-BETA PLASMAS 285
O.Gruber, G.Becker, H.Herold.

2.2.7. TWO-DIMENSIONAL COMPUTER CALCULATION OF TOROIDAL PINCH EXPERIMENTS 289
F.Hofmann and D.W.Ignat.

2.2.8. THE TOROIDAL Z-PINCH PROGRAM AT LOS ALAMOS 293
D.A.Baker, L.C.Burkhardt, J.N. Di Marco, P.R.Forman, A.Haberstich, R.B.Howell, H.J.Karr, L.W.Mann and J.A.Phillips.

2.3. THETA-PINCHES

2.3.1. PLASMA DYNAMICS AND CURRENT SHEATH STRUCTURE IN COLLISIONFREE THETA-PINCHES 299
K.Höthker, K.J.Dietz, K.H.Dippel, E.Hintz.

2.3.2. THE PRODUCTION OF WEAKLY COMPRESSED HIGH-BETA PLASMAS BY SHOCK HEATING IN HIGH-VOLTAGE THETA-PINCHES 303
M.Keilhacker, M.Kornherr, H.Niedermeyer, F.Söldner, K.-H.Steuer.

2.3.3. SHOCK HEATING AND PLASMA SHEATH SCALING IN LOW DENSITY THETA PINCHES 307
M.Keilhacker, M.Kornherr, G.Maret, H.Niedermeyer, K.H.Steuer.

2.3.4. ION HEATING IN A STRONG MAGNETIC COMPRESSION WAVE 311
R.Chodura, B.Rothlein.

2.3.5. IMPLODING-LINER FUSION DEVICES 315
J.P.Boris, A.E.Robson, R.A.Shanny, N.K.Winsor.

2.3.6. DYNAMICAL CONTROL OF THETA PINCH PLASMA 319
T.Itagaki, K.Saito, S.Shiina, K.Yokoyama, H.Yoshimura.

2.4. REACTOR ASPECTS

2.4.1. ON THE EFFICIENCY OF VARIOUS DIVERTORS FOR SCREENING A FUSION PLASMA 325
D.Eckhartt, G.Haas, K.U. von Hagenow.

2.4.2. NEOCLASSICAL DIFFUSION OF α -PARTICLES 329
A.Nocentini, M.Tassarotto, F.Engelmann.

2.4.3. CONSIDERATIONS ON A PULSED BELT PINCH REACTOR WITH NORMAL CONDUCTING COILS 333
H.Herold, R.Wilhelm, H.Zwicker.

2.4.4. LOW DENSITY TOKAMAK REACTOR IGNITION BY FAST NEUTRAL INJECTION AND BUILD UP OF A HIGHER DENSITY BY USE OF A MOVING LIMITER 337
J.P.Girard, M.Khelladi, D.A.Marty.

2.4.5. FUSION REACTOR CHARACTERISTICS IN DEPENDENCE ON BETA AND ASPECT RATIO 341
M.Kaufmann, W.Koppendörfer.

2.4.6. BEAM PLASMA TARGET THERMONUCLEAR SYSTEM BASED ON TOKAMAK 345
R.A.Demirkhanov, Yu.V.Kursanov, L.P.Skripal.

2.4.7. REMARKS CONCERNING EXPERIMENTAL SIMULATION OF THE PELLET-REFUELLING 349
C.T.Chang.

2.5. PLASMA FOCUS

2.5.1. EFFECT OF A SPECIAL MAGNETIC FIELD CONFIGURATION ON THE FORMATION OF A PLASMA FOCUS 355
V.D.Ivanov, V.M.Korzhavin, M.P.Moiseeva, N.K.Sucharева, T.I.Filippova.

2.5.2. EVIDENCE FOR A BROAD AND UNIFORM NEUTRON-PRODUCING PLASMA COLUMN IN THE PLASMA FOCUS 359
P.D.Morgan, N.J.Peacock, P.Cloth, H.Conrads.

2.5.3. THE MEASUREMENT OF ION TEMPERATURE AND MAGNETIC FIELD IN A DENSE PLASMA FOCUS 363
M.J.Forrest, B.A.Norton, N.J.Peacock.

2.5.4. ELECTRON DENSITY OF A PLASMA FOCUS AND THE RADIATION EMITTED AT THE PLASMA FREQUENCY AND ITS HARMONICS 367
H.Conrads, D.Gollwitzer, H.Schmidt.

2.5.5. CHARACTERISTICS CURVES AND SCALING LAWS FOR A MATHER TYPE PLASMA FOCUS 371
H.Rapp, M.Trunk.

2.5.6. DIFFUSION AND BEAM HEATING IN THE DENSE PLASMA FOCUS 375
V.A.Gribkov, O.N.Krokhin, G.V.Sklizkov, N.V.Filippov, T.I.Filippova.

2.6. INJECTION

2.6.1. PENETRATION OF SOLID H_2 CLUSTERS IN A PLASMA 381
F.Bottiglioni, J.Countant, M.Fois.

2.6.2. PLASMA BUILDUP IN TOROIDAL REACTORS BY NEUTRAL INJECTION 385
H.D.Falter, W.Henkes.

2.6.3. PRODUCTION OF A QUASI STEADY-STATE HIGH DENSITY MIRROR PLASMA 389
J.Jacquinot, C.Leloup, J.P.Poffé, M. de Prétis.

2.6.4. POLARIZATION PHENOMENA IN PLASMA INJECTED INTO A MAGNETIC TRAP 393
M.Sadowski, E.Skladnik-Sadowska, K.Sudlitz, A.D.Timofeyev.

2.6.5. PLASMA STREAMS IN INHOMOGENEOUS MAGNETIC FIELDS 397
E.T.Karlson.

2.6.6. PHYSICS OF TARGET PLASMAS IN MINIMUM-B GEOMETRIES 401
W.B.Ard, R.J.Colchin, E.C.Crume, J.L.Dunlap, G.R.Haste, N.H.Lazar, J.F.Lyon.

2.7. DENSE PLASMAS

2.7.1. ON HIGH-BETA PLASMA CONFINEMENT IN A POLOIDAL MAGNETIC FIELD 407
B.Lehnert, T.Hellsten, R.Raggi.

2.7.2. THE DYNAMICS OF COOLING OF A DENSE WALL-CONFINED PLASMA 411
P.Z.Chebotarev, D.D.Ryutov, M.D.Spector, G.E.Vekstein.

2.7.3. NONSTATIONARY EXPERIMENTS ON PLASMA CONFINEMENT IN MULTIPLE-MIRROR TRAP 415
V.V.Danilov, E.P.Kruglyakov, E.V.Shun'ko.

2.7.4. NEUTRON PRODUCTION IN HIGH ENERGY-DENSITY EXPLODED-WIRE Z-PINCH PLASMAS 419
D.Mosher, L.S.Lenive, S.J.Stephanakis, I.M.Vitkovitsky, F.Young.

2.7.5. KIEL EXPERIMENTS OF ELECTRICALLY EXPLODED LIQUIDS CONTAINING DEUTERIUM 422
V.Fisher, H. Jäger, W.Lochte-Holtgreven.

3.1. LASERS IN FUSION

3.1.1. X-RAY SPECTROSCOPY OF THE ION POPULATION IN THE PLASMA PRODUCED AT THE SURFACE OF A PLANE MASSIVE TARGET BY INTENSE LASER IRRADIATION 427
M.Galanti, N.J.Peacock.

3.1.2. THE EFFECT OF THE ELECTRON FREE-STREAMING LIMIT ON LASER COMPRESSION 431
D.E.T.F.Ashby, J.P.Christiansen.

3.1.3. INVESTIGATION OF THE FAST ELECTRONS IN A LASER PRODUCED PLASMA BY X-RAY MEASUREMENTS 435
K.Eidmann, R.Sigel.

3.1.4. FUSION ENERGY PRODUCTION IN A SPHERICAL, LASER-HEATED DT-PLASMA 439
J.Laaksonen, J.Virtamo, P.Jauho.

3.1.5. VARIATION OF THE TEMPERATURE OF LASER-PRODUCED PLASMAS WITH LASER PULSE AND TARGET PARAMETERS 443
B.M.Klein, C.M.Dozien, D.I.Nagel and R.R.Whitlock.

3.1.6. X-RAY AND UV EMISSION OF LASER-PRODUCED PLASMAS 447
D.J.Nagel, O.C.Barr, P.G.Burkhalter, G.A.Doschek, C.M.Dozier, U.Feldman, B.M.Klein, J.H.McCrary, J.M. McMahon, R.R.Whitlock.

3.2. NONLINEAR PHENOMENA

3.2.1. INVESTIGATION OF THE MECHANISM OF PLASMA TURBULENT HEATING 453
L.P.Zakatov, D.M.Zlotnikov, Yu.G.Kalinin, A.S.Kingsep, A.G.Plakhov, V.A.Skoryupin.

3.2.2. THEORY OF ION-SOUND RESISTIVITY 457
J.Wesson and A.Sykes.

3.2.3. ANOMALOUS RESISTIVITY AND STABILIZATION OF ION SOUND INSTABILITY 461
D.Biskamp, R.Chodura, C.T.Dum.

3.2.4. THE SPATIAL EVOLUTION OF THE ELECTRON ENERGY DISTRIBUTION UNDER INFLUENCE OF A LARGE AMPLITUDE PLASMA WAREE 465
E.P.Barbian.

3.2.5. COMPUTATION OF ION-ACOUSTIC WAVE EXCITATION AND ITS ANOMALOUS EFFECTS FOR DOUBLE-SIDED LASER-PLASMA INTERACTION 469
H.Wilhelmsson and K.Östberg.

3.2.6. INVESTIGATION OF NONSTATIONARY SELF-FOCUSING OF ELECTROMAGNETIC WAVES IN PLASMA 473
V.A.Isaev, V.N.Kruglov, A.G.Litvak, B.K.Poluakhtov.

3.2.7. SPATIAL GROWTH PROPERTIES OF PARAMETRIC AND BACK SCATTERING PLASMA INSTABILITIES 477
B.D.Fied and G.Schmidt, and R.W.Gould.

3.3. RELATIVISTIC ELECTRON BEAMS

3.3.1. HIGH CURRENT DENSITY ELECTRON BEAM APPLICATION TO FUSION STUDIES 483
G.Yonas, J.W.Poukey, J.R.Freeman, K.R.Prestwich, A.J.Toepfer, M.J.Clauser, E.H.Beckner.

3.3.2. ON INITIATING THE IMPULSES NUCLEAR FUSION REACTION BY MEANS OF DT-MIXTURE COMPRESSING BY THE SHELL HEATED WITH A STRONG RELATIVISTIC ELECTRON BEAM 487
L.I.Rudakov, A.A.Samarsky.

3.3.3. THE EFFECT OF MAGNETIC FIELD ON THE INTERACTION BETWEEN A RELATIVISTIC ELECTRON BEAM AND PLASMA 491
B.N.Breizman.

3.3.4. INVESTIGATION OF PLASMA HEATING BY A RELATIVISTIC ELECTRON BEAM 495
Yu.I.Abrashitov, V.S.Koydan, V.V.Konychov, V.M.Lagunov, V.N.Lukjanov, K.I.Mekler.

3.3.5. PLASMA HEATING BY INTENSE RELATIVISTIC ELECTRON BEAMS 499
W.F.Dove, K.A.Gerber, G.G.Goldenbaum, D.A.Hammer, C.A.Kapentanakos and B.G.Logan.

3.3.6. PLASMA HEATING WITH A RELATIVISTIC ELECTRON BEAM 503
P.Korn, F.Sandel and C.Wharton.

3.3.7. ENERGY SPECTRUM MEASUREMENT OF RELATIVISTIC ELECTRONS IN EXPERIMENTS ON INTERACTION OF HIGH-CURRENT BEAM WITH PLASMA 507
T.S.Gosteva, L.V.Dubovoi, G.R.Zablotskaya, B.A.Ivanov, V.I.Chernobrovin.

3.3.8. INJECTION OF RELATIVISTIC ELECTRON BEAMS WITH ARBITRARY RADIAL PROFILES INTO WARM PLASMAS WITH COLLISIONS 511
G.Kuppers, A.Salat, H.K.Wimmel.

3.4. BEAM-PLASMA INTERACTIONS

3.4.1. FUNDAMENTAL AND SATTELLITE WAVES GENERATION IN MODULATED BEAM - PLASMA SYSTEMS 517
P.Šunka.

3.4.2. MEASUREMENTS OF PHASE AND GROUP VELOCITY OF THE ELECTRON CYCLOTRON INSTABILITY IN A BEAM-PLASMA EXPERIMENT 521
J.A.C.Cabral, M.E.F.Silva.

3.4.3. STATISTICAL ANALYSIS OF THE HIGH-FREQUENCY BURSTS OF A BEAM-PLASMA EXPERIMENT 525
J.A.C.Cabral, M.E.F.Silva.

3.4.4. MECHANISM OF STOCHASTIC OSCILLATION EXCITATION AT DEVELOPMENT OF BEAM INSTABILITY IN PLASMA 529
V.A.Lavrovsky, J.F.Kharchenko, E.G.Shustin,

3.4.5. TRANSFORMATION OF THE ELECTRON BEAM VELOCITIES DISTRIBUTION FUNCTION AT THE INTERACTION OF MODULATED ELECTRON BEAM WITH PLASMA 533
A.I.Rogashkova, M.B.Tseitlin, V.A.Lavrovskiy, J.F.Kharchenko.

3.4.6. ON DECAY INSTABILITY OF LANFMUIR AND ION-SOUND OSCILLATIONS IN PLASMA-BEAM SYSTEM 537
N.G.Matsiborko, J.N.Onishehenko, V.N.Oraevsky, V.D.Shapiro, V.J.Shevchenko.

3.5. RF AND SHOCK HEATING

3.5.1. DIFFERENT THEORETICAL CHARACTERISTICS OF RF HEATING OF HOT ELECTRON-ION TOROIDAL PLASMAS 545
A.M.Messiaen, R.Koch, P.E.Vandenplas, R.R.Weynants.

3.5.2. THE ABSORPTION OF INTENSE ELECTROMAGNETIC WAVES BY DENSE COLLISIONLESS PLASMA 549
Yu.Ja.Brodskii, S.V.Golubev, V.L.Col'tsman, A.G.Litvak.

3.5.3. INVESTIGATION OF THE MAGNETOSONIC PLASMA HEATING IN THE TOKAMAK 553
V.L.Vdovin, O.A.Zinov'ev, A.A.Ivanov, T.A.Kosinova, M.F.Krotov, Ya.R.Rakhimbabaev, V.D.Rusanov, N.V.Shapotkovskii.

3,5.4. RESONANS EXCITATION OF LARGE-AMPLITUDE OSCILLATIONS IN A NON-UNIFORM PLASMA NEAR ION CYCLOTRON RESONANSE 557
L.I.Grigor'eva, B.I.Smerdov, S.A.Sapogov, V.V.Chechkin.

3.5.5. LINEAR DISCHARGE TURBULENT HEATING EXPERIMENT. ION HEATING AND OSCILLATIONS WITH FREQUENCIES NEAR 561
K.Adati, R.Sugihara, T.Uyama, K.Watanabe.

3.5.6. RF TURBULENCE HEATING IN TOROIDAL MACHINE 565
S.Corti, G.Lisitano, G.Pacher, H.Renner, H.Ringler, E.Würsching.

3.5.7. PROPAGATION OF "SWITCH-ON" SHOCK IN A MAGNETIZED COLLISIONLESS PLASMA 569
T.El-Khalafawy, M.El-Nicklawy, M.El-Gwaily, A.Beshara, V.Demchenko and N.I.Rudnev.

3.6. AGAIN ABOUT RF AND SNOCK HEATING

3.6.1. EXPERIMENT ON MAGNETOACOUSTIC EIGENOSCILLATIONS IN A PLASMA CONFINED IN A PURELY POLOIDAL MAGNETIC FIELD 575
M.Bureš, E.Tennfors and B.Thorstensen.

3.6.2. NUMERICAL SIMULATION OF HIGH-FREQUENCY HEATING OF PLASMA 579
Yu.S.Sigov and Yu.V.Khodirev.

3.6.3. PLASMA HEATING AND DAMPING OF THE FAST WAVE NEAR THE SECOND HARMONIC OF THE ION CYCLOTRON FREQUENCY 583
R.Dollinger, M.Kristiansen, M.O.Hagler and J.Bergstrom.

3.6.4. LOCALIZATION OF ELECTROMAGNETIC WAVE ABSORPTION PROCESSES IN A PLASMA OF TOROIDAL DISCHARGE 587
V.E.Golant, M.M.Larionov, L.S.Levin, L.P.Pakhomov, K.A.Podushnikova, V.V.Rozhdestvensky, G.A.Serebreny.

3.6.5. PROPAGATION OF TORSIONAL ALFVEN-WAVES IN INHOMOGENEOUS AXISYMMETRIC MAGNETIC FIELDS 591
G.Müller, E.Räuchle and P.G.Schüller.

3.6.6. EXPERIMENTS ON PRODUCING THE PLASMA OF HIGH-β BY LONGITUDINAL SHOCK WAVES 595
A.G.Es'kov, O.A.Zolotovsky, P.Kh.Kurtmullaev, Ya.N.Lauhin, A.J.Malyutin, A.J.Markin, V.N.Semenov.

3.6.7. SHOCK HEATING IN TOROIDAL SYSTEMS WITH ELONGATED CROSS SECTION 599
A.G.Es'kov, R.Kh.Kurtmullaev, A.I.Malutin, V.N.Semenov, A.L.Chernyakov.

3.6.8. CO_2 LASER BEAM ABSORPTION BY A PLASMA NEAR PLASMA FREQUENCY 603
E.Fabre, C.Stenz, J.Maignan.

3.7. THEORETICAL ASPECTS

3.7.1. STRUCTURE OF A BOUNDARY LAYER SEPARATING A FIELD FREE PLASMA FROM A VACUUM MAGNETIC FIELD 609
R.Gruber, E.G.Weibel.

3.7.2. THE MOTION OF THE CHARGED PARTICLES IN A MIRROR MACHINE IN THE PRESENCE OF THE CYCLOTRON OSCILLATIONS 613
A.V.Timofeev.

3.7.3. COMPUTER SIMULATION OF RF-PLASMA CONFINEMENT 617
J.L.Shohet, A.J.Hatch.

3.7.4. ABSORPTION OF ALFVEN WAVES IN A PLASMA CYLINDER WITH DISTRIBUTED CURRENT 621
Z.Jankovich.

3.7.5. STABILIZATION OF VOLUME FLUTE MODES IN MIRROR MACHINES BY THE ELECTRODE FEEDBACK SYSTEM 625
V.V.Arsenin.

3.8. STABILITY /THEORY/

3.8.1. LOW FREQUENCY STABILITY THEORY OF AXISYMMETRIC TOROIDAL PLASMAS 631
J.W.Connor, R.J.Hastie.

3.8.2. THE INFLUENCE OF HIGH-FREQUENCY ELECTROSTATIC OSCILLATIONS ON THE LOW-FREQUENCY PLASMA INSTABILITY 635
V.Kopecký.

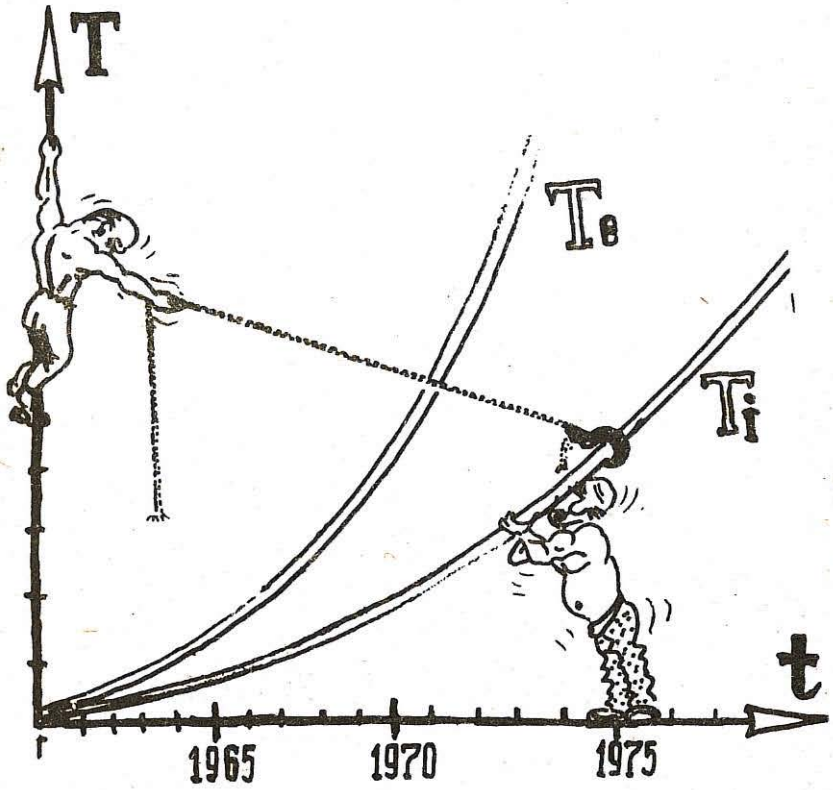
3.8.3. CANONICAL METHOD FOR CALCULATION OF ELECTROSTATIC PLASMA WAVES AND ENERGY-MOMENTUM CONSERVATION LAWS 639
J.Lacina.

3.8.4. CONVECTIVE ION SOUND MODES AND ANOMALOUS SKIN EFFECT 643
F.Santini.

3.8.5. EXCITATION OF ELECTROMAGNETIC WAVES IN PLASMA BY FUSION PRODUCTS 646
T.D.Kaladze, D.G.Lominadze, K.N.Stepanov.

3.8.6. A NUMERICAL INVESTIGATION OF THE STABILITY CRITERION FOR INHOMOGENEOUS NON-MAXWELLIAN VLASOV EQUILIBRIA 650
S.Cuperman, I.Tzur.

1.1. TOKAMAKS: LARGE DEVICES



BEHAVIOR OF IONS IN THE TOKAMAK-4 PLASMA.

E.P.Gorbunov, V.S.Zaverjaev, M.P.Petrov[x].

I.V.Kurchatov Institute of Atomic Energy, Moscow, USSR.

It was suggested in Ref. [1] that when the magnitude of the discharge current J exceeds 150-200ka in the Tokamak-4 device the growth rate of the ion temperature with the current should be greater than $J^{1/3}$ because under these conditions the ions should pass from the plateau region into the collisionless "banana" region. The principal object of the present work has been to test experimentally that conclusion.

The ion temperature was determined from an energy analysis of charge exchange atoms. For this purpose a five channel atomic particle analyzer developed at the Ioffe Institute has been first used. It allows obtaining five fluxes of definite mass atoms simultaneously for five energy ranges. The measurements were carried out in the stationary stage of a discharge near the current maximum. The tipical deuterium energy spectrum measured from a single T-4 operational pulse is shown in Fig.1. For comparison, the deuterium spectrum measured by a single channel analyzer during some 20 pulses in the T-3a device is also shown. Fig.2 illustrates the energy spectrum of deuterium (I) and hydrogen (II) atoms measured in two succesive pulses. In this case deuterium was used as the working gas. But it is seen that the analyzer being adjusted on hydrogen registrated a small flux of fast hydrogen atoms which was 5-7% of that of deuterium atoms. It is likely that hydrogen flux was due to the

---

[x] A.F.Ioffe Physical-Technical Institute

saturation of liner walls with hydrogen during preceeding experiments. It follows from the comparison of these spectra that both hydrogen and deuterium ions of a hydrogen-deuterium plasma are in thermal equilibrium up to the energy $E \approx 4$keV.

Fig.3 is the result of a comparison of the deutron temperatures determined both from the spectrum of charge exchange atoms T_d^a and d-d reaction intensities T_d^n, the latter was determined from neutron flux measurements /2/. In the latter case the ion temperature profile is supposed to be the same as that obtained by L.A.Artsimovich from the solution of the energy balance equation, and shown on Fig.4. It has been also supposed that the profile of the deutron density $n_d(r)$ is parabolic and equals the electron density $n_e(r)$ measured with a microwave interferometer. It follows from Fig.3 that in spite of the fact that the neutron emission is observed to correspond roughly to the deutron temperature T_d^n is ussually less than T_d^a.

It has been shown /3/ that the stationary ion temperature in the plateau region obeys the dependence $T = 5{,}9 \cdot 10^{-7} \cdot \xi$ where $\xi = A^{-1/2}(JH_z\bar{n}_eR^2)^{1/3}$. Fig.5 shows the temperature T^a versus ξ. It is seen that the ion temperature is not observed to increase more repidly than $T = 5{,}9\ 10^{-7} \cdot \xi$ at large values of ξ ($\xi > 9\ 10^8$) corresponding, as a rule, to $J > 150$ka. Moreover, in a number of cases the proton temperature of a hydrogen plasma is found to be lower than that predicted by this dependence, and for equal disharge conditions (J, H_z, n_e) it is close to the temperature of a deuterium plasma. It should be pointed out that in these experiments large amount of multicharged ions could be present in the discharge due to poor vacuum conditions. There is also a reason to expect that the amount

of impurities in hydrogen should be greater than that in deuterinm. This could result in a deviation of T_p^a from the calculated values. Increased interaction between a plasma column and the limiter at large discharge energies could also be a sourse of impurities.

Furthermore, in the presence of impurities the d-d reaction yield should be $(n_d/n_e)^2$ times less compared to a pure deuterium plasma. The value of $\alpha_d = \frac{n_d}{n_e}$ can be evaluated from neutron flux measurements and T_d^a on assuming that the profile $T_d(r)$ corresponds to that shown in Fig.4. In various discharges, α_d varied from 1.0 to 0.2 near the current maximum. It follows from Fig.6 which shows α_d versus the current J that the relative concentration of deutrons decreases, as a whole, with increased discharge energy. With a given kind of impurity ions it is possible to estimate the content of these ions in the plasma. Thus, $\alpha_o = \frac{n_o}{n_e}$ reaches 10-11% for fully ionized oxygen ions while $\alpha_w = \frac{n_w}{n_e}$ is 2% for forty-fold ionized tungsten ions. The calculations have shown that under our conditions the presence of 4-5% of fully ionized oxygen ions may result in the fact that the main plasma ions pass from the collisionless region to the plateau region.

Therefore, the above experiments show that appresiable impurities leading to an increased effective i-i collision frequency in the T-4 plasma did not allow the ion constituent to reach the "banana" region. This factor, however, does not seem to disturb the classical character either of heating or thermal conductivity of ions.

This work was suggested and guided by L.A.Artsimovich. The authors wish to thank V.A.Sadovnikov for his assistance in measurements, and all the stuff of the T-4 device.

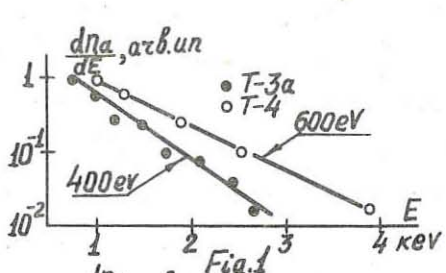


Fig.1

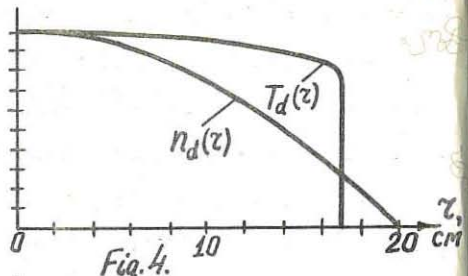


Fig.4.

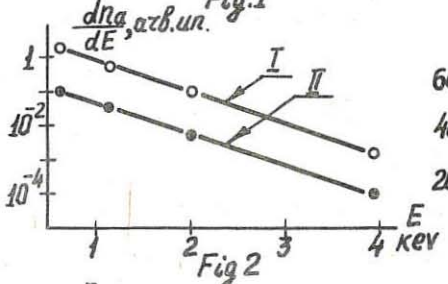


Fig 2

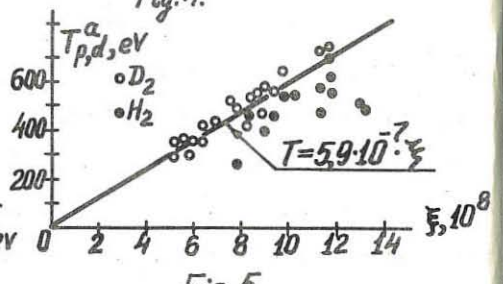


Fig.5

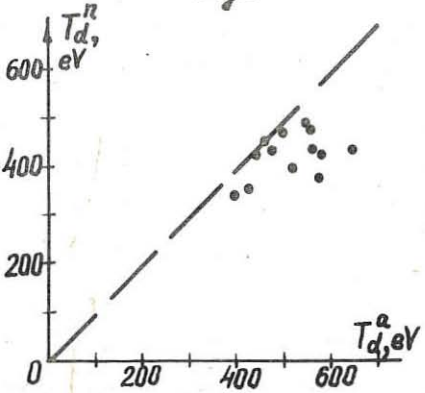


Fig.3

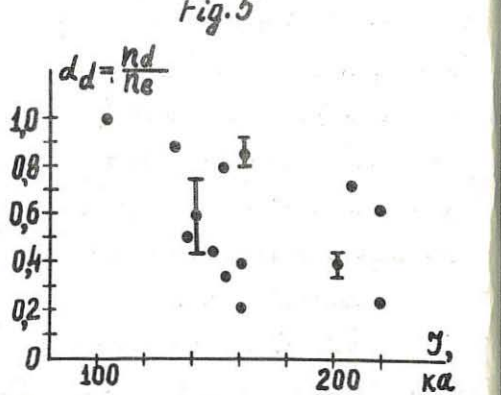


Fig.6.

References.

1. V.S.Strelkov, 5th European Conf. on Controlled Fusion and Plasma Phys., Grenoble (1972), vol.II, p.13.

2. L.A.Artsimovich et al, JETP, 61 (1971), 575.

3. L.A.Artsimovich et al, JETP Lettes, 11 (1970), 449.

6th EUROPEAN CONFERENCE ON CONTROLLED FUSION AND PLASMA PHYSICS

THE CLEO TOKAMAK EXPERIMENT

J W M Paul, A Gibson, J Hugill, J Lang*, P Reynolds P E Stott
UKAEA, Culham Laboratory, Abingdon, Berkshire, England

ABSTRACT We describe the apparatus and how we brought it into operation as a tokamak suitable for neutral injection. Pulses of 100ms with 80kA have been achieved with conductivity temperatures of 130eV and spectroscopic temperatures of 200 ÷ 400eV.

INTRODUCTION

The CLEO experiment is designed to be a high shear stellarator which will extend the programme of the PROTO-CLEO experiment to higher fields and temperatures. However during the construction phase we decided to use the anticipated interval between the completion of the toroidal field system and the helical winding to carry out some exploratory tokamak experiments.

Apart from the obvious aim of commissioning the CLEO machine and its diagnostics, these experiments were designed to answer two questions:

1. Can we obtain gross stability of an iron cored tokamak using a vertical field instead of the usual conducting shell?
2. Can appreciable power be fed into such a plasma using a neutral atom beam without seriously disturbing it?

The answer[1] to both is affirmative and so we can proceed to the new DITE tokamak experiment with more confidence.

APPARATUS

The toroidal field $B_\varphi \leq 2T$ is provided by 24 coils powered by 4 generators in series-parallel deliverying 6MW for 1 second. The low available power necessitated liquid nitrogen cooling and a consequent low repetition rate (4 per hour) at full field. However, the cryostat coils are slim and provide good access particlarly for tangential injection (110mm dia). Electron beam tests showed 0.1% lack of horizontal closure of B_φ which was corrected by applying an additional radial field (B_R). The toroidal field system was brought into reliable operation in January 1973.

For speed of construction the discharge tube was welded from available stainless steel octants (5mm thick) to form a 'lobster back' torus with major radius $r = 0.9m$ and clearance minor radius 0.19m. There is no liner and the torus cannot be baked. Viton vacuum seals are used and the tube is pumped to a working base pressure of 0.2μtorr. Normally gas is admitted by a fast acting valve.

The limiter has upper and lower halves, each consisting of two quadrant arcs of molybdenum (12mm dia) with a preionization filament between them (normal limiter radius $r_L = 0.18m$).

The plasma current is produced by coupling a group of capacitor banks to the

torus through a 0.8 v-s central transformer core with two return limbs. Turns ratio between 10:1 and 16:1 have been used. The capacitor banks, 17kJ at 5kV, 39kJ at 1.5kV and five of 62kJ at 0.5kV are fired in sequence to provide flat-topped current pulses of up to 80kA for 0.1s.

In the absence of a stabilizing shell theory[2] predicts that equilibrium can be obtained by applying a vertical field (B_z) proportional to the plasma current

$$B_z/I = F(r,R,\beta_\theta)$$

with a gradient $-1.9 < m < 0$ where $m = (R/B_z)dB_z/dR$.

The experiment was initially operated using the designed B_z system with $m = -0.7$. An inner B_z coil with an outer return coil was fed in parallel with the transformer primary to ensure $B_z \propto I$, but shunted by an LR circuit to adjust F. Small variation (<10%) in F (e.g. due to β_θ) during the pulse could be obtained by an additional B_z winding powered by a 25kW DC amplifier fed with a plasma position signal proportional to the displacement from equilibrium.

However, early in the programme failure of the inaccessible inner B_z coil forced us to use an alternative system. The stray flux from the core was deliberately unbalanced so as to provide the main vertical field. The outer B_z winding, compensated by a return on the core and shunted, provided adjustment of F. This B_z system has up to 30% variation round the major azimuth and we can only estimate the effective average value and gradient $-0.7 < m < -0.1$. With this system we found that the B_z and B_R required for equilibrium are functions of core bias.

The multi-aperture ion source in the neutral injector, working at 25kV, provides a 40ms pulse of up to 50kW of neutrals into the plasma. The total additional flux of gas from the neutralizer into the torus would give about 50% increase in the usual operating density if it all arrived during the pulse.

Standard tokamak measurement facilities are either available or nearly commissioned. In addition we have operating facilities for measuring (a) the flux of high energy charge exchange neutral atoms resulting from the trapping and slowing down of injected particles, (b) the far infra-red emission near the harmonics of the electron cyclotron frequency, and (c) the fluorescence from neutral hydrogen induced by a dye laser. We also have ready to install a system for measuring the poloidal field by the photon scattering technique.

DISCHARGE CLEANING

A 50Hz AC discharge provided weak baking (< 100°C) for 40 hours and improved the main discharge conductivity temperature from T_σ = 5 to 25eV. More effective discharge cleaning was obtained from 15ms pulses of 15kA at low $B_\varphi \sim$ 0.2T with repetition rates up to 3 per min. After 1500 such discharges in hydrogen the bas

pressure (p_o) was reduced from 1 to 0.5μtorr and tokamak discharges were obtained with 40kA for 40ms with $T_\sigma \sim 90$eV. Cleaning in hydrogen gave rise to OH and to large voltage spikes which damaged the insulation. Discharges in He and Ne were more satisfactory. A total of 5000 cleaning pulses gave $p_o = 0.2\mu$torr and tokamak pulses of 0.1s with 80kA and $T_\sigma \sim 130$eV.

Apart from the first few pulses of the day, cleaning effects cannot be observed spectroscopically. However, there is a clear tendency for the cleaning pulse voltage to become more 'hashy'. Even after exposing the vacuum surfaces to an atmosphere of dry nitrogen, a few hundred cleaning pulses restores clean operation.

ESTABLISHING NORMAL TOKAMAK OPERATION

The initial drastic improvement from $T_\sigma \sim 5$eV to 90eV was accompanied by greater sensitivity to B_z and B_R and by greater difficulty in initiating breakdown.

At this stage four different phenomena prevented normal tokamak operation.

1) Plasma motion of more than 40mm from the tube centre produced a current chop. This lack of equilibrium was eventually corrected by suitable $B_z(t)$.
2) Central equilibrium achieved but with near zero volts and copious hard x-ray emission, sometimes accompanied by regular positive voltage pulses. This is characteristic of appreciable runaway electron current.
3) Central equilibrium suddenly disturbed by strong inward motion accompanied by copious x-rays, and abrupt decrease in resistance and sometimes positive voltage pulses. Again this is characteristic of appreciable runaway.
4) Motion as for (3) above but accompanied by abrupt increase in resistance and definite negative voltage spikes. This phenomenon, which occurred earlier at higher current or pressure, is characteristic of disruptive instability.

The inward motion in (3) and (4) is probably due to a reduction of β_θ by cooling and in case (3) was controlled by the amplifier fed B_z.

At this stage there was no regime between low pressure runaway, (2) and (3), and high pressure disruption (4). The initial pressure 20μtorr was well below normal tokamak operation and the density rose to 10 times the filling pressure.

Further cleaning allowed operation at higher pressure 0.1mtorr and reduced the density rise. This, together with better control of $B_z(t)$ and regular operation at $B_\varphi = 2$T, yielded the desired tokamak conditions.

TOKAMAK CONDITIONS

A typical tokamak pulse of 100ms with 77kA is shown in Fig.1. We have obtained discharges with peak $T_\sigma \sim 130$eV, (assuming parabolic current profile). The absence of appreciable x-ray emission and spectroscopic observations, support the view that this is a normal tokamak discharge without appreciable runaway. The equilibrium is described in an accompanying paper by Hugill et al[2].

We have time resolved the rapid burn through of OI to OV (e.g. Fig.2). This sequence corresponds, on the theory of McWhirter[3], to $T_e \sim 200$ to 400eV. The vacuum UV plate spectra show strong emission of OVII (22Å), OVIII (19Å), CVI (34Å) and with 1% Ne added, Ne X. These lines indicated temperatures of several 100eV. These spectroscopic temperatures are consistent with the usual tokamak condition $\beta_\theta \sim 0.5$ and the usual anomaly factor $T_e \sim 2 \div 3\ T_\sigma$.

The final mean density ($n_e \sim 3 \times 10^{19} cm^{-3}$) is $2 \div 3$ times the pulsed filling pressure but, at the end of the initial ionization phase (1ms burst of H_β emission), n_e corresponds to only half the filling pressure (Fig.2). A pulse of gas, identical to that used for filling, fired into the plasma during the pulse, was fully ionized. There is probably appreciable loss of plasma during the formation phase.

The injection of a 50kW neutral beam into a 200kW discharge, as described by Sheffield et al in an accompanying paper, produced no appreciable disturbance. The observed slowing down of 25keV ions from the beam is consistent with the above temperatures.

Preliminary measurements with the far infra-red detector (1 to 5mm) by Costley of NPL(London) show a level of emission above the classical expectation and also unpolarized.

REFERENCES

1. A Gibson et al, 1973 3rd Int.Symp.on Toroidal Confinement, Garching.
2. Green J M., Johnson J L., Weiner K E., Phys.Fluids 14, 671, 1971.
3. McWhirter R W P., Plasma Diagnostic Techniques, Ch5, Ed. Huddlestone and Leonard, Academic Press 1965.

* Astrophysics Research Division, RSRC, Culham Laboratory.

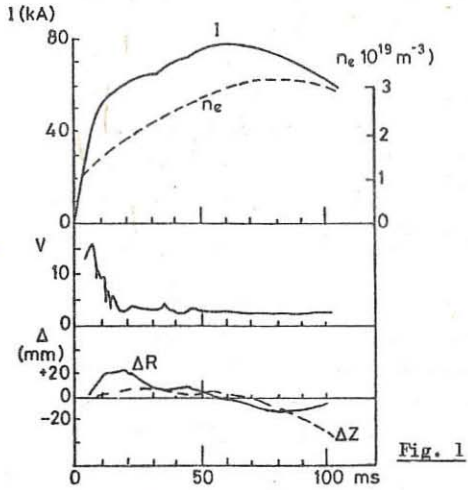


Fig. 1

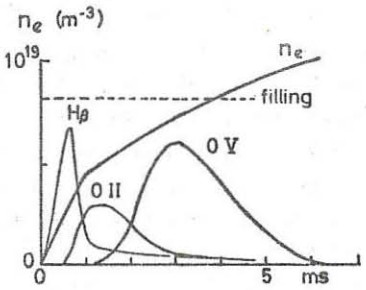


Fig. 2

FIRST RESULTS ON T.F.R.

C. Breton, J.P. Bussac, J.P. Crenn, R. Dei-Cas, M. Delmas,
P. Ginot, M. Huguet, D. Launois, P. Lecoustey, M. Mattioli,
P. Moriette, P. Plinate, Z. Sledziewski, P.H. Rebut,
A. Torossian, J. Tachon,

ASSOCIATION EURATOM-CEA SUR LA FUSION
Département de Physique du Plasma et de la Fusion Contrôlée
Centre d'Etudes Nucléaires
Boîte Postale n° 6. 92260 FONTENAY-AUX-ROSES (FRANCE)

ABSTRACT

The T F R device was completed in the beginning of 73, and the first plasmas obtained.

T F R is a Tokamak with a main radius of 98 cm, and a limiter radius of 20 cm. The toroïdal magnetic field reaches 60 kG on the axis. This apparatus should permit the study of a plasma with the ions in the "banana" regime. This regime should arise for a plasma current greater than 200 kA.

The plasma equilibrium is obtained by means of a thin copper shell and a programmed vertical field. A feed-back control of the plasma position will be added.

The first discharges obtained exhibited a resistive behaviour with a current of 20 kA and a density of 5.10^{13} cm^{-3}. After some discharges we obtained at the same density a current of 50 kA with a few Volts per turn.

The evolution of the plasma is given by the following diagnostics : a multicanal interferometer, magnetic probes, Hβ line and X ray measurements.

The lastest results obtained on T F R will be presented.

CONFINEMENT OF AN ANOMALOUSLY HEATED PLASMA IN A TOKAMAK (T.T.F.)

M. Martone

Laboratori Gas Ionizzati (Associazionte EURATOM-CNEN), C.P. 65
00044 Frascati, Rome, Italy.

ABSTRACT

Fast current diffusion ($\tau < 1$ μsec) in a preionized H_2 plasma (4.5 mTorr) and plasma heating ($\beta_p = 0.4$) has been observed in a tokamak-like experiment (R = 30 cm, a = 4 cm, B_T = 6,2 kG, I_p = 7.6 kA). A theoretical analysis of the current diffusion including ohmic heating gives an increase of the resistivity during the current diffusion phase by a factor ~ 60 with respect to the Spitzer value. After the current diffusion (heating) phase, the plasma current, decoupled from the energy source, decays in a time which depends on the toroidal magnetic field strength.

INTRODUCTION

This experiment has been designed to study the confinement of an anomalously heated plasma in a tokamak-like magnetic configuration. The anomalous heating of toroidal plasma has been studied in many devices / 1 / at low density ($n \simeq 10^{12}$ cm^{-3}), and in linear devices / 2 / at higher density ($n \simeq 10^{14} \div 10^{15}$ cm^{-3}). The main results of such experiments are the observation of a fast plasma heating stronger than the one expected due to classical ohmic heating, and the identification of two regimes of anomalous resistivity depending on the intensity of the electric field applied to the plasma, the low frequency (acoustic) and the high frequency (Buneman) ion wave turbulence regimes. The present experiment works in the ion acoustic turbulence regime, where the conditions for the turbulence to be triggered are: $j_p > n e c_s$, $c_s = \sqrt{\frac{K T_e}{M}}$.

APPARATUS

The toroidal magnetic field (B_T) coils (24 coils, 3 turns each, R_T = 32 cm, r_T = 12 cm) are driven by a condenser bank; the maximum B_T value is 10 kG with a flat top duration (-5% of the maximum value) of 0.2 msec. A 1:1 air core transformer is used to drive the current in the H_2 gas contained in a toroidal pyrex vacuum chamber (R = 30 cm, r = 5 cm) at 4.5mTorr filling pressure. The primary is made by eight copper wires (Ø = 3 mm) along the major circumference of the torus, symmetrically distributed around the minor circumference on a circle of radius 6.2 cm. This primary structure acts also on the plasma as a shell to provide equilibrium. The primary is open for net poloidal current in order to allow the toroidal field to penetrate the vacuum chamber volume. A tungsten limiter is used (a = 4 cm). The transformer is driven by a condenser bank, (4.8 μF, 32 kV) via an inductance L = 4 μh and a resistor R = 1 Ω . When this bank is discharged the current in the primary

reaches I_s = 18 kA in 5 μsec. The start of the plasma preionization current has a delay of about 2 μsec with respect to that of the primary current and reaches the value of 2.4 kA at 5 μsec. At this time the primary is short-circuited through the 1 Ω resistor and the current goes to zero in a time of ~ 1 μsec. The corresponding plasma current variation is 10 kA, the final net plasma current being 7.6 kA (cf. Fig. 2). After the primary current has gone to zero the plasma current decreases on a time scale which depends on the toroidal field.

HEATING PHASE

By means of a magnetic probe inserted radially in the equatorial plane of the torus, the poloidal magnetic field (B_p) profiles across the diameter have been measured at different times after short circuiting the primary (t = 0). These profiles show that the toroidal current, diffuses across the torus radius in a time comparable with the rise time of the total current. Fig. 1 shows the radial profiles of B_p at t = 1 μsec and t = 2 μsec. At t = 1 μsec the current is fully penetrated. Measuring the voltage V_s on the primary and the plasma current I_p just before t = 0 where $\dot{I}_p \simeq 0$ we obtain an initial plasma resistivity $\eta_o = 1.7\ 10^{-4}\Omega$.m, if the preionization current has a radius equal to the limiter radius, corresponding to an initial temperature T_o of about 2 eV.

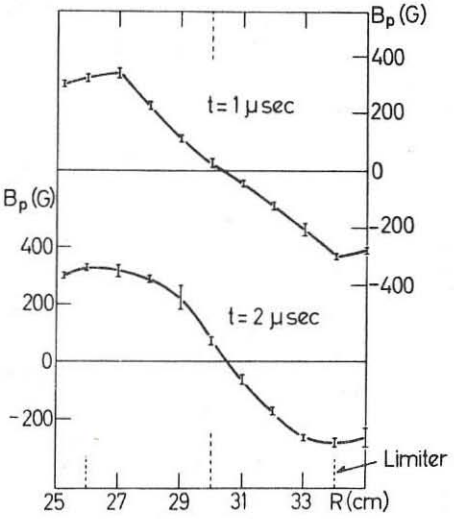


Fig. 1

As at t = 1 μsec the current is completely penetrated into the plasma, it results for its diffusion time $\tau < 1$ μsec. This implies that the resistivity in this phase must be typically $\eta > 6\eta_o$ / 3 /. If, on the other hand, a model with $\eta = \alpha\eta_o\left(\frac{T_o}{T}\right)^{3/2}$ is adopted / 4 / where α is a (constant) enhancement factor with respect to the Spitzer resistivity, diffusion of the current is possible only if $\frac{2}{3}\ \frac{\mu_o a^2 E^2}{\alpha^2 \eta_o^2 n K T_o} \lesssim 1$, where E is the applied electric field. This would yield for the parameters of the experiment $\alpha \gtrsim 60$ and a current diffusion time $\tau = \frac{\mu_o a^2}{\alpha \eta_o} \lesssim 0.2$ μsec. These results indicate that the effective collision frequency $\nu_{ei}^{(eff)}$ is not far from ω_{pi}.

The estimated electron heating is consistent with $\beta_p = 0.4$ measured at the end of the heating phase (t = 2 μsec) corresponding to a temperature of about 10 eV.

CURRENT AND PRESSURE DISTRIBUTIONS IN THE "HIGH ß TOKAMAK" EXPERIMENT TEE

P. Noll, M. Korten, E. Kugler, F. Sand, F. Waelbroeck, G. Waidmann

Institut für Plasmaphysik der Kernforschungsanlage Jülich GmbH
ASSOCIATION EURATOM-KFA

Abstract: Some parameters deduced from poloidal magnetic field profiles obtained in TEE shortly after the fast compression and from equilibrium relations [1] are discussed. In contrast to the screw pinch, these plasmas of lower density are surrounded by a "vacuum" ($\nabla \times B \approx 0$) magnetic field configuration.

A major objective of TEE (fig. 1) [2] is the study of plasma behaviour in a tokamak-like configuration at $\bar{\beta}$ ratios ($\approx 10\%$) close to those required in an economic thermonuclear device. The plasma is heated by fast magnetic compression ($U \lesssim 120$ kV, $\omega = 10^{+6} s^{-1}$) with little consecutive adiabatic compression ($\hat{B}_\varphi \lesssim 10$ kG) in a compact pyrex vessel (R/b = 2.6) surrounded by a partial copper shell which allows a fast programming of the transverse equilibrium field $B_\perp$ [3]. Typically, at the end of the implosion with $\hat{B}_\varphi \approx 4.5$ kG, the plasma aspect ratio $R/a \approx 4$, $q = 2\pi/\iota \approx 1$, the average density $\overline{n_e} \approx 1.5 \cdot 10^{14} cm^{-3}$, the temperature can be varied in the range $30\ eV < T < 150 eV$, and $1.5\% < \bar{\beta} < 12\%$. Higher temperatures and ß's can be produced, but the outward shift of the plasma is then very large.

TEE is similar to a screw pinch. In order to obtain information relevant to Tokamak we had to ensure that the large forcefree currents which flow outside of the main plasma in a screw pinch and affect strongly its equilibrium and stability behaviour [4] are absent here. This was one reason for chosing a low filling pressure p_o: the density close to the wall (some $10^{12} cm^{-3}$) should then be too low to support significant current densities for a long time since v_{De} would be much larger than $\sqrt{kT_e/m_i}$ in the outer regions.

In TEE, in contrast to Tokamak, no energy is fed to the plasma after the heating pulse. Thus, although the plasma energy densities are initially of the order of those reached in quasi-stationary

tokamak operation, internal magnetic probes can be used without being destroyed: the energy deposited on the probe cannot exceed the total initial plasma energy. The probe dimensions are considerably smaller than the plasma cross-section and than the mean free paths. The perturbation caused by the probe is expected to be small during the initial period of plasma confinement, and indeed the signals of external diagnostics are not affected by the insertion of the probe array.

In what follows, we discuss the information which is derived from B_ω-profiles obtained shortly after the end of the heating phase. We can compute the poloidal flux $\psi(\Sigma) = 2\pi \int_{R_o^*}^{R^\pm} B_\omega(R) R dR$ and, assuming nearly circular cross-section for the magnetic surfaces, the toroidal current density $4\pi\, j_\varphi(R^\pm) = \frac{\partial B_\omega}{\partial R} + \frac{B_\omega}{\varrho}$; $R^\pm = R_c(\Sigma) \pm \varrho(\Sigma)$ are the intersections of the surface Σ with the equatorial plane, $R_c(\Sigma)$ = center of Σ, R_o^* = magnetic axis. When an equilibrium is achieved, one obtains from the displacement $\Delta(\varrho) = R_c - R_o^*$ [1]:

$$S(\varrho) = \frac{\bar{p}(\varrho) - p(\varrho)}{B_\omega^2(\varrho)/8\pi} = \frac{R_c}{\varrho} \cdot \frac{d\Delta}{d\varrho} - \frac{\ell_i}{2} = \frac{R_c}{\varrho} \cdot \frac{R^+ B_\omega^+ - R^- B_\omega^-}{R^+ B_\omega^+ + R^- B_\omega^-} - \frac{\ell_i}{2} \quad (1)$$

from which the pressure profile and β_{pol} can be deduced. $S(\varrho)$ can be obtained experimentally with reasonable accuracy (except for $\varrho \ll a$). It offers a sensitive criterium for the relative shapes of current and pressure profiles. Four cases are illustrated on fig.2. In particular, a constant pitch pressureless current distribution leads to a strong decrease $S(\varrho) \propto \varrho^{-4}$ outside of the main plasma, whereas $S(\varrho)$ = const. for $\varrho > a$ when the plasma is surrounded by a vacuum field distribution.

Fig. 3 shows the evolution of the $S(\varrho)$- and of the current density profiles for a case where the $\bar{\beta}$-value was kept small by using a relatively large initial bias field (~500G) before the fast magnetic compression. In this way, and by applying an appropriate external $B_\perp$-field [3], conditions should be established where the cross-section of the magnetic surfaces are reasonably circular. Fig. 4 shows in addition the pressure profile at t = 1.8 /usec deduced from eq. (1). After 1.6 /usec the external value of $S(\varrho)$ is almost constant ($\beta_{pol} \gtrsim 1$) indicating that a radial equilibrium is practi-

cally achieved. This is confirmed by Doppler shift measurements which show that the plasma velocity in the R-direction is strongly reduced after 1.5/usec in accordance with the observed displacement of the magnetic axis. At t = 1.8/usec, the total plasma current $I_p \approx 20$ kA, $\beta_{pol} \approx 1.1$, $(T_e+T_i)/2 = \beta_{pol} \cdot I_p^2/400N \approx 30$eV assuming complete ionisation at p_o=1.2 mtorr, $q \approx 1.4$ on the magnetic axis and reaches 2 at ϱ = 6 cm, the current density in outer regions (ϱ >7cm) is small.

This method was also applied to former experiments with higher $\overline{\beta}$ [5] where other diagnostic methods were used. The results agree with those already published.

The plasma evolution after crowbar is to be studied with an improved set-up. It is hoped to present new results at the conference.

Conclusion. The measured B_ω profiles allow to deduce the distribution of the plasma current and pressure, of q, the total plasma current and energy in TEE at the start of the confinement phase. Whenever a cross-check was possible, good agreement with other diagnostic methods was found. The broad pressure profiles indicate a moderate compression ratio. Weak residual skin effects are still apparent (compare $S(\varrho)$ of fig. 2d and 3), but the current density in outer regions ($\varrho > 7$ cm) is small. The MHD equilibrium and stability behaviour should then be governed by the usual "tokamak" equations with an outer "vacuum" field distribution.

References

[1] V.D. Shafranov, Rev. Plasma Physics, M.A. Leontovich ed. Consultants Bureau, N.Y. vol. 2, p. 103

[2] H.J. Belitz et al., Plasma Physics and Contr. Nuclear Fusion Research, IAEA Vienna (1971), Vol. III, p. 179

[3] F. Sand et al., 3rd Int. Symp. on Toroidal Plasma Confinement, Garching, March 1973, paper A-9

[4] C. Bobeldijk et al., Plasma Physics and Contr. Nuclear Fusion Research, IAEA Vienna (1969), Vol. I, p. 287

[5] F. Waelbroeck et al., 5th Eur. Conf. on Contr. Fusion and Plasma Physics, Grenoble (1972), Vol. I, 9.

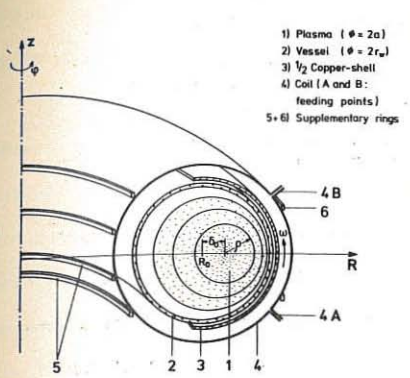


Fig. 1 the TEE experiment: R_o=25cm, r_w=9.5cm, $(LC)^{1/2}$ = 1 /us. The helically wound main coil has an angular pitch $\Delta\varphi$=100° and produces practically no $B_\perp$ inside the vessel ($B_\perp \approx 0.01\ B_\varphi$)

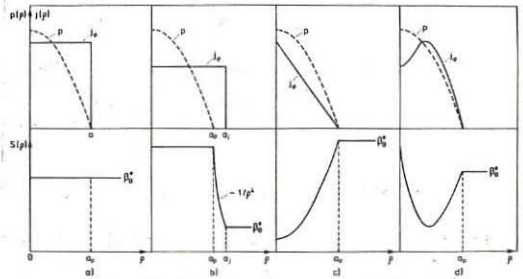


Fig. 2 Schematic profiles $S(\varrho)$ for a parabolic pressure distribution $p(\varrho)$ and 4 different current distributions $j_\varphi(\varrho)$; the shape of $S(\varrho)$ is sensistive to the current distribution. In particular, for the "constant pitch pressureless current" (b), $S(\varrho) \propto 1/\varrho^4$ outside of the confined plasma. A skin effect (d) results in a minimum in the $S(\varrho)$ profile.

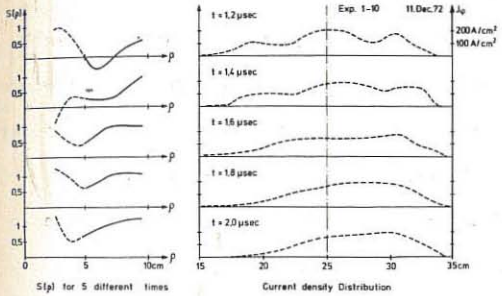


Fig. 3 Experimental evolutions of S (ϱ) and j_φ(R) at the end of the compression phase. After 1.5 /us, the radial equilibrium appears to be reached and that skin currents are practically damped.

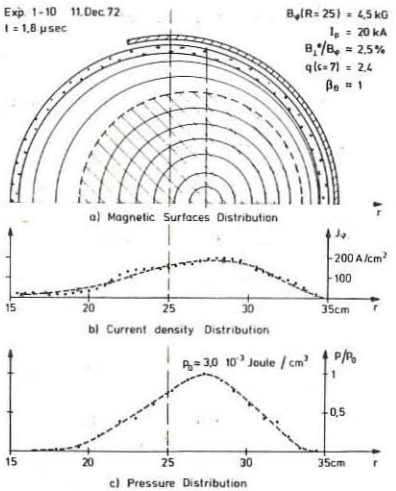


Fig. 4 Pressure and current distributions at the time of maximum field B_φ. In this case, the aspect ratio remains relatively small (R/a ≈4), the current density is small in the outer domain.

Stability and Heating Experiments on the ATC Tokamak

K. Bol, J. L. Cecchi, C. C. Daughney,
R. A. Ellis, Jr., H. Eubank, H. P. Furth, R. A. Jacobsen,*
L. C. Johnson, E. Mazzucato, and W. Stodiek

Plasma Physics Laboratory, Princeton University
Princeton, New Jersey 08540, U.S.A.

The ATC experiment was designed to provide information about two major areas of tokamak research: non-Ohmic heating and MHD stability. The success of the compressional heating method has been described in several publications [1,2], and is also reviewed at the present conference [3]. We will discuss here (1) the MHD stability of the precompression discharge, (2) some new results on the nature of the disruptive instability that occurs in all tokamaks at high gas filling pressure, and (3) some new plasma heating experiments which are now in progress.

1. MHD Stability of the ATC Discharge

Conventional tokamaks utilize a copper shell to provide stability against axisymmetric vertical and horizontal displacements ($n = 0$, $m = 1$) and to improve stability against kink modes ($n = 1, 2, 3, \ldots$; $m = 1, 2, 3, \ldots$). The particular interest of the ATC device from the MHD stability point of view is that the copper shell is eliminated. It is found that a weakly curved vertical magnetic field B_v is sufficient to provide stability against the $n = 0$, $m = 1$ mode. The plasma major radius is determined by proper programming of B_v as a function of time. Recently, the addition of a feedback system has facilitated holding the major radius to within ± 1 cm of any desired position in the range 70-90 cm. Additional stability against vertical displacement of the plasma

* On leave from South African Atomic Energy Board.

column is provided by a system of passive copper loops positioned above and below the vacuum vessel and connected so that they do not link vertical fields.

With respect to the kink modes the ATC discharge is very similar to those reported for conventional tokamaks [4,5]. For a typical precompression regime with $T_e \sim 1$ keV, $T_i \sim 200$ eV, $n_e \sim 2 \times 10^{13} cm^{-3}$, $I_p \sim 60$ kA, $R = 90$ cm, $a = 17$ cm, $B_T = 15$ kG, the limiter q-value is 4.0. At the same toroidal field, discharges can be produced at maximum currents of about 100 kA, corresponding to $q_{lim} = 2.4$. In this case, however, large $m = 2$ perturbations are detected by magnetic pick-up loops. Thomson scattering measurements show that T_e is increased somewhat by the higher currents, but that β_θ and the confinement time are diminished. As reported previously for a copper-shelled tokamak [4], the q-value for optimum energy confinement, falls substantially short of the lowest attainable q-value.

Recent experiments with $B_T = 20$ kG (the full design value of the ATC) have provided 100-kA discharges with $q_{lim} \geq 3$ which show no large $m = 2$ oscillations. Peak precompression temperatures are about $T_e = 1.5$ keV at $n_e = 2 \times 10^{13} cm^{-3}$.

2. Disruptive Instability

The ATC voltage traces under standard conditions are free of "negative voltage spikes" [4], even during the initial current rise. This is probably due to the fact that the plasma does not usually contact the inner and outer limiters during the discharge. By adding small admixtures of neon (about 5%) and operating at high filling pressure, we can, however, produce the usual phenomena [4] of the "high-density limit": cyclical discharge channel contraction in minor radius, followed by rapid re-expansion and negative voltage spikes.

The absence of a copper shell in ATC, provides access for discharge photography in the direction tangential to the major circumference. In Fig. 1 we thus see the minor circumference of the discharge outlined by a bright ring. (The ring represents a relatively low-temperature plasma region, where neutrals are ionized and impurities can remain partly stripped [6].) The figure shows the expansion and "brightening" of the ring in the case of small negative voltage spikes (top) and a large spike (bottom). We will discuss correlation of the optical record with simultaneous measurements on the voltage, current, and harmonic content of the precursor magnetic oscillations. A feature of principal interest is the apparent symmetry of the minor radius expansion, which appears to contradict the interpretation of the disruptive instability as a gross MHD kink mode. The exposure time in Fig. 1 is 20 μsec, so that some "smearing" of rapidly rotating MHD perturbations might be arguable. Recently the study was repeated with 5 μsec exposures, yielding the same results as in Fig. 1.

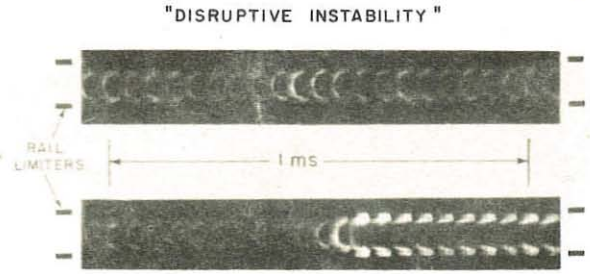


Figure 1.

3. New Heating Experiments

The ATC mechanical structure is being strengthened, to allow compression of 100-kA discharges at the full toroidal field. The possibility of exceeding present compressed plasma parameters ($T_e \sim 2.5$ keV, $T_i \sim 600$ eV, $n_e \sim 10^{14}$ cm^{-3})

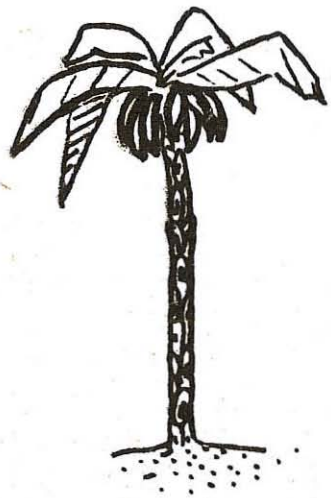
will be investigated. To increase the precompression ion temperature, we are also planning to inject a neutral beam of 5 A, 17 keV.

This work was supported by U. S. Atomic Energy Commission Contract AT(11-1)-3073.

REFERENCES

1. K. Bol et. al., Phys. Rev. Lett. 29, 1495 (1972).
2. K. Bol et. al., Conference on Toroidal Plasma Confinement, Garching-bei-München, Germany (1973).
3. H. P. Furth, Present Conference (Moscow 1973).
4. L. A. Artsimovich, Nucl. Fusion 12, 215 (1972).
5. J. C. Hosea et. al., in Plasma Physics and Controlled Nuclear Fusion Research (International Atomic Energy Agency, Vienna, 1971), Vol. II, p. 425.
6. H. P. Furth, Conference on Toroidal Plasma Confinement, Garching-bei-München, Germany (1973).

1.2. TOKAMAKS: NEOCLASSICAL TRANSPORT



NEOCLASSICAL TRANSPORT PHENOMENA IN A TOKAMAK

U. DAYBELGE

Institut für Theoretische Physik der Ruhr-Universität
463 Bochum, F.R.Germany

ABSTRACT

The distribution function has been found from the drift kinetic equation, in order to calculate the neoclassical transport coefficients. The solutions we obtain are based on exact Fokker-Planck collision terms and a singular perturbation analysis in the phase space. Our results deviate from the ones obtained using model operators or variational techniques.

In the following we consider an axisymmetric toroidal system in which the variation of field strength over a helical line of force can be approximated as $B(s)=B_{min}(1+\varepsilon^2\cos^2\pi s)$, where $\varepsilon^2=2r/R$ and s is the arc length normalized by the field period $L=4\pi^2R/\iota$. If the distribution function F, is expanded as $F=F^M+\alpha F^1+..$, where α is the ratio of electron Larmor radius to a macroscopic length, we can write for the averaged F^1, $f=(2\pi)^{-1}\int_0^{2\pi} F^1 d\phi$ the well-known drift kinetic equation [1] , [2] in the form

$$\frac{\partial f}{\partial s} + \varepsilon\frac{2\pi}{2}\frac{\sin 2\pi s}{1+\varepsilon^2\cos^2\pi s}\frac{1-x^2}{x}\frac{\partial f}{\partial x} - \frac{v_{th}\eta}{\nu_{ei}vx}\left[\bar{C}_{ei}(f)+\bar{C}_{ee}(f)\right] = \frac{E_{\parallel}v_{th}^2}{E_c v}\frac{\partial F^M}{\partial v} \quad . \qquad (1)$$

In (1) we have left the drift term out. The variable x is related to the pitch angle θ by $x=\cos\theta$. Averaging and linearizing the exact Fokker-Planck operators [3]

$$\bar{C}_{ei}(f) = \nu_{ei}(v_{th}/v)^3\frac{1}{2}\left[-2x\frac{\partial f}{\partial x} + (1-x^2)\frac{\partial^2 f}{\partial x^2}\right] \qquad (2)$$

$$\bar{C}_{ee}(f) = \nu_{ee}v_{th}^3/n\left\{8\pi F^M f + \frac{1}{2}\overline{\nabla_v\nabla_v}\int f(x',\varepsilon)\,|\vec{v}-\vec{v}'|\,d^3v' : \nabla_v\nabla_v F^M + \frac{1}{2}\left[\frac{h_2}{v^2}(1-x^2)\frac{\partial^2 f}{\partial x^2} + (v^2h_1+h_2)\frac{\partial^2 f}{\partial v^2} + \frac{2h_2}{v}\left(\frac{\partial}{\partial v}-\frac{x}{v}\frac{\partial}{\partial x}\right)f\right]\right\} \qquad (3)$$

Assuming that the mean free path is much longer than the field period L, we find $\eta \equiv \nu_{ei} L/v_{th} = \nu_{ei}/\omega_{bounce}$ to be much smaller than unity. Therefore, we look for an asymptotic solution for f to lowest order in both η and ε. Further, we adopt the boundary conditions as stated in [1]. With the ansatz $f=f^0 + \eta f^1 + ..$ equation (1) yields

$$Lf^0 \equiv \frac{\partial f^0}{\partial s} + \frac{\pi}{2}\varepsilon^2 \frac{\sin 2\pi s}{1+\varepsilon^2\cos^2\pi s}\frac{1-x^2}{x}\frac{\partial f^0}{\partial x} = 0 \qquad (4)$$

$$Lf^1 - \frac{v_{th}}{vx\nu_{ei}}\left[\bar{C}_{ei}(f^0) + \bar{C}_{ee}(f^0)\right] = \frac{E_{\parallel}}{E_c}\frac{v_{th}^2}{v}\frac{\partial F^M}{\partial v} \qquad (5)$$

First, we look for an "outer solution" that is valid for $|x| \sim 1$, namely when x is far away from the "trapped particle region" defined as $|x| \leq \varepsilon/\sqrt{1+\varepsilon^2}\sin\pi s$. We note in (4) that for $|x| \sim 1$ the equation of characteristics is $x = \text{Const.} + O(\varepsilon^2)$, and f^0 is independent of s. Using this information in (5) and annihilating Lf^1 through an integration over the characteristics for $0 \leq s \leq 1$, we find the classical Spitzer-Härm problem. Its solution by the Chapman-Enskog-Burnett method [3] can be written as

$$(f^0)_{outer} = -\frac{e\langle E_{\parallel}\rangle}{kT} xvF^M \sum_{r=0}^{N-1} \delta^r(N)\, S_{3/2}^{(r)}(v^2) \qquad (6)$$

Here, $S_{3/2}^{(r)}$ is a Sonine polynomial, and $\langle E_{\parallel}\rangle \equiv \int_0^1 E(s)ds$. The coeffi cients $\delta(N)$ of the N'th approximation are found as $\delta^r = (-1)^r 3D_{or}/2D$ where D is the determinant of the matrix a_{ij}, and D_{or} is the minor of a_{or}. In terms of matrices H_{rs} of 3 we can write $a_{ij} = H_{ij}^{ei} + H_{ij}^{ee}$. The form of the outer solution shows that it is not valid inside the "boundary layer" of trapped particle region. For the "inner region" where $|\tau| \equiv |x|/\varepsilon \sim 1$ we construct an inner solution $\Pi(v,\tau;\varepsilon;\eta)$. Again substituting $\Pi = \Pi^0 + \eta\Pi^1 + ..$, we transform (4) and (5) as

$$\hat{L}\Pi^0 \equiv \frac{\partial \Pi^0}{\partial s} + \frac{\pi}{2}\sin 2\pi s \frac{1}{\tau}\frac{\partial \Pi^0}{\partial \tau} = O(\varepsilon^2) \qquad (7)$$

$$\hat{L}\Pi^1 - (1/2\tau\varepsilon^3)(v_{th}/v)^4(vh_2\nu_{ee}/n\nu_{ei}+1)\frac{\partial^2\Pi^0}{\partial\tau^2} = O(\varepsilon^{-1}). \qquad (8)$$

We consider in (8) that the integral operator become negligible in comparison to the derivative inside the boundary layer. The equation of the perturbed characteristics is $\xi = \tau^2 + \frac{1}{2}\cos 2\pi s = \text{const.}$. Their deviation from the true characteristics is of order ε^2. Over the perturbed separatrix $\xi = \frac{1}{2}$. After annihilation of $\hat{L}\Pi^1$ through

an integration along a characteristic for s from 0 to 1, the dominating term is $\int_0^1 (\Pi^0_{\tau\tau} / \tau)\, ds$. If the integrand is expressed in terms of s and ξ then the result is

$$\frac{d^2\Pi^0}{d\xi^2} + \frac{k^2}{2}\,\frac{F(k)}{E(k)}\,\frac{d\Pi^0}{d\xi} = 0 \qquad (9)$$

Here, F and E are Elliptic integrals of the first and second kind, respectively. We also define $k^2 \equiv 2/(2\xi+1)$. Using relations given for elliptic integrals the solution of (9) is (for untrapped particles)

$$\Pi^0 = D_2 + 2\,D_1 \int_k^1 \frac{dk}{k^2\,E(k)} \qquad (10)$$

To determine the constants of integration in (10) we have to use both the boundary conditions over the separatrix and the matching conditions at $k \to 0$ (or $\tau \to \infty$, or $x \to 0$). Since the integral diverges for $k \to 0$, we write the integral in the form

$$\Pi^0 = D_2 + 2\,D_1 \left[-\frac{2}{\pi k} \Big|_k^1 + \int_k^1 dk\,(1/E - 2/\pi)/k^2 \right] \qquad (11)$$

The new integral in (11) is convergent for all k. Its value can be approximated as $I(k) = .15915 - .03195k^2 + .20099k^3 + .31080k^4 + .18168k^5$. From our definitions for ξ and k it also follows that

$$k^{-1} = (|x|/\varepsilon)\left[1 + (1+\cos 2\pi s)/4(x/\varepsilon)^2 + \ldots\right] \quad (\text{for } x/\varepsilon \to \pm\infty)$$

Comparison of the outer solution (6) and (11) with the last expansion reveals that the distribution function can be written as (for untr.p.)

$$f^0 = -\,\operatorname{sign}(x)\, F^M v \frac{e\langle E_{\parallel}\rangle}{kT} \sum_{r=0}^{N-1} \delta^r(N)\, S^{(r)}_{3/2} \left[-1 + \frac{\pi}{2}\, I(1) + \frac{1}{k} - \frac{\pi}{2} I(k) \right] \qquad (12)$$

In (12) we set $D_2 = 0$, from a consideration of the distribution function of the trapped particles which must vanish and the continuity of the distribution function on the separatrix.

Now, we would like to find the contribution of the other driving force, namely of the "drift term" in the kinetic equation. This term will be responsible for the radial flux of the electrons. For this purpose the drift velocity is written as $V_D = -\{(1+x^2)/2\Omega r\} v^2\, \partial h/\partial \theta_p$, where $h \equiv 1 + (\varepsilon^2/2)\cos\theta_p$ with the poloidal angle θ_p. On expressing the position dependence by θ_p instead of s in the kinetic equation, the proper ordering with respect to η leads to

$$\frac{\partial f^0}{\partial \theta_p} - \varepsilon^2 \frac{1-x^2}{4x} \frac{\sin\theta_p}{h} \frac{\partial f^0}{\partial x} = \frac{1-x^2}{x} \frac{v}{2\Omega} F_r^M \frac{\partial h}{\partial \theta_p} \qquad (13)$$

$$\frac{\partial f^0}{\partial \theta_p} - \varepsilon^2 \frac{1-x^2}{4x} \frac{\sin\theta_p}{h} \frac{\partial f^0}{\partial x} = \frac{v_{th}}{\nu_{ei} vx} \left[\bar{C}_{ei}(f^0) + \bar{C}_{ee}(f^0) \right] - 2 \frac{E_\parallel}{E_c} F^M \qquad (14)$$

Using the method of characteristics the solution of (13) is found as $f^0 = xhvF_r^M/\Omega + g(\lambda)$, where $\lambda = (1-x^2)h = \text{const.}$ is the equation of the exact characteristics. Our task now is to determine the unknown function g. Neglecting smaller terms, in the outer limit ($x \sim 1$) we infer from (13) and (14) that

$$(\bar{C}_{ei} + \bar{C}_{ee}) \left[vxF_r^M/\Omega + g(x) \right] = 2 \frac{\nu_{ei} vx \langle E_\parallel \rangle}{v_{th} \overline{E_c}} F^M \qquad (15)$$

Again, this classical problem can be solved by successive approximations as

$$(f^0)_{outer} = \frac{\varepsilon^2}{2\Omega} vx F_r^M \cos\theta_p - \frac{e\langle E_\parallel \rangle}{kT} xvF^M \sum_{r=o}^{N-1} \delta^r S_{3/2}^{(r)}(v^2) \qquad (16)$$

A similar inner limit process would lead us again to lowest order in ε to $\int_{-\pi}^{\pi} d\theta_p \, \Pi_{\tau\tau}/\tau = 0$, where the path of integration is a perturbed characteristic whose equation is, via (13) $\xi_1 = 2x^2/\varepsilon^2 - \cos\theta_p$. Over the separatrix of trapped particle boundary $\xi_1 = 1$. Substitution of Π^0 into the integral expression yields $\partial^2 g/\partial\xi_1^2 + (k^2 F/4E)\partial g/\partial\xi_1 = 0$. Its solution can be written as $g = D_2' + 4D_1' \int_k^1 dk/k^2 E(k)$, where $k^2 = 2/(1+\xi)$. Repeating the matching process one finds the uniform lowest order solution as

$$f^0 = vhxF_r^M/\Omega - \varepsilon \frac{|x|}{x} \frac{\pi}{2} \left[vF_r^M/\Omega - \frac{e\langle E_\parallel \rangle}{kT} vF^M \sum_{r=o}^{N-1} \delta^r S_{3/2}^{(r)}(v^2) \right] \int_k^1 dk/k^2 E(k) \, . \qquad (17)$$

Here, we note that the integral expression in (17) can be transformed into the integral $\int_\lambda^\lambda d\lambda/\langle q \rangle$ uniformly, neglecting terms of order ε^2, to compare our result with [4]. Our derivation does not include a numerical factor in front of the gradients as in [4], as a result of C_{ee}. We note that the effect of C_{ee} is included in δ^r but no where else (neglecting terms higher order in ε). The case of $\nu_{ee} \neq \nu_{ei}$ is excluded. The numerical discrepancy between this result and 4 might lie in the variational technique used there.

The author is grateful to Prof. Pfirsch for an enlightening talk.

---

[1] F.L.Hinton and C.Oberman, Nucl. Fusion 9, 319 (1969).

[2] U.Daybelge, Phys. Rev. Letters 27, 916 (1971).

[3] I.P.Shkarofsky, T.W.Johnston, and M.P.Bachynski, The Particle Kinetics of Plasmas (Addison-Wesley, Reading, Mass. 1966)

[4] M.N,Rosenbluth,R.D.Hazeltine,F.L.Hinton,Phys.Fluids 15,116 (1972).

Radial Transport of Ions in Tokamaks Including Diffusing Oxygen and Carbon Impurities.

D.F.Düchs

Max-Planck-Institut für Plasmaphysik, 8046 Garching bei München, Germany

H.P.Furth and P.H.Rutherford

Plasma Physics Laboratory, Princeton University, Princeton, U.S.A.

Oxygen [1] and carbon [2] impurities have been observed to constitute about 5 % of the ions in Tokamak discharges. In numerical models previously only the ionization and recombination, and the corresponding energy losses, of spatially fixed oxygen has been taken into account [3]. Neglecting the diffusion of the impurities, however, seems to be unrealistic at least for the region near the limiter.

For present-day Tokamak parameters the time scale for impurity ion diffusion is estimated to $\tau_{Diff} \sim$ 20 msec. The stripping of carbon and oxygen, however, takes place in shorter periods: $\tau_{ion} \sim 3$ msec. We, therefore, adopt the following simple model: The total amount of impurities at radius r is determined by solving a diffusion equation for the sum $O(r) \equiv \Sigma O_i(r)$, where O_j stands for the j-th stage of ionization of oxygen (or carbon):

$$\frac{\partial O}{\partial t} = \frac{-1}{r} \frac{\partial (r\Gamma)}{\partial r} \qquad (1)$$

The flux Γ is defined in Eq.(7).

The distribution among the different stages of ionization, however, is computed from rate equations of the type

$$\frac{\partial O_j}{\partial t} = n_e O_{j-1} S_{j-1} - n_e O_j (S_j + \alpha_{j-1}) + n_e O_{j+1} \alpha_j . \qquad (2)$$

The ionization rate coefficients S_j are taken from Ref. [4], the radiative recombination coefficients α_j from Ref. [5]. Collisional recombination is negligible.

Although in standard operating regimes, the total power loss by radiation is $\lesssim$ 30% of the input power [2], it can have a marked effect on the T_e-profile since the line radiation should originate mostly from the outer region where partially stripped ions are present due to lower temperature.

Thus, we include in the electron energy balance the loss terms for ionization, line and continuum radiation as given in Ref. [5] as well as bremsstrahlung.

Recent calculations [6], [7], of the neoclassical transport of impurities yield for the particle flux of an ion species

$$\Gamma_j = \sum_k C_{jk} \left[Z_j Z_k n_j \frac{\partial n_k}{\partial r} - Z_k^2 n_k \frac{\partial n_j}{\partial r} \right]. \qquad (3)$$

Some additional terms involving temperature gradients which have small numerical coefficients in Connor's [6] paper have been omitted for the present version of our model. The sum is to be taken over all other ion species present. Under the condition

$$\sum_i O_i Z_i^2 >> n_p (m_p/m_O)^{1/2},$$

the coefficient C_{OP} for impurity-proton collisions has been derived [6], [7] in the banana regime as

$$C_{OP}^{ban.} = 1{,}46 \cdot 4\sqrt{2\pi}\, \ell n\Lambda (r\, m_p/RT_i)^{1/2} (e/B_\theta)^2 (0{,}53\, n_p + \Sigma O_i Z_i^2)/(3 \cdot \Sigma\, O_i Z_i^2). \qquad (4)$$

References [6] and [7] only consider in detail the case of a single high-Z impurity component. We generalize their solutions to roughly include collisions between different impurity ions:

$$C_{OO}^{ban.} = 1{,}46 \cdot 4 (2\pi r\, m_O/RT_i)^{1/2} (e/B_\theta)^2 \ell n\Lambda/3 \quad . \qquad (5)$$

Since the experiments mostly operate in plateau rather than banana regime we also correct the above coefficients to

$$C_{OP} = C_{OP}^{ban}/(1 + \nu_i^*), \quad C_{OO} = C_{OO}^{ban}/(1 + \nu_i^*) \qquad (6)$$

with

$$\nu_i^* = 4 (R^3\pi)^{1/2} B_z\, n_i \ell n\Lambda Z_{eff}\, e^4/3\, B_\theta r^{1/2} T_i^2.$$

Z_{eff} is defined in Eq. (10), the other symbols have their usual meaning. The total flux of impurities needed in Eq. (1) then is given by

$$\Gamma = \Sigma\, \Gamma_j \qquad (7)$$

summed over all impurity ion species.

Since the equilibration times between all ion components are very short

compared with electron-ion equilibration time we have set all ion temperatures equal ($T_p = T_0 \equiv T_i$) and have treated only a single ion energy equation. The ion thermal conductivity depends on the impurities in a way described by Connor [6]. We have also included a modification of the ion energy transport equation which is due to the fact that the outwardly diffusing protons will carry out more energy than is brought in by the incoming high-Z ions.

Since we are here mainly interested in the impurity ion diffusion we take for the electron transport the simplest model that gives reasonable agreement with the experimentally observed parameters. For both the electron diffusion coefficient D and the electron thermal conductivity κ_e, we employ the "pseudo-classical" form [8], [9]

$$D = \kappa_e = \gamma(Z_{eff})\rho_{e\theta}^2/\tau_e \qquad (8)$$

where

$$\rho_{e\theta}^2 = 2\, m_e T_e \cdot (c/eB_\theta)^2,$$

and

$$\tau_e = 3(m_e T_e^3/2\pi)^{1/2}/4n_e e^4 \ell n\Lambda.$$

The function $\gamma(Z_{eff})$ describes the classical dependence of the resistivity $\eta_{//}$ on Z [$\eta_{//} = \gamma(Z_{eff}) \cdot m_e/n\tau_e e^2$]

$$\gamma(Z) = Z(0.457/(1{,}077 + Z) + 0{,}29)$$

The total electron particle and energy flux is given, respectively, by

$$\begin{aligned} n_e v_e &= -D \frac{\partial n_e}{\partial r}, \\ Q_e &= -n_e \kappa_e \frac{\partial T_e}{\partial r} - \frac{3}{2} T_e D \frac{\partial n_e}{\partial r}. \end{aligned} \qquad (9)$$

The effect of the impurities on the electron transport (other than ionization and radiation losses) is taken into account through

$$Z_{eff} = \sum_{\substack{\text{all} \\ \text{ions}}} n_i Z_i^2/n_e = 1 + \sum_{\text{impurities}} Z_i (Z_i - 1) O_i/n_e. \qquad (10)$$

Our model includes also recycling (influx of cold neutrals = outflux of plasma, of hot, and of cold neutrals) cold neutral gas and four generations of charge exchange created hot neutrals.

In the supplementary paper numerical results, e.g. on inward diffusion of oxygen or carbon, the radial distribution of Z_{eff} and of O, and of losses due to impurities, as well as the effects on radial profiles of n and T_e,) are presented.

References:

[1] W.Stodiek, Proc.5th Europ.Conf.on Contr.Fusion and Plasma Physics, Grenoble, France, 1972, Vol.II, p.1

[2] L.L.Gorelik, S.V.Mirnov, V.G.Nikolaevsky, V.V.Sinitsyn, Nucl.Fusion 12, (1972), p. 185

[3] D.F.Düchs, Bull.Am.Phys.Soc.,Ser.II,(1970),Vol.15, No.11, p.1488

[4] W.Lotz, MPI für Plasmaphysik, Garching, Report IPP 1/62, 1967

[5] D.Düchs, H.R.Griem, Phys.Fluids 9, (1966), p.1099

[6] J.W.Connor, to be published

[7] D.Sigmar, to be published

[8] S.Yoshikawa, Phys.Rev.Letters 25, (1970), p.353

[9] L.A.Artsimovich, JETP Letters, 13, (1971), p.70

"This work was performed under the terms of the agreement on association between the Max-Planck-Institut für Plasmaphysik and EURATOM".

EFFECT OF MAGNETIC FIELD IRREGULARITIES ON PLASMA DIFFUSION

G. Casati (+), M. Dobrowolny (++), E. Lazzaro (+), A. Orefice (+)

(+) Laboratorio CNR di Fisica del Plasma-Via Celoria16, Milano, Italy
(++) Istituto di Fisica dell'Università dell'Aquila-L'Aquila, Italy

Abstract - An analysis is given of the particle collisional diffusion in toroidal plasmas with small, space dependent magnetic field perturbations superimposed on an axisymmetric magnetic field.

In the present paper we investigate some effects on particle collisional diffusion of magnetic field perturbations in axisymmetric toroidal plasmas. The results presented here refer to the plateau regime of neoclassical diffusion [1] . Extension of the theory to the banana regime appears to be worthwhile and is presently in progress. The aim is that of having a picture of the diffusion processes in realistic toroidal magnetic fields. It is in fact well known that, even in axisymmetric toroidal systems, deviations from symmetry may arise from a number of effects, such as the discrete nature of the coils, connections of main coils, stray fields due to gaps in the shell, losses in the iron core of the transformer, control field windings, and so on. Deviations from symmetry have been considered in the previous literature with models referring specifically to Stellarator fields [2] , or reproducing ripples in the toroidal magnetic field of a Tokamak configuration [3] . In the neoclassical plateau regime, the Stellarator diffusion turns out to be of the same order as the plateau diffusion of a Tokamak configuration, while the ripple diffusion is negligible [4] . We consider here more general magnetic field perturbations than in the previous models, and, in particular, show that a radial magnetic field component (even very small) may give rise to particle transport across unperturbed magnetic surfaces which is easily greater than that obtained in axisymmetric fields. The model we take for the magnetic field can be written as

$$\underline{B}(r,\vartheta,z) = (1-\epsilon\cos\vartheta)\left[B_{o\vartheta}(r)\,\hat{\underline{\vartheta}} + B_{o_z}\underline{\hat{z}}\right] + \delta\underline{B}(r,\vartheta,z) \qquad (1)$$

where r,ϑ,z are radial, poloidal and toroidal coordinates, $\epsilon = r/R$ is the inverse aspect ratio and $\delta\underline{B}$ represents the deviation from the axisymmetric magnetic field. Note that, with respect to previous work, no specific assumption is made on the direction of $\delta\underline{B}$

Max-Planck-Institut für Plasmaphysik
8046 Garching bei München

and on its space dependence. In magnitude, we refer to a situation where

$$B_{oz} \gg B_{o\vartheta} \gg \delta B \tag{2}$$

Consequently, starting as usual from the drift kinetic equation, we add a $\delta B/B$ expansion ($\delta B/B < \epsilon$) to the usual toroidal expansion. The resulting equation for the perturbed distribution function f_{1j} of species j particles can be written

$$\frac{v_{/\!/}\Theta + v_o}{r}\frac{\partial f_{1j}}{\partial \vartheta} + (v_{/\!/} - \Theta v_o)\frac{\partial f_{1j}}{\partial z} + \nu_j f_{1j} = \\ = -\left(v_{/\!/}\,\delta B_r/B_{oz} + \alpha_{jr}\right) f_{oj}\,(v_o + U_j)\, e_j B/cT_j \tag{3}$$

where: $\Theta = B_{o\vartheta}/B_{oz}$; $\alpha_{jr} = -(2R\Omega_j)^{-1}(v^2 + 2v_{/\!/}^2)\sin\vartheta$ is the usual toroidal drift; f_{oj} is a local maxwellian; $v_o = cB^{-1}d\phi_o/dr$ is the rotation velocity corresponding to the equilibrium radial electric field and $U_j = c\,T_j\,n_o'/e_j\,B\,n_o$ is the particle diamagnetic velocity. A "τ-approximation" for the collisional term (collision frequency ν_j) has been used, as it sufficient for the plateau regime[1]. By introducing now Fourier expansions in ϑ and z in Eq. (2), i.e.:

$$f_{1j}(r,\vartheta,z) = \sum_{n,l=-\infty}^{+\infty} F_{nl}(r)\,\exp\left\{i(n\vartheta + lz/R)\right\} \tag{4}$$

$$\beta_j(r,\vartheta,z) \equiv v_{/\!/}\,\delta B_r/B_{oz} + \alpha_{jr} = \sum_{n,l=-\infty}^{+\infty} \beta_{nl}(r)\,\exp\left\{i(n\vartheta + lz/R)\right\} \tag{5}$$

one easily derives

$$F_{nl} = -\,e_j\,B(cT_j)^{-1}(v_o + U_j) f_{oj}\,A_{nl}\,\beta_{nl} \tag{6}$$

with

$$A_{nl} = \left\{\nu_j + i\,r^{-1}\left[v_{/\!/}\Theta(n + ql) + v_o(n - q\Theta^2 l)\right]\right\}^{-1} \tag{7}$$

Eqs. (6) and (7) can now be used to calculate the particle flux across an unperturbed magnetic surface:

$$\Gamma_j = R^{-1}\int_0^{2\pi} d\vartheta \int_0^{2\pi R} dz \int_{-\infty}^{+\infty} dv_{/\!/} \int_0^{\infty} dv_\perp^2 \left(1 + \epsilon\cos\vartheta\right) f_{1j}\,\beta_j \tag{8}$$

The final result is conveniently written as:

$$\Gamma_j = -\pi^{3/2}\frac{r}{\Theta}\, n_{oj}\, v_{thj}\,\frac{e_j B}{cT_j}(v_o + U_j)\left\{\gamma_{j1} + \gamma_{j2} + \gamma_{j3}\right\} \tag{9}$$

where:

$$\gamma_{j1} = \left(\rho_{Lj}/R\right)^2 e^{-\gamma^2}\left(1 + 2\gamma^2 + 2\gamma^4\right) \tag{10}$$

$$\gamma_{j2} = 8\gamma^2 \sum_{n=0}^{\infty} \sum_{\ell=-\infty}^{+\infty} P_{n\ell}\, Q_{n\ell}^2 \exp\left\{-(Q_{n\ell}\gamma)^2\right\} \left(\delta B_{rn\ell}/B_{oz}\right)^2 \qquad (11)$$

$$\gamma_{j3} = 4(\rho_{Lj}/R)\gamma e^{-\gamma^2}(1+2\gamma^2)\, \mathrm{Im}\left(\delta B_{r1o}/B_{oz}\right) \qquad (12)$$

Here ρ_{Lj} is the particle Larmor radius, $y = v_o/\Theta v_{thj}$ and

$$P_{n1} = \left| n + ql \right|^{-1} \; ; \; Q_{n1} = (n - q\Theta^2 l)\ (n+ql)^{-1} \qquad (13)$$

Imposing now ambipolarity, one derives, as usual, $v_o \cong - U_i$. It is easily seen, upon evaluation of Eq. (9) for electrons, that the term γ_{e1} corresponds to the usual plateau value of the flux and the other two terms represent the new contribution due to the radial component of the perturbed magnetic field. Of these, γ_{e3} is obviously zero unless $\delta B_r(r,\vartheta,z)$ contains a term proportional to $\sin\vartheta$, while γ_{e2} is different from zero for quite general situations. For this reason the estimates that follow will be based on this term. Notice furthermore that γ_{e2} is independent from toroidicity and would be found also in the case of a cylindrical plasma. It is of interest to compare the $(\delta B_r/B)^2$ contribution with the neoclassical plateau diffusion for parameter values of actual Tokamas. Taking T3 parameters as an example ($\epsilon = 0.12$, $T_i/T_e = 1/2$, $q=3$, $r=12$ cm, $B_{oz} = 2.\ 10^4$ gauss, $T_e = 5$ keV) we can write

$$\gamma_{e2}/\gamma_{e1} \sim 3\ 10^3\ n^2/(n+ql)^3\ \ (\delta B_{rnl}/B)^2 \qquad (14)$$

n,l representing a typical space periodicity of the perturbation. Eq. (14) allows us to discuss the particle diffusion as a function of the geometry of the magnetic perturbation. From the structure of the result it is seen that when $n + ql \sim 1$, and $n \sim 1$, $\delta B_r/B > 2\ 10^{-2}$ is needed to have a particle flux exceeding the plateau value. Furthermore, radial magnetic perturbations of this order, which cannot certainly be excluded, give particle fluxes much higher than the plateau value when $n + ql$ is smaller than unity. On the other hand, it is also seen that $n + ql \gg 1$, as could be obtained from a strong toroidal dependence of the magnetic perturbation, would much reduce the effect of radial magnetic field components.

REFERENCES

[1] A.A. Galeev, R.Z. Sagdeev: Sov. Phys. JEPT 26, 233 (1968).

[2] L.M. Kovrizhnikh: Sov. Phys. JETP 29, 475 (1969).

[3] T.E. Stringer: Nucl. Fus. 12, 689 (1972).

[4] T.E. Stringer: Proceedings III International Symposium on Toroidal Plasma Confinement, F1-I, Garching, March 1973.

EFFECT OF NON-AXISYMMETRY ON THE TRANSPORT COEFFICIENTS OF A TOROIDALLY CONFINED PLASMA

R.K. Varma and A. Sen
Physical Research Laboratory
Ahmedabad 380009
India

Abstract: We calculate the effect of magnetic field ripples on the particle transport for toroidally confined plasmas. The Vlasov equation is solved for the non-axisymmetric perturbations over the axisymmetric state which is taken to be a function of the constants of motion. The diffusion co-efficient obtained is found to be proportional to the fraction of the magnetic energy in the ripple and also has geometric factors which could make it significant.

INTRODUCTION

Axisymmetry appears to be an important characteristic of Tokamak type confinement schemes for fusion plasmas. It is therefore important to assess the effects of any departure from axi-symmetry on the confinement characteristics of the system. Non-axisymmetry can result from magnetic field perturbations due to the finite number of coils [1] as well as due to electrostatic field fluctuations arising out of turbulence [2,3] . It could acquire significant proportions in the scaled up versions of the present generation of Tokamaks.

In this paper we have studied the effect of magnetic field ripples on the particle transport in a Tokamak geometry. In the next section we give a brief outline of our method of calculation. The expressions for the diffusion coefficients are presented and discussed

in Sec. 3.

2. PROCEDURE

We consider a fully ionised collisionless plasma confined in a Tokamak field $\underset{\sim}{B} = (0, B_\theta, B_\varphi)$ where B_θ is the poloidal magnetic field and $B_\varphi \simeq B_0/(1+\epsilon\cos\theta)$ is the toroidal magnetic field; $\epsilon = \frac{r}{R}$ and the usual tokamak coordinates are chosen.

A magnetic ripple $\tilde{B}_\varphi = \tilde{B}_0 \cos n\varphi$ is assumed which, consistent with $div\, \underset{\sim}{B} = 0$ gives $\tilde{B}_r = \frac{1}{2} n \epsilon \sin n\varphi$ ($\tilde{B}_\theta$ is assumed to be zero). Starting with the linearised Vlasov equation we write down a formal solution for the perturbation $\tilde{f}$ in the distribution function due to the ripple:

$$\tilde{f} = -\frac{e}{mc} \int_{-\infty}^{t} dt' \, \underset{\sim}{v} \times \tilde{\underset{\sim}{B}} \cdot \frac{\partial f_0}{\partial \underset{\sim}{v}} \quad , \tag{1}$$

where the integration is carried over the unperturbed orbits of the particles. f_0 is the stationary distribution function and is taken to be a function of the constants of motion $f_0 = f_0(\mathcal{E}, \mu, P_\varphi, P_\theta)$ where $\mathcal{E}$ the energy and P_φ the canonical angular momentum are the exact constants of motion; μ is the magnetic moment invariant and P_θ is a constant of motion in the limit of large aspect ratio. We express $\partial f_0/\partial \underset{\sim}{v}$ as

$$\frac{\partial f_0}{\partial \underset{\sim}{v}} = m \underset{\sim}{v} \frac{\partial f_0}{\partial \mathcal{E}} + mR \hat{\underset{\sim}{e}}_\varphi \frac{\partial f_0}{\partial P_\varphi} + mr \frac{\partial f_0}{\partial P_\theta} + \frac{m \underset{\sim}{v}_\perp}{B} \frac{\partial f_0}{\partial \mu} \tag{2}$$

where all the derivatives on the right, being constants of motion, can be pulled out of the time integral.

In general, $\tilde{f}$ consists of contributions $\tilde{f}_T$ and $\tilde{f}_P$ from trapped

and passing particles, respectively. We calculate here f_p and evaluate corresponding particle flux defined through

$$\Gamma = \left(\frac{1}{2\pi}\right)^2 \int d\theta\, d\varphi\, dv_m\, v_r\, \tilde{f}_p \qquad (3)$$

where v_r is radial drift velocity. All quantities involved have been expanded in the perturbation $\tilde{B}_0$ and the toroidicity ϵ, and only the lowest order terms in these are retained in the evaluation of Γ.

3. RESULTS

The particle flux Γ is obtained in the following form

$$\Gamma = -\left(D_{P_\varphi} + D_{P_\theta} + D_\mu\right) \frac{\partial N}{\partial r} \qquad (4)$$

where D_{P_φ}, D_{P_θ} and D_μ are identified as the contributions to diffusion co-efficient arising out of the P_φ the P_θ and the μ dependences of the distribution function respectively, and are given as

$$D_{P_\varphi} = \frac{\pi n b^2 \epsilon^2}{48}\left[\frac{W_+}{\ell_+} I_+ + \frac{W_-}{\ell_-} I_-\right]$$

$$D_{P_\theta} = \frac{\pi b^2 \epsilon}{8\,\Omega^3}\frac{v_E^2}{\omega_c} J_0 + \frac{\pi b^2}{8\omega_c R}\left[\frac{W_+^2}{\ell_+} J_+ + \frac{W_-^2}{\ell_-} J_-\right]$$

$$D_\mu = \frac{\pi n b^2 \epsilon^2}{48}\left[\frac{W_+}{\ell_+} K_+ + \frac{W_-}{\ell_-} K_-\right]$$

$b = \frac{\tilde{B}_0}{B}$, $v_E = \frac{c}{B}\frac{d\Phi}{dr}$ (Φ is the electrostatic potential) and ω_c is

the larmor frequency. Also $W_{\pm} = \frac{v_E}{r \ell_{\pm}}$ and $\ell_{\pm} = \frac{\Theta}{r} \pm \frac{n}{R}$. The $I_{\pm}$ J_o , $J_{\pm}$, $I_{\pm}$ and $K_{\pm}$ are velocity integrals involving the equilibrium distribution.

We make the following comments.

1. Diffusion is proportional to the fraction of the magnetic energy in the ripple (b^2 dependence)
2. There is a strong dependence on the azimuthal rotation velocity v_E . This effect arises out of a resonance between the ripple periodicity and that of this rotation.
3. As $v_E \to 0$, both D_{ρ_φ} and D_{μ} vanish but there is a part of D_{ρ_θ} that survives.
4. For large n, the diffusion coefficients become independent of n.

REFERENCES:

1. Stringer T.E., Nucl. Fusion 12, 689 (1972)
2. Kadomtsev, B.B., Plasma Turbulence, Academic Press (1965)
3. Gratzl H., Nucl. Fusion 12, 683 (1972)

EQUILIBRIUM AND ENERGY BALANCE IN TOKAMAKS

Y.N.Dnestrovskii, D.P.Kostomarov, N.V. Karetkina
N.L. Pavlova, A.M.Popov

Moscow State University, Moscow, U.S.S.R.

1. Plasma equilibrium in torus in the presence of external magnetic field and conducting shell with finite conductivity is studied by numerical methods. Investigation of such a problem for perfectly conducting toroidal shell has been described in our report [1], where the necessary equations were given. The problem is solved by numerical integration of the time-dependent magnetohydrodynamic equations with some mechanism of kinetic energy absorption. Boundary conditions on the thin toroidal shell take into account its finite conductivity, distribution of fields in vacuum outside the torus and the magnetic field of the external current carrying conductors. The system may be added by electrotechnical equation, describing the feedback devices. Plasma equilibrium in vertical stabilizing field with dipole-like configuration was investigated. Existence of equilibria states in sufficiently broad region of magnitude of the parameter β_J in the same external magnetic field was established. The value of the displacement of the plasma centre relative to the centre of chamber depending on value of the field and magnitude of the parameter β_J was found. The equilibrium form of the plasma cross-section is changed with adding of multipole components of magnetic field. As quadrupole component increases the small plasma cross-section is stretched in the vertical direction. In fig. 1-3 density level lines of plasma (ρ = const) are shown for three magnitude of ratio $\nu = H_4/H_2$ quadrupole and dipole components of the field (ν = 0,2 and 4) when $R/a = 4$, $\beta_J = 3$, $H_2/H = 0.02$ (H is the longitudal magnetic field). The marked ellipticity appears when $\nu \sim 2$, however, already when $\nu \sim 4$ plasma become unstable and the equilibrium is distroyed.

2. The problems connected with the injection of a hot neutral beam into the plasma and with heating of plasma at the expense of the beam energy was investigated. The quantity of the captured particles and their region of localisation depending on energy of

neutrals E, beam dimensions, angle of injection α, plasma and magnetic field parameters are determined at the initial stage of calculations. The beam is supposed to have a rectangle cross-section $\ell \times h$. Then analysis of energy balance of plasma with transmission the energy from the captured hot ions to the ions and electrons of plasma is carried out on the base of our prerious model [2,3]. The stationary temperatures of ions and electrons depending on the current i of the neutral beam are shown in fig.4 as example, when E = 20 kev, α = 43°, ℓ = 20 cm, h = 20 cm (the beam passing through the plasma along a chord), R = 70 cm, a = 20 cm, H = 12 kgs, current in plasma is equal J = 100 ka for two magnitudes of plasma density n = 1 and 2 (n is the maximum density in 10^{13} cm^{-3}). In these conditions thermoconductivity of electrons is several times of the thermoconductivity of ions [3], therefore the heating of electrons by the beam energy is essentialy less then the heating of ions. When n = 1 about 80 p.c. of beam neutrals are ionized and 65 p.c. are captured, when n = 2 95 p.c. are ionized and 80 p.c. are captured.

3. The charge-exchange of plasma ions with "cold" neutrals of residual gas accelarates the thermoexchange with the wall. Up to now the role of this effect was small [4], however, with the increasing of ion temperature and transition into "banana" region the energy loss by means of neutrals may become the basic cause of losses. For investigation of this question, it was carried out the solution of the system of the energy balance equations with kinetic equation for neutrals [3]. At the next figers the dependences Te and T_i (fig.5) and τ_E and β_J (fig.6) on plasma current are shown for T - 4 device [5] with parameter R = 90 cm, a = 17 cm, H = 40 kgs without neutrals (No = 0) and when density of neutrals in vacuum is equal No = 5 (in 10^9 cm^{-3}) and their vacuum temperature To = 10 ev. Continuous curves correspond to n = 5, dotted curves to n = 3. Under the calculations the plasma density was not changed in time, and it's distribution on radius was assumed to be parabolic. In fig. 7 the neutral density distributions and their temperatures are shown when J = 150 ka and the same values of plasma density. The ion temperature profile is also shown for comparison when n = 5.

It should be note that when No = 5 and n = 5 the neutral density in the centre of plasma is about $10^8 cm^{-3}$, and when n = 3 is

about $3 \cdot 10^{8} cm^{-3}$. Such values of density were observed in experiment. Curves at the fig.5 are pessimistic from the point of view of plasma heating. However it should be taken into account that the absorption of neutrals by plasma at the expense of ionisation is increased with the temperature increasing (in our case at the increasing of the current J from 150 ka to 350 ka for n = 5 coefficient of absorption of neutrals was increased from 0.35 to 0.66) So the neutral density in vacuum should be decreased. Moreover, when $n > 5$ in spite of multiple charge-exchange, the density of neutrals in the centre of plasma is small. Therefore the increasing of plasma dimentions also brings to the decreasing of role of neutrals in total energy balance.

References

1. Y.N. Dnestrovskii, D.P. Kostomarov, A.M. Popov. V. Eur. Conf. on Contr. Fusion and Plasma Phys., Grenoble 1972, p.36.

2. Y.N. Dnestrovskii, D.P. Kostomarov, N.L. Pavlova, IV Eur.Conf. on Contr. Fusion and Plasma Phys., Roma, 1971, p.17.

3. Y.N. Dnestrovskii, D.P. Kostomarov, N.L. Pavlova, Atomnaja Energia, 32, 301 (1972).

4. L.A. Artsimovich, A.V. Glukhov, E.P. Gorbunov, M.P. Petrov, IV Eur. Conf. on Cont. Fusion and Plasma Phys., Roma, 1971, p. 18.

5. L.A. Artsimovich et. al., Plasma Phys. and Contr. Nucl. Fusion Res., Vienna IAEA, 1971, vol. 1, p. 443.

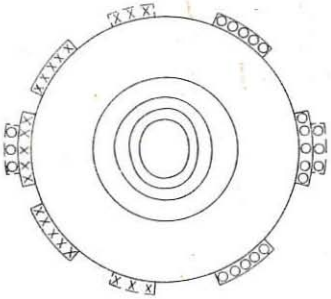


Fig.1

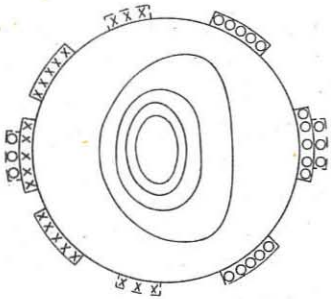


Fig. 2

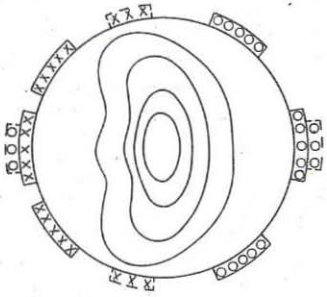


Fig. 3

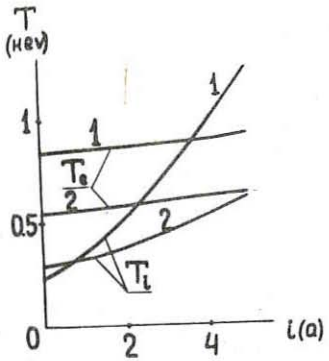


Fig. 4.

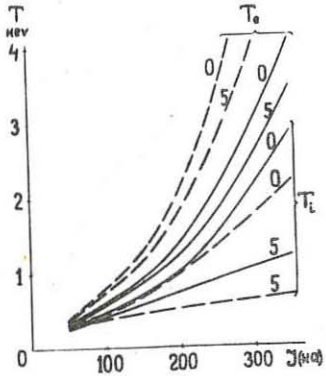


Fig. 5.

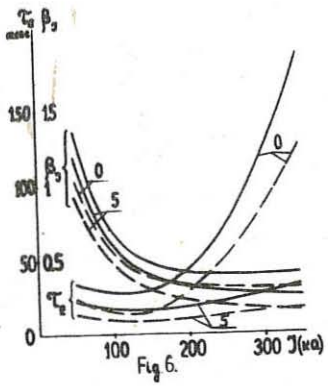


Fig 6.

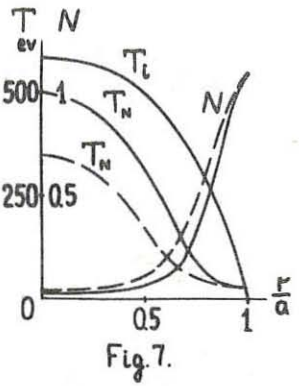


Fig. 7.

MHD SIMULATION OF ANISOTROPIC TOROIDAL PLASMAS

W. Sharp and J.C. Taylor

Department of Natural Philosophy, Glasgow University, Scotland

1. Introduction

The purpose of the MINTOK code is the numerical simulation of widely different physical experiments. Recently, we have concentrated increasingly on Tokamak systems and diffusive quasi-equilibria. The calculation of diffusive effects present certain difficulties even when they alone are present in the system; specifically, explicit algorithms suffer severe δt restrictions. These difficulties increase when other effects are also present. This is the problem of many - timescales or "stiffness". For these reasons the Mintok calculation is mainly implicit. The mathematical and numerical details of the calculation have been described in reference [1], so we shall only restate the basic equations and describe a typical simulation. Space limits us to presenting only a few representative results.

In [1] page 99 we stated that the Tokamak regime "...seems unlikely to be calculable by the present method". Recent experience now suggests that the calculation can cope with this computationally difficult regime. This point is amplified in a later section.

2. Equations

We seek the solution of the following MHD equations for a one-fluid magnetoplasma

$$\dot{\rho} + \nabla\cdot\rho\underset{\sim}{v} = 0$$

$$\dot{\underset{\sim}{v}} + (v\cdot\nabla)\underset{\sim}{v} = \rho^{-1}\Gamma\left[J\times B - \tfrac{1}{2}\beta\nabla p\right] \qquad (1)$$

$$\dot{T} + (v\cdot\nabla)T = (\gamma-1)\left[-T\nabla\cdot\underset{\sim}{v} + 2t^{\circ}(\underset{=}{\eta}:\underset{\sim}{J}\cdot\underset{\sim}{J})/\beta\rho t_{\eta}\right]$$

$$\underset{\sim}{E} + \underset{\sim}{v}\times\underset{\sim}{B} = \underset{=}{\eta}\cdot\underset{\sim}{J}\,t^{\circ}/t_{\eta}$$

plus Maxwell's equations. In the above all quantities are non-dimensional, $\Gamma = (t^{\circ}/t_{\alpha})^{2}$ where t_{α}, t_{η} are the Alfven and resistive diffusion times while t° represents a time to be specified by the code-user (normally one of t_{α}, t_{η} t_{μ}). Thus for example $t_{\alpha} = L^{\circ}/V_{\alpha}$, $V_{\alpha}^{2} = B^{\circ 2}/2\rho^{\circ}$. Note that a tensor resistivity is used. Thermal conductivity and viscosity are now being added.

The equations are expressed in toroidal co-ordinates (r, θ, z) where

r : distance from toroidal axis, θ : angle around it and z is such that $dz = R\,d\phi$, R being the torus major radius and ϕ rotation about the symmetry axis. Both toroidal and cylindrical geometry can be treated together by using the z metric function $N = 1 - \alpha r \cos\theta$, $\alpha = a/R$ so that $\alpha = 0$ corresponds to the cylindrical case.

3. Numerical experiment. Data and results

The data for a typical toroidal equilibrium calculation is given in the following table.

Char. Paras.	Timescales Char. Speeds	Initial Conditions $r\ [0,1], \theta\ [0,2\pi]$	Boundary Conditions $t>0, r=1, \theta\ [0,2\pi]$
Hydrogen Plasma	$t_\alpha = 1.5\ \mu s$	$v_r = 0$	$v_r = 0$
$n^o = 10^{21}/m^3$	$t_{th} = 6.4\ \mu s$	$v_\theta = 0$	$B_r = 0$
$T^o = 10^4\ ^oK$	$t_\eta = 31\ \mu s$	$B_r = 0$	$B_\theta = 0.1$
$B^o = 0.1\ w/m^2$	$v_\alpha = 69$ km/s	$B_\theta = 0.1\ r$	$B_z = 1/(1-\alpha r \cos\theta)$
$L^o = 0.1$ m	$v_{th} = 16$ km/s	$B_z = 1/(1-\alpha r \cos\theta)$	
$\rho^o = 1.7\ kg/m^3$		$j_r = 0$	
$j^o = 0.8\ MA/m^2$		$j_\theta = 0$	
$v^o = 3.2$ km/s		$j_z = 0.2$	$\beta^o = 0.04$
$t^o = 31\mu s = t_\eta$		$T = \left(1 - \frac{0.02 r^2}{\beta^o}\right)^{1/2}$	$\alpha = 0.1$

In this, β^o is the system β, $\alpha = a/R$ inverse aspect ratio, v_α and v_{th} are the Alfvén and thermal velocities. Note that the above "equilibrium" is inaccurate in that div $B \neq 0$ initially but is $0(\alpha)$. This can be avoided, but the satisfaction of $J \times B - \nabla p = 0$ then cannot be achieved with simple forms for ρ and T. For the present therefore we make the choice as above. The simulation is followed for one characteristic diffusion time ($31\mu s$) and the resulting motion represented by a set of graphs of which we show only 4 of the more interesting here.

Figure 1: $v_r(t;\ \theta = 0,\ r)$ $r = .26,\ .58,\ .89$

Evolution of v_r in time at $\theta = 0$ and for 3 radial positions.

$\Delta r = 2/19$, $\Delta\theta = \pi/15$, $\Delta t = 0.01$(——) and $= 0.02$(- - - -)

Since the plasma is initially at rest the small values of v_r are not surprising (multiply by 3.2 km/sec to get physical value). We note the sudden change over a non-dimensional time $\simeq 0.15$ after which smoother variation ensues. Of course this is not a very severe calculation in that the "severity

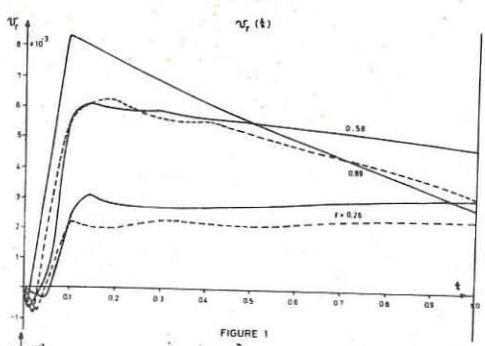


FIGURE 1

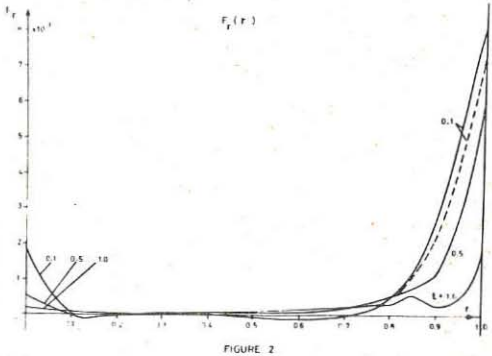


FIGURE 2

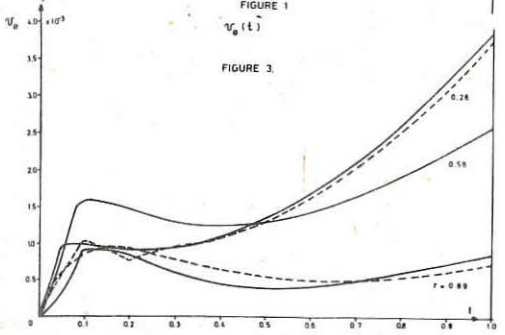


FIGURE 3

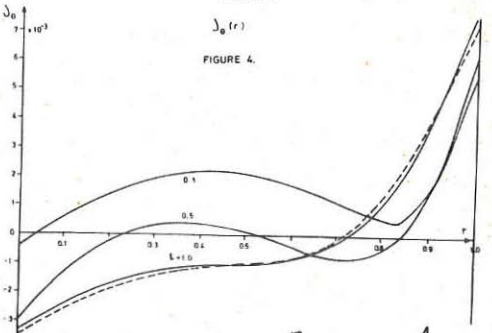


FIGURE 4.

index" $\Gamma \equiv (t^*/t_\nu)^2 \sim$ 400 here. However we have done runs with $\Gamma = 2.5 \times 10^4$ with apparent success. Most of the runs to date have been to test the numerics, in particular the consistency of the solutions obtained with different space or time steps. Figure 1 provides such a comparison between different time steps. Although agreement seems rather poor this is only because v_r is so small, further Δr is quite large. The important feature is that v_r seems to decrease in the outer layers of plasma and in fact this trend is maintained for larger times.

Figure 2: $F_r(r; \theta = 0, t_i)$ $t_i = 0.1,\ 0.5,\ 1.0$

where $\underset{\sim}{F} = \Gamma \rho^{-1}(J \times B - \tfrac{1}{2}\beta \nabla p)$. Thus $\underset{\sim}{F}$ measures the local imbalance between plasma and magnetic forces. For $t = 0.1$ there are 2 graphs corresponding to 2 values of Δr . The pairs at $t = 0.5$ and 1.0 are indistinguishable. Here the message seems clear, that the initial imbalance damps out increasingly with time. This is for $\Gamma \sim 400$ but the same has been found larger Γ . It is clear however that for large enough $\Gamma \sim 10^6$ say, this approach must become numerically impossible[1] without some sort of modification. We believe we have found this and it entails only a very simple change, namely to systematically increase the value of Γ as the motion, and the

corresponding calculation, proceeds. Corresponding to the actual experiment there is a (usually large) value of $\Gamma = \Gamma_{exp}$ say. Then if we can calculate through time, simultaneously increasing Γ until we are calculating with Γ_{exp}, we have achieved a realistic simulation. The procedure corresponds in fact to varying the timescale t^o of the calculation in accord with its evolution from rapid Alfven-scale to slow diffusion-scale motion. The graphs of Figure 1 suggest why this idea makes sense. They show the early rapid rearrangement followed by a much slower-varying phase. Such effects have in fact been reported in experimental devices[2].

Figure 3:

Whereas F_r appears to decrease with time (Figure 2) this is not the case for F_θ. Correspondingly v_θ increases with t. So far we have not followed the motion long enough to confirm the expected levelling out when $v_\theta \sim \iota \propto v_{th}/2\pi$ and the possible formation of a weak shock. More detailed results indicate a strongly sheared poloidal flow over wide ranges of the experimental parameters. We have in fact come across no exception. One consequence of this is that we are now adding viscosity terms to the velocity equation.

Figure 4: $J_\theta(r;\ \theta = 0,\ t)$

There are two main features here. The first is a mild skin-effect, the localization of a poloidal current layer near the outer wall. The second is the change of sign of $J_\theta(r)$ over the radius as $t \to 1.0$. The mechanism for this seems fairly clear. J_θ is essentially $\nabla_r B_z$ and B_z evolves mainly by resistive diffusion. In particular B_z decays slowly where η is small; lastly $\eta \sim T^{-3/2}$. Thus where T is large η is small and the more permanent is $\underset{\sim}{B}$. Now near the wall $(r = 1)$ is small and hence $\dot{T} \propto \rho^{-1}\eta J^2$ is large. Thus T increases faster near the wall than further into the plasma. Thus B_z tends to remain fairly constant in the wall layer. This is found to be the case in the discharge centre. also The result is that as time goes on $B_z(r)$ develops a trough (with much larger gradients near $r = 1$). Thus we can expect $J_\theta(r)$ to change sign and to be largest in a skin layer as in Figure 4.

References:

1. W. Sharp and J.C. Taylor Comp.Phys.Comm. 4, 95 (1972)

2. W. Stodiek Proc. of 5th Eur.Conf.Contr.Fus.Plasma Phys. (1972) p.10.

1.3. TOKAMAKS: NEWS AND VIEWS...



6th European Conference on Controlled Fusion and Plasma Physics

NEUTRAL INJECTION ON THE CLEO TOKAMAK

J. Sheffield, D. Aldcroft, J. Burcham, H.C Cole, M. Cowlin, E. Speth†, and P.E. Stott

U.K.A.E.A., Culham Laboratory, Abingdon, Berkshire, England.

ABSTRACT: Neutral hydrogen beams of 50kW power have been injected into plasmas produced by 200kW of ohmic heating. The beam trapping efficiency is ~ 70%. Fast ions ($E_i < E_{io}$) are detected, thus power is transferred to the plasma. No ill effects are observed. An improved system, delivering 100kW of neutrals, has been installed.

INTRODUCTION: The arrangement of the injector and high energy detector on the Tokamak is in Figure 1. Injection access is an 11cm diameter aperture at 135cm, 55% - 60% of the total beam is within this solid angle. The normalised signal level on calorimeter C, is 1.0 without plasma or B_{TOR}, and with B_{TOR} alone it is 0.6. The effective neutralization efficiency is therefore 60%. This is less than the expected fraction (70→ 75%) [1] owing to reionization of some of the beam in the input tube with subsequent deflection by B_{TOR}. Typical Tokamak conditions are R = 90cm, a = 18cm, B_{TOR} = 20kG, $\bar{n}_e \simeq 2X10^{13}cm^{-3}$(duration 50→ 100msec), I_{TOR} ~ 60→ 80kA ($\bar{T}\sim 10^2$eV.) [6,7]. Under these plasma conditions, and with injection, the normalized signal on Calorimeter C drops to < 0.03, therefore the neutral beam is ionized by the plasma. We calculate that for typical Tokamak conditions 70% of the injected neutrals E_{io}(10→ 30keV) are trapped (ionized on contained orbits.) Thus in total ~ 25% of the ion beam power at the source ends up contained in the high energy ions in the plasma.

To date the peak power has been 140kW (65% H_1^+, 20% H_2^+, 15% H_3^+) ~ 5.5A equivalent at E_{io} = 25keV, duration 40msec. The estimated trapped power is therefore 35kW. The addition of this power to the 200kW of ohmic power is expected [1,2,3] to raise the plasma temperature by ~ 5%. This requires that the trapped ions are contained long enough to slow down and transfer their energy to the plasma. Evidence for this containment has been obtained with a fast particle

detector. At the moment there is no accurate measurement of temperature to demonstrate heating, but it is encouraging that no serious instabilities or other side effects have been observed during injection.

FAST NEUTRAL PARTICLE DETECTOR: (Figure 1.) Charge exchange neutrals from the plasma are collected at an angle to the toroidal axis similar to the injection angle. The neutrals ionized in a stripping cell are then deflected by a magnet into a scintillator (Ne 102) and photomultiplier. The main interference was from X-rays this was reduced to an acceptable level by a large lead shield. The injector was operated at E_{io}= 24 keV (~ 4A) and the detector was set to detect ions at respectively 24, 21, 18 and 15 keV. The nominal detection channel was ± 1 keV, but in fact the presence of a small signal, starting coincident with the beam, was observed with the detector set at 30 keV, i.e. above the injection energy. This signal is believed to be due to ionization of some of the neutrals E_i < 24 keV in the deflection chamber, where the gas pressure was not negligible. Thus at each setting we expect to receive some signal from lower energy neutrals. This is a possible explanation of the long tail on the signal at 18 keV, Figure 1. Indications that the fast ions are contained comes from; detection of ions substantially below the injection energy; and at these lower energies, there is a signal ~ 1msec after the beam is switched off, and there is a small but detectable delay (~ 0.5msec) of the signal relative to the beam. With the detector set at 24 keV there is no measurable delay. There is no signal coincident with the injected beam unless the good plasma conditions, as above, are established.

The finite rise time, presumably partly due to the stacking time of ions, is irreproducible. The probable explanation is a variation on this timescale of the beam species.

The measured delay times imply a total slowing down time ~ 2→ 4msec, this is consistent with the formula of Spitzer[4]

$\tau_{SD} \sim \frac{3X10^{8} Te(eV)^{\frac{3}{2}} sec}{n_e(cm^{-3})\ ln\ \Lambda}$, for $T_e \sim 200eV$, $\bar{n}_e \sim 2X10^{13} cm^{-3}$

The neutral density at which the charge exchange time $\tau_{CX} \sim \tau_{SD}$ is $n_n \sim (2.5 \rightarrow 5)\ X\ 10^{9} cm^{-3}$. This is larger than that commonly experienced in Tokamaks[5], therefore we would expect most of the trapped energy to be transferred to the plasma.

IMPROVED INJECTION SYSTEM: We have tested and installed an injector with an 8 cm diameter extraction system containing 349 apertures, illuminated by a 12 cm diameter plasma source[3]. The beam characteristics are shown in Figures (2) and (3). With this new system we have the possibility of trapping 70 kW of fast ions, the increased power should allow us to make a more detailed study of the containment of the fast ions and will improve our chances of detecting neutral particle heating of the plasma.

†On attachment from I.P.P. Garching, West Germany.

ACKNOWLEDGEMENTS: We would like to thank our many colleagues in the CLEO group and in the Neutral Injection Study Group, for their help and encouragement. Particular thanks are due to R. Crawford for his contribution to the construction of the apparatus.

REFERENCES:

[1] Aldcroft, D. et al (1973) Submitted to Nuclear Fusion (and CLM P-314. 1972).

[2] Gibson, A. et al (1973) 3rd Int. Symp. on Toroidal Confinement Garching. B16-I.

[3] Aldcroft, D. et al (1973) 3rd Int. Symp. on Toroidal Confinement Garching, B.24.

[4] Spitzer L (Jr) (1960) Physics of Fully Ionized Gases (Interscience)

[5] Stodiek, E. (1972) 5th Eurpoean Conf. on Contr. Fusion and Plasma Physics, Grenoble, 2. 1.

[6] Hugill, J. et al (1973) Plasma Equilibrium in Cleo Tokamak. This conference.

[7] J.W.M. Paul, et al (1973) The Cleo Tokamak Experiment. This conference.

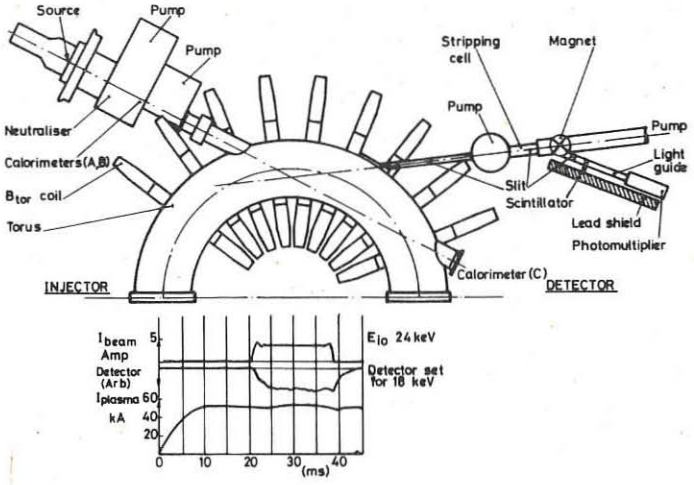


Figure 1.

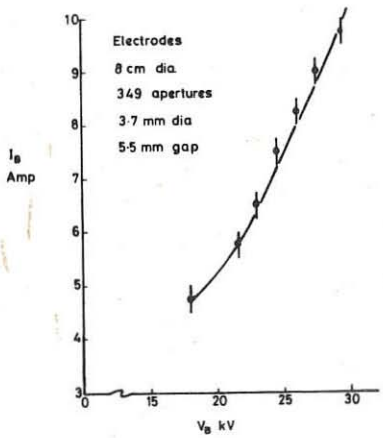


Figure 2.

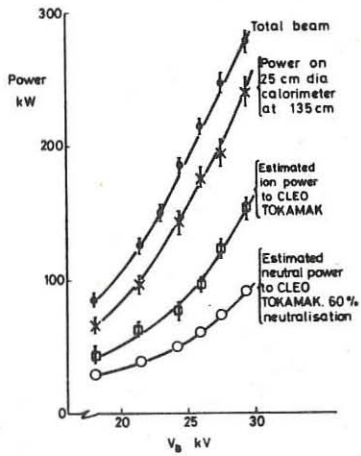


Figure 3.

PLASMA COLUMN PERTURBATIONS PRECEDING TO DISRUPTIVE INSTABILITY IN T-6 TOKAMAK

V.S.Vlasenkov, V.A.Krupin, V.M.Leonov, V.G.Merezhkin, V.S.Mukhovatov

I.V.Kurchatov Institute of Atomic Energy, Moscow, USSR

The kinklike perturbations of a plasma column in tokamaks and relatively slow increase of them before onset of the disruptive instability were observed in [1-3]. Here we present the results of investigations of plasma column perturbations fast-growing just before the negative voltage spike. The experiments were performed with hydrogen plasma in the T-6 Tokamak (R_o = 70 cm, b = 25cm) in the following range of parameters: $p_o = 1.5\ 10^{-4}$ Torr, H_o= 5-10 kG, $J \simeq 40$ kA, $q(a) = 2-4$.

Fig. 1 shows the tipical unstable discharge. One can see a slow growth of plasma density oscillations before the spike and quasistationary oscillations after the spike. The spike is accompanied by the decrease of β_J by ~0.15 and of the mean electron density by ~30%. The electron temperature in the centre of the column also decreases. It follows from the fact that C V light emission from the centre of plasma is decreased whilst that of C IV is increased.

A detailed study of the plasma column perturbations was carried out in the discharges when the spikes were relatively small but have a good reproducibility. In Fig. 2 one can see that the disruptive instability is accompanied by a decrease of n_e in the centre of plasma column by ~30%. The total number of charge particles is reduced by ~6%. The modulation depth of mean electron density increases up to ~25% during 1-2 oscillation cycles before each spike and then decreases (Fig. 3). The maximum modulation

depth is practically independent on the oscillation behavior at the preceding stage of the discharge. The correlation of the phase shift oscillations at $x = 2$ cm and $x = 16$ cm implies the existance of a regular structure of plasma surface perturbations before the spike. The estimates show that the amplitude ξ_o of surface helical perturbations could be ~ 0.5 a at the instant of the spike.

It should be noted that a relatively slow decrease of the voltage precedes to a sharp voltage spike. Sometimes such a decrease is not accompanied by a sharp spike (the so-called minor spike). The fast growth of oscillations accompanied by increasing of frequency starts simultaneously with the slow voltage decrease. Fig. 4 gives the magnetic probe signals $\tilde{H}_\varphi(t)$ integrated with $\tau \simeq 1$ msec, $U(t)$, $\Phi(t)$, top limiter - liner current $J_1(t)$ and bottom limiter - liner current $J_2(t)$ during the minor spike (initial conditions are the same as in Fig. 2). In this case magnetic field perturbations have helical stucture with $m = 4$ and $n = 1$. If the cleanliness of the discharge chamber was insufficient the fast-growing mode with $m = 3$ was observed in the same regime which led to the major spike. The minor azimuthal angle between perturbation maxima on the outer surface of torus is about 130° for $m = 4$ and about 160° for $m = 3$ corresponding to kinklike modes with $n = 1$ following the magnetic field lines at $a/R_o \simeq 2/7$ and $l_i/2 + \beta_J = 0.8 - 0.9$. The perturbations registrated by magnetic probes at the instant of the major spike are more unregular than in the minor one. Estimates of the velocity of the mode rotation yields $(3 - 5) 10^5$ cm/sec and the direction of rotation corresponds to the direction of the electron diamagnetic

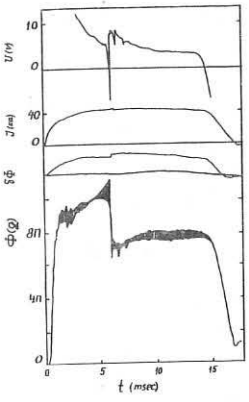


Fig. 1

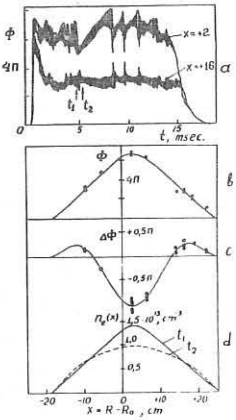


Fig. 2

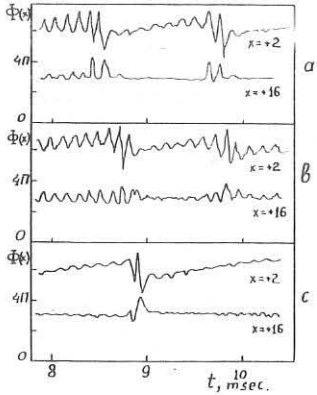


Fig. 3

Fig. 1. The discharge voltage U(t), The plasma current J(t), the diamagnetic signal $\delta\Phi(t)$ and the phase shift $\Phi(t)$ of microwaves probing the plasma in vertical direction with $x = R - R_o = 2$ cm as functions of time for the discharge produced at $a = 15$cm and $q(a) = 3.6$. The plasma diameter $2a$ was taken to be equal to the rail limiter spacing.

Fig. 2. The oscillograms of $\dot{\Phi}(t)$ at $x = 2$ cm and $x = 16$ cm, values of $\dot{\Phi}$ as a function of x at the time t_1 before the spike and at the time t_2 after the spike and the radial profiles of electron density $n_e(x)$ at the times t_1 and t_2. $a = 20$ cm, $q(a) = 3.2$.

Fig. 3. The short-time behavior of $\dot{\Phi}(t)$ expanded in time for three successive discharges. The initial conditions are the same as in Fig. 2.

---

drift. The increase of the limiter - liner current at the instant of the spike (up to 1 kA) takes it possible to suppose that plasma - wall and plasma - limiter interactions play the essential role in the process of the spike.

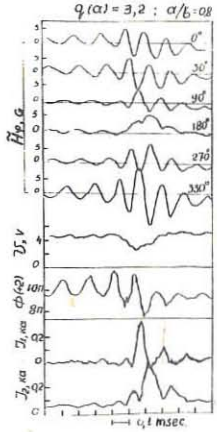


Fig. 4

The streak photographies of the plasma column show the same behavior of perturbations before both minor and major spikes. But in the first case the growth of the perturbations is delayed during the spike whilst in the second case the growth of those is continued and leads to broadening of the plasma up to the chamber wall. The growth rate is about $5 \cdot 10^4$ sec^{-1} - ten times less than maximum increment of kink mode $\gamma_{max} \simeq H_\varphi / \sqrt{8\pi\rho}\, a$.

Thus, the essentially nonlinear phase of surface kinklike perturbations precedes to the disruptive instability in tokamak discharges. The perturbation amplitude ξ_0 can reach (0.2 - 0.5)·a. The phase of the fast growth of the perturbations is lasted for 1 - 2 periods of oscillation (~ 100 μsec).

References.

1 . N.D.Vinogradova and K.A.Rasumova. In Plasma Phys. and Contr. Nuclear Fusion Res., IAEA, Vienna, v. 2, 1966, p. 617.

2 . S.V.Mirnov and I.B.Semenov. Atomn. Energ. 30 (1970) 129; Zh. Eksp. Teor. Fiz. 60 (1971) 2105.

3 . J.C.Hosea et al. In Plasma Phys. and Contr. Nucl. Fusion Res., IAEA, Vienna, v.2, 1971, p. 426.

VACUUM BUBBLES IN TOKAMAK PLASMAS

B.B.Kadomtsev, O.P.Pogutse

I.V.Kurchatov Institute of Atomic Energy, Moscow, USSR

The kink instability of a tokamak plasma is considered without a restriction imposed by the linear approximation. It is shown that helical modes develop into "bubbles"(a kind of plasma-free helical "snakes" penetrating under the plasma surface.).

It is known that the kink instability of the tokamak plasma is almost insensitive to toroidality of the plasma column. Therefore, a simplified model will be used ,namely, we shall consider a straight perfectly conducting plasma column of radius a located inside an ideally conducting outer wall of radius b. The spacing between the plasma and the conducting outer wall is assumed to be vacuum.Let the period of all perturbations be $L = 2\pi R$, simulating a toroidal plasma column of major radius R.

Let us consider the kink instability in the simplest case when the current distribution is uniform.The lines of force have equal pitch in this case,the distribution of the azimuthal field B_0 is shown in Fig.1a. If a perturbation constant along the line of force is produced on the plasma surface (Fig.2 a),then in the case of equal pitches of the lines the perturbation can be enlarged and pulled up to the centre without disturbing the magnetic field (Fig.2d). In the final state we again arrive at an equilibrium configuration with cylindrical

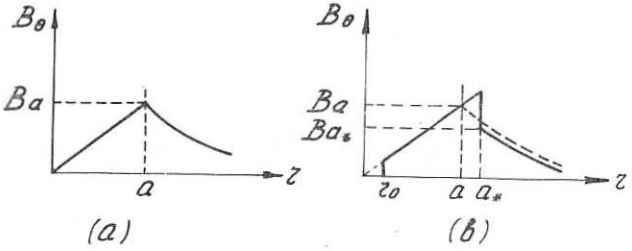


Fig.1

symmetry. In this case, however, there is a bubble of radius r_0 in the centre of the plasma (Fig.2 d). The field distribution takes the form shown in Fig.1 b where a_* is the new radius of the plasma column. The pitch of the lines of force inside the plasma is the same as before. As is seen in Fig.1b the surface currents are produced both on the bubble surface and plasma boundary.

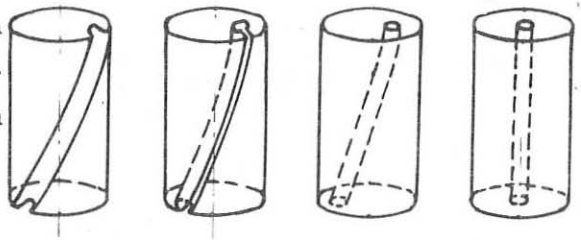


Fig.2

The energy of the new configuration is lower than the initial one. This fact can be easily demonstrated in the case of "frozen-in" fluxes. Let us consider this case more closely. First of all note that $B_\theta \ll B$ for tokamaks and plasma motion may be assumed imcompressible. Hence, the cross section of the plasma is constant so that $\pi a^2 = \pi a_*^2 - \pi r_0^2$. Conservation of the cross section area leads to the conservation of the longitudinal field flux when the bubble penetrates the plasma. A more complicated situation occurs with an azimuthal flux. In the initial state this flux per unit length outside the plasma is equal to $\Phi = \int_a^b B_\theta dr = B_a a \ln \frac{b}{a}$, $B_\theta = B_a \frac{a}{r}$ (where B_a is the field magnitude on the plasma boundary.). To follow the azimuthal flux let us consider a thin vertical foil drawn between the plasma boundary and perfectly conducting outer wall. When the helical deformation takes place a part of the foil penetrates together with the bubble under the plasma surface. In the final state (Fig.2 d) the flux $\frac{\pi r_0^2}{L} B_0$ per unit length passes through the foil inside the bubble. Hence, the azimuthal flux out-

side the plasma is equal to

$$B_a^* a_* \ln\frac{b}{a_*} + \frac{\pi r_0^2}{L} B_0 = B_a a \ln\frac{b}{a} \qquad (1)$$

Now it is not difficult to find the energy variation per plasma unit length, caused by the bubble

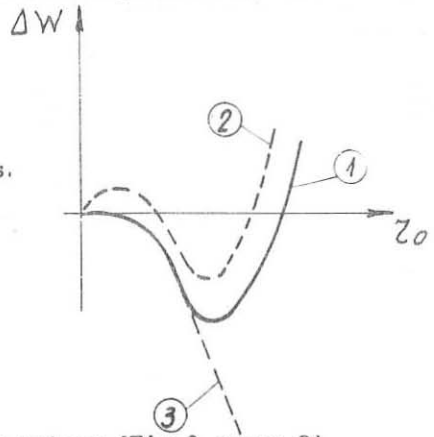
$$\Delta\bar{W} = \bar{W}_{II} - \bar{W}_I = \frac{1}{8\pi}\int_{II} B_\theta^2 dS - \frac{1}{8\pi}\int_I B_\theta^2 dS \qquad (2)$$

State I corresponds to the situation without a bubble, State II is that with a bubble. Figs 1a and 1 b illustrates the form of the distribution B_θ. At $r_0 << a$ this energy variation is equal to

$$\Delta\bar{W} = -\frac{1}{4} B_a^2 a^2 \left(\frac{r_0}{a}\right)^4 \qquad (3)$$

i.e. it equals the energy of the azimuthal field, which is released by the bubble. We have seen that the energy is lowered as the small bubble appears.

Fig. 3 (curve 1) shows the form of $\Delta\bar{W}$ for r_0 being not very small.



Generation and evolution of bubbles can be analysed in detail with the ideal hydromagnetic equations.

It was found that in the linear instability domain, linear perturbations naturally develop into bubbles, the number of the bubbles being equal to the mode number m. When the plasma is linearly stable a potential barrier arises, (Fig. 3, curve 2) and bubbles whose radius is very small cannot appear.

We have considered above the case of fixed fluxes, however, the experiments are carried out with the given total current. In this case the plasma is found to be more unstable. The largest

difference takes place for m = 1. in the case of the given current the energy ΔW has no minimum at all when one bubble is produced (Fig.3,curve 3). It is quite natural to associate the bubble evolution with the appearance of large negative voltage spikes observed experimentally in the presence of the so-called disruptive instability. In fact, as we have already pointed out the appearance of the bubbles is accompanied with a negative current generated on the plasma boundary (Fig.1 b). If a negative surface current touches the limiter it should vanish. Disappearance of the negative current leads to generation of a positive current in the deeper layers an negative voltage spikes.Thus, one of the causes responsible for the disruptive instability may be the usual kink instability which developes up to the bubble generation.

INVESTIGATION OF HF PLASMA HEATING AND OF PLASMA BEHAVIOUR IN THE TM-3 TOKAMAK

V.V.Alikaev, Yu.I.Arsen'ev, G.A.Bobrovskii, V.I.Poznyak,
K.A.Razumova, Yu.A.Sokolov.
I.V.KURCHATOV INSTITUTE OF ATOMIC ENERGY, Moscow, USSR.

Abstract. The additional heating by means of high-power hf radiation which is made resonant at the low hybrid frequency was investigated.

One of the possible methods of plasma heating is the heating by means of the linear transformation of electromagnetic waves into the short wave plasma oscillations in the vicinity of low hybrid resonance. One can expect essential collisionless absoption of such oscillations, in particular, on the ion cyclotron frequency harmonics. We used for the input of hf energy one of the diagnostic ports ($20\times120 mm^2$) which could excite waves with the wide spectrum $K_z > K_o$ and $\vec{E} \parallel \vec{H}$. The power of the hf generator was not more than 100kW, the pulse duration was 1ms. Under the chosen frequency the low hybrid resonance can be achieved at the electron density $n_e \approx 10^{14} cm^{-3}$ and at the main magnetic field $H \approx 40 kOe$.

The absorption of hf radiation of the low power ($P \approx 1W$) was investigated with $n_e \approx 10^{12} \div 10^{13} cm^{-3}$, $T_e \approx 300 \div 800 eV$. Under these regimes the ratio of the signals received by the loop with and without plasma was $A = \frac{1}{3} \div \frac{1}{15}$ and decreased with the density increase.

The investigations with the generator of high power were carried out in two types of regimes: far from the low hybrid resonance regime ($H \approx 10 kOe$, $n_e \approx 10^{12} cm^{-3}$) and in the vicinity of that. In the

latter case we have achieved $n_{e\ max} \approx 10^{14} cm^{-3}$ (H=30÷35kOe), provided that the distribution of n_e is parabolic, without lack of stability. Essential absorption of the hf power was observed inside the whole range of the plasma parameters under the investigation.

In the regimes of the first type the phenomena observed are following (Fig.1):

1. The intensity of H_α and impurity lines and the electron density do not change when the hf generator is switched on.

2. The outward shift of the plasma column increases during the hf pulse and then slightly decreases during the rest of the discharge (curve a).

3. During the hf pulse the loop voltage increases and the plasma current derivative changes. The latter corresponds to the decrease of the current (curves c and d).

4. The decrease of the radius of the cross section of plasma with the conductivity $> 2.10^{15}$ CGSE is registrated during the hf pulse by the additional sinusoidal loop voltage of the frequency of 5.5kc [1]. The decrease is about 35% at the end of the hf pulse in a good accordance with the observed shift. Taking into account the density invariability and the insignificant change of perpendicular energy of the plasma, one can conclude that anomalous resistance appears on the periphery of the plasma column.

5. Comparatively hard X-ray radiation (>100keV) appears when hf power is applied. It continues till the end of the tokamak discharge, slightly decreasing after the hf pulse and increasing at the end of the discharge (curve b). Without the application of hf power there is no X-radiation from the plasma of low density even

at the end of the discharge.

The above mentioned effects of the hf power on the plasma are reduced when the plasma density is increased.

6. A small increase of plasma perpendicular energy is registered by the diamagnetic method. The received additional energy is $(1\div2).10^{14}$ eV.cm^{-3}.

7. The ion energy distribution in the mentioned regimes can be approximated by the two-Maxwellian distribution [2]. During the hf pulse the part of ions of energy more than 300÷500eV increases (Fig.2), the distribution yet remains Maxwellian. The Figure 2 shows also that additional energy is confined for about 1 ms. But the heating of the ions corresponds only to a small part of additional energy of plasma, providing the diamagnetism rise. Thus we have to suggest electron heating by hf power.

In the vicinity of the low hybrid resonance only the diamagnetism rise (by the same value) and the increase of the part of hot ions (with energy more than 300eV) are observed. The other above mentioned phenomena do not appear.

To explain the absorption of hf power all over the regimes we cannot apparently attract the simplest collisional damping of the ordinary waves. The linear transformation is not possible too if there is only radial gradient of density, and the resonance conditions are not achieved in the experiment. One can suppose the longitudinal gradient of the density near to the limiter. In that case the linear transformation is possible at some points of the lines of equal density under $n_e \gtrsim n_c$ (n_c - the cutoff density) [3].

The decayed instability is the alternative explanation of the absorption. The turbulence of the plasma column periphery, provided by it, could explain some of the above mentioned phenomena.

We wish to thank Dr. A.A.Ivanov for useful discussions.

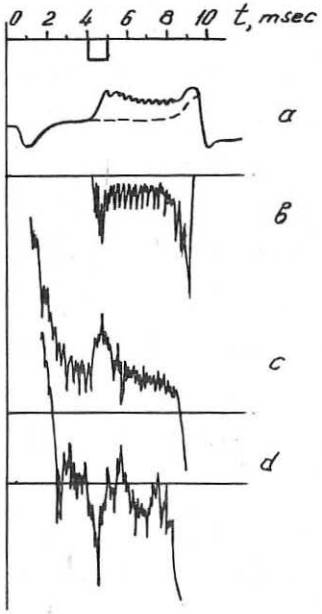


Fig. 1

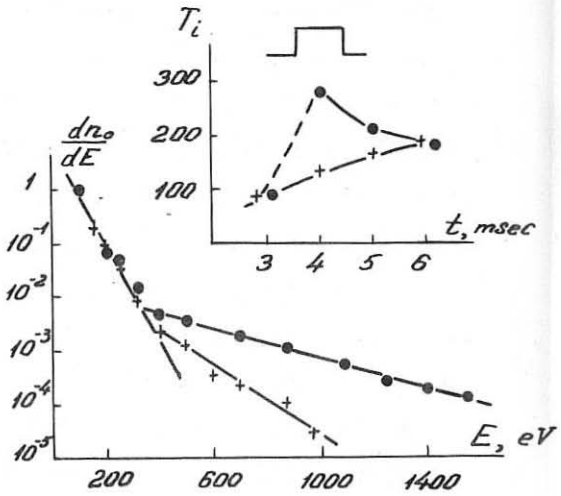


Fig. 2

References.

1. D.P.Ivanov et al. "Diagn. plasmy", Atomizdat,M., 1963, p.292.

2. G.A.Bobrovskii et al. JETP 59 (1970) 1103.

3. A.D.Piliya, V.I.Fedorov. JETP 60 (1970) 389.

ORMAK AND NEUTRAL INJECTION

C. F. Barnett, L. A. Berry, C. E. Bush, J. D. Callen, J. F. Clarke,
R. J. Colchin, R. A. Dory, A. C. England, J. T. Hogan, G. G. Kelley,
J. R. McNally, Jr., M. Murakami, R. V. Neidigh, M. Roberts
J. A. Rome and W. R. Wing

Oak Ridge National Laboratory*
Oak Ridge, Tennessee 37830 U.S.A.

Abstract. The plasma conditions attained in the ohmically heated ORMAK experiment provide a satisfactory base for neutral injection heating. Plasma flows and radial electric fields of the same magnitude as those expected to result from neutral injection have been observed in ORMAK. They appear to have no deleterious effect on the plasma.

Introduction. As of the writing of this paper the ORMAK experiment is being modified to accept two 125 kW neutral beam injector modules[1]. Experimental results are expected by August and will be included in the oral presentation. In this paper we will concentrate on those properties of the existing ORMAK plasma which might be expected to influence the outcome of the neutral injection experiment.

ORMAK Plasma Conditions. The overall energy balance in ORMAK has been shown to depend heavily on n_0, the density of neutral atoms in the plasma[2]. When charge exchange dominates the ion energy loss process, the bulk ion temperature can be found by equating the electron-ion heat transfer rate to the charge exchange losses:

$$3\left(\frac{m}{M}\right)n_e \nu_{ei}(T_e - T_i) = n_0 \sigma_{cx} v_i n_i \times (T_i - T_0) \qquad (1)$$

This equation can be solved for T_i using the fact[3] that the function $f_A = (T_e/T_i - 1)/(T_e/T_i)^{3/2}$ is approximately constant ($f_A = .38$) over the range of experimental temperatures. Calculations of neutral transport in the plasma and observations of the Doppler width of H_α light from the plasma core indicate that the neutral temperature T_0 is between 1/3 to 1/2 of T_i. Therefore, we will replace $T_i - T_0$ in Equation (1) by αT_i. If $\alpha = 1$, all of the ion energy is lost per

charge exchange collision. The bulk ion temperature is then $T_i = 2.76 \sqrt{n_e/\sigma n_0}$ eV. Experimental ion temperatures are shown in Fig. 1 as a function of $\sqrt{n_e/n_0}$. The electron density was obtained from a microwave interferometer and the neutral density from an absolutely calibrated neutral particle spectrometer. Figure 1 indicates the dominance of charge exchange losses even though the data shown were obtained for plasma currents between 60 and 160 kA. Computer simulation of the plasma including transport losses which depend on plasma current gives very good agreement with the experimental data[2].

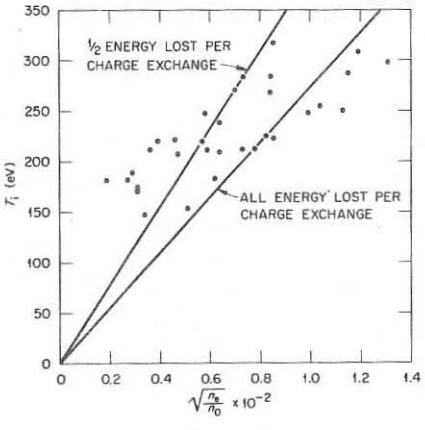


Figure 1

The detailed mechanism determining the level of neutrals in the plasma is unclear. However, we have observed experimentally that the central neutral density is inversely proportional to n_e^2. Figure 2 shows this dependence using the same data as in Fig. 1. The implication of this data is that charge exchange losses decrease rapidly as the plasma density increases.

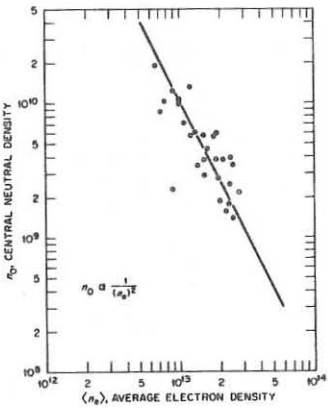


Figure 2

Expected Plasma Conditions with Injection. We have used the ORNL simulation code to obtain a prediction of the ion temperature to be expected with injection heating in the presence of neutrals. The code uses the transport coefficients found to fit the ohmically heated plasma parameters[2].

The calculation is pessimistic in that the beam particles are assumed lost at each charge exchange with no account taken of the significant probability of retrapping. Ion temperatures in excess of 1 keV are obtained with $n_0 = 8 \times 10^8$ cm^{-3}.

This calculation does not include any anomalous processes produced by the injected beam. At the level of injection expected in ORMAK, significant perturbations in the plasma current distribution, momentum, radial electric field and net charge can be expected[4]. The first of these can be minimized by injection of the two beams. The latter three are related by the equation for equilibrium flow in a collisionless toroidal plasma[5].

$$u_{\parallel} = - \frac{T_i}{B_p} \left\{ \frac{n'}{n} - .17 \frac{T_i'}{T_i} - \frac{E_r}{T_i} \right\} \qquad (2)$$

Since Equation 2 should apply in the ORMAK plasma, we expect the neutral injection process to modify the toroidal flow either by direct momentum input or by changing E_r. However, we have observed both poloidal and toroidal flows in ohmically heated ORMAK which have the same magnitude as the flows which could be produced by neutral injection[4].

Observations of Plasma Flow in ORMAK. Figure 3 shows the poloidal rotation inferred from Doppler shift measurements of the H_α radiation of neutrals inside the plasma. It is only observed at the beginning and end of a discharge when the ion temperature is low and when pulses of runaway electrons appear at the limiter. A linear relationship is obtained between the poloidal velocity and the number of runaway electrons striking the limiter.

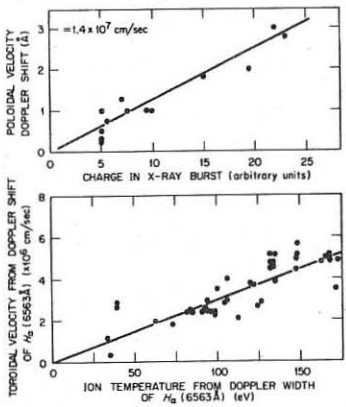


Figure 3

This leads us to assign this poloidal rotation to an $E_r/B_{Toroidal}$ flow in a positive radial electric field. No deleterious effect on the plasma was noted during this rotation although the electric field inferred for the highest velocities measured is 2000 V/cm which is comparable to the fields expected with injection.

The toroidal flow which is observed during the hot ion phase of the discharge is shown in Fig. 3 as a function of the Doppler temperature of the neutrals. The linear relationship shown is predicted by Equation 2 if E_r/T_i is small with respect to (n'/n). It may be that the observed toroidal flow is the equilibrium neoclassical flow. However, inserting values for n'/n obtained from the ORNL simulation code in Equation 2 gives values of $u_\parallel$ a factor of 2 lower than those observed experimentally. In any case the observed toroidal flows are comparable with those which might be produced by neutral injection and again no deleterious effects are seen.

REFERENCES

[1] L. D. Stewart, et al., Third Int. Symp. on Toroidal Plasma Confinement, Garching, Germany (1973).

[2] G. G. Kelley, et al., IBID.

[3] L. A. Artsimovich, Nuclear Fusion, 12, 215 (1972).

[4] J. D. Callen, J. F. Clarke, and J. A. Rome, Third Int. Symp. on Toroidal Plasma Confinement, Garching, Germany (1973).

[5] M. N. Rosenbluth, et al., Fourth Int. Conf. on Plasma Physics and Controlled Nuclear Fusion Research, Madison, Wisconsin (1971).

*Operated by Union Carbide Corporation for the U.S. Atomic Energy Commission.

Report on the Alcator Experiment[+]

The Alcator Group[(o)]

Massachusetts Institute of Technology, Cambridge, Massachusetts 02139

United States of America

[+] Sponsored by the U. S. Atomic Energy Commission

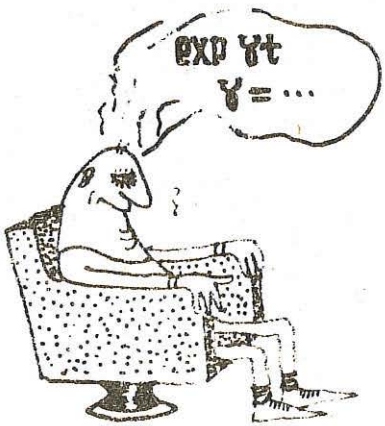
[(o)] U. Ascoli-Bartoli*, R. Blanken, P. Brossier**, B. Coppi, A. Hugenholtz***, L. Lidsky, B. Montgomery, L. Ornstein***, R. Parker, K. Thomassen, R. Taylor, L. Smullin, H. Van der Ven***, R. Van Heiningen***

* C.N.E.N. (Italy) - Euratom Association

** C.E.A. (France) - Euratom Association

*** F.O.M. (Netherlands) - Euratom Association

1.4. TOKAMAKS: STABILITY, STABILITY, STABILITY...



EQUILIBRIUM AND LOCALIZED CRITERIA ON MAGNETIC SURFACES WITH CROSS SECTIONS OF ARBITRARY SHAPE

C. Mercier

ASSOCIATION EURATOM-CEA SUR LA FUSION
Département de Physique du Plasma et de la Fusion Contrôlée
Centre d'Etudes Nucléaires
Boîte Postale n° 6. 92260 FONTENAY-AUX-ROSES (FRANCE)

INTRODUCTION.-

A first type of localized criterion is known from 1961 [1] and has been thoroughly studied. Let us call it the criterion of the first kind. A more precise localization around a magnetic line leads to a localized criterion of the second kind which may be more or less stringent according to the cases considered [2]. For the analytic treatment of these criteria, one needs to know the properties of the M.H.D. equilibria on the magnetic surface around which the perturbations are localized. This has been done for the surfaces which are near the magnetic axis by expanding the equilibrium parameters in powers of the distance from this axis. It has been shown that for these surfaces near the magnetic axis, the two criteria are identical [3]. We shall introduce a new method of expansion which will be valid in symmetry of revolution with cross section of arbitrary shape and this method will allow us to study the properties of the criteria of both the first and the second kinds.

CRITERIA OF THE FIRST AND SECOND KINDS.-

The nested magnetic surfaces are represented by [4] $\psi(\vec{r})$=constant. If the magnetic field $\vec{B}$ is given by $\vec{B}=\text{grad}\chi \times \text{grad}\psi$ a magnetic line is defined by the intersection of two surfaces (μ_o) $\psi=\psi_o$; $\chi=\chi_o$. The perturbations $\vec{\xi}$ will be localized if they vanish outside the surfaces ($\psi_o \pm \varepsilon$) close to the surface $S_o(\psi=\psi_o)$. Let us define the variable $(\psi-\psi_o)/\varepsilon=t$. Then $\vec{\xi}=o$ for $|t|>1$.

Another type of localization may restrict the displacements to be around a closed magnetic line corresponding to a magnetic surface for which the rotational transform is rational. One may then define this localization by $(\chi^\circ-\chi_o^\circ)/\varepsilon'=x$ with $\vec{\xi}=o$ for $|x|>1$. χ_o° defines with ψ a magnetic field with constant rotational transform ($\chi_o^\circ=\chi_o$ on S_o). The criterion of the first kind corresponds

to $\varepsilon << o$ and $\varepsilon' >> \varepsilon$ while the criterion of the second kind corresponds to $\varepsilon << o$ and $\varepsilon' \lesssim \varepsilon$. In the first case, the perturbation is practically constant along a magnetic line and principally in $\vec{S}_o$ in a direction perpendicular to the magnetic line $\vec{\xi} \sim \text{grad } p \times \vec{B}$. On the contrary the perturbation of the second kind is of the ballooning type which means that it is variable along a magnetic line. In the first case one can proceed completely to the minimization and obtain a criterion which must be satisfied on any closed magnetic line.

It is possible to reduce the minimization in the second case to a problem of minimization with a single function. If the shear is zero, the problem is much simplified and it remains only to minimize an integral of the type

$$I = \oint \left[A^2(l) \left| \frac{dg}{dl} \right|^2 + B|g|^2 \right] dl$$

along the closed magnetic line. This latter part is carried out numerically. The case of zero shear is physically interesting because one can show that this is the limiting case of shear tending to zero. If the shear has a non-zero value, one can find a criterion majorant and a criterion minorant : so it is always possible to stabilize these perturbations with a sufficiently high shear.

METHOD OF EXPANSION IN THE NEIGHBOURHOOD OF ANY MAGNETIC SURFACE IN SYMMETRY OF REVOLUTION.-

In a meridian plane, the section of a magnetic surface is a closed curve (c) which we will define by the data of its radius of curvature as a function of the curvilinear abscissa s. A point P in the space is located by the meridian plane which contains it (zOx) and its distance $PM = \rho_1$ to the curve (c), the point M being defined by its curvilinear abscissa s on (c).

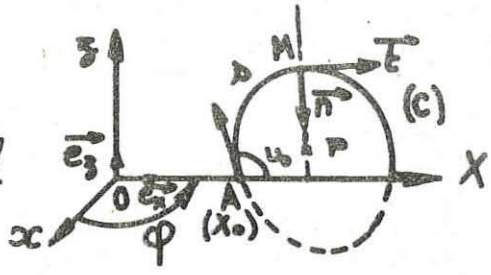


Fig: 1

The coordinates (s, ρ_1, ϕ) of the point P are related to the Cartesian Coordinates by

$$x + iy = (\chi_0 + \rho_1 \sin u + \int_0^s \cos n \, ds) e^{i\phi} = \chi e^{i\phi}$$

$$Z = (z_0 - \rho_1 \cos u + \int_0^s \sin u \, ds) \quad \text{where } u = u_0 - \int_0^s \frac{ds}{R(s)}$$

The system is triorthonormal because we have

$$dS^2 = (1 - \frac{\rho_1}{R(s)})^2 \, ds^2 + d\rho_1^2 + \chi^2 d\phi^2$$

It is then possible to expand the system of M.H.D. equilibrium equations in the neighbourhood of the surface S_0 which is characterized in this system by $\rho_1 = 0$. For instance, the function ψ will be expanded as follows $\psi = \psi_1 \rho_1 + \psi_2 \rho_2 \ldots\ldots$ ψ_1 and ψ_2 are periodic functions of s.

The equilibria thus defined in the neighbourhood of S_0 depend upon an arbitrary function ψ_1 representing the poloidal magnetic field tangent to S_0 and surface quantities like $(\frac{\iota}{2\pi})_0$, $\left|\frac{d}{d\psi}(\frac{\iota}{2\pi})\right|_0$, $(\frac{dP}{d\psi})_0$.

APPLICATION TO LOCALIZED CRITERIA.-

The criterion of the first kind has been studied with this method in many cases of different cross section shapes. One important result should be pointed out : the order relative to the aspect ratio in the criterion changes depending upon whether the cross section has, or has not, an axis of symmetry parallel to OZ. Against these localized perturbations, non-symmetric cross sections have thus stabilization properties quite different from symmetric cross sections. This result is very similar to that found in the neighbourhood of a magnetic axis where the influence of triangular terms is more important by one order. The application to the localized criterion of the second kind with circular cross section (radius ρ_0) for S_0 shows that this criterion is *essentially different from the first kind* when we are far from the magnetic axis (non negligible pressure gradient) with an important variation of the poloidal magnetic field on S_0 $|B_p = B_{p_0}(1 - \nu \cos \theta)|$. *Figure 2* represents the safety factor q versus $\tilde{\beta} \simeq -\frac{q}{2} \frac{1}{\langle B \rangle^2} \langle \frac{L_0}{2\pi} \frac{dP}{dl} \rangle_0$ for

various values of ν(L = Length of the torus). The stable region corresponds to high values of q. We have also drawn lines parallel to the $\tilde{\beta}$ axis representing the stability limit for the criterion of the first kind with the same values of the parameters. Note that the stability regions are identical for $\tilde{\beta} = 0$.

References.-

[1] C.Mercier - C.R.Acad.Sci.Paris 252, 1577 (1961) ; Nuclear Fusion Suppl.part 2, 801 (1962) and 1, 47 (1960) ;

[2] C.Mercier - Sherwood Meeting 1972 ; Report EUR.CEA.FC-692.

[3] G.Laval et al. - Phys.Rev.Letters 24, 1229 (1970).

[4] C.Mercier, H.Luc - International School of Plasma Physics, Vienna 1971 (to be published).

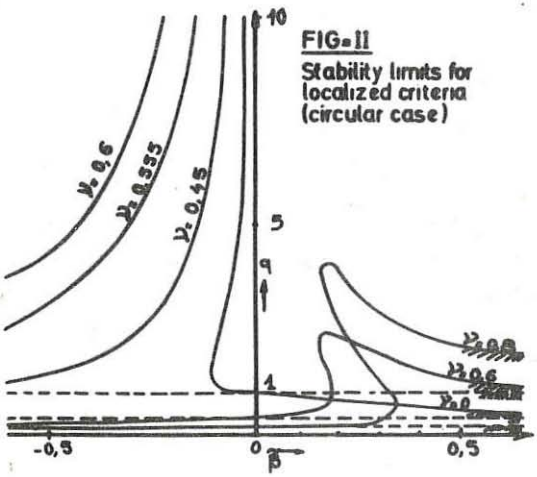


FIG.II
Stability limits for localized criteria (circular case)

EFFECT OF PARABOLIC CURRENT ON THE STABILITY OF M.H.D. EQUILIBRIUM IN TOKAMAK WITH NON CIRCULAR CROSS SECTION.

by

P. Grelot - J. Weisse

ASSOCIATION EURATOM-CEA
Département de Physique du Plasma et de la Fusion Contrôlée
Service IGn - Centre d'Etudes Nucléaires
B.P.85 - Centre de Tri - 38041
GRENOBLE CEDEX (France)

In this investigation the stability limit of the M.H.D. equilibria is given by Mercier's criterium /1/ calculated along the magnetic axis of the configuration.

In the comparison of the stability zones the plasma cross-section is taken as constant. This cross-section is normalized to : the small radius of the equivalent circular Tokamak has a unit value, so that the large radius of Toroid R_G is directly related to the aspect ratio.

The geometric values which appear directly in the most general form of Mercier's criterium are the following :

- the aspect ratio R_G.
- the ellipticity of the magnetic surfaces in the neighbourhood of the magnetic axis
- the inclination of these magnetic surfaces
- the amplitude of the triangular distortions of the magnetic surfaces
- their relative inclination in relation to the elliptic terms.

The effects of the first two factors and some effects of the fourth have been studied in some detail by LUC /2/, in as much as the analytical expansions used proved adequate ($R_G > 3$; low distortion).

An overall study of various shell shapes has been done /3/, /4/, /5/, /6/ with "flat" current profile :

$$j_\phi = j_o \{(1 - \beta) \frac{R_G}{R} + \beta \frac{R}{R_G}\} \qquad (1)$$

A more general (and much more realistic) current density profile is taken by choosing functional values :

$$\overline{B^2} = (\frac{R}{R_G} B_\phi)^2 = B_o^2 + \lambda F + \mu F^2 \qquad p = p_1 F + p_2 F^2 \qquad (2)$$

where F is the flux function.

The "flat" current profile discussed earlier corresponds to $\mu = p_2 = 0$, and is defective in that it does not cancel out at shell level, but is in fact often more important than along the magnetic axis.

So as not to substantially modify calculation methods, we have retained a residue of "flat" current (current at boundaries is < 5 % of its value in the centre of the machine) and studied the two following situations :

1/ $\lambda << 2 \mu F_{max}$ $\qquad p_2 = 0 \qquad (3)$

a pressure profile linear in terms of F is introduced ($p_1 \neq 0$)

2/ $\frac{\lambda}{2} << \mu F_{max} \frac{R_G}{R_M} + 2 \mu_o p_2 F_{max} \frac{R_M}{R_G}$ $\qquad p_1 = 0 \qquad (4)$

Results obtained are the following :

- An attempt to scan the stability limit curve by means of pressure profile purely linear in terms of F (first situation) is soon limited by the equilibrium condition ($p > 0$). This is particularly true for shell shapes ③ and ⑤ where the scanning is so slight that these shells are without interest.

The results relating to the second situation (pressure quadratic in terms of F) have been indicated on Fig. 2 and suggest the following remarks :

- The overall appearance of the stability zones as well as their relative positions are maintained.
- The characteristics in I_o^2 and β compared with those for the flat current profile have been subjected to an overall decrease of one order of magnitude. One exception is the circular shell which is twice as insensitive to this phenomenon. This can be explained by the fact that this type of current profile smoothes out the magnetic surfaces about the axis.

As a conclusion we may say that the study of a parabolic current profile does not invalidate the results and general aspect obtained with the flat current profile.

However, with a flat profile in every case :

Operating with a strong current ($\beta^* < 1$) or operating with strong β ($\beta^* > 1$)

a noticeable improvement in the performance of traditional Tokamaks (circular cross-section) could be anticipated by acting on the shape of the shell (gain 3 in current, gain 2 in β).

This position must be revised with more realistic current profiles.

In particular, for strong β regimes, this method cannot be expected to bring any appreciable improvement over circular cross-section.

Any effect due to shape can only be used to advantage with strong current (in other words, low β).

Références.

/1/ - C. Mercier, Fus. Nucl. 4 (1964), p. 213.
/2/ - H. Luc, EUR/CEA/FC N° 569.
/3/ - R.Y. Dagakvan and al. Trieste IC/70/120.
/4/ - G.D. Jukes, Nucl. Fus. 10 (1970, p. 131.
/5/ - P. Grelot, J. Weisse, 5th Eur. Conf. Grenoble 72. Tome 1, p. 24.
/6/ - P. Grelot, J. Weisse, 5th Eur. Conf. Grenoble 72. Tome 2, p. 231.

Figures - remarks.

Equilibrium stability zones shown on Fig. 2 have been plotted in the plane (I_o^2, β).

$$I_o^2 = \left(\frac{R_G}{a}\right)^2 \frac{B_\theta}{\langle B_\phi{}^2 \rangle}$$

where a is the small radius of the Tokamak of equivalent circular cross-section.

β represente the mean value of local β in the cross-section.

On figure 2, we have indicated :

⊘ point $\beta^* = 1$

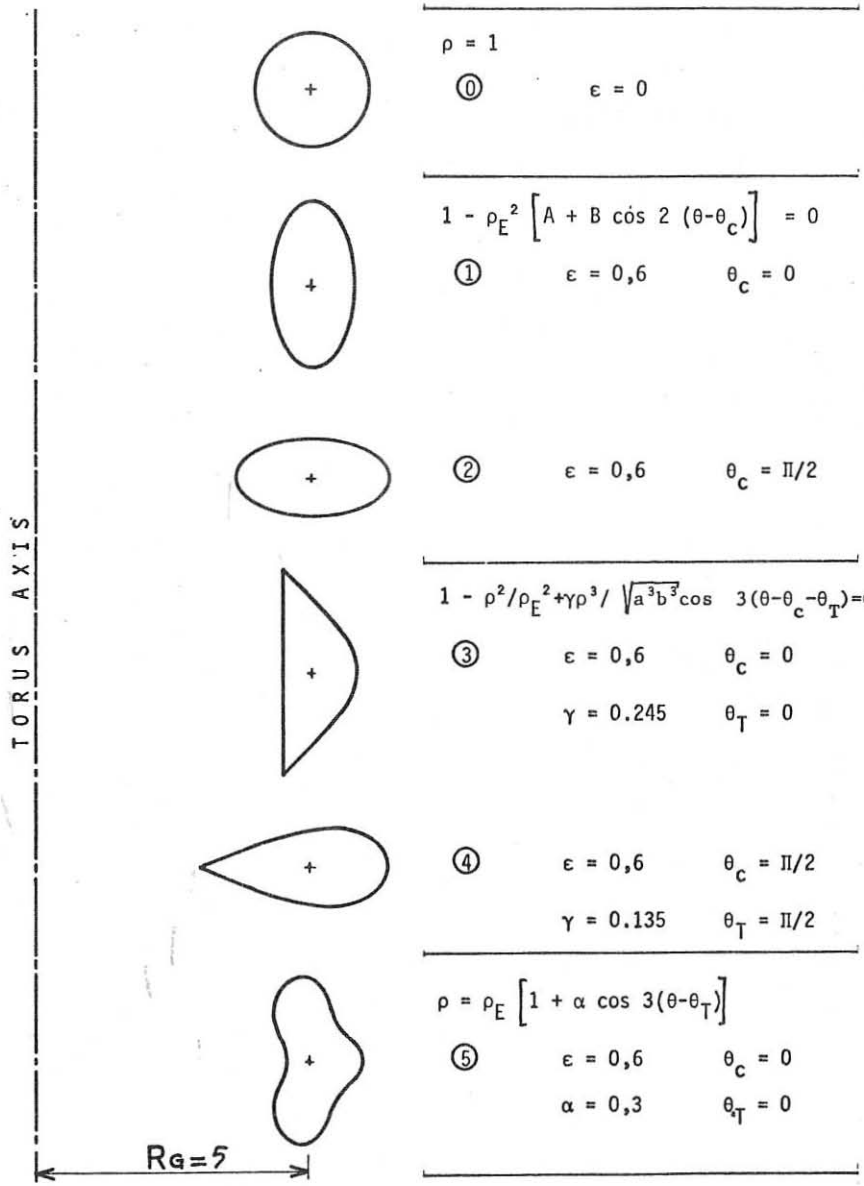
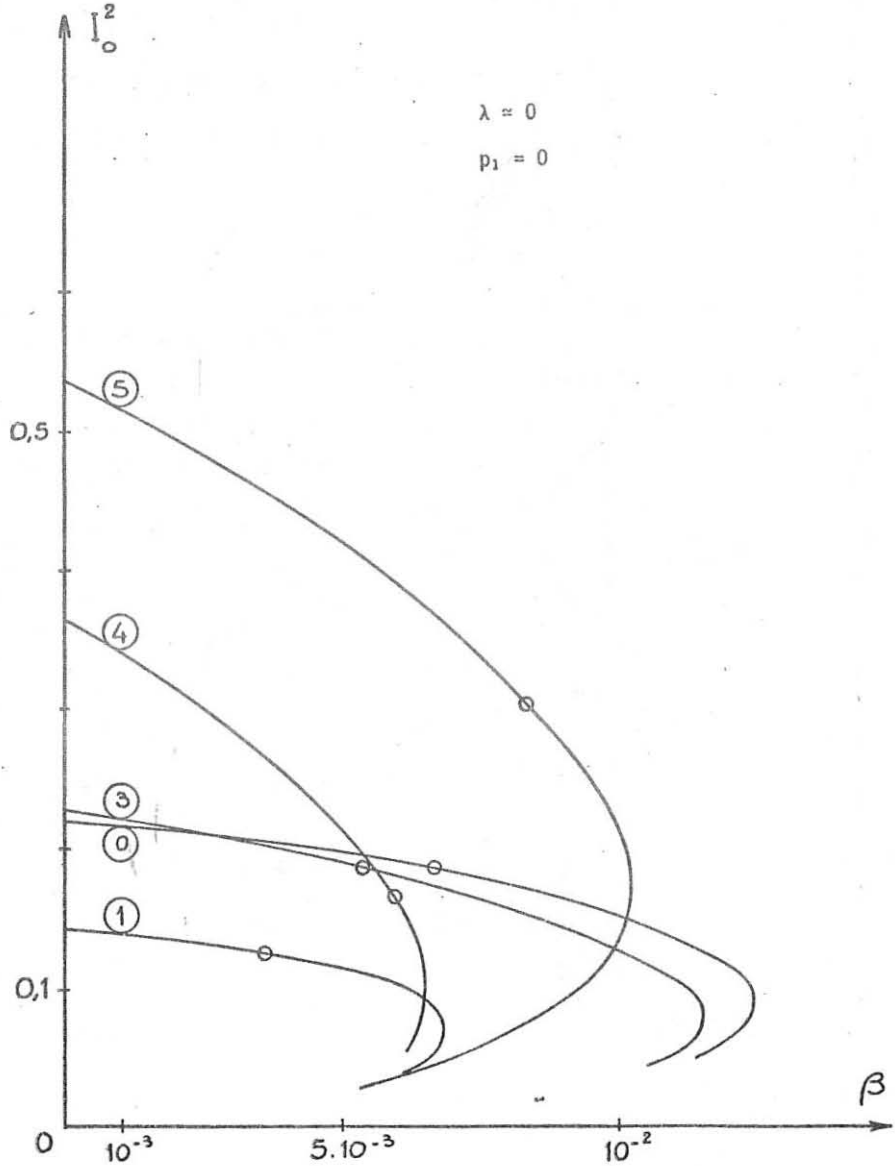

TORUS AXIS
Rg=5
ρ = 1
⓪ ε = 0
1 - ρE² [A + B cós 2 (θ-θc)] = 0
① ε = 0,6 θc = 0
② ε = 0,6 θc = Π/2
1 - ρ²/ρE² + γρ³/ √a³b³ cos 3(θ-θc-θT)=0
③ ε = 0,6 θc = 0
γ = 0.245 θT = 0
④ ε = 0,6 θc = Π/2
γ = 0.135 θT = Π/2
ρ = ρE [1 + α cos 3(θ-θT)]
⑤ ε = 0,6 θc = 0
α = 0,3 θT = 0

Figure 1

Figure 2

"PARABOLIC" CURRENT PROFILE



MHD MODAL ANALYSIS OF TOKOMAK LIKE PLASMA WITH VARIOUS CURRENT DENSITY PROFILES

W.Grossmann, S.Ortolani*

Max-Planck-Institut für Plasmaphysik, Euratom Association, Garching bei München, FRG.

Abstract: An analysis of MHD stability for a cylindrical Tokomak plasma with realistic current density profiles is presented. The results show that the various current profiles lead to stability criteria significantly different from those of earlier considerations /1/.

In a recent report,/2/, the MHD stability of kink modes in a cylindrical Tokomak plasma was considered. Various realistic forms of the axial current density profile have been analysed which correspond to the various phases of operation during a typical Tokomak discharge. For example, a current density profile which is peaked near the limiter (profile I) corresponds to the phase where the "skin effect" is observed. After the "skin effect" has disappeared, a more or less uniform current density is assumed (profile II); uniform over the major part of the plasma and uniformly vanishes at the limiter. Finally two profiles which are peaked on the plasma axis (profiles III and IV) are chosen to represent later times during the discharge. The profiles are shown schematically in fig.1, normalized to maximum values and as function of normalized radius $\tilde{r}$ ($\tilde{r}$ = radius/limiter radius R_L). The model consists of a constant axial magnetic field, a density profile of the form $\rho = \rho_o(1 - \tilde{r}^4)$ where ρ_o is the plasma centerline value, plus the above mentioned current density profiles. The external region outside the limiter is treated by assuming a small but finite constant conducting density of plasma (3 orders of magnitude less than ρ_o) and vacuum magnetic field profiles bounded externally by a perfectly conducting wall. The advantages and disadvantages of treating the external region in this manner are discussed in /3/; however, we mention that the present choice is probably more realistic than the assumption of a zero density pure vacuum external region/1/.

*) Centro Gas Ionizzati-CNR (Universito di) Padova, Italy.

We investigate the stability by numerically integrating the linearized ideal MHD incompressible equations of motion posed as an eigenvalue problem for the growth rate γ and boundary value problem for the radial perturbation eigenfunction ξ_r. The governing equations and method of solution are described in /2/ and we give here only a brief discussion of the results. Assuming a periodicity condition on a plasma cylinder allows a topological torus to be constructed which has a major radius R_T and allows q at the limiter to be defined as:

$$q\ (R_L) = \frac{R_L}{R_T} \cdot \frac{1}{\mu}\ , \text{ where } \mu = \frac{\mu_o\ I_z}{2\pi R_L B_o}$$

and where I_z = total axial current, μ_o = permeativity and B_o=axial magnetic field. The dimensionless axial wavenumber for the perturbations is defined $\tilde{k} = N.q\,(R_L)$, where N is the number of full wavelengths along the topological torus. In the following, the aspect ratio R_T/R_L is taken to be 5 and μ is set equal to 0.2 giving a q at the limiter of unity. The following calculations are made with constant total current for all cases of current density profiles; q at the limiter is the same for all cases.

Shown in fig.2 are the results for the m = 1 mode for all four profiles; given are the growth rates as a function of N for the free boundary model (including external region-full curves) and the fixed boundary model (limiter taken as perfect conductor-dashed curve plus right hand portion). The external region (wall radius/limiter radius = 1.5) opens up the longwavelength part of the spectrum to instability and in this region dominates the stability. For large N there is no appreciable effect on the stability for case III and IV and this can be explained by examining the typical case IV m = 1 eigenfunctions shown in fig.3. For small N the radial extent of ξ_r is great whereas for large N the m = 1 ξ_r is localized near the center of the plasma corresponding to the region where the Suydam criterium is violated.

The effect of the external conducting wall on m = 2 and 3 stability for profiles I and II is less than that for the m = 1 mode due primarily to the more internal localization of the eigenfunctions. This is in disagreement with /1/, however, there a test eigenfunction was assumed which guaranteed an influence from the wall. Our $m \geq 2$ eigenfunctions are in all cases much more localized than those found in/1/.

To illustrate this point we show the m = 2 and 3 eigenfunctions for profile IV in fig.4. Here ist is seen that extreme localization of the perturbations well within the plasma occurs and that the contribution of ξ_r in the outside region is negligible.

Holding the total current constant one can then examine the spacing between the various growth rate envelopes for different m numbers for the different profiles. We find for the values of plasma parameters chosen here that islands of stability exist seperating the unstable envelopes of m = 1,2 and so on for type I and II profiles. However, for type III and IV, overlapping occurs and we show the results for the profile IV in fig.5 for fixed boundary. Here we see that one can find values of N where both m = 1 and 2 are unstable; similarly m = 2 and 3 can be simultaneously unstable.

If we now attempt to compare the results of our calculations to past and recent experiments in Tokomak experiments /4,5/, we notice that in our calculations the higher m modes always occur (at constant current) at high N values. In the experiments, however, $m \geq 2$ modes have been observed at low N; in fact N = 1 seems to be prevalent. More precise tailoring of the numerical calculations to particular experiments is necessary before any true comparison can be made. On the other hand, as shown in /2/, the inclusion of a uniform rotation on the plasma equilibrium leads to a shifting of all higher m mode unstable evelopes to lower $\tilde{k}$ or N values. In /4,5/ it was observed that the $m \geq 2$ perturbations rotate in the poloidal direction.

Finally we show the results of an attempt to determine a stability criterion for stability against m = 1 for type IV profiles. Considering only the fixed boundary case we show in fig.6 the results of plotting the maximum growth rates $\tilde{\gamma}_{max}$ as a function of μ. This could be equivalent to a variation of total current. Extrapolation of this linear curve to zero growth rate for m = 1 yields a value of μ =o.o2 and is equivalent for the given profile to a value of q at the limiter of 10 and about 0.7 on the axis. Thus, for this case, q = 1 at the limiter is not the trigger value of the m = 1 mode. We conclude by restating that the inclusion of realistic current density profiles in a more exact MHD treatment leads to results which differ from earlier considerations.

We investigate the stability by numerically integrating the linearized ideal MHD incompressible equations of motion posed as an eigenvalue problem for the growth rate γ and boundary value problem for the radial perturbation eigenfunction ξ_r. The governing equations and method of solution are described in /2/ and we give here only a brief discussion of the results. Assuming a periodicity condition on a plasma cylinder allows a topological torus to be constructed which has a major radius R_T and allows q at the limiter to be defined as:

$$q\ (R_L) = \frac{R_L}{R_T} \cdot \frac{1}{\mu}\ , \text{ where } \mu = \frac{\mu_o\ I_z}{2\pi R_L B_o}$$

and where I_z = total axial current, μ_o = permeativity and B_o=axial magnetic field. The dimensionless axial wavenumber for the perturbations is defined $\tilde{k} = N \cdot q\,(R_L)$, where N is the number of full wavelengths along the topological torus. In the following,the aspect ratio R_T/R_L is taken to be 5 and μ is set equal to 0.2 giving a q at the limiter of unity. The following calculations are made with constant total current for all cases of current density profiles; q at the limiter is the same for all cases.

Shown in fig.2 are the results for the m = 1 mode for all four profiles; given are the growth rates as a function of N for the free boundary model(including external region-full curves) and the fixed boundary model(limiter taken as perfect conductor-dashed curve plus right hand portion). The external region (wall radius/limiter radius = 1.5) opens up the longwavelength part of the spectrum to instability and in this region dominates the stability. For large N there is no appreciable effect on the stability for case III and IV and this can be explained by examining the typical case IV m = 1 eigenfunctions shown in fig.3. For small N the radial extent of ξ_r is great whereas for large N the m = 1 ξ_r is localized near the center of the plasma corresponding to the region where the Suydam criterium is violated.

The effect of the external conducting wall on m = 2 and 3 stability for profiles I and II is less than that for the m = 1 mode due primarily to the more internal localization of the eigenfunctions. This is in disagreement with /1/, however, there a test eigenfunction was assumed which guaranteed an influence from the wall. Our $m \geq 2$ eigenfunctions are in all cases much more localized than those found in/1/.

To illustrate this point we show the m = 2 and 3 eigenfunctions for profile IV in fig.4. Here ist is seen that extreme localization of the perturbations well within the plasma occurs and that the contribution of ξ_r in the outside region is negligible.

Holding the total current constant one can then examine the spacing between the various growth rate envelopes for different m numbers for the different profiles. We find for the values of plasma parameters chosen here that islands of stability exist seperating the unstable envelopes of m = 1,2 and so on for type I and II profiles. However, for type III and IV, overlapping occurs and we show the results for the profile IV in fig.5 for fixed boundary. Here we see that one can find values of N where both m = 1 and 2 are unstable; similarly m = 2 and 3 can be simultaneously unstable.

If we now attempt to compare the results of our calculations to past and recent experiments in Tokomak experiments /4,5/, we notice that in our calculations the higher m modes always occur (at constant current) at high N values. In the experiments, however, $m \geq 2$ modes have been observed at low N; in fact N = 1 seems to be prevalent. More precise tailoring of the numerical calculations to particular experiments is necessary before any true comparison can be made. On the other hand, as shown in /2/, the inclusion of a uniform rotation on the plasma equilibrium leads to a shifting of all higher m mode unstable evelopes to lower $\tilde{\kappa}$ or N values. In /4,5/ it was observed that the $m \geq 2$ perturbations rotate in the poloidal direction.

Finally we show the results of an attempt to determine a stability criterion for stability against m = 1 for type IV profiles. Considering only the fixed boundary case we show in fig.6 the results of plotting the maximum growth rates $\tilde{\gamma}_{max}$ as a function of μ. This could be equivalent to a variation of total current. Extrapolation of this linear curve to zero growth rate for m = 1 yields a value of μ =o.o2 and is equivalent for the given profile to a value of q at the limiter of 10 and about 0.7 on the axis. Thus, for this case, q = 1 at the limiter is not the trigger value of the m = 1 mode. We conclude by restating that the inclusion of realistic current density profiles in a more exact MHD treatment leads to results which differ from earlier considerations.

References: 1) Shafranov,V.D., Soviet Phys.-Tech.Phys.15, 175(197o) 2) Grossmann,W., S.Ortolani, IPP-Report 1/132(1973); 3) Crow,J.E., D.C.Robinson, IPP-Report 1/127(1972),paper C 1; 4) Mirnov,S.V., I.B. Semenov, Sov.Phys. JETP, 33, 1134(1971); 5) Hosea,J.C., et al., Princeton Univ., MATT-855(1971).

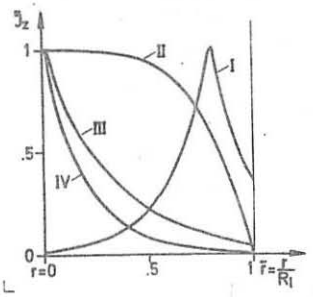


Fig. 1

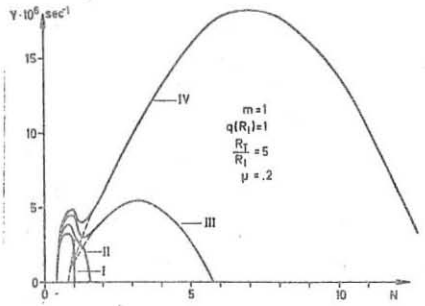


Fig. 2

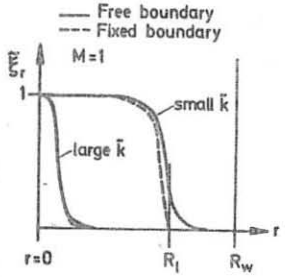


Fig. 3

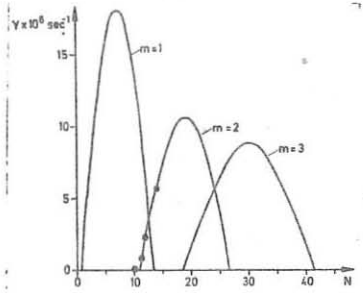


Fig. 4

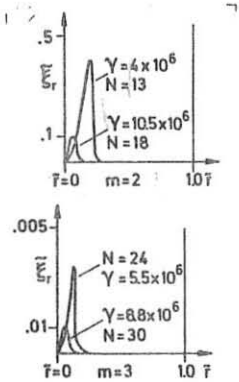


Fig. 5

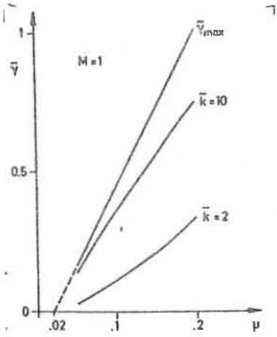


Fig. 6

KINK INSTABILITIES IN HIGH β TOKAMAKS AND BELT PINCHES*

J. P. Freidberg, F. A. Haas+ and B. M. Marder
Los Alamos Scientific Laboratory, University of California

Abstract. It is shown that kink instabilities in a high β sharp boundary Tokamak ($\beta \sim a/R$) are strongly destabilized by toroidal effects. For either $\beta \sim a/R$ or $\beta \sim 1$ (Belt Pinch) moderate ellipticity has a stabilizing effect on kink modes whereas large ellipticity is strongly destabilizing.

1. Introduction. We present the results of three separate calculations whose combined aim is to provide some insight into the effects of toroidicity and ellipticity on kink instabilities in high β plasmas. Using the sharp boundary, thin-skin, ideal MHD model we have examined the long wavelength kink instability in (1) a high β circular Tokamak ($\beta \sim a/R$), (2) a high β elliptical Tokamak ($\beta \sim a/R$) and (3) a straight Belt Pinch with simulated toroidal effects ($\beta \sim 1$). Existing theories are almost entirely concerned with the low β Tokamak ordering, $\beta \sim (a/R)^2$ [1,2] although there has been some work at higher β's [3]. Our primary objective is to determine that configuration which leads to the highest critical β, stable against long wavelength kink modes. A second objective is to test whether $q = 1$ is sufficient for kink stability in high β circular and elliptical plasmas.

The calculations are performed by expressing the normal component of plasma displacement as a Fourier series and minimizing numerically over the Fourier coefficients. This technique has been described earlier [4] and has the advantage of allowing a large number of harmonics in the minimization (typically 10-40).

2. High-β Circular Tokamak. Defining the plasma to have minor radius "a" and major radius "R" ($\varepsilon = a/R$), we work in coordinates (r, θ, ϕ) based on the center of the cross-section. The plasma contains only a toroidal field B_ϕ, but the vacuum has both toroidal ($\hat{B}_\phi$) and poloidal ($\hat{B}_\theta$) components. The equilibrium quantities have the ordering: $B_\phi \sim \hat{B}_\phi \sim 1$, $\hat{B}_\phi - B_\phi \sim \varepsilon$, $\hat{B}_\theta \sim \varepsilon$, $\beta \sim \varepsilon$, where $\beta = 1 - B_\phi^2/\hat{B}_\phi^2$. To leading order the safety factor q at the surface is defined by

$$q = \frac{1}{2\pi} \varepsilon \hat{B}_\phi \int_0^{2\pi} \frac{d\theta}{\hat{B}_\theta(\theta)} .$$

The normal displacement at the surface is written in the form

$$\xi(\theta, \phi) = \exp(in\phi) \sum_m{}' \xi_m \exp(im\theta) ,$$

where the ξ_m's are undetermined coefficients over which the minimization is performed (m = o is excluded) and n is the mode-number the long way. Results for

n = 1, 2 and 3 are presented as a series of marginal stability lines in a plot of β/ε versus q (see Fig. 1). For each n the region of stability lies below the curve. The worst mode is n = 1, and at sufficiently low β the model is unstable below the Kruskal-Shafranov limit (q = 1) and stable above, which is consistent with earlier work. We observe that there is a limiting β (= 0·21ε) above which the n = 1 kink mode is unstable for all q. Along the n = 1 marginal line the eigenfunction is found to be predominately m = 2. The results indicate that toroidal effects strongly destabilize the kink mode.

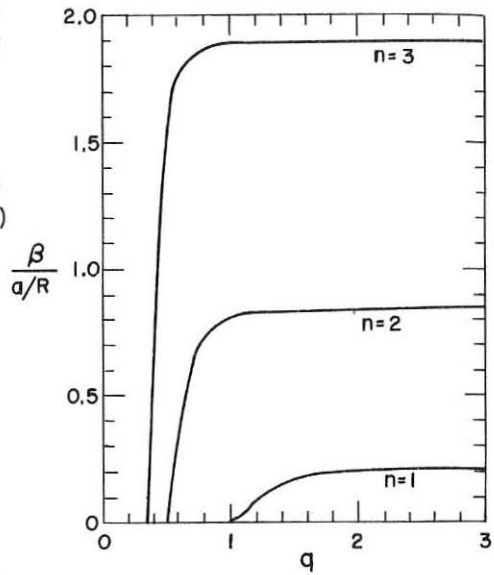


Fig. 1. Marginal stability curve.

3. High-β Elliptical Tokamak. Assuming the plasma to have elliptical cross-section with semi-axes a, b, and major radius R, we work in elliptic coordinates (u, v, ϕ) based on the center of the minor cross-section. Taking a/b $\sim$ 1 the other equilibrium quantities are ordered as for the previous calculation. The safety-factor q is again defined as the appropriate average over the plasma surface. The normal displacement at the surface is written as

$$\xi(v,\phi) = \exp(in\phi) \sum_m{}' \xi_m \exp(imv) ,$$

where as before the ξ_m's are determined by a numerical minimization. For a given a/b the β/ε versus q dependence is qualitatively the same as that shown in Fig. 1. For the limit $q \to \infty$ Fig. 2 shows the dependence of critical β on a/b for the n = 1 marginal line. The highest value of β (= 0·37ε) is found for b/a = 2·2, corresponding to a vertical rather than a horizontal ellipse. Figure 3 shows the variation of critical q for stability with ellipticity as $\beta/\varepsilon \to 0$. In this case for either vertical or horizontal ellipses the critical q is a symmetric increasing function of ellipticity.

4. Belt Pinch. We have performed the sharp boundary stability analysis for arbitrary β and finite ellipticity on a straight periodic system. This calculation is motivated by the conjecture that q = 1 is sufficient for stability of the $\beta \sim 1$ Belt Pinch [5] against kink modes. The coordinate system and perturbation are

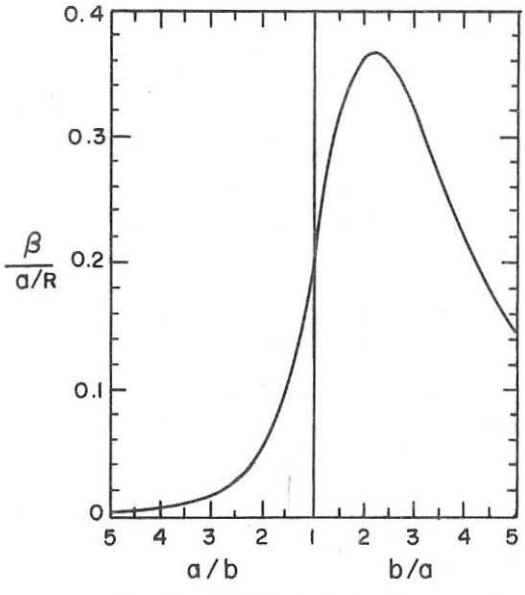


Fig. 2. Critical β vs a/b as q → ∞.

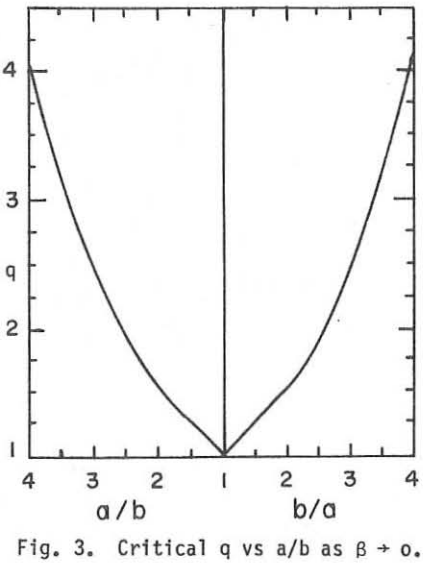


Fig. 3. Critical q vs a/b as β → o.

the same as in the elliptical Tokamak. Figure 4 illustrates critical β versus q for various b/a. For fixed β the critical q is a strongly increasing function of ellipticity.[6]

By introducing toroidal effects in an ad-hoc manner we obtain some insight into the stability of a high β toroidal Belt Pinch. Toroidal equilibria are only possible for $\beta \leq \frac{1}{2} \varepsilon/q_e^2$ where q_e is the product of q and a decreasing function of b/a. It is found that the desirable equilibrium property associated with ellipticity (i.e., high β at q = 1) is almost nullified by instability. Our results indicate that a small increase in critical β can be achieved for b/a ≈ 2. However, the critical β rapidly decreases for higher ellipticity. In Fig. 5 we illustrate the combined stability results and toroidal equilibrium condition. Stable equilibria are possible below the appropriate R/a and b/a curves.

Summarizing, our results indicate that q >> 1 is required for stability of highly elliptical systems. Combined with the toroidal equilibrium constraint this places a severe restriction on β.

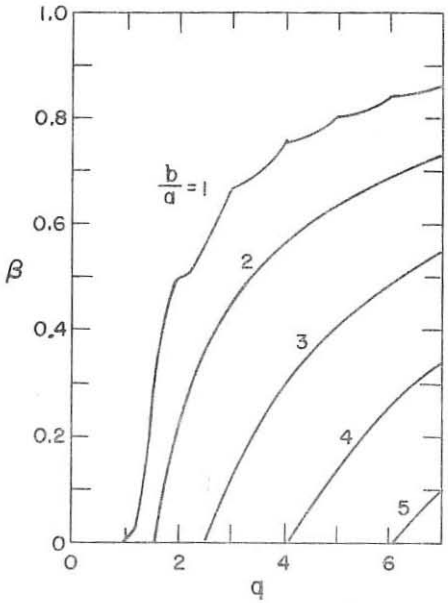


Fig. 4. Critical β vs q for various b/a.

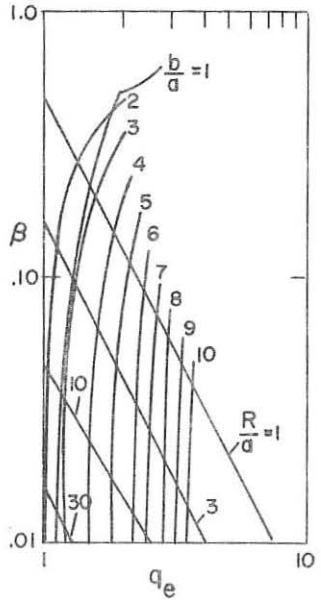


Fig. 5. Combined equilibrium and stability results.

References

1. A. A. Ware, F. A. Haas, Phys. of Fluids 9, 956 (1966).

2. K. E. Weimer, J. L. Johnson, J. M. Greene, E. A. Frieman, Proc. of the Fifth European Conference on Controlled Fusion and Plasma Physics I, 27 (1972).

3. G. Bateman, Phys. of Fluids 14, 1506 (1971).

4. J. P. Freidberg, Phys. of Fluids 14, 2454 (1971).

5. H. Zwicker and R. Wilhelm, Proc. of the Fifth European Conference on Controlled Fusion and Plasma Physics II, 59 (1972).

6. G. Laval and R. Pellat, EUR-CEA-FC-575, Dec. (1970).

*Work performed under the auspices of the U. S. Atomic Energy Commission.

+On leave from Culham Laboratory UKAEA.

Stability Criteria for General MHD Equilibria

D. Lortz

Max-Planck-Institut für Plasmaphysik, Garching b.München
Federal Republic of Germany

Abstract: It is shown that the energy variation can be estimated by an integral containing only surface quantities, thus leading to a one-dimensional problem which can be treated like the cylindrically symmetric case. The result is a new sufficient stability criterion which admits a non-vanishing current density on the magnetic axis.

Let us write the energy variation [1] in the form

$$2\delta W_{F1} = W_1 + W_2, \quad W_2 = \iiint \gamma p \, (\operatorname{div} \vec{\xi})^2 \, d^3\tau$$

$$W_1 = \iiint \left[\vec{Q}^2 + \vec{\xi} \cdot (\vec{Q} \times \vec{j}) + (\vec{\xi} \cdot \nabla p) \operatorname{div} \vec{\xi} \right] d^3\tau, \quad \vec{Q} = \nabla \times (\vec{\xi} \times \vec{B}).$$

We use Hamada coordinates [2] θ, ζ, v defined by

$$\vec{B} \cdot \nabla\theta = \dot{\chi}, \quad \vec{j} \cdot \nabla\theta = \dot{I}, \quad (\nabla\theta \times \nabla\zeta) \cdot \nabla v = 1$$

$$\vec{B} \cdot \nabla\zeta = \dot{\phi}, \quad \vec{j} \cdot \nabla\zeta = \dot{J}, \quad \dot{p} = \dot{I}\,\dot{\phi} - \dot{J}\,\dot{\chi}$$

where ϕ and χ are the longitudinal and azimuthal fluxes and J and I the respective total currents inside a magnetic surface bounding the volume v. (Dots denote partials with respect to v.)
In these coordinates we find

$$W_1 = \iiint \{ \vec{Q}^2 + \xi^v [\vec{2j} \cdot \nabla\mu + 2\dot{p}\,\dot{\xi}^v + \xi^v (\ddot{I}\dot{\phi} - \ddot{J}\dot{\chi})] \} \, d^3\tau$$

$$\xi^i = (\xi^\theta, \xi^\zeta, \xi^v), \quad \mu = \dot{\phi}\,\xi^\theta - \dot{\chi}\,\xi^\zeta$$

$$\vec{Q}^2 = (Q^\theta)^2\, g_{\theta\theta} + (Q^\zeta)^2\, g_{\zeta\zeta} + (Q^v)^2\, g_{vv} +$$

$$+ 2(Q^\theta Q^\zeta g_{\theta\zeta} + Q^\theta Q^v g_{\theta v} + Q^\zeta Q^v g_{\zeta v}),\quad Q^v = \vec{B}\cdot\nabla\,\xi^v$$

$$Q^\theta = \frac{\partial\mu}{\partial\zeta} - (\dot{\chi}\,\xi^v)^{\cdot}\ ,\quad Q^\zeta = -\frac{\partial\mu}{\partial\theta} - (\dot{\phi}\,\xi^v)^{\cdot}$$

We thus see that the θ,ζ-dependence occurs only in the components of the metric tensor in the term $\vec{Q}^2$. The $\vec{Q}^2$-term can be estimated as follows:

$$L_1(Q^\theta)^2 + L_2(Q^\zeta)^2 + \frac{L_3}{(2\pi)^2}(Q^v)^2 \geq \vec{Q}^2 \geq M_1(Q^\theta)^2 + M_2(Q^\zeta)^2 + \frac{M_3}{(2\pi)^2}(Q^v)^2 \qquad (1)$$

where the L's and M's depend on v only and where

$$L_1 = \max_{\theta,\zeta}\ (g_{\theta\theta} + \alpha^2|g_{\theta\zeta}| + \beta^2|g_{\theta v}|)$$

$$L_2 = \max_{\theta,\zeta}\ (g_{\zeta\zeta} + \frac{1}{\alpha^2}|g_{\theta\zeta}| + \gamma^2|g_{\zeta v}|)$$

$$L_3 = (2\pi)^2 \max_{\theta\ \zeta}\ (g_{vv} + \frac{1}{\beta^2}|g_{\theta v}| + \frac{1}{\gamma^2}|g_{\zeta v}|)$$

α,β,γ are arbitrary real functions of θ,ζ,v

$$M_1 = \frac{1}{3}\min_{\theta,\zeta}\ \frac{1}{|\nabla\theta|^2},\quad M_2 = \frac{1}{3}\min_{\theta,\zeta}\ \frac{1}{|\nabla\zeta|^2}\ ,\quad M_3 = \frac{1}{3}\min_{\theta,\zeta}\ \frac{(2\pi)^2}{|\nabla v|^2}$$

Having thus arrived at a separable problem, we can put

$$\xi^v = \mathrm{Re}\ \xi(v)\exp 2\pi i(m\theta + n\zeta)$$

$$\mu = \mathrm{Re}\ \frac{w(v)}{2\pi i}\exp 2\pi i\ (m\theta + n\zeta)$$

and minimize W_1 algebraically with respect to w for $n^2 + m^2 \neq 0$:

$$W_1 \geq W_o = \int_o^V (F\,\dot{\xi}^2 + G\,\xi^2 + 2\,H\,\dot{\xi}\,\xi)\,d\,v \qquad (2)$$

where V is the total volume of the plasma and

$$F = \frac{M_1 M_2}{a^2}(n\dot{\phi} + m\dot{\chi})^2$$

$$G = \frac{1}{a^2}\left[M_1 M_2 (n\ddot{\phi}+m\ddot{\chi})^2-(m\dot{I}+\dot{J}n)^2-2(m\dot{I}+\dot{J}n)(-M_1 n\ddot{\chi}+M_2\ddot{\phi}\, m)\right]$$

$$+ \dot{I}\ddot{\phi}-\dot{J}\ddot{\chi}+M_3(n\dot{\phi}+m\dot{\chi})^2$$

$$H = \frac{1}{a^2}(n\dot{\phi}+m\dot{\chi})\left[M_1 M_2 (n\ddot{\phi}+m\ddot{\chi})+M_1\dot{I}n-M_2\dot{J}\, m\right]$$

$$a^2 = M_1 n^2 + M_2 m^2 ,$$

For $n = m = 0$ we find

$$W_1 = \dot{p}(V)\xi^2(V) + \int_o^V \left[M_1(\dot{\chi}\xi)^{\cdot 2}+M_2(\dot{\phi}\xi)^{\cdot 2}+(\ddot{J}\dot{\chi}-\ddot{I}\dot{\phi})\xi^2\right]dv \qquad (3)$$

Let either $\dot{I}(V) = \dot{J}(V)=0$ with vacuum outside the plasma or $\xi(V)=0$. Then W_1 in eq.(3) is positive if

$$\frac{\pi^2}{4V^2}\dot{\phi}^2 \min_v M_2 - \ddot{I}\dot{\phi}+\ddot{J}\dot{\chi} > 0 \qquad (4)$$

For $m = 0$ W_o in eq.(2) is positive if

$$\frac{\pi^2}{4V^2}\dot{\phi}^2 \min_v M_2-\frac{\dot{J}^2}{M_1} + M_3\dot{\phi}^2 + \dot{J}\ddot{\chi}-\dot{\phi}\ddot{I} > 0 \qquad (5)$$

otherwise we have the sufficient condition

$$-\frac{1}{C^2}\left[\dot{I} + \dot{J}\kappa - 2M_1\kappa\ddot{\chi} + 2M_2\ddot{\phi}\right](\dot{I}+\dot{J}\kappa)+\dot{I}\ddot{\phi}-\dot{J}\ddot{\chi}$$

$$+ M_3(\kappa\dot{\phi}+\dot{\chi})^2-\left[\frac{1}{C^2}(\kappa\dot{\phi}+\dot{\chi})(M_1\kappa\dot{I}-M_2\dot{J})\right]^{\cdot} > 0 \qquad (6)$$

$$C^2 = M_1\kappa^2 + M_2, \quad \kappa = \frac{n}{m} .$$

In the neighbourhood of the magnetic axis condition (4) is always satisfied and inequality (6) reduces to

$$-\dot{p}\,(3|\nabla\zeta|^2\,\dot{p} + \ddot{\phi}\dot{\phi}) > 0 \qquad (7)$$

Unlike the sufficient criteria *[3], [4]* known so far condition (7) can be satisfied if $\dot{J} \neq 0$ on the magnetic axis. For an axisymmetrix system with radius R of the magnetic axis and

circular near-axis cross sections we have on the magnetic axis (v=0)

$$|\nabla\zeta|^2 = \frac{1}{4\pi^2R^2}\left[1 + \left(\frac{4B}{Rj}\right)^2\right], \quad \dot{\phi}(0) = \frac{B}{2\pi R}, \; \dot{J}(0)=\frac{j}{2\pi R}, \; \dot{\chi}(0)=\frac{j}{4\pi}.$$

In this case condition (7) can only be satisfied if $\dot{I}(0) \neq 0$ because otherwise $\ddot{\phi}(0)= 3B/(4\pi^3R^4)$.

The one-dimensional form (2) is also useful for deriving necessary conditions. Note that for n m $\neq$ 0 W_2 can be made arbitrarily small. Using the left inequality of (1) we see that all we have to do is replace the M's by the L's. As an example, consider the case $(\dot{\chi}/\dot{\phi})^{\cdot} \equiv \dot{p} \equiv 0$, which according to Mercier's criterion [5],[6] is marginal, and let $\kappa = -\dot{\chi}/\dot{\phi} + \varepsilon$. Then up to linear terms in ε

$$W_o = -2\varepsilon \int_o^V \dot{J}\,\xi\,(\dot{\phi}\xi)^{\cdot}\,d\,v. \qquad (8)$$

The integral (8) can have either sign if $\dot{J}\,\dot{\phi} \neq 0$. Since the contribution from the surrounding vacuum is $O(\varepsilon^2)$, this case is unstable.

References:

/1/ Bernstein, I.B., Frieman, E.A., Kruskal, M.D., Kulsrud, R.M., Proc.Roy.Soc. A244 (1958) 17.

/2/ Hamada, S., Nucl. Fusion 2 (1962) 23.

/3/ Solovev, L.S., Soviet Phys.JETP 26 (1968) 1167.

/4/ Lortz, D., Rebhan, E., Spies, G., Nucl.Fusion 11, (1971) 583.

/5/ Mercier, C., in Plasma Physics and Controlled Fusion, (Proc.Conf. Salzburg, 1961) Nucl.Fusion Suppl. Part 2 (1962)801.

/6/ Solovev, L.S., Soviet Phys.JETP 26, (1968) 400

"This work was performed under the terms of the agreement on association between the Max-Planck-Institut für Plasmaphysik and EURATOM".

Stability of Trapped Particle and Drift Wave Normal Modes with Estimates of Anomalous Transport

W. Horton* and D.W. Ross

Center for Plasma Physics and Thermonuclear Research, University of Texas at Austin, Texas 78712

Abstract: Results are given for the domain of instability in tokamaks for normal modes of the dissipative trapped particle modes /1/ and the collisionless drift waves. Estimates of the anomalous transport are given.

From the anomalous transport estimates one finds that the very low frequency ($\omega < \omega_{bi} = \epsilon^{1/2} v_{Ti}/qR$), long wavelength modes are potentially the most danerous, and hence it is of primary interest to determine the stability boundaries for these modes. A mode is said to exist when an exponentially growing radial normal mode is shown to occur for the assumed profiles. Much of the work, presented follows from numerical integration of the mode equations which are of the form $\Lambda^2\, d^2\Phi/dr^2 + Q(\omega,\ell,r)\Phi=0$ with appropriate finiteness or outgoing wave energy boundary conditions which determine the radial mode and the growth rates. The details of the numerical integration and eigenvalue search procedures are given elsewhere /2,3/.

Dissipative Trapped Ion Mode. The local condition for instability with $\eta = d\ell nT/d\ell n\, n = 0$ in the dissipative trapped ion mode is /4/ that $\nu_i/\epsilon\omega_{bi} < 0{,}4(m_e/m_i)^{7/8}\tau^{7/16}$ with $\tau = T_e/T_i$, or in terms of an ion temperature threshold $T_i > T_c(\text{kev})$ we have /3/

$$T_c = 2.4 \times 10^{-2}\, \bar{z}\, n_{13}^{1/2}\, q^{1/2}\, R^{1/2}\, A^{7/36}/\epsilon^{3/4}\tau^{7/32} \qquad (1)$$

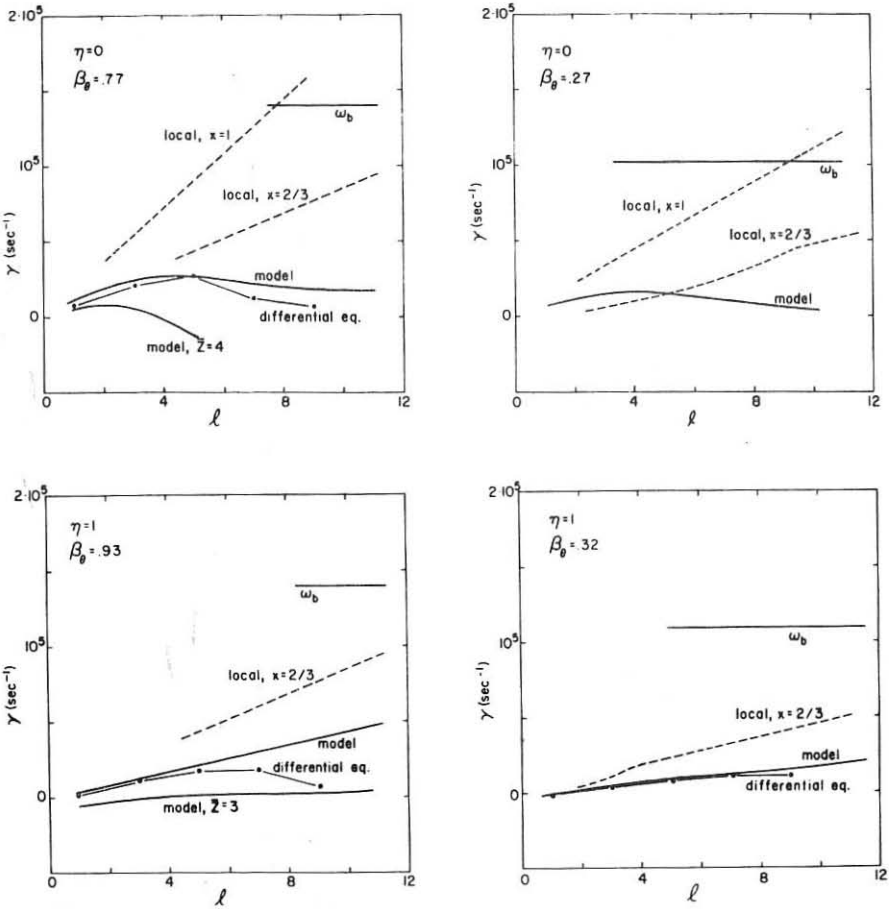
where n_{13} is density in units of 10^{13}cm^{-3}, R is the major radius in cm, A is average ion atomic mass and $\bar{z} = \Sigma\, n_i z_i^2/\Sigma\, n_i z_i$. In addition, the mode occurence requires sufficiently large minor radius to allow $\omega_\ell < \omega_{bi}$ for the first few ℓ-modes. Thus, qualitatively the modes occur for densities and temperatures of relevance to tokamaks only for a limited range of machine parameters typical of the large tokamaks (e.g.Ormak) and feasibility experiments but are excluded in smaller tokamaks and at reactor sizes.

The model profiles used with $x = r/a$ are $n(x) = n_o \exp\left[-(x/.8)^{1/2}\right]$, $T(x)=T_o\left[1-\eta+\eta n(x)/n_o\right]$ and $q(x)= q(a)\left[(x^2+x_q^2)/(x_q^2+1)\right]$ where the parameters η and x_q control the temperature gradient and troidal current profile respectively. The normal mode equation includes the ion-Landau resonances of the passing particles through the $Z(\omega/\omega_{bi}|m-\ell q|)$ - functions and the collisional and grad-B drift mechanisms with $\langle(\omega-\omega_{Tj})(\omega-\omega_{Dj}+i\nu_j/\epsilon)^{-1}\rangle_{Max}$ $(\omega-\omega_{Tj})(\omega-\omega_{Dj}+i\bar{\nu}_j/\epsilon)^{-1}$ with the coefficients in the averages chosen to agree with the expansion for $\bar{\nu}_i/\epsilon,\ \bar{\omega}_D \ll \omega \ll \bar{\nu}_e/\epsilon$.

From the solutions of the normal mode equation we have found the following: (a) without a temperature gradient ($\eta=0$) the unstable modes tend to localize near the boundary where the local instability condition is satisfied by a wider margin. The cut-off density or threshold T_i remains essentially as given by Eq.(1) with no appreciable stabilization occuring from the radial

mode structure or the shear. (b) with the temperature gradient (η=1) the local stability theory predicts a substantially lower T_i threshold due to the now destabilizing ion resonance; however, the radial mode is now spread over the plasma column and radial effects are appreciably stabilizing with the result that the ion threshold temperature is found to be approximately $\simeq 0{,}4\ T_c\ (\eta=0)$.

From noting that the radial wave number is determined by the rational surfaces we construct a simple model dispersion relation /3/ namely, $-\Lambda^2 k_r^2 + \bar{Q}(\omega,\ell) = 0$ with $k_r = \pi\ell(dq/dr)$, which predicts well the calculated mode growth rates as shown in the figures and label model.



In the figures we show the growth rates calculated for the tokamak parameters a = 45 cm, R = 130 cm, B = 50 KG, $n \cong 10^{14}$ cm^{-3} and $T_i = T_e \gtrsim 5$ kev. As predicted by the model dispersion relation the growth rate increases as ℓ rather than ℓ^2. As a consequence the estimated diffusion rate $D = \sqrt{2\epsilon}\ \gamma/k_\parallel^2$ is dominated by $\ell = 1$ and, in this example, gives a confinement time $\tau_p \simeq 15/\gamma$.

Dissipative Trapped Electron Mode. Sagdeev and Galeev /4/ have emphasized the importance of this mode as occuring in tokamaks to high desities. The mode is susceptible to shear stabilization /4/. For profiles with $\eta > 0$ the mode exhibits a density threshold which is computed for the parameters given above.

Collisionless Drift Mode. At values of shear where the trapped electron modes are stabilized /4/ by the radial wave energy transport to regions of resonant ion absorption, the large m-modes ($k_\perp \rho_i \sim 1$) become collisionless for $\nu_e/\omega_{be} < q\,(m_e/m_i)^{1/2}\,\epsilon^{-3/2}$ and have a large average $k_\parallel$ in the mode. The principal observations and assumptions for the nonlinear theory are that there are a large number $(r_n/\rho_i)^2$ of uncorrelated, weakly interacting $(W/nT_e < \rho_i^2\tau/r_n^2)$ modes for which the electric field approaches a Gaussian-normal distribution. For the strongly magnetized electrons in the normally distributed, random electric field the propagator becomes $(\omega - k_\parallel v_\parallel + ik_\perp^2 D_\perp)^{-1}$. Solutions of the normal mode equation show that as the level of turbulence rises the last mode to be stabilized by the orbit diffusion has $k_\perp \rho_i \tau^{1/2} \simeq 1$ for which marginal stability occurs when $D_\perp = \gamma_L/k_\perp^2 (k_\perp \rho_i \tau^{1/2} = 1)$. The resulting diffusion coefficient is given by

$$D \simeq \nu_e\, r_n^2\, \frac{(m_e/m_i \Theta\xi)^{3/2}\,\left[1-(\xi/\xi_c)^{3/2}\right]}{1 + \nu_e/\nu^*} \qquad (2)$$

where

$$\nu^* = (\nu_e \rho_e^2/r_n^3)\,\Theta\xi\,(m_i/m_e)^{3/2} \text{ and } \Theta = B_p/B$$

and the shear is $S = \Theta\xi = \Theta\left|d\ell n\ q/d\ell n\ n\right|$ with $\xi = \xi_c$ being the critical shear. The banana regime of Eq. (1) arises when the collision rate is insufficient to maintain the Maxwellian background distribution in the presence of the fluctuations and a partial plateau is formed. For $\nu_e > \nu^*$ the diffusion scales essentially as the neoclassical plateau rate but enhanced by a factor of $(R/r_n)\Theta^{-1/2}$.

This work was performed under the auspices of the U.S.Atomic Energy Commission.

+Present address: Max-Planck-Institut für Plasmaphysik, 8046 Garching, West-Germany.

References:

/1/ B.B.Kadomtsev and O.P.Pogutse, Nucl. Fusion 11, 67(1971)

/2/ N.T.Gladd and W.Horton, "Critical Shear and Growth Rates for Drift Modes in a Nonuniform, Current-Carrying Plasma," to be published in Phys.Fluids, 16, (1973).

/3/ N.T.Gladd and D.W.Ross, University of Texas Report No.61, 1973 and D.W.Ross, University of Texas Report No.64, 1973.

/4/ R.Z.Sagdeev and A.A.Galeev, Comments on Plasma Physics and Controlled Fusion 1, 23 (1972).

1.5. STELLARATORS



ENERGY CONTAINEMENT IN THE WENDELSTEIN II B STELLARATOR WITH OHMIC HEATING

G. Grieger, H. Hacker, G. Pacher, H. Renner, H. Ringler,
E. Wuersching

Max-Planck-Institut für Plasmaphysik, Garching b. München,
Euratom Association Federal Republic of Germany

Abstract

For quasistationary conditions in the W II b stellarator with B_o = 0.7 T the energy containment time $\tau_E' (=\frac{WE}{P_{OH}})$ was determined for hydrogen plasmas with $T_e \simeq$ 150 eV. It was found to be about $10\tau_{Bohm}$ in magnitude. The comparison of temperatures determined from conductivity and laser scattering gives Z_{eff} = 2.2.

The Wendelstein II b stellarator (R = 0.5 m, r = 0.09 m) is equiped with two air core transformers: OH 1 for preionizing and preheating, OH 2 for quasistationary operation. The main field B_o is limited to less than 1.5 T. The helical windings (ℓ= 2, m = 5) can produce a shear-free field with the rotational transform ι_o < 0.5. The maximum limiter aperture is 13 cm. Preliminary experiments in this device have been reported elsewhere (1), in which it was found that the containment properties deteriorate at rational values of the total rotational transform $= \iota_o + \iota_p$, ι_p representing the contribution of the plasma current I_p (2). Intensive cleaning of the system using a 100 Hz discharge improved the discharge appreciably, so that it became possible to continue the heating current for 10 - 20 msec. in spite of the low voltage available from OH 2.

Vertical Field

At low toroidal fields it became very evident that compensation of

the vertical field produced by the plasma current loop is necessary. The displacement of the magnetic axis of the stellarator by a vertical field is given by $\Delta = \frac{R}{\iota_o} \frac{B_z}{B_o}$. Fig. 1 shows the current development in dependence on B_z. Insufficient compensation of the vertical field causes the elliptical magnetic surfaces to touch the nearly circular limiter, resulting in a decrease of the effective plasma radius. The available ohmic power is then insufficient to overcome the decreased containment at rational ι. Similar conditions result from a decrease of the limiter radius at smaller currents. Feedback control of the vertical field (for our plasma L = 1.96 μH, giving $B_z(T) = 7.26 \times 10^{-4} I_p(kA)$) allows higher plasma currents and therefore better energy transfer to the plasma.

Pulsed Gas Valve

During the long discharges obtained with the pulse-cleaned machine, the neutral gas pressure drops by a large fraction, resulting in decreased plasma density late in the discharge. This is accompanied by the production of runaway electrons. An additional neutral flux from a fast-acting valve compensated the loss of neutral gas and thereby improved the discharge parameters appreciably.

Plasma Production and Diagnostics

After firing a Bostick gun, OH 1 is used to preionize the plasma at $p_{H_2} = 2 \times 10^{-5}$ torr. The fast-acting valve delivers additional particle flux during the main current phase of OH 2. In Fig. 2, a typical discharge is presented with $\iota_o = 0.1$. The density given is peak density n_e calculated from a five channel microwave interferometer (3). Electron temperatures are conductivity temperatures for Z = 1. The given rotational transform ι obtains from ι_o and ι_p with an assumed channel of radius 5 cm. Fig. 3 shows temperature and density profiles obtained by Thomson scattering at t = 10 ms. Remarkable agreement with the microwave profile is observed. The

asymmetry of the profile results from a 5 mm shift of the magnetic surfaces relative to the torus center. It is noteworthy that the diameter of the plasma is pinched to 7 cm (with limiter diameter of 11 cm). At r = 4 cm, an electrostatic analyzer gives ion temperatures of 35 eV. Fig. 4 presents J and ι, calculated assuming constant Z over the cross-section, and referred to the effective circular magnetic surfaces. From the comparison of laser and conductivity temperatures, $Z_{eff} = 2.2$ ($R_{exp} = 0.8$ mΩ, $R_{spitzer} = 0.36$ mΩ).

Integration over the plasma volume gives the energy content $W_e = 1.15$ J. The power input N amounts to 11.5 kW, giving $\tau_E' = \frac{W_e}{N} = 100$ µs. The energy loss to the ions amounts to 650 W, and an upper limit for radiation losses is estimated (Hinnov /4/) as 1 kW assuming 10 % O. This indicates only a small influence of these processes on the real energy containment time.

τ_E' agrees with pseudoclassical values for $c^2 = 10$, and β_θ reaches 0.75 at r = 4 cm, indicating Tokamak-like behaviour. Note, however, that the current is increased over the plasma current to account for ι_o ($\approx 1/3$).

Conclusion

Experiments to date with the ohmic-heated stellarator W II b show good agreement of containment with pseudoclassical scaling (5). The measurement of particle containment time from the absolute intensity of H_α radiation is in preparation. This information should clarify the discrepancy between the estimated particle and measured energy containment times (5). Spectroscopic measurements are planned to investigate the effect of impurity radiation on the power balance. Numerical circulation for W II b plasmas using the Duechs code including the effect of oxygen are in preparation.

References

(1) G.Grieger, R.Jaenicke, C.O.L.Juulman, C.Mahn, H.Renner, H.Ringler, G.Schilling, G.H.Wolf, and J.Hugill, Plasma Physics, 15, 151 (1973)

(2) P.Barberio-Corsetti, IPP Report II/206 (1972)

(3) J.G.Wegrowe et al., Verhandl.d.DPG (VI) 7, 115 (1972)

(4) E.Hinnov, MATT 194 (1963)

(5) G.Grieger, III. Int.Symp.on Tor.Plasma Conf., 1973, D 3

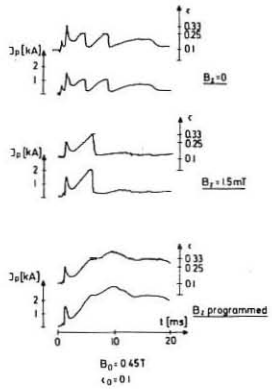


Fig. 1

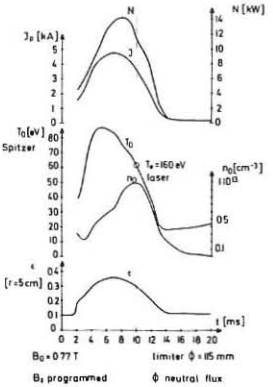


Fig. 2

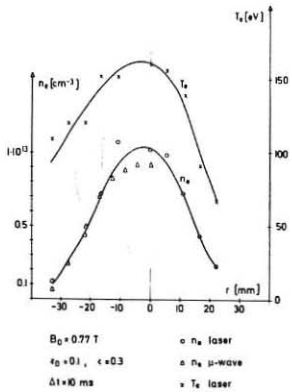


Fig. 3

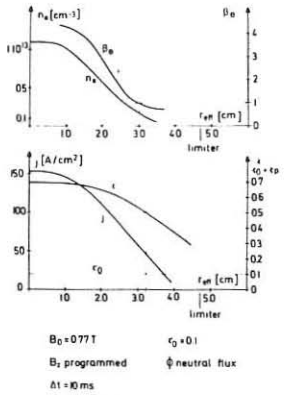


Fig. 4

ENERGY CONFINEMENT DURING HF HEATING OF PLASMA IN "URAGAN" STELLARATOR.

A.G.Diky, S.S.Kalinichenko, I.I.Konovalov, S.S.Ovchinnikov, O.S.Pavlichenko, V.K.Pashnev, A.S.Slavny, V.A.Suprunenko, V.F.Tarasenko, V.T.Tolok, O.M.Shvets.

Physical-Technical Institute, Kharkov, USSR.

In our previous report at Garching we have presented preliminary results of investigations of HF heating of plasma in "Uragan" stellarator. Having used the method of excitation of the ion cyclotron or ion-ion hybrid waves in toroidal traps which had been developed earlier [1] we obtained in the stellarator "Uragan" [2] a plasma with the gas-kinetic pressure value near to limited by an equilibrium ($n_i \simeq 2 \cdot 10^{12} cm^{-3}$, $T_i \simeq 500 ev$, $\beta \simeq 10^{-3}$). In this report we present the results of investigations of energy confinement in such hot-ion plasma.

For HF heating of plasma the axial-nonsymmetric waves with m=1 were used. This waves were excited by the coil which created the transverse HF magnetic field in plasma and provided energy input to the major mode. It was shown earlier [3] that such wave is excited most effectively and propagates freely in a toroidal magnetic field. This wave provided uniform plasma heating over the whole length of "Uragan" stellarator; this fact was confirmed by measurements of plasma gas-kinetic pressure by means of means of a series of diamagnetic loops arranged over the machine length. The energy of this wave was thermalized without "magnetic beach" application and was realized in our opinion on inhomogeneitics of stellarator magnetic field. The choice of m=1 mode was determined by the fact that in this case the HF field strength had a maximum

near a plasma axis. The calculations showed that exciting device for m=1 mode transfers maximum energy into more dence plasma than device for excitation of m=0 mode.

More experiments were performed when ion-cyclotron waves were excited (fig.1a). A number of experiments on excitation of ion-ion hybrid waves in a deuterium-hydrogen plasma were made too(fig.1b). In the last case the wave energy thermalization was provided due to existence of resonance conditions ($K_\perp \to 0$) on a plasma axis [4]. Figs.1a,b show that at resonance values of magnetic field strength H_0 a plasma gas-kinetic pressure increased and reached the values approximating the critical ones from the point of view of plasma equilibrium in stellarator. Fig.2 shows a dependence of maximum gas-kinetic pressure on magnetic field strength and demonstrates the constancy of value of $\beta_{max} = \frac{(nT)_{max}}{H_0^2/8\pi}$ (the solid curve shows the relationship $(nT)_{max} \sim H_0^2$).

Fig.3 illustrates a time behaviour of HF current, electron density, "diamagnetic" temperature $(T_e + T_i)_\perp$, electron temperature and intensities of spectral lines D_β and CIII4647 Å in a typical regime (H_0=7kOe, ε =0,58; p =5.10^{-5}torr; deuterium). The asterisk shows a value of ion temperature obtained from the analysis of a spectrum of energies of deuterium atoms. The appropriate energy spectrum of deutrons is shown on fig.4. It follows from these measurement that the value of nT during a first millisecond is determined mainly by hot ions.

The possibility of fast cutoff of input HF power enabled one to observe a free decay of plasma diamagnetism. During the decay of nT plasma density was practically unchanged, the electron temperature was rather low, therefore the decrease of plasma diamagnetism was the result of ion cooling. Evaluations of deuterium atoms consentrations showed the resonant charge exchange contribution into ion cooling to be negligibly small. From measurements of decay rate of

$n_i T_i$ the ion energy life time was determined as $\tau_E^i \equiv \frac{n_i T_i}{\frac{d}{dt}(n_i T_i)}$ (Arrows on fig.3 shows the moment of HF pulse cutoff at these measurements) Fig.5 shows the dependence of the measured value of τ_E^i on i on temperature (H_0=7kOe; $\mathcal{E}$ =0,58).

In the regimes iunder investigation the ion-ion collision frequency is such that ion thermal conductivity has to comply with the regime of Galeev-Sagdeev "plateau" 5 . In these conditions the ion energy lifetime is described by the relation $\tau_E^i \sim H_0^2 a^2 i\, T_i^{-3/2}$ (a is the plasma radius, i is the rotational trnsform angle). The solid curve in fig.5 shows the calculated dependence of τ_E^i upon ion temperature. Fig.6 gives the measured dependence of τ_E^i upon the product $a^2 i$ at a constant value of T_i . One can see fair agreement between experimental data neoclassical theory predictions.

Thus in this work we showed:

1) The effective method of plasma HF heating for a closed magnetic trap has been developed, This method allowed to obtain the value of nT , which approximated to limiting value from the viewpoint of equilibrium in stellarator, and to perform a direct measurements of τ_E^i in the stellarator.

2) The energy lifetime of the decaying ion-hot-plasma in the stellarator is determined by the ion thermal conductivity which is near to neoclassical value.

REFERENCES.

1. S.S.Ovchinnikov et al."Plasma Physics and Controlled Nuclear Fusion", v.3, p.597 (Vienna, 1972).

2. A.G.Dikiy et al."Plasma Physics and Controlled Nuclear Fusion", v. 3 ,p.151 (Vienna, 1972).

3. S.S.Ovchinnikov et al. Pisma s Zh. Eksper. i Teor.Fiz. 12, 277 (1970).

4. V.F.Tarasenko et al. The Fifth European Conference on Plasma Physics and Controlled Nuclear Fusion Research, v.7, p.113 (Grenoble, 1972).

5. A.A.Galeev, R.Z.Sagdeev. Zh.Eksper. i Teor.Fiz., 53, 348 (1907).

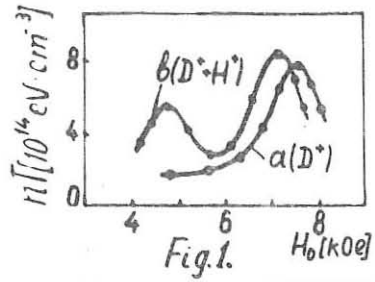


Fig.1.

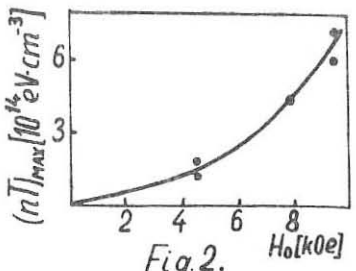
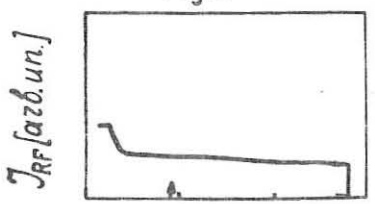
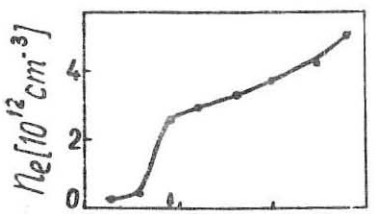
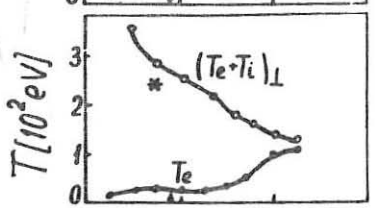


Fig.2.







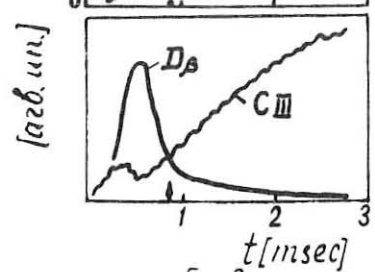


Fig 3.

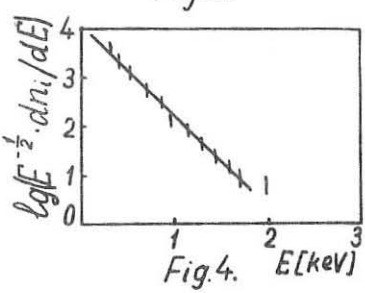


Fig.4.

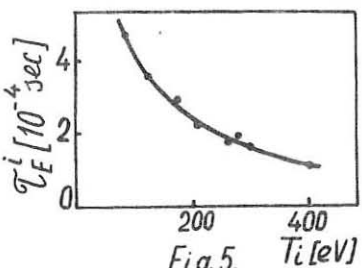


Fig.5.

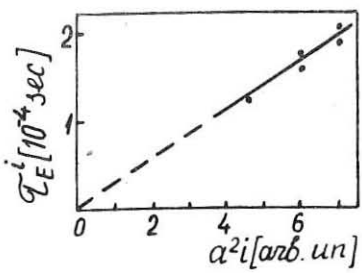


Fig.6.

RECENT RESULTS FROM THE GARCHING HIGH-BETA STELLARATOR TORUS ISAR T 1.

E.Fünfer, M.Kaufmann, W.Lotz, J.Neuhauser, G.Schramm

Max-Planck-Institut für Plasmaphysik, Euratom Association

Garching bei München, F.R.G.

Abstract: Experiments with the complete high beta stellarator torus ISAR T 1 are reported. The theoretically predicted M&S like equilibrium with ℓ=1 helical field and small ℓ=2 field was established and further improved by various magnetic field corrections. The plasma life time seems to be limited by m=1 MHD instabilities in qualitative agreement with theory.

I. Introduction: After linear preexperiments with ℓ=1 helical field /1/ and a short toroidal sector experiment /2/ the complete high beta Stellarator torus ISAR T 1 is now in operation. The toroidal equilibrium is provided by a combination of a first order helical field with ℓ=1 symmetry and small ℓ=2 admixture, the plasma column being a toroidal corkscrew with elliptical deformation. Further details and references concerning equilibrium and stability of this configuration are found in /1-6/. The normalized plasma deformation δ_ℓ and the coordinate system used below are defined by the following expression for the plasma surface (neglecting toroidal effects):

$$r_p = \bar{r}_p[1 + \delta_1 \cos(hz - \theta) + \delta_2 \cos(hz - 2\theta) + \delta_o \cos h_o z]$$

II. Experimental set-up and Plasma Parameters

1) The main data of the ISAR T 1 toroidal theta pinch are: bank energy 0.5...2.6 MJ, R_T= 135 cm, r_{coil} = 11 cm, r_{tube} = 4,6 cm, B_{max} = 14...34 kG, T/4 = 5...7.5 µs. The ℓ=1 and ℓ=2 fields are generated by helical windings (radius 6.6 and 7.5 cm). In the first experiment the main field was also modulated by small copper inserts ($\tilde{B}/B \approx 4$ %). This very small ℓ=0 component contributes only at very high beta. All field admixtures have 24 field periods around the torus.

It was shown by vacuum magnetic field calculations that, with the high helical currents necessary for equilibrium ($J_1, J_2 \geq 50$ kA for B_o = 14 kG), the magnetic axis is shifted outwards and the separatrix becomes rather small. The magnetic axis can be centered again

by a transverse field of some hundred gauss parallel to the main axis which, in experiment, is provided by a pair of nonhelical wires (- 400 G... + 400 G). In Fig.1, cross sections of magnetic surfaces along one period (relative distance $\pi/2h$) are shown for different bias field (top: 150 G, bottom 500 G).

2) The density was measured with an infrared laser interferometer (λ = 3.4 μ) and a microwave interferometer (λ = 1 mm); the electron temperature T_e was determined from the time dependence of different oxygen and carbon ion lines and (T_e+T_i) was calculated from the toroidal drift of the pure theta pinch. Stereoscopic streak pictures were used to determine the plasma motion at different phases around the torus.

3) Most discharges were done with 0.5 MJ and 17 mTorr D_2 filling pressure. Under these conditions by varying the degree of preionization α and applying a toroidal bias field parallel to the main field of up to 600 G the following range of plasma parameters was achieved: n_{max} = 0.9... 1.8 x $10^{16}cm^{-3}$, $T_e \approx T_i \approx$ 15... 100 eV, $\beta \approx$ 6... 70%. With an appropriately chosen set of α and bias field a bell shaped density profile with a mean radius of r_o = 1.3...0.9cm was achieved over the whole range of beta values available.

III. The Toroidal Equilibrium As in the preceeding sector experiment it was shown that the toroidal drift can be compensated by a combination of mainly ℓ=1 and ℓ=2 fields. Nevertheless, several improvements were necessary:

1) Helical m=1 oscillations with a wavelength equal to the field period were caused by the shock heating in the circular toroidal quartz tube as in all preceeding experiments. At beta near one the first overswing sometimes touched the tube wall. By lowering beta and/or carefully adjusting the time delay between main and helical field (some 100 ns) the early wall contact was avoided.

2) A transverse drift of the total plasma ring parallel to the main axis was observed corresponding to a force of about one fourth of the toroidal drift force. We suppose that a transverse interference force is produced by a z-modulation of the ℓ=1 field because of z-dependent helical mirror currents in the corrugated coil (ℓ=0 inserts). By readjusting the current distribution in the ℓ=1 windings resulting

in a helix rotation of 15^{o} the transverse force was compensated.

3) At intermediate beta (10...30%) and long life time (20...30 μs) the plasma seemed to be lost along magnetic field lines rather than by MHD instability, if no transverse field was applied. For very high beta there was no essential effect.

4) In general the stellarator fields induce a toroidal net current which has to be compensated by an externally applied voltage. It turned out, that residual currents of several 100 A had already a measurable effect on the plasma position. On the other side one has to realize that the Kruskal limit for currents on the surface of the compressed plasma is of the same order. Thus it is necessary to compensate very carefully after each change of the experimental set up. For easier experimental work an automatic compensation has to be built.

After these improvements plasma life times up to 4 toroidal drift times were achieved (see Fig.2, $\beta_{max} \approx 0.3$). We got for the equilibrium ($\beta = 0.7$) from the field components necessary the following plasma distortions: $\delta_1 = 1.9$, $\delta_2 = 0.35$, $\delta_o = 0.066$. Experimental values were ($t \approx 3$ μs): $\delta_1 = 1.8 \pm 0.2$ cm, $\delta_o = 0.07 \pm 0.02$, δ_2 measurement is not completed. For a pure $\ell=1$, $\ell=2$ system the product $\delta_1 \cdot \delta_2$ necessary for equilibrium was theoretically 0.4, while experimentally $\delta_1 \cdot \delta_2 \approx 0.6$ was needed. Since there was also a small force $F_{1/o}$ from the $\ell=1$, $\ell=0$ interference ($F_{1/o} \approx 0.3\ F_{1/2}$), it is concluded that the helical fields must be slightly higher than predicted by the linearized theory. Indeed, the helical distortions are relatively high in our case ($\delta_1\ \bar{r}_p\ h \leq 0.33$).

IV. Stability of the improved Equilibrium m=1: The existence of stable, damped m=1 oscillations with wavelength equal to the helical period (see III,1)) proves at once the stability against short wavelength m=1 modes. Their frequency agrees quantitatively with theory. On the other hand, the plasma seems to be lost by a very long wavelength m=1 instability, if beta is high. Indeed, we calculate from theory that modes with more than about five helical field periods become increasingly unstable in qualitative agreement with experiment.

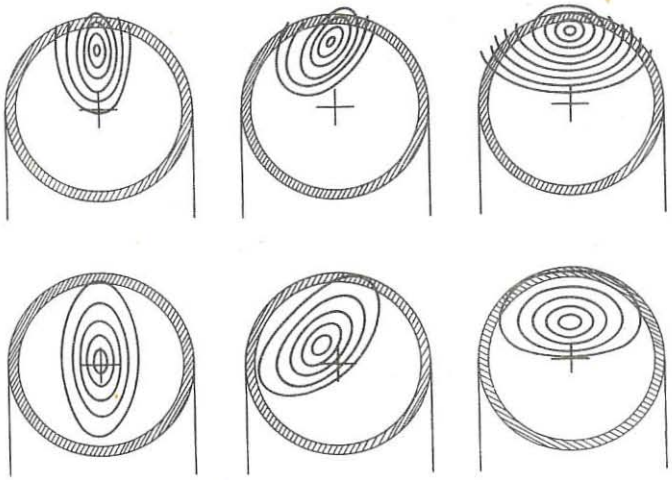


Fig. 1

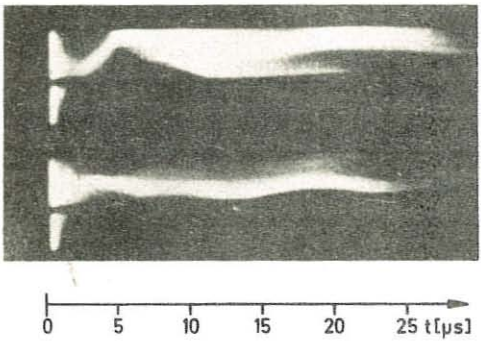


Fig. 2

References:

/1/ Fünfer,E., M.Kaufmann, W.Lotz, J.Neuhauser, Plasma Phys.Contr. Nucl.Fus.Res., IAEA Vienna (1971), Vol.III, CN 28/J-3 (see also Rep. IPP 1/130 (1973); /2/ Fünfer,E., M.Kaufmann, W.Lotz, M.Münich, J.Neuhauser, G.Schramm, U.Seidel; Proc.2nd Top.Conf.Pulsed High-Beta Plasmas, W.Lotz, Ed., Garching (1972), IPP 1/127, A 2; /3/ Kaufmann, M.; Proc. 3rd Int.Symp.Toroidal Plasma Confinement, Garching,(1973),A2-I; /4/ Freidberg,J.P.; same conference as /1/, CN 28/J-5; /5/ Ribe,F.L., M.N.Rosenbluth; Phys.Fluids 13, 2572 (1970); /6/ Weitzner,H.; same conference as /1/, CN 28/J-6.

LASER PLASMA CONTAINMENT IN TOR-I STELLARATOR

E.D.Andrjukhina, G.S.Voronov, U.V.Kholnov, I.S.Shpiegel
Lebedev Physical Institute, Moscow, USSR

Functional dependences of plasma containment time on plasma parameters and confining magnetic field characteristics have been studied. Ion flows and longitutinal current have been measured.Experimental dependences are shown not to coincide with the conclusions of neoclassical theory.

Consequent comparison of plasma diffusion with the results of neoclassical theory for stellarators has been carried out in the experiment on "Porto-Cleo" stellarator /I/. In this work the experimental life time was plotted as the function of parameters combination $\chi = \frac{R}{\iota \lambda_{ei}}$ the ratio of connection length to the electron-ion mean free path. The satisfactory agreement with the theory was obtained at $10^{-2} \leq \chi \leq 10^{2}$.

It was important for us to obtain the dependence of plasma decay velocity not on the parameters combination, but to study functional life time dependences on all plasma parameters and the confining magnetic field characteristics, which determine plasma diffusion according to the theory.

Laser injection method /2/ allowed to change plasma parameters in the range $n_e = 5 \cdot 10^{10} - 10^{12}$ cm^{-3}, $T_e = 0.5 - 3$ eV, $T_i = 5 - 60$ eV, magnetic field in the stellarator TOR-I varrying in the range B=3.5 - 12 kG, $\iota = 0.04 - 0.3$. This variation range of plasma parameters and ι corresponded to $1 \leq \chi \leq 10^{3}$. As a rule, it is impossible experimentally to change only one plasma parameter,having the other constant, to obtain the life time dependence on this parameter.To determine such dependences we used multeparametrical method of minimal squares errors. The functional life time dependences on plasma parameters, magnetic field and rotational transform angle were obtained with the help of a computer. At the experimental condition plasma life time is determined by theoretical diffusion coefficient for hydrodynamics region /3/.

$$\tau_{theor} = const \; \frac{B^2 \iota^2 T_e^{3/2}}{n_e (T_e + T_i)} \; ; \quad \iota \ll 1 \, , \; T_i > T_e \qquad (I)$$

Thus τ_{exp} can be represented in the form

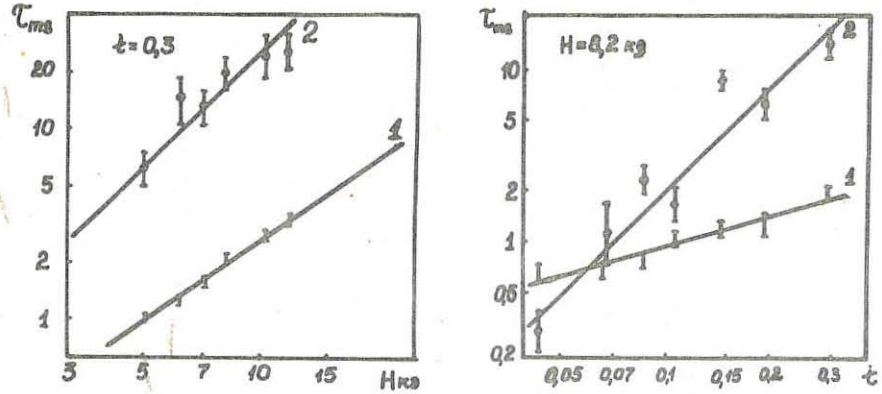
$$\tau_{exp} = const \; n_e^{\alpha_1} T_e^{\alpha_2} T_i^{\alpha_3} B^{\alpha_4} \iota^{\alpha_5} \qquad (2)$$

Experimental values of exponents α_i were determined by the multiparametrical method of the minimal squares errors using 200 experimental points, corresponding to different combinations of plasma and magnetic field parameters. The values of n, T_e, T_i and τ_{exp} were measured in each pulse simultaneously for a fixed moment of time. Electron temperature was measured by a conductivity method, ion temperature was determined by a multi-grid probe with the modulation of analysing voltage, plasma density was measured by Fabri-Pero interferometer and the plasma potential - by a single probe.

The calculations of exponents α_i for experimental τ_{exp} values showed, that the experimental dependence can be represented in the form

$$\tau_{exp} = const\ n_e^{-0,04} \cdot T_e^{-0,22} \cdot T_i^{0,08} \cdot B^{1,4} \cdot \dot{\iota}^{0,7} \qquad (3)$$

Thus the rate of the plasma losses does not depend on plasma parameters and is determined only by the characteristics of confining magnetic field. The comparison of experimental data with the conclusions of the theory is given in fig.1 and 2, where dependencies τ_{exp}(1) and



τ_{theor}(2) on magnetic field and $\dot{\iota}$ are represented. In this Figures τ_{theor} was calculated according to formula I, averaging of τ_{theor} and τ_{exp} was carried out over all plasma parameters. Mean square variations shown for τ_{theor}, correspond to the range of plasma parameter variations, as n_e, T_e and T_i are included into the calculation formula for τ_{theor}. The comparison of experimental and theoretical dependencies in these Figures show, that their pitch, determining the value of exponent is significantly different, especially for the dependence on $\dot{\iota}$. It is impossible at present to explain such

a difference between experimental data and theoretical dependence, but some conditions should be pointed out, which can influence plasma diffusion in our experiments. We carried out the comparison with the hydrodynamic scaling of plasma containement but only electrons were in the region of hydrodynamics and ions remained in "plato" region, because $\frac{\lambda ei}{\lambda ie} = \sqrt{\frac{T_i}{T_e}}\ 10^{-2}$ and $T_i > T_e$. However, plasma potential in our experiments was negative, life time value was close to thouse calculated according to the electron diffusion coefficient, that is the diffusion was determined by electrons and in this sense the comparison with the theory was justified.

If ions are on "plato", then their loss from the trap can appear to be higher due to the mechanism, described in paper /4/ . This creates assymetry of the function of velocity distribution in space, which leads to the longitudinal ion flow, measured in /4/ for collisionless plasma. It was interesting to make analogous measurements for collision frequencies in "plato" region and obtain the dependence of longitudinal ion flow, $\frac{V_z}{V_{T_i}}$ on $V_E/\Theta V_{T_i}$, where $V_E = \frac{1}{c}\frac{E}{H}$, V_{T_i} - thermal ion velocity up to the full distruction of "bananas" during the ion shift into a high collision region.

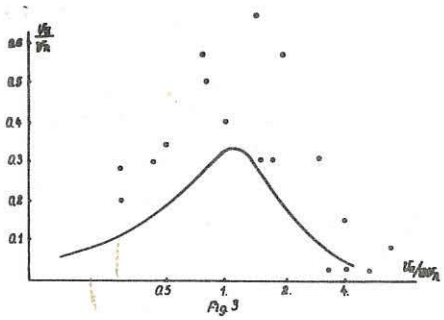


Fig 3

The value of the electric field was determined by the plasma potential measurements, the flow velocity V_z by the ions velocities distribution measurements. The obtained experimental data and theoretical dependence are given in fig.3. There is a qualitative agreement of these dependences, quantative difference not exceeding factor 2. As it was expected, with ion transfer into the hydrodynamics region (which corresponded to $n_e = 10^{12}$ $T_i = 5$ eV) the ion flow disappeared.

According to the theory /5/, the plasma diffusion must lead to the longitudinal current in toroidal systems if asymuth component of the magnetic field exists. In our experiments the longitudinal current measurements were made in the above mentioned range of plasma parameter variations. The measurement system allowed to register current of about 10^{-3}A.

It gives the opportunity to measure currents of a factor lower then the expected according to the calculations from the experimental value of diffusion velocity. Theoretically, this value should not change during the confinement process, if plasma loss velocity does not vary. However, we always measured damping current, the value of which increases with the increasing of the initial plasma density at the moment of injection. This current fell down with the time constant 0.2-0.5 msec and became lower than the installation sensitivity. The measured current had the direction, counter to the asymuth magnetic field, its damping velocity decreasing with B and t growing. Although the absolute value of this current is of the factor, expected according to the calculations, the fast damping of it in time and its dependence on initial conditions makes it possible to assume, that it is connected with the nonstationary state of the plasma during the filling process of the trap.

References:

I.R.A.E.Bolton, I.Hugil, D.I.Lees, W.Millar, P.Reynolds IV Conf. on plasma physics, Madison, USA CN-28/H-6.

2.E.D.Andrukhina, M.A.Bloch, G.S.Voronov, O.I.Fedyanin, Yu.V.Kolnov, I.S.Shpigel, V.Europ. conf. on Plasma Phys. Grenoble, France, 1972 v.I, p.81.

3.Pfirsch D., Schluter A. Max-Plank Inst. Rep. MPI/PA/7 1962.

4.M.S.Berezhetsky, S.E.Grebenshthikov, J.A.Kossy, I.S.Sbitnikova, I.S.Shpigel. ZETP, 62, 2, 1972.

5.A.A.Galeev. ZETF 59, (1970) 1378.

T.E.Stringer IV Conf. on Pl.Phys. Madison USA IAEA/CN-28/F3.

A Stellarator Field Produced by Twisted Coils

S. Rehker, H. Wobig

Max-Planck-Institut für Plasmaphysik, Garching b. München
Federal Republic of Germany

Abstract: With the increasing size of Stellarator experiments the construction of the helical windings becomes more and more difficult. It is therefore of interest to find other methods of producing the helical fields. In the Tor - 2 experiment [1] the helical fields are produced by planar elliptical coils. Numerical calculations for this system were reported in [2]. As already pointed out by the authors [3], a modulation of the elliptical coils out of their plane appreciably increases the rotational transform. Since this modulation of the coils turns out to contribute the greatest part of the rotational transform, we investigated the case of circular, but twisted coils in greater detail. Fig. 1 shows a circular, but twisted coil.

For a straight Stellarator a short analytical calculation gives the relation between the geometry of the current lines on a cylinder with radius a and the properties of the magnetic field. Current lines with the modulation $z = z_0 \sin n(\varphi - \alpha z)$, $n = 1, 2 \ldots$ in the z-direction produce the rotational transform ω per period:

$$\omega = (\alpha z_0)^2 (n\alpha a)^2 [K_n'(n\alpha a)]^2 \left\{ \frac{2}{n!} \left(\frac{n}{2}\right)^{n+1} [(1 - \frac{1}{n})(\alpha r)^{2n-4} + \ldots] \right\}$$

If these circular coils are replaced by elliptical coils with the mean radius a ($a = \frac{r_{min} + r_{max}}{2}$), the necessary modulation to create the same value of the rotational transform is roughly $\frac{z_0}{2}$. Therefore, the advantage of having circular coils is reduced by the need for larger modulation compared with equivalent elliptical coils. For the numerical calculation each coil is described by the following formulas:

$$x(\Theta) = r(\Theta) \cos(\Theta + \Theta_n) \; ; \; y(\Theta) = r(\Theta) \sin(\Theta + \Theta_n)$$

$$z(\Theta) = f_n(\Theta) \sin(\Theta + \Theta_n) + c_n(\Theta) \sin 2(\Theta + \Theta_n) + e_n(\Theta) \sin 3(\Theta + \Theta_n) + \ldots$$

with

$$r(\Theta) = b \cdot \left(1 + \gamma \cos(\Theta + \Theta_n) + \varepsilon \cos 2(\Theta + \Theta_n) + \mu \cos 3(\Theta + \Theta_n)\right)^{-\frac{1}{2}}$$

$b, \gamma, \mu, \varepsilon$ are constants and the phase angle describes the position of the n^{th} coil. The z -axis of the coordinate system is tangent to a toroidally closed line. The amplitude functions f_n, c_n, e_n, g_n are either constant or equal to $1 + \delta \cos \Theta$ In the latter case the modulation is adjusted to the toroidal geometry and the modulation of the coils is smaller at the inside of the torus than at the outside.

Fig. 2 shows a set of $l = 2$ coils and Fig. 3 the calculated magnetic surfaces. The aspect ratio of the coil system is 2.22. The line S is the mapping of the positive r-axis after one revolution around the torus, the angle between S and the positive r-axis being a rough measure of the rotational transform. If the coils are adjusted to the toroidal geometry by the factor $1 + \delta \cos \Theta$, the magnetic surfaces are shifted to the inside of the torus (Fig. 4). Since the equilibrium position in a finite ß-plasma is shifted outwards by the parallel secondary currents, this inward shift of the vacuum field is a very helpful by-product of the modification of the coils. In Fig. 5 the magnetic surface of an $l = 3$ Stellarator are shown. The maximum amplitude of the coils is the same as in the $l = 2$ system (Fig. 2).

The superposition of the $l = 2$ and the $l = 3$ systems also yields magnetic surfaces.

The rotational transform in the $l = 2$ and $l = 3$ systems described above could be increased to $\iota \approx 0.2 - 0.25$, while in a system with larger aspect ratio $\left(\frac{R_o}{r_{coil}} = 5.4\right) \iota = 0.5$ could easily be reached. The magnetic well depth of the $l = 2$ configuration Fig. 3 is 11 %.

In conclusion we may say that circular but twisted coils produce toroidal magnetic surfaces with values of the rotational transform high enough for Stellarator experiments.

References

[1] M.A. Ivanovskii, S.N. Popov, A.P. Popryaduhkin, Prepring FIAN 94 (1968) 42

[2] Y.N. Petrenko, A.P. Popryaduhkin, Proc. of the III rd Symposium on Toroidal Confinement, Garching 1973, Paper D 8

[3] H.Wobig, S.Rehker, Proc. of the 7 th Symposium on Fusion Technology, Grenoble 1972

"This work was performed under the terms of agreement on association between the Max-Planck-Institut für Plasmaphysik and EURATOM".

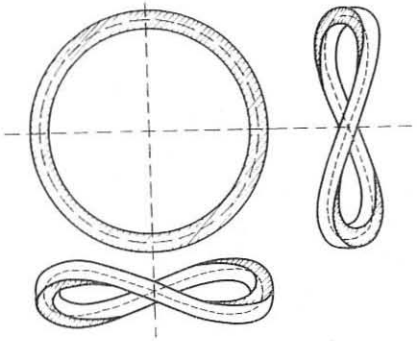


Fig. 1

$\ell = 2$ coil

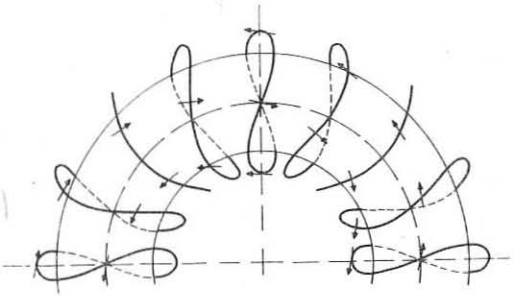


Fig. 2

$\ell = 2$ coil system

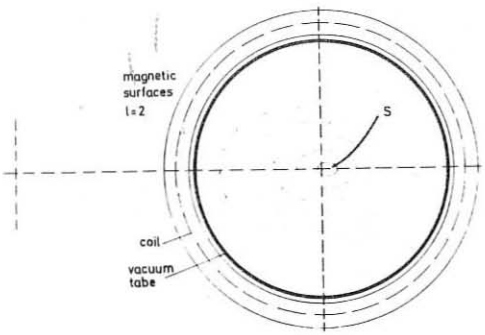


Fig. 3

Magnetic surfaces
of the $\ell = 2$ system

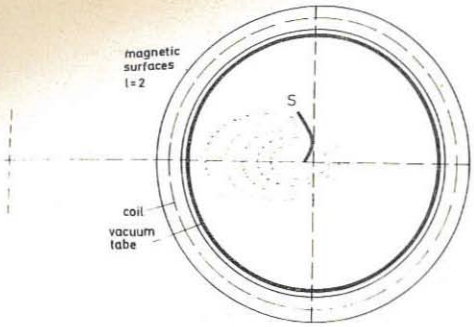


Fig. 4

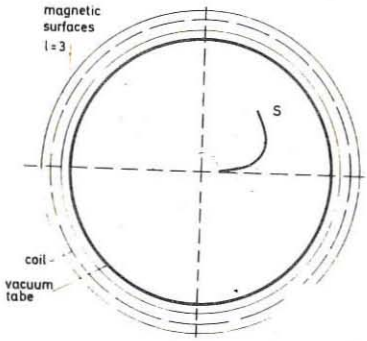


Fig. 5

Magnetic surfaces
of the $\ell = 3$ system

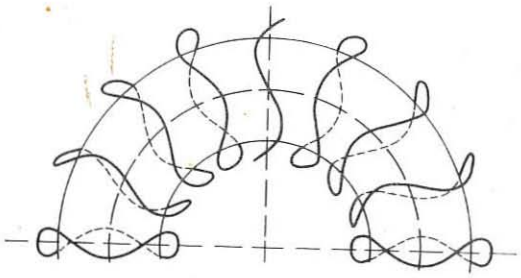


Fig. 6

$\ell = 3$ system

FLUCTUATIONS AND CONTAINMENT OF PLASMA IN JIPP L=3 STELLARATOR

T. Dodo*, M. Fujiwara, K. Miyamoto, A. Ogata
Institute of Plasma Physics, Nagoya University, Nagoya, JAPAN

Abstract: Fluctuations and anomalous loss of xenon afterglow plasma in l=3 stellarator are observed. This instability is caused from the difference of $E_0 \times B_0$ drift velocity between ions and electrons due to the finite Larmor radius effect.

In the early time of the afterglow in JIPP stellarator, the convective loss of plasma and the fluctuation are observed[1]. The fluctuation causes also rapid loss of plasma and after the cease of this fluctuation the decay time of the plasma becomes one order of magnitude longer (Fig. 1). After the decay of the convective cells of X_e plasma at the three corners of l=3 stellarator, the plasma has still negative potential for several milliseconds. The equipotential surfaces have triangular shape as the magnetic surfaces (Fig. 2). The low frequency ($\sim$4 kHz) fluctuation appears at 0.5 ms after switching off the ECRH power and grows very rapidly until 2 ms, then the amplitude becomes smaller and the frequency becomes lower ($\sim$1 kHz) (Fig. 3). This fluctuation propagates in the direction of $E_0 \times B_0$ rotation of the plasma and is expressed as $\exp.i(m\theta + n\phi - \omega t)$, m=2 and n=-1, where θ is in the poloidal direction and ϕ is in the toroidal direction.

The fluctuation is not localized at the steep density gradient but covers the region where the static electric field exists (cf. Figs. 4 and 2). The phase is nearly constant in the radial direction. The velocity of $E_0 \times B_0$ rotation at 2 ms ($\sim 4\times10^4$ cm/s) is

lower than the drift velocity due to the density gradient ($\sim 10^5$ cm /s). These features indicate that the Kelvin-Helmholtz instability is not responsible for this fluctuation[2].

The instability and anomalous loss of weakly ionized rotating plasma by the radial electric field have been discussed extensively.

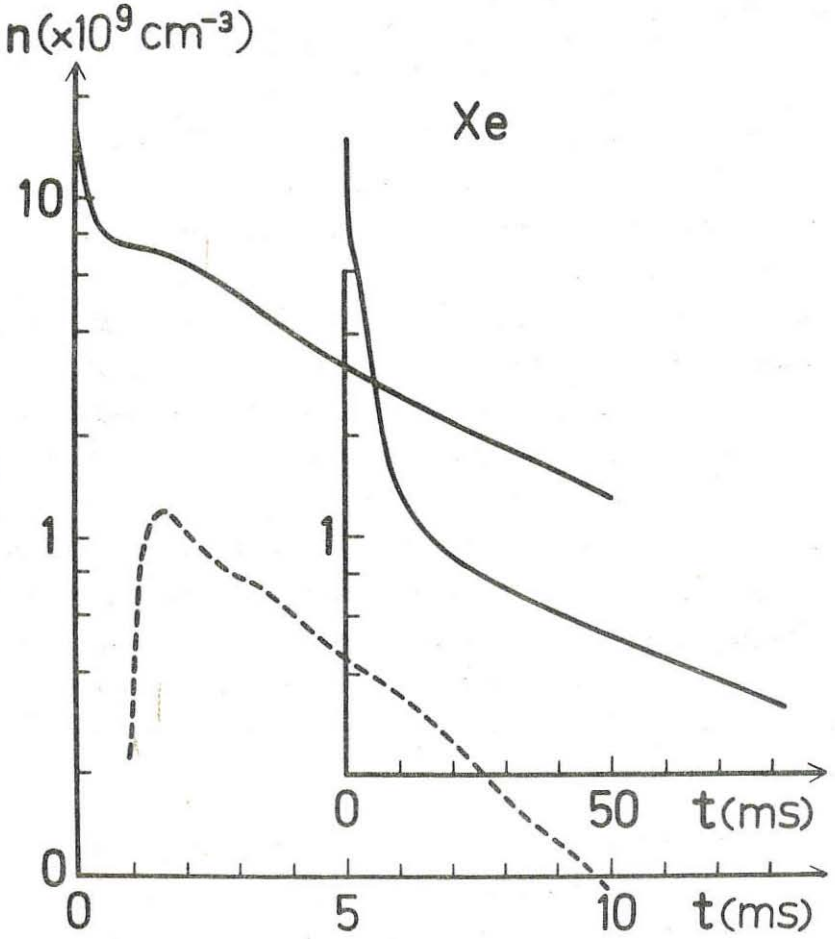


Fig. 1. Time variations of the density of X_e plasma (solid lines) and the amplitude of density fluctuation (dotted line).

This instability is caused from the difference of rotation velocity between ions and electrons due to the collision between ions and neutrals. In the present experiment, $(\omega_c \tau_{coll})_{ion}$ is much larger than 1 but the ion Larmor radius (∿1 cm) is comparable to the extension of the electric field (∿2 cm). Therefore, the rotation velocity of ions is lower than that of electrons due to the finite Larmor radius effect. The centrifugal force causes also the lowering the rotation velocity of ions. The detailed discussion will be reported later.

[1] M.Fujiwara, K.Miyamoto, Nuclear Fusion 12 (1972), 587.
[2] For example: D.L.Jassby, Phys. Fluids 15(1972)1590.
[3] For example: E.B.Hooper,Jr., Plasma Phys. 12 (1970),855.
* Permanent address: Central Research Lab.,Hitachi Ltd., Kokubunji, Tokyo.

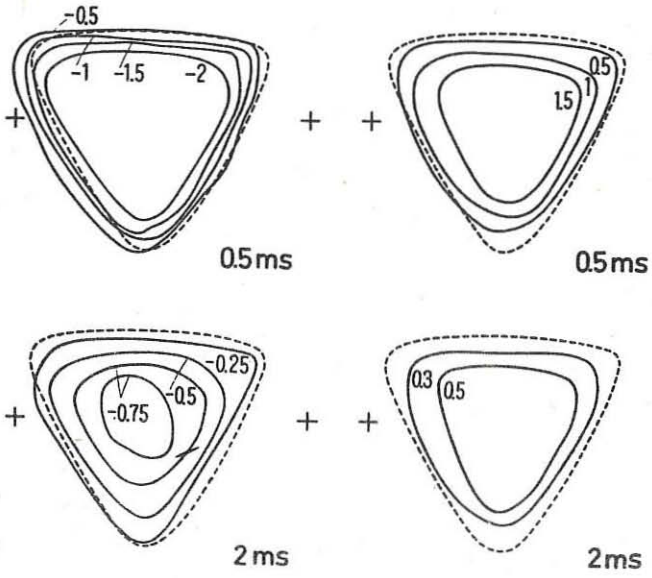
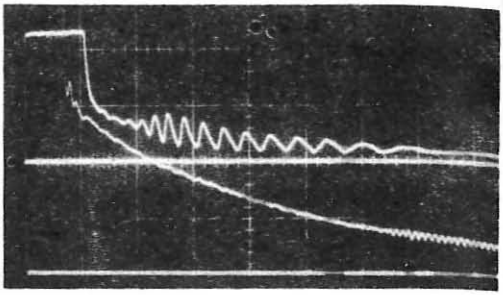


Fig. 2. Distribution of floating potentials (left hand side) and the densities at the times 0.5 ms and 2 ms after switching off the ECRH power. The numbers in the figures of the floating potential are in volts. The major axis of the torus is on the left hand side. The distance between the mark "+" is 10 cm.

Fig. 3. The density fluctuations on the separatrix of the magnetic surface. The upper trace; 0.2V/div, 1 ms/div: the lower trace; 0.01/div, 10 ms/div.



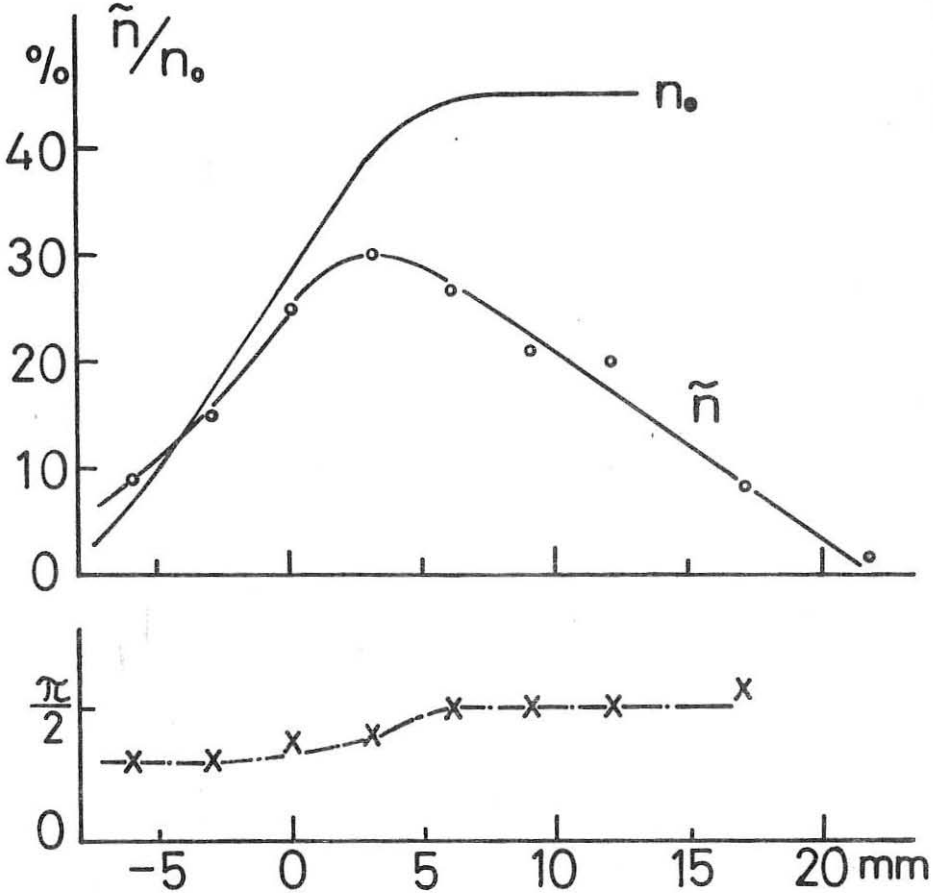


Fig. 4. The radial variation of the amplitude (the upper figure) and the phase. The origin of the abscissae is on the separatrix.

PLASMA CONFINEMENTS BY HYBRID STELLARATOR FIELD OF ℓ=2 AND ℓ=3

M. Fujiwara, K. Kawahata, A. Mohri and K. Miyamoto

Institute of Plasma Physics, Nagoya University, Nagoya, Japan

Abstract

Dependence of plasma confinement on the rotational transform angle and shear as well as the magnetic well depth is studied using J.I.P.P. stellarator which equips both ℓ=2 and ℓ=3 helical windings. Effect of shear on the resonant loss of rational surface is studied.

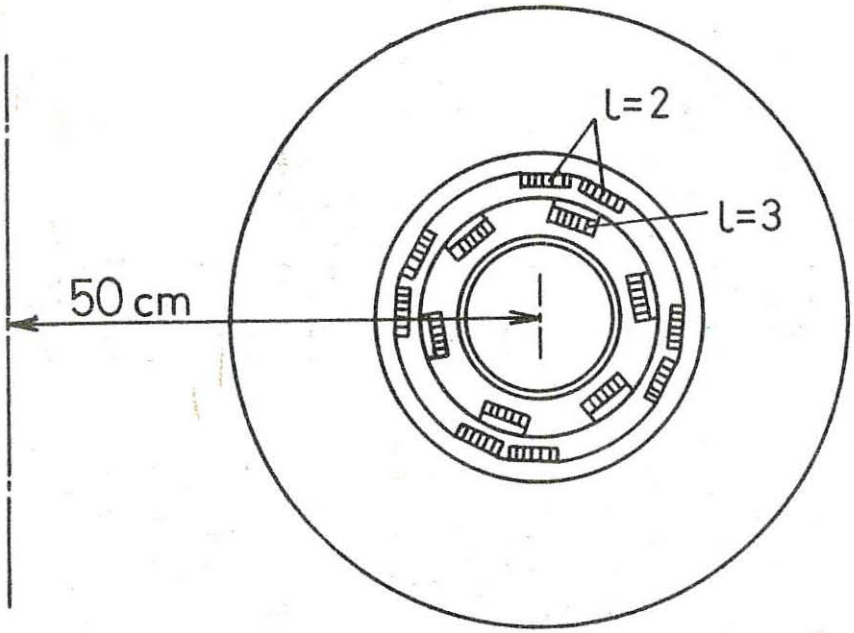


Fig.1. Schematic drawing of J.I.P.P. stellarator

J.I.P.P. stellarator device [1],[2],[3] is circular in shape and has ℓ=2 helical winding with 4 field periods and ℓ=3 helical winding with 8 field periods (Fig.1). The major radius is 50 cm and the maximum toroidal field is 4 KG in quasi-stational operation (5 s per minute). The inner radius of the stainless steel vacuum vessl is 7 cm. The ℓ=2 helical winding has a minor radius of 12.8cm with 30 kilo-ampere-turn and the ℓ=3 helical winding has a minor radius of 9.5 cm with 14 kilo-ampere-turn. Therefore the rotational transform angle and shear are variable independently (ι=0 ∿ 0.6, shear parameter θ = 0 ∿ 0.1, see Fig.2).

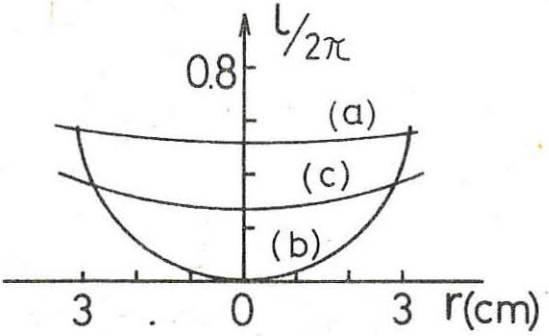


Fig.2 Radial dependence of the rotational transform angle in the cases of (a) ℓ=2 ($I_{h2}/I_t = 1.35$), (b) ℓ=3 ($I_{h3}/I_t = 2.9$) and (c) hybrid one ($I_{h2}/I_t = 1.04$, $I_{h3}/I_t = 1.04$), where I_{h2} and I_{h3} are the currents of helical coils of ℓ=2 and ℓ=3 and I_t is the current of the toroidal coil.

The plasma source used here is an electron cyclotron resonant heating with frequencies of 2.45 GHz (B_{ce}∿0.87 KG) and 9.4 GHz (B_{ce}∿ 3.4 KG). In the case of ECRH with 2.45 GHz, the microwave power of about 300 W is fed through a coaxial cable and a loop antena during about 10 ms.

Figure 3 shows a typical singnal of the ion saturation current

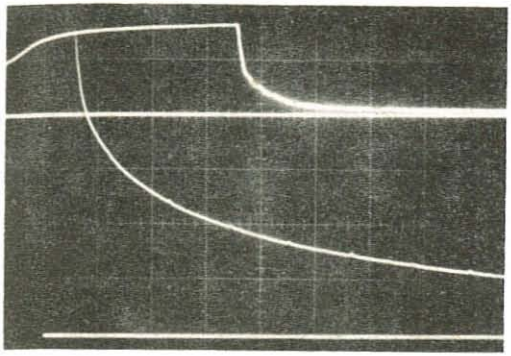


Fig.3. Typical signal of ion saturation current of Xe plasma produced by ECRH ($I_{h2}/I_t = I_{h3}/I_t = 1.2$). Upper trace (40 μA/div, 2 ms/div) and lower trace (1 μA/div, 5 ms/div).

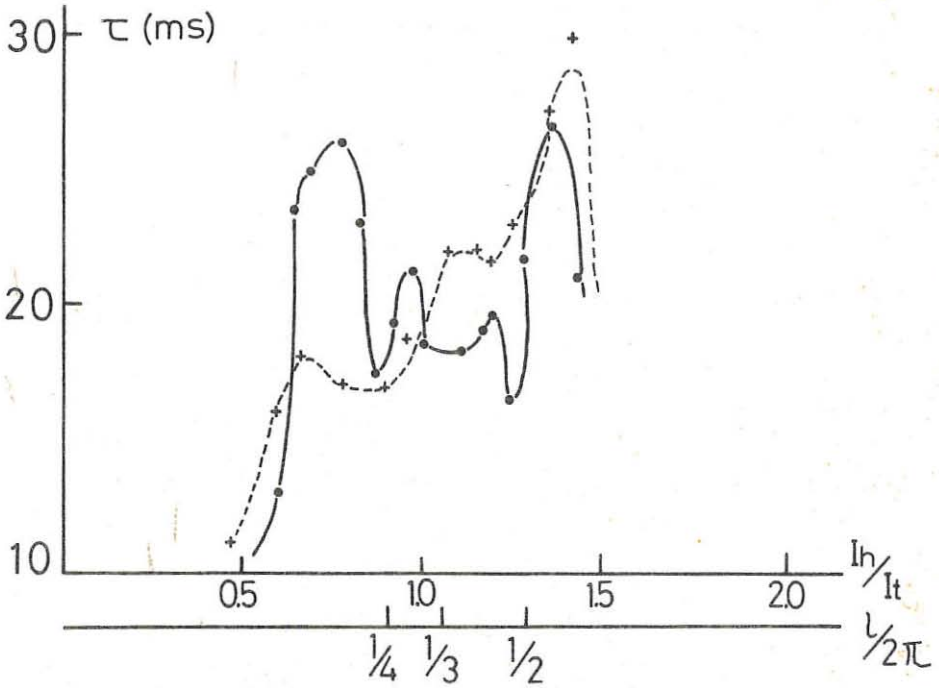


Fig.4. Dependence of confinement time on rotational transform angle on axis. Curve (ℓ=2) is of the case of ℓ=2 stellarator field and curve (ℓ=2 + ℓ=3) is of the hybrid case ($I_{h2} = I_{h3}$).

of a Langmuir probe, when Xe gas of 1.8×10^{-5} torr is used. After the power is turn off, the density decreases with two different decay time constants. During about 1.5 ms after that, the density decays rapidly and then later decreases much more slowly. In the early period, the strong convective cells are observed [1]. The plasma parameters are Te=1∿0.6 eV, $n_e \sim 10^9/cm^3$ in the later period. The degree of ionization is 2∿0.2 %

When the plasma is confined in the ℓ=2 stellarator field, the confinement time τ in the later period becomes small near the rational transform angle as is observed in Wendelstein [4] and Tor-1 [1]. (Fig.4). When the ℓ=3 stellarator field is superposed in addition to the ℓ=2 stellarator, the shear is introduced, and the observed resonant losses near the rational transform angle are reduced as is shown in Fig.4 . The detail investigation of the effect of rotational transform angle and shear on the plasma confinement are being continued intensively.

Reference

[1] K. Miyamoto, A. Mohri, N. Inoue, M. Fujiwara, K. Yatsu, Y. Terashima, R. Itatani; Plasma Physics and Controlled Nuclear Fusion Research, vol.III, p.93, Internal Atomic Energy Agency, Vienna, 1971.

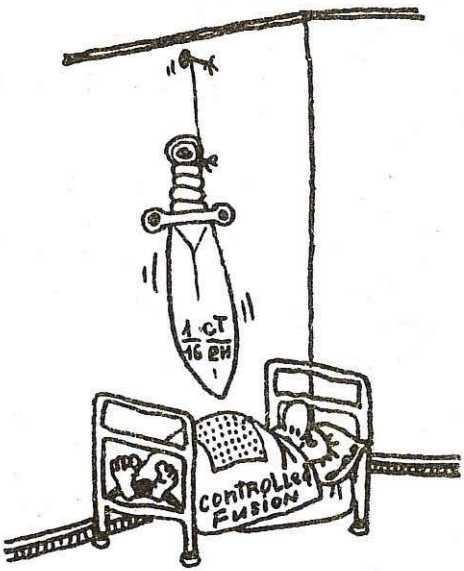
[2] M. Fujiwara and K. Miyamoto; Nucl. Fusion, 12, 587 (1972).

[3] K. Miyamoto; Proceedings of 3 rd International Symposium on Toroidal Plasma Confinement, D-2, Max-Planch Inst. Plasma Phys. Garching/Munchen 1973.

[4] G. Grieger, W. Ohlendorf, H. D. Pacher, H. Wolig, G. H. Wolf; Plasma Physics and Controlled Nuclear Fusion Research, vo.III, p.37, Internal Atomic Energy Agency, Vienna, 1971.

[5] D. K. Akulina, E. D. Andryukhina, Yu.I. Nechaev, O. I. Fedynin, Yu. V. Kholnov; ibid, vol.III, p.21.

1.6. INTERNAL RINGS, TRANSPORT



Sixth European Conference on Controlled Fusion and Plasma Physics
Moscow, USSR - 30 July - 3 August 1973

NEUTRAL INJECTION AND OHMIC PLASMAS IN THE CULHAM LEVITRON

M.W. Alcock, R.E. Bradford, R. Freeman, D.P. Hammond, A.C. Riviere, D.R. Sweetman
UKAEA Culham Laboratory, Abingdon, Berkshire, England

Abstract

Initial results are presented on the production of plasma by neutral injection and by ohmic heating. The observed containment times of the order of 0.1 second, are consistent with the results of FM1 at Princeton at the equivalent toroidal field strength. No anomalous loss of hot ions was observed but a negative plasma potential considerably greater than kT_e/e was present during injection.

The Culham Superconducting Levitron Experiment is now in operation [1] and initial experiments are being carried out on plasmas produced by neutral injection and ohmic heating. The neutral injection method is of particular interest because of the degree of control it offers, the lack of runaway phenomena and the ion heating it provides. It is also one of the most promising methods of heating for both large experiments and reactors.

A description of the Levitron has been given elsewhere [2]. At the present time a temporary toroidal winding capable of carrying up to 40 kilo-amp turns is in use in place of the final winding (900 kAT) and for the experiments described here the ring was operated at a current of 300 kAT. No difficulty has been found in stabilising the ring and the residual fluctuations in ring position are less than 10^{-3} cm. The base pressure, as measured by a shielded ion gauge near the plasma position, is approximately 6×10^{-9} torr and it is possible to raise the pressure by feeding in gas through a series of holes arranged symmetrically around the major azimuth. This arrangement avoids serious non-uniformity in gas pressure.

At the moment the diagnostic facilities include secondary emission detectors (SED's) to observe the fast atom flux produced by charge exchange of trapped 5 keV ions. These are placed in pairs to measure the hot ion density on the small and large major radius sides of the ring ('inner' and 'outer') at four azimuthal positions. Correlation of the SED signals with photon emission indicates that during plasma production using neutral injection alone the SED signal due to photo-electrons is much smaller than that due to fast atoms. There are also 12 limiter probes (scrapers) placed symmetrically around the major azimuth. These can be biased to collect ions or electrons and adjustment of individual probes by only a few mm (equivalent to the accuracy of their location on a circle) is sufficient to equalise the observed currents. The average electron density on the small major

radius side of the ring is measured by means of a confocal-mirror Fabry-Perot 4 mm microwave cavity. This is able to detect plasma densities as low as $10^9 cm^{-3}$. Finally, a single probe was inserted into the edge of the plasma on the large major radius side of the ring. This was connected by a capacitor divider network so that a measure of plasma potential was obtained.

The production of plasma by neutral injection into closed line systems has been discussed previously [3,4]. The condition for exponentiation of the cold plasma produced by ionization by the hot ions is given by

$$I_o > \frac{V}{d} \frac{e}{\sigma_{ti}} \frac{\sigma_x}{(\sigma_i + \sigma_x)} \left(\frac{1}{\tau} - n_o \overline{\sigma_e v_e} \right) \quad \text{Amps} \qquad \ldots (1)$$

where I_o is the beam current (amps equivalent), V the plasma volume, d the trapping length, n_o the gas density, σ_{ti} the cross section for beam trapping by cold ions, σ_i for production of cold ions by hot ions, σ_x for charge exchange of hot ions with the gas, and $\overline{\sigma_e v_e}$ the rate coefficient for ionization by electrons. τ is the cold ion containment time. If this condition is not achieved the hot ion density will be so low that there is little heating of the electrons by classical heat transfer. If we neglect electron ionization then under our conditions the critical τ is $0.2/I_o$ seconds for a background gas of hydrogen and $4/I_o$ for helium. The present experiments were carried out using a 5 keV H^o beam equivalent to about 20 mA and with helium as the background gas. Under these conditions τ required for exponentiation is about 200 seconds and an auxiliary form of electron heating is therefore essential.

If the background gas pressure is raised to the point where beam trapping is by collision with gas molecules then the beam current trapped is given by

$$I_t = I_o n_o \sigma_o d \quad \text{Amps} \qquad \ldots (2)$$

where σ_o is the cross section for ionization of beam atoms on gas molecules.

In the absence of the loss of hot ions by any means other than charge exchange the equilibrium SED signals will be directly proportional to I_t. Equation (2) shows I_t will increase linearly with gas pressure and this behaviour is clearly shown by the results in Fig.1 where SED signal current is plotted against the gas pressure. These results show that there is no anomalous loss of hot ions in a time comparable to the charge exchange time ($\sim$ 10 msec) at the lowest pressure. The points below 10^{-7} torr indicate the change from trapping by gas collision on helium to the trapping by Lorentz ionization and by collisions with background gas (N_2).

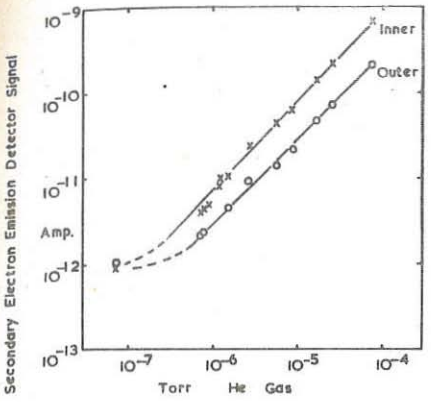


FIG.1

The cold plasma density is given by

$$n_e = \frac{I_t}{V} \frac{\sigma_i + \sigma_x}{e\,\sigma_x} \tau \quad cm^{-3} \qquad \ldots (3)$$

At the highest pressure the electron density measured by the interferometer was approximately 3×10^9 cm^{-3} and this, by means of (2) and (3), implies a τ of approximately 100 msec. These results were taken at a ratio of toroidal current I_t to poloidal current I_p of 0.08 and are consistent with the results of Chen et al [5]. During beam injection the plasma potential became negative and increased approximately linearly with I_t to -180 volts. This potential was considerably greater than kT_e/e since under the present conditions heating of the electrons by the hot ions would be negligible and T_e would be, at most, only a few eV. The measurement was made near the edge of the plasma and further measurements are needed to establish the total charge on the plasma. The charging of the plasma is believed to be due to the charge separation occuring at the point of injection [6] and the preferential loss of hot ions to the scrapers on the outer surface of the plasma.

Given the cold plasma confinement time of about 0.1 sec and the presently available toroidal field and beam current, to satisfy the build-up condition given above it is necessary to raise the electron temperature. Experiments have been started using ohmic heating from a 5 kAT peak-to-peak, 50 Hz modulation of the toroidal field which drives currents in the poloidal direction in the plasma. By this technique we have succeeded in producing a plasma density of 7×10^9 cm^{-3} at a low gas pressure (3×10^{-7} torr). The plasma density increased with the square of the amplitude of the field modulation. The variation of plasma density and therefore containment time with toroidal field strength is shown in Figure 2. There appears to be a threshold between 2400 and 3600 amp-turns for any appreciable plasma to be formed.

In summary we have observed trapping and containment of hot ions from neutral injection into a toroidal experiment with an indication of a resultant plasma potential. The secondary cold plasma has a lifetime of the order of 100 msec.

Preliminary ohmic heating experiments show that plasmas can be obtained at low gas pressures of the order of a few times 10^{-7} torr. In future experiments it is intended to raise the target plasma density to the value at which injected hot ions give up their energy to the plasma before being lost by charge exchange. It should then be possible to maintain the plasma by neutral injection alone.

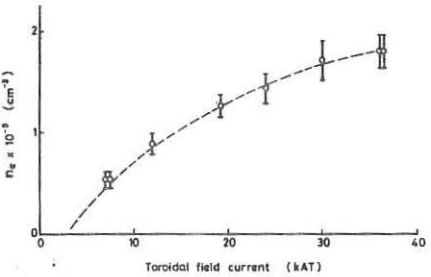


FIG.2

References

[1] A.C. Riviere, D.R. Sweetman, 5th Eur. Conf. on Controlled Fusion and Plasma Physics, Grenoble, August 1972 p.95.

[2] S. Skellett, 7th Symp. on Fusion Technology, Grenoble, October 1972, p.251.

[3] R.J. Bickerton, D. Drogman, Nuclear Fusion 6 287 (1966).

[4] A.H. Futch Jr., C.C. Damm, Plasma Physics 9 423 (1967).

[5] K. Chen, D. Meade, M. Okabayashi, J.A. Schmidt and S. Yoshikawa, Paper C8, Third Int. Symp. Tor. Plasma Conf., Garching March 1973.

[6] J.G. Cordey, M.J. Houghton, Bull. Am. Phys. Soc. Series II 16, 1235 (1971) and J.D. Callen, J.F. Clarke, ibid, p.1261.

Critical β for Quadrupole Configurations.

E. Rebhan, D. Lortz

Max-Planck-Institut für Plasmaphysik, 8046 Garching b.München
Federal Republic of Germany

Abstract: A sufficient stability criterion is applied to straight quadrupole configurations. Defining β = (total internal energy)/(total magnetic energy), complete MHD stability can be achieved up to $\beta \approx 1$ if the poloidal current is sufficiently large. The results obtained can qualitatively be transferred to toroidal configurations.

A recently developed stability criterion [1] is applied to straight quadrupole configurations.
Let us first consider the equilibrium. In two-dimensional equilibrium ($\frac{\partial}{\partial z} \equiv 0$) using a flux function F ($\underline{B} = \nabla z \times \nabla F + B_z \cdot \nabla z$, $\underline{j} = -(p' + B_z B_z') \cdot \nabla z - B_z' \cdot \nabla z \times \nabla F$) we have the equation

$$\Delta F = (k^2 - \lambda^2) F \tag{1}$$

where the special assumption

$$p' = -k^2 F, \qquad B_z B_z' = \lambda^2 F \tag{2}$$

is made. For $k^2 - \lambda^2 \gtrless 0$, in cylindrical symmetry solutions of (1) are given by the modified Bessel functions of order zero: $I_o(\sqrt{k^2-\lambda^2}\, r)$, $K_o(\sqrt{k^2-\lambda^2}\, r)$

Superimposing solutions with different centers of symmetry, we obtain quadrupole solutions:

$$F = \left[I_o(Qr_1) + I_o(Qr_2)\right] K_o(Q) - \left[K_o(Qr_1) + K_o(Qr_2)\right] I_o(Q)$$
$$Q = \sqrt{k^2-\lambda^2}, \quad r_1 = \sqrt{(x+1)^2 + y^2}, \quad r_2 = \sqrt{(x-1)^2+y^2} \tag{3}$$

From the separatrix whose X-point is at $x = y = 0$, the pressure goes down in both directions. When $p = 0$ is reached, the solution (3) must be continued by a vacuum.

Turning to the question of stability, we consider the quantity

$$A = -2\,(p' + B_z B_z')\frac{\kappa}{|\nabla F|^3} = +\frac{2Q^2 \kappa F}{|\nabla F|^3} \tag{4}$$

κ is the curvature of the flux lines $F = \text{const}$

$$\kappa = -\underline{n}\left[(t\nabla)\underline{t}\right], \underline{n} = \frac{\nabla F}{|\nabla F|}, \quad \underline{t} = \frac{\nabla z \times \nabla F}{|\nabla F|}$$

According to ref. [1] complete stability is obtained if on each field line inside the plasma

$$\langle a \rangle = \int_{F=\text{const}} a\, dx < \alpha_o \tag{5}$$

where

$$a = \left(\int_{F=\text{const}} |\nabla F| dl \right)^2 \cdot A,$$

where for $F = \text{const}$

$$dx = \left(|\nabla F| / \int_{F=\text{const}} |\nabla F| dl\right) \cdot dl$$

and where α_o is the lowest eigenvalue of the problem

$$y''(x) + (\alpha + a - \langle a \rangle)\, y(x) = 0 \tag{6}$$
$$y(x+1) = y(x)$$

According to (3) - (6), stability depends only on the combination $Q = \sqrt{k^2 - \lambda^2}$ of k and λ. This suggests that stability up to high β-values can be achieved by letting the pressure gradient ($\sim k^2 |\nabla F|$) become large together with the meridional current ($\sim \lambda |\nabla F|$), while keeping Q fixed.

The criterion (5) was evaluated numerically for the solutions (3). It is found that for each Q there exists a $F^*(Q) > 0$ such that for all field lines

with $|F| < F^*(Q)$ the criterion is fulfilled. Since $p = p_o - \frac{k^2F^2}{2}, p_o$ can be chosen such that $p = 0$ for $F = \pm F^*$ and $p > 0$ for $|F| < F^*$.

Defining

$$\beta = \int_{V_{P\ell}} p \, d^3\tau \Big/ \int_{V_{P\ell}} \frac{B^2}{2} \, d^3\tau$$

we get

$$\beta = (\lambda^2+Q^2) \cdot \frac{\int_0^{F^*} dF \int_{F=\text{const}} dl (F^{*2}-F^2)/|\nabla F|}{\int_0^{F^*} dF \int_{F=\text{const}} dl (|\nabla F|^2 + \lambda^2 F^2)/|\nabla F|} \tag{7}$$

Numerical plots of β as a function of λ and Q are shown in Fig. 1.

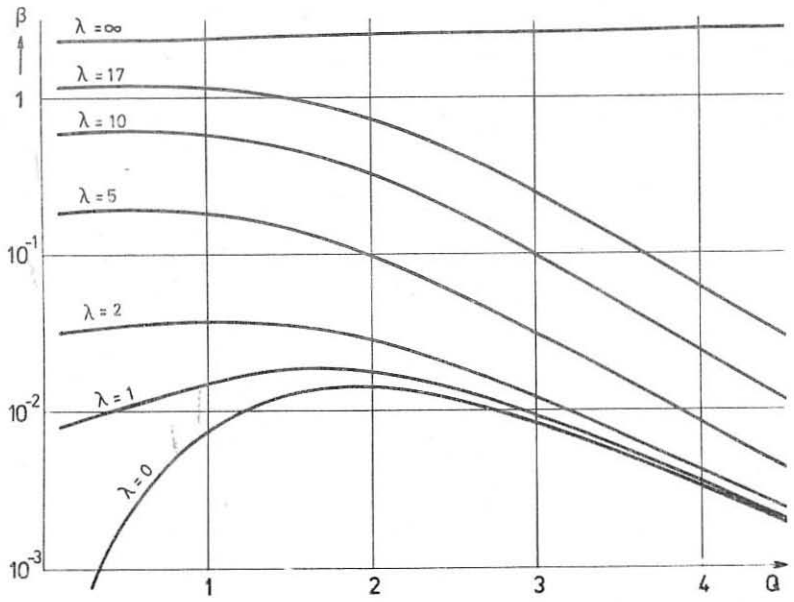


Fig. 1

Without meridional current ($\lambda=0$) β has a maximum value of $\approx 1.5 \times 10^{-2}$ at $Q \approx 2$. With increasing poloidal current (increasing λ) higher β values are reached which for $\lambda \gtrsim 10$ attain the order of magnitude $\beta = 1$. The maximum thereby shifts towards $Q = 0$, which means that the meridional magnetic field is almost vacuum.

It should be stressed that the stability found here is not marginal but real positive. A qualitative transfer of the results to toroidal axisymmetric quadrupoles is thus possible. In both linear and toroidal configurations the energy variation obeys the inequality

$$\delta^2 W > \frac{1}{2} \int (\alpha_o - \langle a \rangle) \frac{|\nabla F|^2 (\xi \cdot \nabla F)^2}{\left(\int_{F=\text{const}} |\nabla F| \, dl\right)^2} \, d^3\tau$$

where A_{tor} is given by a formula similar to (4) in axisymmetry. With vanishing toroidal curvature $(A_{tor} - A) \to 0$ and $(\alpha_o^{tor} - \alpha_o) \to 0$. Since in the linear quadrupole inside the plasma $\alpha_o - \langle a \rangle > 0$, because of continuity this will be true also for small toroidal curvature. Thus, even if toroidicity were to have a destabilizing effect, there would still be a domain of stability. It can be expected that in axisymmetric quadrupoles as well stability is possible up to $\beta \approx 1$.

[1] D.Lortz, E.Rebhan, G.Spies, Nuclear Fusion 11, 583 (1971)

"This work was performed under the terms of the agreement on association between the Max-Planck-Institut für Plasmaphysik and EURATOM".

Plasma Confinement Properties in FM1-Spherator

K.Chen, D.Meade, M.Okabayashi, J.Schmidt, and S.Yoshikawa

Plasma Physics Laboratory, Princeton University

Princeton, New Jersey 08540, U.S.A.

Abstract: Plasma confinement time in FM-1 was investigated at high electron temperature(T_e=10-100eV). The confinement time is consistent with the assumption of τ=150-300τ_B.

The plasma confinement properties at electron temperature, T_e, less than 5eV has been investigated and reported at the previous conference at Grenoble.[1] It was found that the plasma decay time follows pseudo-classical scaling when the electron temperature is less than 1eV with the plasma density $n_e=1\times10^{11}cm^{-3}$. At higher electron temperature($T_e\geq$1eV), the confinement time was approximate by the empirical formula $\tau=300\tau_B$. The main purpose of the present experiment is to investigate whether this empirical formula still is valid at higher electron temperature (T_e=10-100eV).

High electron temperature plasma was produced by applying a short pulse of high power microwaves (electron cyclotron resonance) to the preionized helium plasma ($n_e=1-2\times10^{11}cm^{-3}$, T_e=1eV). Since the electron temperature decays rapidly mainly due to ionization energy loss, it is almost impossible to obtain the confinement time at constant plasma parameters. Therefore, the following procedure was adapted in these experiments. The time dependence of observable parameters, such as plasma density, absolute intensity of light emitted from plasma, electron temperature, ion temperature and loss rate are compared with predictions obtained with the assumption of a confinement time scaling. For helium plasma, the absolute value of 4686Å was

monitored, the electron temperature was measured by Langumuir probes, and the neutral gas pressure was measured by a fast ionization gauge. Ion temperature was measured from the Doppler broadening of 4686Å by using a pressure swept Fabry-Perot interferometer. The instrumental width allowed a measurement of the ion temperature down to 0.1eV.

Numerical predictions were made using a zero dimensional computer code, which included charge exchange, ionization and reconbination processes. Since at low electron temperature (1-5eV) a Bohm type scaling law was observed, a similar scaling was assumed for the plasma confinement time at high electron temperature (>10eV). Figure 1 shows the comparison of experimental results and numerical calculations. The preionized plasma (n_e=1.5×$10^{10}$$cm^{-3}$) was heated with a 2msec, 5kW pulse at 10GHz. The electron temperature increases up to 50-100eV from 1eV during the heating pulse, according to the numerical calculations. Probe measurements showed the electron temperature was 50-70eV just after the end of the pulse and droped to 10eV after 20msec. As shown in Fig.2, due to the ionization of residual neutral gas, the plasma density goes up to 7-8×$10^{10}$$cm^{-3}$ at 15msec after the end of heating pulse. The light intensity of 4686Å reaches a masimum at 7msec. The solid lines show the predicted values of plasma density and absolute light intensity assuming different values of Bohm-like confinement scaling. Reasonable agreement between the experimental results and calculations was obtained with the assumption of τ=150-300τ_B. This confinement time is consistent with the value obtained around T_e=1-5eV, which was previously reported. The time dependence of the ion temperature is also shown in Fig.1. The numerical curves were obtained assuming that ions were heated through classical electron-ion collisional coupling. It was found, contrary to our prediction, that ion temperature

peaked just after the end of the microwave heating pulse and decayed with a time constant of 5msec. This result suggests that during the high power microwave heating ions gain energy by a process other than electron-ion collisional coupling. Preliminary experimental results show the rate of ion heating is strongly dependent on the input microwave power and that a threshold power level esists. This indicates the ion heating mechanism may be related to parametric heating processes.

In conclusion, an experiment was carried out to investigate the plasma confinement time at higher electron temperature range (T_e=10-100eV). It was found that the Bohm type scaling law (τ=150-300τ_B) found at lower electron temperature is still consistent with the experimental results.

This work was supported by U.S. Atomic Energy Commission Contract AT(11-1) -3073. Use was made of computer facilities supported in part by National Science Foundation grant NSF-GP579

1. M.Okabayashi, J.Schmidt, J.Sinnis, and S.Yoshikawa, in Proceedings of The Fifth European Conference on Controlled Fusion and Plasma Physics, Grenoble 1972, Vol,I,p92.

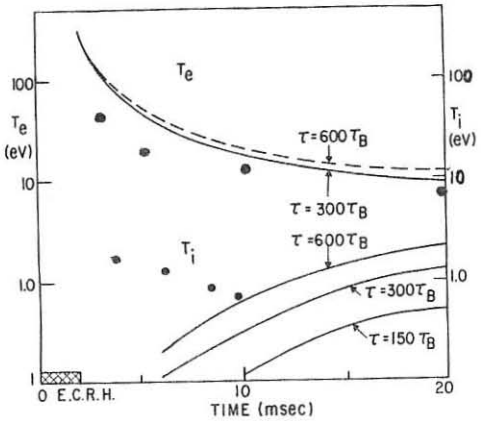


Fig.1. Comparison of numerical calculation and experimental results. Lines are numerical results. Large black dots are electron temperature measured by probes. Small black dots are ion temperature measured by Doppler broadening.

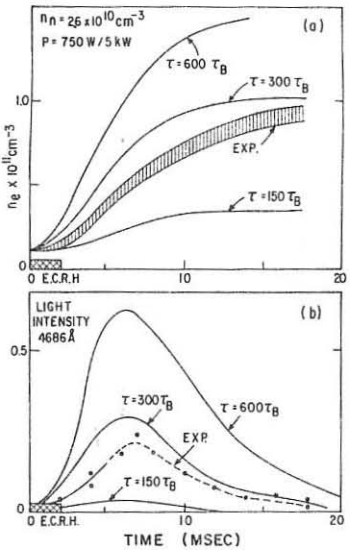


Fig.2.(a). Comparison of plasma density. (b). Comparison of absolute intensity of 4686Å.

OBSERVATION OF DRIFT INSTABILITY DUE TO PARTICLE TRAPPING IN A CORRUGATED GEOMETRY

P. Deschamps, R. Gravier, C. Renaud, A. Samain

ASSOCIATION EURATOM-CEA SUR LA FUSION
Département de Physique du Plasma et de la Fusion Contrôlée
Centre d'Etudes Nucléaires
Boîte Postale n° 6. 92260 FONTENAY-AUX-ROSES (FRANCE)

Magnetic field configurations used for confinement, which are periodic along the field lines divide particles into two classes i) circulating particles which are not reflected at the field maxima, ii) trapped particles localized in the field depressions. If these depressions are shallow enough, even a small collision rate can efficiently scatter the particles from one class out into the other.

As was first pointed out by Kadomtsev and Pogutse [1] this scattering is a dissipative mechanism capable of driving unstable the oscillations associated to the plasma radial pressure gradient.

In order to investigate this effect the 5 m long homogeneous magnetic field in ODE which had previously been used to study the collisionless drift waves [2], was modified to produce a spatial dependence approximated by $B = B_o(1-\varepsilon \cos \frac{2\pi z}{L})$ with three field periods ($\varepsilon \sim 0.12$, L=1.20 m, $B_o \leq 3750$G). The main plasma parameters remained as described in reference [2], with constant density along the axis ($n_o \sim 5 \times 10^8 - 2 \times 10^{10}$ cm^{-3}, $T_e \sim 10$ eV, $T_i \sim 2$ eV, $\nabla n_o/n_o \sim \nabla T/T \sim -1.3$ cm^{-1}, $p_o < 10^{-6}$ torr).

Under certain conditions which have been partly investigated as of now, low frequency instabilities arise, which are maximum in the density gradient at r $\sim$ 0.8 cm. These instabilities can be compared to the collisionless drift waves appearing in homogeneous field, at the same magnitude of B_o. In both cases the waves propagate azimuthally in the electron drift direction and are standing waves radially and along the axis. However the distributions of the fluctuating density amplitudes (n_1) along the field line differ. A typical example for m = 1 modes is recorded on fig. 1, using a probe moving over 2.90m, parallel to the machine axis. The measurements show that

the new mode exhibits maxima localized in the magnetic troughs and that the oscillations extend in phase all over the machine length.

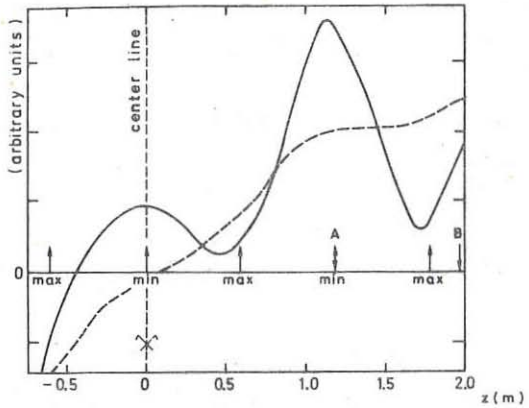


Fig.1_ AXIAL DISTRIBUTION OF FLUCTUATION AMPLITUDES
—— with FIELD CORRUGATIONS
--- without CORRUGATIONS

As an indication of the instability strength the relative amplitude of the "trapped" drift mode (n_1/n_o) measured at position A (see fig. 1) and that of the collisionless drift mode measured at position B are plotted against the on-axis density on fig.2. The density is measured both by a cavity and by Langmuir probes. Only the "trapped" drift mode appear to be sensitive to plasma density within one order of magnitude variation.

When the magnetic field is varied, at a cavity measured density of $\sim 1.5\ 10^9 cm^{-3}$, both situations are stable below 1100 G, the fluctuation amplitudes reach a maximum around 1350 G (ky ai = $\frac{m}{r}$ ai $\sim$ 0.18; ai:ion Larmor radius). Above 1500 G the "trapped" drift mode vanishes whereas the collisionless drift mode still remains close to its maximum value. The "trapped" drift mode frequency is the lowest throughout, especially when its amplitude is large, for instance 75 kHz at 1350 G instead of 90 kHz for the col-

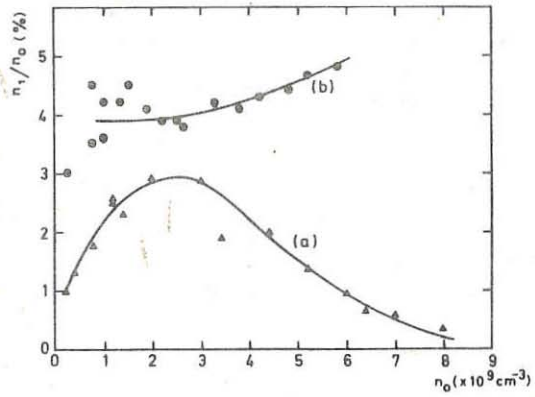


Fig.2_ INFLUENCE OF DENSITY ON THE DRIFT INSTABILITY AMPLITUDE
a) with ±12 % FIELD CORRUGATIONS
b) without CORRUGATIONS
B_o = 1350 G ; $T_e \simeq 9$ eV , m=1

lisionless drift mode.

As an attempt to compare with Kadomtsev's trapped drift mode we have computed, in order of magnitude, the contribution to the imaginary part of the dispersion relation coming from the trapped electrons(not to be confused with the linear growth rate). Using Kadomstev's notations this expression reads

$$W(\omega/\nu_{ef}) = I_m\{ X \int_0^{\infty} \frac{\omega-\omega_e^*(1+\eta(v^2-3/2))}{\omega + i\nu_{ef}/v^3} e^{-v^2} v dv \int_{-v\epsilon^{1/2}}^{v\epsilon^{1/2}} dv_{//} \}$$

where $v \equiv v_\perp/v_e$, $\eta \equiv d\,\mathrm{Log}\,T_e/d\,\mathrm{Log}\,n_o$ and where the v^{-3} dependence has been kept in ν_{ef}. For trapped electrons we assumed $v_{//}^2 << v_\perp^2$. Spatial dependences are ignored in the integrals and supposed to be taken up by X of order unity. Fig.3 is a plot of W versus ω/ν_{ef} for $\omega \sim 0.8\,\omega^*$ and $\eta \sim 1$ ($\nabla T_e/T_e \sim \nabla n_o/n_o$). The dependence on the density is qualitatively that found in the experiment on fig. 2 but the optimum value of ω/ν_{ef} for instability lies in the range 0.1-0.2 whereas the experimental value is 2-3. The instability is observed for a density lower than expected from the above estimate.

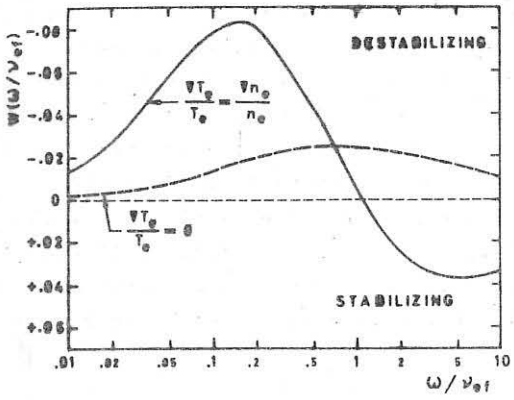


Fig.3_INFLUENCE OF TRAPPED ELECTRONS ON THE DRIFT INSTABILITY
$\epsilon = 0.12$, $\omega = 0.8\,\omega^*$

When $\eta=0$, again for $\omega \sim 0.8\omega^*$, fig. 3 also indicates that if the temperature gradient is removed ($\nabla T_e/T_e \sim 0$) the strength of the instability should be less.

In our experiment the cancellation of the temperature gradient can be achieved by heating selectively the outer part of the plasma at the electron cyclotron frequency -see reference [3] for a description of this technique - making it possible to check for the destabilizing influence of the temperature gradient. On fig.4 as η varies continuously from ~ 0.2 to ~ 0.8 the instability amplitude is plotted against a temperature gradient dependant parameter

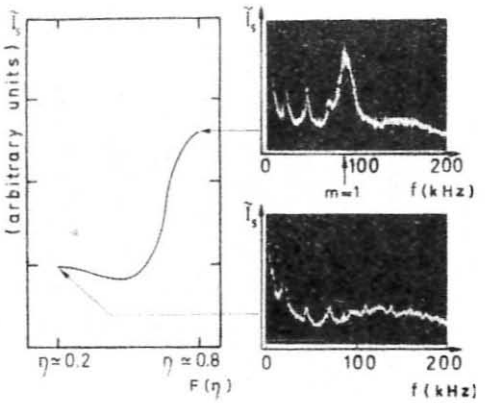


Fig. 4 – INFLUENCE OF THE ELECTRON TEMPERATURE GRADIENT ON THE TRAPPED DRIFT INSTABILITY

$n_o \simeq 2.5 \times 10^9 cm^{-3}$; $B_o \simeq 1350$ G

namely Langmuir probe floating potential for experimental convenience at $B_o = 1350$ G.

In the homogeneous field case on the contrary, the temperature gradient was observed to stabilize the collisionless drift wave [3] as expected theoretically.

To summarize the observations, a drift instability has been observed in a corrugated shearless field in ODE under conditions where the bounce frequency for electrons (2-3 10^6 rad/s) is larger than either the wave frequency or the effective collision frequency ($\nu_{ef} \sim 1.2 \times 10^5\ s^{-1}$ at $2 \times 10^9\ cm^{-3}$). In spite of discrepancies with rough numerical estimates the wave retains qualitative features of the trapped particle instability predicted by Kadomtsev and Pogutse in 1966.

REFERENCES

[1] B.B. Kadomstev and O.P. Pogutse, Sov. Physics J.E.T.P., 24, 1172 (1967)/ Zh. E.T.F. 51, 1734 (1966)/.

[2] P. Brossier, P. Deschamps, R. Gravier, R. Pellat, C. Renaud, Phys. Rev. Let. 26, 124 (1971).
R. Boissier, P. Brossier, P. Deschamps, R. Gravier, R. Pellat, C. Renaud, Proc. 3rd Int. Conf. on Quiescent Plasmas (Elsinore 1971) 246.

[3] P. Brossier, P. Deschamps, R. Gravier, R. Pellat, C. Renaud, Submitted to Phys. Rev. Let. and to XIth C.I.P.I.G. (Prague 1973).

INFLUENCE OF THE SLOW INHOMOGENEITIES ON TRANSPORT PHENOMENA IN THE HIGH TEMPERATURE PLASMA IN THE STRONG MAGNETIC FIELD

Yu.A.Dreizin, A.M.Dykhne
I.V.Kurchatov Institute of Atomic Energy,
Moscow, USSR

Drift approximation analisis of the motion of electrons in time-independent random potential φ is given. The coefficient of electron diffusion $\mathcal{D}_\perp$ across magnetic field depends on free path ℓ, Larmor radius r_H, a characteristic scale a of inhomogeneities and there dimensionless amplitude $\Delta \sim \frac{e\varphi}{T}$, as shown on Fig.1.

1. For the calculation of transport coefficients in a turbulent plasma it is necessary to find the spectrum of turbulent waves, and then to solve the problem of scattering of plasma particles by these waves. If the magnetic field is absent and waves energy is less than thermal energy of plasma, scattering of particles by waves may be calculated by perturbation theory /1/.

In magnetized plasma the picture of particle's interaction with low frequency waves significantly differs from usual picture of scattering by waves provided that Larmor radius is less than the wave length. In particular, for applicability of perturbation theory the smallness of the wave energy as compared with the plasma thermal energy is not sufficient.

We shall consider here the influence of random, static, threedimensional isotropic plasma inhomogeneities on the diffusion of electrons across the magnetic field. In ous previous article /2/ this problem was investigated in hydrodynamical approximation $\ell \ll a$. In the

present work this restriction is removed.

2. Let us consider weak inhomogeneities, $\Delta = \frac{e\varphi}{T} \ll 1$, where T - electron temperature. A homogeneous magnetic field is strong enough so that inequalities $r_H = \frac{c\sqrt{mT}}{eH} \ll a$, $r_H \ll \ell$ are valid. The former permits to use drift approximation. Let $\bar{r}(t)$ represent the trajectory of an electron moving in potential φ and colliding with plasma particles. We wish to estimate the transverse electron diffusion coefficient $\mathcal{D}_\perp$:

$$\mathcal{D}_\perp = \lim_{t\to\infty} \frac{\langle (\bar{r}_\perp(t) - \bar{r}_\perp(0))^2 \rangle}{4t}$$

Neglecting electron-electron collisions we may connect the diagonal component of conductivity tensor $\sigma_\perp$ with $\mathcal{D}_\perp$ as in a homogeneous plasma: $\sigma_\perp = \frac{\langle n \rangle e^2}{T} \mathcal{D}_\perp$, where $\langle n \rangle$ -mean number density of electrons. It can be shown that other components of $\hat{\sigma}$ don't change significantly due to inhomogeneities with $\Delta \ll 1$.

3. Let us consider first the collisions case. Conservation of the adiabatic invariant and energy of an electron results in conservation of $E_\parallel = \frac{m v_\parallel^2}{2} - e\varphi(\bar{r})$. If $E_\parallel$ is sufficiently small, than the motion of electron will be confined in space. Electrons with such $E_\parallel$ are trapped. For electrons with $E_\parallel \gg T\cdot\Delta$ almost everywhere $E_\parallel > -e\varphi(\bar{r})$ holds. This region of $E_\parallel$ corresponds to untrapped electrons. Finally electrons with $E_\parallel \sim T\cdot\Delta$ we shall call half-trapped ones - there motion is not confined in space, but forbidden domains where $-e\varphi(\bar{r}) > E_\parallel$ are not too rare (fig.2). So far as $\Delta \ll 1$ almost all electrons are untrapped and statistical weights of trapped and half-trapped electrons are small, $\sim \sqrt{\Delta}$. It is convenient to consider the diffusion of untrapped $(\mathcal{D}_{\perp u})$ and halftrapped $(\mathcal{D}_{\perp h})$ particles separately and then find $\mathcal{D}_\perp$ as $\mathcal{D}_\perp = \mathcal{D}_{\perp u} + \sqrt{\Delta}\,\mathcal{D}_{\perp h}$ (trapped particles don't contribute to $\mathcal{D}_\perp$).

4. Untrapped particles. Let an electron move with velocity $v_\parallel \gg v_{th}\sqrt{\Delta}$, $v_{th} = \sqrt{\frac{T}{m}}$. It drifts across $\bar{H}$ with a velocity $u \sim \frac{c\varphi}{aH} \sim$

$\sim V_{th}\frac{r_H}{a}\Delta$. The correlation between drift velocities vanishes when the particle passes a distance $\sim a$ along $\bar{H}$. From this we may estimate $\mathcal{D}_{\perp u}(v_{\parallel})$ as $u^2\frac{a}{v_{\parallel}}$. Taking average over particles with different we obtain $\mathcal{D}_{\perp u}\sim u^2\frac{a}{V_{th}}\ln\frac{1}{\sqrt{\Delta}}\sim V_{th}\frac{r_H^2}{a}\Delta^2\ln\frac{1}{\sqrt{\Delta}}$

Now let us take into account collisions between electrons and ions. It may be shown that when $\ell\lesssim\frac{a^3}{r_H^2\Delta^2\ln\frac{1}{\sqrt{\Delta}}}$ our estimation of $\mathcal{D}_{\perp u}$ fails. Really, after collision an electron moves back along $\bar{H}$ through the same inhomogeneities, and correlation of transverse displacements before and after collision results in increase of $\mathcal{D}_{\perp u}$. An estimation of $\mathcal{D}_{\perp u}$ in this case may be fulfilled in the same manner as in /2/:

$$\mathcal{D}_{\perp u}\sim\frac{a^{4/3}u^{4/3}}{\ell^{1/3}V_{th}^{4/3}}\sim V_{th}\frac{r_H^{4/3}}{\ell^{1/3}}\Delta^{4/3}$$

5. Half-trapped particles. Let $\ell=\infty$. An electron travels along reflects from boundaries of forbidden domains (mirrors) and drifts with the velocity u. The resulting motion of an electron resembles the random walk rather than the motion between two mirrors (fig.2).

An electron drifts across $\bar{H}$ during the correlation time $\sim\frac{a}{u}$ characteristic distance $\sim a$. So $\mathcal{D}_{\perp h}\sim ua\sim V_{th}r_H\Delta$. The half-trapped particle becomes untrapped one due to scattering at the small angle $\sim\sqrt{\Delta}$. Time interval before such collision becomes less than drift time at distance $\sim a$ when $\ell\lesssim\frac{a^2}{r_H\Delta^2}$. This leads to another expression: $\mathcal{D}_{\perp h}\sim u^2\tau_{\sqrt{\Delta}}\sim V_{th}\ell\frac{r_H^2}{a^2}\Delta^3$, where $\tau_{\sqrt{\Delta}}$ time before scattering at the angle $\sim\sqrt{\Delta}$ occurs. On fig.1 dependence of $\mathcal{D}_{\perp u}$, $\sqrt{\Delta}\mathcal{D}_{\perp h}$ and their sum $\mathcal{D}_{\perp}$ on ℓ is presented.

Literature

1. A.A.Vedenov, in " Вопросы теории плазмы " ed. by M.A.Leontovich, Moscow, 1963.
2. Yu.A.Dreizin, A.M.Dykhne. ЖЭТФ 63, 242, (1972).

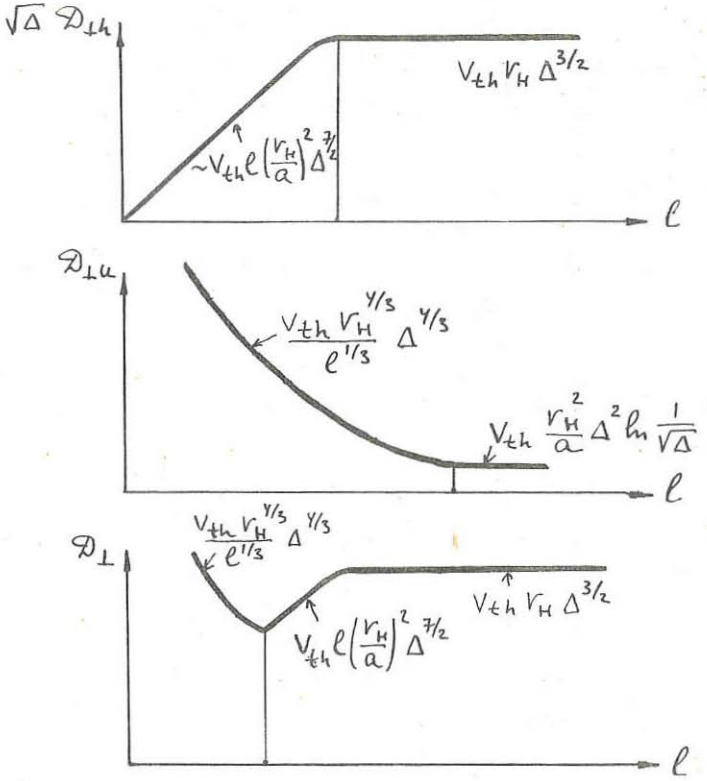

$\sqrt{\Delta}\,\mathcal{D}_{\perp h}$
$V_{th} r_H \Delta^{3/2}$
$\sim V_{th} \ell \left(\frac{r_H}{a}\right)^2 \Delta^{7/2}$
ℓ
$\mathcal{D}_{\perp u}$
$\frac{V_{th} r_H^{4/3} \Delta^{4/3}}{\ell^{1/3}}$
$V_{th} \frac{r_H^2}{a} \Delta^2 \ln \frac{1}{\sqrt{\Delta}}$
ℓ
$\frac{V_{th} r_H^{4/3} \Delta^{4/3}}{\ell^{1/3}}$
$\mathcal{D}_\perp$
$V_{th} r_H \Delta^{3/2}$
$V_{th} \ell \left(\frac{r_H}{a}\right)^2 \Delta^{7/2}$
ℓ

Fig 1.

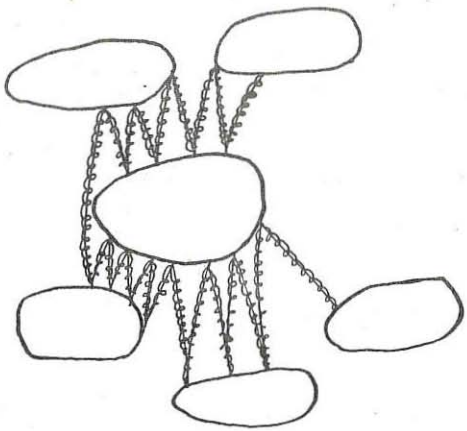


Fig. 2.

1.7. TOKAMAKS: NEW TRENDS



EXPERIMENTS ON THE TO-1 TOKAMAK HAVING AN AUTOMATIC SYSTEM FOR CONTROLLING THE EQUILIBRIUM.

L.I.Artemenkov, P.I.Koslov, P.I.Melikhov, V.S.Svishev.

I.V.Kurchatov Institute of Atomic Energy
Moscow, USSR.

ABSTRACT:

The present experiments (H_o = 8kG, I_p = 15 – 20kA) on TO-1 device have demonstrated that in uncased Tokamak having an automatic system the plasma parameters are sufficiently high and there are the possibilities for their improvements.

An impedance automatic control system is used on the uncased TO-1 Tokamak for providing major radius plasma column equilibrium [1]. The early experiments [2] showed that the system was operable but the plasma had low parameters. Short low- conductivity and low-temperature discharges were produced because of the imperfect outgassing of the chamber and the vertical plasma column shift. Measurements of the residual gas spectrum gave an indication of the presence of the high-molecular components. It was cleared up that the vertical plasma column shifts had been caused by the imperfection of the structure of the magnetic fields in the device, which was easily compensated by supplying a current pulse to special corrective coil. The discharge pulses with duration up to 400 msec and mean conductivity up to 5.10^{16} CGSE were obtained due to the improved chamber outgassing and providing a pulse correction.

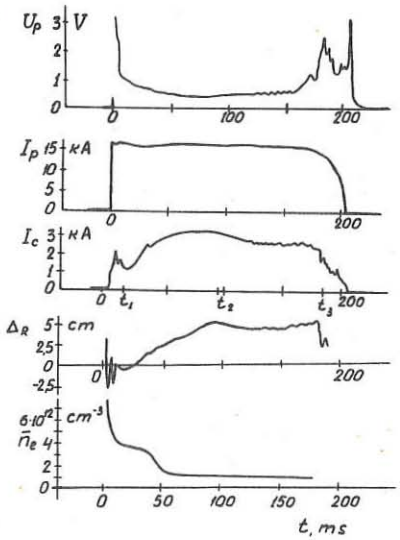


Fig.1. Discharge voltage, current, corrective coil current, plasma column shift and electron density.

The experimental results shown below are obtained at the 8.2kG longitudinal magnetic field and whith the gain factor of the con-

trol system being K=1.8 (in our case K=2.5 corresponds to the superconductive slitless shell).

Fig.1 shows a typical set of discharge oscillograms at the initial pressure of hydrogen $P_o = 4.10^{-4}$ torrs and the equivalent time constant of the control coil τ_e= 200msec. It follows from the interferometric measurements that the initial electron concentration in the discharge first falls rapidly with a time constant of about 10 msec and then substantially slower. This fall may be accounted for presumably by the sorption of the hydrogen coming in the form of ions or charge exchange neutrals by the chamber surface, which results in the concentration fall time being close to the time of ion diffusion. Further, this process is slowing down due to the increase in the reverse flow of hydrogen from the chamber surface to the plasma.

It can be seen from the oscillograms that there are three principal stages in the discharge[3]. In the initial stage ($0-t_1$) the plasma column is macro-unstable, interacts strongly with the diaphragm, which is indicated by intensive impurity lines, and has low conductivity. The duration of this stage depends substantially on P_o, decreasing with the decrease in pressure, and slightly on τ_e. The energy distribution of charge exchange atoms at $P_o=8.10^{-4}$torrs differs from the Maxwellian one, which is characteristic of unstable regims[4].

In the second stage (t_1-t_2) the plasma column is macroscopically stable, interacts weakly with the diaphragm and displaces to the outer wall of the chamber. The plasma conductivity and energy content increase while the radius decreases.

In the third stage (t_2-t_3) the discharge voltage increases, intensive impurity lines appear, the plasma column does not practically shift and touches the diaphragm with its outer side.

Fig.2 shows the dependence of

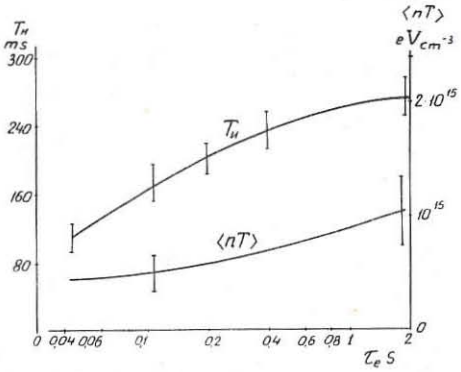


Fig.2. Dependence of the pulse duration and plasma energy content on τ_e, $P_o = 4.10^{-4}$tor.

the discharge macrocharacteristics on the equivalent time constant τ_e changing in the range of 0.04 - 2 sec.

It is seen that the discharge duration T and mean energy content determined from the diamagnetic effect increase monotonously. The increase in the conductivity averaged over the pulse is also observed. These changes give an evidence that the thermoisolation of the plasma column improves with the increase of τ_e.

To minimize the energy losses from the plasma in the third discharge stage the attempt was made to confine the plasma column near the geometrical axis of the chamber by its pulse shift along the major radius. For this purpose 2 msec voltage pulses were simaltaneously supplied at the moments t_1, t_2 and t_3 (Fig.3) to the in-

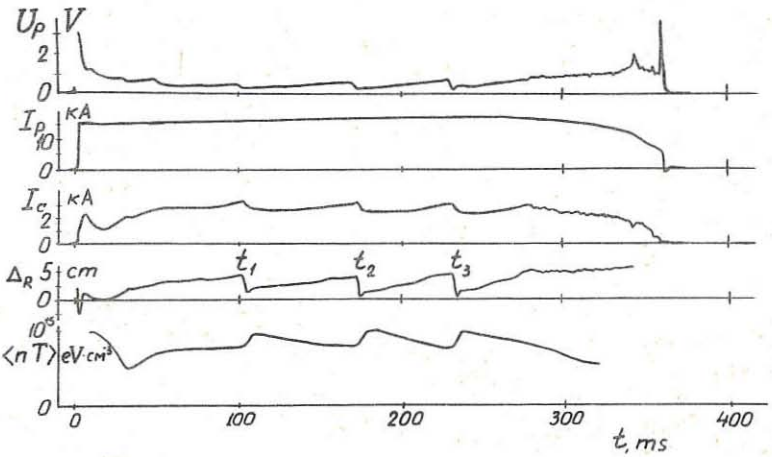


Fig.3. Discharge characteristics; t_1, t_2 and t_3 are the moments of pulse supplying at the regulators.

puts specially provided for all the regulators. It is seen that the plasma column conductivity and energy content calculated by the diaphragm radius increased additionally after the pulses had ceased. It follows from these data that the energy lifetime increases by 2 to 3 times after the plasma column has been taken from the diaphragm.

In our experiments the recurrence of plasma pulses is reasonably good if the chamber is outgassed and corrective magnetic fields are properly selected. The deviation of the corrective magnetic

field by 10 percent of the optimal value or deterioration of the vacuum conditions results in the decrease in the pulse duration by 2-3 times.

That the discharge ceases with a magnetic flux still existing in the iron core seems to be due to developing instabilities. The measurement of the plasma column skin-radius at 8 khz indicates (Fig.4) that in this case the plasma column radius is decreased and stability margin q is near unity by the time the pulse ceases. When the discharge ceases because of the saturation of the iron core $q > 2$ during all the discharge pulse.

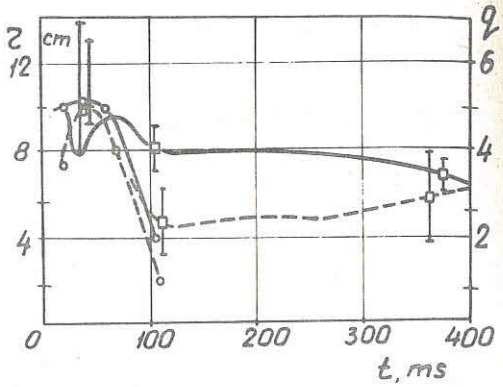


Fig.4. Plasma column radius (solid line) and stability margin (dashed line) —□— $P_o=4.10^{-4}$ torr —○— $P_o=8.10^{-4}$ torr

The plasma parameters on the Tokamak with the automatic system for controlling the equilibrium could be improved by increasing the gain factor of the regulators. The limitations could arise due to the instability of the controlling system or due to distortion of the magnetic surfaces at large β_J.

The assistance of N.N.Shwindt with the measurements of the impurity line intensities is gratefully acknowledged.

REFERENCES:

1. О.І.Кухтенко, Ю.І.Самойленко. Автоматичне керування плазмовими об'єктами. Вісник Академії Наук Української РСР, 3, 1971.

2. Л.И.Артеменков и др.Труды IУ Международной конференции МАГАТЭ по физике плазмы и управляемому термоядерному синтезу,1971,С -28,С-3.

3. Л.И.Артеменков, Козлов П.И., Мелихов П.И., Мухин П.А., Пашков Л.Н. Письма в ЖЭТФ, 17, 5, 1973 г.

4. Н.В.Иванов, И.А.Кован, П.И.Козлов, Е.В.Лось, В.С.Свищев, Н.Н.Швиндт, Письма в ЖЭТФ, 16, 88, 1972 г.

6th European Conference on Controlled Fusion and Plasma Physics, Moscow, 1973

PLASMA EQUILIBRIUM IN CLEO-TOKAMAK

J. Hugill, J.W.M. Paul, G.W. Reid and P.E. Stott
U.K.A.E.A. Culham Laboratory, Abingdon, Berkshire, England

ABSTRACT

Tokamak discharges of up to 77kA (q = 4) lasting for > 110ms are obtained in a stainless steel vacuum vessel ($\tau \approx 0.5$ms), using an externally applied vertical field for equilibrium. Various field configurations with slopes ($m = \frac{R}{B}\cdot\frac{dB}{dR}$) from - 0.75 to + 1.6 have been used.

INTRODUCTION

The principal features of Cleo-Tokamak have been described[1]. Equilibrium is obtained in a stainless steel torus, without a liner or copper shell, by applying vertical field from external windings. The limiter, consisting of 1.2cm diameter molybdenum rod radiussed to 18cm, is in two halves which can be separated vertically to control the plasma diameter. Diameters of 30cm and 36cm have been used, and lately the lower half of the limiter has been completely withdrawn without affecting the discharge noticeably. At the larger diameter the minimum distance of the plasma boundary from the vacuum vessel wall is $\lesssim$ 1 cm. The maximum toroidal field is 20kG, and the machine is usually operated at this value, for which the q = 1 current is 360kA at r_{plasma} = 18cm. The working gas is hydrogen except where stated.

DIAGNOSTICS

The main diagnostics used for equilibrium studies are a Rogowski for plasma current, gap volts, $\int$ndl from 2mm and 4mm microwave zebra-stripe interferometers and coils on the outside of the vacuum vessel measuring the position of the current channel. The outputs of three such coils placed at different azimuthal positions around the torus, differ by < 1cm, showing that the current channel moves in a horizontal ring concentric with the major axis, i.e. parallel to B_φ.

START-UP AND CONDITIONING

The conductivity temperature, T_σ, increased from 7eV to 90eV[1], during the first few thousand discharges, as described in[1]. Initially the current is well centred in the vacuum vessel for a range of vertical field, and with the radial field arising from B_φ field errors and the non-symmetrical position of the core bias winding, uncompensated. As T_σ increases it is necessary to compensate the radial field and adjust the vertical field correctly to position the discharge centrally.

At present typical discharges have $T_\sigma \sim 130$eV[1] at peak current. The

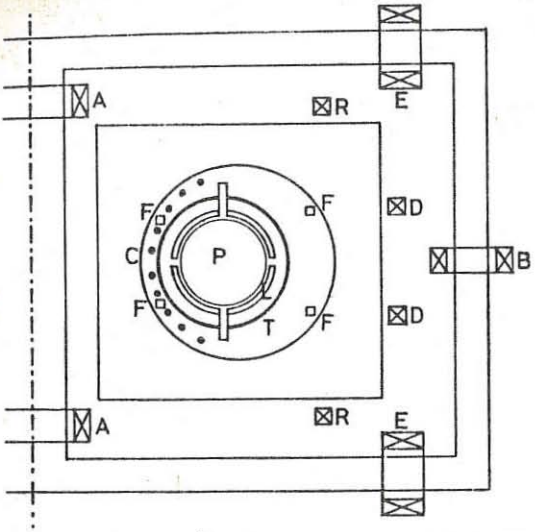


Fig. 1 Showing the various windings on the apparatus:
A, B, E windings on the core;
C, D vertical field winding;
R radial field winding;
F feedback winding;
P plasma region;
T vacuum torus;
L limiter.

The iron core has two external limbs.

current rises to $\gtrsim$ 80% of its peak value in 10ms during which time the density is increasing rapidly. In this phase the plasma position is usually well-centred, even when the vertical field is not quite correct and only starts to move appreciably at later times. We believe that neutral gas inflow and/or ionization processes within the plasma column still have a beneficial effect on the equilibrium in centring the discharge to some extent.

EXTERNAL VERTICAL FIELD SYSTEM

The theoretical work of Greene et al.[2] was used as a basis for designing the vertical field system. An isolated, perfectly conducting, current-carrying plasma with a radius of 18cm, a parabolic current distribution and $\beta_\theta = 0.5$, should require a vertical field of 3.87G/kA plasma current for equilibrium. The field gradient, $m = \frac{R}{B}\frac{dB}{dR} < 0$ for vertical stability and $m > -1.9$ for horizontal stability.

External vertical fields arise from several circuits. In general the vacuum fields of the currents are modified by the presence of the iron transformer core. The most important of the windings producing vertical field are shown in Fig. 1. The vertical field winding itself is in two sections with 10 turns at C, and 10 turns at D. Currents are in opposite directions in each so that the winding does

---

[1] Value in the centre of the discharge assuming a parabolic current distribution with the same diameter as the limiter, and a corresponding radial variation of conductivity and temperature, Z = 1.

not link the core. The field produced is 9.0 Gauss/kA-t, with m = - 0.75, so it should provide stability for radial and vertical motion.

The primary winding on the transformer core, and the plasma current itself also provide vertical fields of order 1.0 Gauss/kA-t with typically 2:1 azimuthal variation because of the azimuthal nonsymmetry of the core.

EXPERIMENTAL RESULTS

Three configurations of vertical field have been used. Originally the primary had 10t on the centre limb of the core and 2t total on the outer vertical limbs. The fields of the primary and the plasma current itself nearly cancel, producing no net effect on the equilibrium. About 40% of the primary current through the vertical field winding (adjusted by means of a parallel shunt) is required to centralise the discharge. The corresponding vertical field at the plasma is 3.2 Gauss/kA of plasma current, with m = - 0.75. Best conditions, obtained after 3500 shots are: I_{peak} = 44kA, pulse length > 50ms, $\bar{n}_e \sim 1.7 \times 10^{13}$ cm^{-3}, $T_\sigma \sim$ 90eV at peak current.

After some 4000 shots the inner half of the vertical field winding failed. Operation was continued using the outer half compensated by 10t placed on the horizontal limbs of the transformer at E in Fig. 1. This gives a smaller vertical field with positive slope: 2.6 Gauss/kA-t, m = + 1.6. This field is too small for equilibrium, and the plasma moved outwards until disruptive instabilities occurred. Since m > 0, vertical instability of the current channel was anticipated, but not observed. However, the discharge was extremely sensitive to exact compensation of the radial field. The best conditions obtained in helium are: I_{peak} = 32kA, $T_\sigma \sim$ 74eV, pulse length 45ms.

At present a completely different configuration is used. The primary winding is positioned on the horizontal limbs of the transformer. The vertical fields from the primary and plasma together now amount to 2.4 Gauss/kA of plasma current, 70% of the field required for equilibrium, but with a 1.0 Gauss/kA variation in azimuth: m ~ - 0.45 ± 0.3. The remainder of the vertical field is provided by 10t at D and 10t at A, Fig. 1, suitably shunted. The combined vertical field is estimated to be 3.2 Gauss/kA with slope m = - 0.3 ± 0.2. The best conditions obtained after 11,000 shots, are: I_{peak} = 77kA, $\bar{n}_e = 2.5 \times 10^{13}$ cm^{-3}, $T_\sigma \sim$ 130eV, pulse length > 110ms. The pulse is terminated after a rapid outward motion of the plasma when the transformer core is nearly saturated.

CONCLUSIONS

Tokamak equilibrium is obtained in a simple stainless steel vacuum vessel without using a copper shell by applying the correct amount of vertical field. Fields with radial slopes, between m = - 0.75 and m = + 1.6 have been used successfully. Azimuthal variations of ~ 30% do not seem to have any detrimental effect. There is some evidence that other processes such as ionization at the plasma boundary are partly effective in positioning the current channel.

ACKNOWLEDGMENTS

The authors gratefully acknowledge the work of the Cleo Engineering and Design team and the Cleo Operations team in making this work possible.

[1] A. Gibson et al. "The Cleo Tokamak Experiment" Garching Conference on Toroidal Confinement (1973).

[2] J.M. Greene, J.L. Johnson and K.E. Weimer "Tokamak Equilibrium" Phys. Fluids 14, 671 (1971).

EFFECT OF SHAPING FIELDS ON DOUBLET DISCHARGES

T. Ohkawa, T. H. Jensen, M. S. Chu, R. K. Fisher, and C. L. Hsieh

Gulf General Atomic Company
San Diego, California, USA

Abstract: The effects of the external shaping field on Doublet II discharges are studied both experimentally and theoretically. With an appropriate shaping field, a long-lasting Doublet configuration has been obtained.

INTRODUCTION

Axisymmetric toroidal configurations with noncircular cross sections have potentially a great advantage of being able to confine plasmas with a higher β over the configuration with circular cross sections. Doublet configurations which have three magnetic axes have already been discussed.[1,2]

Since the main part of the poloidal magnetic field is produced by the plasma current, the configuration must be in a stable mhd equilibrium. The shape of the equilibrium configuration depends on the magnetic boundary condition, the current distribution of plasma and to a lesser extent on β. The magnetic boundary condition may be determined either by a conducting wall which dictates the shape of the outermost flux surface, by an external field, or a combination of both. The conducting wall has the advantages of being simple and of providing stability against an axisymmetric displacement of plasma. The disadvantages are the limit on experimental time due to the skin effect of the wall and the impracticability of changing the shape readily. The external field method is more complicated in that the current in the coils must be programmed to be proportional to the plasma current. Also the circuitry must be designed to insure against the instability.

The current distribution in the plasma is determined by the temperature distribution for slow discharges where inductive effects are negligible. The temperatures of the flux surfaces free from the limiter are governed by the balance between the ohmic heat input and the heat transport across the magnetic field. Whereas the temperature of the flux surfaces eclipsed by the limiter depends on the balance between the ohmic and cross field heat input and the heat loss due to the parallel heat conduction to the limiter. For most experimental conditions, the temperatures of the eclipsed flux surface stays very much lower than those of the free surfaces. Therefore, the calculation of mhd equilibrium with the assumption that the outermost free flux surface is a free boundary with a vacuum region outside of it is a good approximation.[3] Because of the inherent

nonlinearity of the problem, the solution is not unique even when a linear equation is used inside the free boundary. Some of the results of these theoretical calculations and the comparison with the experimental results obtained in the Doublet II device where the boundary condition is given by a conducting wall has already been reported.[4-6] In this paper, the results, both theoretical and experimental, with the superposition of an external field on Doublet II plasma will be discussed.

DOUBLET II

The device[3] and the behavior of the discharges have been reported earlier.[4-6] It was found that the discharges in several msec make the transition from Doublet to Droplet configuration, i.e, plasma current flows mainly inside the separatrix which intersects the limiter.

A set of shaping coils designed to give a combination of a vertical and a quadrupole field in the plasma region has been installed. Because of the presence of the copper field shaper, the shaping field cannot be programmed and is dc. However, by maintaining a constant value for the plasma current, the relative strength of the field produced by the plasma current and the external field may be kept constant except early in the discharge.

The magnetic characteristic of a discharge with an external field are shown in Fig. 1. Toroidal field of 6.7 kG and hydrogen filling pressure of 1×10^{-3} Torr are used. The external field is a mirror-shaped vertical field and is about 60 G in the plasma region. The top trace shows the plasma current reaches 110 kA at 12 msec. The second trace is the loop voltage and shows no visible spikes. The conductivity temperature estimated without the corrections due to impurities or toroidal effects at the peak of the current is approximately 100 eV. Two typical traces of the magnetic probe signals are also shown. One (B_{23}) is located on the median plane and the other (B_{15}) is near the bottom elliptic magnetic axis. The relative sizes of these signals stay roughly constant except in the early phase of discharge, indicating the magnetic configuration is maintained for 20 msec. Also these signals do not show fluctuations. A similar discharge without the external field shows a very small signal on the median probe B_{23}, which is the indication of Droplet discharge. The fact that the signal of probe B_{23} became about half as large as the signal of probe B_{15} indicates the configuration is significantly affected by the shaping field.

Magnetohydrodynamic equilibrium calculations were made to be compared with the observed magnetic field distribution. The external field is added to the calculation described earlier.[7] The adjustable parameters, β_p (poloidal β) and γ (the ratio of current density at the elliptic axes and the free boundary)

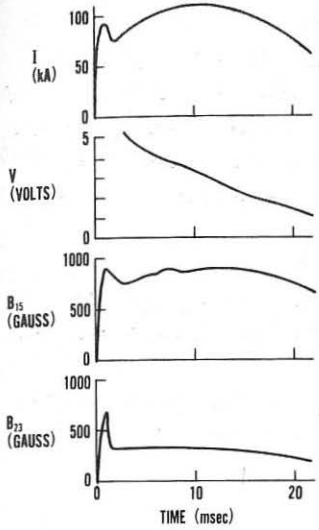


Fig. 1

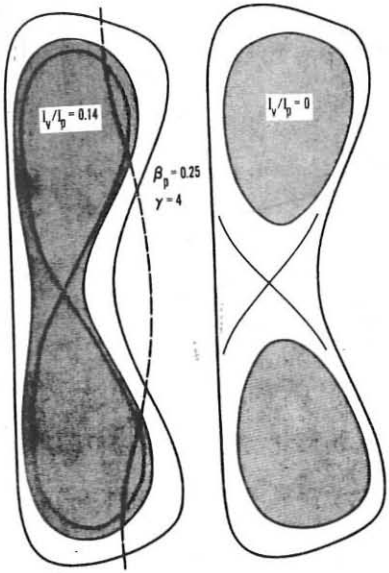


Fig. 2

are chosen to fit the measured magnetic field distribution. Two magnetic configurations corresponding to the discharge shown in Fig. 1, and a similar one without the external field are depicted in Fig. 2. The dotted line indicates the shape of the external magnetic field. The effect of the external shaping field is apparent in the figure. The Droplet configuration is converted to a Doublet configuration by the external field.

The survey of the calculated configurations shows that the discharge with the present copper shaper and limiter system should take the Droplet form unless the current density is uniform or of skin distribution ($\gamma \leq 1$). The experimental results support this result. However, with external shaping field, a Doublet configuration may be obtained with a peaked current distribution ($\gamma > 1$), according to the calculation. The configuration shown in Fig. 2 confirms the prediction, since the best fit with the observation is obtained with $\gamma = 4$, and the configuration is a Doublet.

In summary, the effects of the external shaping field are studied both experimentally and theoretically. With an appropriate shaping field, a long-lasting Doublet configuration has been obtained.

Work supported by the U.S. Atomic Energy Commission, Contract No. AT(04-3)-167, Project Agreement No. 38.

REFERENCES

[1] T. Ohkawa, Kakuyugo-Kenkyu 20, No. 6, 557 (1968).

[2] Tihiro Ohkawa and Torkil H. Jensen, Plasma Physics 12, 789 (1970).

[3] Arthur A. Schupp, Torkil H. Jensen, and Tihiro Ohkawa, in the IEEE Transactions on Nuclear Science, Vol. NS-18, No. 4 (August 1971), pgs. 55-59.

[4] T. H. Jensen, et al., in Proceedings of Fifth European Conference on Controlled Fusion and Plasma Physics, Grenoble, France (Aug. 21-25, 1972) Vol. I, pg. 4.

[5] R. K. Fisher, et al., Bull. Am.Phys. Soc. Vol. 17, 1056 (1972).

[6] "Characteristics of Doublet II Discharges," by T. Ohkawa, et al., Invited paper at the Third International Symposium on Toroidal Plasma Confinement, Garching, Germany (March 26-30, 1973).

[7] Ming Sheng Chu and D. Dobrott, Bull. Am. Phys. Soc. Vol. 17, 1056 (1972), and Ming Sheng Chu and T. H. Jensen, Bull. Am. Phys. Soc. Vol. 18, 708 (1973).

THE FIRST EXPERIMENTAL RESULTS IN FINGER RING TOKAMAK

A.V.Bortnikov, Yu.T.Baiborodov, N.N.Brevnov, V.G.Zhukovskii, L.E.Zakharov, D.V.Orlinskii, V.I.Pergament, N.K.Romanovskii, N.I.Sokolov, A.M.Us

I.V.Kurchatov Institute of Atomic Energy, Moskow, USSR

L.A.Artsimovitch and V.D.Shafranov have shown[1] that it is possible to increase the maximum current in the Tokamak by altering the shape of the plasma ring cross section, namely, elongating it along the axis of symmetry. In this report some experimental results of the investigation of the form of plasma cross section in finger ring Tokamak are represented[2].

Design of the divice. Fig.1 shows the main design features of the finger-ring Tokamak. The major radius R_0=36 cm. The dimansion of the working volume is limited by the tungsten limiter along the major radius $2l_r$=14 cm, along the main axis of symmetry $2l_z$=56 cm. The degree of alongation is l_z/l_r=4. Maximum longitudinal magnetic field is 15000 Oe at the axis. An electric field is excited by means of the air-core transformer. A rectangular vacuum chamber is made in the form of two semitoroids of stainless steel 5 mm thick. A copper shell inserted into the chamber is supposed to produce the elongating shape of the plasma ring cross

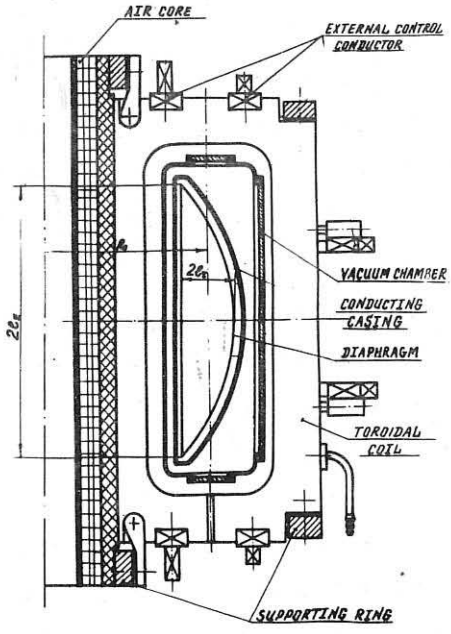


Fig.1

section and to maintain it in equilibrium. The skin time τ_s is less then the current pulse duration τ but $\tau_s > \tau$ when the shell is cooled by liquid nitrogen. To maintain the equilibrium in the first case an additional magnetic field can be generated with the help of six current loops.

The fact that the below results were obtained under poor vacuum conditions (the chamber was not baked) did not prevent the main aim of the preliminary experiments: pre-start-up check and determination of the degree of plasma column cross section elongation.

Experimental results. Fig.2 presentes typical traces taken with the current loops being switched off and warm shell. The duration of a discharge current pulse did not exceed 15 msec. This value is close to the skin time of a warm conducting shell.

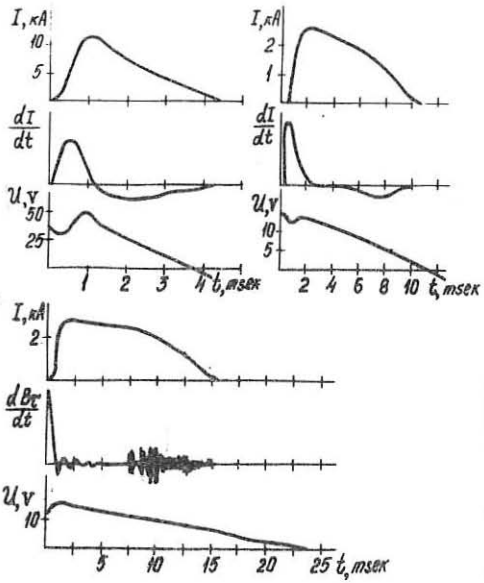


Fig.2

The location of the current centre as well as the degree of plasma column elongation was determined from probe measurements /3,4/. Eleven magnetic probes (Fig.3) were placed near (0,5 cm) the inner surface of the shall. A typical traces of a magnetic probe signal dB /dt from the central plane is shown in Fig.2. It is seen that about 10 msec. after the beginning of the discharge intense oscillations generate as the current aharply decreases. Appearance of the oscillations and decrease in the discharge current

at a positive loop voltage indicate that the lack of equilibrium take place. A number of integral plasma characteristics can be determined from tangential and normal components of the magnetic field measured along a contuor enveloping the current. The distribution of the tangential magnetic field B_φ along the contour is given

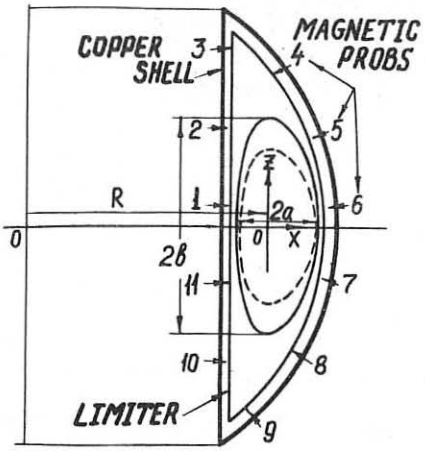


Fig.3.

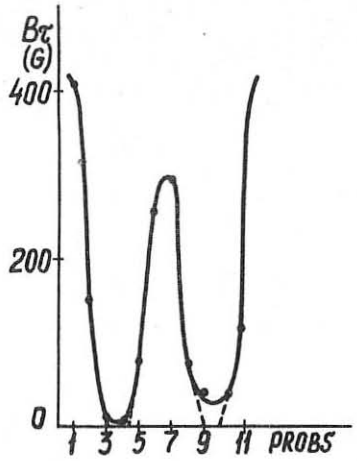


Fig.4.

in Fig.4 The estimations based on this distribution (the normal component near the shell walls is supposed negligibly small) show that the centre of the current channel is near the axis (R=36,5 cm, Δ 0,5 cm) during almost the entire discharge time. These estimation assumed the plasma current to be uniform, the plasma column cross section to cunsist of too semi-ellipsoids with common major semiaxis and different minor semiaxis, the plasma to accupy the space between the major semiaxis and the limiter (this is the minimum elongation case). Since B_φ is small near the tops of the shell it is difficult to measure it with sufficient accuracy. To evaluate a pos-

sible error the field B was assumed to be zero in this part of the contour. (Dotted line in Fig.4). The corresponding shape of the plasma column is also designated by the dotted line in Fig.3. The degree of elongation is $b/a = 2$. Taking into account the measured values (solid lines) $b/a = 2{,}6$. Thus, the minimum degree of elongation determined from magnetic probe measurements 2. Fig.5 shows a

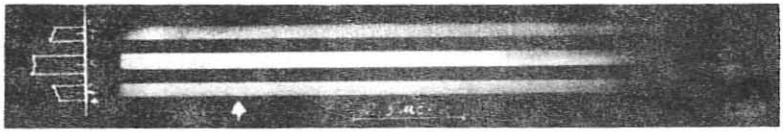


Fig.5

photograph of the discharge taken in visible light. Assuming the light emmission intensity is proportional to the current density one may conclude that the plasma column is stretched along the main axis of the device symmenty.

The current, probe and photographic measurements taken together show that formation and behavior of the plasma column in a finger-ring model Tokamak are consistent with theoretical predictions: the plasma column is elongated along the main axis of the symmetry, being in equilibrium during the shell skin time.

Acknowledgement. The authors are very thankful to academician L.A.Artsimovitch for the formulation of the problem and V.D.Shafranov for very useful discussins.

References:

1. L.A.Artsimovitch, V.D.Shafranov. JETP Pis'ma, 15, 72 (1971).
2. A.V.Bortnikov et al. "First International Symposium on Toroidal Plasma Confinement", Garching, Report B-5 (1973).
3. V.D.Shafranov, Plasma Physics, 13, 757 (1971).
4. V.D.Shafranov, L.E.Zakharov, JTP, 43, N2, 225 (1973).

DYNAMIC STABILIZATION OF A PLASMA IN STELLARATOR AND TOKAMAK MACHINES

by

R.A.Demirkhanov, A.G.Kirov, V.N.Zharikov, N.I.Malikh, L.F.Ruchko, G.I.Astapenko, V.A.Zhdanov

Sukhumi Institute of Physics and Technology of the State Committee on Utilization of Atomic Energy, Sukhumi, USSR

ABSTRACT: The paper gives the results of experimental investigations of plasma dynamic stabilization in stellarator (R-O) and tokamak (RT-4) machines at small q by means of a H.F. quadrupole magnetic field and a H.F. magnetic field of zero mode type.

It follows from the theory[I] that the MHD stability of a magnetized plasma with a current at small q can be improved using H.F. fields with megacycle ranges of frequencies of relatively small magnitude.

The paper describes the results of experimental studies on dynamic stabilization of magnetized toroidal plasma columns with a quasistationary current by means of a helical H.F. quadrupole magnetic field (R-O machine) and a H.F. field of zero mode (RT-4 machine). The aim of these researches is to reduce the safety factor q. Though the R-O machine is of stellarator type, the conclusions on the MHD stability of a plasma in it, as a matter of fact, can be applied to the systems of tokamak type.

The machine "R-O" is a l = 3 stellarator. A rotating helical H.F. quadrupole magnetic field is generated in it by a special helical windings. "RT-4" is a small tokamak without a liner, in copper casing which is in direct neighbourhood to the plasma. The copper casing serves also as a primary winding of an air transformer to excite both quasistationary and longitudinal H.F. currents in the plasma. The basic parameters of the machines are given in the table.

	d(cm)	D(cm)	B_z(kGs)	I_p(ka)	τ_{I_p}(mSec)	$\tilde{B}_\varphi$(Gs)	ω (sec^{-I})
R-O	I0	I00	I0	5	I	300	$3.I0^6$
RT-4	9	40	20	25	0,7	700	$2.I0^5$

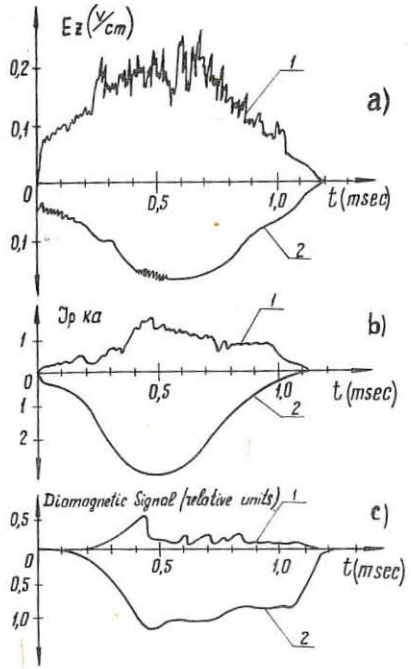


Fig.I.
I - Regime without a H.F. field,
2 - Regime with a H.F. field.

The R-O experiments have been carried out with the stellarator rotating transform angle $i = \pi$. Helium served as an operating gas. It follows from the experiments that when the H.F. field is absent, there exists the threshold value of I_{pcrit}, above which the current in the plasma does not rise on increasing the voltage on the loop. On increasing B_z, the critical current value grows. At $Ip = Ip_{crit}$, a strong helical instability of a plasma column of m = 2 mode is observed. In such a case, for the traces of the voltage on the loop (Fig.Ia), of the current in the plasma (Fig.Ib), of the diamagnetism (Fig.Ic) and the plasma density, we observe intense low frequency oscillations and "spikes". In such regimes, the plasma temperature ($n_e = 10^{13} cm^{-3}$) does not exceed $Te \approx 20$–30 eV.

On superposing a stabilizing H.F. quadrupole magnetic field on a current-carrying plasma column, the level of low frequency oscillations considerably reduces (Fig. Ia, b, c). The helical structures on scanning the plasma column luminosity dissapear simultaneously. In a stabilized regime the quasistationary current in the plasma may exceed the threshold current value Ip_{crit} several times. The threshold dependence of the column macroscopic stability upon the ratio $\frac{\langle \tilde{B}_\varphi^2 \rangle}{B_3^2}$, (Fig. 2), is characteristic for a stabilized regime of the discharge. The plasma diamagnetic temperature in a stabilized regime at $n_e \approx 2{,}5 \cdot 10^{13} cm^{-3}$ reaches $T_{diam} \approx 100$ eV. In a stabilized regime at $\frac{\langle \tilde{B}_\varphi^2 \rangle}{B_3^2} \approx 0{,}4$ and $q_{eff} \approx 1$, the H.F. field pressure and the current field pressure, too, are essentially less than the plasma pressure, i.e., $\tilde{\beta}\varphi \approx \beta_3 \gg 1$.

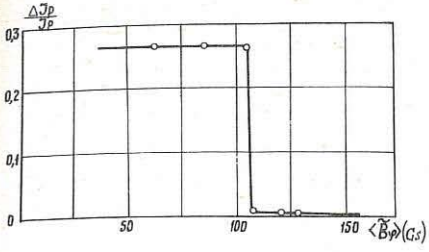


Fig. 2.

The current discharge experimental study in RT-4 shows that a typical tokamak regime is realized in it[2]. The plasma column radius is $a_{pl} \approx 3{,}5$ cm. The typical experiments have been carried out at B_z = I5 kGs, hydrogen being an operating gas. Two different regions of regimes have been observed in the experiments. At $q > 3$, the discharge is stable, all the diagnostic signals are smooth. The plasma density in such conditions is $n_e \approx 3 \cdot 10^{13}$ cm^{-3}, and the plasma electron temperature determined from the conductance is $T_\sigma \approx 60$ eV, being measured spectroscopically, $T_e \approx 90$ eV. The energetic life time $\tau_E \approx 30$–40 μ Sec. On increasing the quasistationary current, i.e. reducing $q (q < 3)$, the discharge becames unstable. In diagnostic signals (Ip, U , n_e, H_β, OII , E_γ – soft X-ray emission) there arise low frequency oscillations, sharp spikes of the voltage are observed which indicate the change of the plasma column structure, as it is typical for tokamaks. At $q < 3$ the temperature and τ_E is much smaller.

In the regimes with $q < 3$, the H.F. current packet has been generated through the plasma column (Fig. 3c). On switching the H.F. current, the low frequency oscillations in all of the diagnostic signals reduce; the voltage loose sharp "spikes"(Fig. 3b). (In Fig.3b, as distinguished from Fig.3a, the signals are filtered

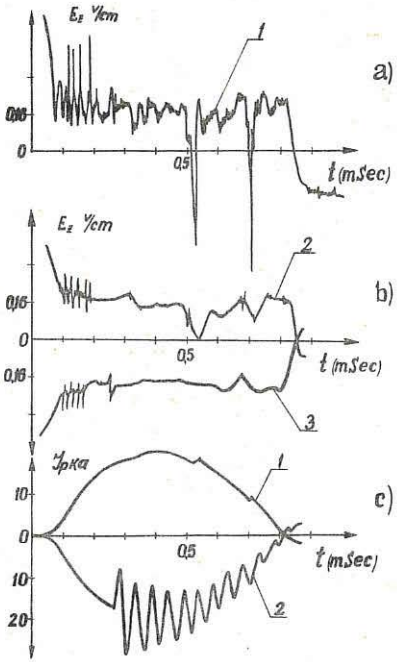


Fig.3. B_z= I5 KGs.
I – Discharge without a H.F. current.
II – Discharge with a H.F. current.

taking away the frequency equal to the H.F. field frequency). The characteristic feature of the stabiliztion regime is (similar to the conditions in R-0) the threshold dependence of the stabilization onset upon the ratio $\frac{\beta_\varphi}{\beta_3}$. In RT-4 at $q \approx 2$, the stabilization occurs at $\frac{\beta_r}{\beta_3} \approx 1/3$. On the basis of the experimental results obtained in RT-4, one can conclude that the H.F. longitudinal current presence in tokamaks can avoid the "spike" instability rise and contribute to lowering the safety factor q.

References

1. V.P.Sidorov, T.R.Soldatenkov, Nuclear Fusion, 12, 73 (1972).
2. L.A.Artsimovich, Nuclear Fusion, 12, 215 (1972).

An Axisymmetric Divertor in a Tokamak with a Tear Drop-like Cross Section (DIVA)

M. Yoshikawa, Y. Shimomura, H. Maeda, A. Kitsunezaki, and S. Mori
Japan Atomic Energy Research Institute, Tokai, Japan

Studies made in designing the axisymmetric divertor in a Tokamak device with a tear drop-like cross section are described.

1. Introduction

A Tokamak device (DIVA) with an axisymmetric divertor shown schematically in Figs.1 and 2 has a tear drop-like cross section with a major radius of 60cm and an average aspect ratio of 5.5. The toroidal field is 10kG. The objective of the experiment is to study plasma confinement in a Tokamak with a tear drop-like cross section and to examine the effect of a divertor on the confined plasma.

The equilibrium of the plasma is maintained by the divertor hoop and a copper shell covered by gold. A steady vertical field can also be applied. A set of movable shell may be placed at two positions. For plasma confinement without the diverter in operation the movable shell is placed at the "closed" position as shown in Fig. 2. The operation of the divertor is studied by moving the movable shell vertically to the "open" position. Particles escaping the confinement are guided along flux lines to the divertor plate. The plate is made of titanium and is periodically refreshed by flushing titanium alloy wires. Gold-plated limiters shown in Fig. 2 are manually movable.

We shall describe below considerations made in designing the divertor.

2. Magnetic Flux Required Between the Plasma and the Wall

The difference $\psi_{wall}-\psi_{plasma}$ in the flux function ψ between the plasma and the wall should be large enough to ensure that the bulk of particles lost from the confinement reach the divertor region. An analysis is made by assuming a collisional loss along flux lines with a time constant $\tau = 1.03\tau_{ii}\log_{10}R_m=\alpha T_i^{3/2}/n$ and a diffusional loss across flux lines with a banana diffusion coefficient times an anomaly factor γ, that is, $D=\gamma D_{banana}=1.12\gamma a_{ep}^2\varepsilon^{1/2}(1+T_i/T_e)/\tau_e=\gamma\delta n/T_e^{1/2}B_p^2$, where a_{ep} is the electron gyroradius in the poloidal magnetic field B_p, ε the inverse aspect ratio, and R_m the mirror ratio. The transport equation in the divertor flux surfaces is solved including the effect of a singularity in the flux volume $dV/d\psi \propto (\psi-\psi_s)^{-1+2/m}$ near the separatrix $\psi=\psi_s$ with the multipolar order m. Figure 3 shows, for various values of m, $\Phi_{wall}/\Phi_{plasma}$ the ratio of particle loss flux to the wall to the total loss flux as a function of $\psi_{wall}-\psi_{plasma}$. The unit of ψ is $\psi_1=\{2\alpha\delta\gamma T_{iav}^{3/2}/T_{eav}^{1/2}\}^{1/2}=23\gamma^{1/2}A^{1/4}Z^{-1/2}\varepsilon^{1/4}(\log_{10}R_m)^{1/2}(1+T_{iav}/T_{eav})^{1/2}\cdot(T_{iav}/T_{eav})^{3/4}T_{eav}(eV)^{1/2}$ G-cm. Here A and Z are the mass and the charge number,

respectively, of the ions. The figure shows that $\psi_{wall}-\psi_{plasma} > 2.5\psi_1$ is required for $\Phi_{wall}/\Phi_{plasma} < 0.01$. When a Bohm-like diffusion is assumed instead in the divertor flux surfaces a similar treatment can be made. Table I lists the maximum values of $\gamma=D/D_{banana}$ and $\gamma'=D/D_{Bohm}$ allowable for $\Phi_{wall}/\Phi_{plasma} < 0.01$.

A simple orbit analysis shows that the maximum separation between the drift and the magnetic surface is given by $\Delta\psi = \{(1-B_0/B_d)^{1/2}+(B_0/B)(1-B/B_d)^{1/2}\}$ (mv/e). Here B is the total magnetic field at the position where the separation is concerned, B_0 is the field at the intersection of the particle orbit with the median plane, and B_d the field at the divertor. The separation is the largest for $B = B_0$ and is $(2mv/e)(1-B_0/B)^{1/2}$. For a typical case of $B_d = 2B_0$ and $B_p = 2000$ G the separation is 1 cm and 0.3 cm for hydrogen ions of 100 eV and 10 eV, respectively, in energy.

3. Trapping Efficiency of Neutral Particles at the Divertor

The trapping probability on titanium of hydrogen ions with energies above 3 keV is over 0.9 up to a dose of 10^{19} cm^{-2}. Although no measurement has apparently been reported in the 100 eV range, the trapping efficiency should be substantial since the range of ions is more than a few lattice constants.

Trapping in the divertor of neutral particles backscattered at the divertor plate can be provided with a moderate sticking probability on titanium evaporated on the inner surfaces of the vacuum chamber. A Monte-Carlo calculation has been made on backstreaming process. The time-integrated influx N_{total} and backstreaming flux N_{back} to the plasma are shown in Fig.4 as a function of time. Table II summerizes the backstreaming fraction for H, H_2, O, and CO. The fraction can be held below 10 %. The sputtering yield of titanium by 100 eV hydrogen ions is in the range of 10^{-3}.

4. Backstreaming of Neutral Particles upon Ionization near the Divertor

The mean energy of neutral particles produced at the divertor plate by ion impact is in the range of 1-5 eV. These particles may be ionized when passing through the plasma near the divertor. A small fraction of those ions may enter the main bulk of the plasma. The plasma density near the divertor can be estimated as $n_d = (B/B_p) \cdot (S/2\tau_n v_i^* d) n_e$, where S is the cross-sectional area of the plasma, τ_n the particle confinement time, v_i^* the ion velocity at the electron temperature, d the width of the plasma sheet near the divertor, and n_e the plasma density of the confined plasma. The calculated probability of local ionization is shown in Table III. Most of particles in the eV energy range can go through the local plasma and then are absorbed in the aforementioned way. At the thermal velocity the ionization probability becomes substantial as shown in Table III.

5. Methane Problem

Titanium surfaces have practically no sticking probability with methane and worse can produce hydrocarbons upon interaction with hydrogen. The methane released from the surface at thermal velocity has a higher possibility of being locally ionized as seen in Table III.

The methane production can be limited by the supply of carbon. The major supply of carbon is the alloy wires which have carbon content of 150-300 ppm. A calculation shows that the total number of carbon atoms from the above source and others amounts to 20 % of that of hydrogen ions in the confined plasma. Since only a small fraction of carbon from the alloy wires would be available for the methane production and a small part of ions produced by local ionization will actually enter the plasma, the impurity level of the confined plasma would be much less than the above figure. Furthermore the Monte-Carlo calculation shows that the backstreaming fraction at 5 msec of methane molecules at the thermal velocity is less than 20 %, even if the sticking probability is assumed to be zero. This should help further reduce the backstreaming.

References

1. A.Kitsunezaki, H.Maeda, Y.Shimomura, and M.Yoshikawa presented at the International Symposium on Toroidal Plasma Confinement (Garching,1973) G-2

Cases	Case I T_e=300eV, T_i=100eV	Case II T_e=100eV, T_i=100eV	Case III T_e=30eV, T_i=10eV
	Plasma thermally well insulated from the wall	Electrons in the divertor flux surfaces cooled	Plasma poorly insulated from the wall
$\gamma = D/D_{banana}$ [1]	$\gamma < 90$ [1]	$\gamma < 30$ [1]	$\gamma < 900$ [1]
$\gamma' = D/D_{Bohm}$ [2]	$\gamma' < 0.01$ [2]	$\gamma' < 0.03$ [2]	$\gamma' < 0.6$ [2]

Table I Requirement for the diffusion coeficients in the divertor flux surfaces for particle flux to the wall to be less than 1 % of the total loss flux.
Assumed parameters in 1) hydrogen (A=Z=1), $\psi_{wall}-\psi_{plasma}$=2000G-cm, ε=0.2, and R_m=1.7
Assumed parameters in 2) hydrogen (A=Z=1), B=10kG, wall-plasma distance 2cm, τ_n=3msec minor radius 11cm, and R_m=1.7

Species	Sticking probability	Time 5 msec	Time ∞	Species	Sticking probability	Time 5 msec	Time ∞
H at 323 K	0.1	0.200	0.20	O at 323 K	0.1	0.095	0.20
	0.2	0.095	0.10		0.2	0.070	0.10
	0.3	0.070	0.07		0.3	0.060	0.07
H_2 at 323 K	0.05	0.25	0.35	CO at 323 K	0.1	0.080	0.20
	0.1	0.15	0.20		0.3	0.050	0.07
	0.2	0.10	0.10		0.5	0.025	0.01

Table II Time-integrated fraction N_{back}/N_{total} of backstreaming particles (see Fig.4)

Electron temperature		300eV		100eV		30eV	
Energy of atoms		5 eV	323 K	5 eV	323 K	5 eV	323 K
Species of atoms	H	0.02	0.13	0.03	0.19	0.004	0.02
	O	0.10	0.57	0.13	0.65	0.040	0.23

Table III Probability of local ionization of atoms emitted from the divertor plate Assumed parameters are $n_e=3\cdot10^{13}cm^{-3}$, $\tau_n=3$ msec, hydrogen(A=Z=1), and $B/B_p=2.85$

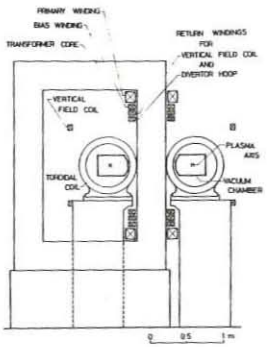


Fig.1 Cross section of the device

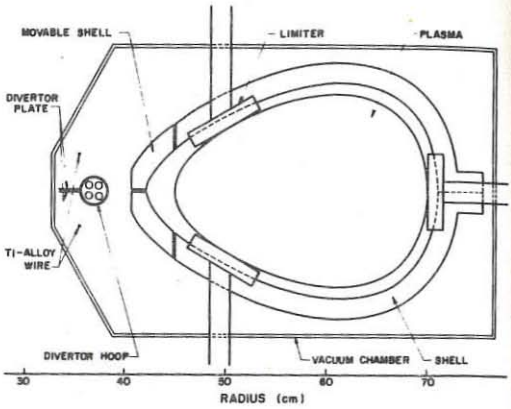


Fig.2 Cross section of the vacuum chamber

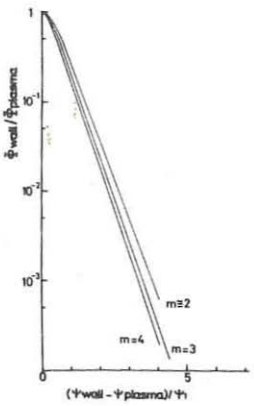


Fig.3 Ratio of particle flux to the wall to total particle loss flux

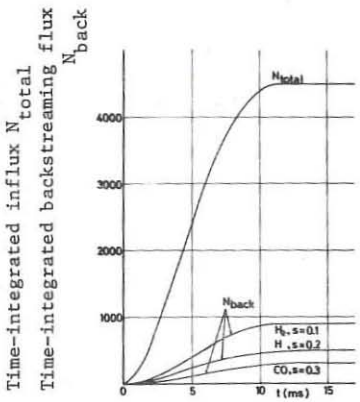


Fig.4 Time-integrated influx and backstreaming flux to the plasma

STUDY OF DYNAMIC STABILIZATION CONDITIONS OF TOROIDAL DISCHARGE IN MODULATED LONGITUDINAL MAGNETIC FIELD

M.A.Vasilevsky, E.G.Komar, I.M.Roife, E.V.Seredenko

D.V.Efremov Scientific Research Institute of Electrophysical Apparatus
Leningrad

In previous studies with Toloscope-device on dynamic stabilization (DS) of a toroidal discharge in a longitudinal magnetic field [1,2,3] one of the DS schemes based on the excitation of magnetosound oscillations of plasma column was used. In these experiments radial oscillations with $\omega > \gamma_{K\Phi}$ ($\gamma_{K\Phi}$ - instability increment of Kruseal-Shafranov at $q < 1$) at modulation of quasi-constant current was excited. In this case the current developed in plasma coincides in direction with an external magnetic field. Such a DS-scheme, besides the improvement of plasma column stability, provides the additional direct heating of ion component. In the above experiments the additional heating caused by radial oscillations was noted.

As known there exists another similar DS-scheme based on the modulation of a longitudinal magnetic field (a.c. current of the plasma is directed in the small circle of the torus and is perpendicular to the magnetic field). E.G.Komar was the first to propose this stabilization scheme in 1961. The studies conducted, for example, [4,5] showed its efficiency.

Our paper presents some results of the investigation of this DS-scheme on the Toloscope-device, having a toroidal quartz chamber with large and small diameters of

about 60 cm and 6 cm, respectively. The chamber is surrounded by a copper shell providing equilibrium and serving as a single-turn solenoid of constant and alternating magnetic fields. Quasi-constant current pulses with duration of about 100 μsec and alternating magnetic field pulses ($\omega = 7 \cdot 10^6$ sec^{-1}) of about 250 μsec were switched on at a flat part of the pulse of the quasi-constant magnetic field.

Fig.1 gives the distribution of fields over the section of the chamber for one of the regimes of the stabilised discharge: quasi-constant current $I_{-} = 6$ kA, quasi-constant field $H_{z-} = 400$ oe, the mean value of the alternating magnetic field outside the discharge $\bar{H}_{z\ell_{\sim}} = 240$ oe, the working gas (hydrogen) pressure $P = 2 \cdot 10^{-3}$ torr ($n \simeq 2 \cdot 10^{14}$ cm^{-3}).

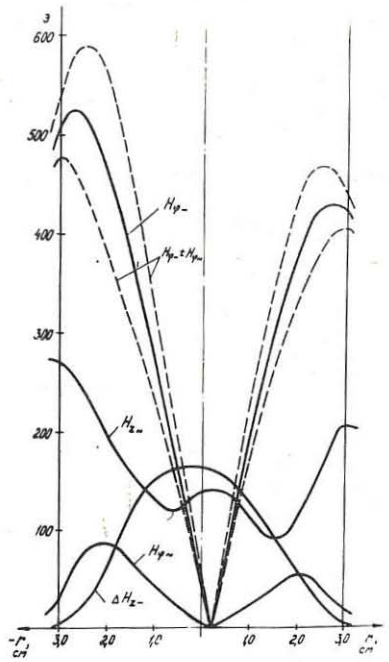


Fig.1

The distribution of the alternating magnetic field $H_{z_{\sim}}$ over the chamber section points out to its skinning. The rise of $H_{z\sim}$ in the centre of the chamber is defined by the oscillations of plasma column with frequency ω. The same oscillations define the appearance of alternating component of current field $H_{\varphi_{\sim}}$. The value radial oscillations $\varepsilon = \frac{\Delta a}{a}$ of plasma column can be estimated with the help of an ideal

MGD-model as $\frac{H_{z\sim}|_{z=0}}{2\bar{H}_{ze-}}$. The shape of the curve $\Delta H_z(z)$ makes it possible to estimate $\beta_\varphi \sim 0{,}8$. The asymmetry of curves relative to the small circle of the torus is defined by the toroidal-shape of the system. Taking the value of ε as a parameter and using the results of the experiments one can plot boundaries of stability regions on the plane $H_{\varphi-}$ - H_{z-} - similar to [2,3]. These regions are shown in Fig.2.

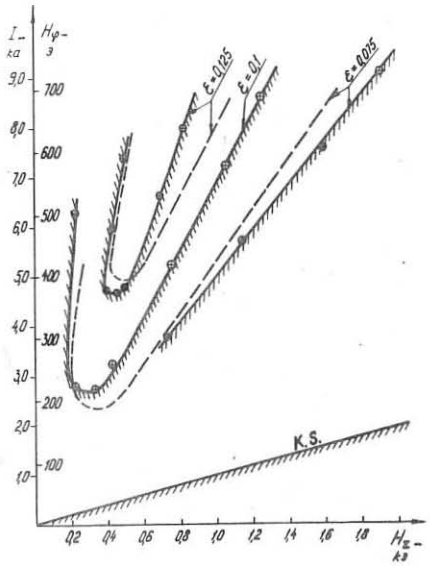


Fig.2

In the same fig. the curve K.S., where q=1, is given. Shading of boundaries is directed to the side of stability regions. Dotted lines show boundaries obtained for the scheme [2,3]. The close coincidence of the boundaries of stability regions by parameter ε for these DS - schemes proves once more the defining role of the radial oscillations for obtaining the plasma column stability.

The difference between the DS-schemes under consideration is that if for the scheme [2,3] as shows Fig.3 (for $H_{z-} > H_{\varphi-}$) the required stabilization value $H_{\varphi\sim} \simeq Const H_{z-}$ (dotted curves), then for the present scheme $H_{z\sim} \simeq Const H_{\varphi-}$ (solid curves). Namely, the required stabilization value $H_{z\sim}$ is practically independent on the field H_{z-}. Thus, the latter scheme can be effectively used in systems with high magnetic fields also.

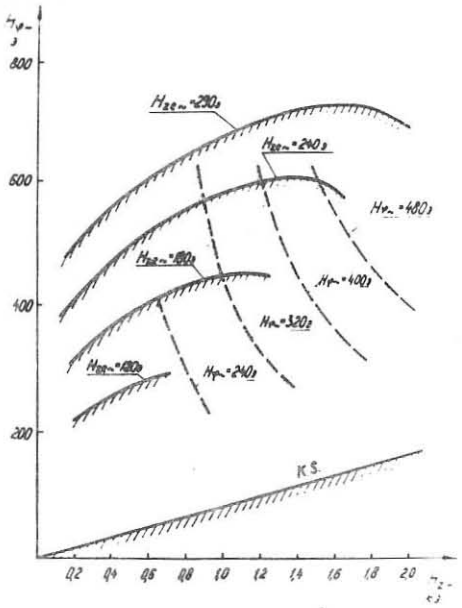


Fig.3

In our experiments we could obtain at relatively small fields $H_{z\sim} \lesssim 300$ oe the stabilized plasma column with current $I_- \simeq 9$ kA in fields H_{z-} up to 2 koe. At the same time in experiments [2,3] at $H_{z-} \sim 2$ koe we had to produce fields $H_{\varphi\sim}$ of much higher value to stabilize $I_- \lesssim 5$ kA.

It should be noted that in the experiments with the Toloscope-device small dimensions of the chamber and the decrease of conductivity $\sigma_\perp$ at the increase of H_{z-} and hence the reduced skinning of field H_{z-} led to the reduction of $H_{z\sim}$ at $H_{z-} \gtrsim 2$ koe ($H_{\varphi-} \lesssim 600$ oe) and respectively to the reduction of stabilization efficiency in this region of H_{z-}.

REFERENCES

1. M.A.Vasilevsky, I.M.Roife, E.V.Seredenko, rep. CN-28/Y-12, Madison, 1971.

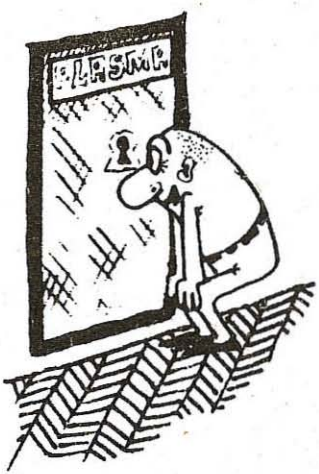
2. I.M.Roife, M.A.Vasilevsky, E.V.Seredenko, Proceedings V European Conference, v.1, p.75, Grenoble, 1972.

3. M.A.Vasilevsky, I.M.Roife, E.V.Seredenko, JTPh (USSR), 2320, 1972.

4. H.A.B.Bodin at all, Proceedings III European Conference, p.76, Utrecht, 1969.

5. G.Becker at all, Rep. CN-28/B-9, Madison, 1971.

1.8. TOKAMAKS: DIAGNOSTICS



NEUTRAL DENSITY DETERMINATION BY SCATTERING OF VACUUM-UV RADIATION

C.Breton and R.Papoular

ASSOCIATION EURATOM-CEA SUR LA FUSION
Département de Physique du Plasma et de la Fusion Contrôlée
Centre d'Etudes Nucléaires
Boite Postale n° 6. 92260 FONTENAY-AUX-ROSES (FRANCE)

Abstract.- The purpose of the diagnostic method to be described is to determine the spatial distribution of the neutral atoms density in a plasma machine, without having recourse to any conspicuous assumption regarding the statistical distribution of excited populations.

PRINCIPLE.-

Let a beam B of wavelength λ_b and bandwidth Δ cross a section C of the plasma, through a point P where the electron and neutral densities are respectively N_e and $N_1(cm^{-3})$. The neutral species to be measured is supposed to occur essentially in the ground state and to have a resonant frequency $1/\lambda_b$, corresponding to a transition with an absorption oscillator strength f_{1-2} and an Einstein emission coefficient A_{2-1} and a Doppler width $\Delta_D(H_z)$. If Δ is larger than the largest of A or Δ_D, and if I is the spectral radiance (photons Hz^{-1} cm^{-2} s^{-1}) of beam B and $S(cm^2)$ its cross-section at P, then, the number of photons per second which are absorbed in, and subsequently scattered by, a portion of length l(cm) of the plasma, centered on P, is

$$\Phi_s = 2.5 \times 10^{-2} \; I \; Sl \; N_1 f_{1-2} \quad (s^{-1}). \qquad (1)$$

Let Ω_d be the solid angle subtended by mirror M_d at point P, R_d its reflectance and η the quantum efficiency of the detector D, then

$$\Phi_d = \phi_s \; \frac{\Omega_d}{4\pi} \; R_d \; \eta \qquad (s^{-1}) \qquad (2)$$

is the number of photons detected per second. This is only true, of course, provided the optical thickness of the path from souce

to detector is much less than 1. Let T(s) be the duration of the exciting uv emission and RC > T the integration time constant of the electronics associated with the detector. Then, the signal delivered by the latter is

$$V_s = (\phi_d\ T)\frac{e}{C}\ M \qquad (v) \qquad (3)$$

where e is the electron charge, C is in Farads and M is the internal multiplication factor of the detector. For this signal to be detectable, it must emerge from the noise, which is mainly composed of Johnson and current noise ($V_{J,C}$), and shot noise, $R(\overline{\Delta i^2})^{1/2}$, where $\overline{\Delta i^2}$ is the mean square fluctuation of the current i_p in the detector, due to self-emission of the plasma at the resonant wavelength λ_b. In a Tokomak, this emission is due to excitation by electrons and may be estimated from

$$\phi_p = \overline{N_1\ N_e}\ Q_{1-2}\ U \qquad (s^{-1}), \qquad (4)$$

where Q_{1-2} is the excitation rate coefficient (cm^3s^{-1}) and $\overline{N_1\ N_e}$ the mean product of neutral and electron densities (cm^{-3}) in the plasma volume U(cm^3) encompassed by the acceptance angle of the detector. Then,

$$i_p = \phi_p\ e\ \frac{\Omega_d}{4\pi}\ R_d\ \eta\ M \qquad (A) \qquad (5)$$

and $\overline{\Delta_i}^2 = 2\ e i_p\ \delta\ M$, where δ is the bandwidth of the electronics (Hz). *Assuming shot noise is dominant over all other sources of fluctuations in the plasma or electronics,* the minimum detectable neutral density is given by $V_s = R(\overline{\Delta i^2})^{1/2}$, i.e.

$$(N_1)_{min} = \frac{40\ RC}{TIS1f}\left(\frac{8\pi\overline{N_a N_e}Q_{1-2}U\delta}{\Omega_d R_d \eta}\right)^{1/2} \quad (cm^{-3}) \qquad (6)$$

APPARATUS.-

We have built a high-radiance laser-plasma source emitting a continuous spectrum which behaves like that of a black body of temperature about 5×10^6°K over the range from 900 to 2000Å at least [1]. When actuated by an Nd-glass laser of 10 J and 40 ns, it emits a pulse of about 100 ns, with a spectral radiance of

3×10^{13} photons sr^{-1} $\mathring{A}^{-1}$ at $\lambda = 1200\mathring{A}$. A spherical concave mirror, 40 mm diameter, with a reflectance of 50 % at $1216\mathring{A}$ (Lyman α) subtending an angle of 10^{-1} sr at the source, can deliver a beam carrying 1 photon Hz^{-1} per pulse, and having a cross-section of 1 cm^2 at a distance of about 1 m. Somewhat better performance has been obtained by using a CO_2 - TEA laser of 10^J-0,2 μs, which is also much more practicable.

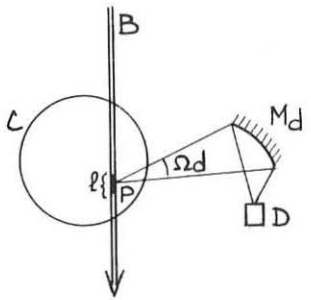
As a detector, we have used a proportional counter filled with NO at a few torrs, closed by a MgF_2 window of 20 mm useful diameter, and having a quantum efficiency > 0.4 at $1216\mathring{A}$.

The above source and detector can be used to measure the density of neutral hydrogen atoms by resonant scattering of Lyα. In a typical case, $\overline{N_1 N_e} = 5.10^{23}$ cm^{-3}, $Q_{1-2} = 3 \times 10^{-8}$ cm^3 s^{-1}, U = 100 cm^3, R = 10^5 Ω, C = 10^{-10} F, δ = 2.5×10^4 Hz, IST = 1 Hz^{-1}, l = 2 cm, f = 0.42, $\Omega_d = 10^{-2}$ sr, R_d = 0.5, η = 0.4, M = 1, so that, from (6), $(N_1)_{min} = 10^{10}$ cm^{-3}, with V_s = 55 μV and $V_{J,C} \simeq 20\mu V$. $(N_1)_{min}$ could be reduced to $\simeq 10^9$ cm^{-3} just by increasing the diameter of the source condenser mirror to 12 cm. Another factor 3 should be gained through improving the mirror reflectance to 90 % and operating the laser at its maximum energy of 15^J.

EXPERIMENTAL TEST.-

To test the feasibility of the proposed diagnostic, we have used the existing apparatus as described above to measure low densities of neutral Xenon, which has a resonance transition (^1S_o-$^1P_1$) at $1296\mathring{A}$, near the hydrogen Lyα, with f_{1-2} = 0.19. The conditions were : R=$10^6\Omega$, C=10^{-10}F, δ=10^5Hz, η=0.2, IST=0.3Hz^{-1}, l=1 cm, $\Omega_d=5\times10^{-3}$, R_d=1 (no mirror). The pressure was varied from 3×10^{-2}torr to 3×10^{-7}torr. For an atomic density of $10^{10}cm^{-3}$, the signal delivered was about 200 μV, of which about 100 μV were due to spurious scatter of incident light on the chamber walls. The electronics noise was 14 μV. The variation of the signal with gas pressure are as predicted by theory and the absolute values of the signal are in order of magnitude agreement with the calculation.

[1] C.Breton and R.Papoular, C.R.Académie Sc.(Paris) 1972, Report EUR.CEA.FC-667 (Oct.1972).



A KINETIC MODEL FOR THE NEUTRAL GAS BETWEEN PLASMA AND WALL

S. Rehker, H. Wobig

Max-Planck-Institut für Plasmaphysik,
Garching, Federal Republic of Germany

The role of the neutral particles penetrating a plasma is of interest for two reasons: firstly, because of charge exchange and excitation processes the neutral particles contribute to the energy losses, and secondly the charge exchange neutrals are used for diagnostic purposes[1]. A macroscopic description of the boundary layer of neutrals is given in[2], Y.N. Dnestrovskii et al.[3] consider the Boltzmann equation for the neutrals. In this paper we also start from the Boltzmann equation with charge exchange and ionization as elementary processes and take into account different reflection mechanisms on the wall. The plasma distribution functions are Maxwellian.
The time independent kinetic equation is

$$\underline{v}\cdot\nabla f_o = -\int |\underline{v}-\underline{v}'| \left[\sigma_{eo} f_e + \sigma_{io} f_i\right] d^3\underline{v}' \cdot f_o + \int |\underline{v}-\underline{v}'| \, \sigma_u \left[f_o(\underline{v}')\, f_i(\underline{v}) - f_o(\underline{v})\, f_i(\underline{v}')\right] d^3\underline{v}' \qquad (1)$$

σ_{eo}, σ_{io}, σ_u are the cross-sections for ionization and charge exchange. f_o, f_i, f_e are the distribution function for neutrals, ions and electrons.

In the following we consider the one-dimensional problem with a homogeneous plasma background. The kinetic equation becomes

$$v_x \frac{\partial f_o}{\partial x} = -N(\alpha+c) f_o + N \frac{e^{-\left(\frac{v}{v_i}\right)^2}}{(\sqrt{\pi} v_i)^3} C \int f_o(\underline{v}')\, d^3\underline{v}' \qquad (2)$$

N = plasma density, α= ionization rate, C = charge exchange rate, v_i = thermal velocity of ions.

The boundary conditions are

$$x = o \; : \; f_+(o,\underline{v}) = f_+^{\,o}(v) + R_i f_-(o,\underline{v}) \quad \text{(ideal reflection)}$$

or

$$f_+(o,\underline{v}) = f_+^{\,o}(\underline{v}) + R_D F_o(v) \iiint v_x f_-(o,v)\, d\underline{v}^3 \quad \text{(diffuse reflection)}$$

$f_+^{\,o}(v)$ is the distribution of the "injected" particles, the distribution function f_+ of all particles coming from the wall also contains the reflected neutrals. $F_o(v)$ is the distribution determined by the details of the reflection mechanism, for example, a Maxwellian with wall temperature.

The distribution of the particles impinging on the wall is found from equation (2).

$$f_-(o,\underline{u}) = \frac{e^{-u_y^2 + u_z^2}}{(\sqrt{\pi} v_i)^2} \; \frac{c}{c+\alpha} \int_o^\infty \frac{e^{-u^2}}{\sqrt{\pi}} \; n(z') \; \frac{e^{-\frac{z'}{|u|}}}{|u|} \, dz' \qquad (4)$$

$$\underline{u} = \frac{\underline{v}}{v_i} \; , \; z = \frac{\alpha+c}{v_i} Nx, \; n(z) = \text{density of neutrals.}$$

The density $n(z)$ can be found from the integral equation

$$n(z) = \beta \int_c^\infty \int_o^\infty \frac{e^{-u^2 - \frac{z-z'}{u}}}{\sqrt{\pi}\, u} \, du \cdot n(z') dz' + \int_o^\infty F_+(o,u) e^{-\frac{z}{u}} \, du \qquad (5)$$

$$\beta = \frac{c}{c+\alpha} \; ; \; F_+(o,u) = \iint f_+(o,v) dv_y dv_z \quad \text{(reduced distribution function)}$$

This integral equation was solved numerically together with the boundary conditions (3) and the eq. (4) for $f_-(o,u)$. We replaced the integral equation by a set of 40 linear algebraic equations. Since the kernel $K(z,z')$ of the integral equation (5) has a logarithmic singularity, we replaced the matrix elements $K(i,i)$ by $\frac{1}{2} K(i,i+1)+K(i,i-1)$. By changing the number of equations from 40 to 80 we checked the accuracy of this approximation.

From the result of (5) the distribution function of the "escaped" neutral particles $f_-(o,u)$ be found. If $n(z)$ is constant in space, the integration in eq. (4) yields a Maxwellian for f_-. But due to

the inhomogeneity of n(z) $f_-(o,\underline{u})$ deviates from a Maxwellian. This has to be taken into account if one wants to measure the ion temperature from f_-.

Fig. 1 shows a solution of (5) without reflection on the wall ($F_+=F_+^o$). n(z) consists of two parts: the cold neutrals coming from the wall ($v= 0.1v_i$) provide for the rapid decay of n(z) for $z \ll 1$. The tail of n(z) for $z \geq 1$ is produced by the hot neutrals after charge exchange. The reflection mechanisms modify the density in the neighbourhood of the wall (Fig. 2). The density profile with hot injected neutrals ($v= 10v_i$) is shown in Fig. 3. For comparison we show the solution of (5) with a delta like plasma distribution which was used in [3]. The distribution function of the "escaping" neutrals is shown in Fig. 4. The reflection on the wall does not modify this curve essentially. The equivalent Maxwellian has a smaller shape than ln F_- , an approximation of the tail of ln F_- by a straight line yields an ion temperature which is smaller than the real one.

REFERENCES

1 W. Stodiek et al.: IAEA-CN-28/C-10 Fourth Conf.Proc. I (465), Madison, 1971

2 B. Lehnert: TRITA-EPP-72-05, Royal Inst. of Technology, Stockholm, 1972

3 Y.N. Dnestrovskii et al.: Atomnaya Energya 32 (301-305), French Translation EUR-CEA-FC-645-TR (1972)

"This work was performed under the terms of agreement on association between the Max-Planck-Institut für Plasmaphysik and EURATOM".

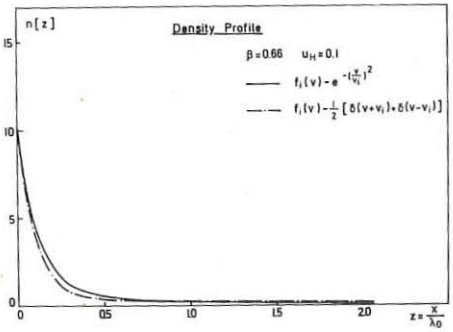


Fig. 1

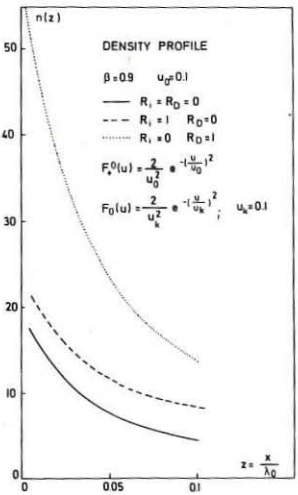


Fig. 2

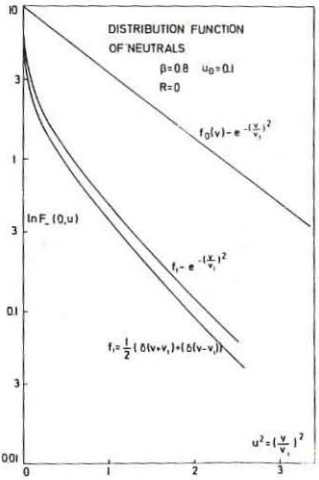


Fig. 4

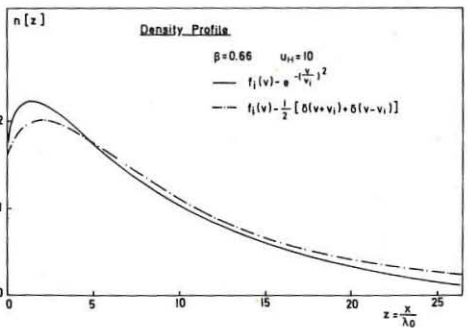


Fig. 3

MEASUREMENT OF THE MAGNETIC FIELD DIRECTION IN A TOKAMAK PLASMA USING THE POLARIZATION OF AN IMPURITY LINE

J. Fujita[+)] and K. McCormick

Max-Planck-Institut für Plasmaphysik Garching, Germany

Abstract

A method for measuring the poloidal magnetic field in a Tokamak discharge is described. The field resolution expected for typical plasma parameters is indicated. Test results for a part of the diagnostic apparatus are shown.

One of the most important diagnostics in Tokamak research which has not yet been carried out is the measurement of the current distribution in a Tokamak plasma. This parameter enters into experimental determinations of the skin effect, resistivity and the safety factor q.

The radial current distribution can be determined from the profile of the poloidal magnetic field using Ampere's law. The poloidal field B_p causes the orientation of the total magnetic field to assume an angle Θ with respect to the toroidal field B_T. Quantitatively, $\Theta = B_p(r)/B_T(r) = r/Rq(r)$, where r and R refer to the minor and major radius respectively. Thus, knowing B_T and Θ, B_p may be calculated. It is the purpose of this experiment to measure Θ. The method described here takes advantage of the Zeeman effect.

In particular, observed in a direction transverse to the magnetic field, the unshifted component (π) of a normal Zeeman triplet is polarized parallel to the field, whereas the shifted components (σ) are polarized perpendicular to the field. Using an appropriate filter one can look at one of these components and therewith measure the orientation of the magnetic field from the direction of polarization. Spatial resolution can be achieved by observing line radiation from impurity atoms locally introduced into the plasma via neutral beam injection.

Figures 1 and 2 illustrate the experimental setup. A neutral lithium beam, capable of being scanned radially, is injected into the plasma along a line perpendicular to both the equatorial plane

of the torus and the axis of the optical system. Line radiation emitted at 6708 Å is gathered by an f/10 lens (for example) from a volume determined by the beam width and imaged aperture diameter (nominally 10 mm and 6 mm, respectively). After passing through a series of relay lenses (not shown), the π component is separated from the σ components (for B_T = 26 kG, the σ components are spaced 1.1 Å apart) by a 50 mm diameter, pressure-scanned Fabry-Perot (FP) with a FWHM bandpass of 0.5 Å and a free spectral range of approximately 16 Å. Unwanted orders of the FP are suppressed by a three period 10 Å bandwidth interference filter. The filtered light then continues through a Faraday rotator (FR) (consisting of a 25 mm diameter, 200 mm long Schott Type SF 59 glass rod contained within a 240 mm long solenoid of 300 turns of 1.6 mm diameter wire), into a half wave plate (used for zeroing) and is split into two beams having mutually perpendicular directions of polarization by a Wollaston prism of 20° output divergence. Each beam is detected by an EMI 9658 A photomultiplier whose quantum efficiency is about 10 % at 6708 Å.

The difference signal between the two photomultipliers is fed to the servoamplifier (capable of delivering $\pm$ 20 amperes with a time constant $< 10^{-3}$ sec), which drives the FR so that the direction of polarization is brought back to zero to give a null signal at the output of the differential amplifier. The FR current necessary to achieve this situation is directly proportional to the angle through which the magnetic field rotates due to the poloidal component. Thus by monitoring this current on an oscilloscope, a continuous time history of B_p is obtained for one position in the plasma. A profile of B_p is built up by scanning the beam radially, several shots being necessary at each position to attain the desired field resolution.

Based on a theoretical extrapolation to higher energies of an experimentally determined electron excitation cross section for the Li 6708 Å line [1], a 20 keV, 0.7 mA neutral beam passing through a plasma with T_e=1 keV and n_e=10^{13} cm^{-3} should produce a photon flux of 10^{14} photons/cm^3 -sec into 4π steradians. Taking into account the beam volume viewed, the solid angle subtended by the lens and the attenuation of the various elements in the optical train, a PM photocathode signal current of roughly 2.5 x 10^7 photoelectrons/sec should result. Assuming that the input noise to the differential

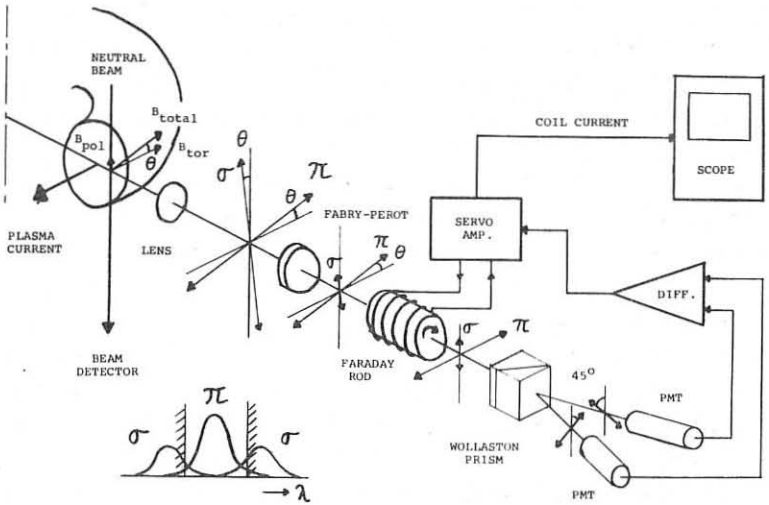


Fig. 1 CONCEPTUAL VIEW OF THE EXPERIMENTAL SYSTEM USED FOR MEASURING THE MAGNETIC FIELD DIRECTION

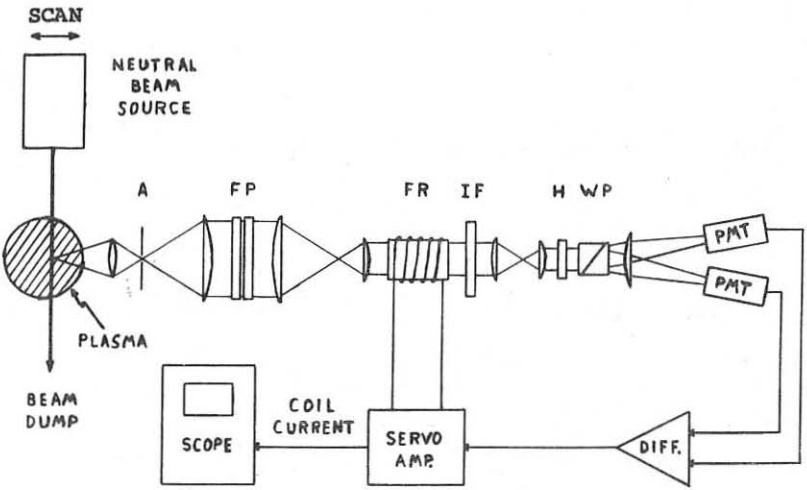


Fig. 2 SCHEMATIC DIAGRAM OF OPTICAL SYSTEM LAYOUT A-Aperture, FP-Fabry Perot, FR-Faraday Rotator, IF-Interference Filter, H-Half Wave Plate, WP-Wollaston Prism, PMT-Photomultiplier

amplifier is due entirely to photon statistics, and defining the minimum resolvable angle of rotation θ_{min} to be that where the (difference) signal-to-noise ratio is unity, then θ_{min} scales as the inverse square root of the photoelectron current and the integration time constant τ. In this case, for $\tau = 10^{-3}$ sec, $\theta_{min} \simeq 0.14^{o}$. For reference with respect to PULSATOR, the value of θ at the limiter (r = 12 cm, R = 70 cm) for q = 3 is approximately 3.3^{o}.

The optical train-feedback system minus the Fabry-Perot has been tested by modulating the direction of polarization with a second FR and observing the response of the servo amplifier output. Currents to the respective FR[s] are shown in Fig. 3. The constant of proportionality [at 6328 Å] between the FR current and the angle of rotation for each FR is also indicated. Note that the overall detection system time constant is $\leq 10^{-3}$ s. Here the light source is a He-Ne laser whose output has been attenuated to yield a photocathode current of approximately 10^{8} photoelectrons/sec.

A lithium ion source using a Lisitano coil has been constructed and is currently undergoing testing.

+) Institute of Plasma Physics, Nagoya University, Nagoya, Japan

References

[1] McCavert, P. and Rudge, MRH, J.Phys. B 5 (1972) 508

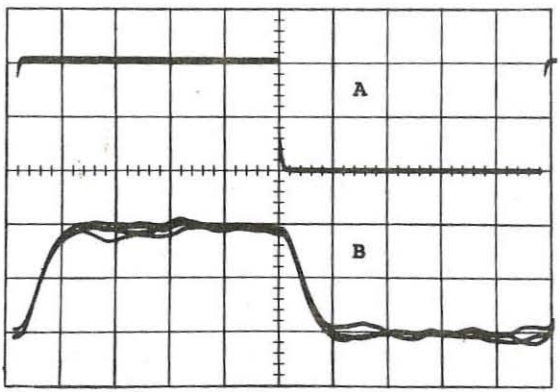


Fig. 3 CURRENTS TO FARADAY ROTATORS
Vertical - 2 A/div., Horizontal - 2 ms/div.
A: Modulation Current → 0.5°/A
B: Servo Amp. Current → 0.53°/A

Poloidal Field Measurements in the ST Tokamak by Harmonic Generation at the Upper Hybrid Layer

R. Cano[†], I. Fidone[†], and J. Hosea

Plasma Physics Laboratory, Princeton University, USA

The initial experiments [1] on local generation of the harmonic wave in the ST tokamak with an electromagnetic wave propagating along the major radius R revealed that the harmonic power characteristic matched the predictions of the theory for generation at the upper hybrid layer [2]. However, the observed minimum of the harmonic power component ratio $P_{ord}/P_{ext} \sim 10^{-2}$ was too large to permit the harmonic polarization measurements which are required to specify the poloidal magnetic field $B_y(r)$. Experimental improvements have resulted in a substantial reduction in the minimum of P_{ord}/P_{ext} (to $\sim 10^{-3}$) so that we are now able to resolve changes in polarization which although the measurements are preliminary, are commensurate with the expected poloidal effect at the upper hybrid layer.

The method used here is discussed in detail elsewhere [3]. Briefly, a locally generated extraordinary wave with frequency Ω, propagating in a plasma with $\omega_p << \omega_c \lesssim \Omega/2$, maintains its initial polarization. Therefore, remote polarization measurements yield the direction of the confining magnetic field at the point of generation.

In Ref.3, the case of a linearly polarized harmonic is discussed. For elliptical polarization, the direction of the local magnetic field is obtained from the rotation of the ellipse. The measurement of the rotation in this case requires the simultaneous detection of the amplitudes and phases of the harmonic electric field components. Let θ be the angle of the magnetic field with respect to the z axis (defined here as the horizontal polarimeter axis) and $E_\perp$, $E_\parallel$, and ψ be the wave components and their relative phase in the local magnetic field frame. Then correspondingly in the laboratory (polarimeter) frame

$$\frac{|E_z|^2}{|E_y|^2} = \frac{|E_{||}|^2}{|E_{\perp}|^2}\left(1 - 2\frac{|E_{\perp}|}{|E_{||}|}\theta\cos\psi + \frac{|E_{\perp}|^2}{|E_{||}|^2}\theta^2\right), \qquad (1)$$

and

$$\tan\chi = \left(|E_{\perp}|\,\theta/\,|E_{||}|\right)\sin\psi + \text{constant}, \qquad (2)$$

where θ is assumed small and χ is the relative phase between E_y and E_z. In the absence of plasma current, the polarimeter is rotated to give $\theta = 0$ and the polarimeter measurements of $|E_z|^2/|E_y|^2$ and χ give the ellipticity $\varepsilon = |E_{||}|/|E_{\perp}|$ and the constant of Eq.(2).

Figure 1 gives the present experimental arrangement. A carcinotron (f = 33.6 GHz) modulated at 50 kHz and delivering up to 15 watts of incident power is used in place of the lower power klystron of the initial experiments [1]. Improved horn allignment and the addition of a microwave absorber provide the reduced ellipticity already mentioned. The polarimeter is now rotatable to permit θ scans and finally, a phase comparator has been added to give the phase χ simultaneously with the amplitude measurements.

In Fig.2, $|E_z|^2/|E_y|^2$ is plotted versus θ at two times for a helium discharge with the magnetic field on the vessel axis set at $B_z(x = 15\text{cm}) = 14.1$ kG. The experimental points are found to fit parabolic curves as predicted by Eq.(1) with $\psi \cong \pi/2$. The axes of the polarimeter and of the ellipse coincide at the minimum of $|E_z|^2/|E_y|^2$. Rotation of the magnetic field due to plasma current is measured by the shift of the minimum between the zero current (t = 0) and the maximum current (t = 6ms) cases. This shift of $\sim 1.5^\circ$ is in good agreement with the value expected at the upper hybrid layer, r $\approx$ 20 cm, which for the selected B_z is outside the limiter so that $\theta \sim I_z/5rB_z \sim 1.2^\circ$.

Figure 3 presents the measured values of χ versus θ for the discharge conditions of Fig.2. Within the experimental errors, $\tan\chi \sim \chi$ is proportional to θ. The separation at $\theta \sim 0$ between the two curves yields the angle of rotation of the magnetic field whereas the slopes give the ellipticity at the respective

times; $\varepsilon \sim 6.4 \times 10^{-2}$, 7.5×10^{-2} in reasonable agreement with the values obtained from direct calibration of the detected amplitudes of $\varepsilon \sim 4 \times 10^{-2}$, 4.6×10^{-2} for t = 0, 6 msec.

By varying the level of the toroidal field for a fixed polarimeter position and constant incident frequency, a preliminary measurement of the radial profile of $\theta = B_y/B_z$ may now be obtained. Combining these measurements of θ with the location of the upper hybrid layer deduced from Thomson scattering measurements of the electron density profile for similar discharge conditions gives the poloidal field profile plotted in Fig.4. The expected peak in B_y (in Fig.4, $\theta = B_y/14.1 \times 10^3$ G) is clearly observed as is the 1/r variation outside the current channel.

The location of the peak in Fig.4 is indicative of a rather flat current distribution. However, remaining uncertainties in the measurements of θ plus the need for more exact density profile measurements taken simultaneously with the θ data preclude a definite determination of the current distribution at this time.

The results reported here demonstrate that the harmonic polarization is in fact sensitive to the poloidal field at the upper hybrid layer. Future experiments are planned at twice the present incident frequency for which we expect to reduce further the harmonic ellipticity and obtain more reliable density profiles so that a quantitative measurement of the poloidal field profile, or equivalently the current density profile, may be obtained.

This work was supported by U. S. Atomic Energy Commission Contract No. AT(11-1)-3073 and by the Association C. E. A.-EURATOM, Fontenay-aux-Roses, France.

†Permanent address: Centre d'Etudes Nucleaires, Fontenay-aux-Roses, France.

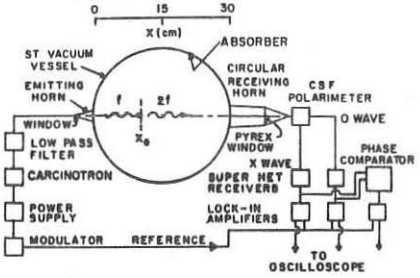


Fig. 1

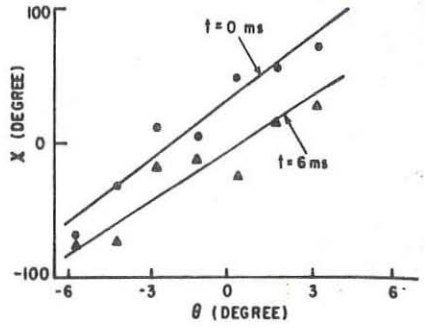


Fig. 3

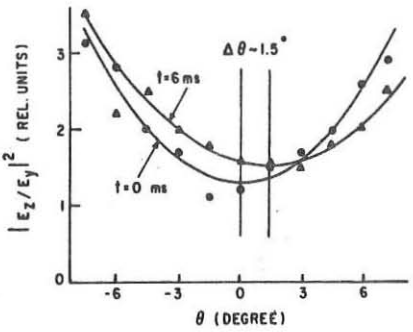


Fig. 2. $|E_z/E_y|^2$ versus θ for a helium discharge (B_z = 14.1 kG, a = 10.6 cm). For t = 0, I_z = 0 and for t = 6 msec, I_z = 26 kA and $n_e(r = 0) = 7 \times 10^{12}$ cm^{-3}.

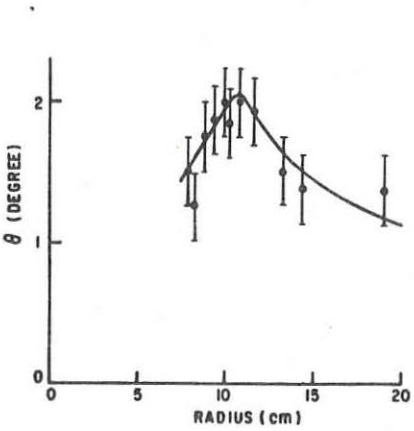


Fig. 4

References

[1] R. Cano, C. Etievant, and J. Hosea, Phys. Rev. Lett. 29, 1302 (1972).

[2] I. Fidone, G. Granata, and J. Teichmann, Phys. Fluids 14, 737 (1971).

[3] R. Cano, I. Fidone, and M. J. Schwartz, Phys. Rev. Lett. 27, 783 (1971).

Space Potential Measurements in the ST Tokamak

F. C. Jobes and J. C. Hosea
Plasma Physics Laboratory, Princeton University
Princeton, New Jersey 08540, USA

As previously reported [1, 2], the heavy-ion beam probe has been employed successfully on the ST tokamak to determine the density perturbation produced by the low frequency oscillatory instabilities and as well the contribution of the measured radial electric field to the mode frequency (monitored with magnetic loops located outside the plasma column). We are now using the ion beam probe to make a systematic investigation of the space potential both as a function of time and discharge conditions. . Of particular interest is the dependence of the space potential on the concentration of runaway electrons in the ST plasma and its behavior leading into and during the disruptive instability. Also, we are improving the frequency response of the feedback circuit to enable us to measure the effect of the low frequency oscillatory instabilities on the space potential so that an estimate of the diffusion caused by these instabilities may be made.

Figure 1 presents the heavy-ion beam probe system presently being used on the ST tokamak. A singly ionized thallium beam is injected at the top of the plasma column and is partially ionized to the second level of ionization along its path through the plasma. The secondary ions coming from the vicinity of the detector line (located by the detector-source geometry and the beam energy) are collected on a split-plate detector after passing through an electrostatic analyzer. Due to the change in charge at the detector line, the secondary beam energy differs from that of the injected primary beam by the space potential V_{pl}. Uncorrected, this causes the secondary beam to move along the major

radius R across the ϕ split in the detector plates. The secondary beam intensity difference from the two plates is, in practice, fed back to the electrostatic analyzer so as to keep the beam centered on the split. Then, the fed back potential is directly proportional to the space potential. (On-line computers facilitate the data collection and display.)

At present, our results are preliminary but certain patterns are beginning to emerge. For the usual discharge conditions which have been studied - B_ϕ = 14 kG, $I_\phi \sim 10 - 30$ kA, $p = .1 - 4 \times 10^{-5}$ Torr in hydrogen and helium, $T_e(r=0) \sim 500$ eV, and $n_e \sim .5 - 2 \times 10^{13}$ cm^{-3} - we find that V_{pl} is negative, peaking to a value of ~ -200 V at the center of the plasma during the constant current phase of the discharge. As $I\phi$ falls at the end of the discharge, V_{pl} peaks more negatively at the center of the plasma and becomes slightly positive out toward the plasma boundary. During the initial current phase, we have thus far been unable to observe a positive potential. In fact, no positive potentials have been observed which could produce large ion velocities in the ion diamagnetic drift direction such as have been reported for the Ormak device [3]. It is possible that sharp pressure gradients as have been observed in ST are responsible for these large ion velocities.

By varying the beam energy, a two dimensional scan of the space potential over the cross-section can be obtained. Figure 2 presents such a scan for the special case of a small radius discharge. (This radius selection permits a scan over most of the discharge column.) Here V_{pl} (plotted as $-V_{pl}$ peaks quite negatively (< -1 kV) to an amplitude several times that of T_e ($r = 0$) in eV and is approximately symetric about the center of the plasma except on the inside of the column where a trail off toward the inside limiter is apparent.

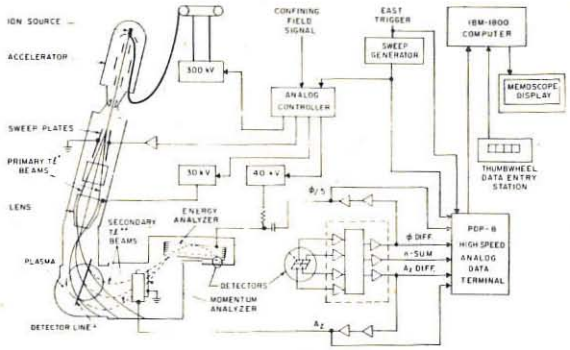


Fig. 1 Ion Beam Probe System

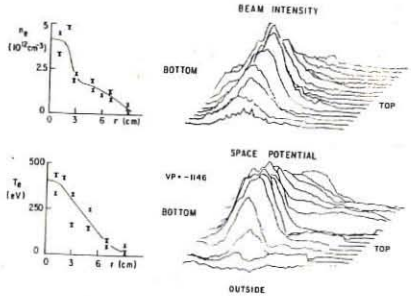


Fig. 2 Density and space potential scans over the cross section of a He discharge, and associated laser temperature and density measurements. The space potential is plotted inverted. [a = 6cm, Iϕ = 9kA, Bϕ = 14kG]

1.9. TOKAMAKS: EQUILIBRIA (THEORY)



STATIONARY CONVECTION IN TOKAMAK PLASMAS

E.K. Maschke and R.B. Paris

ASSOCIATION EURATOM-CEA SUR LA FUSION
Département de Physique du Plasma et de la Fusion Contrôlée
Centre d'Etudes Nucléaires
Boîte Postale n° 6. 92260 FONTENAY-AUX-ROSES (FRANCE)

ABSTRACT

During its time evolution a Tokamak plasma may become locally unstable according to ideal MHD theory (e.g. $q_{axis}<1$, or skin effect). If viscosity and resistivity are taken into account, a quasi-stationary convective motion is possible, which is characterized by a critical Rayleigh number and leads to enhanced thermal transport.

In the time evolution of the experimental Tokamak profiles of density n and electron temperature T_e two anomalous phenomena appear: the rapid disappearance of the skin effect [1-3], and the flattening of the T_e profile near the axis [4] when $q_{axis}<1$. In both cases the plasma is locally unstable according to ideal MHD theory. The unstable situation is approached relatively slowly in the course of Ohmic heating. Near the stability limit, viscosity, resistivity, and thermal conductivity are important, and in analogy with Bénard convection one might expect the onset of stationary convection rather than violent turbulence.

In the present paper we show that in a situation where the plasma is slightly unstable according to ideal MHD theory, taking account of viscosity and resistivity leads to a theory which is formally analogous to the theory of Bénard convection. Instead of an instability driven by gravitational and thermal effects, we consider an interchange type instability driven by unfavourable average curvature of the magnetic field lines. We show that it is possible to define a Rayleigh number which contains the resitivity instead of the thermal conductivity. Here we limit ourselves to the discussion of a slab model which may be applied to the skin-effect situa-

STATIONARY CONVECTION IN TOKAMAK PLASMAS

E.K. Maschke and R.B. Paris

ASSOCIATION EURATOM-CEA SUR LA FUSION
Département de Physique du Plasma et de la Fusion Contrôlée
Centre d'Etudes Nucléaires
Boîte Postale n° 6. 92260 FONTENAY-AUX-ROSES (FRANCE)

ABSTRACT

During its time evolution a Tokamak plasma may become locally unstable according to ideal MHD theory (e.g. $q_{axis}<1$, or skin effect). If viscosity and resistivity are taken into account, a quasi-stationary convective motion is possible, which is characterized by a critical Rayleigh number and leads to enhanced thermal transport.

In the time evolution of the experimental Tokamak profiles of density n and electron temperature T_e two anomalous phenomena appear: the rapid disappearance of the skin effect [1-3], and the flattening of the T_e profile near the axis [4] when $q_{axis}<1$. In both cases the plasma is locally unstable according to ideal MHD theory. The unstable situation is approached relatively slowly in the course of Ohmic heating. Near the stability limit, viscosity, resistivity, and thermal conductivity are important, and in analogy with Bénard convection one might expect the onset of stationary convection rather than violent turbulence.

In the present paper we show that in a situation where the plasma is slightly unstable according to ideal MHD theory, taking account of viscosity and resistivity leads to a theory which is formally analogous to the theory of Bénard convection. Instead of an instability driven by gravitational and thermal effects, we consider an interchange type instability driven by unfavourable average curvature of the magnetic field lines. We show that it is possible to define a Rayleigh number which contains the resitivity instead of the thermal conductivity. Here we limit ourselves to the discussion of a slab model which may be applied to the skin-effect situa-

tion in Tokamaks. The flattening of the T_e profile for $q_{axis}<1$ will be treated in a later publication. From the velocity of convection and the perturbed temperature the effective heat flow due to convection may be calculated. This requires a nonlinear treatment of the type used in [6] for the Bénard problem.

We describe the plasma by the equation of motion and Ohm's law :

$$\rho\left(\frac{\partial}{\partial t} + \vec{V}\cdot\nabla\right)\vec{V} = -\nabla p + (\nabla\times\vec{B})\times\frac{\vec{B}}{4\pi} + \rho\nu\nabla^2\vec{V} \qquad (1)$$

$$\frac{\partial\vec{B}}{\partial t} + \eta\nabla\times(\nabla\times\vec{B}) = \nabla\times(\vec{V}\times\vec{B}) \qquad (2)$$

where η the resistivity and ν is the viscosity [7].

We first consider a cylindrical plasma in equilibrium, with $\vec{V}_o=0$, subjected to a perturbation of the form $\exp\{im\theta+ikz+\sigma t\}$ chosen to be nearly constant along field lines in the region of interest, viz. $(m/r)B_{o\theta}+kB_{oz}\simeq 0$. Introducing $W = rV_{1r}$, $\Omega=r(\nabla\times\vec{V})_r$, $\omega_z=(\nabla\times\vec{V})_z$ we obtain the following system of linearized equations :

$$(\nu D-\sigma)\{DW - \frac{4k^2}{\frac{m^2}{r^2}+k^2}\,\frac{1}{r}\,\frac{dW}{dr} + \frac{4mk}{\frac{m^2}{r^2}+k^2}\,\frac{\Omega}{r^2}\} - \sigma\frac{2k}{\frac{m^2}{r^2}+k^2}\left(\frac{k}{r}\frac{dW}{dr} - \frac{m}{r^2}\Omega\right)$$

$$+ \frac{1}{\rho_o}\{(\frac{m^2}{r^2} + k^2)2B_{o\theta}B_{1\theta} - \frac{im}{r}\frac{d}{dr}[B_{1r}(rB_{o\theta})'] - ikr\frac{d}{dr}[B_{1r}B'_{oz}] = 0 \qquad (3)$$

$$\left.\begin{aligned}
&(D-\frac{2}{r}\frac{d}{dr} - \frac{\sigma}{\eta})(rB_{1r}) - \frac{2im}{r}B_{1\theta} = 0\\
&(D-\frac{2}{r}\frac{d}{dr} - \frac{\sigma}{\eta})(rB_{1\theta}) + \frac{2im}{r}B_{1r} = \frac{1}{\eta}\,Wr\left(\frac{B_{o\theta}}{r}\right)'\\
&(D - \frac{\sigma}{\eta})B_{1z} = \frac{1}{\eta}\,W\,\frac{1}{r}\,B'_{oz}
\end{aligned}\right\} \qquad (4)$$

$$(\nu D - \sigma)\Omega = -2ik\nu\omega_z - iB_{1r}\left[\frac{m}{r}B'_{oz} - \frac{k}{r}(rB_{o\theta})'\right] \qquad (5)$$

$$\left.\begin{aligned}
(\nu D - \sigma)\omega_z = &-\frac{1}{r}\frac{d}{dr}r\left[\frac{B_{1r}}{r}\frac{d}{dr}(rB_{o\theta}) + iB_{oz}(kB_{1\theta} - \frac{m}{r}B_{1z})\right]\\
&- \frac{im}{r}\left[\frac{d}{dr}(B_{oz}B_{1z}) + \frac{1}{r^2}\frac{d}{dr}(r^2B_{o\theta}B_{1\theta})\right]
\end{aligned}\right\} \qquad (6)$$

where

$$D = \frac{1}{r}\frac{d}{dr}\,r\frac{d}{dr} - \frac{m^2}{r^2} - k^2 \quad .$$

We now consider an equilibrium with skin effect and apply the above equations to an interval of the order of the skin depth d about $r = r_o$. Thus, passing to a slab model we find

$$\mathcal{D}(\mathcal{D} - \tfrac{\sigma}{\eta})(\mathcal{D} - \tfrac{\sigma}{\nu})\, W = -\frac{2K^2}{\nu\eta}\,\frac{B_{o\theta}B'_{o\theta}}{\rho_o r_o}\, W \qquad (7)$$

with $K^2 = \frac{m^2}{r_o^2} + k^2$ and $\mathcal{D} = \frac{d^2}{dr^2} - K^2$. Using the equilibrium equation we can relate $B'_{o\theta}$ to the pressure gradient p'_o, assuming B_{oz}=const. Eq.(7) is formally analogous to the equation of Bénard convection in a liquid layer heated from below. Therefore we may use the solution of this problem given in [5] and define a Rayleigh number for the cylindrical shell

$$\mathcal{R}_{cyl} = \frac{2(-p'_o)d^4}{\rho_o r_o \eta\nu} \quad . \qquad (8)$$

If we assume "rigid" boundary conditions [5], then the critical Rayleigh number for the onset of stationary convection is

$$\mathcal{R}_{crit} = 1707 \quad . \qquad (9)$$

We now simulate the toroidal configuration by replacing, in the expression for the curvature of the field lines, the cylindrical V" by the toroidal V" to obtain the average toroidal curvature. In this way we find for the Rayleigh number in the toroidal case

$$\mathcal{R}_{tor} = \frac{q^2-1}{|q^2-1|}\,\frac{2p'_o B_{oz} d^4}{RB_{o\theta}\rho_o\nu}\sqrt{\frac{|q^2-1|}{q^2}} \quad . \qquad (10)$$

If q>1 in the region of the skin effect, then the average curvature is unfavourable for stability on the inner side of the skin layer ($p'_o>0$). For $\mathcal{R}_{tor} > \mathcal{R}_{crit}$ convective motion can ensue . For example, with q=3 at the skin layer $r=r_o$ and T_e=100 eV, r_o=20 cm, $n = 5\cdot 10^{13}\,cm^{-3}$

d=1 cm and $p_o'/\rho_o \simeq kT_e'/m_i$, the condition $\mathcal{R}_{tor} > \mathcal{R}_{crit}$ becomes $T_e' r_o / T_e \gtrsim 10^{-2}$. It follows that a finite pressure gradient has to be exceeded in order to drive the convective motion.

The resulting enhanced heat transport can be calculated if the Rayleigh number is just supercritical, because the amplitude of the motion is then sufficiently small to enable the use of a non-linear perturbation analysis [6]. This contrasts with theories where viscosity is ignored, resulting in the prediction of strong turbulence, which makes an accurate quantitative calculation of heat transport difficult. This non-linear theory will be presented in a following paper.

In conclusion, we have shown that stationary convection is possible in situations where ideal MHD theory would predict instability. This type of theory might explain the rapid disappearance of the skin effect and the flattening of the T_e profile observed in Tokamak plasmas.

REFERENCES

[1] N.J. Peacock et al., Nature 224, 488 (1969).

[2] D.F. Düchs, H.P. Furth, P.H. Rutherford, Plasma Physics and Controlled Nuclear Fusion Research, Proc. Conf. Madison (1971), Vol. I, p. 369, IAEA, Vienna 1971.

[3] C. Mercier, Soubbaramayer, V European Conf. Controlled Fusion and Plasma Physics, Grenoble (1972) Vol. II, p. 157.

[4] W. Stodiek, V. European Conf. Controlled Fusion and Plasma Physics, Grenoble (1972), Vol.II, p.1.

[5] S. Chandrasekhar, Hydrodynamic and Hydromagnetic Stability, Clarendon Press, Oxford 1961.

[6] A. Schlüter, D. Lortz, F. Busse, J. Fluid Mech. 23, 129, (1965).

[7] S.I. Braginskii, Reviews of Plasma Physics, ed. by M.A.Leontovich, Vol.1, p.205, Consultants Bureau, New-York 1965; for the cylindrical case with $\nabla.\vec{v}=o$ and $v_z \simeq o$, the complete form of the viscosity tensor may be included in eq.(1), resulting in an additional term expressible as a gradient. This subsequently disappears when the curl of eq.(1) is taken.

Multipole Tokamak Equilibria with Finite ß.

W. Feneberg, K. Lackner

Max-Planck-Institut für Plasmaphysik, 8046 Garching bei München,
Federal Republic of Germany

Abstract: We describe a method for the computation of plasma configurations with various current profiles and finite poloidal ß, held in equilibrium by given external currents. Applications to configurations combining the elliptic and triangular deformations desirable for stability with magnetic divertors are given.

The recent interest in Tokamak devices with shaped crossections [1], [2] and with axisymmetric "magnetic" divertors [3] as well as the desired long time scales for the experiments, which preclude the use of conducting walls for field shaping, require the knowledge of equilibrium configurations formed by applied currents in external conductors. Such configurations, together with the required external currents can be computed either by separate solution of the "inner" (plasma) problem and continuation to the outside as improperly posed initial value problem, by prescribing flux surfaces outside the plasma which are afterwards substituted by conductors ("virtual casing", [4], [5]), or by prescribing the external field a priori by its sources and solving simultaneously the inner and the outer problem [6]. The second and third scheme lead to a nonlinear problem for all current distributions, as the position of the plasma surface depends on the solution itself, and thus require iterative methods for the solution. The first method is inherently unstable and usefull only if conductors are to be arranged continuously on a flux surface closer to the plasma than the first predicted singularity. Similarly the virtual casing method is restricted to external conductors arranged on a flux surface.

Consequently we have developed a program implementing the third scheme. Results for the case of force-free equilibria, and current distributions of the type

$$j_{tor} \sim 1/r \quad \text{for } \psi \geq \psi_c \quad \text{and } j_{tor} = 0 \quad \text{for } \psi < \psi_c \qquad \ldots\ldots (1)$$

together with an outline of the method have been given already previously [3]. The program has now been extended to current distributions of the type

$$j_{tor} = c_{0p} \cdot r + c_{1p} \cdot (\psi - \psi_c) \cdot r + c_{0F}/r + c_{1F} \cdot (\psi - \psi_c)/r \quad \text{for} \quad \psi \geq \psi_c \qquad \ldots\ldots (2)$$

$$j_{tor} = 0 \quad \text{for} \quad \psi < \psi_c$$

which include thus finite β_p effects (both para and diamagnetic cases), and which can describe current distributions peaked either at the plasma surface or at the magnetic axis. According to the general method described in [5], [6], the coefficients in (2) are varied during the iteration so as to keep constant four parameters $I_i \cdot r_{axis}^n$ where I_i, i = 1, . . 4 are the area integrals over the plasma crossection of the four terms in (2), respectively ($\sum I_i$ = total plasma current); and r_{axis} is the position of the magnetic axis at a particular iteration cycle. Positive values of the exponent n help to stabilize the position of the plasma column and thus to accelerate convergence. The plasma boundary ψ_c is determined by the requirement that it should either pass through a given point on the inside of the torus, or should touch a plane parallel at a given height to the symmetry plane. Physically these restrictions can be thought to be realized by appropriate limiters.

This program has been applied recently to a large number of configurations combining the desired elliptic and triangular deformations [2] with suitably located divertors. The most promising seems to be the configuration proposed in [1] and recently termed "fingerring", with divertors located on top and bottom of the column. Alternative divertor arrangements compatible with the desired deformation of the plasma crossection seem to suffer from either poor stability (divertor on outside), or space limitations and smaller maximum poloidal ß for equilibrium (divertor on inside).

Figure 1 and 2 illustrate the dependence of equilibrium shape and position for a given external conductor arrangement and conductor currents on current distribution and poloidal $\beta_p = 8 \cdot \pi \int pdf / I_p^2$. For both series of runs the height of the plasma column was supposed to be fixed by a rail limiter parallel to the symmetry plane, but quite similar results are obtained if the height is adjusted case by case till the plasma boundary touches the stagnation points on top and bottom (magnetic divertor). The currents in the outer conductors are - 1.6 on the inside, +2.3 on top and - 1.5 on the outside in relative units throughout the 6 cases; the total plasma current in the same units is + 5.25 for the cases in Fig. 1 and 3.0 in Fig. 2.

The cases in Fig. 1 correspond to $\beta_p = 0$ and 3 different current distributions (see 1 d): (a) a slight skin type distribution, (b) $j_{tor} \sim 1/r$ and (c) a distribution peaked at the magnetic axis. As expected, the magnetic surfaces tend to get much more circular as the current peaks in the center.

Fig. 2 illustrates the influence of β_p for current distributions with c_{1p} and $c_{1F} = 0$; (a) $\beta_p = .75$, (b) $\beta_p = 1.8$, (c) $\beta_p = 2.85$. The shift in the plasma position and the increase of the diameter of the plasma column in radial direction with increasing β_p can of course be partially compensated by reducing the plasma current, as has indeed been done already between the cases of Fig. 1 and Fig. 2.

The above examples for the dependence of plasma shape and position on current distribution illustrate the feedback requirements for compensating for changes in the internal parameters of the plasma, and the limits of applicability of simple models allowing only for a particular current distribution (e.g. surface currents) or a particular value of β_p (either 0 or 1). Future calculations will concentrate on examining different external conductor arrangements for their limiting β_p.

References:

1) L.A. Artsimovich, V.D. Shafranov, ZhETF 15, 72 (1972)
2) G. Laval et al. I.C. 70-35, Trieste Report (1970)
3) W. Feneberg, Phys. Letters 36A, 125 (1971)
4) V.D. Shafranov, L.E. Zakharov, Nuclear Fusion 12, 599 (1972)
5) K.v.Hagenow, K. Lackner, 3rd Intern. Symposium on Toroidal Plasma Confinement, Garching (1973)
6) W. Feneberg, K. Lackner, Bull. American Phys. Soc. 17, 1055 (1972).

"This work was performed under the terms of the agreement on association between the Max-Planck-Institut für Plasmaphysik and EURATOM".

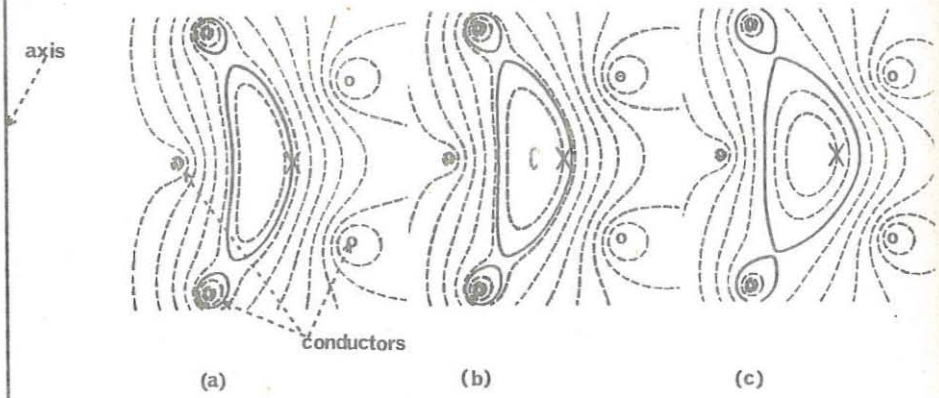
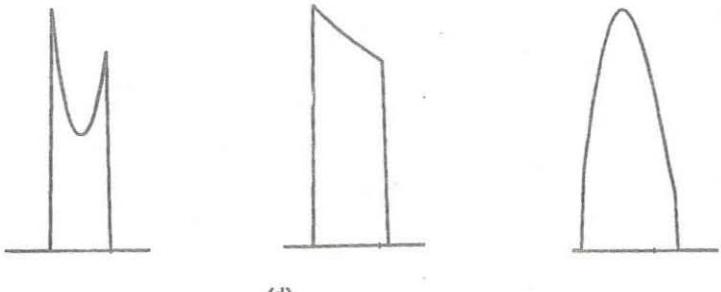


Fig. 1



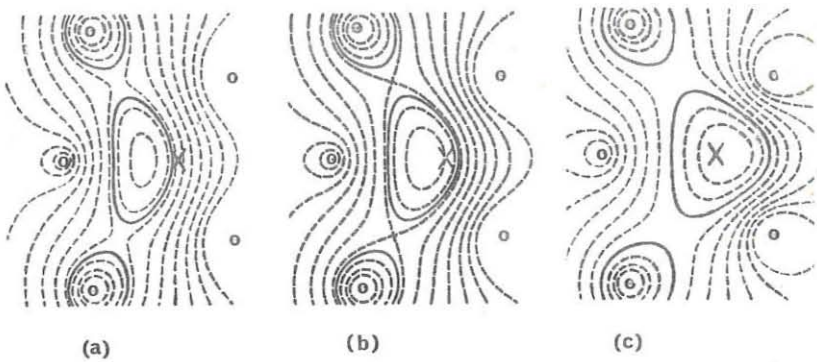


Fig. 2

EQUILIBRIUM ROTATION OF A TOKAMAK DURING NEUTRAL INJECTION

E. Canobbio and O. De Barbieri

Association EURATOM-CEA
Département de Physique du Plasma et de la Fusion Contrôlée
Centre d' Etudes Nucléaires
B.P.85 - 38041 - GRENOBLE (France)

ABSTRACT.- We discuss the steady state rotation velocity of a Tokamak plasma in the plateau regime, in the presence of neutral beams injected for heating purposes.

I. The Ambipolar Condition. A byproduct of plasma heating by neutral injection is plasma rotation, which can be both poloidal (around the magnetic axis) and toroidal (around the major axis). This topic has been considered in Refs./1,2,3/, which, however, disagree as regards the possibility of loosing plasma toroidal momentum. Since the energy of the beam is much larger than the plasma temperature, the slowing-down and the diffusion time of the beam can be taken to be much longer than the diffusion time of the plasma. As a result, when studying plasma rotation : 1) the time evolution of the beam can be disregarded, and 2) the ambipolar condition must be applied to the whole beam-plasma system. The present paper deals with the plateau regime. The corresponding problem in the banana regime, where plasma diffusion during neutral injection is no longer automatically ambipolar, demands a separate analysis.

With the usual toroidal coordinates (r, θ, ϕ) the magnetic field is $\vec{B}=B_\phi(\vec{e}_\phi + \Theta\,\vec{e}_\theta)$, $B_\phi = B_o(1+r\cos\theta/R)^{-1}$, $|\Theta|=r/qR<<1$, R being the major radius. From the conservation of canonical angular momentum of a single particle

$$d_j/dt(1+r\cos\theta/R)m_j v_{\phi j} = e_j B_\theta (1+r\cos\theta/R) v_{Drj}/c,$$

when integrating over the velocity space, summing over the electrons and ions of the plasma, and averaging over a magnetic surface ($\langle ... \rangle \equiv \int_0^{2\pi} ... (1+r\cos\theta/R)d\theta/2\pi$), we obtain for the evolution of the macroscopic toroidal plasma momentum per unit volume :

$$\frac{d}{dt}P_\phi = \langle B_\theta j_r\rangle/c = B_o\Theta\langle j_r\rangle/c + O(r/R) \qquad (1)$$

where $\langle j_r\rangle \equiv e\langle n\bar{v}_{Dri}\rangle - e\langle n\bar{v}_{Dre}\rangle$, and $\bar{v}_{Drj}$ is the usual radial drift velocity in the plateau regime.

Observing that equilibrium requires ambipolarity in the radial direction

$$\partial\langle E_r\rangle/\partial t = -4\pi(\langle j_r\rangle + \langle j_I\rangle) = 0, \qquad (2)$$

where j_I - the current connected with the time derivative of the charge density

$\sigma(r,t)$ deposited by the injected beam - is in general not zero (see below), we conclude that

$$\frac{d}{dt} P_\phi = -\Theta B_o \langle j_I \rangle / c \neq 0. \qquad (3)$$

The presence of j_I is ignored in Refs. /1/ and /2/. It is considered in Ref./3/ although most of the conclusions drawn there are incorrect because Eq.(2) was not exploited properly. Ref./2/, where the dominant terms retained when calculating the rotation decay are proportional to the polarization drift, cannot be used to find the steady state. In addition to the magnetic force $(\vec{j} \wedge \vec{B})$ one could add ion viscosity /4/ to the RHS of Eq.(1). However, perpendicular viscosity is a slow process - proportional to ion Larmor radius squared- which can be neglected in the presence of a pumping beam, and parallel viscosity simply cancels the θ-dependence of the rotations (on a short time scale $\sim \nu_{ii}^{-1}$) leaving the equilibrium value of these θ-averages undetermined.

II. The Source of Plasma Rotation.- The toroidal force per unit volume transmitted via Coulomb collisions by the beam to the plasma is

$$F_\phi(r) = m_b(v_{b\phi} - v_{p\phi})(n_b(r)|v_b|\tau_s/2\pi R)/\tau_s \qquad (4)$$

where $n_b(r)|v_b|\tau_s/2\pi R$ is the density of fast ions accumulated in the plasma in a slowing-down time of the beam, τ_s, and $\vec{v}_{b(p)}$ is the fluid velocity of the beam (plasma). This force can be eliminated by injecting neutrals either radially or by means of pairs of properly dimensionned antiparallel beams tangent to the magnetic axis.

There is also a force in the poloidal direction which at equilibrium is not conveyed to the plasma via the electric field E_r but only via Coulom collisions. This force is the time derivative of the poloidal momentum of diamagnetic origin which is carried by the ion beam:

$$F_\theta(r) = m_b v_{b\perp} \frac{\partial}{\partial t} \left(\langle \Delta r \rangle \frac{\partial}{\partial r} n_b |v_b| t/2\pi R \right). \qquad (5)$$

Here $\langle \Delta r \rangle$, the θ-average of the radial excursion of the fast ions, can be written as (/5/ and /6/):

$$\langle \Delta r \rangle \simeq - \text{sign}(v_{b//} + v_E/\Theta)|v_b|(r/R)^{1/2}/\omega_{cb}\Theta \quad \text{for radial injection,} \qquad (6)$$

$$\simeq - \text{sign}\,(v_{b//} + v_E/\Theta)|v_b|(r/R)/\omega_{cb}\Theta \quad \text{for tangent injection,} \qquad (7)$$

where the subscript // refers to the lines of force, $v_E = -cE_r(r)/B_\phi$, and ω_{cb} is the gyrofrequency of the beam ions. When injecting pairs of antiparallel beams, the toroidal guiding center excursions of the ions of the two beams may balance

but not their Larmor excursions, ρ_b. We take, therefore,

$$< \Delta r > \simeq \rho_b \simeq (|v_b|/\omega_{cb})\sqrt{2Rr_p}/2R \text{ for antiparallel injection.} \qquad (8)$$

Lacking a rigorous derivation of the j_I- current entering into Eqs.(2) and (3) we estimate $< j_I >$ by using the continuity equation :

$$< j_I > \equiv -\frac{1}{r}\int_0^r dr'r'd\sigma(r',t)/dt \simeq -\frac{\alpha e|v_b|}{2\pi Rr}\int_0^r dr'r'<\Delta r>\partial n_b(r')/\partial r' \qquad (9)$$

where the factor α accounts for a possible reduction of the electric charge density $\sigma(r)$ of the beam produced by cross-field diffusion. α is an unknown parameter of the problem which is expected to be not much smaller than unity.

III. Steady State Rotation. In order to have equilibrium in the various injection schemes, the neutral beam must satisfy the conditions which are obtained by equating $- dP_\phi/dt$ (Eq.(3)) to F_ϕ(Eq.(4)) :

a) radial injection : $|v_{b\phi}/v_b| \simeq \alpha \cdot (r/R)^{1/2}$
b) unidirectional parallel injection : $1 \simeq \alpha \cdot (r/R)$
c) antiparallel injection : $\left[n_b v^+_{b\phi} - n_b v^-_{b\phi}\right]/\Sigma n_b |v_b| \simeq -\alpha\Theta(\frac{r_p}{2R})^{1/2}$

Therefore, equilibrium can always be achieved only in case c), while it requires a small α- value (rapid beam diffusion) in case a), and is impossible in case b), the loss of toroidal momentum being too small.

In order to see whether in cases a) and c) the beams alter appreciably the diffusion of the plasma with respect to the $j_I = 0$ case, we use the usual plateau expressions for $< nv_{Drj} >$ in the limit : $|v_E| << |\Theta|(2\,T_j/m_j)^{1/2}$, $\partial T_j/\partial r = 0$, $v_{//j} = 0$. We obtain for the poloidal velocity

$$v_{\theta i} \equiv v_E + v_{ni} \simeq K|v_{ni}| \qquad (10)$$

where $v_{ni} = (T_i/m_i\omega_{ci})\cdot d(\ln n_p)/dr$ is the ion diamagnetic drift velocity and for deuterium antiparallel beams in a deuterium plasma

$$K = 2.10^{12}.\ \alpha\ (\frac{r_p}{r_b})\ (\frac{r_p}{\rho_\theta})(\frac{R}{r_p})\frac{I^{1/2}(A)E^{1/2}(ev)}{n_{p(cm^{-3})}r^2_{p(cm)}T_{i(ev)}} \qquad (11)$$

Here, ρ_θ is the poloidal Larmor radius of the plasma ions, E is the beam energy, and I is the equivalent current of the neutral beams. Using both present devices and reactor parameters, it is easy to see from Eqs. (10) and (11) that the presence of the beam does not change appreciably the value of $v_{i\theta}$ (and of v_E). On

the other hand, cross-field diffusion is enhanced unless $K \ll (m_e T_e^3/m_i T_i^3)^{1/2}$. In present day devices some increase of diffusion cannot be excluded. In this case, however, a knowledge of the value of the α-factor is necessary to settle the question. When injecting radially, the K-factor is $|\Theta|^{-1}$ times larger than that given by Eq.(11). With reactor parameters both injection schemes give no significant increase of diffusion. Finally, concerning plasma equilibrium in the poloidal direction, it can be seen that the magnetic force $< j_r > B_\phi/c$ is balanced by the inertia term, the F_θ-force (Eq. (5)) being negligible.

Acknowledgemt. We greatfully acknowledge Professor M.N. Rosenbluth for stimulating criticism on the results of Ref. /3/.

References.

/1/. J.D. Callen et al, Garching Symposium, March 26-30, 1973, paper E14.
/2/. T.H. Stix, Bull. Am. Phys. Soc., 17(1972) 1063, and private communication.
/3/. E. Canobbio and O. De Barbieri, Garching Symposium, March 26-30, 1973, paper E 11.
/4/. M.N. Rosenbluth et al, Madison Conference (1971) paper CN28/C-12.
/5/. H.L. Berk and A.A.Galeev, Phys. Fluids, 10, 441 (1967).
/6/. T.H. Stix, Plasma Physics, 14 (1972) 367.

THE SIMULATION OF CLASSICAL TOROIDAL PLASMAS IN THE PLANE

D.E. Potter and G.H. Tuttle

Physics Department, Imperial College, London SW7, England

Abstract: A fluid model to describe classical, axisymmetric, toroidal plasmas in the poloidal plane is briefly described. A low but finite beta plasma is assumed so that both the motion of the field lines and the plasma are included. The equations are expressed on an orthogonalised field-line space and solved implicitly on the computer. The simulation has been applied to the Tokamak where the full time-scale of the experiment is followed and the creation of an equilibrium, diffusion, energy losses and decay are studied.

Introduction

Two approaches have been used in studying the macroscopic properties of plasmas in axisymmetric torii. The field structure and distribution of plasma in equilibrium have been studied with time-independent models (sometimes involving iteration) using expansions in the inverse aspect ratio[1,2,3]. The alternative approach has been to follow the full time evolution of the pinch experiment with one-dimensional simulations, assuming a small inverse aspect ratio and averaging around the poloidal plane[4,5]. Here we describe a fluid model which permits the simulation of the plasma in the poloidal plane over the full timescale of the experiment. The simulation admits of an arbitrary aspect ratio, and describes the motion of the field surfaces, the motion of the plasma, the effect of Alfven waves and the diffusion of both the plasma and the field surfaces with respect to the laboratory frame.

Fluid flow across a strong toroidal field

In cylindrical coordinates, the Tokamak and a number of other axisymmetric toroidal systems are characterised by a large vacuum toroidal field B_ϕ. For a sufficiently small beta, the plasma has insufficient energy to compress the toroidal magnetic flux. Expanding in beta and according to Faraday's Law, the quantity rB_ϕ is an invariant over the poloidal plane, so that to the first approximation, the plasma must flow subject to the quasi-toroidal incompressibility condition:

$$\frac{d}{dt}(aB_\phi) = 0 , \qquad \text{or,} \qquad \nabla.\left(\frac{v}{r^2}\right) = 0 , \tag{1}$$

where aB_ϕ is the magnetic flux through a small area element a, r is the distance from the major axis of symmetry and $\underline{v}$ is the fluid velocity. On integrating this equation we define a stream function ψ (a pseudo-scalar in the poloidal plane),

$$v_z = r\frac{\partial\psi}{\partial r} \quad , \qquad v_r = -r\frac{\partial\psi}{\partial z} \tag{2}$$

Thus on the short timescale and in the limit of infinite conduction, the conservation of toroidal magnetic flux restricts the free expansion of the plasma and allows only the interchange of magnetic flux tubes. The equations (2) may be interpreted from the particle point of view as the "E/B" drifts.

More precisely, we include the effects of finite resistivity (η) and toroidal flow v_ϕ and after using the Navier-Stokes equations we obtain expressions for the velocity field of the plasma:

$$v_r = -r\frac{\partial\psi}{\partial t} - \frac{B_r}{B_\phi}v_\phi - \frac{\eta}{B_\phi^2}\{\frac{\partial p}{\partial r} + J B_z + \frac{v_z\xi}{r^2} - \frac{\partial}{\partial r}(\tfrac{1}{2}\rho v^2)\}$$

$$v_z = r\frac{\partial\psi}{\partial r} - \frac{B_z}{B_\phi}v_\phi - \frac{\eta}{B_\phi^2}\{\frac{\partial p}{\partial z} - J B_r - \frac{v_r\xi}{r^2} - \frac{\partial}{\partial z}(\tfrac{1}{2}\rho v^2)\} \tag{3}$$

where $\underline{B}_p = (B_r, o, B_z)$ is the self-magnetic field in the poloidal plane, p is the pressure, J the toroidal current density, ρ the density and ξ is related to the vorticity of the poloidal flow. The first two terms describe toroidal incompressibility and equilibria. The remaining terms following the coefficient η/B_ϕ^2 describe compressibility and the consequent diffusion of the plasma, with the various force terms which lead to that diffusion: namely, the outward pressure, the inward poloidal magnetic field force and the Coriolis and centrifugal forces respectively. It is to be noted that the effects of both toroidal and poloidal currents have here been included.

Evolutionary Equations

The expressions for the velocity field (Eqs.3) are to be coupled with the magnetohydrodynamic equations for the conservation of mass, the adiabatic law for the specific internal energy ε, and Faraday's Law for the toroidal vector potential A which describes the self-poloidal-magnetic field of the plasma. In addition, however, the stream function (Eqs.3) remains to be determined. A vorticity density ξ (a pseudo scalar on the poloidal plane) is therefore defined:

$$\xi = \underline{\nabla} \wedge r^2\rho\underline{v} \tag{4}$$

in a manner such that when applied to the momentum equations of the plasma,

the magnetic force terms $\underline{J}_p \wedge B_\phi$ are eliminated. Time-dependent equations for the 'vorticity' ξ, the vector potential, the density and internal energy density are thus obtained:

$$\frac{d\xi}{dt} = r\underline{B}.\underline{\nabla}\ (rJ) + 2r\ \frac{\partial p}{\partial z} \tag{5}$$

$$\frac{d}{dt}rA = \eta r \nabla^2 A \tag{6}$$

$$\frac{d}{dt}(r^2\rho) = o \tag{7}$$

$$\frac{d}{dt}(\varepsilon r^{\frac{4}{3}}) = \frac{r^{\frac{4}{3}}}{\rho}\ \{\eta\ J^2\} \tag{8}$$

from which the stream function and poloidal magnetic field may be determined:

$$\underline{\nabla} \wedge r^2 \rho \underline{\nabla} \wedge \psi = \xi \tag{9}$$

$$\nabla^2 A = -J, \quad \underline{B}_p = \nabla \wedge A \tag{10}$$

These equations describe advection, Alfven waves associated with the poloidal field, adiabatic and Joule heating, the diffusion of the field lines and, together with equations (3), the diffusion of the plasma.

The equations are simplified and numerical diffusion avoided by expressing the system in the natural coordinates, or orthogonalised field-line space, rather than the laboratory space[6]. The system of equations may then be resolved implicity on the computer to follow the complete evolution of the plasma and field structure in the poloidal plane. Since the natural coordinates are used, more sophisticated fluid and drift models can in principle be applied to provide a detailed representation of toroidal axisymmetric regimes.

Conservation Laws

The form of the equations (5,6,7,8) in the absence of resistivity and in the frame of the fluid, suggest the conservation of a variety of variables. Due to the conservation of toroidal magnetic flux (above), if a is the area of a small fluid element in the poloidal plane, the quantity a/r is conserved as the element moves around the poloidal plane. Similarly,

$$m = \rho r^2, \quad \alpha = rA, \qquad e = r^{\frac{4}{3}}\ \varepsilon \tag{11}$$

are each conserved quantities. Thus for example, if a toroidal ring of plasma is compressed towards the major axis of symmetry (decreasing r), the pressure increases very rapidly:

$$p \propto \rho\varepsilon = me\ r^{-\frac{10}{3}} \tag{12}$$

in agreement with the adiabatic heating mechanism suggested by Johnson et al.[7].

Application

In the first instance, the simulation is being applied to the study of the Tokamak experiment, for which solutions will be presented. Detailed solutions will be published elsewhere.

References

1. Pfirsch, D. and Schluter, A. (1962): Max Planck Institute Report No. MPl/PA/7/62.
2. Stringer, T.E. (1970): Phys. Fluids 13, 1586.
3. Greene, J.M., Johnson, J.L., Weimer, K.E. and Winsor, N.K. (1971): Phys. Fluids 14, 1258.
4. Duchs, D.F., Furth, H.P. and Rutherford, P.H. (1971): paper CN-28/C4 in Fourth Conf. on Plasma Phys. and Contr. Nucl. Fusion Research, Madison, June 1971.
5. Mercier, C., and Soubbaramayer, (1970): p.16 in Proc. IVth European Conf. on Contr. Fusion and Plasma Research, Rome, Sept., 1970.
6. Potter, D.E., and Tuttle, G.H. (1973): "On the Construction of Discrete Orthogonal Coordinates", to be published.
7. Johnson, J.L., Green, J.M., and Weimer, K.E. (1970): p.15 in Proc. IVth European Conf. on Contr. Fusion and Plasma Research, Rome, Sept., 1970

VARIATION OF A TOROIDAL EQUILIBRIUM

M. Bineau

ASSOCIATION EURATOM-CEA SUR LA FUSION
Département de Physique du Plasma et de la Fusion Contrôlée
Centre d'Etudes Nucléaires
Boîte Postale n° 6. 92260 FONTENAY-AUX-ROSES (FRANCE)

I - A toroidal equilibrium in a domain D is defined by functions $\vec{J}(\vec{x})$, $\vec{B}(\vec{x})$, $p(\vec{x})$ related by $\vec{J} \times \vec{B} = \nabla p$, $\nabla \times \vec{B} = \vec{J}$, $\nabla . \vec{B} = 0$. Let $\vec{J}_o(\vec{x})$, $\vec{B}_o(\vec{x})$, $p_o(\vec{x})$ be the functions for such an equilibrium. The variations of these functions are solutions of the set of equations :

$$(1) \qquad \begin{cases} \vec{J}_o \times \vec{B}_1 + \vec{J}_1 \times \vec{B}_o - \nabla P_1 = 0 \\ \vec{B}_1 = \nabla \times \vec{A}_1 \qquad \vec{J}_1 = \nabla \times \vec{B}_1 \end{cases}$$

If Ψ means the azimuthal flux of $\vec{B}$ inside a magnetic surface, an equilibrium should be determined by prescribing two functions of Ψ and by boundary conditions for $\vec{B}$. In the following analysis of the system (1) two functions $a(\Psi)$ and $b(\Psi)$ are taken as parameters. They represent respectively the variations of the functions $p(\Psi)$ and $I(\Psi)$ where $I(\Psi)$ is the azimuthal flux of $\vec{J}(\vec{x})$ interior to the magnetic surface corresponding to the flux Ψ. The boundary conditions are taken in the following way : the vector potential $\vec{A}_1(\vec{x})$ is uniquely determined by the field $\vec{J}_1(\vec{x})$ (a possible form for this relation is :

$$\vec{A}_1 = \frac{1}{4\pi} \int \frac{\vec{J}_1(\vec{x}')}{|\vec{x} - \vec{x}'|} \, d\tau(\vec{x}')) .$$

An analysis of the set of equations (1) is sketched in the following sections and leads to this result :

- When the parameters of the variation $a(\Psi)$, $b(\Psi)$ are fixed, the linearized system admits of at most one solution. In the particular case where the given equilibrium is axisymmetrical the linearized system has an unique solution which is axisymmetrical.

If the given equilibrium is not axisymmetrical the system (1) has in general no solution.

(The statement is valid for a functional space of square summable functions. The method of analysis seems unable to handle the case where the given equilibrium has a magnetic axis unless it

is axisymmetrical. The preceding assertion is therefore restricted to hard-core type equilibrium).

II - The set of equations (1) is first transformed by using coordinates η , θ, Ψ attached to the given equilibrium and such that $\vec{B}_o$ and $\vec{J}_o$ have for expressions $\vec{B}_o = \nabla(\theta - i(\Psi)\eta) \times \nabla\Psi$, $\vec{J}_o = \nabla\,(\theta - j(\Psi)\eta) \times \nabla\, I_o(\Psi)$.
(It follows that $J_o - I_o'(\Psi)\,\vec{B}_o = \nabla\eta \times \nabla\, V_o(\Psi)$ where $V_o(\Psi)$ is the volume interior to the magnetic surface with flux Ψ). At each point $\vec{x}$ of D there is a trihedral of vectors $\frac{\partial \vec{x}}{\partial \eta}$, $\frac{\partial \vec{x}}{\partial \theta}$, $\frac{\partial \vec{x}}{\partial \Psi}$ denoted by $\vec{x}_\eta, \vec{x}_\theta, \vec{x}_\Psi$, and such that $\vec{x}_\eta \times \vec{x}_\theta \cdot \vec{x}_\Psi = V_o'(\Psi)$.)

An auxiliary function $r_1(\vec{x}) = V_o'(\Psi)(\vec{J}_1 - I_o'(\Psi)\,\vec{B}_1).\nabla\eta$ is taken. The system (1) can then be written

$$(2)\quad \begin{cases} a)\ B_o.\nabla\,(p_1 + P_o'\,\vec{x}_\theta \cdot \vec{A}_1) = \frac{\partial}{\partial\theta}(p_o'\,\vec{B}_o \cdot \vec{A}_1) \\ b)\ B_o \cdot \nabla(r_1 + I_o''\,\vec{x}_\theta \cdot \vec{A}_1) = \frac{\partial}{\partial\theta}\left(\frac{V_o''}{V_o'}\,p_1 - I_o''\,\vec{B}_o \cdot \vec{A}_1 + p_o'\,\nabla\eta \cdot \vec{B}_1\right) \\ c)\ \vec{J}_1 - I_o'\,\vec{B}_1 - p_o'\,V_o'\,\nabla\eta \cdot \vec{B}_1\,\vec{x}_\theta = r_1\,\vec{B}_o + V_o'\,\nabla\eta \times \nabla p_1 \end{cases}$$

It is found that the parameters $a(\Psi)$ and $b(\Psi)$ are related to the unknown functions by $a(\Psi) = \int (p_1 + p_o'\,\vec{x}_\theta \cdot \vec{A}_1)\,d\eta\,d\theta$, $b(\Psi) = \int (r_1 + I_o''\,\vec{x}_\theta \cdot \vec{A}_1)\,d\eta\,d\theta$.

When rotational symmetry is assumed equations (2) a and (2) b are explicitly integrable since rotational symmetry implies equality of $\frac{\partial}{\partial\theta}$ with $\frac{V_o'(\Psi)}{i(\Psi)}\,B_o \cdot \nabla$.

(For example $p_1 = a(\Psi) - \frac{p_o'(\Psi)}{i(\Psi)} \int \vec{B}_o \cdot \vec{A}_1 \frac{ds}{|\nabla\Psi|} + 2\pi \frac{P_o'(\Psi)}{i(\Psi)}\,rA_\theta$,

where A_θ, is the azimuthal component of $\vec{A}$ and r is the distance to the axis of symmetry).

Substitution in (2).c of the solution p_1 and r_1 of (2) a and (2)b leads to a Fredholm equation

$$\vec{J}_1 + L(\vec{J}_1) = b(\Psi)\,\vec{B}_o + a'(\Psi)\,\frac{\vec{J}_o - I'_o\,\vec{B}_o}{p'_o}$$

(L is a compact operator on the space L^2 of square summable functions). This equation has an unique solution for arbitrary data $a'(\Psi)$, $b(\Psi)$ provided that the given equilibrium be determined by $p_o(\Psi)$ and $I_o(\Psi)$ or in other words that $a(\Psi) = b(\Psi) = 0$ imply $\vec{J}_1(\vec{x}) = 0$.

III - NON SYMMETRICAL EQUILIBRIUM

For an axisymmetrical equilibrium the field $\vec{J}_1(\vec{x})$ is the solution of a Fredholm equation which is obtained by first solving equations (2).a and (2).b in the form $p_1 = a(\Psi) + f(\vec{J}_1)$, $r_1 = b(\Psi) + g(\vec{J}_1)$ where f and g are compact operators. Such a solution is a priori impossible when there is no symmetry. However a similar transformation of the system (2) can be based on the following idea discussed in the next section : if a solution exists, continuous operators f and g : $\vec{J}_1 \to f(\vec{J}_1)$, $\vec{J}_1 \to g(\vec{J}_1)$ can be found such that p_1 and r_1 are expressible by $a(\Psi)+f(\vec{J}_1)$ and $b(\Psi)+g(\vec{J}_1)$ respectively.

This fact allows replacement of the system (2) by an equation for $\vec{J}_1$:

$$(3) \qquad \vec{J}_1 + L(\vec{J}_1) = b(\Psi)\,\vec{B}_o + a'(\Psi)\,\frac{\vec{J}_o - I'_o\,\vec{B}_o}{p'_o}$$

where $L : \vec{J}_1 \to L(\vec{J}_1)$ is continuous in the space L^2 and small of order β (β is a measure of $\frac{p_o}{B_o^2}$). Inside a radius of convergence for β equation (3) has a unique solution for whatever choice of functions $a(\Psi), b(\Psi)$. Accordingly if a solution exists it is uniquely determined by the data $a(\Psi)$ and $b(\Psi)$. The solution of (3) may be called a pseudosolution of (2). In order for a pseudosolution to be the solution of (2), equivalence of (2).a and (2).b with $p_1 = a(\Psi)+f(\vec{J}_1)$ and $r_1 = b(\Psi)+g(\vec{J}_1)$ must be verified. The condition for this equivalence is expressed by means of an infinite sequence of relations which are conditions for the functions $a(\Psi)$ and $b(\Psi)$. The statement given in the first section is thus justified.

IV Some assumptions are made about the smoothness of the given equilibrium. For example $P_o'(\Psi)$ and $I_o''(\Psi)$ are differentiable functions and vanish on the boundary of D. With respect to the variable Ψ the domain D is an interval Ψ_1, Ψ_2.
Since $\vec{B}_o.\nabla = \frac{1}{V_G'(\Psi)}(\frac{\partial}{\partial\eta}+i(\Psi)\frac{\partial}{\partial\theta})$ equations (2).a and (2).b have the form

$$(4)\quad (\frac{\partial}{\partial\eta}+i(\Psi)\frac{\partial}{\partial\theta})z = c(\Psi)\frac{\partial y}{\partial\theta}$$

where $c(\Psi)$ vanishes on Ψ_1 and Ψ_2. We seek to replace (4) by an expression for z as a functional of y. The functions z and y have representations by means of Fourier series with functions $\exp 2i\pi(n\eta+m\theta)$ and coefficients $z_{nm}(\Psi)$, $y_{nm}(\Psi)$. If (4) has a square summable solution then $y_{nm}(\Psi)$ vanishes at the value Ψ_{nm} of Ψ, the solution of $n+i(\Psi_{nm})m=0$. If (4) has a solution, a possible expression of z is thus

$$z = c(\Psi)\sum_{nm}\frac{y_{nm}(\Psi)-\bar{y}_{nm}}{i(\Psi)-i(\Psi_{nm})}\exp 2i\pi(n\eta+m\theta)+z_o(\Psi)$$

where $\bar{y}_{nm}=0$ if $\Psi_{nm}<\Psi_1$ or $\Psi_{nm}>\Psi_2$ and $\bar{y}_{nm}=y_{nm}(\Psi_{nm})$ if $\Psi_1\leq\Psi_{nm}\leq\Psi_2$. The mapping $y\to h(y) = c(\Psi)\sum\frac{y_{nm}-\bar{y}_{nm}}{i(\Psi)-i(\Psi_{nm})}\exp 2i\pi(n\eta+m\theta)$ is continuous from L_1^2 into L^2 where L_1^2 is the vector space of functions defined on D and normed by $\int(|y|^2+|\nabla y|^2)\,d\tau\,(\vec{x})$.

According to potential theory $A : \vec{J}\to\vec{A}(\vec{J})$ and $A_i : \vec{J}\to\frac{\partial}{\partial x_i}\vec{A}(\vec{J})$ are continuous mappings $L^2\to L_1^2$. The method described above thus allows replacement of equation (2).a by $p_1 = a(\Psi)+f(\vec{J}_1)$ where $f : \vec{J}_1\to f(\vec{J}_1)$ is a continuous mapping $L^2\to L_1^2$. Similarly equation (2)b can be replaced by $r_1=b(\Psi)+g(\vec{J}_1)$ where $g : \vec{J}_1\to g(\vec{J}_1)$ is a continuous mapping of L^2 into itself. The conditions for the equivalence of (2).a and (2).b with the new expressions are $\bar{f}_{nm}(\vec{J}_1)=0$, $\bar{g}_{mn}(\vec{J}_1)=0$ for all n and m.

Arbitrarily Shaped Resistive Tokamak Equilibria

B.J. Green, K.U. v. Hagenow, H.P. Zehrfeld

Max-Planck-Institut für Plasmaphysik, 8046 Garching, FRG

In contrast with the usual treatments of Tokamak equilibria we self-consistently include the effects of resistivity. This makes the problem physically well posed and in particular allows the determination of the current density profiles. Situations of arbitrary cross section and aspect-ratio can be considered.

The problem of toroidal axisymmetric MHD equilibrium has been discussed for some time now. Its usual formulation (e.g. see [1]) consists of the introduction of a stream function (which can be taken identical with the poloidal magnetic flux G), leading to an elliptic partial differential equation

$$\Delta^* G \equiv R^2 \mathrm{div} \frac{\nabla G}{R^2} = -\Lambda\dot{\Lambda} - 4\pi^2 R^2 \mu_o \dot{p} \qquad (1)$$

Here R is the distance from the major axis of the torus, and $\dot{p}$ and $-\dot{\Lambda}/\mu_o$ are the derivatives with respect to G of the pressure and poloidal current, respectively.

Normally the functions Λ and p are arbitrarily prescribed and the boundary-value problem solved. However, the self-consistent inclusion of resistive effects [2,3] determines these functions in terms of more basic quantities maintaining the equilibrium, viz. ring voltage U, electrical conductivity and sources describing the creation and destruction of plasma. The few treatments of this resistive problem have yielded explicit results only for the large aspect-ratio limit with either a circular boundary [2-5] or an elliptical one [3]. This paper indicates how we will treat the problem in full generality, that is, there will be no restriction, in principle, on the form of the plasma boundary or on the toroidal aspect-ratio.

It is convenient to resolve the magnetic field $\underline{B}$ and the current density $\underline{J}$ into meridional and toroidal components

$$B = \frac{1}{2\pi}(\nabla\zeta \times \nabla G + \Lambda \nabla\zeta) = B_M + B_T \qquad (2)$$

$$\mu_o J = \text{rot}\, B = \frac{1}{2\pi}(\dot{\Lambda}\nabla G \times \nabla\zeta - (\Lambda\dot{\Lambda} + 4\pi^2 R^2 \mu_o \dot{p})\nabla\zeta) \qquad (3)$$

where ζ is the azimuthal angle co-ordinate in this axisymmetric situation. From these expressions can be seen not only the implicit dependence of $\underline{B}$ and $\underline{J}$ on Λ and p through solutions of equation (1), but also the explicit one.

The introduction of an anisotropic resistivity ($\eta_{\parallel}, \eta_{\perp}$) is accomplished by the inclusion of an Ohm's Law and the equation of mass conservation (see [2] for details). The Λ and p functions are then given by the following equations

$$\dot{\Lambda} = \frac{\mu_o U}{\eta_{\parallel}\Lambda} \cdot \frac{\tau + q_p}{\varepsilon + (1+\varepsilon)\tau} \qquad \dot{p} = \frac{U\langle 1/R^2\rangle}{4\pi^2 \eta_{\parallel}} \cdot \frac{\varepsilon - (1+\varepsilon)q_p}{\varepsilon + (1+\varepsilon)\tau} \qquad (4)$$

We define averages for any function A and any surface quantity S:

$$\bar{S} \equiv \frac{1}{V}\int_0^V S(\hat{V})\, d\hat{V} \qquad \langle A\rangle \equiv \frac{d}{dV}\int A(x)\, d^3x \qquad (5)$$

The latter integration is to be carried out over the volume V enclosed by a magnetic surface. ε and τ can then be written:

$$\varepsilon \equiv \frac{\langle B_M^2\rangle}{\langle B_T^2\rangle} \qquad \tau \equiv \left(\frac{\eta_{\perp}}{\eta_{\parallel}} - 1\right)\langle 1/R^2\rangle\langle R^2 \cdot B_M^2/B^2\rangle + \langle 1/R^2\rangle\langle R^2\rangle - 1 \qquad (6)$$

$q_p = \langle \underline{v}.\nabla G\rangle / U$ is a dimensionless source-dependent function for a plasma with flow velocity $\underline{v}$.

The partial differential equation expressing the radial force balance becomes

$$\Delta^* G = -\frac{\mu_o U}{\eta_{\parallel}}\left\{R^2\langle 1/R^2\rangle + \frac{1 - (1+\varepsilon)R^2\langle 1/R^2\rangle}{\varepsilon + (1+\varepsilon)\tau}(\tau + q_p)\right\} \qquad (7)$$

For given ring voltage the problem then consists of prescribing a source q_p corresponding to the relevant physical processes, e.g. recycling, neutral injection, recombination etc., and resistivity. The resulting equation for G can then be solved numerically by iterative methods [6].

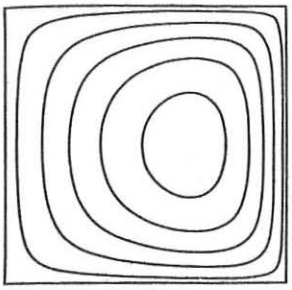


Fig.1

This programme can be carried out in all generality, here for simplicity we give the results of the special case $\tau + q_p = 0$. This condition implies that the poloidal current density is zero (i.e. $\dot{\Lambda} = 0$) and that the toroidal magnetic field is the vacuum field. This is the borderline case between paramagnetic and diamagnetic situations. Positive sources of matter are required to maintain a stationary state.

We consider a torus with square cross section. The magnetic surfaces for such a case with aspect-ratio A = 2 are shown in fig.1.

It should be noted that for large aspect-ratio, $A \gg 1$, $\dot{p}$ is independent of G. However, simplified calculations which assume such a dependence for finite aspect-ratio can be highly misleading. A comparison between two cases, the one with constant, the other with self-consistently determined p, has been made for a large range of aspect-ratio values and for fixed total toroidal plasma current. The results for the pressure and the toroidal current density at A=2 are shown in figs. 2 and 3, respectively. While the differences in the pressure profile are barely discernable, those in the current density profile are significant. Note that each current density curve has been normalized to its value at the outer wall.

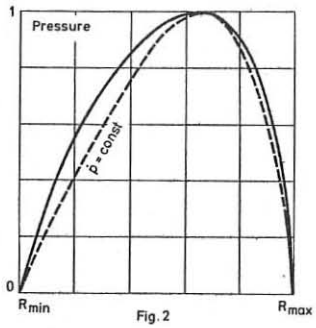


Fig. 2

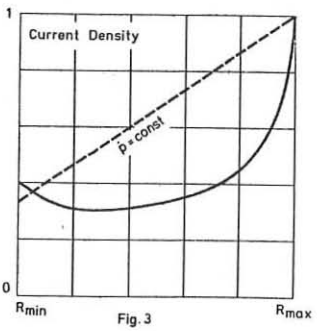


Fig. 3

Further, calculations for the poloidal beta

$$\beta_p = \frac{2\mu_0(\bar{p}-p)}{\langle B_M^2 \rangle}$$

show that this quantity does not vary

greatly from its large aspect-ratio limit ($\beta_p = 1$), in contrast to the situation with a linear pressure function, where β_p is artificially enhanced.

Such discrepancies in the form of the toroidal current density and in the variation of β_p have obvious implications on the stability of these equilibria and on the scaling of future devices.

References:

[1] Shafranov V.D.(1966) "Review of Plasma Physics" 2 Consultants Bureau, New York

[2] Zehrfeld H.P. and Green B.J.(1970) IPP Report III/1, Garching

[3] Grad H. and Hogan J.(1970) Phys.Rev.Letters 24, 1337

[4] Nührenberg J.(1971) Nuclear Fusion 11, 655

[5] Andreoletti J.(1971) Plasma Physics 13, 313

[6] v. Hagenow K.U. and Lackner K.(1973) "Third International Symposium on Toroidal Plasma Confinement", Munich, Paper F7.

The Effect of Plasma Flow on the Toroidal Equilibrium Shift

B.J. Green, H.P. Zehrfeld
Max-Planck-Institut für Plasmaphysik, 8046 Garching, FRG

Neutral injection in toroidal systems leads unavoidably to plasma flow. Such flows affect the position and form of the magnetic surfaces. We show that modifications of the toroidal plasma shift can be of the same order as the no-flow shift. This necessitates a reinterpretation of column position diagnostics in Tokamak systems.

In toroidal equilibrium a plasma is displaced outward with respect to the containing device (i.e. away from the major axis). An expression for this plasma column shift, in the case of large aspect ratio, has been given by Shafranov [1]. Recently equilibrium studies have been generalized to include plasma flows [2] and a new expression for this shift has been obtained.

The treatment of flow effects appears to be of particular importance in toroidal systems where matter is injected to heat the plasma or maintain its density, for the momentum of injected material will be transferred to the plasma column. Systems have been designed in order to eliminate net momentum transfer [3], but it seems that, locally, zero transfer will not be possible [4]. Thus plasma flows will be set up, additional to any generated during the plasma production phase. A complete treatment of such flows involves consideration of the appropriate dissipative processes, however it is the purpose of this note to treat an ideal axisymmetric plasma and indicate the nature of flow effects on the toroidal equilibrium at large aspect ratio. The equilibrium calculation with flow [2] gives for the plasma shift

$$\Delta'(r) = \frac{1}{D_0}\left\{\Delta_s'(r) - \frac{r}{R_0}\left(\frac{\mu_0}{B_M^2}\left(\langle\rho v^2\rangle - \rho v^2\right) - \frac{1}{2}\,\frac{\mu_0}{B_M^2}\langle\rho v_M^2\rangle - \frac{D_0}{\beta}\cdot\frac{v_M^2}{c^2}\cdot\frac{\beta_M^2\left[\frac{v_\perp^2}{c^2} + \frac{v_M^2}{c^2}\left(1-\beta\frac{v^2}{c^2}\right)\right]}{\left(1-\beta_M\frac{v_M^2}{c^2}\right)\left(1-\left(1+\beta\right)\frac{\beta_M}{\beta}\frac{v_M^2}{c^2}\right)}\right)\right\} \qquad (1)$$

where

$$\Delta_s'(r) = -\frac{r}{R_0}\left\{\frac{2\mu_0}{B_M^2}\left(\langle p\rangle - p\right) + \frac{1}{2}\frac{\langle B_M^2\rangle}{B_M^2}\right\} \qquad (2)$$

It should be noted that the corresponding expression for $\Delta'(r)$ in [2] was incorrectly written. Δ_S is the plasma shift where flow effects have been neglected, p is the plasma pressure, ρ the mass density and c the acoustic speed (here assumed constant). The subscripts M,T denote the meridional and toroidal field components respectively, and $v_\perp$ is that component of plasma flow perpendicular to the magnetic field $\underline{B}$.

The $\langle\ \rangle$ denotes a volume average ($V = 2\pi R_o \cdot \pi r^2$)

$$\langle A \rangle \equiv \frac{1}{V}\int_0^V A\, d\bar{V} = \frac{2}{r^2}\int_0^r A(\bar{r})\,\bar{r}\, d\bar{r} \tag{3}$$

so that

$$\langle A \rangle - A = -\frac{1}{r^2}\int_0^r \bar{r}^2 \frac{dA}{d\bar{r}}\, d\bar{r} \tag{4}$$

β_M and β_T are local β values referred to the appropriate component of the magnetic field, and D_o is a function which is related to the characteristic determinant of the general radial force balance equation [2]:

$$D_o(r) = \frac{\left(1-\beta_M\frac{V_M^2}{C^2}\right)\left(1-(1+\beta)\frac{\beta_M}{\beta}\frac{V_M^2}{C^2}\right)}{\left(1-\beta_M\frac{V_M^2}{C^2}\right)\left(1-\frac{V_M^2}{C^2}\right)-\frac{\beta_M}{\beta_T}\frac{V_M^2}{C^2}} \tag{5}$$

The lowest order force balance is expressed by the Bennett pinch relation generalized to include flow effects

$$B_M^2 = \langle B_T^2\rangle - B_T^2 + 2\mu_o(\langle p\rangle - p) + \mu_o\langle \rho v_M^2\rangle \tag{6}$$

Some effects of flow can be seen directly from the expression (1) for Δ'. Here we restrict our attention to subsonic situations, where $v_M^2/c^2 < \beta/(\beta_M(1+\beta))$. Together with (2) to (6), equation (1) then reveals that for fixed current and pressure distribution

(1) purely toroidal flows with decreasing profile of kinetic energy density lead to an enhanced plasma shift,

(2) the plasma shift for flows with radially increasing ρv^2 is <u>always</u> smaller than in the static case, because all flow contributions to Δ' are positive and B_M^2 can only be increased by flow effects.

It should be noted that the modifications of the shift due to flow can be of the same order as the no-flow shift itself and that the effect depends not only on the magnitude of the flow but also on the flow gradients.

To illustrate these points we consider a simple pressure profile which is monotone decreasing in radius, and a toroidal magnetic field:

$$p(r) = p(0)\left(1 - \frac{r^2}{a^2}\right), \quad B_T^2(r) = B_T^2(0)\left(1 + 2\left(\hat{\beta}_M - 1\right)\frac{\beta_T(0)}{\hat{\beta}_M}\cdot\frac{r^2}{a^2}\right) \quad (7,8)$$

a is the wall radius. $\hat{\beta}_M$ is the oft-quoted poloidal beta value ($= \mu_o p(0)/B_M^2(a)$). $\hat{\beta}_M > 1$ corresponds to a diamagnetic, $\hat{\beta}_M < 1$ to a paramagnetic situation.

To exemplify statement (1) above, we consider the purely toroidal flow

$$v_T^2(r) = v_T^2(0)\left(1 - \lambda\frac{r^2}{a^2}\right) \qquad 0 < \lambda \leq 1 \qquad (9)$$

which together with the assumed pressure profile gives a kinetic energy density function which is monotone decreasing in radius. Now the case of purely toroidal flow (i.e. $v_M = 0$) is special in the sence that the Bennett pinch relation is not different from that in the no-flow case. Also, the elliptic nature of the problem remains unaltered for arbitrarily large flows ($D_o = 1$). From the Bennett pinch relation and (2)

$$B_M^2(r) = \frac{\mu_o p(0)}{\hat{\beta}_M}\cdot\frac{r^2}{a^2}, \quad \Delta_s' = -\frac{\varepsilon r}{a}\left(\hat{\beta}_M + \frac{1}{4}\right)$$

where $\varepsilon = a/R_o$. The boundary condition on the plasma shift is $\Delta(a) = 0$ which gives

$$\Delta(0) = \Delta_s(0) + \frac{1}{4}a\varepsilon\hat{\beta}_M\left(1 + \frac{1}{3}\lambda\right)\frac{v_T^2(0)}{c^2} \qquad (10)$$

i.e. a flow-enhanced plasma shift. The outward shift contribution due to flow increases with increasing magnitude of the flow gradient.

To exemplify statement (2) above, we treat again the special case of purely toroidal flow. However, the estimate of the column shift reduction will be conservative, for non-zero meridional flow serves only to enhance this reduction. We take the ρv_T^2 radial profile

$$\rho v_T^2 = \rho(0)v_T^2(0)\frac{r^2}{a^2}\left(1 - \frac{r^2}{a^2}\right), \quad \frac{d(\rho v_T^2)}{dr}\begin{cases} > 0 \text{ as } r^2/a^2 < 1/2 \\ < 0 \text{ as } r^2/a^2 > 1/2 \end{cases} \qquad (11)$$

which has a positive gradient in the main plasma region. As before the Bennett relation is unaltered and integration of (1) gives

$$\Delta(0) = \Delta_S(0) - \frac{a\varepsilon}{12}\hat{\beta}_M \frac{v_T^2(0)}{c^2} \qquad (12)$$

To illustrate more forcefully the effect of gradients in flow kinetic energy, we take as a final example the situation where $v_M=0$ and the displacement is set identically zero. This imposes the following constraint on pressure, magnetic field and flow

$$\frac{d(\rho v^2)}{dr} = -2\frac{dp}{dr} + \frac{B_M^2}{\mu_0 r} \qquad (13)$$

Assuming the pressure and toroidal magnetic profiles

$$p(r) = p(0)\left(1-\lambda\frac{r^2}{a^2}\right), \quad B_T^2(r) = B_T^2(0)\left(1+2(\hat{\beta}_M\cdot\lambda-1)\frac{\beta_T(0)}{\hat{\beta}_M}\frac{r^2}{a^2}\right) \qquad (14)$$

and the condition $v_T(0)=0$, we get

$$\frac{v_T^2}{c^2} = \frac{4\lambda+\hat{\beta}_M^{-1}}{2\cdot\left(1-\lambda\frac{r^2}{a^2}\right)}\cdot\frac{r^2}{a^2} \qquad (15)$$

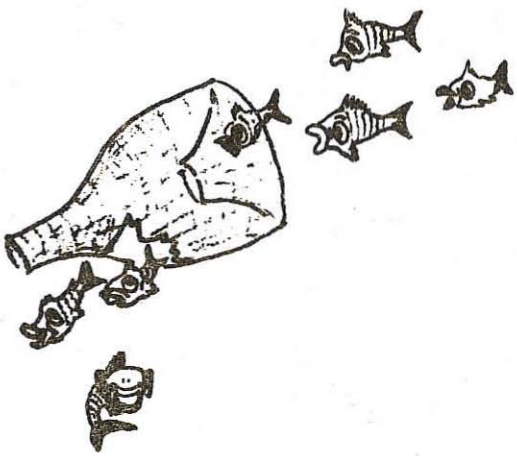
Here the condition for subsonic flow implies a rather flat pressure profile.

This treatment indicates qualitatively the effect of flow on one feature of the toroidal plasma equilibrium viz., the plasma column shift. This quantity plays an important role in the processing of Tokamak experimental data [5,6]. Some Tokamak experiments (see for example [7] have displayed anomalous plasma shifts, and although flow effects were excluded as an explanation, it appears certain that for future experiments involving particle injection, accurate measurements of plasma flow profiles will be necessary.

References

1. Shafranov V.D. (1966) "Reviews of Plasma Physics" 2 Consultants Bureau, New York
2. Zehrfeld H.P. and Green B.J. (1972) Nuclear Fusion 12 569
3. Ohkawa T. (1970) Nuclear Fusion 10 185
4. Callen J.D. and Clarke J.F. (1971) Bull.Am.Phys.Soc. 16 1261
5. Mukhovatov V.S. and Shafranov V.D. (1971) Nuclear Fusion 11 605
6. Artsimovich L.A. (1972) Nuclear Fusion 12 215
7. Artsimovich L.A. et al., (1969) Nuclear Fusion Special Supplement 17

2.1. OPEN TRAPS



INVESTIGATION OF THE INSTABILITY OF COLLISIONAL PLASMA IN PR-6 MIRROR TRAP

B.I.Kanaev, E.E.Yushmanov

I.V.KURCHATOV INSTITUTE OF ATOMIC ENERGY

Moscow, USSR

A B S T R A C T

The previous experiments in PR-6 device have revealed an instability identified tentatively as the drift-cone mode. New experiments involving SHF heating of electrons have confirmed the close tie between the instability and T_e, thus proving the validity of the earlier concept. It is experimentally shown, the instability can be stabilized by slight repopulation of the cold region of the ion distrib. funct. through transverse heating of a small fraction of the electrons.

It was shown earlier /1,2/, that at $n \gtrsim 10^{12}\,cm^{-3}$ and $\mathcal{E}_i \gtrsim 100ev$ the plasma decay in a min B trap was accompanied with the development of an instability (temporarily referred as SCI - sub-cyclotron instability) at the frequency $\omega \simeq 0{,}7\,\omega_{Bi}$ and $k\rho_i \simeq 4$. The SCI brings about intense anomalous losses, which are the more vigorous the hotter the ions are. A positive ambipolar potential seems to be responsible gor the SCI.

The data available allow us to assume, that the SCI by its nature should be none but the drift - cone instability /3/. Compared to the theoretical prototype, however, the "live" instability has several distinctions. First, for the SCI to develop it is necessary the ion distrib. funct. to be more strongly deformed, than with a simple loss cone. Such additional deformation is caused by the ambipolar potential and represents transformation of the loss cone into an onesheet hyperboloid. As a result, the cold end of the distribution turns to be cut off up to energy $e\varphi/(R-1)$. The presence of an appreciable "hole" is a necessary condition for the SCI to appear. Its second prominent feature, unnoticable beforehand, is the tendency to malignant growth /2/ due to SCI capability to deform the distrib. funct. more and more via the electron feedback(the SCI heats the electrons thus increasing the potential, the instability becoming still stronger, and so on).

This is the framework of the concept developed from the preceding work. Among the new experiments one of importance is that with

super-high frequency heating of the electrons in order to obtain weighty pros or cons about the concept as above. According to that, the additional heating of the electrons, increasing the potential, should apparently result in SCI growth. The appearance of such an effect could confirm both the "hole origin" of the SCI and reality of the electron feedback.

To heat the electrons, an SHF puls of 50 μsec. and $\simeq$ 10kw was injected into the trap soon after the plasma decay beginning. Its frequency was 15GHz, near to ω_{Be}. The measurements of T_e after the puls show its increase by a factor of about two; this is also reflected as the plasma potential increase. The results are presented in Fig.1:

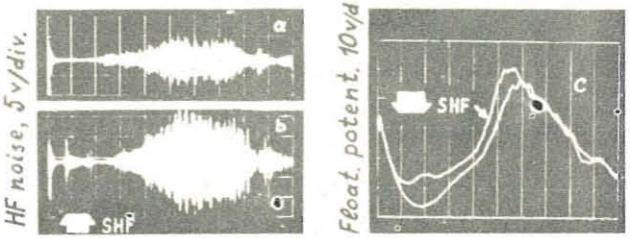


Fig.1. Time scale 50 μsec/div.

(a) growth of the SCI for free decay; (b) the same with SHF applied; (c) superposed signals of the floating potential with the pulse and without it. It is seen, that the effect of the expected SCI enhancement is well manifested.

In general, SHF influences the electrons in two ways. In addition to a certain increase in the total T_e, a relatively small group of electrons acquires high energy transverse to B. The relation between these two kinds of heating depends on a number of conditions, in particular, on the plasma density: the higher the density, the weaker is the anisotropic overheating. The overheated electrons were also produced in the experiment described above, but due to high plasma density they were not very numerous and their excess energy was lost rapidly, therefore their effects were negligible. But when the SHF puls was applied later, at lower density, the overheating was strongly increased, and phenomenon opposit to that described could be observed: the SCI died away.

Such a stabilization results from reverse deformation of the loss hyperboloid towards the hole narrowing or even its entire closing. The deformation is caused by the change in Z-profile of the po-

tential in the central region of the trap due to the appearance of the anisotropic electrons. Before SHF puls the plasma electrons are confined mainly by a high electrostatic barrier, and their distribution is almost Maxwellian, so the potential and electron density profiles are related through Boltzmann law $n_e(z) \sim \exp[\varphi(z)/T_e]$. After the SHF puls a certain fraction of the electrons near the midplane has turned anisotropically heated and is further confined by the magnetic field. The density of the cold Maxwellian electrons decreases by the same value, and in accordance with Boltzmann law it leads to a certain decrease in the potential near the midplane relative to the lateral regions, where there are no overheated electrons. The Z-profile of the potential flattens at the top or even becomes locally concave, thus giving rise to the above deformation of the hyperboloid /4/.

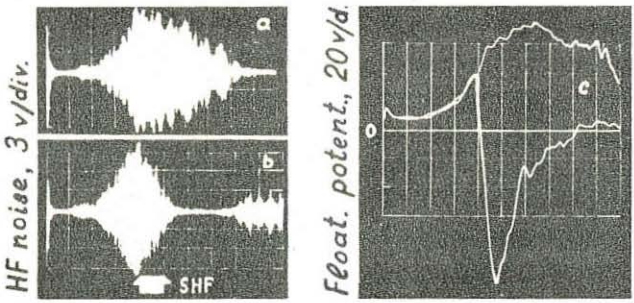


Fig.2. Time scale 50 μsec/div.

The illustration of the stabilization phenomenon is presented by Fig.2. The trace (a) is, as before, a free growth of the SCI; the trace (b) shows the damping effect of the SHF; the trace (c) shows the signals of a floating probe in the midplane without the puls and with it. A deep negative spike reflects appearance of the hot electrons, striking the probe. If the probe is shifted from the midplane, it indicates absence of the hot electrons there and

only slight change in the plasma potential. The trace (c) indicates also a rather rapid relaxation of the overheated group, therefore the damping effect turns out to be temporary.

The damping method described above is closely related by its physics to Post's idea concerned with the addition of small amounts of warm ions to stabilize the loss cone modes /5/. In our case, such an addition represents the ions to be found in the additional volume of accessible V-space, appearing after the SHF puls. It is clear from the geometry, that this addition is small.

The authors are deeply grateful to M.S.Ioffe for fruitful discussions as well as to V.P.Pastuchov, who in particular have pointed out the possibility of favourable deformation of the loss surface at anisotropic heating of the electrons. The work could not be performed also without ingineering help of Yu.T.Baiborodov.

1 Yu.T.Baiborodov et al. Madison conf. CN-28/G-7(1971).

2 B.I.Kanaev, E.E.Yushmanov, Greenoble conf. (1972).

3 R.F.Post, M.N.Rosenbluth, Phys.Fl., 9, 730 (1966)

4 E.E.Yushmanov, Sov.Phys. - JETP 22, 409 (1966).

5 H.L.Berk et al, Novosibirsk conf., CN-24/G-12 (1968).

Sixth European Conference on Controlled Fusion and Plasma Physics
Moscow, USSR. 30 July - 3 August 1973

A COMPUTATIONAL STUDY OF SPACE CHARGE LIMITATIONS IN DIRECT CONVERSION SYSTEMS

F B Marcus† and C J H Watson

UKAEA Culham Laboratory, Abingdon, Berkshire, England

† on attachment from University of Oxford

The direct conversion of charged particle energy into electricity, with high efficiency, is of importance for achieving a net power output at an economic level from mirror-type fusion reactors. To achieve this, a focusing and decelerating electrostatic ion collector has been proposed by R F Post [1,2]. In this paper we present some computer studies of this system, which take into account the high space charge levels appropriate to reactor regimes. These studies confirm and supplement a theoretical analysis which is discussed in [3].

The potential within the collector was assumed to be of the form

$$\Phi = \frac{W_o}{2\pi eN}\left[kz + C \sin(kz) \sinh(kx)\right] + \Phi_{sc} \quad , \quad k = \frac{2\pi}{L}$$

where z is the axial direction, x is the transverse direction, L is the focusing period length, N is the number of periods in which an ion of average energy W_o is decelerated to rest, and C is a constant. Φ_{sc} is the potential due to the space charge, which is assumed to be uniform within a slab of thickness $2h$, and has a density characterised by $\omega_{pi}\tau$, where ω_{pi} is the ion plasma frequency, and $\tau = L/V_o$ is the transit time across one collector period for an ion of average velocity V_o.

Two computer programs were used to trace particle orbits in this field. The first numerically integrates the exact equation of motion in it. The second uses the analytic theory described in [3] to eliminate the component of the motion with frequency $\omega \geq kV$. It is shown in [3] that the low frequency component of the motion is determined by an effective confining potential $\psi(x,W)$, which depends on z only through the slow variation of W, the mean ion energy within one period. The transverse motion within this confining potential is characterised by a dimensionless parameter $q(x,W)$, equal to the magnitude of the peak focusing potential within a given period at that value of x, normalised with respect to W. An optimized collector structure represents the best

compromise between two requirements. (i) In order that a beam edge should exist at a height h, at which the focusing force balances the space charge force, it is necessary that $q(h,W_o) = \omega_{pi}\tau\sqrt{2h/\pi L}$. (ii) Ions which are not in equilibrium at the beam edge execute periodic oscillations about it, and they become defocused if at $x = x_{max}$ (their maximum transverse excursion), $q_{max} \equiv q(x_{max},W) > 0.67$. Thus the collector should be designed so that $q_{max} < 0.67$ until W has fallen to a small fraction of W_o. Optimization with respect to these two requirements gives $h/L \simeq \frac{1}{2}$ and $N \simeq 20$, and these values were assumed in all the computations. If now the equation of motion is written in dimensionless form, using V_o and L as the velocity and length scales, it is seen to depend solely on the parameter $\omega_{pi}\tau$. Particle orbits were obtained from both programs, for a range of $\omega_{pi}\tau$ values (0.2 - 0.5) chosen for their relevance to the reactor situation.

In each case the ion was launched at some point below the equilibrium position $x = h$, and it oscillated about this equilibrium until decelerated and defocused. If the point of launching was fairly close to $x = h$, the orbits predicted by the two programs were essentially identical until the ion was defocused (see Fig.1 below).

If, however, the ion was started nearer to the beam axis, so that the value of q_{max} exceeded 0.45 at some reflection off the potential ψ, then non-adiabatic effects were observed; these caused the orbit to deviate locally from that predicted by the analytic theory. The analytic theory has been modified [3] to take into account these local non-adiabatic jumps, and a 'modified analytical program', which incorporates this, describes ion orbits correctly until defocusing occurs, with an accuracy in z of 10%.

To calculate the mean energy collection efficiency η, two groups of exact orbits were followed for $\omega_{pi}\tau = 0.23$ and 0.46 (which differ by a factor of four in current density) for a range of different initial positions x_o and transverse velocities $V_\perp$. The energy was fixed at the average energy, the initial $V_\perp / V_o$ was varied from -0.10 to 0.10, and x_o was varied from -h to h. In the first group, consisting of 105 particles, there were 4 retrogade orbits, and there were 2 in the second group. These retrogrades were assumed to be collected with average η. The resultant average values of η were 0.85 and 0.45. The modified analytic theory program was run under similar conditions, and for $\omega_{pi}\tau = .23, .23\sqrt{2}, .23\sqrt{3}$, and 0.46, gave η values of 0.86, 0.73, 0.53, and 0.43 respectively, in good agreement with the other results. This latter program

was used in the following studies.

In order to determine the statistically more important processes, an analysis was made of the sequence of events occurring during each of the two groups of 66 trajectories. These were classified in terms of a sequence of the following letter codes: B is an adiabatic bounce, J is a non-adiabatic jump in energy at a bounce, L is a defocusing event, S is a stopping in the last collector period, and J-L or J-S is a non-adiabatic jump followed immediately by a particle loss at the adjacent collector period. For $\omega_{pi}\tau = 0.23$, the sequences and number of occurrences were:

S,2; BL,4; BCL,18; BCS,3; JCL,6; JCS,1; BBS,3; BCJ-L,1; BCJS,2; BJCS,2; CBCL,10; JCJ-S,1; BJCL,3; BBCS,1; JCJCL,1; CBCJ-L,1; BCBCL,3; BJJCS,1; BBJCL,1; BCJJCL,1; BCJCJ-L,1.

In this group only 24% of the ions were collected in the last focusing period. The total inefficiency, $\eta^* = 1-\eta$, of 0.14, resulted primarily from the three most common sequences, BCL, CBCL, and JCL, with η^* equal to 0.06, 0.03, and 0.02. In the $\omega_{pi}\tau = 0.46$ case, the dominant process was a loss on the first bounce, with its η^* equal to 0.27 out of a total η^* of 0.57. The shift in the relative frequency of sequences with increasing $\omega_{pi}\tau$ is directly related to the decrease in efficiency.

To study this effect in isolation from the effect of initial beam divergence, we performed a series of runs with zero divergence. Four groups of twenty ions each were launched at different initial transverse positions. At $\omega_{pi}\tau = 0.23$, $0.23\sqrt{2}$, $0.23\sqrt{3}$, and 0.46, the values of η were 0.94, 0.76, 0.62 and 0.41. For $(\omega_{pi}\tau) = 0.23$, the sequences and number of occurrences were S,1; BL,2; BBS,4; BCS,1; BCL,4; JCS,1; BCJS,2; BJCL,1; BJCS,2; JCJ-L,1; and BCJCS,1. In this group, 60% of the ions were collected in the last focusing period. The total $\eta^* = .06$ resulted primarily from the BL, BCL, and JCJL sequences, with $\eta^* = .01$, .02, and .01. In the $\omega_{pi}\tau = 0.46$ case, the dominant loss process was a loss on the first bounce, with its $\eta^* = .33$ out of a total η^* of .59.

Thus we see that above a certain level of space charge (corresponding to $\omega_{pi}\tau \approx 0.3$) the dominant loss process is a bounce with $q \geq 0.67$ occurring before the particle reaches the last collector period, regardless of the initial beam divergence. Conversely at a sufficiently low space charge level ($\omega_{pi}\tau < 0.25$) and sufficiently low initial divergence, $\eta^* \leq 0.06$, implying that most of the particles reach the last collector period and are then strongly defocused within it. However, even quite modest levels of initial beam diverg-

ence are sufficient to ensure that this does not occur. This greatly simplifies the interpretation of the efficiencies obtained, for if loss typically occurs at a bounce with $q \approx 0.67$, occurring before the last collector period, and the initial beam divergence is negligible, a theoretical argument [3] shows that $\eta^* \approx 2.2(\omega_{pi}\tau)^2$. Under the same conditions, but with finite beam divergence, a rather less rigorous argument indicates the same scaling of η^* with $\omega_{pi}\tau$, but with a slightly different numerical factor. The argument only becomes inapplicable if a significant fraction of the particles reach the last collector period. The computer results confirm this picture well (Fig.2); for the realistic initial beam divergence considered above, $\eta^* = 2.6(\omega_{pi}\tau)^2$, and for zero divergence the points lie between the lines $2.2(\omega_{pi}\tau)^2$ and $2.8(\omega_{pi}\tau)^2$ except at $\omega_{pi}\tau = 0.23$, where the majority of the particles reach the last collector period.

We conclude that for a realistic reactor direct converter, the inefficiency due to the finite space charge only (i.e. ignoring all other loss processes) scales with the total current I as $\eta^* = 1 - \eta = 2.6(\omega_{pi}\tau)^2 = I/2I_c$

where $$I_c = \left(\frac{3600 \text{ Amps}}{1 \pm 0.15}\right)\left(\frac{\text{Perimeter}}{300 \text{ metres}}\right)\left(\frac{2h}{1 \text{ metre}}\right)\left(\frac{W_o}{500 \text{ KeV}}\right)^{\frac{3}{2}}.$$

A more extensive discussion of these results is given in [4].

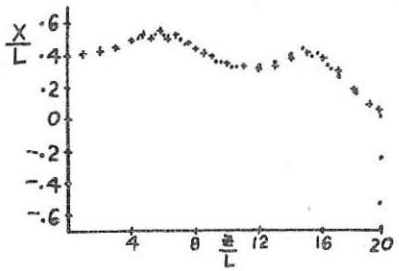


Fig.1. Typical Ion Orbit Exact and Analytical.

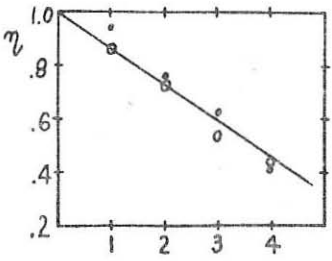


Fig.2. Energy Collection Efficiency vs $[\omega_{pi}\tau/.23]^2$

References

[1] Post, R.F., BNES Nuclear Fusion Reactor Conference, Culham Laboratory, Paper 2-1, 1969.

[2] Moir, R.W., Barr, W.L., Freis, R.P., and Post, R.F., Madison, Proc.IAEA, Vol.III, 1971. Paper CN-38/K-1.

[3] Marcus, F.B., and Watson, C.J.H., Space Charge Limitations in Direct Converter Design. To be published.

[4] Marcus, F.B., D.Phil. Thesis, University of Oxford, England, 1972.

PLASMA CONFINEMENT IN THE PRESENCE OF FEEDBACK SYSTEM IN OGRA - 3 DEVICE .

V.A.Chuyanov, V.Kh.Likhtenshtein, D.A.Panov,
V.A.Zhil'tsov, A.G.Scherbakov.
I.V.Kurchatov Institute of Atomic Energy ,
Moscow , USSR.

A b s t r a c t . In the simple mirror magnetic trap one electrode feedback system increases a flute instability threshold only within a limited range of plasma densities.The feedback system with two electrodes displaced in azimuth by 90° removes this limitation.The density obtained with the feedback "on"exceeds the flute instability threshold by more than a factor of ten. At the highest density achieved plasma losses related with residual oscillations are observed.

The previous experiments on the stabilization of plasma flute instability in the magnetic mirror machines"Ogra-2"/1/ and "Phoenix -2" /2,3/ by feedback and theoretical calculations/4/ as well have shown the certain prospect for a continuation of these works. The Ogra-3 device, the magnetic trap with the simple mirror field generated by superconducting coils and with improved injector of atomic beam with the intensity up to 0.5 eq. amp. at the energy of 20keV has been built.The maximum magnetic field strength in the center of the trap is 24 kgs , the mirror ratio is 2.1.The magnetic field in the median plane of the trap decreases according to the parabolic low $B(z=0) = B_0(1-\beta z^2)$ with the coefficient $\beta = 2.22 \cdot 10^{-3}$ cm^{-2}.The distance between the magnetic mirrors is 44 cm , the radius of the zone filled by the plasma depends on the position of electrodes limiting the plasma and in the present experiment was equal to 8 cm.

In the present experiments the cross-section of the injected beam being equal to $10 \times 20 cm^2$ was decreased up to 4x6cm on the entrance of the trap by meance of diaphragms. Correspondingly the maximum intensity of the beam in the trap doesn't exceed now 25 eq. mA.

The stabilization of flute instability was carried out by the integrating feedback /3/ with measuring the azimuthal component of

the perturbated electrical field. For this purpose the differential signal of two electrostatic probes located symmetrically with respect to the stabilizing electrode was used in each feedback channel. There were used from 1 up to 4 independent feedback channels and from 1 to 4 stabilizing electrodes respectively in those experiments.

The calculations /4/ have shown that in the absence of rotation of the plasma the one-electrode feedback system can stabilize the flute instability only up to densities exeeding the flute threshold no more than 2 times. In the presence of a plasma potential and a rotation of the plasma in the field of own space charge the stable density can be somewhat increased. Experiments with the one-electrode feedback system have confirmed these calculations. The trajectory of build-up on the plane "density-plasma potential" is shown in Fig. 1. The mean density was measured by the flux of charge-exchange neutrals, the potential on the trap axis - by the energy of cold ions streaming out through mirrors and by the shift of oscillation frequency due to the plasma rotation. Boundaries of stability are shown in this Fig as well. According to /4/ they were calculated for different radial distributions of the densityc characterising by coefficients γ /4/. In the stable region the potential is determined by the ion-cyclotron instability and increases together with the plasma density. When the boundary of stability is achieved, the rate of potential growing with the change of density increases and then movement takes place along the boundary of stability, calculated in /4/.

To eliminate this instability it is necessary to have two stabilizing electrodes as minimum located at different azimuths with 90° shift. The experiments with such two electrodes have shown that the instability inherent to one-electrode system is indeed eliminated and the plasma density encreases simultaneously with decreasing the amplitude of oscillations.

But when the density is increased further up to $3n_0$, that in our case corresponds to $3.10^8 cm^{-3}$, an excitation of the second azimuthal mode of the flute instability was found. The increase of the number of electrodes up to 4 permitted to raise the threshold of the second mode up to $4\text{-}5.10^8 cm^{-3}$. (Here everywhere the mean

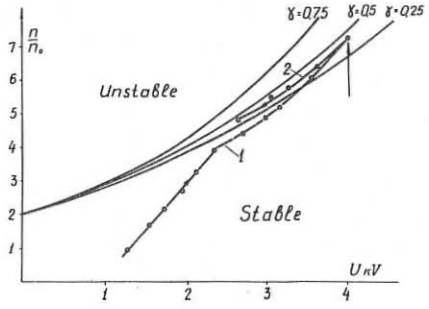


Fig.1 Trajectory of build-up (1) and decay (2) of the plasma on the plane "density-potential". The theoretical boundaries of stability for different radial distributions[14] are shown as well. The arrow indicates the moment when injection is switched off. $n_0 = 1 \cdot 10^8 cm^{-3}$ - the threshold of flute instability.

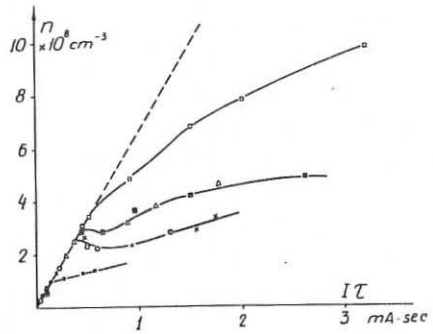


Fig.2 The dependence of the plasma density n on $I\tau$ (I-is the injected beam, τ -is the charge-exchange time) at the different number of stabilizing electrodes. ∘ -without stabilization, O - one electrode, X - two electrodes shifted over 180°, Δ - two electrodes shifted over 90°, ■ - 3 electrodes, □ - 4 electrodes.

densities over the whole cross-section of the plasma were indicated. According with measurements of the radial distribution the plasma density on the trap axis is three times higher). Using the calculations [4] for m=2 it could be expected that for the complete suppression of the second mode it would be necessary to use 6 electrodes. But it should be noted that near the threshold of the second mode the losses associated with it are not great and do not interfere the further build-up of the plasma. The experimental results with the different number of stabilizing electrodes are given in Fig.2.

Let us note that at the injected current being equal to 25 eq. mA, the plasma volume $10^3 cm^3$ and the pressure of the residual gas corresponding to the charge-exchange time 0,2 sec., the plasma density exceeds $10^9 cm^{-3}$ and such effects as the charge-exchange on the injected beam and the pumping-out of the residual gas by the plasma can be important.At these conditions the used technique for measurements of plasma density by charge-exchange neutrals become unreliable and can give highly underestimated results.

Cyclotron harmonics were observed in comparatively narrow ranges of the plasma densities and had no significant effect on its build-up. At the same time the cyclotron instability resulted in the considerable spreading the initial narrow energy distribution of ions and the increase of their mean energy.

Thus ,the plasma losses (Fig.2) have to be connected with the residual low requency oscillations occuring in the plasma due to the limited number of electrodes of the feedback system or the imperfection of its frequency responce [3].

Authors wish to thank I.N.Golovin and V.V.Arsenin for the constant interest in the work and valuable discussions of results.

R E F E R E N C E S

1.Arsenin V.V.,Chuyanov V.A., Zhil'tsov V.A. Plasma Physics and Controlled Nuclear Fusion Research (Conference proceedings,Novosibirsk,1968) v.2, 515-529,IAEA,VIENNA 1969.

2. Chuyanov V.A.,Murphy E.G. Nuclear Fusion,12,177-183 (1972).

3. Chuyanov V.A.,Murphy E.G., Pisma ZhETPh,13 ,553-555 (1971).

4. Chuyanov V.A. V European Conf. on Cont. Fusion and Plasma Physics , Grenoble,1972 , Report N 76.

HOT ELECTRON PLASMA ACCUMULATION IN AN OPEN ENDED MINIMUM B SYSTEM

BY

R. Bardet, P. Briand, L. Dupas, C. Gormezano, G. Melin.

ASSOCIATION EURATOM-CEA
Département de Physique du Plasma et de la Fusion Contrôlée
Service IGn - Centre d'Etudes Nucléaires
B.P.85 - Centre de Tri - 38041
GRENOBLE CEDEX (France)

INTRODUCTION : The CIRCE device is an R.F. supplemented open ended minimum B system. A pulsed cold plasma is created outside of the mirror and is injected parallel to a progressive wave (circularly polarized) at the electron cyclotron resonance in one mirror of the magnetic bottle. Hot electrons plasmas have already been studied in a number of experiments with different aims : target plasma trapping /1/,/2/, high beta stability /1/, R.F. plugging /3/, electron heating effect on power balance in mirrors /4/, etc ...

The main feature of the CIRCE experiment is that the plasma is not created "in situ" and consequently the operating neutral pressure depends only on pumping conditions and not on the ionization requirements. So, the negative potential well /3/, which is established by the equilibrium between the losses of the hot electrons and of the ions, is not perturbed by the cold plasma.

We can also apply the R.F. power longer that the injection time and then we can study, without injecting, the interaction between the plasma and the R.F. field. In particular, we are interested in the diffusion of electrons into the loss cone /5/. To this aim, we must prevent the hot electrons from ionizing the neutral gas : the cold electrons created in this way have an energy comparable to that of the hot ones after a single passage through the resonance zone ; hence, they cannot be distinguished from the primary hot electrons. Roughly, we find that we have to compare $n_e = n_1 \exp(-\frac{t}{\tau_e})$ without ionization to $n_e = n_1 \exp\{(n_o \sigma v - \frac{1}{\tau_e})t\}$ with ionization (n_o being the neutral gas density and σ being the ionization cross section). The higher the electron temperature, the more severe becames the maximum allowable neutral pressure.

With this kind of injection, we can get a good quality factor n_e/n_o /1/ which is necessary to obtain a suitable target plasma for trapping neutrals provided that the electron density be sufficiently high.

DESCRIPTION OF THE EXPERIMENT : The plasma source is located (Fig. 1) in zone 3 : a cold plasma is created at, or near, the electron cyclotron resonance by a polarized progressive wave (15 kW, 16 GHz) /6/. The pressure is sufficiently high ($\simeq 10^{-3}$ Torr) in order that the mean free path of the hot electrons will be lower than

the dimension of the chamber. This cold plasma diffuses along a slowly decreasing magnetic field with a differential pumping system. The main R.F. power (25 kW, 8 GHz) is injected parallel to the cold plasma by a bent wave guide (zone 5) with a small aperture (8 mm) which preserves the polarization.

The diameter of the main chamber is 35 cm. The axial mirror ratios are : $\frac{B \text{ injection}}{B \text{ resonance}} = 1.7$ $\frac{B \text{ mirror}}{B \text{ min}} = 2.6$ $\frac{B \text{ resonance}}{B \text{ min}} = 1.2$. In order to prevent flute instabilities, an hexapolar magnetic field (zone 7) is applied which gives a radial magnetic field Br $\simeq$ 500 Gauss at 5 cm from the axis and Br $\simeq$ 5000 Gauss at the walls. The pumping in the main chamber is done by an oil diffusion pump (zone 11) (10.000 l/s) and by a titanium gettered pump (zone 8) (30.000 l/s). The base pressure in the main chamber is 3.10^{-8} Torr and the operating pressure is near of 10^{-7} Torr. This rise of pressure is mainly caused by wall degassing due to the R.F. field and not by the injected plasma.

DIAGNOSTICS : We describe only the diagnostics now in operation.

Injected plasma : The electron density is measured at two points

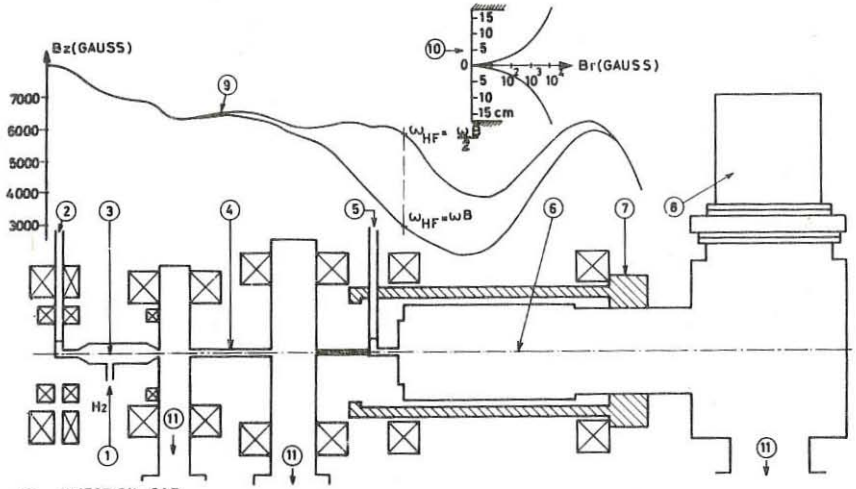
- at the exit of the plasma source by an 8 mm interferometer,
- in the middle of the main chamber by a "Zebra-stripe" interferometer (8 mm) which has the advantage of being linear for a large range of densities.

Hot plasma :

- The electron density is measured by the "Zebra-stripe" interferometer.
- A diamagnetic pick-up loop, external to the plasma, (15 cm from the axis) registers the total stored perpendicular electron energy upon plasma decay.
- The free-free bremsstrahlung is measured with a N_a I (Tl) scintillator covered by a beryllium window. The output of the multiplier is sent to a 400 channel pulse-height analyser.
- The energy and time dependence of the flux of neutral atoms emitted by the plasma is analysed with a CO_2 vapour cell where a fraction of the atoms is reionized. This fraction is electrostatically analysed using a multiplier and a 400 channel pulse height analyser.
- The negative potential well is measured with an electrostatic analyser located at the mirror. The cold electrons created by collisions of energetic electrons with neutrals escape from the negative potential well with an energy equal to this value of the potential well.

RESULTS : The experiment is at its early stage and the parameters have been adjusted mainly to test the diagnostics. With 5,75 kW R.F. power in the plasma source (time duration : 10 ms, repetition rate : 10 Hz) we get a plasma density of $5.10^{12} e/cm^3$ at the exit of the plasma source and $10^{11} e/cm^3$ in the middle of the main chamber,

so we can infer a density of 2.10^{11} e/cm^3 in the resonance zone (Fig. 2a). During the same time interval, with a main R.F. power of 2.65 kW, the product $n_e x l$ (l being the diameter of the plasma) is $4.8.10^{12}$ e/cm^3 (Fig. 2b). We do not know the exact value of l but, probably, it is of the order of 4 cm. The maximum value of the diamagnetism is 185 Gauss (Fig. 2c) which gives β : 0.18. The electron temperature is 35 keV but, as yet, we are not sure that the wall X-rays do not play an important role in the spectrum. From the neutral energy spectrum, we find two ion temperatures : T_i = 150 eV and T_i = 450 eV (with a density smaller by an order of magnitude). After the stop of the R.F. pulse, some instabilities occurs and there are two decreasing times of the density : the first one is 2 ms (for the electrons and for the ions) with a density fall of 2/3, the second one is 60ms for the electrons (Fig. 2d) and 30ms for the ions (Fig. 2a). The negative drop of potential is between 180 and 400 V.



① INJECTION GAZ
GAZ INJECTION

② ARRIVEE H.F (15 KW, 16 GHz)
R.F INPUT (15 KW, 16 GHz)

③ SOURCE DE PLASMA
PLASMA SOURCE

④ ZONE DE DIFFUSION ADIABATIQUE
ADIABATIC DIFFUSION ZONE

⑤ ONDE H.F DE CHAUFFAGE (25 KW, 8 GHz)
R.F HEATING WAVE (25 KW, 8 GHz)

⑥ ZONE D'ACCUMULATION
ACCUMULATION ZONE

⑦ BOBINE HEXAPOLAIRE
HEXAPOLAR COIL

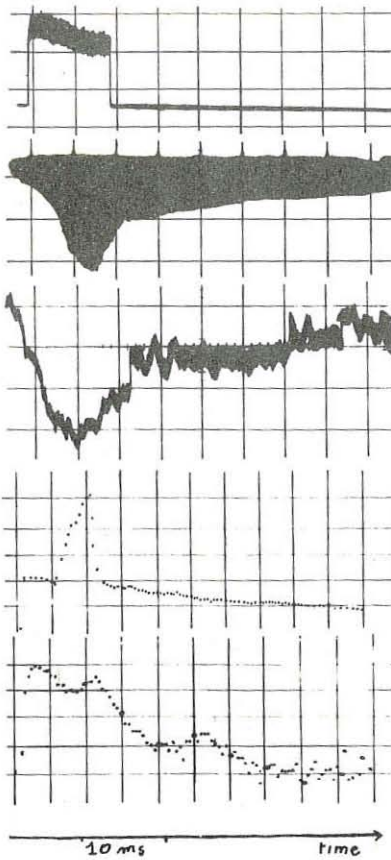
⑧ POMPE A TITANE
TITANIUM PUMP

⑨ CHAMP MAGNETIQUE AXIAL
AXIAL MAGNETIC FIELD

⑩ CHAMP MAGNETIQUE RADIAL
RADIAL MAGNETIC FIELD

⑪ POMPAGE
TO VACUUM PUMPS

FIGURE N° 1



injected plasma interferometry
(exit of the plasma source)
$n_e = 5 10^{12}$ e/cm^3

Fig. 2a

$n_e$xl = $2 10^{12}$ e/cm^3

Zebra-stripe interferometry
(hot plasma)

Fig. 2b

ΔB = 100 Gauss

Diamagnetism

Fig. 2c

100

X-rays time analysis

Fig. 2d

100
10
1

Neutrals time analysis
($E_{analyse}$ = 800 V)

Fig. 2e

REFERENCES :

/1/ - Annual Progress Report - O.R.N.L. 4793 (1972).

/2/ - J. Jacquinot et al. - Vth European Conf. Grenoble, Vol. 1, p. 85 (1972).

/3/ - F. Werkoff - Plasma Phys. 14, 897 (1972).

/4/ - G.R. Haste - Plasma Phys. 14, 729 (1972).

/5/ - A.J. Lichtenberg, G. Melin - Diffusion in E.C.R.H. Magnetic Mirrors
EUR/CEA/FC N° 656 (1972) (to be published in Physics of Fluids).

/6/ - R. Bardet et al. - Description de l'expérience CIRCE.
EUR/CEA/FC N° 653 (1972).

INVESTIGATION OF PLASMA CONFINEMENT BY ELECTROMAGNETIC TRAPS.

O.A.Lavrent'ev, V.A.Sidorkin, V.P.Goncharenko, Yu.S.Asovsky, L.I.Ovcharenko, V.A.Potapenko, I.A.Stepanenko, Yu.I.Pankrat'ev, V.A.Naboka, S.A.Vdovin.

Physico-Technical Institute of Ukrainian Academy of Sciences.

Electromagnetic trap differs advantageously from other thermonuclear systems. It works on principle of the energy recuperation. High-energy charged particles leaving the plasma traverse the moderating electrostatic fields transforming completely their kinetik energy in the potential energy. This potential energy whether goes out of the trap (transforming directly from nuclear reaction energy in electrical energy),or by outer injection retransforms in the kinetic energy of particles and returns in the plasma. Energy recuperation is attained when the plasma ionic component is confined by the field of space electron charge (by the potential well) and the electrons are confined by outer electric and magnetic fields.

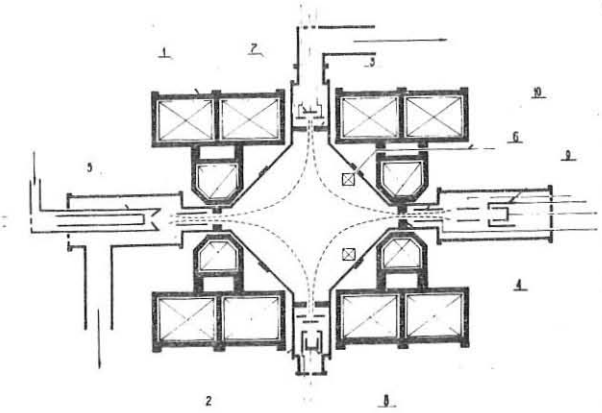


Fig.1. 1. Solenoids. 2. Vacuum chamber 3. Limiting rings. 4. Limiting diaphragms. 5. Electron injector. 6. Axial blocking electrodes. 7. Ringed blocking electrode. 8,9. Electrostatic analyzers. 10.Diamagnetic probe.

Schematic diagram of the electromagnetic trap is showen on the Fig.1. Plasma is formed directly in the volume of confinement by ionization a generator gas with electrons. For that purpose the high-energy electron flow is injected in the trap through one of the magnetic gaps of cusp geometry. The electrons accumulate between magnetic surfaces with negative electrodes blocking the gap, and form the space charge and the potential well of electrons.

Ions generated during ionization of a gemerator gas are accelerated in the potential well. Slow electrons of ionization must be go out of the trap and replace by the fast electrons of outer injection. The electrons of ionization goes out by diffusion through the magnetic field. It was found experimentally that slow spent electrons leave the trap more rapidly then the classical theory of diffusion through magnetic field predict. As it was shown in [2] this process is influenced by diocotron oscillations, developing in the magnetic gaps of the trap, where the negative curvature of magnetic field is insufficient for hydrodynamical instability depression. Diocotron oscillations excite drift of slow electrons blocked in magnetic gap regions between negative electrode and negative space charge. Dipcotron oscillations influence no on fast electrons, that pass through the magnetic gaps at the times less of the characteristic time of instability increase, i.e. the plasma stability and the classical life times of charged particles are maintained. Fast removal of slow electrons permits to force the plasma confining rate in electromagnetic trap that allow to construct the experimental installation having impulsive magnetic fields.

From theoretical values [3,4] it follows that the plasma density in electromagnetic trap is limited by electron space charge deflection in the magnetic gap and its limiting value is $\beta_E H^2/4\pi m_e c^2 \simeq 2.10^4 H^2$ cm^{-3}. This relation was verified experimentally with different installations in magnetic field region 1 - 6,6 kgs. Plasma density was defined by net charged particles yield and with 8-mm interferometer. Plasma density quadratic dependence of magnetic field was prowed experimentally with proportionality constant closed to the theoretical value. The density of 10^{12}cm^{-3} was attained for magnetic field of 6,6 kgs. At a condition of high vacuum the density accumulation was fulfilled at the times of second order. Accumulated plasma density is two order of magnitude higher than the initial density of the neutral gas in the chamber and few order of magnitude higher than the electron density in injecting beam.

Energetic spectra of charged particles was defined with electrostatic multigrid analisator and by passive corpuscular diagnostics.

The electrons going out of the trap at a moment of electrostatic potential collecting from blocking electrodes have the distribution function close to Gaussian one. The curve maximum of increasing time of electrons setting in the trap extends and displaces to less energy. At the injecting energy of 2 kev the electrons have the average energy in the trap equal to 1,8 kev 10 μsec after injection impulse ceasing. Fig.2 shows the typical spectrum of charge exchanged particles, flying from the plasma through the magnetic field layer. It was recalculated for the spectrum of ions circulating in the potential well. Obtained function of the ion energy distribution is close to Maxwellian one. Ion temperature evalu-

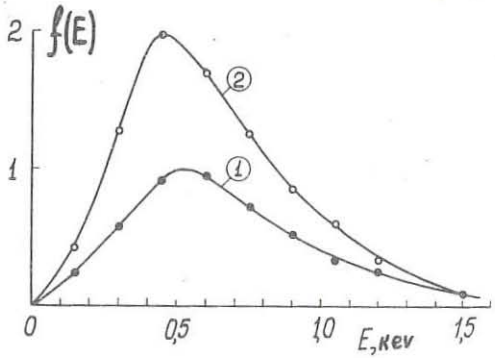


Fig.2. Energy spectrum of charge exchanged particles.
1) $p = 5.10^{-5}$ torr
2) $p = 1.10^{-4}$ torr

ation gives the value of 250 ev that is $^1/_4$ of injecting electron energy.

The plasma decay time was defined be the change of total number of charged particles in the trap.

From decay time the electron life time was defined taking into account the additipnal ionization, and the energetic time was defined taking into account the energy losses by radiation, the recharge and the ionization. Energetic time was evaluated also from the change of energy containing in the plasma electron component. From the cut off at $p \to 0$ the electron life time was defined equal to 1,1 msec and energetic time was 0,7 msec, conditioned only by plasma processes. Obtained times are in satisfactory accord with the values of diffusion classical theory.

REFERENCES

1. Lavrent'ev O.A. et al. U.G.Ph, 8 1963, 452.
2. Pankrat'ev Yu.I. et al. U.G.Ph, 31, 1971, 274.
3. Lavrent'ev O.A. "The magnet trap", num.3,"Naukova Dumka", Kiev, 1968.
4. A.A.Ware, I.E.Faulkner, Nucl.Fusion, 9, 1969, 353.

200 kW NEUTRAL BEAM INJECTION INTO THE 2XII MIRROR DEVICE*

F. H. Coensgen, W. F. Cummins, W. E. Nexsen, Jr.,
A. W. Molvik and T. C. Simonen
Lawrence Livermore Laboratory, University of California
Livermore, California 94550 USA

ABSTRACT: Results on injection of a 10 ampere, 20 keV neutral beam into the 2XII minimum-B mirror device are reported. Beam attenuation exceeding 50% is measured with approximately 10 joules deposited into the 2XII plasma. Particle deceleration at least as fast as Coulomb dynamical friction is observed. The beam does not drive instabilities.

INTRODUCTION: Confinement studies in 2XII have been reported previously [1]. In the operation reported here the injection field was 1 kG and the central field after compression, 5.7 kG. The ion energy was 1 to 2 keV and the plasma was quiescent [1]. Principle plasma diagnostics include: microwave interferometers, 11-channel fast atom detector, Thomson laser scattering, forward angle microwave scattering, RF probes, and visible and vacuum UV monochrometers.

The neutral source [2], delivers 10 amperes for 20 msec into a 10 x 20 cm area at the plasma midplane. Injection is normal to the magnetic field axis. The source is located 340 cm from the plasma in a 3000 liter tank. Beam burial is in a 1500 liter chamber. Both vessels are entensively gettered with fresh titanium before each shot. No increase in charge exchange flux or line radiation, or change in other plasma parameters is detected when the source gas supply is pulsed on, indicating that source gas does not contribute any problems. To facilitate beam injection studies the source is operated with either hydrogen or deuterium and can be modulated with 10 μsec rise and fall times. The beam is monitored by input and output calorimeters, secondary electron emitters, as well as anode current and voltage monitors.

BEAM TRAPPING: Measurements of neutral beam attenuation by the plasma made with a secondary electron detector are shown in Fig. 1. From microwave interferometer measurements of electron line density the expected beam attenuation may be calculated $I/I_o = 1 - \exp(-v_o^{-1} \int nd\ell\, \Sigma \langle\sigma v\rangle)$. A rate coefficient $\Sigma \langle\sigma v\rangle = 1.2 \times 10^{-7}$ cm^3/sec was used to calculate the line in Fig. 1a. These measurements indicate that the beam attenuation is in agreement with microwave measurements and that most of the injected beam is trapped during the period of magnetic compression (400 μsec). Subsequently this part is heated by compression and the energy

*Work performed under the auspices of the U.S. AEC.

distribution spread. In estimating the injected particle energy content this compressional heating is included. Those ions whose large cyclotron orbits carry them to the wall are not included in the energy calculation. In comparison with the 10 joules trapped from the beam, the energy content of a 2 keV 2XII plasma at 2×10^{13} cm^{-3} is 32 joules.

The subsequent deceleration of the injected mono-energetic beam is observed by monitoring the arrival of fast atoms with energies below the injection energy. Our preliminary measurements indicate that the beam slows down at least as fast as expected for Coulomb dynamical friction. Whether an enhanced deceleration exists, due for example to an above thermal fluctuation level, is presently being investigated with more detailed and precise measurements.

INFLUENCE OF INJECTED PARTICLES ON 2XII PLASMA PARAMETERS: Density measurements with and without neutral beam injection show only small differences. Figure 1b indicates that 2×10^{15} particles are trapped. If the angular velocity distribution does not change the resulting density contribution from the beam in the center plane is $\sim 1 \times 10^{12}$ cm^{-3}. However, as discussed above, the trapped ions decelerate rapidly and become part of the plasma ion distribution and consequently are lost at the same rate. Table I and II indicate that the beam does not significantly change $n\tau$.

Coulomb scattering of plasma ions by 20 keV beam particles occurs much slower than particle deceleration by electron dynamical friction. Plasma ion energy could change faster if the beam stimulated high level instabilities. Table II indicates no measurable change occurs with approximately 5-10 joules of 15 keV hydrogen atoms deposited in the plasma. Hydrogen injection permits charge exchange measurements of the deuterium 2XII plasma. The apparent deuterium energy increase in Table I is not ion heating but rather due to the high sensitivity of the charge exchange detector to injected deuterium particles at 90^{o}.

The effect of beam injection on electron temperature for the data of Table I is estimated to be 10%. Such a change is within the uncertainty in the Thomson scattering measurement.

Forward angle scattering of 4 mm microwaves and RF probes located beyond the mirrors show no significant increase in noise in the frequency range $0.2 < \omega/\omega_{ci} < 3$ with neutral beam injection.

TABLE I - TWELVE SHOTS D^0 INTO D^+ PLASMA

	$n \times 10^{-13}$ cm^{-3}	τ μsec	$n\tau \times 10^{-10}$ sec/cm^3	$\bar{E}_i$ keV	T_e eV
Beam Out	1.8 - 2.7	260 - 330	.53 - .88	1.7 - 2.5	42 - 103
Average		300 ± 8	.70 ± .03		69 ± 5
Beam In	2.0 - 3.5	240 - 340	.58 - .97	4.8 - 6.7	45 - 140
Average		285 ± 9	.67 ± .04	see text	73 ± 8

TABLE II - SEVEN SHOTS H^0 INTO D^+ PLASMA

	$n \times 10^{-13}$ cm^{-3}	τ μsec	$n\tau \times 10^{-10}$ sec/cm^3	$\bar{E}_i$ keV	T_e eV
Beam Out	2.4 - 2.7	290 - 355	.74 - .86	1.2 - 2.2	63 - 115
Average		320 ± 10	.79 ± .02	1.7 ± .1	83 ± 5
Beam In	2.1 - 2.6	315 - 370	.71 - .87	1.1 - 1.8	70 - 117
Average		345 ± 8	.81 ± .02	1.4 ± .1	86 ± 10

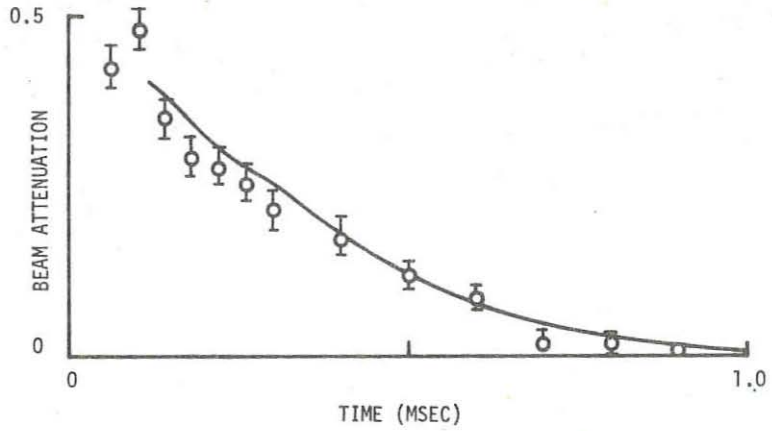
CONCLUSIONS:

* Neutral beam attenuation exceeding 50% has been measured in agreement with calculations.
* Approximately 10 joules is trapped in the plasma.
* Injection of 10 amperes into the dense 2XII plasma ($\omega_{pi} >> \omega_{ci}$) does not drive cyclotron instabilities.
* The experiment is used to determine particle deceleration due to dynamical friction. Our preliminary results indicate deceleration exceeding the Coulomb rate.
* The neutral beam has been used to measure plasma radial density profiles and to probe the ion energy distribution in the plasma interior.

REFERENCES:

[1] F. H. Coensgen, W. F. Cummins, A. W. Molvik, W. E. Nexsen, Jr., T. C. Simonen, Proceedings Fifth European Conference on Controlled Fusion and Plasma Physics, II, 71 (1972).

[2] K. W. Ehlers and W. B. Kunkel; and W. S. Cooper, K. H. Berkner and R. V. Pyle, Proceedings Second International Conference on Ion Sources, Vienna (1972) p 259; and p. 264.



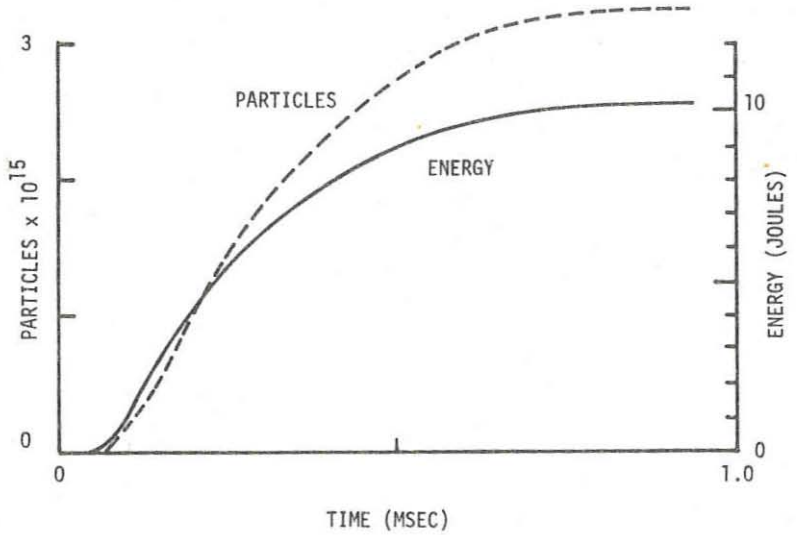


Figure 1 (a) Measured and Calculated Neutral Beam Attenuation;
(b) Calculated Energy and Particles Trapped Versus Time for 5 Amp, 16 keV H^0 Injection.

EXPERIMENTAL INVESTIGATION OF THE QUASI-ELASTIC REFLECTION OF A PLASMA BY A COMBINED HF-MAGNETOSTATIC MIRROR AT ECR

V.D.Dougar-Jabon, K.S.Golovanivsky, L.A.Pokhmelnykh

Plasma Physics Laboratory, Patrice Lumumba University,
Moscow W-302, U.S.S.R.

Abstract: The order of adiabaticity of the reflection of a stationary beam of plasma ($n=10^9$ cm^{-3}) with the ionic longitudinal energy $W_{i\parallel}$ = 0,2 - 1,6 KeV was experimentally investigated. It was found that with a sufficiently small gradient of the magnetic field in the ECR zone, the reflection is quasi-elastic for a wide band of the ionic energy.

The possibility of reflection of a plasma by a combined HF-magnetostatic barrier at ECR was first shown by Consoli and Hall[1]. Though the experiments confirmed this assumption[2,3], the problem of exchange of energy between plasma and the HF field and the final energetical balance under plasma confinement by a combined barrier is still of interest. In the general case, there is a possibility of the plasma getting heated up by the HF energy, nevertheless the numerical calculation of the equation of the motion of the electron ion pair[4] showed the possibility of the reflection of a plasma beam with the minimum of the HF energy loss when we take into account the energy returned by the plasma to the HF field during its backward motion.

The value of the HF power dissipating in the plasma in the process of getting reflected characterises the degree of adiabaticity of the combined barrier. During the onward passage through the resonance zone every electron must collect some transversal energy $W_{e\perp}$ which in a magnetic field of mirror configuration provides for the stopping of the ions of longitudinal energy $W_{i\parallel}$ by the ambipolar mechanism. Using the relation[5]

$$W_{e\perp} = W_{i\parallel} / (R^* - 1) \qquad (1)$$

where R^* is the local mirror value in the plane of stoppage of the plasma flow in relation with that of the resonance value i.e. $R^* = B / B_{res}$, we can find the expression for the HF power

absorbed by the plasma during the onward motion through the resonance zone

$$P_1 = I_i W_{i\parallel} / q(R^*-1) \qquad (2)$$

where I_i is the ionic flow in the plasma and q the ionic charge. During the backward motion of the reflected plasma through the ECR zone the exchange of energy between plasma and HF field is characterised by the power P_2, which can be either positive (recuperation of the energy) when the energy gets transferred from plasma to the field, or negative when the energy transfer is in the opposite direction. The final energetic balance during the reflection will be characterised by the power collected by the plasma during the whole process from the field

$$P = P_1 + P_2 \qquad (3)$$

For the evaluation of the adiabaticity of the combined barrier it is convenient to introduce a new coefficient of recuperation

$$\eta = -\frac{P_2}{P_1} = 1 - \frac{P}{P_1} \qquad (4)$$

which quantitatively characterises the value of the recuperated energy from the plasma or the energy gained by the plasma during the second passage of the plasma through the resonance zone. Taking into account (2) this coefficient gets the form

$$\eta = 1 - \frac{P q (R^*-1)}{W_{i\parallel} I_i} \qquad (5)$$

The second term in the right hand side of (5) is always positive, and therefore the maximum value of η can be unity, which corresponds to the case of an absolutely elastic reflection of the plasma flow by the combined barrier. The region $0 < \eta < 1$ corresponds to the process of partial recuperation, i.e. when the plasma on its backward motion does not give back the whole of the energy which it gained during its onward motion. The value of η is less than zero when plasma absorbs additional energy during its backward motion.

The experiments were conducted on the device described in /6/: A PIG source produced an argon plasma flow with the density $(5.10^7 - 5.10^8)$ cm^{-3}, and longitudinal energy of the ions in the range (0,3 - 1,6)KeV and the thermal energy of the electrons

(20 - 40)eV depending upon the regime of the source. The flow propagated along a glass tube of diameter 5 cm. The residual pressure in the system did not exceed 1.10^{-5} torr. The system of magnetic coils formed a magnetic field of mirror configuration. The value of the magnetic field in the middle plane of the cavity was equal to the ECR value of 848 Gs.,while the gradient of the magnetic field could be varied in the interval (10 - 40)Gs/cm. A generator with variable power upto 10 watts and a frequency of 2375 MHz excitedthe cylindrical cavity producing in it a HF field of the mode TE_{111} with the electrical vector perpendicular to the direction of the plasma flow.

The ionic flow I_i, the longitudinal energy $W_{i\parallel}$ and the stoppage plane of the plasma were found with help of the multigrid energy analyser, movable along the axis of the glass tube. The stoppage plane was observed to be situated at a distance of 5-6 cm from the resonance plane. Knowing this, we could calculate the local mirror value R*.

The absolute value of the HF power loss in the plasma is defined by the expression

$$P = P_o \, (1 - E^2 / E_o^2) \qquad (6)$$

where E_o and E are the amplitudes of the electrical components of the HF field in the empty cavity and with the plasma respectively, and P_o is the power dissipated in the empty cavity, which is defined by the usual methods. This expression is correct under the conditions $E^2/E_o^2 \simeq Q/Q_o$, which were fulfilled in the experiments. The absolute value of E was measured by a calibrated square-law detector.

The experimental results obtained under three different longitudinal gradients of the magnetic field in the resonance region: 10, 30 and 40 Gs/cm. are shown in Fig.1. The results show that for all gradients not exceeding 32 Gs/cm. and the longitudinal energy in the interval of 0,3 - 1,6 KeV practically the whole of the transversal energy gained by the electrons in their first passage through the resonance plane is recuperated during their second passage on the backward motion. When the gradient of the magnetic field was equal to 40 Gs/cm. and the energy of

the ions was less than 1,0 KeV an effective recuperation was noticed. With the ionic energy more than 1,0 KeV the degree of recuperation decreases sharply and it takes the value upto $\eta \cong 0,3$ when $W_{i\parallel} = 1,6$ KeV, i.e. the electrons conserve about 70% of the energy gained by them during the onward motion. From the obtained results it follows that there is some physical mechanism which automatically controls the phase of the transversal velocity of the electrons in such a manner, that the electrons on their second passage through the ECR zone lose their transversal energy. This mechanism enables the quasi-elastic reflection of the plasma when the magnetic field seem by the particles changes sufficiently slow.

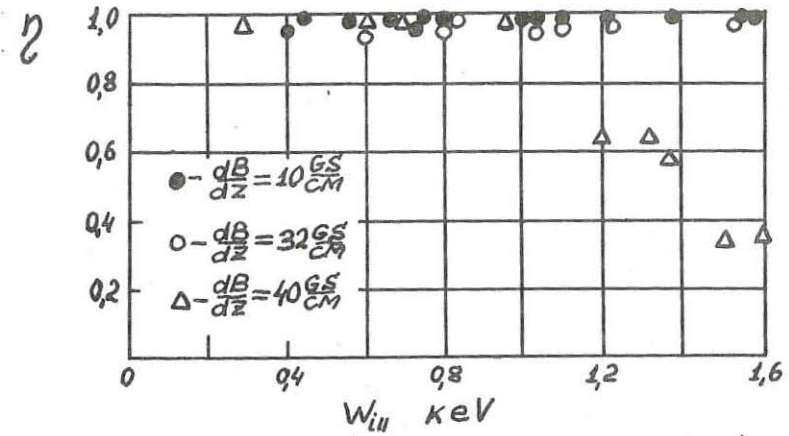
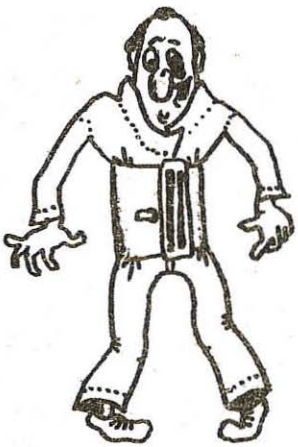


Fig.1.

REFERENCES:

1. T.Consoli, R.B.Hall. Fusion Nucleaire, 3, 237, 1963.
2. R.Bardet, T.Consoli, R.Geller. Nuclear Fusion, 4, 48, 1964.
3. K.S.Golovanivsky, V.D.Dougar-Jabon. Phys.Lett., 34A, 222,1971.
4. V.P.Milantiev, V.A.Tourikov. V European Conf. on Contr. Fusion and Plasma Phys. Grenoble, 1972.
5. K.S.Golovanivsky, L.A.Pokhmelnykh. V European Conf. on Contr. Fusion and Plasma Phys., Grenoble, 1972.

2.2. TOROIDAL PINCHES



Sixth European Conference on Controlled Fusion and Plasma Physics
Moscow, USSR. 30 July - 3 August 1973.

FURTHER STUDIES OF A HIGH-BETA REVERSED FIELD PINCH

C.W. Gowers*, J.W. Long†, A.A. Newton, D.C. Robinson, A.J.L. Verhage, H.A.B. Bodin.

UKAEA, Culham Laboratory, Abingdon, Berkshire, England.

*AWRE, Aldermaston, Berkshire and †Oxford Polytechnic.

ABSTRACT. Studies of the development of the density and temperature distributions during the decay of a stable reversed field pinch are reported. The measurements are compared with numerical simulations of field, thermal and particle diffusion, from which the energy confinement time is deduced. The data can be explained on a classical basis.

INTRODUCTION. Reversed field configurations with $\beta_\theta \sim 0.6$ and initially possessing hollow pressure, density and temperature profiles are generated in HBTX [1]. For peak plasma currents of 40 kA the plasma is observed to be stable for 30-40 μsec, the decay time of the fields. The stability during this period is discussed elsewhere [2].

RESULTS. Fig.1(a) shows the observed radial pressure distribution at different times, obtained from scattering measurements of $T_e(r)$ and $n_e(r)$ assuming $T_e = T_i$ ($\tau_{ei} \sim$ 1-2 μsec). The mean electron temperature of about 7 eV agrees well with the conductivity temperature and this suggests that impurities are unimportant. Previous measurements for a stabilized pinch showed that, before the onset of instability, the total radiated energy was small compared with the thermal energy

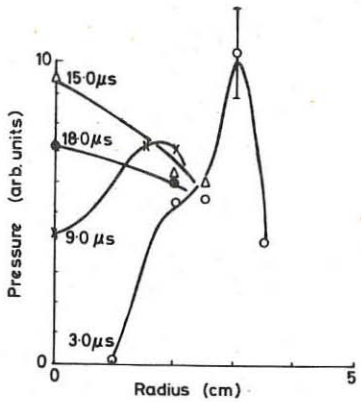


FIG.1(a) Measured evolution of pressure distribution

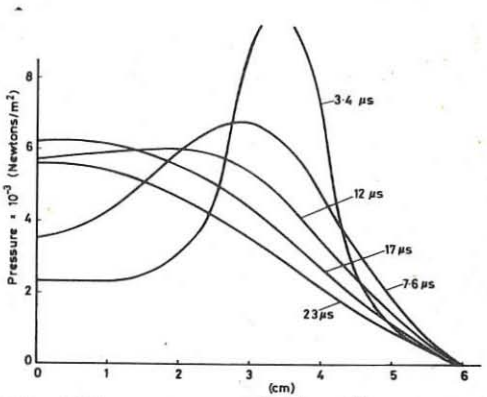


FIG. 1(b) Computed evolution of pressure distribution

of the plasma. The evolution of the pressure distribution was calculated numerically assuming field diffusion alone, using the measured field configuration at 3.4 μsec as the initial conditions together with the conductivity temperature. The predicted decay of the current and external B_z agrees well with experiment. The evolution of the computed pressure distribution is shown in Fig.1(b), and is to be compared with the measured curves in Fig.1(a); there is general agreement - it is seen, for example, that experimentally the pressure fills in at the predicted time.

Fig.2 shows the measured electron density distribution at various times; although no detailed measurements were possible in the outer regions, estimates of the total number of charged particles contributing to the plasma energy at times later than 20 μsec show that there are about half the number at early times. If recycling can be neglected on these short time scales then the particle confinement time can be deduced; the value increases from 16 μsec at 5 μsec (after initiation of the discharge) to 26 μsec at 15 μsec.

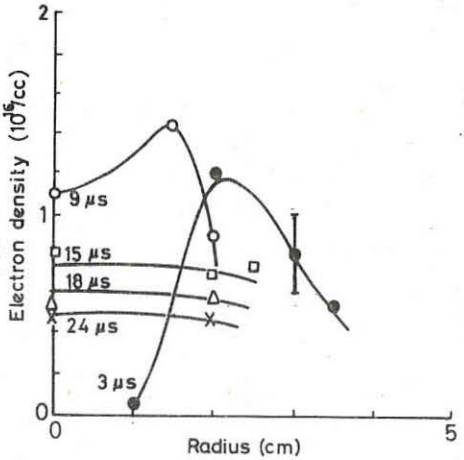


FIG.2 Measured density distribution at different times

Fig.3(a) shows the measured radial electron temperature distribution at different times. The temperature on axis rises rapidly between 10 and 15 μsec, which may be explained because the initial trapped core of neutral particles [3] (which comprises 10-20% of the total number) disappears at about 5 μsec, and subsequent ohmic energy input goes into heating the plasma rather than ionization. The final temperature on axis exceeds the peak value at early times and this leads to an increase in β_θ towards unity. (This was predicted previously [2] from the classical diffusion process.)

A new computation has been carried out with a recently developed two fluid code, including field and heat diffusion; radial pressure balance is maintained (important for high-β simulations). The measured magnetic field and temperature distributions at 3.4 μsec are used as the initial conditions. Results obtained in conditions comparable to those of Fig.3(a) are shown in Fig.3(b) for the evolution of the radial temperature distribution. The principle features - rise in

temperature and β_θ and decay of total current and the final values reached agree with observations.

Fig.4 shows the evolution of β_θ, the total plasma energy, E, the ohmic power input W (from field decay), the current I, and the energy confinement time τ_E calculated on a simple model assuming field diffusion alone. The scattering data for β_θ and E are shown for comparison. The value of τ_E is calculated from the expression

$$\frac{dE}{dt} + \frac{E}{\tau_E} = 2\pi \int_0^{r_w} (E_\theta j_\theta + E_z j_z)\, r\, dr$$

$$+ 2\pi \int_0^{r_w} rv \frac{\partial p}{\partial r}\, dr \qquad (\gamma = 5/3)$$

- where the first term on the right hand side is the ohmic input and the second the work done by adiabatic compression or expansion; v is the radial velocity, p the pressure, E and j the electric field and current density respectively. Uncertainties arise because the conductivity temperature is assumed constant (although, Fig.3(a), T_e rises and due to dynamic effects at earlier times. It is seen on Fig.4 that τ_E rises to a value exceeding 10 μsec at 24 μsec.

CONCLUSIONS. Studies of the time variation of the radial electron density and temperature distributions in a stable reversed field

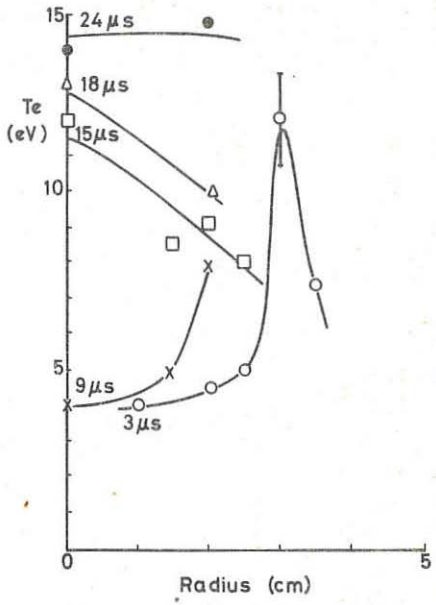


FIG.3(a) Measured evolution of the temperature distribution

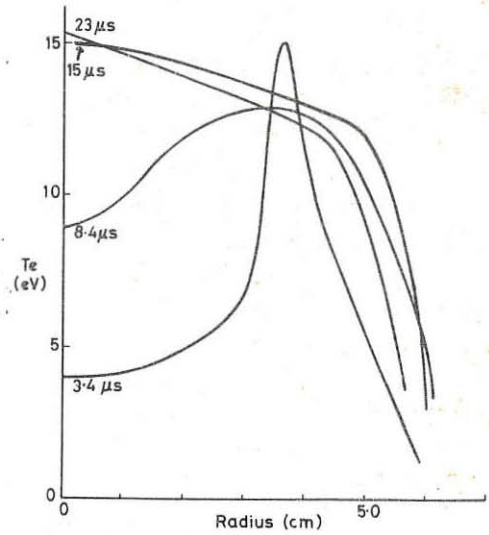


FIG.3(b) Computed evolution of the temperature distribution

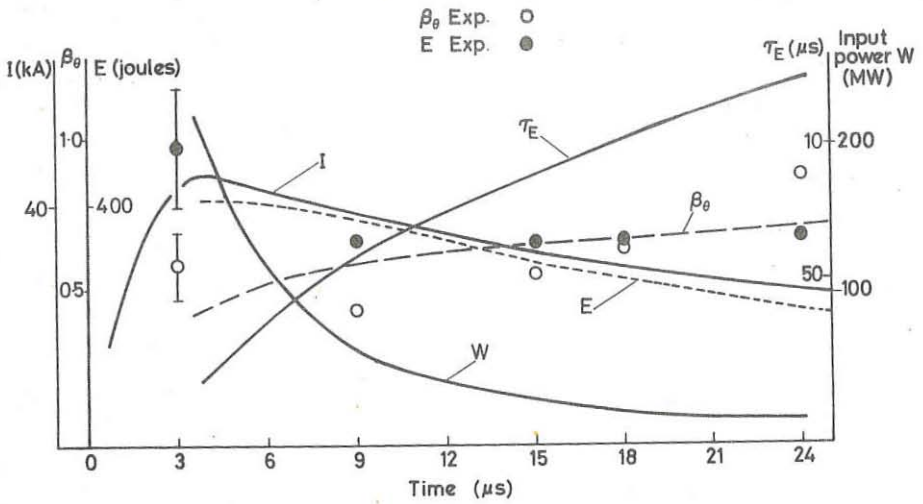


FIG.4 Time variation of input power, w, plasma energy, E, β_θ and energy confinement time calculated from experimental data; direct experimental measurements of β_θ and E are shown for comparison, as is the plasma current.

pinch which lasts for the classical decay time of the fields (30-40 μsec) have been described. The main features, including the increase of β_θ with time, are in agreement with the results of numerical simulations. The data has been analysed to yield values of the energy confinement time of 12-15 μsec, which confirms preliminary estimates [1] the particle confinement time is estimated to be somewhat longer. The observations can be explained on a classical basis.

REFERENCES.

[1] Robinson, D.C. et al 5th European Conf. Grenoble, 1972, p.47, Vol.II.

[2] Crow, J.E. and Robinson, D.C. 3rd Symp. on Toroidal Plasma Confinement, Garching, 1973. Paper A4.

[3] Crow, J.E. et al 3rd Symp. on Toroidal Plasma Confinement, Garching, 1973. Paper A5.

Sixth European Conference on Controlled Fusion and Plasma Physics
Moscow, USSR - 30 July - 3 August 1973

RESISTIVE INSTABILITIES IN DIFFUSE PINCHES

J.E. Crow, J. Killeen†, D.C. Robinson
UKAEA Culham Laboratory, Abingdon, Berkshire, England.
†Lawrence Radiation Laboratory, Univ.of California,USA

Abstract

The effect of finite resistance on the stability of diffuse pinches such as Tokamak and the Reversed Field Pinch is studied in conditions where the ratio of the skin diffusion time to Alfvén transit time, S, varies from $10^2 \rightarrow 10^5$.

Introduction

Detailed studies have been made of the growth of M.H.D. instabilities both theoretically and experimentally [1]. There is good agreement between theory and experiment for the growth rate and wavelength of such instabilities for a variety of field configurations; however, detailed studies of the field disturbances or eigenfunctions reveal discrepancies between theory and experiment. Localised modes are readily modified by such effects as finite larmor radius, resistance and viscosity; in addition gross modes can be affected by finite resistance and in particular in situations where S is not large for example in the HBTX [2] (10^2 - 10^3) and the outer regions of a Tokamak (10^3 - 10^4).

Calculations

The growth of resistive instabilities and the effect of resistivity on M.H.D. instabilities has been studied using an initial value method to solve the incompressible cylindrical plasma case. The growth rate, eigenfunctions and perturbed fields are all obtained as a function of m, the azimuthal mode number, k the wavenumber and S. The procedure has been tested using the Lundquist fields [3] or Bessel function model (which is a realistic reverse field configuration for $R_{wall} < 3.5$) for which the marginal stability points for the resistive tearing mode have been calculated analytically [4]. True resistive tearing mode behaviour with growth rate $\propto S^{2/5}$ is only obtained for $S > 10^5$ and this is illustrated in Figure 1 where the curve for k = 0.1 is unstable on ideal M.H.D. and that for k = 0.4 is only resistively unstable. It is also to be noted that for relatively low values of S the resistive modes can grow faster than ideal M.H.D. modes. Figure 2 shows the growth rate for m = 0,1 for the above field configuration with $B_z(o) = 1$, as a function of the position of the conducting wall for S = 100. For this configuration m = 0 is always stable on ideal M.H.D.; the ideal M.H.D. m = 1 mode has a critical position for the conducting wall only slightly larger (3%) than that for the resistive mode. The position where the longitudinal flux,

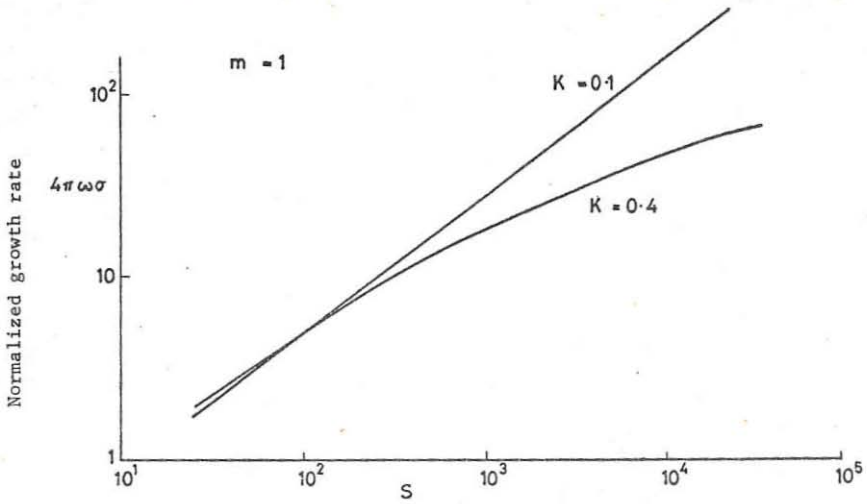


FIG.1

Φ, decreases to zero (a necessary M.H.D. stability criterion is that Φ should be positive) is marked on the figure.

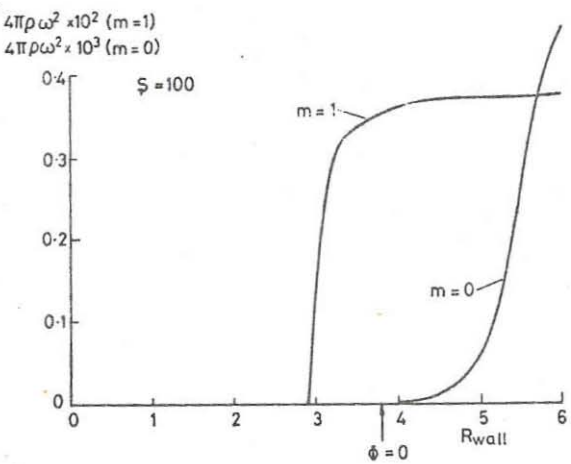


FIG.2

A reversed field configuration defined by a pitch variation satisfying necessary ideal M.H.D. criteria [5] and a pressure profile to satisfy the Suydam criterion can be M.H.D. stable with values of $\beta_\theta \lesssim 0.45$. Such configurations, with variable β_θ, have also been studied for resistive instabilities with essentially the same conclusion as above - a bigger band of unstable wavenumbers is obtained but the position of the conducting wall for stability can be up to 15% less than that for ideal M.H.D. stability. The form of the field disturbances for a typical resistive instability is shown in

Fig.3, which illustrates the tearing mode characteristic of the perturbed radial field, b_r, which does not change sign at the singular surface $F = \underline{k}.\underline{B} = 0$. Though observation of b_r seems to be a useful means of distinguishing between a resistive and an ideal M.H.D. mode, at moderate values of S the resistivity effectively broadens the eigenfunctions associated with ideal M.H.D. instabilities so that the point where b_r changes sign is no longer observable. This is illustrated in Fig.4 for S = 100 and 1000.

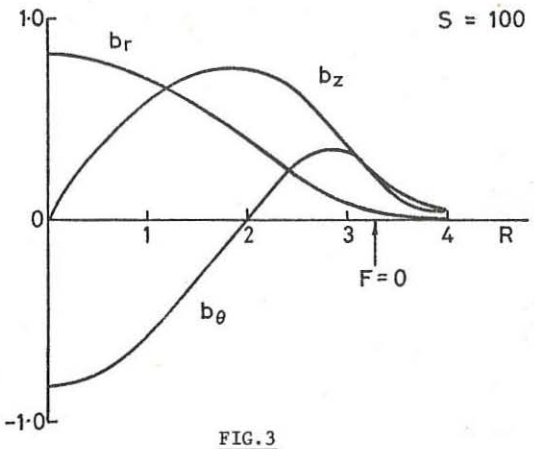


FIG.3

Tokamak configurations with $j_z \sim j_o (1 - r^4/a^4)^2$ have also been studied for S = 100 and 10^5. In contrast to the usual stability windows which appear [6] at values of q in excess of (1), 2, 3 the present calculations show considerable overlap of the various azimuthal modes and windows are apparent in this case only as reduced growth rates.

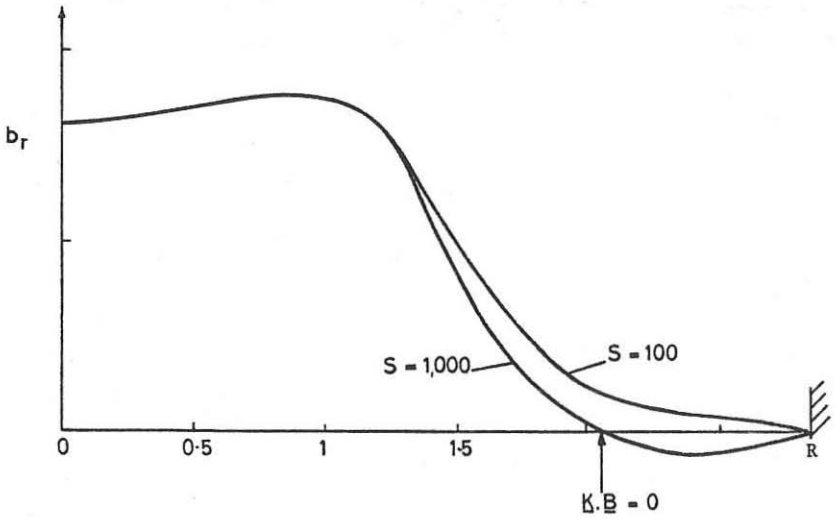


FIG.4

Conclusions

The effect of finite resistance on the reverse field pinch is such as to require closer proximity of the conducting wall to the plasma (up to 15%) to ensure complete stability. M.H.D. disturbances at low values of S resemble resistive modes and the true resistive instabilities can grow faster than their M.H.D. counterparts. The effect of resistivity in a specific Tokamak current configuration is to reduce or destroy the stability windows at larger values of q.

References

[1.] J E Crow, D C Robinson, 2nd Topical Conference on Pulsed High-Beta Systems, Garching, Paper C1 (1972).

[2.] D C Robinson et al., Vth European Conference on Controlled Fusion and Plasma Physics, Grenoble 1972, p.47, vol.II.

[3.] D Voslamber, D K Callebaut, Phys.Review 128, 2016 (1962).

[4.] R D Gibson, K J Whiteman, Plasma Physics 10, 1101 (1968).

[5.] D C Robinson, Plasma Physics 13 439 (1971).

[6.] V D Shafranov, Zh.Tech.Fiz. 40 241 (1970).

STABILITY, RADIATION LOSSES AND EQUILIBRIUM IN THE GARCHING BELT PINCH ISAR IV.

H. Krause, R. Wilhelm, H. Zwicker.

Max-Planck-Institut für Plasmaphysik, Euratom Association, Garching bei München, FRG.

Abstract: Stability for m=1 modes at $q \lesssim 1$ is investigated. For $q<1$, clear m=1 modes are observed while for $q \approx 1$ stability is much better. The influence of preionisation and of oxygen impurity cooling on the temperature behaviour is measured and compared to calculations.

Introduction. Theoretical considerations and first experimental results [1-4] indicate that the β limit can be increased considerably in a Tokomak with elongated plasma cross section. Investigations in Garching [5] had shown a grossly stable plasma for about 80 µsec for initial $\beta \approx 70$ % and for q-values between 3.5 and 1.8 during the entire observation time. In order to confirm the theoretical picture and to find optimal conditions of operation the q-value was reduced in a new series of experiments. In addition, plasma parameters and radiation cooling were investigated in more detail.

Stability. Fig. 1 shows a typical q(t) behaviour at a filling pressure of $p_o = 50$ mTorr D_2 as it was evaluated from the measured plasma current and the optically observed plasma dimensions. q(t) is below 1 for 40 µsec with a minimum at $q \approx 0.3$. The side on framing picture of the plasma belt shows clearly the development of an m=1 mode after about 25 µsec under these conditions. In contrast to this behaviour the plasma belt is much more stable if the minimum of q(t) just touches the value q=1 as it is shown in Fig. 2. But also in this case weak m=1 instability is indicated at later stages of the discharge ($t > 40$ µsec).

Heating and radiation cooling. The fast magnetic compression heating is essentially determined by the initially induced electric field E which at a given bank voltage is much smaller in the belt pinch than in a usual θ-pinch. Consequently preionisation and impurity radiation loss are of great importance. For this reason the ionisation degree of the predischarge and the O_2 impurity level were measured for two different preionisation methods. In addition the electron temperature was measured by laser scattering and the time behaviour of OII and

OIII lines in the main discharge during the time up to the field maximum (7 μsec).
For a filling pressure of p_o = 20 mTorr D_2 and an initial electric field of E≈ 100 V/cm the results are given in table 1.

ion. degree	O_2 impurity	T_e (6.5 μsec)
≤ 2 %	≈ 0.1 %	5 eV
≤ 21 %	1.5 %	20 eV

Table 1

The results show that in spite of the low impurity level the bad preionisation reduces the fast compression heating sharply. This is mainly due to the field penetration during the initial stages which in turn reduces the initial β. With a better preionisation the temperature is increased roughly by a factor of 4. Neglecting impurity losses, rough calculations give $T_e = T_i \approx 30$ eV for these conditions. Consequently we believe the measured temperature is limited essentially by radiation losses. Therefore the time behaviour of T_e was measured for this case by laser scattering at the natural impurity level of 1.5 % O_2 and at an increased value of 3 % O_2. The result is given in Fig. 3.
At 1.5 % O_2, T_e starts with about 20 eV, shortly before the end of the adiabatic compression (7 μsec), and decays to very small values within 20 μsec. Fig. 4 gives the measured cooling rate $1/T_e \cdot dT_e/dt$ as a function of T_e. The calculated rate for 1.5 % oxygen [6] line radiation without any heating is also plotted. Evaluation of the heating rate as the difference between the curves gives reasonable agreement with Spitzer resistivity down to about 8 eV. This indicates that the results of the simplified model for radiation cooling [6] are essentially correct. Consequently the calculated condition for burning through OII - OVI ($T_e + T_i > 120$ eV at $T_{e_o} < 20$ eV for 1 % O_2) should apply.

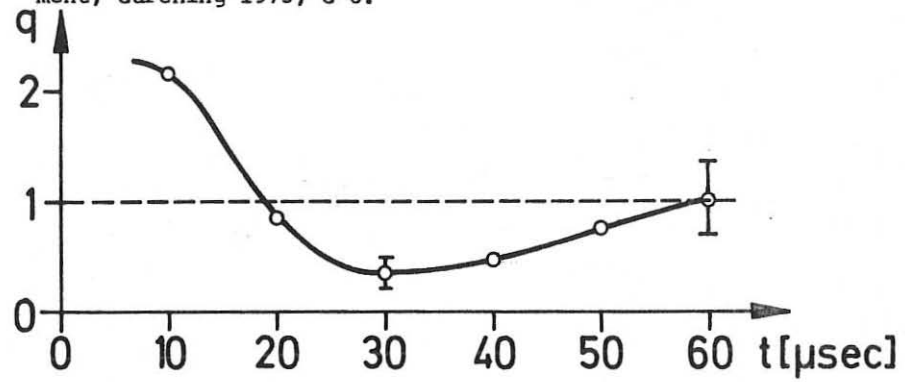
Equilibrium. The measurements indicate high eccentricities (20-50) at large radial compression ratios (5-10) for the plasma belt. This is in contradiction with equilibrium calculations [7]. They show radial compression ratios <2 for any height. This discrepancy could be overcome by assuming force free currents around the dense core [8]. Such force free fields are indicated also experimentally by diamagnetic probe measurements. Also numerical calculations for the initial sta-

ges of the belt pinch [9] give additional currents outside the dense plasma.

Conclusions: The experiments have shown that the Kruskal-Shafranov limit remains valid for highly elongated plasma cross sections. Radiation cooling is the main energy loss in the present small belt pinch. Fast initial pulse heating should overcome this barrier in the 1 MJ belt pinch II [10]. The high eccentricity, necessary for high-β containment, presumably is obtained by force free currents outside the dense plasma.

References:

[1] Kolb,A.C., M.P.Young, Plasma Physics and Contr.Nucl.Fusion Research (Proc.Conf.Novosibirsk, 1968) 2 (Vienna 1969) 567.
[2] Artsimovich,L.A., V.D.Shafranov, JETP 15/1972/72;
[3] Plantikow,U., J.Schlüter, 3rd Int.Symp.on Toroidal Plasma Confinement, Garching 1973, A-6.
[4] Wilhelm,R., H.Zwicker, Plasma Physics and Nuclear Fusion Res., 1971, I, 259;
[5] Zwicker,H., R.Wilhelm, 5th Europ.Conf. on Contr.Fusion and Plasma Physics 1972, II, 59;
[6] Engelhardt,W., G.Bateman; paper presented at this conference;
[7] v.Hagenow,K.-U., K.Lackner, 3rd Int.Symp. on Toroidal Plasma Confinement, Garching 1973, F-7.
[8] Lackner,K.; private communication;
[9] Ignat,D.W., F.Hoffmann, Lausanne report LRP 61/73;
[10] Wilhelm,R,; H.Zwicker, 3rd Int.Symp.on Toroidal Plasma Confinement, Garching 1973, G-6.



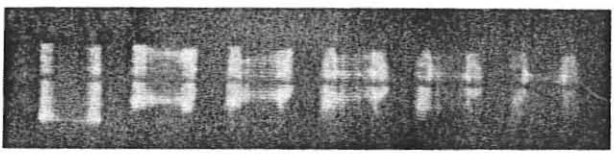


Fig. 1

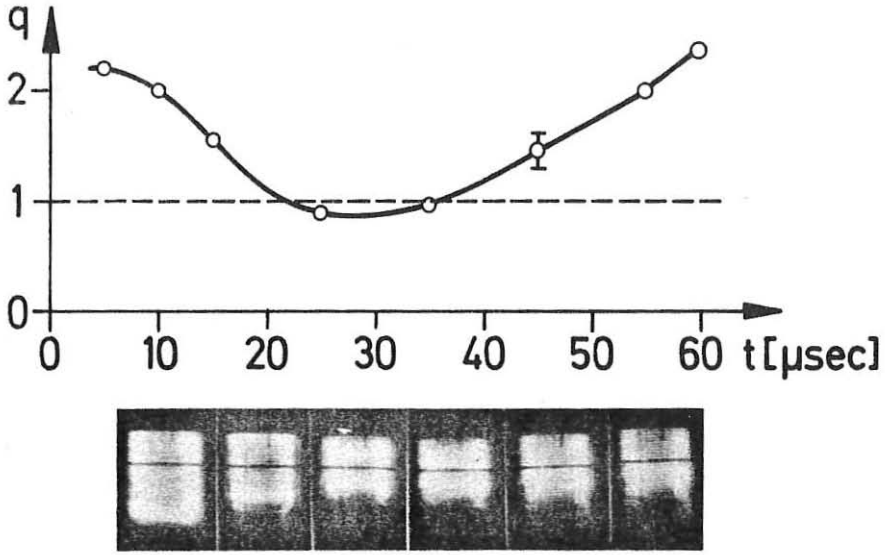


Fig. 2

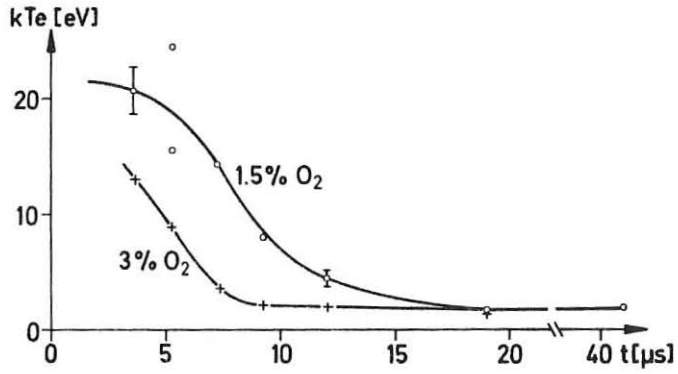


Fig. 3

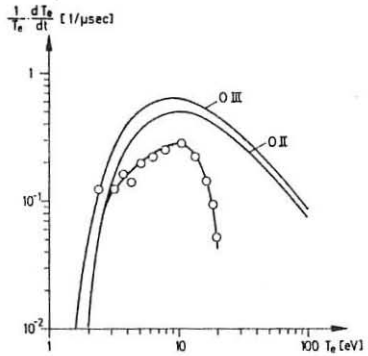


Fig. 4

PLASMA COOLING BY IMPURITY RADIATION

W.Engelhardt and Glenn Bateman

Max-Planck-Institut für Plasmaphysik, Euratom Association,

Garching bei München, F.R.G.

Abstract: Plasma cooling by impurity radiation and ionization is considered as an initial value problem. Given the initial temperatures and a fixed concentration of oxygen impurity, we calculate the temperature reached after complete ionization of the impurity.

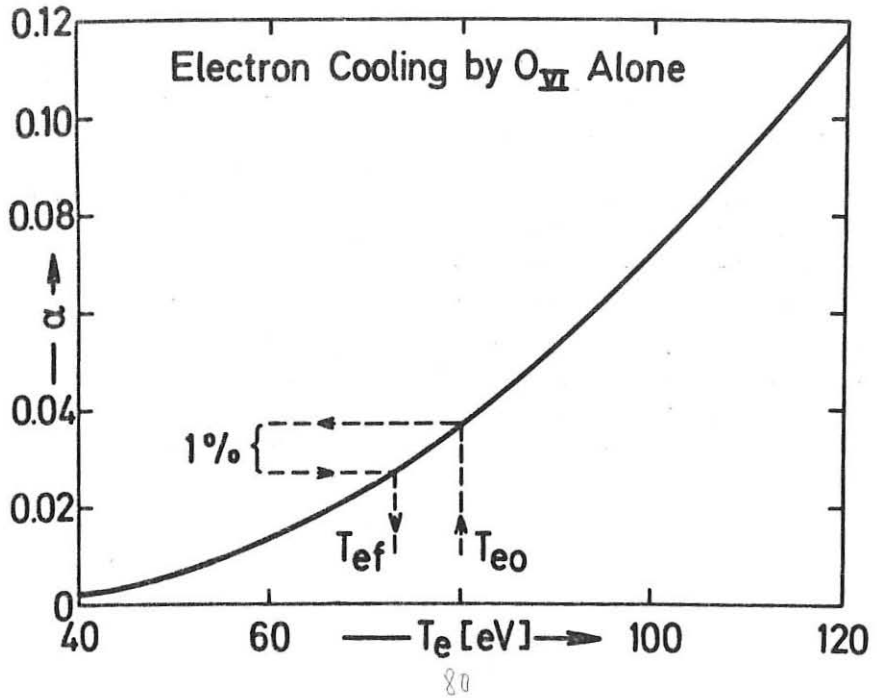
Introduction: In many experiments, energy is deposited in the plasma first as an initial pulse (a shock or initially turbulent heating for example) followed by a slow heating process (e.g. high temperature Ohmic heating). Similarly, for radiation cooling there is a period of rapid energy loss before the impurity atoms are ionized almost completely - a given ion may be excited and radiate many times before it is ionized. In order to estimate the total amount of energy lost because of the impurity, we suppose that the initial heating pulse is much shorter than the time needed for the impurity to be fully ionized and that the long term heating rate is negligible during this time. Thus we make a simple global estimate for the total energy input needed to "burn through" a given amount of oxygen impurity and reach any desired final temperature.

We assume a uniform fully ionized hydrogen plasma with fixed density and a fixed concentration of oxygen impurity. We consider spectral line radiation in the approximation of the corona model, ionization by electron impact, and classical electron-ion energy equipartition.

Using only these three processes, the hydrogen density scales out of the problem. We use the simplified radiation rate suggested by Düchs and Griem /1/ and the ionization rates tabulated by Lotz /2/. The radiation rates for O_{II} - O_{VI} are all about the same (within the factor of 3 accuracy claimed). The rates for O_{VII} and O_{VIII} are neglected, since they are orders of magnitude smaller, and so the calculation is stopped after O_{VI} is burned through. Recombination is neglected in order to establish a clear initial value problem;

it should be important only below 50 eV.

Cooling of coupled and uncoupled species: Before considering the classical equipartition time, let us consider the extreme cases of $\tau_{eq} = \infty$ and $\tau_{eq} = 0$. When $\tau_{eq} = \infty$ the energy reservoirs are completely uncoupled so that all of the energy loss comes from the electrons alone. This may apply for example, when the electron temperature is larger than 50 eV, in which case the classical equipartition time is longer than the time to burn through O_{VI}. When $\tau_{eq} = 0$, by any unspecified mechanism, we have $T_e = T_i$ at every instant. In the case $\tau_{eq} = \infty$, the energy lost by radiation and ionization of O_{VI} alone may be determined from a single curve as shown in fig.1. This curve represents the temperature needed to just burn through α % of O_{VI} and simultaneously cool completely. The curve for $\tau_{eq} = 0$ (not shown) is twice as high.



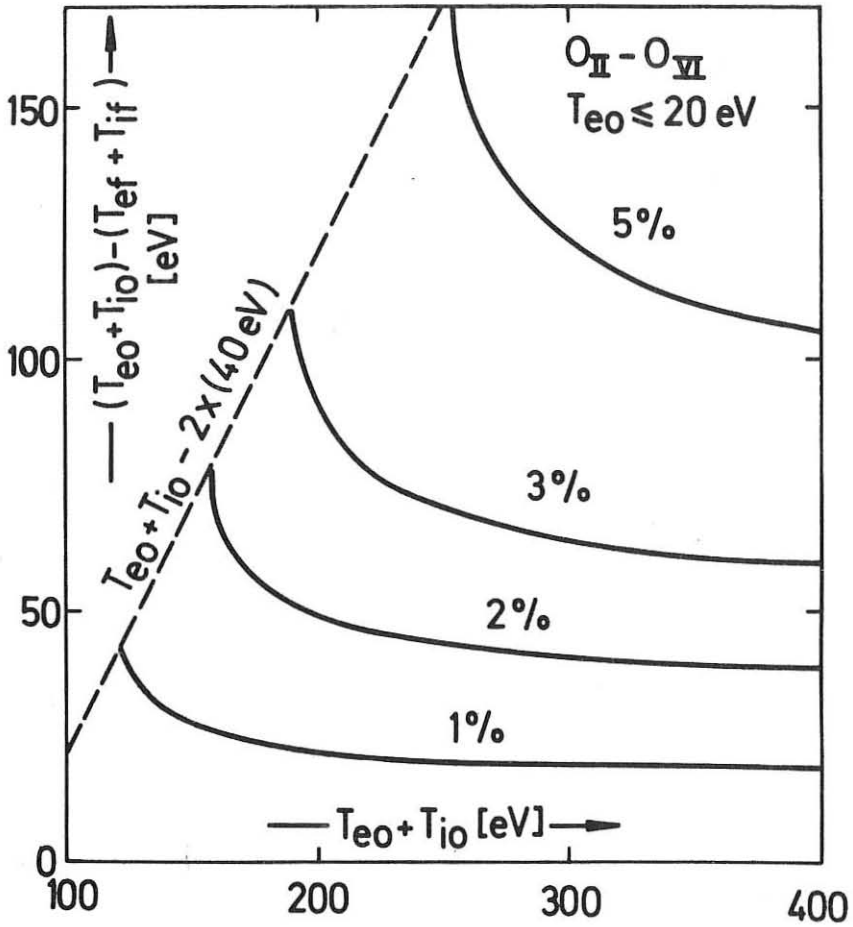
To use this curve start with the point on the curve corresponding to the initial temperature T_{eo}, subtract the amount of oxygen impurity α, and read off the corresponding final temperature T_{ef}. If the oxygen impurity begins in an ionization stage lower than O_{VI} there is a negligible increase in the amount of radiated energy, because the lower stages burn through very fast, but one should subtract the additional energy needed for ionization from the initial temperature T_{eo} and account for the energy going into the newly produced electrons before determining the final temperature by the above method. For example, when starting with O_{II}, use the procedure

$$T_{oe} \rightarrow \frac{T_{eo} - 188\alpha}{1 + 4\alpha} \xrightarrow{\text{Fig.1}} T_{ef} \quad \text{eV}$$

Cooling and Classical Equipartition: Now consider the classical equipartition time in the most interesting case where the electrons are initially cold (as in a shock heated plasma). As the electrons gain energy from the ions, T_e passes through the range where the radiation loss rate is the greatest and the ionization rate is the slowest. Then the energy lost while burning through the lower ionization stages is comparable to that lost while burning through O_{VI}. For this reason, we consider the full set of ions (O_{II} - O_{VI}) rather than O_{VI} alone. In fig.2 we show the total energy lost in terms of the initial combined temperatures $T_{eo} + T_{io}$. These results are valid for any $T_{eo} \leq$ 20 eV, where the classical equipartition time is much shorter than the cooling time. From these cooling curves, each for a given impurity concentration, the experimentalist can estimate the threshold initial temperature needed to reach any final temperature at all (above T_{ef} = 40 eV, where recombination becomes important) after the transient nonequilibrium phase is over.

References:

/1/ Düchs,D. and H.R.Griem,; Phys.Fluids 9, 1099 (1966)
/2/ Lotz,W., IPP 1/62 (1967); Z. für Physik 216, 241 (1968).


$O_{II} - O_{VI}$
$T_{eo} \leq 20$ eV
5%
3%
2%
1%
$T_{eo} + T_{io} - 2x(40\,eV)$
$-(T_{eo}+T_{io})-(T_{ef}+T_{if})$ [eV]
$T_{eo} + T_{io}$ [eV]
0
50
100
150
100
200
300
400

THE INFLUENCE OF A LONGITUDINAL HIGH FREQUENCY CURRENT ON PLASMA STABILITY IN A COMBINED PINCH

G.G.Zukakishvili, I.F.Kvartskhava, E.K.Tikhanov.

Sukhumi Institute of Physics and Technology of the State Committee on Utilization of Atomic Energy, Sukhumi, USSR.

ABSTRACT The paper gives the experimental data on the MHD instability stabilization in a combined pinch by a longitudinal h.f. current. The instability is of m=1, the wavelength $\lambda = 2L$ type/1/.

The experiments have been carried out in the quartz discharge chamber with the diameter of 6.5cm; the magnetic field strength H_z=65 kOe; the z-pinch current I_z=5 - 50kA; the θ-pinch coil length L =21cm. The currents have similar cycles (T=19μsec) and are switched simultaneously. The temperature of a preliminary plasma is ~ 3ev. The combined pinch parameters are determined in a basic θ-pinch ($H_z^2 \gg H_f^2$); at the initial D_2 pressure of $8 \cdot 10^{-2}$mm Hg, the density $n_e \simeq 10^{17} cm^{-3}$, the electron temperature $T_e \simeq 100ev$, and the ion temperature $T_i \simeq 400ev$. Due to the high ion temperature, the end losses resulted in the rapid decrease of the plasma column radius and the corresponding variation of the stability conditions. With I_z given, the instability developes at the critical pinch radius (the radius values calculated in accordance with the critical current, are given by points in Fig.1).

The h.f.current I_z with the amplitude up to 25kA, is generated by the discharge of 0.2μF capacity. On replacing the pinch by the metal rod, this current will have the frequency $\omega_s = 3.8 \cdot 10^6 sec^{-1}$ (with the Q-factor being equal to 22). On discharging in a preliminarily heated plasma, the frequency rises up to $4.7 \cdot 10^6 sec^{-1}$,

and Q-factor dropped to 10. After the first halfcycle, the current flowed in a plasma wall-side layer of $\leqslant$1cm thickness; its resistivity being equal to $\sim 10^{-2}$ohm (derived by the circuit Q-factor regarding the outer circuit resistance), which is in accordance with the classical values of skin-layer depth and resistance at $T_e \sim$ 3ev. On imposing the h.f.current on Θ-pinch or a combined pinch, ω_s takes an intermediate value of $4.3 \cdot 10^6 sec^{-1}$, which indicates the presence of a part of the current flowing in a dilute plasma between the pinch and the chamber wall. The h.f. current density distributions along the radius (Fig.2) and the discharge photoes (Fig.4C and 4D) confirm this conclusion. In the beginning of each halfcycle, the current arises near the wall(Fig.2) and proceeds to the axis with the speed determined by the plasma conductance. In the second halfcycle, when the total current decreases, in the circuit, the reversed current flows by the wall (reversed skin/2/). As the magnetic field dissipation time is larger than the h.f. circuit halfcycle, a system of recurrent opposite currents is formed in the discharge volume/3/. The plasma average resistivity of $\sim 1.6 \cdot 10^{-1}$ohm$\cdot$cm (at Q-factor being equal to 5 - 6) is 20 times the classical value if to consider that the plasma temperature does not exceed 3ev. This agrees with the results from /3,4/. Fig.4 shows slot photo-scannings of pinch plasma luminosity (4A), of a combined pinch in an instable regime (4B) and of Θ-pinch with the h.f.current (4C, 4D) taken from the side in the central section. It is shown that at the h.f.current amplitude exceeding the critical value, the plasma column is stable. On increasing the delay between the Θ-pinch and the h.f.current, the pinch oscillations of ω_s frequency are observed. They are related with the plasma column radius decrease (see above) and the respective worsening of

stabilization conditions. Fig.3 shows time-resolved Schlieren photoes obtained with He-Ne laser/1/. The comparison of Fig.3B to 3C shows that on superposing the h.f. current on the combined pinch, the instability rises 1.5 μsec later. During this time, $I_z/I_z \simeq 1.5$ and $\omega_s \simeq (2-3)\omega_i$ (ω_i being the MHD instability increment). Further, I_z/I_z reduces as a result of decaying I_z, while ω_i grows due to pinch radius decrease and stabilizations conditions are violated.

An anomalous resistance of a low density intermediate plasma seems to be related to the ion-sound instability rise (as $V_{Te}=\sqrt{\frac{KT_e}{m_e}} > V_D=\frac{j}{ne} > V_{Ti}=\sqrt{\frac{KT_e}{m_i}}$ are satisfied at $T_e > T_i$). In such a case, the h.f. current reaches the pinch surface and stabilizes it. A marked part of h.f.current energy is absorbed by a dilute plasma.The qualitative analysis shows that the intermediate plasma density grows due to particle diffusion from the pinch and to ablation of the substance from the walls, electron heating and equalization of T_e to T_i, after some time, must lead to the ion-sound instability collapse and the h.f.current skinning in a wall-side region. Thus, the energy sorption in a dilute plasma and the h.f. current subsequent skinning (especially on growing the specific power) can limit the chances of the pinch dynamic stabilization methods.

REFERENCES

1. I.F.Kvartskhava et al., Plasma Physics and Controlled Nuclear Fusion Research. 1, IAEA, Vienna (1971) 183.
2. I.F.Kvartskhava et al., Nuclear Fusion, 11, (1971) 349.
3. O.Gruber, Zeitschrift fur Physik, b.251, h.4 (1972) 333.
4. E.M.Little, A.A.Newton, W.E.Quinn, F.L.Ribe. Plasma Physics and Controlled Nuclear Fusion Research. II, IAEA, Vienna (1969) 555.

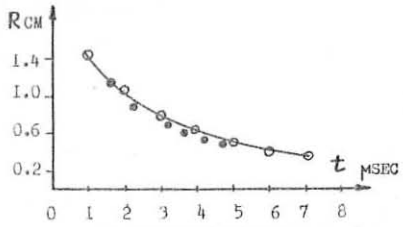


FIG.1. THE DEPENDENCE OF PLASMA COLUMN RADIUS UPON TIME H_z=65kOe; P=8·10^{-2}mm Hg.

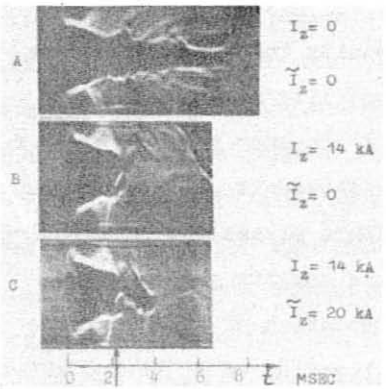


FIG.3. SCHLIEREN PHOTOGRAPHS OF THE PLASMA. THE END VIEW. THE H.F. CURRENT SWITCHING MOMENT IS INDICATED BY THE ARROW. H_z = 65 kOe, P = 8 · 10^{-2} mm Hg.

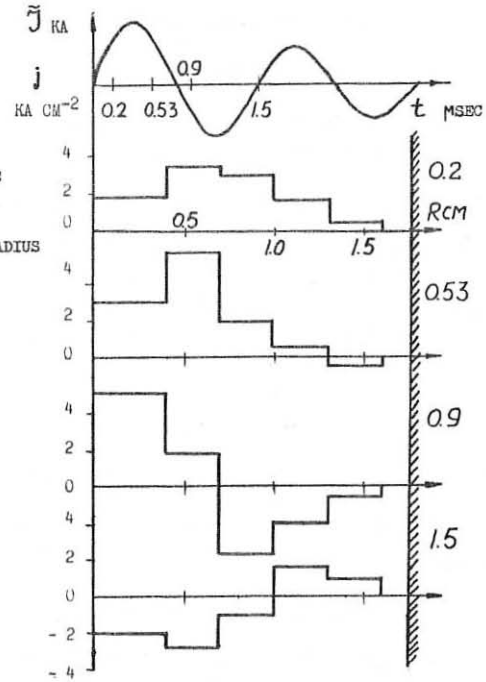


FIG.2. THE CURRENT DENSITY RADIAL DISTRIBUTION. THE CHAMBER DIAMETER 3.6cm, P = 5·10^{-1}mm Hg, H_z= 40 kOe.

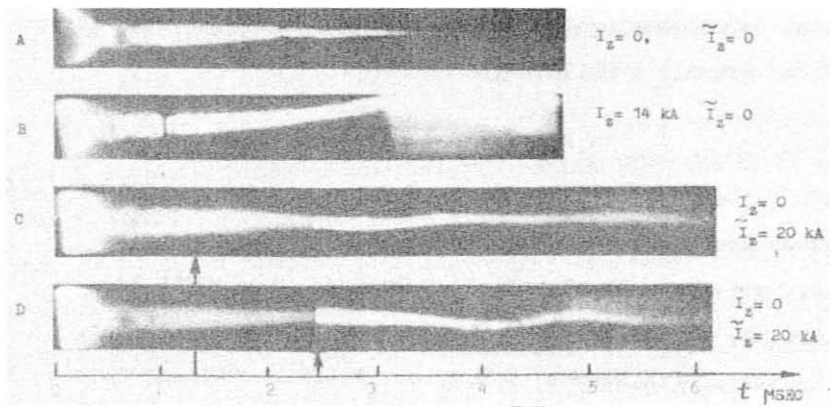


FIG.4. PLASMA PHOTOES FROM THE SLOT. SIDE VIEW. THE ARROWS INDICATE H.F. CURRENT SWITCHING MOMENTS. H_z= 65 kOe, P = 8·10^{-2} mm Hg.

ASPECTS OF DYNAMIC STABILIZATION OF HIGH-BETA PLASMAS

C. Gruber, G. Becker, H. Herold

Max-Planck-Institut für Plasmaphysik, Euratom Association,
Garching bei München, FRG.

Abstract: Dynamic stabilization of an unstable toroidal screw pinch by $\tilde{B}_z$ is demonstrated. Working in resonance with the m=0 mode the $\tilde{B}_z$ amplitude necessary for stabilization is reduced. The plasma heating rate inherent in the $\tilde{B}_z$ stabilization scales with the square of the growthrate and is independent of the stabilizing frequency.

1. Introduction. Dynamic stabilization of the helical m=1 instability has been studied in a linear screw pinch by three methods [1,2,3].

1) HF axial currents $\tilde{I}_z$ were superimposed to study stabilization by dynamic shear. The growth of the m=1 mode is suppressed [1,2], but the $\tilde{I}_z$ causes large HF power losses in the tenuous plasma.
2) Superimposed axially homogeneous HF magnetic fields $\tilde{B}_z$ enforce m=0, k=0 oscillations of the plasma (amplitude $\tilde{r}_p$). The m=1 instability is stabilized by coupling of the m=0 and m=1 modes [1,2,4]. Provided that the breakdown limit at the tube wall is not exceeded [1,2] and that $\omega_s < \omega_k$ holds (ω_s stabilization frequency; ω_k radial oscillation frequency of the plasma column, $\omega_k = B_z/\sqrt{\rho_\ell}$; ρ_ℓ line mass) the power losses in the plasma are small compared with those in 1).
3) A standing wave magnetic field was applied [3]. In contrast to theoretical predictions neither stabilization of the m=1 mode of a screw pinch nor dynamic equilibrium of a toroidal theta pinch sector could be achieved.

According to these experimental results the $\tilde{B}_z$ method proves to be most advantageous from an economic point of view.

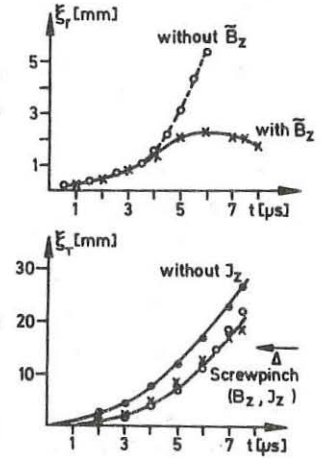
2. $\tilde{B}_z$ stabilization of a toroidal screw pinch sector

In order to investigate toroidal effects with $\tilde{B}_z$ stabilization axially homogeneous HF fields were applied to a toroidal screw pinch. Combining the stabilizing condition from our linear experiments [1,2]

(1) $\quad \Lambda = \tilde{r}_p/r_p \geq 2\ \omega_i/\omega_s$,

the m=1 growthrate ω_i and the toroidal equilibrium condition it can be estimated that for technical reasons dynamic stabilization is fea-

sible only with large aspect ratios A ($A=R_T/r_c$, R_T large torus radius, r_c coil radius, r_p plasma radius). Therefore to save costs the experiments were performed on a torus sector at plasma parameters similar to those in our linear experiments (sector angle 21 °, R_T=400 cm, r_c=5.5 cm, $T_e \approx T_i \approx 25$ eV, q=0.3 and $n=2\times10^{16}$ cm^{-3} on axis). A $\tilde{B}_z$ field that is homogeneous at the plasma surface was generated by a high Q capacitor bank ($\varepsilon=\tilde{B}_z/B_z \leq 0.2$, $\omega_s=5.5\times10^6$ s^{-1}) [3]. Densitometric evaluation of smear pictures yields $\delta \approx \varepsilon$ for $\omega_s \approx 0.2\ \omega_k$ in agreement with [1,2]. The time behaviour of toroidal drift ξ_T and m=1 motion ξ_r was determined by stereoscopic smear pictures at several axial positions. Figure a) demonstrates the stabilizing effect of the $\tilde{B}_z$ field ($\omega_i=6\times10^5$ s^{-1}). Dynamic stabilization obeys condition (1) which was found in linear experiments, i.e. evidently no essential toroidal effects are observed with large aspect ratio. The toroidal drift, however, is not influenced by the HF fields (Fig. b). The transition of the screw pinch into the equilibrium position at a toroidal displacement Δ=1.5 cm (according to Shafranov) cannot be observed. The frequency of the major radius oscillations of the plasma ($\sim 1/\sqrt{A}$) is so small that only the first overshooting of the column occurs within the observation time. By this experiment dynamic stabilization of the m=1 mode has been demonstrated also on a toroidal plasma.



3. $\tilde{B}_z$ stabilization in the resonant case $\omega_s=\omega_k$

According to 1. 2) the enforced m=0 oscillations in the $\tilde{B}_z$ method play the role of an oscillator between the external driving force and the m=1 mode to be stabilized. This method is particularly economic with small oscillator damping, because here the driving HF circuit has not to produce the dynamic force, but has only to supply the damping losses. Moreover it is advantageous to produce a given δ by the smallest possible ε, e.g. by working in resonance ($\omega_s=\omega_k$). This helps to reduce HF power loss in the external circuit, to avoid breakdown and to fulfill simultaneously the stabilizing condition (1). Therefore resonance experiments at ω_k between 10^7 and 2.4×10^7 s^{-1} and $\varepsilon \leq 0.1$ were performed

on a linear screw pinch with $T_e \approx T_i \approx 20$ eV and $\vartheta = 0.2$ (theta coil length 100 cm, $Q = 14$ to 22). No parametric resonances were observed and should only occur at $\varepsilon_c = 4\lambda/\omega_k > 0.2$ [2] with the measured damping of the m=0 oscillation and with the attainable ε values (damping coefficient $\lambda = 7 \times 10^5$ to 1.5×10^6 s^{-1} for $\delta > 0.1$). For the oscillating amplitude δ is found

(2) $\quad \delta = \alpha\, \varepsilon$

with $\alpha = 2$ to 3 after a few cycles. By solving the m=0 equation of motion with $\tilde{B}_z$ [2] it was found that δ depends on ε, λ and ω_s/ω_k (the inductive coupling of the plasma to the external circuit has been taken into account). Thus for instance $\alpha = 1$ at $\omega_s = 0.2\ \omega_k$ and $\alpha \approx \omega_k/8\lambda$ at $\omega_s = \omega_k$ with $\varepsilon < \varepsilon_c$. These results agree well with the measured ones. Magnetic probe and continuum measurements show that there exist small radial phase differences in the m=0 motion. The wings of the Gaussian-like profiles where most of the mass is located oscillate with twice the amplitude of that of the axial region. Nearly all the mass oscillates with a phase shift of 90 degrees against the driving force. Furthermore the experiments show that the stabilizing condition (1) obtained earlier at $\omega_s \leq 0.5\ \omega_k$ is also valid at the resonance, although no longer all the mass oscillates in phase. That means, the ε values necessary for stabilization were about a factor 2 to 3 smaller than in the non-resonant case according to the large α values. At resonance the damping of the HF current with plasma (due to energy transfer to the m=0 oscillations) is a factor three larger than in the vacuum case. Furthermore the power loss in the plasma increases with larger $\tilde{r}_p$ and with ω_s. The losses can roughly be described by

(3) $\quad \tilde{P} = \rho_\ell\, \lambda\, \omega_s^2\, \tilde{r}_p^2$

which is the average power loss per cycle of an oscillating plasma cylinder.

4. Prospects of dynamic stabilization

The following estimates of the power need of the HF bank, heating of plasma and scaling laws are made using the results of the $\tilde{B}_z$ stabilization of the m=1 mode on a screw pinch. These results should, however, be valid in general for all MHD modes that are coupled to an intermediate oscillator and that obey a stabilizing condition similar to (1). An estimate using the data of our experiments and

those of a fusion plasma shows that for $\omega_i > 10^4\ s^{-1}$ the losses due to m=0 damping are large compared with the ohmic losses in the electric circuit. Thus the HF losses are only weakly determined by the Q value of the HF circuit. Inserting (1) into (3) yields

(4) $\quad \tilde{P} = 4\ \rho_\ell\ \lambda\ r_p^2\ \omega_i^2$.

According to this the power loss depends only on ω_i for a given λ, but is independent of ω_s. When looking for the optimum working parameters with respect to plasma losses, ω_s can be chosen free under the condition $\omega_s > 10\ \omega_i$. Moreover it is advantageous to work at the smallest possible circulating power ($\sim \epsilon^2\ \omega_s$) with respect to investment costs and losses in the HF circuit. Combining (1) and (2) yields

(5) $\quad \epsilon^2\ \omega_s \geq 4\ \omega_i^2 / (\omega_s\ \alpha^2)$

Concerning the circulating power and the breakdown at the wall [1,2] preference should be given to working in resonance ($\alpha > 1$).
Since the power losses in the plasma that heat the dense plasma are relatively high, the $\tilde{B}_z$ scheme may simultaneously serve as a very efficient heating and stabilizing method. This is a particularly interesting prospect for the heating of plasma in cases where the usual heating methods are insufficient and where the plasma has to go through unstable regimes. From (4) an e-folding time τ of the plasma energy

(6) $\quad \tau = (\beta/32) \cdot (\omega_k^2/\omega_i^2)/\lambda$

is obtained. For fusion plasmas with $\omega_k = 5 \times 10^7\ s^{-1}$, $\beta = 0.2$ and $\lambda \approx 2 \times 10^6\ s^{-1}$ (from collision free theta pinch experiments) one estimates, for instance at $\omega_i = 4 \times 10^5\ s^{-1}$ an e-folding time of 50 µs. A more detailed calculation of the heating rate is presently impossible, since the m=0 damping mechanism in a fusion plasma is still unknown. One should also mention that this application of dynamic stabilization does not influence the energy balance of fusion reactors substantually.

References

[1] G.Becker, O.Gruber, H.Herold, 4th Intern. Conf. Plasma Phys. and Contr. Nucl. Fus. Res., Vol. I, 277 (1971), IAEA, Vienna

[2] O.Gruber, Z. Physik 251 (1972), 333

[3] G.Becker, O.Gruber, H.Herold, 5th Eur. Conf. Contr. Fus. and Plasma Phys., Vol. I and II, Paper 53 (1972), Grenoble

[4] G.Becker, ibid, Paper 52

TWO-DIMENSIONAL COMPUTER CALCULATION OF TOROIDAL PINCH EXPERIMENTS

F. Hofmann and D.W. Ignat
Centre de Recherches en Physique des Plasmas
Avenue des Bains 21 , 1007 Lausanne, Switzerland

Abstract: A two-dimensional, three-fluid, magnetohydrodynamic computer code has been developed for numerical calculation of toroidal pinches with arbitrary cross section and aspect ratio. The code has been applied to the study of the initial phase of a toroidal screw pinch with highly elongated plasma cross section (belt pinch).

Introduction

Toroidal plasma confinement devices with non-circular cross section are presently being studied very actively at a growing number of Laboratories[1-4]. At Lausanne, the time evolution of a "belt pinch" has recently been computed[5], using a one-dimensional model[6]. The results of that calculation, in particular the temperature of the plasma after compression, are in good agreement with the latest measurements[7] on the Garching experiment.

One of the important phenomena that cannot be studied with a one-dimensional model, however, is the motion of plasma in the direction of the major axis of the torus. Yet, axial plasma motion is crucial in determining stability, since the Kruskal-Shafranov factor (q) is roughly proportional to the axial height of the plasma, for highly elongated cross sections[1]. Therefore, in order to be able to study the time evolution, and the approach to equilibrium, in both radial and axial dimensions, we have developed a two-dimensional magnetohydrodynamic computer code.

Physical Model

We consider the following set of basic equations:

$$\frac{\partial n}{\partial t} = -\nabla \cdot (n \vec{v}) - n\,(\alpha n - \sigma n_H)$$

$$\frac{\partial n_H}{\partial t} = -\nabla \cdot (n_H \vec{v}_H) + n\,(\alpha n - \sigma n_H)$$

$$\frac{\partial \vec{v}}{\partial t} = -(\vec{v}\cdot\nabla)\vec{v} - \lambda(\vec{v}-\vec{v}_H) + \frac{1}{nm}\left\{-\nabla(2nT) + \frac{1}{\mu_0}(\nabla\times\vec{B})\times\vec{B} + \nabla\cdot\left[\mu(\nabla\vec{v}+\vec{v}\nabla)\right] - \frac{2}{3}\nabla\left[\mu(\nabla\cdot\vec{v})\right]\right\}$$

$$\frac{\partial \vec{v}_H}{\partial t} = -(\vec{v}_H\cdot\nabla)\vec{v}_H + \lambda_H(\vec{v}-\vec{v}_H) + \frac{1}{n_H m}\left\{-\nabla(n_H T) + \nabla\cdot\left[\mu_H(\nabla\vec{v}_H + \vec{v}_H\nabla)\right] - \frac{2}{3}\nabla\left[\mu_H(\nabla\cdot\vec{v}_H)\right]\right\}$$

$$\frac{\partial \vec{B}}{\partial t} = \nabla\times(\vec{v}\times\vec{B}) - \frac{1}{\mu_0}\nabla\times\left[\eta(\nabla\times\vec{B})\right]$$

$$\frac{\partial T}{\partial t} = -(\vec{v}\cdot\nabla)T + \frac{2}{3}\frac{1}{2n+n_H}\left[-2nT(\nabla\cdot\vec{v}) + \nabla\cdot(Q\nabla T) + W\right]$$

where n is the number density, $\vec{v}$ the velocity, $\vec{B}$ the magnetic field, and T the average temperature defined as $T = (nT_e + nT_i + n_H T_H)/(2n + n_H)$. α is the recombination rate coefficient, σ the ionization rate coefficient, μ the viscosity, λ the friction coefficient, and η the resistivity. The index, H, refers to the neutral gas component. W is a heat source, due to ionization, recombination, friction between ions and neutrals, Joule heating, and viscuous heating. Q is an average thermal conductivity (divided by the Boltzmann constant) defined as $Q = (nQ_e + nQ_i + n_H Q_H)/(2n + n_H)$. The rest of the symbols have their usual meaning. Cylindrical symmetry, $\frac{\partial}{\partial\theta} = 0$, quasi-neutrality, and ideal gases are assumed. Plasma rotation and Hall currents are neglected. The equations listed above are written in finite difference form (in cylindrical geometry) and solved on a fixed Eulerian mesh. Hyperbolic terms are treated explicitly, whereas parabolic terms are treated implicitly by a modified ADI method.

Results

Using the physical model outlined above, two-dimensional (r,z) numerical calculations were carried out, simulating the toroidal screw pinch described in Ref.1. Initial conditions were 50 mTorr D_2, 20 % preionized. Flux surface boundary conditions ($B_r = 0$) were assumed at both the inside and outside walls of the discharge chamber. This assumption differs from the actual experimental setup[7] which uses a constant current surface on the inside and a constant flux surface on the outside. Energy losses due to impurity radiation (e.g., oxygen) are neglected in

the present calculation.

Fig. 1 shows the evolution of the pinch in the upper half of the (r,z) plane. The instantaneous position of the plasma is indicated by lines of constant density , $n_e = 5 \times 10^{15}$ cm^{-3}. The maximum electron density of the compressed plasma is about 2×10^{16} cm^{-3}. The first maximum compression occurs at 2.1 μs. Note that the width of the belt changes in time due to radial bounce oscillations. Considerable distortion of the cross section and the beginning of an axial contraction are seen in the Figure.

Analysis of magnetic field distributions reveals the presence of force-free currents in the tenuous plasma both inside and outside the dense plasma belt. This seems to be confirmed by recent experimental evidence[7]. Calculations covering longer periods of time are presently under way and will be discussed at the Conference.

This work was supported by the "Fonds National Suisse de la Recherche Scientifique".

References

1. R. Wilhelm and H. Zwicker, in "Plasma Physics and Controlled Nuclear Fusion Research" (IAEA, Vienna, 1971), Vol I, p. 259.

2. K.H. Dippel, et al. "Third International Symposium on Toroidal Plasma Confinement", Garching, 26-30 March, 1973, paper G7.

3. T. Ohkawa, et al., ibid., paper B17-I.

4. A.V. Bortnikov, et al., ibid., paper B5.

5. F. Hofmann, Nuclear Fusion (to be published).

6. F. Hofmann, in "Proceedings of the Fourth European Conference on Controlled Fusion and Plasma Physics" (C.N.E.N., Rome 1970), p. 153.

7. H. Krause, R. Wilhelm and H. Zwicker, private communication.

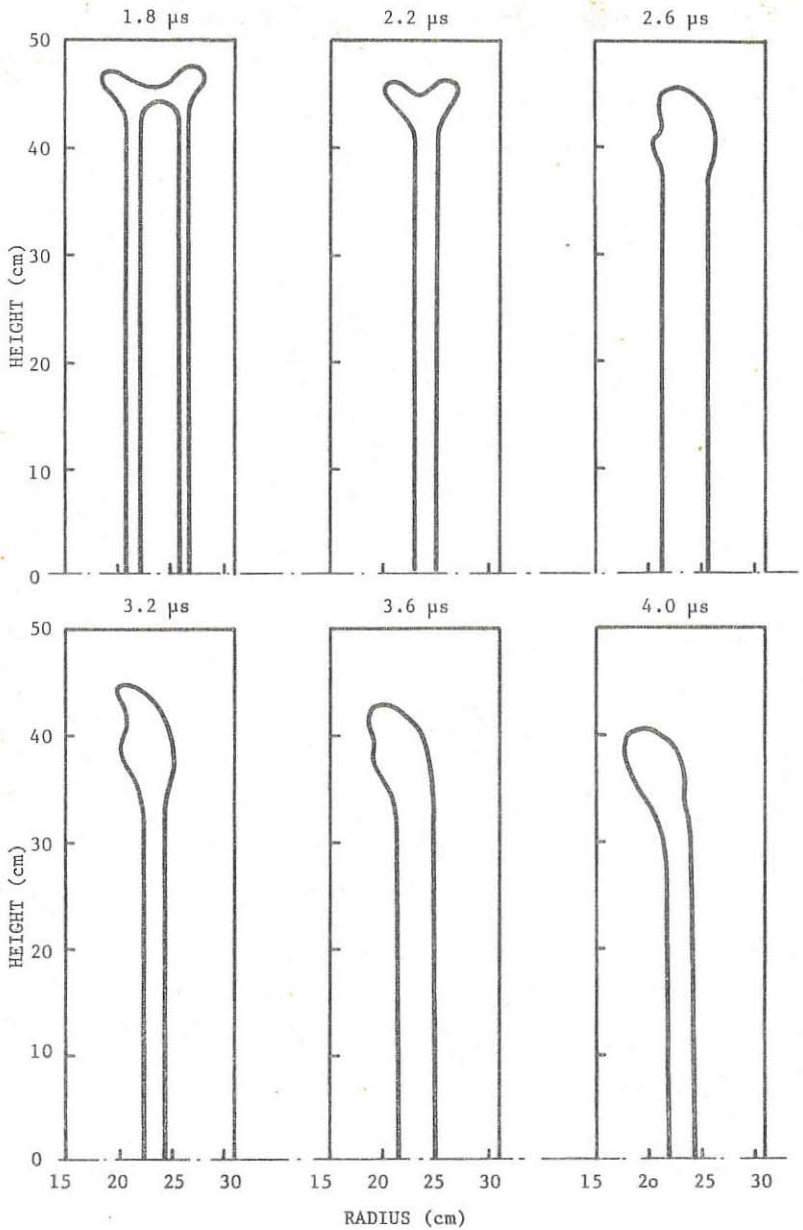


Fig.1.: Equi-Density Lines in a Belt Pinch, at Various Times

THE TOROIDAL Z-PINCH PROGRAM AT LOS ALAMOS*

D. A. Baker, L. C. Burkhardt, J. N. Di Marco, P. R. Forman, A. Haberstich, R. B. Howell, H. J. Karr, L. W. Mann and J. A. Phillips

Los Alamos Scientific Laboratory, University of California
Los Alamos, New Mexico 87544 U.S.A.

Experimental and theoretical studies of the diffuse Z pinch are described. The dependence of stability on B_z field magnitude, B_z reversal and I_z crowbar are discussed.

The Z-pinch group at Los Alamos is investigating the properties of a diffuse pinch with a reversed toroidal field external to the plasma. The ZT-1 experiment has discharge currents of 200 kA with rates of rise of $\sim 1.5 \times 10^{12}$ A/sec, and initial deuterium gas fillings of 2.5 to 30 mTorr. The initial toroidal bias magnetic field ranges up to 5 kG and can be rapidly reversed to 5 kG. Fully stable profiles have not yet been achieved but improvement in plasma behavior is noted when field reversal is applied.

As previously reported [1] a grossly stable plasma is observed at high values of initial bias magnetic field. Analysis of magnetic probe data shows these pinches are unstable to localized modes in the vicinity of the pitch minimum. Reversing the magnetic field in the region external to the pinch removes the pitch minimum. However, with high bias fields, the reversed B_z penetrates only $\sim$ 4 mm inside the ceramic wall. Calculations indicate fewer unstable modes and reduced growth rates when compared with the non-reversed case. A time history of the unstable modes reveals that the pinch goes through a series of stages. Before the external field has reversed by more than one-third of the value of the initial bias field (1 to 2 μsec), the analysis shows a wide range of wave numbers (-0.3 to -0.65 cm^{-1}) of the unstable modes. Streak photographs show a band of light on the wall at this time. The light then diminishes in intensity and the probe analysis shows a reduced range of unstable wave numbers (-0.3 to -0.35 cm^{-1}) with growth times of $\sim$ 50 μsec. At 6 to 8 μsec the streak photographs show a bright band structure and the analysis indicates an extended range of unstable wave numbers (-0.25 to -0.70 cm^{-1}) with growth times of $\sim$ 0.5 μsec.

Reduction of the initial bias field allows the reversed B_z to penetrate 1.0 to 1.5 cm from the wall. But this reduction results in a kink instability which moves the plasma column to the wall in 1 to 2 μsec.

Other parameters are being explored to obtain fully stable reversed field profiles. For example, the degree of preionization also affects the pinch stability. The onset of the kink instability at low bias fields, as observed by the spontaneous reversal of the I_θ current in the B_z windings, can be delayed by a factor of three by reducing the degree of preionization. The reason for this behavior has not yet been explained and the effect of field reversal is to be explored.

Explosively driven crowbar switches have been installed in the four feed plates of the torus primary. With these switches the discharge current decays with an e-folding time of about $\leq$ 120 μsec for the first 20 μsec. At high bias field the plasma pressure profiles deduced from magnetic probe data remain essentially constant for the first 8 μsec, even though the plasma is unstable to local modes. This is to be contrasted with a drop in pressure by a factor of five during this time, without crowbars.

Differential soft x-ray measurements using scintillators in conjunction with thin aluminum foils (6.25×10^{-4} and 1.27×10^{-3} cm) have been made. The signals are characterized by a large amplitude pulse followed by a low level tail. The signal can be interpreted as being due to an initial electron temperature of about 1 keV which rapidly decreases to $\leq$ 100 eV in about 2 μsec or as a burst of $\sim$ 10 keV x-rays resulting from runaway electrons. In either case these measurements are difficult to reconcile with the magnetic probe data. Thomson scattering experiments are in progress to resolve this question.

Using our two-fluid code a study is being made of the pinch with anisotropic, time-dependent transport coefficients. With perpendicular resistivity at one Bohm the I_θ current falls rapidly with the implosion and the magnetic field profiles become diffuse as in the experiment. However the I_θ then rises indicating a rapid leakage of flux from the plasma column. At 1/200 Bohm I_θ has the proper time dependence but the B_z and B_θ profiles are sharp and do not resemble the diffuse profiles found in ZT-1.

A numerical stability study has been made on linear Z-pinch equilibria having hollow pressure profiles and reversed longitudinal field in the outer region of the plasma. The reversal is necessary for stability of configurations having a vacuum field region outside the pinch [2]. Configurations have now been found which are stable for $m \geq 0$ with β_θ values as high as .6. The Robinson limit of $\beta_\theta \leq .5$ for $m = 0$ is approximate and can be exceeded. We find that the depth of the pressure minimum on axis has little effect on the location of the conducting wall required for stability. Higher β_θ's can be obtained with a flat profile on axis but we have chosen hollow profiles to extend stable times against diffusion.

The MHD stability of a linear diffusing pinch has been calculated using both simple diffusion and a fully hydromagnetic model. Assuming classical diffusion only, the results indicate that stability can be maintained for a time sufficient to satisfy the Lawson criterion.

The first unstable modes to appear are Suydam modes in the outer region of the pinch. Their onset is delayed in some cases by allowing the total z current and external θ current to decay exponentially in time.

The growth rates and widths of these localized modes can be predicted without going through the normal mode analysis by expanding the f and g functions, appearing in the energy integral, about the singularity r_s where $k B_z + m B_\theta / r_s = 0$. An analytic expression for the growth rates of symmetric Suydam modes is then obtained.

Figure 1 shows a comparison between growth rates obtained by the normal mode analysis and by the analytic solution for a typical diffusing pinch. The discrepancy at small r is due in this particular case to the fact that Suydam modes are highly asymmetric in that region. Suydam modes are either single or double humped, depending on the value of the shear at the singularity.

---

*Work performed under the auspices of the U.S. Atomic Energy Commission.

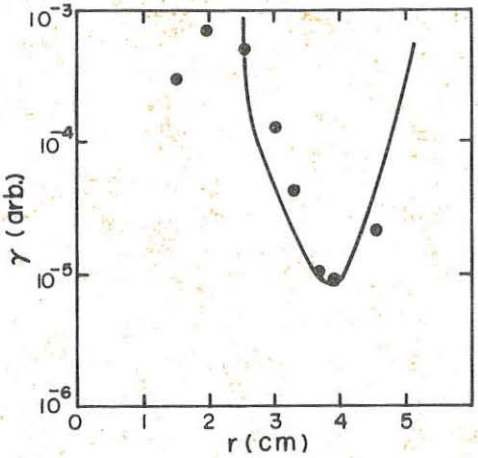


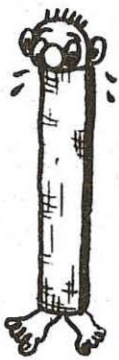
Fig. 1. Growth rates of unstable Suydam modes. Circles are the normal mode analysis, curve is analytic solution.

References:

1. L. C. Burkhardt, et al., Proceedings of the Second Topical Conference on Pulsed High-Beta Plasmas, July 3-6, 1972, W. Lotz, Editor, Garching bei München IPP 1/127.

2. D. C. Robinson, Plasma Physics 13, 439 (1971).

2.3. THETA-PINCHES



PLASMA DYNAMICS AND CURRENT SHEATH STRUCTURE IN COLLISIONFREE THETA-PINCHES

by

K. Höthker, K.J. Dietz, K.H. Dippel and E. Hintz

Institut für Plasmaphysik der Kernforschungsanlage Jülich GmbH

ASSOCIATION EURATOM/KFA

Jülich/Germany

I. INTRODUCTION.

Previous investigations at this laboratory /1,2,3/ were concerned with the scaling laws which govern the dynamic behaviour of the plasma, the ion heating, and the diffusion of the magnetic field in the piston region during the implosion phase of a low density theta-pinch. Initial densities ($10^{12}\text{cm}^{-3} \lesssim n_{e1} < 10^{13}\text{cm}^{-3}$), implosion velocities ($\lesssim 10^{8}\text{cm sec}^{-1}$) and the initial magnetic field were choosen such that the mean free path of the inward moving ions and the ion cyclotron radius were large compared to the radius R of the discharge tube.

Under such circumstances one may expect that the ions behave as free particles. Assuming further that they are reflected elastically when they encounter the piston one obtains the following relations for the magnetic field of the piston B_p and for the piston velocity u_p:

$$B_p = (c \cdot E_p)^{1/2} \; (16 \; n_1 \; m_i)^{1/4}; \quad E_p = (1/c) \; B_p \cdot u_p$$

where E_p is the electric field at the plasma boundary.

Measurements showed that the scaling goes as expected from the equations. The same was true for the absolute values. The mean ion energies measured after the fast magnetic compression phase were also in agreement with the predictions of the free particle model. From the observed diffusion rates of the magnetic field it was possible to determine the effective electrical conductivity σ_{eff} or the effective electron-ion-collision frequency ν_{eff} in the current sheath, which came out as: $\nu_{eff} \approx \omega_{pi}$ (ω_{pi} is the ion plasma frequency). In this paper we present results of experimental studies which were concerned with a more detailed investigation of the piston-induced radial plasma flow and of the electron density, the electron temperature, and the magnetic field distribution in the piston region; this was done for one set of initial conditions: $n_{e1} = 5 \cdot 10^{12}\text{cm}^{-3}$, $u_p \approx 5 \cdot 10^{7}\text{cm/s}$, $T_{e1} = 2{,}5$ eV; $B_1 < 10$G.

PLASMA DYNAMICS AND CURRENT SHEATH STRUCTURE IN COLLISIONFREE THETA-PINCHES

by

K. Höthker, K.J. Dietz, K.H. Dippel and E. Hintz

Institut für Plasmaphysik der Kernforschungsanlage Jülich GmbH

ASSOCIATION EURATOM/KFA

Jülich/Germany

I. INTRODUCTION.

Previous investigations at this laboratory /1,2,3/ were concerned with the scaling laws which govern the dynamic behaviour of the plasma, the ion heating, and the diffusion of the magnetic field in the piston region during the implosion phase of a low density theta-pinch. Initial densities ($10^{12}\mathrm{cm}^{-3} \lesssim n_{e1} < 10^{13}\mathrm{cm}^{-3}$), implosion velocities ($\lesssim 10^{8}\mathrm{cm\ sec}^{-1}$) and the initial magnetic field were choosen such that the mean free path of the inward moving ions and the ion cyclotron radius were large compared to the radius R of the discharge tube.

Under such circumstances one may expect that the ions behave as free particles. Assuming further that they are reflected elastically when they encounter the piston one obtains the following relations for the magnetic field of the piston B_p and for the piston velocity u_p:

$$B_p = (c \cdot E_p)^{1/2}\ (16\ \ n_1\ m_i)^{1/4};\quad E_p = (1/c)\ B_p \cdot u_p$$

where E_p is the electric field at the plasma boundary.

Measurements showed that the scaling goes as expected from the equations. The same was true for the absolute values. The mean ion energies measured after the fast magnetic compression phase were also in agreement with the predictions of the free particle model. From the observed diffusion rates of the magnetic field it was possible to determine the effective electrical conductivity σ_{eff} or the effective electron-ion-collision frequency ν_{eff} in the current sheath, which came out as: $\nu_{eff} \approx \omega_{pi}$ (ω_{pi} is the ion plasma frequency). In this paper we present results of experimental studies which were concerned with a more detailed investigation of the piston-induced radial plasma flow and of the electron density, the electron temperature, and the magnetic field distribution in the piston region; this was done for one set of initial conditions: $n_{e1} = 5 \cdot 10^{12}\mathrm{cm}^{-3}$, $u_p \approx 5 \cdot 10^{7}\mathrm{cm/s}$, $T_{e1} = 2{,}5$ eV; $B_1 < 10$G.

PLASMA DYNAMICS AND CURRENT SHEATH STRUCTURE IN COLLISIONFREE THETA-PINCHES

by

K. Höthker, K.J. Dietz, K.H. Dippel and E. Hintz

Institut für Plasmaphysik der Kernforschungsanlage Jülich GmbH

ASSOCIATION EURATOM/KFA

Jülich/Germany

I. INTRODUCTION.

Previous investigations at this laboratory /1,2,3/ were concerned with the scaling laws which govern the dynamic behaviour of the plasma, the ion heating, and the diffusion of the magnetic field in the piston region during the implosion phase of a low density theta-pinch. Initial densities ($10^{12}\text{cm}^{-3} \lesssim n_{e1} < 10^{13}\text{cm}^{-3}$), implosion velocities ($\lesssim 10^{8}\text{cm sec}^{-1}$) and the initial magnetic field were choosen such that the mean free path of the inward moving ions and the ion cyclotron radius were large compared to the radius R of the discharge tube.

Under such circumstances one may expect that the ions behave as free particles. Assuming further that they are reflected elastically when they encounter the piston one obtains the following relations for the magnetic field of the piston B_p and for the piston velocity u_p:

$$B_p = (c \cdot E_p)^{1/2} \; (16 \; n_1 \; m_i)^{1/4}; \quad E_p = (1/c) \; B_p \cdot u_p$$

where E_p is the electric field at the plasma boundary.

Measurements showed that the scaling goes as expected from the equations. The same was true for the absolute values. The mean ion energies measured after the fast magnetic compression phase were also in agreement with the predictions of the free particle model. From the observed diffusion rates of the magnetic field it was possible to determine the effective electrical conductivity σ_{eff} or the effective electron-ion-collision frequency ν_{eff} in the current sheath, which came out as: $\nu_{eff} \approx \omega_{pi}$ (ω_{pi} is the ion plasma frequency). In this paper we present results of experimental studies which were concerned with a more detailed investigation of the piston-induced radial plasma flow and of the electron density, the electron temperature, and the magnetic field distribution in the piston region; this was done for one set of initial conditions: $n_{e1} = 5 \cdot 10^{12}\text{cm}^{-3}$, $u_p \approx 5 \cdot 10^{7}\text{cm/s}$, $T_{e1} = 2{,}5$ eV; $B_1 < 10$G.

II. APPARATUS.

The experimental set up and the diagnostic methods are described in /2/. The local electron density and temperature were measured at the radii r=8cm and r=6cm by means of Thomson scattering, the magnetic field was measured along the tube radius by means of probes.

III. RESULTS.

1. Plasmadynamics. Fig. 1 shows $n_e(t)$, $T_e(t)$, and B (t) at r=8cm. Similar observations at r=6cm together with probe measurements along r permit the conclusion, that the first two peaks of $n_e(t)$ are the result of a nearly stationary spatial structure $n_e(r)$ propagating at constant velocity u_s towards the axis. Only adiabatic electron heating is observed. The third density peak coincides with the magnetic piston; its velocity seems to oscillate around a mean value $u_p = u_s/2$, shape and amplitude vary with time. Integrating the particle flux at r=8cm in time shows, that only ≈10% of the particle flux passes through this point at a velocity u_s, while the bulk follows with the magnetic piston at $u_p = u_s/2$. The total line density $N = 2\pi \int nr\, dr$ is conserved to within 15%. In Fig. 2 we have tried to illustrate the temporal evolution of the events in a r-t diagram, including also some other observations. From this one gets at least an approximate understanding of how the physical processes develop: On the first few cm of its way the piston reflects the incident particles elastically generating a density front with $u_s = 2u_p$. Then the reflection properties suddenly change, probably because of the onset of microinstabilities in the current sheath. The particles may be trapped in the piston region or just penetrate deeper into the piston because the sheath broadens. In the latter case the delayed occurrence of the second peak may just be a transit time effect. However, on the basis of the existing experimental data we shall not attempt to describe the complicated dynamic behaviour of the piston and the resulting plasma flow ahead of it, in particular, since according to the r-t diagram and according to the shape of the 3rd density pulse the first plasma pulse, after reflection at the axis, should encounter the piston near r=8cm, and an interpretation of the observations is therefore very difficult.

2. Structure of the current sheath. Fig. 1 showed the magnetic field signal at r=8cm and the electron temperature derived from light scattering measurements as a function of time. The B (t) curve

is a superposition of several oscillograms. The observed rapid heating of the electron gas in the piston can be explained by Coulomb collisions only up to a T_e-value of 8 eV, measured at the first bend of B (t) (at t = 280 nsec). Beyond this point the electrical conductivity is anomalously low, indicating that electric field fluctuations are strongly enhanced. This is in agreement with the observation /2/ that the effective electron-ion-collision frequency derived from measured diffusion rates is of the order $\nu_{eff} \approx \omega_{pi}$. A quantitative comparison of measured heating rates with j^2/σ_{eff} is not possible with the existing experimental data.

The measured velocity distribution of the electrons for T_e = 60 eV is shown in Fig. 3. It is worthwhile mentioning that the maximum temperature of about 1 keV measured with Thomson scattering agrees quite well with the temperature obtained previously from soft x-ray measurements using the foil absorption technique.

One may expect that the microturbulence in the current sheath develops from an ion sound instability. Classical heating in the initial phase should result in $T_e/T_i \gg 1$. The sharp decrease of the drift velocity at the end of the classical regime indicates the beginning of turbulent heating, the ratio v_d/c_s (with $c_s = T_e/m_i$) is always above the threshold for ion sound instability (Fig. 4). For the subsequent increase of the drift velocity we do not have a satisfactory explanation; it may be of significance that it occurs when the ß-value exceeds 1. It may further be noteworthy that a strong thermal skin effect is observed; heat conduction apparently does not contribute to the temperature rise in the first, classically heated part of the piston.

IV. CONCLUSIONS.

In the first phase of the fast magnetic compression of a non-magnetized, collision-free plasma in a theta-pinch, a two velocity flow ahead of the piston is induced as described by the "free particle" model. This phase is interrupted because of a sudden change in the reflection properties of the piston - probably due to the onset of current driven instabilities in the piston region. The bulk of the particles is trapped in the current sheath. As a result of the strongly enhanced, turbulent resistivity electrons are heated to temperatures above 1 keV.

REFERENCES: /1/ P. Bogen et.al. Proc. Conf. Madison 1971, Vol.3, 277, IAEA Vienna 1971. /2/ K.J. Dietz, K. Höthker, Paper D1, and /3/ K.J. Dietz, K.H. Dippel, E. Hintz, Paper D2, Proc. 2nd Top. Conf. on Pulsed High-ß-Plasmas, IPP-Report 1/127, Garching 1972

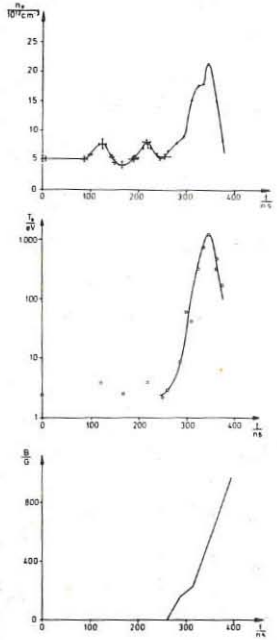


Fig.1 $n_e(t)$, $T_e(t)$, and B(t) at r=8 cm

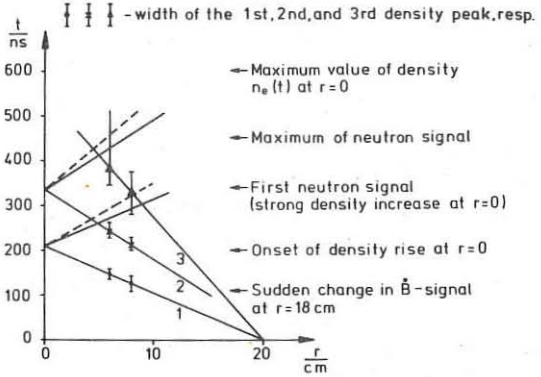


Fig.2 r-t-diagram of 1st, 2nd, and 3rd density disturbance and correlation to other observations(---t(r) in case of expansion with sound velocity)

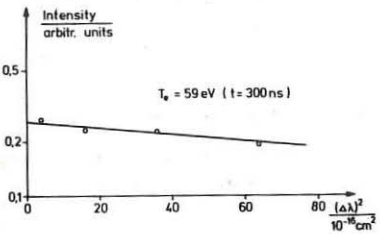


Fig.3 Semilogarithmic plot of scattered light intensity against wavelength

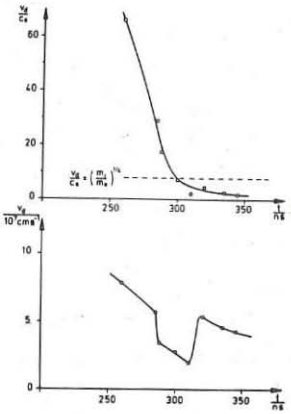


Fig.4 Drift velocity v_d and v_d/c_s as a function of time

THE PRODUCTION OF WEAKLY COMPRESSED HIGH-BETA PLASMAS BY SHOCK HEATING IN HIGH-VOLTAGE THETA PINCHES

M.Keilhacker, M.Kornherr, H.Niedermeyer, F.Söldner, K.-H.Steuer

Max-Planck-Institut für Plasmaphysik, Euratom Association

Garching bei München, F.R.G.

Abstract: In the Garching 500 kV-Theta-Pinch (coil diameter 43 cm) which furnishes a fast rising almost trapezoidal magnetic field pulse shock heating without adiabatic compression produces $\beta \approx 1$ plasmas with compression ratios between 2 and 3. The compressed plasma density is typically $10^{14} cm^{-3}$ and the ion temperature 2 keV, while the electrons are cold.

Introduction - Wall Stabilization of High-β Tori

In high-β stellarators [1,2] helical fields are used to produce toroidal equilibrium. Theory and experiment indicate that these helical fields excite MHD-instabilities if the plasma is strongly compressed and thus far from the conducting wall. The latter situation holds for present theta pinches which heat the plasma by a combination of shock heating and adiabatic compression resulting in a large compression ratio $\varkappa$ ($\varkappa = r_W/r_p$ is the ratio of wall and plasma radii). In this case the dominant unstable modes must be feedback stabilized which is technologically difficult and expensive.

On the other hand, if the plasma is only weakly compressed the most dangerous m=1 mode may be stabilized by image currents that are induced in the conducting wall. According to theory [3] this wall stabilization is proportional to $\beta^2 . \varkappa^{-4}$ and therefore becomes effective only for a high-β plasma with small compression ratio. For realistic parameters $\varkappa$ should be about 2 - 3 to make the wall term dominate the destabilizing terms.

In this paper we discuss the production of weakly compressed high-β plasma by shock heating in high-voltage theta pinches.

Free Particle Model of Shock Compression

a) Step pulse of magnetic field: We take the model of an imploding sheath separating the piston magnetic field and the plasma that bounces off the ions at twice the implosion speed u (free particle model). Assuming a step pulse for the piston field B_S the compres-

sion ratio after shock compression is

$$\varkappa_S = \left(\frac{f+2}{2}\right)^{1/2} = \begin{matrix} 1.4 & f = 2 \\ 1.6 & f = 3 \end{matrix} \quad \text{for} \qquad (1)$$

while the ion temperature (keV) is (for f = 2 and deuterons)

$$kT_S = 2 \times 10^7 \, n_S^{-1/2} \, E_\theta \qquad (2)$$

with f = degrees of freedom after compression, n_S = density after shock compression (cm^{-3}), and $E_\theta = u\, B_S$ = electric field at plasma boundary (kV/cm).

b) Finite rise of magnetic field: In a more sophisticated model including a finite rise τ of the driving field Freidberg and Morse have shown [4] that the final temperature and plasma radius are independent of τ as long as τ is less than about 30% of the piston transit time r_w/u.

c) Subsequent adiabatic compression: If the shock heating (eq.(2)) is followed by adiabatic compression one finally gets the relation (for f = 2)

$$kT = 0.7 \times 10^7 \, n^{-1/2} \, \varkappa^3 \, E_\theta \qquad (3)$$

where n, kT and $\varkappa$ are the plasma parameters after adiabatic compression. If the finite inductance of the theta pinch coil is taken into account the electric field at the coil, $E_{\theta,c}$, necessary to reach a certain temperature kT is about twice as large as the field E_θ resulting from eq.(3).

High-Voltage Theta Pinch Experiment

In the Garching high-voltage theta pinch [5] a coil of 43 cm ø and 100 cm length is energized by four Blumlein lines that are charged to 125 kV each and connected in series at the coil (maximum field amplitude 5.5 kG).

A radially homogeneous magnetic field free initial plasma of densities n_o between 1 and 6 x $10^{13} cm^{-3}$ ($T_{eo} \approx 1 - 2$ eV, degree of ionization 20 - 50%) is produced by z-pinch preionization of deuterium gas at filling pressures around 1 mtorr [6].

At these densities the implosion time is about 300 ns which is much longer than the rise time of the piston magnetic field (see Fig.1). Therefore in this experiment one expects strong shock heating with-

out substantial adiabatic compression resulting in a "fat" high temperature theta pinch plasma.

Experimental Results

The time development of the magnetic field profiles was measured by magnetic probes, the neutron flux with a calibrated plastic scintillator, density and electron temperature by Thomson scattering of laser light.

Fig. 2 shows typical radial magnetic field profiles during compression of a plasma with $n_o = 2 \times 10^{13} cm^{-3}$ (1.6 mtorr D_2). The magnetic piston which is a relatively thin sheath starts to implode with a velocity of about $7 \times 10^7 cm/s$ then decelerates and finally is stopped by the kinetic pressure of the compressed plasma.

This is also illustrated in the top part of Fig.3 where the position at which the magnetic field has half the value of the outside field B_s is plotted as a function of time ("smear picture" of magnetic piston). The bottom part of Fig.3 shows the corresponding neutron yield.

These and other measurements indicate the following picture of shock compression at initial densities in the range 10^{13} to $10^{14} cm^{-3}$: In contrast to lower densities (see paper by Keilhacker et al., this conference) where the density jump coincides with that of the magnetic field resulting in a low-β plasma ($\beta \leq 0.5$) at higher densities and correspondingly smaller current sheaths the ions are elastically reflected by the magnetic piston thus moving ahead of the magnetic field and separating from it (free particle model). In this case a $\beta \approx 1$ plasma is formed. The neutron flux starts when the accelerated ions reach the axis.

For the above example ($n_o = 2 \times 10^{13} cm^{-3}$) the density of the compressed plasma is about $10^{14} cm^{-3}$. The ion temperature as calculated from the neutron flux is about 2 keV, while the electrons remain cold. The rise in density yields a compression ratio of 2.2, while the radial magnetic field profiles indicate a larger compression. This is probably due to a decrease in initial plasma density near the tube wall.

The weak magnetic field gradients behind the piston that change

sign at around 600 ns indicate the presence of plasma outside the $\beta \approx 1$ plasma column. The properties and the origin of this plasma will be investigated in forthcoming experiments.

References: [1] Burnett,S.C. et al.; Plasma Physics and Contr.Nucl. Fusion Res., 3, 2o1 (1971).[2] Fünfer,E., et al.,Proc.2nd Topical Conf.on Pulsed High-Beta Plasmas, Garching, Report IPP 1/127, 21, (1972). [3] Weitzner,H., Ref.[1], 223 (1971),[4] Freidberg,P.,et al., Ref.[2], 139(1972), [5] Keilhacker,M., et al., Ref.[2], 127 (1972). [6] Lange,F.D., et al., Verhandl. DPG (VI) 8, 746 (1973).

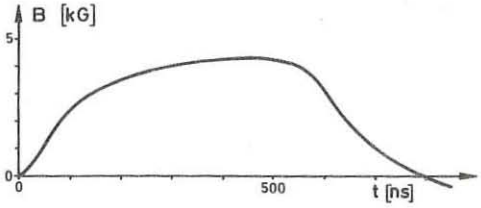
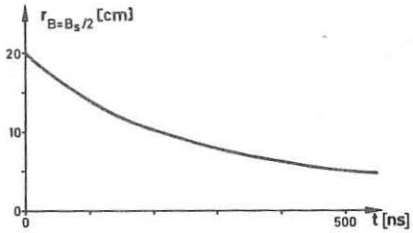


Fig.1: External magnetic field



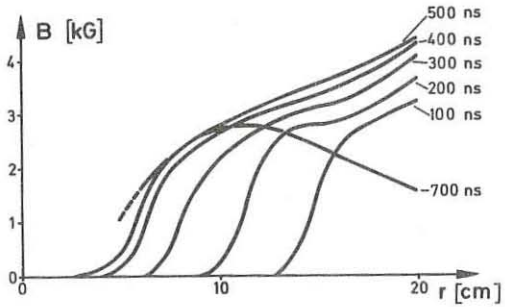


Fig.2: Radial magnetic field profiles for initial density of 2×10^{13} cm^{-3}

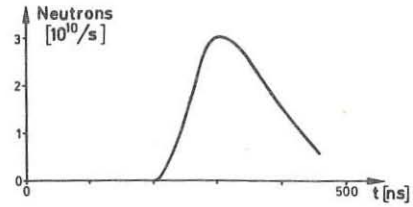


Fig.3: "Smear picture" of magnetic piston and neutron yield for initial density of 2×10^{13} cm^{-3}

SHOCK HEATING AND PLASMA SHEATH SCALING IN LOW DENSITY THETA PINCHES

M.Keilhacker, M.Kornherr, G.Maret, H.Niedermeyer, K.-H.Steuer

Max-Planck-Institut für Plasmaphysik, Euratom Association
Garching bei München, F.R.G.

Abstract: Investigation of shock compression over a wide range of initial densities shows that at low densities ($n_o \leq 2.10^{12} cm^{-3}$) the snow plough model applies, at higher densities ($n_o \geq 10^{13} cm^{-3}$) the free particle model. In the first case the compression results in a $\beta \leq 0.5$ plasma, in the latter β is about 1.

Introduction

Fast magnetic compression of low density plasmas at the moment is the most effective way of heating a plasma to thermonuclear temperatures. In this paper we investigate the problems connected with shock heating of low density plasmas covering a wide range of initial densities ($10^{11} \leq n_o \leq 6.10^{13} cm^{-3}$). In particular we study the formation of the piston sheath in order to find out whether the ions are swept up within the magnetic piston (snow plough model) or whether they are elastically reflected (free particle model). Furthermore we look for a limiting density below which effective plasma compression becomes impossible due to strong broadening of the current sheath by anomalous field diffusion and try to derive scaling laws for this critical density.

Shock Heating Experiment

Shock compression is investigated in a high-voltage theta pinch (charging voltage up to 500 kV, coil diameter 43 cm, coil length 100 cm) /1/. The rise of the magnetic field is 3.10^{10} G/sec, the maximum amplitude 5.5 kG and the pulse length 0.5 µsec.

To cover a wide range of initial plasma densities two types of preionization are used:

1) Photoionization by UV-radiation producing a radially homogeneous magnetic field free plasma with densities $10^{11} \leq n_o \leq 2.10^{12} cm^{-3}$ /1/.

2) Z-Pinch preionization at pressures around 1 mtorr producing a highly ionized plasma with densities $10^{13} \leq n_o \leq 6.10^{13} cm^{-3}$ /2/.

Experimental Results

Fig.1 shows typical radial magnetic field profiles during the compression of a very low density plasma. The magnetic field penetrates down to the axis. Simultaneously the density on axis rises and the neutron yield strongly increases. This indicates that the plasma is collected within the magnetic piston. The sheath implodes with a velocity of about 10^8 cm/sec corresponding to an ion kinetic energy of 10 keV. The ion temperature calculated from the neutron yield is also about 10 keV in agreement with the above picture of snow plough compression.

During implosion the current sheath broadens due to anomalous diffusion thereby strongly heating the electrons. Shortly after maximum compression the electron temperature is 700 eV. This temperature is in agreement with energy balance calculations assuming the same effective collision frequency ν_{eff} for parallel heat conduction as for ohmic heating, the latter being determined from the experimentally observed diffusion rate ($\nu_{eff} \approx 0.3\ \omega_{pi}$).

After a strongly dynamic phase the plasma comes into pressure equilibrium while the external magnetic field slowly diffuses into the plasma ($\beta = 0.5$ at max. external field). These β-values decrease with decreasing initial density and charging voltage.

The compression of higher density plasmas differs from this model of snow plough compression. The magnetic field does not reach the axis although a rise of density on axis connected with simultaneous neutron emission is observed (see paper by Keilhacker et al., this conference). In this case the piston elastically reflects the ions which then move ahead of the piston. This results in a $\beta=1$ plasma. The ion temperature is about 2 keV while the electrons on axis remain relatively cold.

A more detailed description of sheath formation and shock compression results from numerical calculations (see paper by Chodura and Röthlein, this conference).

Plasma Sheath Scaling

In the low density regime measurements give the following relation for the sheath width

$$\Delta \sim n_o^{-0.5} \cdot m_i^{-0.5} \cdot U_o^{0.4} \cdot t$$

Fig. 2 shows the tickness of the current sheath at half the tube radius, $\Delta R/2$, resulting from this relation. The compression time to half the tube radius is calculated from a modified snow plough model that takes into account the experimental result that the sheath growes linearly with time. The initial density at which $\Delta R/2$ becomes $R/2$ we define as "critical density" below which shock compression becomes ineffective due to diffusion (region II). The sheath widths of region Ia represent a result of numerical plasma simulation which indicates that the sheaths become stationary at a width $\Delta \approx 1/2\ c/\omega_{pi}$ /3/. The measured sheath widths at higher densities (Z-pinch preionization) are in agreement with this prediction.

Conclusions

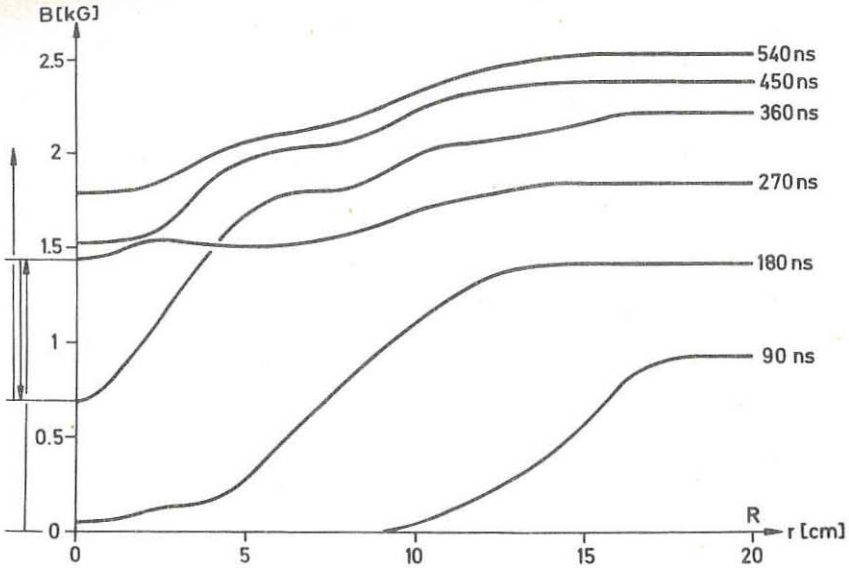
At very low densities the plasma is swept up in the current sheath and the compression can be described by a modified snow plough model. At higher densities the current sheath is smaller being only some fraction of the coil radius. This means that the ions are accelerated in the sheath in a time short compared to the compression time i.e. they are elastically reflected by the piston (free particle model).

References:

/1/ Keilhacker,M., et al., Proc. 5th Europ.Conf.on Contr.Fusion and Plasma Physics, paper 47 (Grenoble 1972)

/2/ Lange,F.D., et al., Verhandl. DPG (VI) 8, 746 (1973)

/3/ Biskamp,D., R.Chodura, 2nd Topical Conf. on Pulsed High-Beta-Plasmas, Report IPP 1/127, 143 (1972).



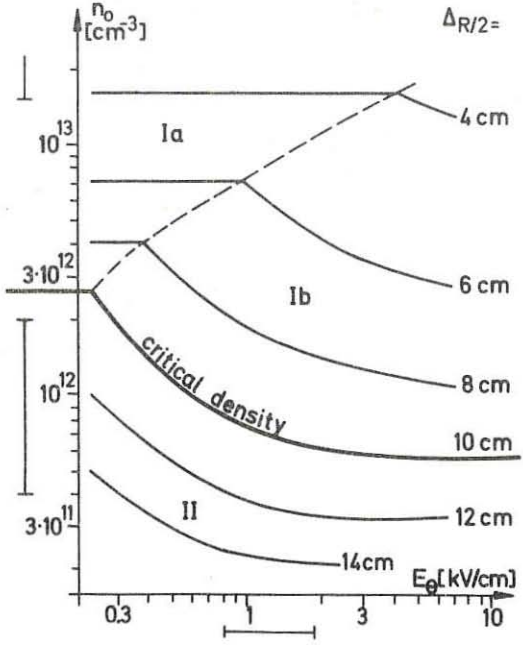


Fig.1: (above)
Radial magnetic field profiles (n_o=7.1o^{11}cm^{-3}, deuterium, U_o = 230 kV)

Fig.2: (left)
Sheath widths in the Garching 500 kV-Theta-Pinch (R = 20 cm, deuterium). The bars show the experimentally investigated parameter range.

ION HEATING IN A STRONG MAGNETIC COMPRESSION WAVE

R.Chodura, B.Röthlein

Max-Planck-Institut für Plasmaphysik, Euratom Association

Garching bei München, F.R.G.

Abstract: Ion heating by fast magnetic compression is investigated in a hybrid numerical model. This model consists of particle description for the collisionfree ions and dissipative fluid description for the electrons[1,2]. Time behaviour of plasma dynamics during and after compression, field profiles and ion heating rates are given.

Introduction: Ion heating by plasma compression in a fast rising magnetic field is a basic process in high-beta experiments. Since the final state at the end of the heating stage determines equilibrium and stability in the subsequent confinement period it is desirable to get information about this state in a numerical simulation experiment.

Most experiments operate at zero bias and large driving magnetic fields leading to very high currents and Hall fields in the front of the implosion pulse. In fact, the potential jump of the Hall field across the front is so large that it acts as a reflecting piston on the ions accelerating them to twice the piston velocity. Thus a precursor of reflected ions is formed in front of the piston. Assuming axial symmetry the precursor passes through the axis, hits the piston, is reflected again and so on until a state of highly disordered motion is reached.

Model: In order to follow this process numerically a fluid description is inapplicable because of the multi-streaming of the ions. Therefore, the motion of the ion component was treated by a collisionless particle-in-cell method. Electrons, because of their small gyroradius and mean free path, were treated as a fluid. Dissipation in the electron component by resistivity and radial heat conduction was included by using an effective collision frequency for Coulomb and collective collisions. Electron inertia was ignored.

The problem was studied in one-dimensional cylindrical geometry. The mean radial motion of electrons and ions was coupled by the quasineutrality condition. The external magnetic field was assumed to rise linearily with time from zero without limitation. Other parameters are given in fig.1.

Results: At the beginning of the implosion the piston acts as a snow-plough i.e. collects plasma particles without reflection. It lasts for a time of about $t \sim 60$ (in units $\omega_{ce}^{-1/2}$ where ω_{ce} is the electron gyro-frequency in the external field) until particle reflexion sets in at $r \sim 0.7$ (in units of the initial plasma radius R). Still then the piston is only partially reflecting becoming more and more compact as it moves further inward. The reflected ions precursor reaches the axis at about $t \sim 100$. (A "free-particle model" assuming a perfectly reflecting piston from the beginning would give a slightly larger time). After passing through the axis the precursor hits the piston again at t = 107 and r = 0.26, penetrates into the pistonregion and is again reflected inward at t = 115 and r = 0.43. Soon after this time the mean radial velocity becomes positive at all places in the plasma. At t = 132 the precursor plasma beam goes through the axis for the second time and again is turned inwards at t = 177 and $r \sim 0.48$. With time growing this regular motion is increasingly smeared out. A third bounce can be noticed at t = 252. Fig. 1 shows the time behaviour of the overall plasma motion. (r,t)-traces are plotted for the outer plasma boundary (10 % initial density), the place of current maximum and for an individual ion which was snow-plowed by the piston. The minima of this traces are correlated with the bounce times of the precursor as described above.

Fig.2 shows the radial distributions of magnetic field B, density n and radial ion temperature T_{ir} at the end of the computer run t = 260. The magnetic field profile keeps its slope nearly constant for all the time since the first compression being only shifted towards the axis. At times of maximum compression the field profile forms a hump in front of the main rise but also then it stays away from the axis, implosion energy being counterbalanced by electron and ion pressure. The low field region may be something narrower in reality because electron pressure is overestimated in the model due to neg-

lection of axial heat conduction. Profiles of density and ion temperature are still time-dependend due to some residual ordered motion.

Ion temperature is strongly anisotropic: Nearly all the thermal energy resides in the radial degree of freedom. This is a consequence of the conservation of generalized angular momentum in collisionless ion motion which prohibits a thermal spread of azimuthal velocities.

Fig.3 shows the time behaviour of the thermal ion energy content of the system. Apart from the peaks at maximum compression the thermal energy tends to a value of about $2.5 \cdot 10^{-2}$ which is still only 1/3 to 1/2 of the total kinetic energy of the ions and about 1/2 of the free particle energy $\frac{1}{2} n_o R^2 m_i (R/t_{f.p})^2$.

The model will be used to discuss experimental results.[3]

References:

[1] Chodura,R., K.Graf Finckenstein, Report IPP 1/113, Institut f. Plasmaphysik, Garching, Germany (197o);

[2] Forslund,D.W., J.P.Freidberg, Phys. Rev. Letters 27, 1189(1971);

[3] Keilhacker,M., et al., This proceedings.

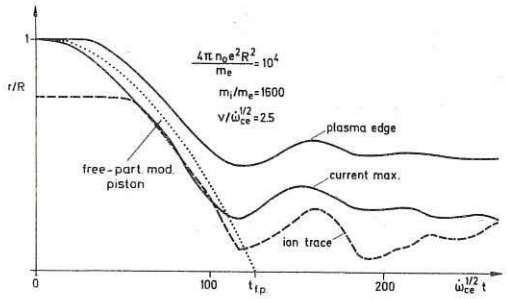


Fig. 1: (r,t) diagram of plasma boundary, maximal current and of the piston in a "free particle model" together with the orbit of an individual ion.

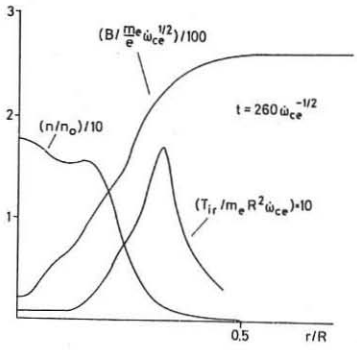


Fig. 2: Radial profiles of magnetic field B, density n and radial ion temperature T_{ir}.

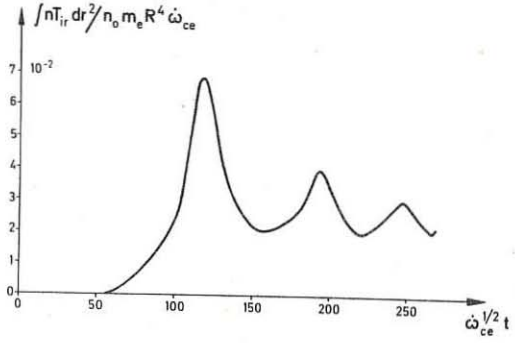


Fig. 3: Time dependence of thermal ion energy.

IMPLODING - LINER FUSION DEVICES

J. P. Boris, A. E. Robson, R. A. Shanny, N. K. Winsor
Naval Research Laboratory, Washington, D.C. 20390

ABSTRACT - We consider fusion systems based on the adiabatic compression of plasma by megagauss magnetic fields generated by electromagnetically imploded metal liners in θ-pinch and cusp geometry.

INTRODUCTION - The almost universal acceptance of 100 kilogauss as the design magnetic field for fusion reactors places an upper limit of 10^{14} - 10^{16} on the plasma density, according to the β-value of the confinement system. Confinement times of 10^{-2} - 1 second are therefore needed to meet Lawson's criterion, requiring quasi-stationary magnetic fields and complicated confinement geometries.

Magnetic fields over 10^7 gauss can be produced by flux compression with imploding liners.[1] If we exclude explosive systems and consider only experiments in which the implosion is driven electromagnetically,[2,3] we can probably take 3.10^6 gauss as the maximum field that can be generated in a reproducible fashion. This field contains a $\beta = 1$ plasma at 10 keV and 10^{19} cm^{-3}, for which the Lawson time is only 10^{-5} second. The short confinement time is fortunately compatible with the necessarily transient method of producing the high magnetic fields. Furthermore, we need only consider rather simple, axially-symmetric confinement systems.

The application of flux compression techniques to plasma confinement has been discussed by Linhart et al[4] and some experiments have been performed by Thomson et al.[5] However, this work has not received serious consideration as a means of producing controlled thermonuclear power because it involved compression by explosives. More recently, the application of electromagnetic flux compression to plasma has received active consideration by Velikhov[6] and by the controlled fusion group at the Naval Research Laboratory.[7,8]

LINUS THETA PINCH - Theoretical and computational studies have been performed on the dynamic compression of plasma by the magnetic field inside a liner in long theta pinch geometry. If the system is long enough that end losses may be neglected, the compression is followed by a symmetrical expansion. A characteristic liner velocity v_∞ is defined by $v_\infty = (3/8\pi)^{\frac{1}{2}} B_o/b\rho^{\frac{1}{2}}$, where B_o is the confining magnetic field at peak compression, ρ is the density of the liner material and b is a thickness parameter, given by $b = (r_1^2 - r_o^2)^{\frac{1}{2}}/r_o$ where r_1 and r_o are respectively the outer and inner radii of the liner at peak compression.

A "dwell time" during which the plasma remains close to peak compression is defined by $t_d = r_o/v_\infty$ and, with $B_o^2/8\pi = 2\, n_o T_o$, we find $n_o t_d \propto B_o r_o \rho^{\frac{1}{2}} b/T_o$, where T_o is the temperature at peak compression.

By integrating the thermonuclear reaction rate in the plasma over the compression and expansion cycle, we obtain $Q = B_o r_o \rho^{\frac{1}{2}} f(b,T_o)$, where Q is now the ratio of neutron energy to the liner energy characterized by v_∞.

The function $f(b,T_o)$ has a broad maximum for $T_o = 20$ keV and increases less than linearly with b. Typically, for $T_o = 20$ keV and $b = 3$, $f = 0.12$ giving $Q = 0.12\, B_o r_o \rho^{\frac{1}{2}}$ (B_o in MGauss, r_o in cm, ρ in gm-cm^{-3}). Putting $Q = 1$, $B_o = 3$ MGauss and $\rho = 8.9$ gm-cm^{-3} (copper liner) we obtain $r_o = 0.9$ cm. The energy invested in the system is 14 MJ/meter and the corresponding value of v_∞ is 1.2×10^5 cm-sec^{-1}.

The simplified analysis assumes a perfectly conducting, incompressible liner. Diffusion of the confining field into the liner reduces the efficiency of the compression. The field at the inner surface of the liner depends, as a function of time, on the zero-order dynamics and the penetration is calculated taking into account the temperature-variation of conductivity. At $B_o = 3$ MGauss, the fraction of liner energy lost through field diffusion is $\sim 50\%$; the fraction increases rapidly if B_o is increased, so apart from other effects (such as liner vaporization), these efficiency arguments probably set an upper limit on the field at ~ 3 MGauss. The liner velocity is then always subsonic and compression of the liner material is adiabatic. Compression absorbs only $\sim 10\%$ of the energy of a copper liner, but becomes a serious (although largely reversible) energy loss in lithium.

In a finite length system, end losses account for a fraction ξ of the total energy, and Q must be increased to $1 + \xi$ to break even. The characteristic length L corresponding to a free effusion time t is $L = 2 c_s t$, where c_s is the plasma sound speed (10^8 cm sec^{-1} at 10 keV). Thus for $t = 10^{-5}$ sec, $L = 20$ meters. However, the total energy of the system is a minimum when $\xi = \frac{1}{3}$, requiring that the length of the LINUS theta pinch be ~ 60 meters. This length would of course be reduced if means could be found to reduce the end losses without compromising the hydromagnetic stability of the plasma.

A more detailed description of a long theta pinch, in which the liner is driven from an inductive energy store, has been obtained from the LINUS-0 code.[7,8] Incorporation of the external circuit equation provides an even more detailed treatment of the liner dynamics. The stability of the liner has also been examined. The unmitigated Rayleigh-Taylor instability has been found to be the most destructive to the integrity of the liner, but rotation has been shown to be capable of complete stabilization.[8]

THE LINUS FLYING CUSP - The principle of flux compression may also be applied to cusp geometry if the liner now consists of two short cylinders, or rings, containing oppositely directed flux that are imploded towards a central point. If the "hole" in the bottle is one gyro-diameter wide at the ring cusp, and the line cusps are of the same area as the ring cusp, it can be shown that $nt \propto B_o^3 r_o^2 / T_o^2$, and the total energy in the system at peak compression is $\propto B_o^{-2.5}$. These expressions illustrate the advantage in applying megagauss fields to the cusp geometry.

The compression is now quasi-spherical. Furthermore, the relatively high plasma loss rate through the cusps automatically leads to an unsymmetrical compression and expansion. A simple model of the dynamics shows that the total energy is a minimum when the characteristic loss time at peak compression is equal to the dwell time. To obtain $Q = 1$ with a maximum field $B_o = 3$ MGauss, we require only $r_o = 4$ cm and the total system energy $\sim$ 100 MJ. This would represent an extremely compact fusion feasibility experiment.

A two dimensional MHD code describing the compression of plasma by liners in cusp geometry is being prepared. In this program the solution of the magnetic field profiles, the time dependent plasma configuration, and the self consistent liner motions and deformations are all treated independently. The separation of time scales for these three phenomena makes the numerical solution of these problems particularly simple. Further extensions of the code to realistic end losses and magnetic field diffusion are also planned.

The application of these principles to a fusion reactor has several interesting features not found in more conventional approaches. The use of the liner as an energy transfer stage allows efficient use of adiabatic compression as a plasma heating method, and could use a relatively inexpensive energy source such as an inductive store. The liner in a reactor would be lithium of sufficient thickness at peak compression to act as neutron absorber as well as heat transfer medium. The problem of the "first wall" would be eliminated by replacing the "wall" at each cycle. Induced radioactivity would be greatly reduced. Finally, the cusp configuration offers the possibility of quite compact reactors of modest energy output.

REFERENCES

1. H. Knoepfel, Pulsed High Magnetic Fields, N. Holland-American Elsevier 1970.
2. E. C. Cnare, J. Appl. Phys. 37, 3812 (1966).
3. S. S. Alikhanov et al, J. Sci. Instr. Series 2, 1, 543 (1968).
4. J. G. Linhart et al, Nuclear Fusion Supplement Pt II, 733 (1962).

5. D. B. Thomson et al, Proceedings of a Conference on Megagauss Magnetic Fields Generated by Explosives and Related Experiments, Frascati, Italy, Sept 21 - 23 1965, EUR 2750e, Brussels 1966, p 491.
6. E. P. Velikhov, invited comments, Fifth European Conference on Controlled Fusion and Plasma Physics, Grenoble, France 21 - 25 August 1972.
7. J. P. Boris and R. A. Shanny, Proceedings of the Fifth European Conference on Controlled Fusion and Plasma Physics, Grenoble, France 21 - 25 August 1972 Paper 20.
8. N. K. Winsor, J. P. Boris and R. A. Shanny, Proceedings of the International Summer School of Plasma Physics, Varenna, Italy (September 1972, in press).
9. N. K. Winsor, D. L. Book and J. P. Boris, Bull. Am. Phys. Soc. II 17, 1030 (1972).

Dynamical Control of Theta Pinch Plasma

by

T.Itagaki, K.Saito, S.Shiina, K.Yokoyama amd H.Yoshimura

Department of Physics and Atomic Energy Research Institute,
College of Science and Engineering, Nihon University, Tokyo

Abstract: The effect of suppression of ballooning motion by a h.f. magnetic field is investigated in a modified theta pinch plasma. The field configulation of theta pinch is deformed by means of a copper sheet, which is rolled around the discharge tube and has a longitudinal cut.

Recently the investigation of dynamical stability and equilibrium of a toroidal high-β configulation has been reported.[1~4] As the preliminary experiment of dynamical toroidal confinement,we make a theta pinch plasma in linear geometry with mirror field configulation (mirror ratio 1.5, the maximum field strength 10 kG at the midplane, half period 25 μsec and distance between two mirror points 24 cm), which is modified by means of a copper sheet. The discharge tube of Pyrex glass has inner diameter 10 cm and length 150 cm. The copper sheet (length 37 cm, width 27 cm and thickness 0.25 mm) is rolled around the discharge tube, having a longitudinal gap of angle of about 60 degrees (fig.2). The h.f. magnetic field $\tilde{B}$ produced by the discharge current of a cable condenser (the maximum field strength 1.1kG for charging voltage 30 kV, angular frequency $\omega = 7.5 \times 10^6$ rad/sec or $\nu = 1.2$ MHz and e-folding time 5 μsec) is superimposed in the central part of the mirror field. The radial distribution of the vacuum magnetic field are shown in fig. 1. Helium gas is used at 100 mTorr. The preheating is done by Z-discharge.

When $\tilde{B}$ is not superimposed, the plasma column shows ballooning motion due to the field gradient. The motion at the midplane is caused toward the gap side during about 1 μsec just after the contraction and then slowed down due to the end effect.[5] The h.f. magnetic field pushes the plasma column to the opposite side of the longitudinal gap. In this case, the cross section of plasma column is nearly circular. The plasma density profile was measured from axial direction by means of a ruby laser Mach-Zender Interferometer.

The evolution of density profile is also consistent with the foregoing results, obtained by streak photograph analysis. (fig. 4 and 5).

The equilibrium position can be estimated from the effective potential energy $U_e = U_0 + \bar{f}^2/2\rho\omega^2$,[6] where U_0 is a quasi stationary potential, f the h.f. force on the plasma column per unit length, ρ the line mass of the plasma column and ω the frequency of the h.f. field. Using a simplified model of the plasma column (no end loss and sharp boundary), we estimated $\bar{f}^2$ as

$$\bar{f}^2 = \frac{4r^2}{\mu^2}\left\{\frac{1}{2}(\tilde{B}_1 B_{01} - \tilde{B}_2 B_{02})^2 + \frac{3}{8}(\tilde{B}_1^2 - \tilde{B}_2^2)^2\right\}$$

$\tilde{B}_1$ and $\tilde{B}_2$ are $\tilde{B}$ on the plasma boundary of the gap side and the one of the opposite side, respectively. B_{01} and B_{02} have also the similar mean with respect to the quasi stationary field B_0. r is the radius of the plasma column. μ is the free space permeability. We put $U_0 = -\rho\alpha\xi$, where α is the acceleration determined from the streak photograph and ξ the displacement of the plasma column. The agreement of the estimated value with the experimental one is fairly good. In this theory, the amplitude of h.f. force should have gradient oppose to it of the quasi stationary potential for existence of equilibrium. In fact, we found that the h.f. force was not effective in experiment, in which the metal sheet was removed to flatten the gradient of the h.f. force.

The observation by magnetic probe shows that $\tilde{B}$ and its gradient are remarkably intensified by production of the plasma column (fig. 3). When the plasma column is replaced by a metal tube with radius of 2.6 cm, such a intensification of the h.f. field is not observed. The metal tube has larger radius compared with radius of half value of the plasma density. The observed intensification of the h.f. magnetic field (~ 1.2 MHz) may be related to a resonance to the radial oscillation of the plasma column (~ 0.8 MHz) and the position of the h.f. skin current.

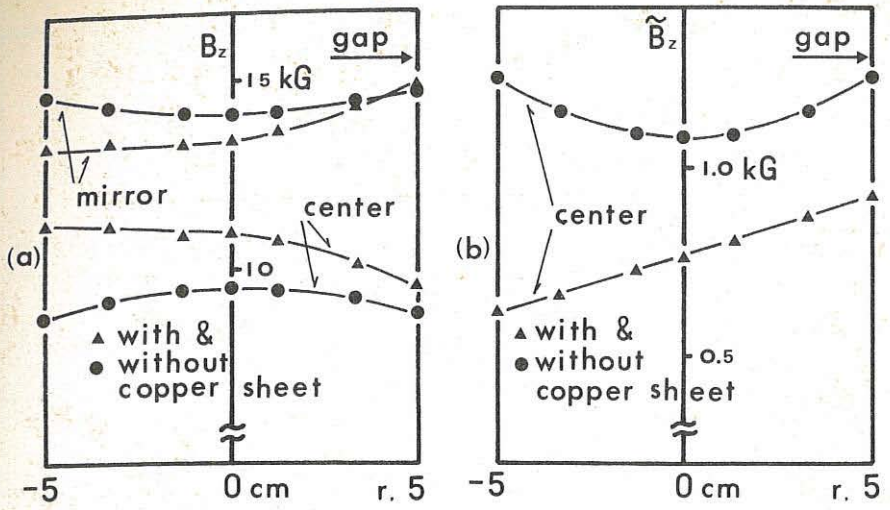


Fig.1. (a) B component produced by main discharge.
(b) $\tilde{B}$ component of the high frequency field.

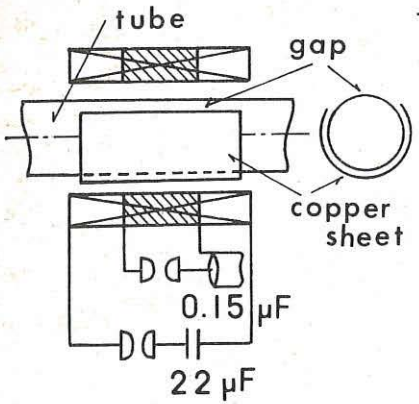


Fig.2. Experimental device

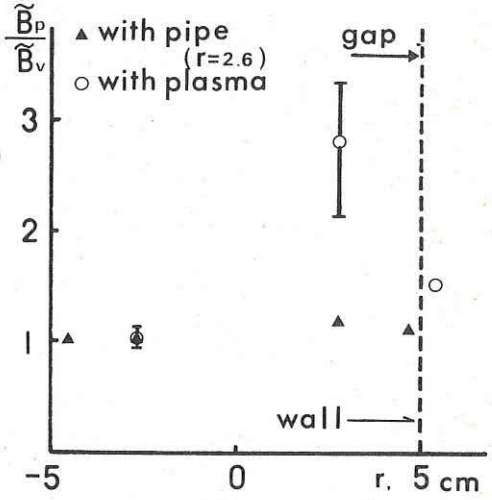
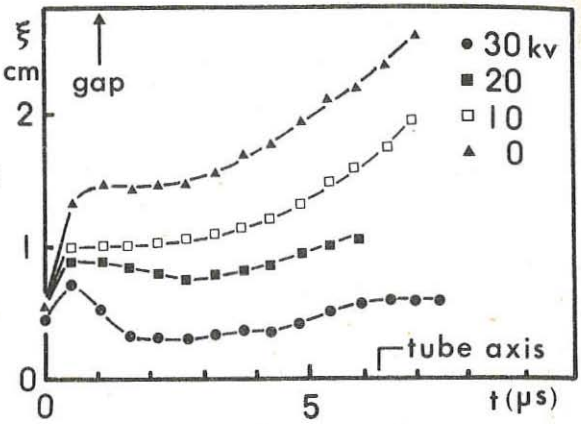


Fig.3. The ratio of the high frequency vacuum field to the high frequency field with plasma and with copper pipe.

Fig.4. The motion of the plasma column with and without the high frequency field. The parameter is the charging voltage of the bank for dynamical control.



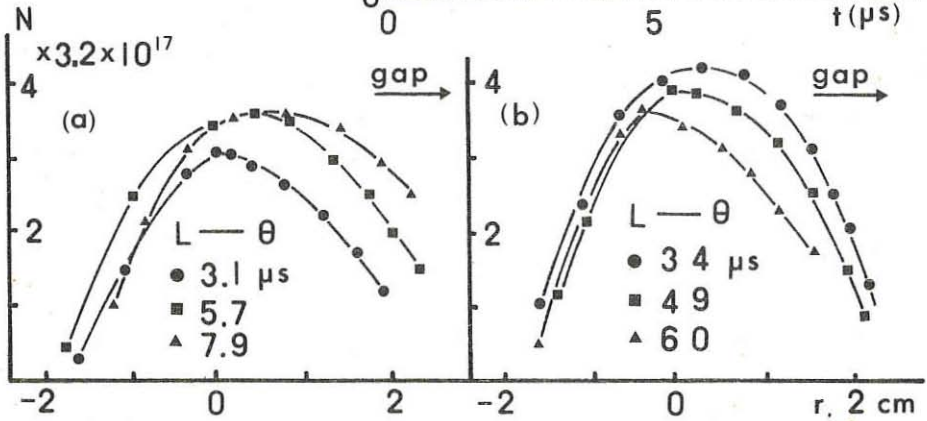


Fig.5. Radial distribution of the total density of the plasma column, (a) without and (b) with the high frequency field. L-θ shows the time between the start of θ pinch and laser illumination.

Reference

1) G.Berge: Phys. Of Fluids 13 1031 (1970)

2) G.H.Wolf and G.Berge: Phys. Rev. Letters 22 1096 (1969)

3) G.Becker, O.Gruber and H..erold: Proc. of the Second Topical Conf. on Pulsed High-Beta Plasmas (Garching, July 1972) p.233

4) I.R.Jones: Phys. Rev. Letters 28 135 (1972)

5) T.Miyamoto, S.Hamada and H.Ohnishi: J. Phys. Soc. Japan 23 1131 (1969)

6) L.D.Landau and E.M.Lifshits: Mechanics (Pergamon Press, London, 1960) p.94

2.4. REACTOR ASPECTS



ON THE EFFICIENCY OF VARIOUS DIVERTORS FOR SCREENING A FUSION PLASMA

D. Eckhartt, G. Haas, K. U. von Hagenow
Max-Planck-Institut für Plasmaphysik, EURATOM Association
Garching b. München, F. R. G.

Abstract: The various divertors proposed in the literature differ in the spatial variation of their conductance to the divertor for plasma particles outside the separatrix. We present a simplified model of the boundary region of a fusion reactor under the action of these divertors and compute the radial profiles of plasma and neutral particle density.

In order to protect a fusion plasma by means of a divertor from wall effects of the vacuum chamber, the existence of a plasma layer outside the separatrix is required, the "screening-layer". This layer has to be opaque for material which is desorbed or sputtered from the wall. Hence, the "effective pumping speed" or conductance to the limiter for plasma particles should not be too large. On the other hand, the radiation losses from the impurities in the screening layer itself should not be intolerably large. This means that the mean life time of the impurity ions in the screening layer should not be too long to keep their density down and, moreover, the electron density in the screening layer should be sufficiently small to reduce the radiation per impurity ion.

It appears that these requirements can be met best by a screening layer of relatively large thickness but small electron density. The various divertor schemes which have been proposed in the literature, are tested in this respect assuming - as a first order approximation - the following model of the plasma boundary: The flux of hot ions with constant temperature from a toroidal plasma is driven radially outwards by Bohm-type diffusion and balanced by flow into the divertor and by charge exchange losses with the cold neutral working gas. The density of the neutral gas attains a prescribed value far away from the separatrix, i. e., in a region where the hot plasma density is negligibly

ON THE EFFICIENCY OF VARIOUS DIVERTORS FOR SCREENING A FUSION PLASMA

D. Eckhartt, G. Haas, K. U. von Hagenow
Max-Planck-Institut für Plasmaphysik, EURATOM Association
Garching b. München, F. R. G.

Abstract: The various divertors proposed in the literature differ in the spatial variation of their conductance to the divertor for plasma particles outside the separatrix. We present a simplified model of the boundary region of a fusion reactor under the action of these divertors and compute the radial profiles of plasma and neutral particle density.

In order to protect a fusion plasma by means of a divertor from wall effects of the vacuum chamber, the existence of a plasma layer outside the separatrix is required, the "screening-layer". This layer has to be opaque for material which is desorbed or sputtered from the wall. Hence, the "effective pumping speed" or conductance to the limiter for plasma particles should not be too large. On the other hand, the radiation losses from the impurities in the screening layer itself should not be intolerably large. This means that the mean life time of the impurity ions in the screening layer should not be too long to keep their density down and, moreover, the electron density in the screening layer should be sufficiently small to reduce the radiation per impurity ion.

It appears that these requirements can be met best by a screening layer of relatively large thickness but small electron density. The various divertor schemes which have been proposed in the literature, are tested in this respect assuming - as a first order approximation - the following model of the plasma boundary: The flux of hot ions with constant temperature from a toroidal plasma is driven radially outwards by Bohm-type diffusion and balanced by flow into the divertor and by charge exchange losses with the cold neutral working gas. The density of the neutral gas attains a prescribed value far away from the separatrix, i. e., in a region where the hot plasma density is negligibly

small. The temperature of the neutral gas is equal to that of the wall. The flow of hot ions into the divertor is determined by the conductance outside the separatrix, or rather by its reciprocal, the average time of flight, or life time, which an ion spends in the screening layer. This life time depends on the mean path length of an ion along the magnetic lines of force which connect into the divertor. If there exists a magnetic mirror at the divertor throat, the path length is longer according to the transparency of the mirror. The plasma boundary layer is treated in plane geometry, the coordinate x being the radial distance from the mean radius of the separatrix r_p, normalised to r_p. The particle balance in stationary state is then determined by the following set of equations (where the prime denotes differentiation with respect to x):

$$N''(x) = \frac{r_p^2}{D} N(x) \left[f(x) \cdot V + n_c(x) \cdot R_{ex} \right]$$

$$n_c(x) = \frac{4 r_p R_{tot}}{\bar{v}} \cdot n_c(x) \cdot N(x)$$

where $N(x)$: density of the hot plasma ions with thermal speed V,

$n_o(x)$: density of the neutral gas atoms with thermal speed $\bar{v}$,

D: constant diffusion coefficient,

$(f(x) \cdot V)^{-1}$: mean life time of a hot ion in the screening layer,

R_{ex}: rate of charge exchange processes between hot ions and cold atoms, and

R_{tot}: total rate of ionization processes of the cold gas atoms.

These equations have been solved numerically by assuming the following parameters of the hot plasma inside the separatrix of a toroidal fusion reactor, and for the cold neutral gas outside the separatrix, resp.: major plasma radius $R = 10^3$ cm, average radius of the separatrix, $r_p = 1,25 \cdot 10^2$ cm, particle confinement time 1s, average plasma density $3 \cdot 10^{14}$ cm^{-3}, constant plasma temperature 20 keV, diffusion coefficient $D = 0,78 \cdot 10^4$ cm^2/s $= 1/160 \cdot D_{Bohm}$, neutral gas density at the wall $n_o(x_w) = 10^{11}$ cm^{-3}, wall temperature, $T_W = 0,1$ eV.

In the case of a Stellerator-divertor [1], all magnetic field lines outside the separatrix pass through the divertor on each revolution around the major torus axis. Hence the conductance to the divertor, $(f \cdot V)$, is simply given by a step function. The radial dependences of plasma and neutral gas density for this

case are shown in Fig. 1. The cold gas density extends far beyond the separatrix into the hot plasma region. Therefore, this type of divertor cannot screen the plasma from wall originated impurities under the conditions assumed. Moreover, the desorbed and sputtered atoms are expected to have a higher mean energy than T_W and will be more slowly ionized due to the absence of resonant charge exchange processes. As seen from Fig. 2, the situation can be slightly improved by increasing the mean life time of the ions in the screening layer, this increase is brought about by taking into account the rotational transform of the magnetic field lines and the existence of a magnetic mirror at the entrance of the divertor.

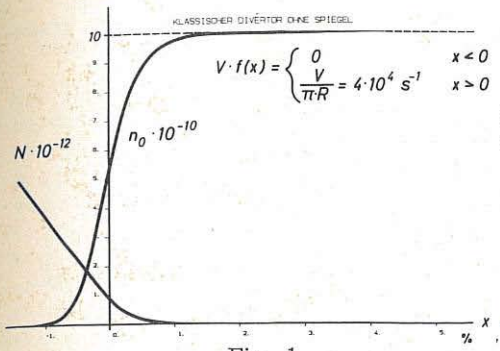


Fig. 1

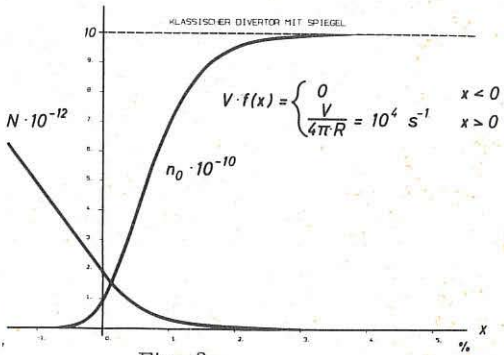


Fig. 2

Another extrem case is shown in Fig. 3, where we took a functional dependence of the conductance that corresponds to a "continuous" divertor of the Torsatron-type [2]. Here the mean life time decreases as one goes away from the separatrix, first slowly and then more rapidly. The resulting screening layer is completely opaque. On the other hand, previous estimates for a similar system showed, that the radiation losses from impurities in the screening layer might become very high in this case, as the residual electron density is still rather large in the regions where ionisation of impurities is likely to occur. This slow decay of the hot plasma density is related to the x^2-dependence of the conductance to the limiter outside the separatrix. Therefore, it would be interesting, to study a divertor whose conductance rises with a smaller power of the normalised distance x. Such a behaviour is expected from a "bundle-divertor" [3] where the conductance might be approximated by the formula

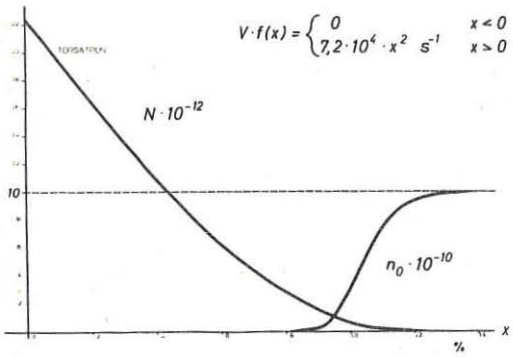


Fig. 3

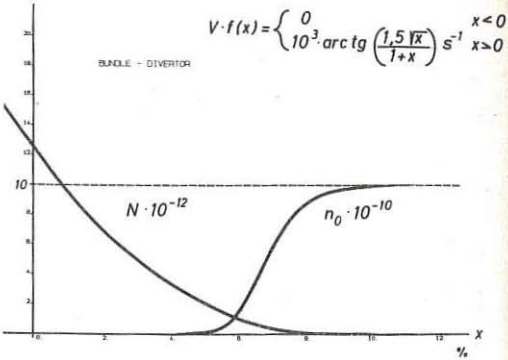


Fig. 4

shown in the insert of Fig. 4. However, as seen from this figure, a situation develops which lies in between the case of the "classical" divertor of the Stellarator-type and the "continuous" divertor of the Torsatron. But it is conceivable that the desired density profiles could be established by proper shaping of the bundle of diverted field lines and of the pumping surfaces inside the divertor. For example, part of the diverted field lines might pass through the divertor without intersecting one of the pumping surfaces and the ions would be guided back into the hot plasma along these field lines without being pumped off.

We plan to continue this investigation by including the slow ions formed by the charge exchange and by a more detailed treatment of the radiation and ionisation processes of the impurity atoms and ions.

References:

[1] L. Spitzer, Phys. Fluids 1 (1958) p. 262

[2] C. Gourdon, D. Marty, E. K. Maschke, J. Touche, Proceedings IV. European Conference on Controlled Fusion and Plasma Physics, Rome (1970) p. 35

[3] C. Colven, A. Gibson, P. E. Stott, Proceedings V. European Conference on Controlled Fusion and Plasma Physics, Grenoble (1972) p. 6.

NEOCLASSICAL DIFFUSION OF α-PARTICLES

A. Nocentini, M. Tessarotto
Istituto di Meccanica dell'Università, Trieste, Italy

and F. Engelmann
Laboratori Gas Ionizzati (Associazione EURATOM-CNEN), Frascati, Italy

ABSTRACT: A generalization of neoclassical diffusion theory to a 3-component plasma, containing also α-particles generated in fusion events, has been elaborated. The resulting diffusion of the α-particles can again be made intuitive using a simple random-walk model.

The collisional diffusion of energetic α-particles which are generated by fusion processes in a DT plasma confined in toroidal geometry can be readily calculated by generalizing the well-known neoclassical transport theory for the banana regime (cf., e.g., ref. /1÷4/) to a multi-component plasma. Starting from the set of Boltzmann equations for the plasma components, it is easy to see that the conservation of momentum in collisional interactions implies that the particle transport is ambipolar also in a multi-component plasma. The flux of α-particles is obtained expanding in the usual way /3/ for small deviation of the drift surfaces from the magnetic surfaces and small collision frequency. As the α-particles generated in fusion events are highly energetic - they have initially an energy $U_{\alpha,0} = 3.5$ MeV satisfying

$$U_{\alpha,0} > \bar{U}, \quad \kappa T_i \tag{1a}$$

with

$$\bar{U} = \left(\frac{3\sqrt{\pi}}{4}\,\frac{m_\alpha}{m_i}\right)^{\frac{2}{3}} \left(\frac{m_\alpha}{m_e}\right)^{\frac{4}{3}} \kappa T_e, \tag{1b}$$

T_e and T_i the electron and ion temperatures, respectively, and m_e, m_i, m_α the masses of electrons, ions, and α-particles - their collisional interaction is mainly with electrons. A physical and formal difference with respect to the case of interactions of electrons and ions of approximately equal energy derives, however, from the fact that in the regime (1a) the dominating collisional effect the heavy particles are subject to, is momentum (and, hence, energy) transfer to the electrons, the corresponding collision frequency being

$$\nu_{\alpha e}^{(s)} = \frac{4\sqrt{2\pi}}{3}\,\frac{Z_\alpha^2 e^4 \ln\Lambda}{m_\alpha\, m_e} \left(\frac{m_e}{\kappa T_e}\right)^{\frac{3}{2}} n \tag{2}$$

with $Z_\alpha = 2$ the charge number of the α-particles and n the electron density, the rest of the notation being standard. Scattering in angle occurs only with a frequency which for energies U_α of the α-particles larger than $\bar{U}$ is typically by a

factor $\left(\frac{m_\alpha}{m_e}\right)^{\frac{1}{2}} \left(\frac{k T_e}{u_\alpha}\right)^{\frac{3}{2}}$ smaller, due to collisions of the α-particles with the plasma ions. Taking the zeroth-order distributions of the plasma electrons and ions Maxwellian and that of the α-particles isotropic, one obtains, to lowest significant order, for (moderately) small $\varepsilon = \frac{r}{R}$ (with R the major radius of the torus and r the radial coordinate), such that $\varepsilon > (\frac{m_\alpha}{m_e})^{1/3}(\frac{k T_e}{u_{\alpha,0}})$, and small α-particle density an average flux of α-particles in radial direction

$$\Gamma_\alpha = -0{,}53 \frac{q^2 \nu_{\alpha e}^{(s)}}{\varepsilon^{\frac{1}{2}} \Omega_\alpha^2} \frac{d}{dr} \int d^3v\, v^2 f_\alpha^{(0)}(v) - 1{,}6\, \varepsilon^{\frac{3}{2}} \frac{E}{B_p} \int d^3v\, f_\alpha^{(0)}(v) \qquad (3)$$

where q is the safety margin, Ω_α the cyclotron frequency and $f_\alpha^{(0)}$ the zeroth-order distribution of the α-particles, B_p the poloidal magnetic field, and E the toroidal electric field. The corresponding supplementary contribution to the average flux of electrons is

$$\Delta\Gamma_e = -0{,}53\, z_\alpha \frac{q^2 \nu_{\alpha e}^{(s)}}{\varepsilon^{\frac{1}{2}} \Omega_\alpha^2} \frac{d}{dr} \int d^3v\, v^2 f_\alpha^{(0)}(v) - 1{,}46\, z_\alpha \varepsilon^{\frac{1}{2}} \frac{E}{B_p} \int d^3v f_\alpha^{(0)}(v). \qquad (4)$$

The fluxes Γ_α and $\Delta\Gamma_e$ contain, as usual, a ("diffusive") part related to radial gradients and a term describing the Ware effect /5/. The ambipolarity of the diffusive fluxes is explicitly seen, for the fluxes connected with the Ware effect it follows through an adjustment of the ion flux. It is also to be noted that for all energies $\varepsilon_\alpha = \frac{m_\alpha}{2} v^2$ satisfying relation (1a) the zeroth-order α-particle distribution is approximately given by

$$f_\alpha^{(0)}(v) \approx \frac{I_\alpha}{4\pi \nu_{\alpha e}^{(s)} v^3}, \qquad (5)$$

where I_α is the generation rate per unit volume of the α-particles, so that one has

$$\int d^3v\, v^2 f_\alpha^{(0)}(v) = \frac{I_\alpha}{\nu_{\alpha e}^{(s)}} \frac{u_{\alpha,0}}{m_\alpha}. \qquad (6a)$$

with

$$\equiv 3 n_\alpha \frac{k T_\alpha}{m_\alpha}$$

$$n_\alpha \equiv \int d^3v f_\alpha^{(0)}(v) = \frac{1}{2} \frac{I_\alpha}{\nu_{\alpha e}^{(s)}} \ln \frac{u_{\alpha,0}}{u} \qquad (6b)$$

the density of energetic α-particles and $\frac{3}{2} k T_\alpha$ their average kinetic energy.

The above result for the diffusive flux of α-particles differs in structure from that of a two-component plasma by the appearance of a factor $\varepsilon^{-\frac{1}{2}}$ rather than $\varepsilon^{-\frac{1}{2}}$. Furthermore, it is determined by parameters typical for the dynamics of the α-particles. This is due to the fact that the fastest stochastic process, which is connected with the presence of the α-particles, under the conditions considered, is related to the collisional effect of the electrons on the α-particles.

In fact, taking as the spatial step of a random walk process the maximum deviation of the α -particles from the magnetic surfaces $\Delta r_\alpha \approx \frac{q}{\varepsilon^{1/2}\Omega_\alpha}\left(\frac{u_{\alpha,o}}{m_\alpha}\right)^{1/2}$ and as the corresponding time step $\Delta t = 1/\nu_{\alpha e}^{(s)}$ one obtains, noting that only a fraction $\varepsilon^{1/2}$ of the particles contributes, a diffusion coefficient

$$D \approx \varepsilon^{1/2}\frac{(\Delta r_\alpha)^2}{\Delta t} = \frac{q^2 \nu_{\alpha e}^{(s)}}{\varepsilon^{1/2}\Omega_\alpha^2}\frac{u_{\alpha,o}}{m_\alpha}, \qquad (7)$$

leading to a diffusive flux

$$\Gamma_\alpha^{(d)} \approx D\frac{dn_\alpha}{dr}. \qquad (8)$$

This is, apart from numerical coefficients, the same result as the first term of Eq. (3) (cf. also Eqs (6)). The proportionality of $\Gamma_\alpha^{(d)}$ to $\varepsilon^{-1/2}$ rather than to $\varepsilon^{-3/2}$ is, hence, explained by the fact that, when the dominant collisional process is a drag, the relevant time step is given by ν^{-1} (rather than ε/ν appearing if scattering in angle is important).

In the Ware term of the α -particle flux an analogous modification appears. The dominant part of the modification of the electron Ware flux, caused by the presence of the α -particles, has in contrast the usual structure as it derives from the effect of electrons colliding with ions, the α -particles entering through their effect on the electron distribution. It is, hence, a cross effect, which expalins why there is, already to the order considered, a modification also of the ion Ware flux.

Quantitatively, the collisional transport of energetic α -particles as given by Eq. (3) is a small effect as long as the single-particle confinement of the α -particles is good, i.e., for $\Delta r_\alpha/a \ll 1$ with a the minor radius of the torus. It may, however, become important for a relatively small enhancement of diffusion above the collisional value as $\Delta r_\alpha/a$ is never very small, even when toroidal systems with dimensions typical for a reactor are considered.

REFERENCES

/1/ A.A. Galeev and R.Z. Sagdeev: Zh. ETF 53, 348 (1967) (Sov.Phys. JETP 26, 233 (1968)).

/2/ P.H. Rutherford: Phys.Fluids 13, 482 (1970).

/3/ E.A. Frieman: Phys.Fluids 13, 490 (1970).

/4/ M.N. Rosenbluth, R.D. Hazeltine, and F.L. Hinton: Phys. Fluids 15, 116 (1972).

/5/ A.A. Ware: Phys.Rev.Letters 25, 916 (1970).

CONSIDERATIONS ON A PULSED BELT PINCH REACTOR WITH NORMAL CONDUCTING COILS.

H. Herold, R. Wilhelm, H. Zwicker.

Max-Planck-Institut für Plasmaphysik, Euratom Association, Garching bei München, FRG.

Abstract. An energy balance for two belt pinch reactor systems is made. Additional heating with 10 % efficiency is included. It is shown that systems with about 400 MW_e output should be possible at $M \approx 2.4$. Comparison with pulsed Tokomaks shows some advantages of the belt pinch systems.

Pulsed toroidal systems with high aspect ratio need for normal-conducting coils unrealistic large dimensions for reasons of ohmic losses in the coils. In the compact belt pinch geometry this is not necessarily true. Therefore the question for a pulsed, normal-conducting high β-reactor in belt pinch geometry is investigated.

1. Pulsed belt pinch systems

The basic geometry of the main coil and the plasma is given in Fig.1. The coil aspect ratio $A = R/r_1$ is assumed to be $A = 3$. The plasma compression ratio $\varkappa = r_1/r_p$ before the axial contraction is assumed to be $\varkappa = 4$. For reasons of high-β stability we have further $\Pi = 4$ R. Then the basic geometry is determined by the major radius R and the coil thickness Δ.

The system operates at T = 15 keV with a pulse length τ and a period τ_o. The ratio $p = \tau/\tau_o$ is the pulse factor which is assumed to be $p = 0.1$. For the energy balance all mean powers are related to the period τ_o. For the thermal power $\bar{P}_{th}$ the 14.1 MeV neutrons and the 4.8 MeV breeding energy of the $Li^6(n,\alpha)$ reaction is taken into account. α-particle energy has been fully neglected. For the magnetic energy the whole coil volume was used and the thermal plasma energy was neglected. The resulting error is less than 10 % for our conditions.

In every cycle the magnetic energy E_B, the ohmic losses E_Ω and if necessary, the energy E_H for additional heating (besides fast compression) is recovered with an efficiency ε while E_{th} is converted with the efficiency η.

Under these assumptions the multiplication factor M describing the excess of electrical energy over losses is given by

$$M = \frac{\tau \cdot \overline{P}_{th}}{\overline{P}_B + \overline{P}_H + \overline{P}_O} + \varepsilon$$

The pulse length τ is limited by the condition that only a fraction of 16 % of the DT filling gas is burned.

Case A: We consider a system where the coil is within the blanket directly at the wall of the vacuum vessel. For reasons of the Li breeding rate this limits the thickness of the coil to about 3 cm Cu. In the belt pinch geometry considered, however the inner wall intercepts only 23 % of the neutron flux. Therefore the inner coil wall can be made rather thick. The other parts of the coil can be made of 3.5 cm Cu plus 4 cm Mo which after G. Bell et al. [1] gives sufficient breeding rates in the blanket which may compensate for the neutrons lost for breeding in the thick inner wall of the coil. In this way the ohmic losses can be made sufficiently small for a positive energy balance.
Assuming a coil temperature of 500 °C, $\beta = 0.7$, $\overline{P}_w = 900$ W/cm^2; $\eta = \varepsilon = 0.4$ the multiplication factor M(R) was calculated for the case that heating up to 10 keV, where α-particle heating starts, is produced by fast magnetic compression. Fig. 1 curve a gives the result. It shows that for such a pulsed system already at a major radius of 2-4 meters a positive energy balance should be possible.
For the same system furthermore shock heating to 2 keV and an additional heating from 2 to 10 keV is considered with an efficiency of 10 %. The necessary additional energy E_H changes the energy balance of the system and gives M(R) as it is shown in curve b of Fig. 1. Also in this case M values around 2 should be obtained at R = 4-6 m.

Case B: Here a system is considered with an inner blanket of 40 cm thickness between the coil and the vacuum vessel. This provides for sufficient tritium breeding [2] and allows much thicker coils which reduce the ohmic losses. Current diffusion for the thick coil walls was taken into account for the ohmic losses.
Furthermore: $\beta = 0.7$; $\overline{P}_w = 225$ W/cm^2, $\eta = \varepsilon = 0.4$; A = 3, $\kappa = 4$, p = 0.1, $T_{coil} = 500$ °C. Including additional heating from 2 to 10 keV with 10 % efficiency for such a system M, τ, n_e, and the electrical output $\overline{P}_{el}$ were calculated as a function of the major radius R. Fig. 3 gives the result. Also here small size systems ($R \approx 4$ m) should be possible with an output of about 400 MW_e and an overall efficiency of about

20 - 25 %. Besides the small size they would have the advantage that the fields are relatively small ($B \approx 2.5$ T) and that the problems of limiter and divertor may be avoided.

2. Comparison with circular cross section

For the energy balance of such a system one has to regard that β is limited to $\beta = (\kappa A q^2)^{-1}$ and that κ may be small. Fig. 4 gives an example for the most favourable case with inner blanket and otherwise the same conditions as in the belt pinch system case B. Fig. 4 shows that at a reasonable $q = 2$ economically interesting M values cannot be achieved even at large R. Thus a purely pulsed Tokomak reactor with resistive coils appears not to be feasible.

3. Economic considerations

Compared to a conventional Tokomak reactor with superconducting coils, working in quasi DC mode the pulsed belt pinch concept has some economically important features: The belt pinch needs no injection system and possibly no divertor and because of the high-β the core dimensions can be relatively small. On the other hand the larger circulating power P_c demands a power plant of higher capacity, since P_c must go through the thermal/electric conversion. Also the magnetic energy store must be much larger.

The capital costs K for the reactor core per kW_{th} are mainly determined by the magnetic field costs. They scale roughly as

$$K \sim \frac{1}{\beta\, P_w^{1/4}\, P_{th}^{1/4}\, p^{1/2}}\; f\,(D, A, \kappa, r_p)$$

The factor f depends mainly on the thickness D of the blanket inside the coils, typically $f_{Tok}/f_{Belt} \approx 2$. Inserting relevant numbers K_{Tok}/K_{Belt} is about 5 to 6 for the same P_w and P_{th}. This number has to be multiplied by another factor of at least 3 which regards the price relation of superconducting to resistive windings. It is likely that this substantial cost saving for the belt pinch reactor core can make up for the cost increase associated with the higher P_c and the larger energy store. A more precise cost estimate has to wait for a detailed design study of the pulsed belt pinch reactor.

References

[1] Bell, G.I., W.H. Borkenhagen, F.L. Ribe, Nucl. Fus. React. Conf., Culham, p. 242 (1969)

[2] Burnett, S.C., W.R. Ellis, T. Oliphant, F.L. Ribe, Proc. 2nd Top. Conf. Pulsed High-β Plasmas, Garching, G II, (1972)

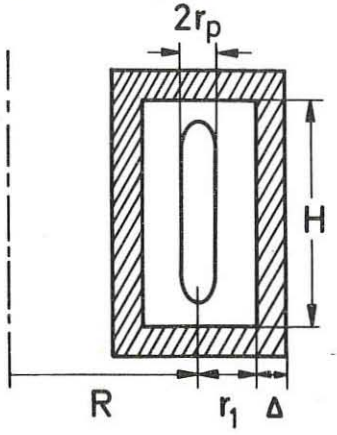


Fig. 1

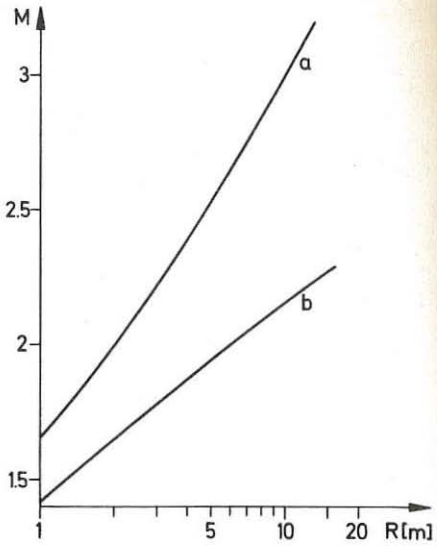


Fig. 2

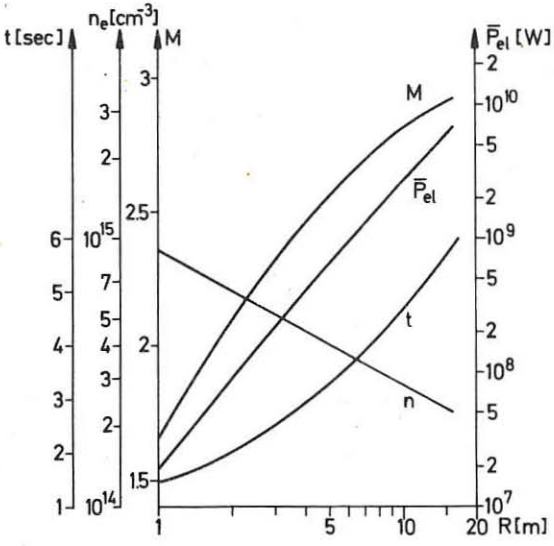


Fig. 3

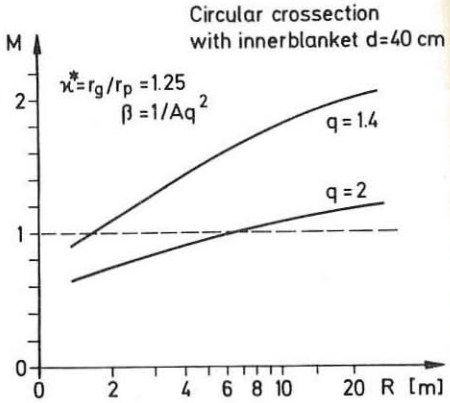


Fig. 4

LOW DENSITY TOKAMAK REACTOR IGNITION BY FAST NEUTRAL INJECTION AND BUILD UP OF A HIGHER DENSITY BY USE OF A MOVING LIMITER

J.P.Girard, M.Khelladi, D.A.Marty

ASSOCIATION EURATOM-CEA SUR LA FUSION
Département de Physique du Plasma et de la Fusion Contrôlée
Centre d'Etudes Nucléaires
Boite Postale n° 6. 92260 FONTENAY-AUX-ROSES (FRANCE)

In a previous paper [1] we have shown with the help of a simple global balance model the possibility to reach the ignition of a low density (3-4 10^{13} cm^{-3}) Tokamak reactor. This requires the use of fast neutral injection at rather modest energy (100 kev) and current of order of 300 A.

Nevertheless from a practical point of view such a reactor has to work at higher density 10^{14}-210^{14} cm^{-3}. So it is interesting to check if it is possible to bring and heat cold fuel in a low density reactor in order to increase the density without extinction and without equilibrium violation.

PROPOSED METHOD.-

We consider a Tokamak reactor in which the plasma radius a is adjustable by means of a moving limiter, the major radius R_0 remaining constant. To suppress the skin effect Kadomtsev [2] has proposed such an idea which we will test but we will use it essentially for obtaining a higher density plasma.

In a first step an ohmically heated small radius plasma is built. Then, by use of the moving limiter the plasma radius is increased so that the density gradient at the boundary of the plasma remains constant. Such an operation is achievable if we inject cold gas from outside to build the density. Simultaneously fast neutral injection allows a significant temperature increase and a natural maximum energy deposit in an area which moves slowly with the limiter. The expansion speed must not be too fast if we want the plasma center to be hot enough to be self-sustained by α particles heating. On the other hand it must not be too slow so that to avoid an overheating of the plasma center because of β_θ limitation.

An attempt of an optimized solution of this problem has been tried numerically with a cylindrical model in the case of a "banana" regime dependance for the ion thermal conductivity.

EXPANSION WITH A CONSTANT SAFETY FACTOR VALUE (q=3).-

The Tokamak reactor under consideration has the following main characteristics : a = 300 cm, R_o = 1125 cm, B_ϕ = 60 kGs. Fig.1 shows for different q values the different domains where the ignition is possible. We can see that even for q=3 the ignition domain is still fairly large. This is interesting because we can consider a realistic q value of 3. Lower q could provided M.H.D. instabilities, the plasma being far from the "conducting" shell in the beginning of the expansion. To build the density with such a Tokamak we start with a limiter radius of 90 cm so that we can get a good fast neutral beam capture in the energy range 100-150 keV. It is to be noticed that this radius is close to those chosen for a near future ignition Tokamak [3]. The main current is raised so as to keep q constant at the plasma edge (q=3). Its value is 7.5 10^5 A at the beginning of the expansion and 8.33 10^6 A at the End. For a mean initial density $\bar{n}$ = 7.10^{13} cm^{-3} the ohmic stationnary state has been found to give the following modest results ($\bar{T}_e$=$\bar{T}_i$=630 eV). Then the nearly perpendicular injection and the expansion start. A D-T mixture of 80 % D and 20 % T has been found good enough to prevent an overheating of the plasma center (75 % D and 25 % T is thermically unstable before the end of the expansion) and avoid an extinction of the plasma center at the end of the expansion (85 % D and 15 % T). To keep the same fuel composition inside the plasma two beams having the following characteristics are used : 8 A/meter of

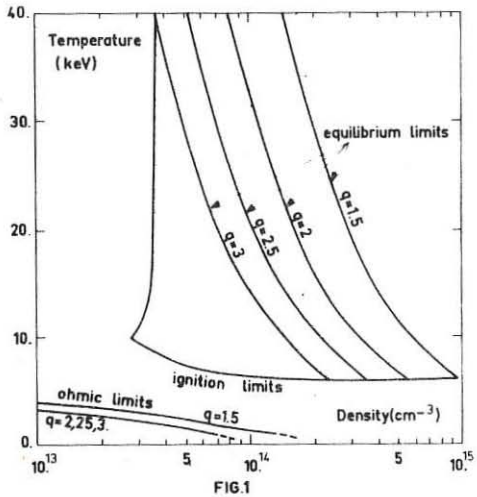


FIG.1

machine of D_0 at 100 keV and 2 A/m of T_0 at 150 keV. This corresponds to an injected power of 1100 kW/m. The density is built by different processes : *1)* fast ions which are thermalized, *2)* a certain quantity of cold gas (D_2^o-T_2^o) brought by the injectors. This gas load, equivalent to the fast neutral load is 3.10^{19} molecules/s.m, *3)* but an additional gas souce of 3.10^{19} particles/s.m is needed to reach a mean density of $10^{14}cm^{-3}$ at the end of the expansion. Fig.2 presents the successive density and ion temperature profiles during the phase of expansion. The final density profile is smooth, whereas the ion temperature profile is rather peaked due to a certain overheating by α-particles in the center of the plasma. Radiation losses due to impunities and a change in the composition of the fuel due to the burning of the fuel could suppress such an overheating. The total expansion duration is 13 s and no skin effect has been observed during all this time.

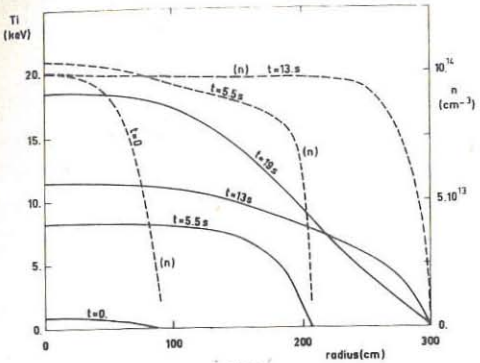


FIG.2

EXPANSION WITH VARYING q.-

If it is necessary to start the expansion with a rather high q value (q=3) because of M.H.D. instabilities, it is however possible to decrease q during the expansion since the plasma gets closer to the "conducting" shell, so that to diminish ion conduction losses and mainly to increase the equilibrium limit. We have considered the case where the main current is raised from 7.5 10^5 A (a= 90cm, q=3) to 12.5 10^6A (a=300 cm, q=2). Simultaneously the needed fast neutral current gets smaller since the ion conduction losses are decreasing as q^2. It value has been taken $I_{beam} = I_{beam(t=0)} \frac{q^2}{q^2(a=90cm)}$, $I_{beam(t=0)}$ being the initial current. The expansion phase is now about 14 s and the fast neutral current decreases from 12 A/m to 5.5. A/m. This corresponds to a mean injected power of 850 kW/m

which is smaller than previously. Fig.3 presents the density and ion temperature profiles evolution which keep quite the same shapes as previously.

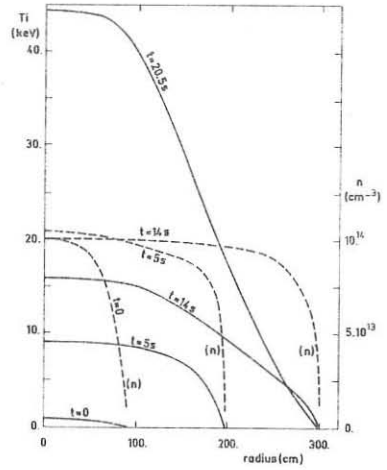


FIG. 3

CONCLUSION.-

Finally we can say that the proposed method for building a thermonuclear high density reactor type Tokamak plasma by means of a moving limiter keeps the main advantage of fast neutral injection at relatively low energy (100-150 keV). Two cases have been successfully tested with our numerical code. In the first case the high density (10^{14}cm^{-3}) plasma ignition has been obtained with an injected power of the order 78 MW in a Tokamak having a constant q value of 3. In the second case the required total injected power is about 60 MW, the q value varying from 3 to 2 while the limiter radius varies from 90 cm to 300 cm during the phase of expansion which lasts about 13 s. It must be precised that the non existence of the "banana regime" does not allow the low density plasma ignition [1], but using a moving limiter we might obtain ignition with fast neutrals injection at the same energy but with much higher density.

References.-

[1] J.P.Girard and all, 5th European Conf. on Controlled Fusion and Plasma Physics, Grenoble 1972, p.241.

[2] B.B.Kadomtsev in I.N.Golovin and all, Nuclear Fusion Reactor Conference (Proc.Conf.Culham 1969, p.194).

[3] P.H.Rebut, M.Huguet - private communication.

FUSION REACTOR CHARACTERISTICS IN DEPENDENCE ON BETA AND ASPECT RATIO.

M. Kaufmann, W. Köppendörfer

Max-Planck-Institut für Plasmaphysik, Euratom Association,

Garching bei München, F.R.G.

Abstract: The choice of suitable parameters, determined by technological requirements on one side and by plasma stability properties on the other side, allows to show that high beta large aspect ratio stellarators with superconductive coils can well compete with low beta stellarators and tokamaks with respect to the reactor boiler costs.

1. Introduction: The following considerations deal with certain reactor aspects of high beta stellarator type equilibria. Modified $\ell = 1$ high beta stellarator plasmas are experimentally investigated in Los Alamos /1/ and Garching /2/ and theoretically at the New York University /3/, and elsewhere. Results of these efforts show that such equilibria are only conceiveable if the plasma aspect ratio is typically equal or greater than hundred.

Mainly economic reasons, however, have led to the general opinion that stationary fusion reactors with such large aspect ratios have no chance if the total output is below 20 gigawatts, a limiting value which is set by network and environmental restrictions /4,5,6/. One argument were given e.g. by Carruther /6/ who concluded from optimization considerations that the plasma radius has to equal approximately the blanket thickness. This statement leads together with the limitation of the total power, to moderate aspect ratios of typically below 20 for stationary reactors.

Ribe /7/ has nevertheless proposed a slim high beta stellarator for a pulsed reactor. Certain advantages of this proposal like reduced average wall loading, shock heating, no need for divertors, no fueling problems stand opposite to disadvantages like periodic pulse load, fast circuits for magnetic energy storage and the need of insulators in the high energy neutron flux region. This proposal has brought about that a high beta reactor is usually thought to be a fast pulsed reactor.

The object of this paper is to show that high beta reactors are not

limited to low aspect ratios, because a cost optimization is not necessarily identical to Carruthers mentioned requirement. If superconductor costs are a considerable fraction of the total boiler costs stationary high beta reactors with aspect ratios of hundred can well compete with fat low beta stellarators and tokamaks.

In the following a definition of the problem and its independent variables will first be given. They will be used for an adequate description of the more important features of a fusion reactor. It allows if simplified restrictions from plasma stability theory are taken into account an interesting comparison between low beta and high beta toroidal fusion reactor concepts. In addition the problem of the start up of such a high beta fusion reactor is briefly scetched.

2. The Definition of Suitable Parameters: Technological requirements determine the essential reactor quantities: total thermal power L, admissible wall power loading P_w and blanket thickness D. The plasma parameters determining hydromagnetic equilibrium and stability, can sufficiently be described by the aspect ratio $A = \frac{R_t}{R_p}$, the plasma β which is the ratio of the plasma thermal pressure to the total pressure and the compression ratio $K = \frac{R_w}{R_p}$. The radii are: R_t the torus large radius, R_w the small radius of the first wall and R_p the small plasma radius. For convenience it is appropriate to introduce in addition a length $D_o = \frac{1}{2\pi}\left(\frac{L}{P_w}\right)^{1/2}$. All other parameters can be expressed by the six quantities L, P_w, D, A, β, and K provided the plasma temperature is fixed, which is assumed to be 15 keV.

3. Boiler Costs of Fusions Reactors: The boiler costs divide into magnet and blanket costs. The most recent supercondutor cost estimate have been given by Lubell and coworkers /8/. It comprises material, fabrication, reinforcement structure, cryogenic and electric insulation and refrigeration. Helical field coils are not included. The magnet costs C_m divided by the reactor power L are expressed by the quantities defined in section 2 are:

$$C_m^* = \frac{C_m}{L} = 1.9.10^3 \frac{K\left(1+\frac{D}{D_o}\left(\frac{A}{K}\right)^{1/2}\right)^{8/5}}{\beta^{4/5} P_w^{3/5} A^{1/5}} \quad \text{in } \frac{\$}{Mw} \qquad (1)$$

The dependence on beta is evident, whereas the dependence on the aspect ratio for low aspect ratios is proportional to $A^{-1/5}$ and for large aspect ratios proportional to $A^{3/5}$ depending on whether $\frac{D}{D_o}\left(\frac{A}{K}\right)^{1/2}$

is small or large compared to one. Reactors are usually in the intermediate regime, so the full expression has to be used. The blanket costs are proportional to the blanket volume V_B, which is in order to obtain specific costs devided by L:

$$V_B^* = \frac{V_B}{L} \approx \frac{D}{P_w}\left(1 + \frac{D}{2D_o}\left(\frac{A}{K}\right)^{1/2}\right) \quad \text{in} \quad \frac{m^3}{MW}$$

For rough estimates /9/ this volume can be multiplied by 10^4 in order to obtain $^{\ell}/_{MW}$.

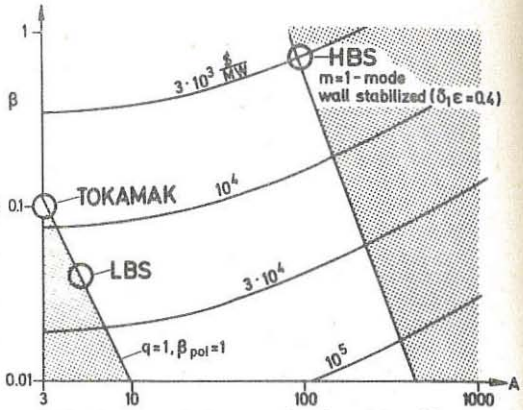
It is advantageous to describe the reactor dimensions, the plasma density and the magnetic field by the chosen quantities as shown in the table.

4. Comparison between low Beta and High Beta Toroidal Reactors: In the figure isocost curves of superconductors are shown as functions of β and A for $L = 10^4$ MW, $P_w = 10 \frac{MW}{m^2}$, D = 1.5 m and K = 2. Boundaries from plasma stability theory mark the position of high beta stellarators (HBS) and low beta stellarators (LBS) and tokamaks. For high beta stellarators this boundary is given by the conditions under which the most dangerous m = 1 modes can just be wall stabilized /4/ (stability on the right). In order to charakterize the limits of low beta tori the $\beta_{pol} = 1$ and q = 1 boundary for tokamaks was taken (stability on the left). This boundary is very close to the limit for a $\ell = 2$ stellarator, stable in consequence of a sufficient criteria /10/. As a difference it is assumed that the aspect ratio for a Tokamak can be made smaller compared to a low beta stellarator. The figure gives clear evidence that low superconductor costs favour high beta stellarators. Even if blanket costs are higher for high beta tori the total boiler costs (see table last line) could still favour large aspect ratio stellarators.

5. Remarks on the Start-Up of a High-Beta-Stellarator Reactor: The wall stabilized HBS equilibrium requires to keep β above a distinct critical value. Shock heating is the only examined way to provide instantly a high beta plasma. To reach the ignition point directly by shock heating, however, is a severe technical problem because the electric field has to be about 10 kV/cm. A more realistic start up procedure could be: shock heating up to 1 keV and an additional slow heating methode e.g. neutral injection. According to the small curvature neoclassical effects are estimated to enhance diffusion only

when the temperature is above ignition. The start up problems may be further eased by starting with reduced densities. During heating the superconductor magnetic field would have to be suppressed by a normal conducting coil system.

	HBS	LBS	TOKAMAK
$B[T]=\frac{1.63}{\beta^{1/2}}\left(\frac{A\kappa^3 R_w^3}{L}\right)^{1/8}$	3.3	8.7	5.8
$n[m^{-3}]=2.22\cdot10^{20}\left(\frac{A\kappa^3 R_w^3}{L}\right)^{1/4}$	$6.7\cdot10^{20}$	$3.1\cdot10^{20}$	$2.8\cdot10^{20}$
$R_p[m]=\frac{1}{2\pi}\left(\frac{L}{R_w\,\kappa A}\right)^{1/2}$	0.36	1.6	2.1
$C_M^n + C_B^n\ [\frac{\$}{MW}]$	6.1	19	9.8



Costs of superconductors as a function of A and β
(L=10 GW $P_w=10\frac{MW}{m^2}$ D=1.5 m $\kappa=2$)

References:

1) Burnett,S.C., et al., Proc.5th Europ.Conf.on Contr.Fus.Plasma Phys., Grenoble, 2, 35 (1972); 2) Fünfer,E., et al., Proc. 2nd Top. Conf.Puls.High-Beta Plasmas, Garching, A 2 (1972); 3) Weitzner, H., Plasma Phys. Contr.Nucl.Fus.Res.; IAEA (1971), III, CN-28/J-6; 4) Carruthers,R., P.A.Davenport, J.T.D.Mitchell, UKAEA Culham Report CLM-R 85; 5) Golovin,I.N.; Yn.N.Dnestrovsky, D.P.Kotomarov, Proc. Nucl.Reactor Conf. , UKAEA Culham, p.194 (1969); 6) Carruthers,R., Proc.Nucl.Fusion Reactor Conf. UKAEA Culham, p.337 (1969); 7) Burnett,S.C., et al.; 2nd Top. Conf. Pulsed High Beta Plasmas, Garching G 11 (1972); 8) Lubell, M.S., H.M.Long, J.N.Luton jr., W.C.T.Stoddart, Oak Rigde Nat.Lab.Rep. ORNL-TM-3927; 9) Steiner,D., Oak Ridge Nat.Lab.Rep. ORNL-TM-2360; lo) Nührenberg,J., private communication.

BEAM - PLASMA TARGET THERMONUCLEAR SYSTEM BASED ON TOKAMAK.

R.A.Demirkhanov, Yu.V.Kursanov, L.P.Skripal

Sukhumi Institute of Physics and Technology of the State Committee on Utilization of Atomic Energy, Sukhumi, USSR.

ABSTRACT: A stationary system in which DT reactions occur as a result of bombarding tritium plasma target by beam of accelerated deuterons is considered. The system can serve as an energetic reactor or a breeder.

A prospect of developing the injectors of neutral particles with intensity of tens of equivalent amperes and energy of hundreds of kev, makes it worth to evaluate the scope of the system: beam-plasma target[1] as an energy source. The paper gives the calculations of physical parameters of a plasma-beam reactor in which a tokamak plasma is used as a target.

For the given power level of reactions with respect to the power of plasma thermal losses, $Q = R_1 W/P_{pl}$, where $R_1 = IB(1-\alpha)$ is the reaction rate, $P_{pl} = 3nTV/\tau$, W - is the reaction energy; τ, T, V are the energetic life time, the temperature and the volume of a plasma, respectively; I is the injected deuteron flux, B is the reaction probability per deuteron, α - is a relative concentration of deuterons in the target, - we have the following estimations of beam and target parameters:

$$n\tau = \frac{3(n\tau_1)\,T_e\,Q}{\alpha_1(1-\alpha)\,WB} \qquad (1)$$

$$B/E \geq Q/(1-\alpha)W \qquad (2)$$

$$I/V = \alpha_1 n^2/(n\tau_1) \qquad (3)$$

Here, $\alpha_1 = I\tau_1/nV$ - is a relative concentration of high energy deuterons, and τ_1 is the deuteron stopping time. B and $n\tau_1$ are

calculated in[2,3] under the assumption of Coulomb mechanism of deuteron stopping. The condition (2) sets the lower limit for the target electron temperature; this limit has the minimum at $E \simeq 200$ kev.

The region of $n\tau$ and T_e values satisfying (1) and (2) for E = 200 kev, W = 22,4 Mev, Q=2, is given in Fig.1 (region C). The minimum of T_e is 6,5 kev. The minimum of $n\tau$ ($\simeq 10^{13}$ cm^{-3}sec) is reached at $T \simeq 9$ kev and $\alpha = \alpha_i = 1/3$. The comparison to the dependence of $n\tau$ upon T in a thermal reactor (curve A) shows that at moderately small α_i ($\alpha_i \geq 5 \cdot 10^{-2}$) Lawson curve for a beam reactor lies lower than for a thermal one.

The position of C boundary depends on a number of factors. The deuteron stopping increase as a result of collective processes, presence of heavy impurities, etc., result in decrease of reaction probability B and, threby, makes the region C closer to the boundary A of a thermal reactor.

Increase of Q also results in getting the regions C and A closer. On the contrary, on decreasing the ratio Q/W, the boundary

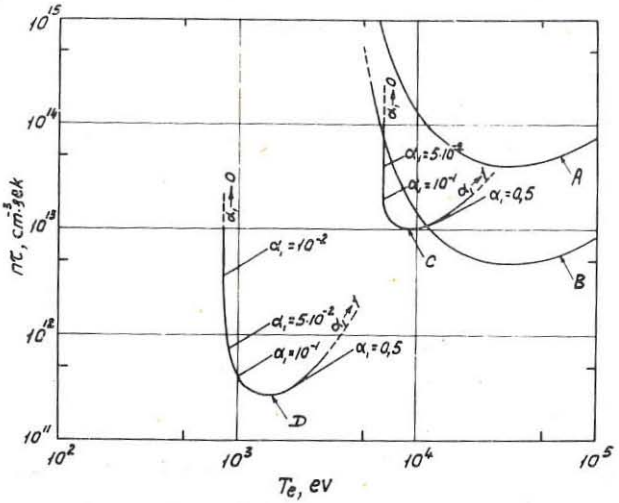


Fig. 1

C can be transported to the region of lower values of $n\tau$ and T_e. This chance can be realized if to increase W_{nucl} due to the fission reaction energy.

A combined system of fusion and fission reactors with autonomous cycles of tritium and splitting fuel breeding has been considered in [4], where it was concluded that on choosing the fuel doubling time of 2-3 years, the ratio of fusion and fission reaction rates R_1/R_2 can be close to 1.

Using this conclusion and substituting the value of $W = 22.4 + \frac{R_1}{R_i} 200 \simeq 222,4$ Mev into (1) and (2), we get the region D of $n\tau$ and T_e values for Q=2 (see Fig.1), which is realized in available Tokamaks. In such a case, the value Q= 20 corresponds to the region C .

For comparison, Lawson curve for a thermal reactor (curve B) with Q = 2 and W = 222,4 Mev, is given. It is obvius, that decrease of $n\tau$ and T_e in a beam combined system is more effective than in the system based on the thermal reactor.

Table 1 gives the calculated parameters of the beam reactor based on Tokamak with $Q/W = 0,09$ Mev^{-1}, E = 200 kev.

T a b l e 1

$n\tau$ (cm^{-3}sec)	2.10^{13}
Plasma concentration (cm^{-3})	10^{14}
Electron temperature (kev)	6,5
Plasma major radius (cm)	150
Minor radius (cm)	30
Safety factor (q)	1
Stabilizing magnetic field (kgs)	50
Injected beam equivalent current (amperes)	20

The basic assumptions of the calculations are the following:

1. Energetic deuterons are confined in the target up to complete stopping as a result of Coulomb collisions.
2. Plasma stability at q=1 is realized by using of h.f. stabilization or feedbacks.
3. The similarity law for τ corresponds to the neoclassical theory with the coefficient normalized over the results of Tokamak-3 experiments.
4. Generation of a beam of D_0 atoms with energy of 200 kev and equivalent current of ~10 amperes becomes possible with the efficiency of 80%.

Conclusions

The beam-plasma target system based on Tokamak can demonstrate of positive power with dimensions and plasma and magnetic field parameters, as they are considered in models under construction (T-10, PLT-1). The construction of neutral atom injector and energy converters with necessary efficiencies represents a realizable problem. Combining the plasma-beam system with the fission reactor creates the prospects for building a small-scale energetic complex with the maximum efficiency of fuel consumption and the fuel doubling time of 2-3 years.

References

1. Л.А.Арцимович. Управляемые термоядерные реакции. Физматгиз, М.1961.
2. J.M.Dawson et al. Phys. Rev. Lett. 26, 1156 (1971).
3. Р.А.Демирханов и др. Атомная энергия 34, № 5, 1973 г.
4. L.M.Lidsky. Nuclear Fusion Reactor Conf. Sept. 1969. Culham Labor. Abingdon.

Remarks Concerning Experimental Simulation of the Pellet - Refuelling

C.T. Chang

Danish AEC Research Establishment Risö, Roskilde, Denmark

Abstract The physical processes and the time scales involved in the ablation of a pellet are greatly influenced by the plasma state in the reactor. Proper experimental simulation, therefore, needs a careful study.

Introduction Injection of a pellet consisting of deuterium or deuterium-tritium mixture has been suggested as a possible means of refuelling a steady-state fusion reactor[1]-[3]. Approximately, the process might be divided into two stages: (a) the initial or unshielded stage where direct impact of energetic particles from the fusion plasma plays a main role, problems such as the possible cracking and disintegration due to thermal stress, the charge of the pellet, the time t_o required to establish a shield etc. might require some consideration; (b) the shielded stage where the transport of energy from the fusion plasma is modulated by an intermediate medium, possibly a layer of plasma vapor, cold compared with the fusion plasma, hydrodynamic effect such as the expansion of the vaporized cloud, the possible occurrence of interface instabilities, etc. might be of importance.

The initial stage Since the physical phenomena involved, such as the secondary electron emission, penetration depth, sputtering, etc. depend on the type and energy of the projectiles involved, it will be worthwhile to compare the expected plasma parameters in a foreseeable fusion reactor with those in some of the present experimental apparatus, see Table 1. The parameters listed are for the first three devices based on data given in ref. 4, and the two remaining devices those available at Risö.

As an illustration, let us estimate the time t_o required to establish a shield. For projectiles with impact energy around 10 keV, ion pair production might be of importance. Using the formula for stopping power[5] and considering the process as a random walk, we find the average displacement in the pellet $\bar{\Delta r} \approx 7 \times 10^{-6}$ cm for

projectile energy of 20 keV. Relating the speed u_s of the "ionization front" to the ion thermal energy flux F_i, the energy required for pair-production W_o(=36 ev)[5] and the particle density of the pellet n_s($\approx 10^{22}$cm^{-3}), we find $u_s = F_i/w_o n_s \approx 300$ cm/sec. and $t_o = \bar{\Delta r}/u_s = 20$ nsec, ($\ll$ the stipulated penetration time $t_p \approx 1$ msec[2]). If all the ablated material were at the density n_s, to reach a pressure of 18 atm. of the fusion plasma, the temperature of the ablated vapor T_1 need only to be 10^{-3}ev which is much lower than the expected energy of the emitted secondary electrons[6]; the occurrence of the expansion process is to be expected. Accordingly, one might conclude that so far as ablation of the pellet is conserned, events occurring in this stage can be ignored. A second thought shows that it cannot be so, this is because whatever knowledge acquired here, e.g. the charge of the pellet, etc. is to be used as the initial condition for the subsequent stage. In this respect, for electrons with impact energy around 20 keV, we might expect the pellet to be negatively charged[6]. For comparison, if experiments were carried out in Zeta, at the indicated ion and electron thermal energy flux, F_i and F_e, we might expect t_o to be controlled by the sputtering process and the pellet could be charged positively instead.

The shielded stage Assuming an isotropic process, the ablation rate G is related to the rate of change of the pellet radius, $\dot{r}$. Under the requirement that the penetration time $\tau_p <$ the disintegration time τ_d (= b/u_o, where b is the required penetration depth, and u_o the injection speed of the pellet), the penetration speed u is related to the drag by

$$m_p \dot{u} = C_D \rho_o A u^2 \qquad (1)$$

where ρ_o is the mass density of the fusion plasma, $m_p(t)$ and $A(t)$ are the mass and the projected area of the pellet respectively. The drag coefficient, $C_D(M, \lambda/r_p)$, is a function of the Mach number M and the Knudsen number, λ/r_p of the flow. At the injection speed of 10 km/sec[2], the ion kinetic energy flux $n_i m_i u^3/2$ is six order of magnitude smaller than its thermal energy flux, F_i, shown in Table 1, consequently, the energy equation can be written as

$$\Sigma \lambda_j \left[n_j v_j (kT_j)/2 \right]_o = hG/4\pi r_i^2 + p_c(\dot{r}_i) \qquad (2)$$

where $r_1(t)$ is the radius of the ablated envelope the subscript "j" refers to the type of particle concerned, λ_j, its corresponding heat transfer coefficient and is a function of the projectile energy. The "overall heat of ablation" per particle is given by

$$h = h_s + h_i + 3kT_1/2 + m_p u_1^2/2 \qquad (3)$$

where h_s and h_i are the sublimation and ionization energy of the pellet; the last two terms represent the average thermal and kinetic energy of the ablated vapor. If the evaporated cloud should expand as rapidly as $u_o/10$, the energy flux due to expansion $p_o(\dot{r}_1)$ is still two orders of magnitude lower than F_i, neglecting the last two terms in eqs. (2) and (3), we still have three unknowns T_1, r_1 and G. If we know where the ablated mass should go (for example the suggested "θ-pinch end-loss mechanism"[2]),the mass conservation law gives an additional restriction, but it also brings an extra unknown n_1, the number density of the ablated vapor. To make a complete description, some stipulations regarding the physical processes occurring at the inner and outer boundaries of the evaporated zone must be made; their appropriate formulation as well as the expression of the mass conservation equation depend on the plasma state of the ablated vapor zone, and the information obtained from the initial unshielded stage.

As a reminder, we might mention that because the dependence of the ablation rate G on local values of the thermal energy fluxes F_e and F_i, the decoupling between the ablation and the deceleration process is possible only when the density and temperature profile of the fusion plasma are overlooked.

Conclusion The above intuitive reasoning indicates that the physical processes involved in the pellet-refuelling problem is greatly influenced by the plasma state, the β-value of the reactor; the size, the speed and direction of injection of the pellet, etc.. Since no device at the present can simulate completely the plasma environment in a fusion reactor, the proper choice of a suitable experimental program clearly deserves further study.

References:

1) L. Spitzer, Jr., D.J. Groove, W.E. Johnson, L. Tonks and W.F. Westendorp, Report NYO-6047, U.S. A.E.C., pp 196-229 (1954).

2) D.J. Rose, Culham Laboratory Technology Division, Memorandum No. 82 (1968).

3) S.L. Gralnick, Plasma Laboratory Report No. 58, School of Engineering and Applied Science, Columbia University, New York (1972).

4) R.S. Pease, in Peaceful Uses of Atomic Energy, Proceedings of the 4th International Conf. Geneva, Sept. 1971, vol. 7, p.431.

5) A. Dalgarno, "Range and Energy Loss" in Atomic and Molecular Processes, edited by D.R. Bates (Academic Press, 1962).

6) O. Hachenberg and W. Bauer, "Secondary Electron Emission from Solids" in Advances in Electronics and Electron Physics, vol XI (Academic Press, 1959).

Table 1. Plasma Parameters in Some Typical Devices as compared with a 5 GW Fusion Reactor

	kT_e, ev.	kT_i, ev.	n, cm^{-3}	B, kG	β	p, atm.	λ, cm	F_e Watt/cm^2	F_i Watt/cm^2	$\bar{v}_e$ cm/sec	$\bar{v}_i$ a) cm/sec	ρ_i, mm	ω_{pe} sec^{-1}
5 GW Reactor	2^4 Δ)	2^4	2.8^4	100	0.075	18	5.7^6	4.2^9	7.0^7	9.5^9	1.6^8	3.4	9.4^{11}
Zeta	200	200	10^{14}	3	0.10	6.3^{-2}	1.6^1	1.5^6	2.5^4	9.5^8	1.6^7	11	5.6^{11}
θ-m θ pinch	200	200	4^{16}	25	0.40	25	4	6.0^8	10^7	9.5^8	1.6^7	1.7	1.1^{12}
Puffa-tron	20	500	10^{14}	15	0.05	8.2^{-2}	$(\lambda_1^{16}=10^4)$	4.8^4	4.9^4	3^8	3.5^7	2.5	5.6^{11}
Shoek Machine	10	10	10^{17}	-	-	3.2	4^{-3}	1.7^7	3.9^5	2.1^8	4.9^6	-	1.8^{12}

Legend: $p = n(kT_i + kT_e)$, plasma pressure,
λ, mean free path
F_e, electron thermal energy flux
F_i, ion thermal energy flux
$\bar{v}_e$, electron thermal velocity
$\bar{v}_i$, ion thermal velocity
ρ_i, ion Larmor radius
ω_{pe}, electron plasma frequency

a) For the first three devices, $m_i = m_d$, and the last two devices, $m_i = m_p$.

Δ) $2^4 = 2 \times 10^4$

2.5. PLASMA FOCUS



EFFECT OF A SPECIAL MAGNETIC FIELD CONFIGURATION ON THE FORMATION OF A PLASMA FOCUS

V.D.Ivanov, V.M.Korzhavin, M.P.Moiseeva, N.K.Suchareva, T.I.Filippova

I.V.Kurchatov Institute of Atomic Energy, Moscow, USSR.

A b s t r a c t. An attempt is made to apply an external magnetic field of a specially chosen geometry for controlling the position of a plasma focus (P.F.) in devices of the noncylindrical Z-pinch.

The main experimental technique used was laser interferometer measurements with a resolution of 2 nsec.

In the plasma focus devices the plasma focus occurs near the surface of the inner electrode (the anode)[1]. To decrease the influence of surface evaporation on the P.F. parameters the anode is usually provided with a certain groove or hole in the axial zone[1,2].

L.A.Artsimovich suggested to use a weak external magnetic field of a specially chosen configuration for affecting the dynamics of the plasma sheath motion so that the high temperature region of the P.F. should be formed at a given distance from the anode surface. To solve our problem it would be advantageous to utilize the geometry of opposite fields. On this case the component H_z is zero in the symmetry plane. As a result, by varying the position of the magnetic windings it is possible to shift the symmetry plane, and consequently, to displace the position of the P.F. as well.

The experiments were carried out in the 50kj LV-2 device[3]. The main parameters of the device are as follows. The anode is 480mm in diameter, the initial voltage - 24kv, the maximum current - 1.2 Ma, the deuterium pressure - 0.5-1 torr.

The magnetic field was generated by two flat windings, their pitch being proportional to R. In this case H(R) in the symmetry plane was close to $\frac{1}{R}$ for R>3cm. The field strength was varied from 0 to 4.5kOe. The experiments were carried out in parallel both without external fields (H=0) and with a uniform external magnetic field (H).

In addition to conventional oscillographic measurements of the discharge current, voltage, neutron and x-ray emission, photographs taken by thin aluminium filter pinhole cameras and measurements of integral neutron yield by the induced Ag^{109} activity, the laser beam interferometer measurements with a resoltion of 2 nsec. were also carried out. The instruments were described in detail in[3,4].

All the experiments can be devided into three groups:

"a" - those with the longitudinal magnetic field ($H_z \neq 0$).

"b" - those with the opposite field geometry ($H_R \neq 0$).

"c" - those without an external magnetic field (H=0).

Figs. 1,2,3,4 present the corresponding experimental results.

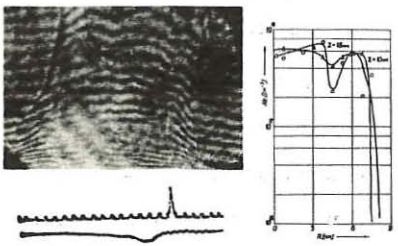


Fig.1 H_z=370 Oe

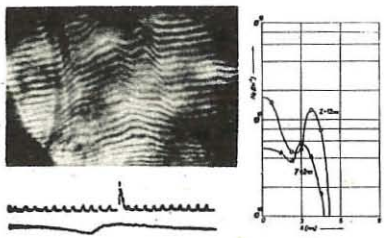


Fig.2 H_R=620 Oe

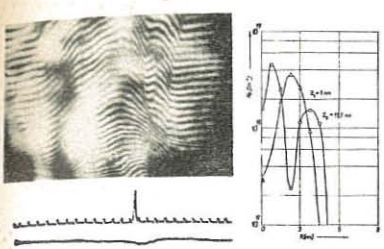


Fig.3 H_R=620 Oe

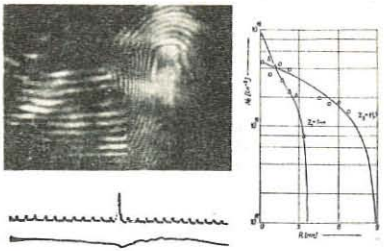


Fig.4 H=0

In the case "a", the pinch increases in diameter, it becoming more straight, i.e., it is more stable with respect to m=0,1, the plasma density however, decreases. The neutron yield is observed to reduce simultaneously, and high x-ray emission characteristic of the "c" near the anode disappears.

A few pinhole images of the pinch show that the x-ray emitting region near the anode is of a ring shape whose diameter is rather large (~7÷10cm).

Different width and depth in the density valley inside the pinch over two cross section (Z=10mm, Z=18mm) (Fig.1) should be related to different diffusion coefficients of the captured magnetic field. Solution of the corresponding equations allows the conclusion that the temperature over the cross section of Z=10mm becomes 3,5 times lower than that over Z=18mm.

Figs.2 and 3 correspond to the case "b". The minimum radius and maximum density of the plasma take place in the symmetry plane of the opposite magnetic field. The neutron emission decrease as in the case "a", while it is less critical with respect to the field strength (see Fig.5).

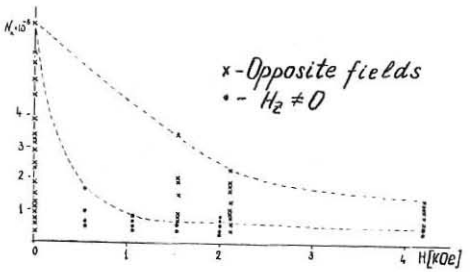


Fig.5

X-ray emission of the anode is sufficiently decreased or entirely disappears. However no bright glow corresponding to a high degree of compression was observed in the region of the symmetry plane.

C o n c l u s i o n. The geometry of opposite field with a given $H \sim \frac{1}{R}$ used in the plasma focus devices really decreases the anode erosion. Unfortunately, this leads to a partial decrease in the plasma parameters in the high temperature zone.

Discussions with V.A.Gribkov were most helpful.

References.

1. N.V.Filippov,et al. Nuclear Fusion Supplement part 2, 577, 1962.
2. V.I.Agafonov, et al. Plasma Phys. and Contr. Nucl. Fusion Research, IAEA, 2, 1962, p.21.
3. N.V.Filippov, et al. Plasma Phys. and Contr. Nucl. Fision Research, IAEA, v.1, p.573, 1971.
4. V.A.Gribkov, et al. JETP Lett 15, 329, 1972.

EVIDENCE FOR A BROAD AND UNIFORM NEUTRON-PRODUCING PLASMA COLUMN IN THE PLASMA FOCUS

Joint European Programme on Plasma Focus

P.D. Morgan (*,+), N.J. Peacock
The Culham Laboratory, Abingdon, Berks., U.K.

P. Cloth, H. Conrads
IPP-IRE, Ass. EURATOM-KFA, Jülich, Germany

Ch. Maisonnier, F. Pecorella, J.P. Rager, M. Samuelli
Laboratori Gas Ionizzati (Ass. EURATOM-CNEN), Frascati, Italy.

ABSTRACT

Holographic interferometry, time of flight measurements on the fusion reaction neutrons and time-resolved x-ray imagery have been used to specify some of the parameters of the plasma during the late-time history of the dense pinch in the 120 kJ Plasma Focus at Frascati. The measured parameters are in agreement with the model of a broad and uniform plasma column which is turbulently heated after the break-up of the pinch.

INTRODUCTION

One of the first goals of the Joint European effort on Plasma Focus is to check by direct measurements on the Frascati device / 1 / the validity of the model / 1 / proposed to account for the neutron emission. Following this model, most of the neutrons would be of thermonuclear origin, and a small fraction only would be produced at the time of maximum compression, whereas the bulk of neutron emission would originate later from a diffuse plasma of considerably larger dimensions, lower density, and higher temperature resulting from efficient turbulent heating during the radial expansion of the plasma column.

The present experimental effort is aimed at assessing the importance of ion beams in the plasma and defining the region of electron density by holographic interferometry. Also, the location of hot electrons and hot ions is found by soft-x-ray and by neutron imaging techniques respectively.

Preliminary results using the first three methods are given hereafter. It is anticipated that final density measurements and more x-ray measurements will be included in a supplement paper.

(*) *Royal Holloway College (London)*
(+) *Supported by USAF under contract F.44620-71-C-0098*

HIGH ENERGY IONS

The method for measuring the number of high-energy ions is based on the intensity of (D,Li^7) reactions. The method has been used successfully for tracing in a Focus device / 2 / the number of ions with energy exceeding 300 keV, where the reaction cross-section becomes substantial. Lithium deuteride is placed in the anode and lithium hydride in the cathode, both on axis. Three time-of-flight spectrometers are used for analysing the neutron spectrum and are placed at 8 m, 13 m, and 20 m respectively from the Focus. The arrangement has a threshold sensitivity for detecting neutrons from the (D,Li^7) reactions which is about 10^8 neutrons per discharge.

The neutron spectra recorded on the Frascati Focus show little evidence of ions having energies above 300 keV. Over more than 50 discharges with pressures varying between 0.5 and 2 Torr, only one case indicates the presence of a few (D,Li^7) neutrons above threshold. The bulk of neutrons are from (D,D) reactions. By contrast, on the Jülich Focus the (D,Li^7) reactions exceed the (D,D) reactions by a factor of five. The total neutron yield is about equal for both experiments ($\sim 2 \times 10^{10}$).

DENSITY MEASUREMENTS

Fig. 1 is a schematic diagram of the apparatus used for the holographic interferometry. 1 - ruby laser, / 3 /; 2,7-expansion telescopes; 3,5-pellicle beam splitters; 4-photo-diode; 6-mirror arrangement to equalise the scene and reference paths; 8-hollow wedge; 9-lens focusing plasma plane onto diffuser; 10-1mm pinhole; 11-camera; 12-diffuser; 13-lens to expand reference beam to fill film 14. The input apertures of the camera are closed by narrow-band interference filters.

The double-exposure holograms were recorded on Kodak SO-243 film. Background fringes were introduced by replacing the initial air filling in the hollow wedge with helium, between exposures. Electron-density profiles were obtained from the interferograms after an Abel-inversion, / 4 /.

In particular, the diffuse-pinch phase, during which maximum neutron emission occurs, has been investigated. Preliminary results show clearly the presence of a broad, well-defined column of plasma during this phase, with peak electron densities approximately two orders of magnitude lower than those in the dense pinch; there is evidence that the line density remains constant. Fig. 2 shows an electron density profile obtained at the maximum intensity of neutron emission, with an inset showing a typical neutron signal. The radius of the column is 1.9 cm and the peak electron density is $\sim 3.2 \times 10^{17}$ cm^{-3}. It can be seen that the plasma boundary is sharp and that the electron density within the column is, to a first approximation, constant. The line density, $N_e = 2\pi \int_0^R n_e(r)\, r\, dr$, is $\sim 2.7 \times 10^{18}$ cm^{-1} and the column length is ~ 3 cm. In order to account for the neutron yield of 4.8×10^{10}, observed on the discharge pertaining to the density profile, a deuterium ion temperature

of 8 keV is necessary for a thermal plasma with an emission time of 100 nsec. At even later times in the discharge, during the decay of the second neutron burst, the plasma expands to a diameter which is larger than the width of the field of view of 5.7 cm. For example, 60 - 100 nsec after peak neutron intensity, the recorded fringe shifts become assymmetric about the electrode axis and are irregular across the field of view. This indicates that during this phase the plasma column breaks up shortly after the peak neutron emission.

SOFT x-RAYS

Fig.3 is a 50 ns exposure, soft x-ray image centered on the maximum of the second neutron burst shown inset on Fig. 2.

Fig. 3 shows a diffuse plasma of much larger diameter than the 2 mm dimension of the plasma column at maximum compression, / 5 /. The latter appears in the picture as a black filament at the centre. This is due to early charge depletion of the x-ray intensifier (channel plate) by the much higher emissivity of the denser plasma. A systematic investigation of the spatial and temporal evolution of the x-ray emitting volume is in progress.

CONCLUSION

A well-defined, hot plasma column of about 4 cm in diameter with a mean density of 2.3×10^{17} cm^{-3} exists at the time of maximum neutron intensity. No gross density perturbations within the column are observed. There is no evidence of high energy ion beams in the plasma. These results are in agreement with the model previously proposed / 1 /.

REFERENCES

/ 1 / Ch. MAISONNIER, et al.: Proc. of Vth European Conf. on Controlled Fusion and Plasma Phys. Vol. II, p. 183 - Grenoble 1972.

/ 2 / H. CONRADS et al.: Phys. Fluids 15, 209 (1972).

/ 3 / P.D. MORGAN and N.J. PEACOCK: J. Phys. E: Sc. Instr. 4, 671 (1971).

/ 4 / K. BOCKASTEN: J. Opt. Soc. Am., 5, 943 (1961).

/ 5 / Ch. MAISONNIER et al.: Proc. Conf. Plasma Physics and Controlled Thermonuclear Research, Vol. I, p. 511 - Madison (1971).

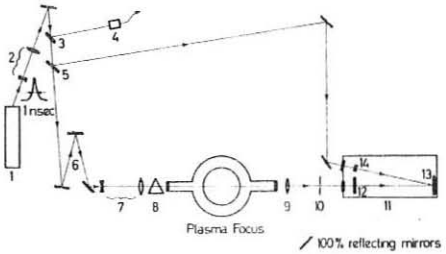


Fig. 1 - SCHEMATIC LAYOUT OF HOLOGRAPHIC OPTICS.

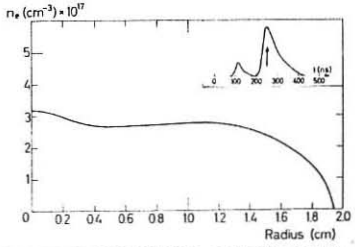


Fig. 2 - ELECTRON DENSITY PROFILE AT THE TIME OF MAXIMUM NEUTRON EMISSION INSET TYPICAL NEUTRON SIGNAL

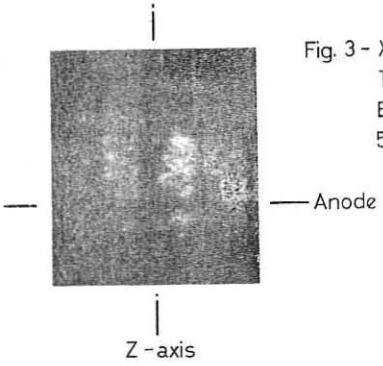


Fig. 3 - X-RAY IMAGE DURING THE SECOND NEUTRON EMISSION (EXPOSURE 50 ns).

Sixth European Conference on Controlled Fusion and Plasma Physics
Moscow, USSR. 30 July - 2 August 1973.

THE MEASUREMENT OF ION TEMPERATURE AND MAGNETIC FIELD IN A DENSE PLASMA FOCUS

M J Forrest, B A Norton*, N J Peacock

UKAEA Culham Laboratory, Abingdon, Berkshire, England.

*Royal Holloway College, Englefield Green, Surrey, England.

ABSTRACT. Recent measurements of ion and electron temperatures in pure deuterium plasma by laser scattering give T_i = 3 keV, T_e = 2 keV in contrast to results in Ne doped plasma [1] where T_i = 0.7 keV and T_e = 2.25 keV. The magnetic field during pinch collapse has been estimated from measurements of the Zeeman splitting of the CV 2271 Å line to be between 0.8×10^6 and 2×10^6 Gauss.

1. INTRODUCTION. This paper describes two separate aspects of work on a Mather-type plasma focus - the ion temperature measurement by means of scattering and an estimate of the magnetic field from the observed Zeeman effect.

2. ION TEMPERATURE MEASUREMENTS. When the correlation factor for scattering $\alpha = (k\lambda_D)^{-1} > 0.5$ (k^{-1} being the scale length for scattering and λ_D the Debye length) the scattered spectrum is influenced by density fluctuation due to ion motion. In the present experiments the scattered light is collected at 45° to the laser beam, giving $\alpha \sim 2$.

A 6 joule 20 nsec pulse from a ruby laser was used to irradiate the pinch on and transverse to the axis of symmetry of the electrodes at a distance of 12 mm from the anode. The laser beam was focused to 3 mm, larger than the plasma focus, to accomodate irreproducibility in the location of the dense plasma. A multichannel echelle spectrometer with a channel resolution of 1.8 Å was used to record the scattered spectrum.

Using 2.5 torr deuterium filling pressure with 4% neon the form of the scattered spectrum was, as predicted by Evans[2], sensitive to the temperatures of the ion species present and to ratio of deuterium temperature T_i to electron temperature T_e. Experimental points matched a double humped shaped curve symmetrical about the laser frequency. In one case the computed curve which fitted the data best yielded $n_e \simeq 2 \times 10^{19}$ cm^{-3}, $T_e \simeq 2.25$ keV, $T_i \simeq 0.7$ keV, $T_{Ne} \simeq 9$ keV. These values of n_e, T_e, T_{Ne} agree with those determined previously by interferometric[3] and spectroscopic[4] techniques. The total scattered light was found to be equivalent to that expected for a thermal plasma during the dense pinch.

With a pure deuterium plasma at 3 torr filling pressure the plasma was much less reproducible, only a few per cent of the discharges resulting in a detectable scattered spectrum. Fig.1 shows an example of one of these spectra. The flat top

bell-shaped symmetry about the laser frequency is characteristic of $T_e/T_i \leq 1$. The best fit curve to the experimental points gives $T_i \simeq 3$ keV and $T_e \simeq 2$ keV. Scattering was not observed other than at the dense pinch phase. Within the accuracy of the measurement, the intensity of the scattered light was no greater than expected from a thermal plasma. The parameters determined from the scattered light spectrum, assuming a thermal plasma, are in good agreement with those derived previously using X-ray spectroscopy and Laser Interferometry. In the case of the Neon doped plasma $T_e > T_i$ while in the pure deuterium plasma $T_i > T_e$, the latter consistent with results of Bernard [5].

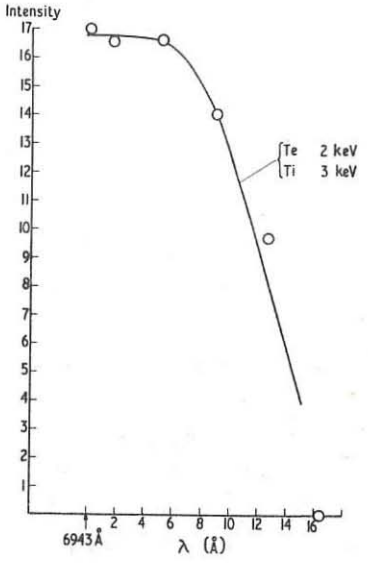


Fig.1

Scattered spectrum in deuterium with no rare gas additives; filling pressure 3.0 torr D_2. The solid curve is calculated for the values of electron and ion temperatures indicated.

3. MAGNETIC FIELD MEASUREMENT. The magnetic field during the radial implosion is inferred from measurements of the Zeeman splitting of the CV 2s ^3S - 2p $^3P^o$ multiplet transition in an experiment carried out using 2.5% ethylene in 2.1 torr deuterium. Most ions capable of providing visible transitions at which magnetic splitting may be large will be rapidly 'burnt through' at the high temperatures involved. Carbon V, with an ionization potential of 392 eV, has an ionization time of a few nsec in the focus when $n_e \sim 10^{19}$ cm^{-3} and $T_e \sim 1$ keV, and the 2s - 2p multiplet transition in C V at 2271 Å and 2279 Å was found to satisfy the requirements that the Zeeman splitting was comparable to or larger than the other broadening effects, namely mass-motion, thermal and Stark broadening. The Doppler thermal width of the 2271 Å line with $T_i \sim 1$ keV is ~ 1.6 Å. Stark broadening is described by the impact approximation and a suitable scaling of the half-width parameters for the 2s - 2p transition in Helium given by Griem [6] leads to a dispersion half width of ~ 1.04 Å for an electron density of $\sim 3 \times 10^{19}$ cm^{-3}. Uncertanties in T_i or n_e of 100% will result in an uncertainty in the width of the

overall thermal-Stark profile of about 50%, but it is still smaller than the expected Zeeman splitting of several Å.

The multiplet has been observed in time-integrated grazing incidence spectra and the short wavelength 2s $^3S_1$-2p $^3P^o_2$ transition was discernable above the background emission about 100 nsec before and up to the time at which the main neutron burst began. A thin section of this pinched column was viewed across a diameter of the imploding plasma, and consequently one portion of the shock front was advancing and the other receding in the direction of view, and this mass-motion resulted in a red and a blue shift of the short wavelength component about the 2271 Å position.

The implosion velocity has been measured by Laser interferometry [1] and is $\lesssim 3 \times 10^7$ cm sec^{-1}.

Measurements on a thin plasma slice, 4 mm long in the axial direction and 0.01 mm wide, were made with a calibrated monochromator and photomultiplier arrangement (10 nsec rise-time) focused onto the centre of the pinch, and a rotatable quartz-stack polarizer. A scan was carried out on the 2271 Å component, using a bandwidth of 0.8 Å and the polarizing stack, in order to detect isolated wavelength regions with predominantly π or σ emission. At 2272 Å, mainly π component radiation was observed, while σ emission predominated at < 2265 Å. Ratios of the intensities of π and σ components are shown in Table 1 at various times before the neutron pulse. The field is estimated by comparing these ratios to the calculated ones for various values of magnetic field.

The magnetic splitting is described by the weak field approximation as the energy level shifts are less than the multiplet splitting of the 2p levels for fields below about 3×10^6 Gauss.

Calculations of the Zeeman pattern for the described conditions with a compression velocity of 2×10^7 for various fields (Fig.2) show that fields > 10^5 gauss must be present to permit any discrimination between π and σ components. An upper limit for H is set at 2×10^6 gauss due to the fact that no π emission was observed at ≤ 2265 Å, but due to uncertainties in the compression velocity, it is not possible to predict the precise Zeeman pattern.

Evidence of magnetic splitting greater than the half-width of the line profile in the non magnetized case sets the lower value of the field at $\sim 0.8 \times 10^6$ gauss.

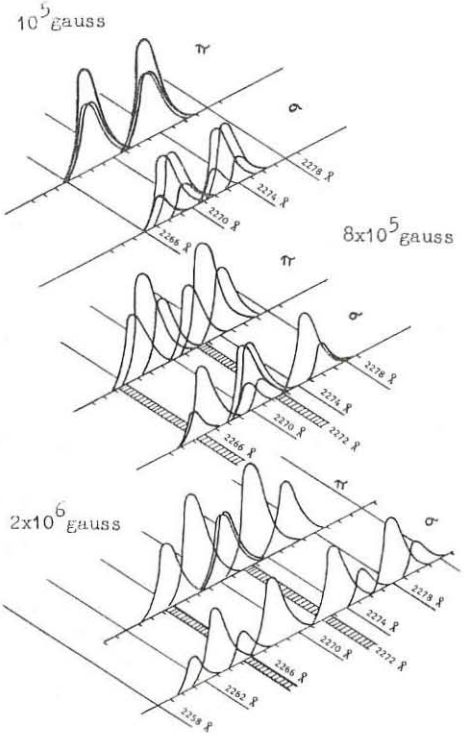
4. CONCLUSIONS. Scattering measurements show that in pure deuterium T_i = 3 keV and T_e = 2 keV compared with Neon doped deuterium when T_i = 0.7 keV and T_e = 2.25 keV. The magnetic field is estimated from the observed Zeeman splitting to lie between 0.8×10^6 and 2×10^6 gauss.

TABLE 1

Mean Ratio of Measured Intensities of π and σ Components

Time before neutrons	Iπ/Iσ (2272Å)	Iπ/Iσ (2268Å)	Iπ/Iσ (2265Å)
20 nsec	2.9 ± 0.5	1.0 ± 0.1	0.08 ± 0.02
40 nsec	$5.4^{+0.1}_{-1}$	1.0 ± 0.1	$0.063^{+0.06}_{-0.03}$
60 nsec	12.0^{+5}_{-6}	1.3 ± 0.2	$0.9^{+0.09}_{-0.04}$
100 nsec	$2.6^{+0.4}_{-0.6}$	0.8 ± 0.3	0.2 ± 0.1

Fig.2 π and σ components of CV 2s-2p in various magnetic fields, $n_e = 3 \times 10^{19}$ cm^{-3}, $T_i \lesssim 10^3$ eV. Shaded portions depict regions in which observed emission was predominantly from π or σ components. (the weakest σ components are not shown).



REFERENCES

[1] Peacock, N.J. et al, Proc. 5th Europ. Conf. on Cont. Fus. and Plasma Phys. Vol. pp.66, CEA, Grenoble.

[2] Evans, D.E. (1970) Plasma Phys. Vol.22 pp.573-584.

[3] Peacock, N.J. et al,(1968) Proc. IAEA 3rd Conf. Plasma Phys. and Cont.Fus.Res. (Novosibirsk paper CN-24/G-4).

[4] Peacock, N.J. et al (1971) Plasma Phys. and Cont.Nuc.Fus. Res.Vol.1, pp.537-51 IAEA, Vienna.

[5] Bernard, A. et al (1972) Proc. 2nd Topical Conf. on Pulsed High Beta Plasmas P. El, Published by Max Planck Inst., Garching, IPP 1/127 July 1972.

[6] Griem, H.R. U.S. NRL Report 6084 Washington D.C. 1964.

ELECTRON DENSITY OF A PLASMA FOCUS AND THE RADIATION EMITTED AT THE PLASMA FREQUENCY AND ITS HARMONICS

H. Conrads, D. Gollwitzer

Institut für Plasmaphysik, Association EURATOM-KFA
Postfach 365 - 517 Jülich 1 (West Germany)
and

H. Schmidt
Institut für Plasmaforschung, Universität, Stuttgart,
Pfaffenwaldring 38 - 7 Stuttgart 80 (West Germany)

ABSTRACT

The electron density of a plasma focus has been measured as a function of time during 150 nsec, when the focus is formed reaching a peak density of 5.10^{19} per cm^3 on axis. The absolute intensity of the radiation has been measured in the spectral range of 0.5 µm - 12 µm, where the plasma frequency and its harmonics are positioned.

1. EXPERIMENTAL ARRANGEMENT

The measurements have been performed with the DPF Jül I - device having the following specifications: U = 40 kV, C = 22 µF, length of electrodes: 3 cm, diameter: outer one 11 cm, inner one 5 cm with LiH-insert, pressure 0.5 Torr - 6 Torr D_2.

For measuring the time dependence of the electron density two different methods had to be used: interferometry (Mach-Zehnder) and refraction by the plasma. The probing radiation has been taken from an Argon-laser emitting at 0.541 µm. The radiation has been recorded by an image convertor camera in smear-mode having a time resolution of about 100 p sec. For measuring the refraction of the plasma the smear camera was imaging a plane 2 m apart from the plasma. This arrangement was sensitive enough to record 0.5 m rad refraction of the Argon-laser beam by the plasma.

The absolute intensity emitted by the plasma in the spectral range between 0.6 µ and 12 µ has been recorded by a system as shown in Fig. 1. For measuring the intensity between 0.6 µm and 1 µm the photodiode was

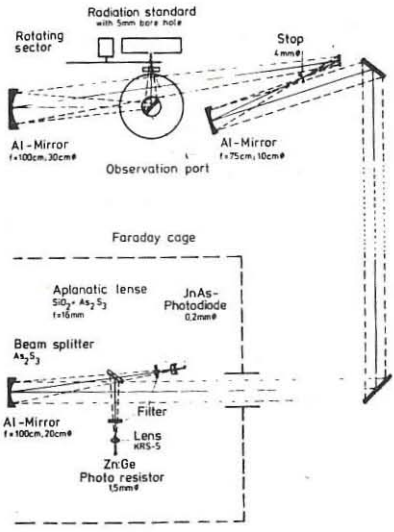


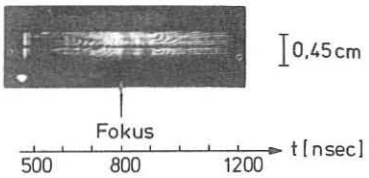
Fig. 1

replaced by a photomultiplier. A spectral resolution was obtained in the range between 0.6 µm and 3 µm by interference filters and between 5 µm and 12 µm by combining a long-pass-interference filter with In - As and BaF_2 respectively.

2. RESULTS

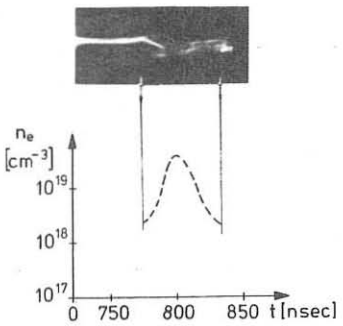
Fig. 2 shows a typical interferogramme. 10 nsec before the plasma reaches its highest compression according to smear pictures of the selfluminosity of the focus the fringes are lost. 50 nsec later they are appearing again. The fringe shift corresponds to an increase of the electron density from 10^{17} per cm^3 to 2.10^{18} per cm^3 and later on to a decrease of the same order of magnitude. This interferometric method is no longer applicable for the time, when the density is increasing far beyond 2.10^{18} per cm^3, because strong refraction is taking place. For a probing laser beam of low divergency it can be assumed, that the product of the refraction angle and the critical electron density corresponding to the laser frequency is almost equal to the maximum of the electron density. Fig. 3 shows the refraction as a function of time and the corresponding electron density, and Fig. 4 the electron density as a function of time from both measurements. The laser beam limited to a diameter of 2 mm at the plasma was pointing at an area of 10 mm above the anode on axis. At this position the electron density is increasing within 60 nsec almost two and a half orders of magnitude reaching a peak density of 5.10^{19} electrons per cm^3.

Measurements of the radiation emitted by the plasma focus were made "end on", in order to cover the plasma layer close to the anode. This layer is of particular interest regarding the lithium ions released by the anode and being ac-



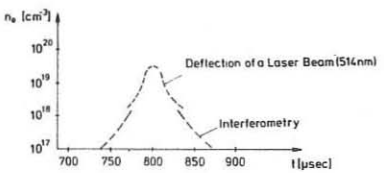
Interferogram Recorded by a Smear Camera (p_1 = 8,7 Torr ; z = 0,8 cm)

Fig.2



Electron Density as a Function of Time Obtained by the Deflection of a Laser Beam (514nm) (p_1=6 Torr; z = 0,7cm)

Fig. 3



Electron Density as a Function of Time

Fig. 4

celerated up to 1 MeV. Fig. 5 shows the emitted radiation as a function of the wavelengths. The emission between 0.6 µm and 1.5 µm has been also observed "side-on" and in neither case can the intensity be explained by a thermal plasma. After dropping 4 orders of magnitude between 1.5 µm and 5.5 µm the emission decreases with $1/\lambda^2$ in the range between 5 µm and 12 µm. Most likely the $1/\lambda^2$ - emission is due to an optically thin plasma of an electron density below 10^{19} per cm^3 being placed along the line of sight in front of a denser plasma. For evaluating the non-thermal radiation the thermal part has to be subtracted per wavelength unit from the measured intensities. An upper limit of the thermal radiation is a $1/\lambda^2$ decay fitted to the intensity at the shortest measured wavelength at 0.6 µm (curve 1) and a lower limit is a fit to the intensity at 5.5 µm (curve 2). Fig. 6 shows the resulting intensity of the non-thermal radiation for both cases. It peaks between 1.25 µm and 1.5 um. Such an emission was typical for a plasma diameter up to 1.5 mm on axis.

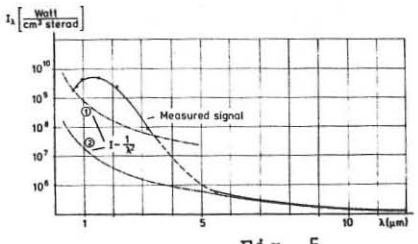


Fig. 5

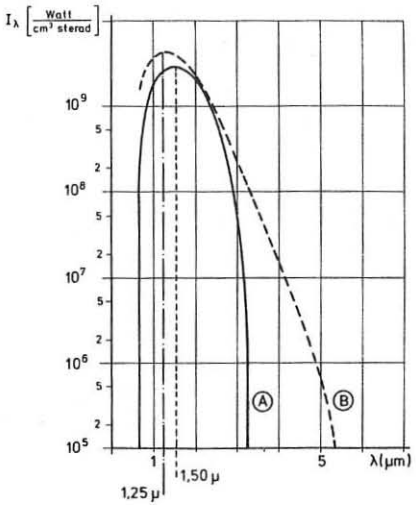


Fig. 6
Curve A corresponds to curve 1 in Fig. 5

3. DISCUSSION

Interferometry and refraction measurements show, that the electron density can reach values of 5 10^{19} per cm^3 at a distance of 1 cm from the anode. It can be expected that this value might increase in the vicinity of the anode. The measured radiation of the plasma is covering the spectral range from below the plasma frequency to its higher harmonics. The observed emission between 1.25 µm and 1.5 µm exceeds the thermal emission by at least a factor of 10. It is known, that the electrons in a plasma focus have an energy distribution with an $E^{-3.3}$ - slope for energies between 60 keV and 350 keV / 1 /. The enhanced emission in the infrared could be assigned to a turbulent plasma. In such a plasma low frequency inhomogeneities can couple a electrostatic wave to an electromagnetic

wave radiating close to the plasma frequency ω_p. Also two electrostatic waves can couple to one electromagnetic wave emitted close to twice the plasma frequency $2\omega_p$. Since the electrostatic waves have to be only weakly Landau-damped for producing enhanced emission the frequency of each must be in the range of $\omega_p < \omega \lesssim 1.5\,\omega_p$ / 2 /. At the present we cannot distinguish between the two cases. However, these experiments are being continued.

REFERENCES

/ 1 / H.L.L. van PAASSEN, R.H. VANDREE, and R.S. WHITE: Phys. Fluids 13, 10 (1970)

/ 2 / P.A. STURROCK, R.H. BALL, and D.E. BALDWIN: Phys. Fluids 8, 1504 (1965).

Characteristic Curves and Scaling Laws for a Mather Type Plasma Focus

H. Rapp and M. Trunk

Institute for Plasma Research, University of Stuttgart, BRD

Abstract: From experimental and theoretical studies for a focus machine of the Mather type, characteristic curves and scaling laws are established. Neutron and X-ray radiation characteristics are presented and results of MHD calculations are interpreted.

In order to establish scaling laws for a plasma focus device with a long accelerator, the neutron output was measured as a function of the deuterium filling pressure p, accelerator length l, and capacitor energy E_c. The electrical parameters of the current circuit remained constant. The capacitance and inductance of the storage system was 225 μF and 20 nH, respectively. In Fig. 1 the characteristic curves for two different capacitor energies are presented as functions of the product, pl. In the diagram, circles are the mean values and error bars are the standard deviations of the mean values. For each set of parameters, a series of 15 shots was made without changing the gas filling. The optimum pressure shifts with bank energy as

$$E_1/E_2 = p_1 l_1 / p_2 l_2 \ .$$

This agrees with the shift of the maximum of the stored magnetic and kinetic energy at the moment of pinch as calculated from "snow-plough" theory. The product pl represents the mass of the gas in the whole coaxial tube. The shifting law describes a still unknown optimum balance between the driving magnetic forces and inertia of the gas. We can regard the left side of the maximum of each characteristic curve as the kinetic energy dominated regime and the right side as the magnetic energy dominated regime /1/.

The neutron output N at optimum pressures scales with bank energy E according to a power law

$$(N/N_0) = (E/E_0)^m \ ,$$

with m=2.1 ± 10 %. This law has been established for energies between 20 kJ and 45 kJ but also agrees well with the results from our smaller focus with only 12 kJ. It also corresponds with results of other institutes with bigger machines up to 120 kJ.

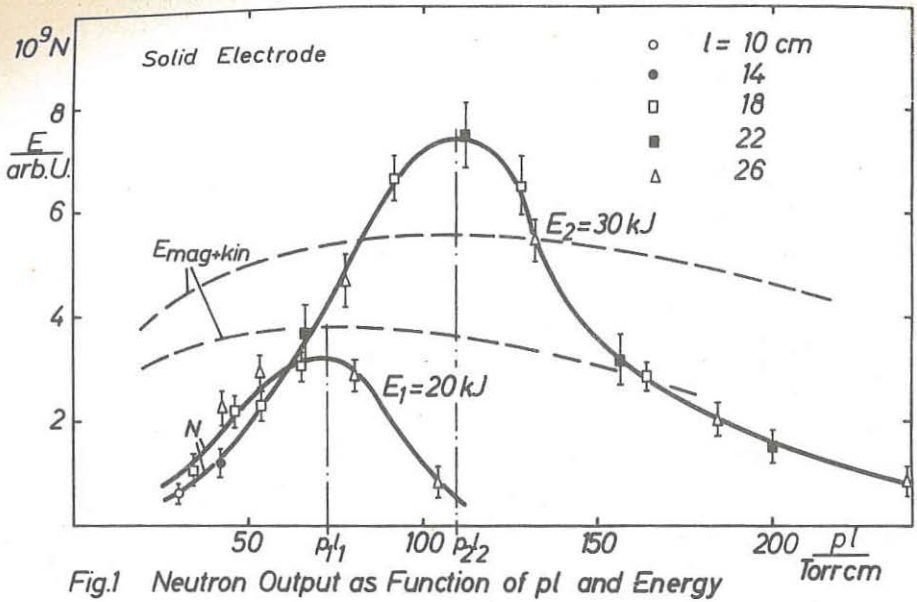


Fig.1 Neutron Output as Function of pl and Energy

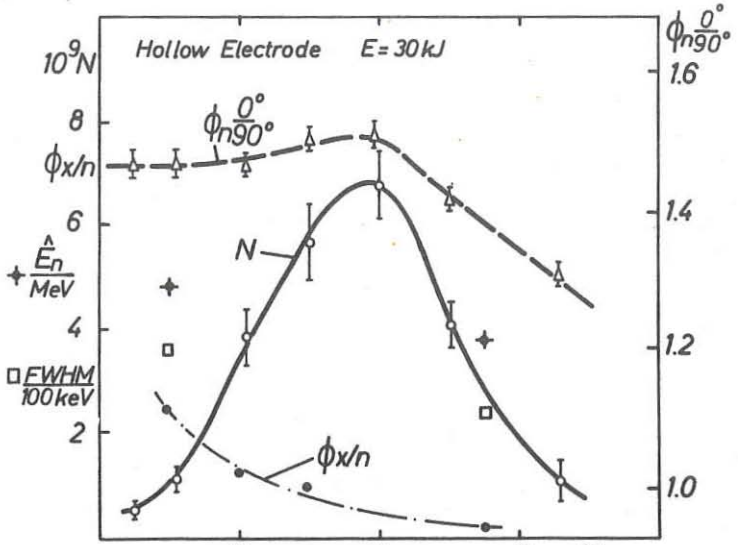


Fig.2 Characteristic Curve and Typical Correlated Signals

In Fig. 2 some typical observations are correlated to a characteristic curve, which has been obtained with a hollow inner electrode. From the time integrated neutron flux anisotropy, $\phi_n\ 0^o/90^o$, it is clear that the plasma becomes more isotropic for pressures higher than the optimum pressure. Independent of the pressure range, the anisotropy is always rising with neutron output. It reaches the value of 1.8 . The mean ratio, $\phi x/n$, of the peak fluxes of the hard X-rays to neutrons behind a wall of 5 cm lead declines rapidly with increasing pressure. The intensity of the hard X-rays is a measure for the induced axial pinch voltage. This voltage can damage the collector and the gun isolator, especially if short electrodes and low pressure are used. With solid electrodes, multiple pinches sometimes occur in the optimum and high pressure regions.

In the low pressure region the end-on neutron spectrum has a full width at half maximum (FWHM) of about 460 keV and a spectral shape which is similar to that resulting from a 3-dimensional monoenergetic ion distribution with a high energy tail. The maximum neutron energy, $\hat{E}_n$, reaches 3.6 MeV. In the high pressure region FWHM is less than 250 keV and $\hat{E}_n$ is less than 3.2 MeV. The spectral shape becomes similar to a neutron spectrum for a 2-dimensional Maxwellian ion distribution. The most probable end-on neutron energy of 2.65 MeV in the laboratory frame remains constant. This value corresponds well with our result of 8.8×10^7 cm/s center-of--mass velocity determined from side-on neutron flux measurements using shadow bars at different axial positions.

In parallel to the measurements, MHD calculations /2/ similar to those first used by Potter /3/ were carried out. Theoretically predicted dynamics of the focus discharge agree quantitatively with the experimental results, whereas due to the relatively coarse mesh used in the calculations the calculated plasma variables are only in qualitative agreement with the observed values. Fig. 3 shows some results of these calculations as functions of pl at the moment of the highest temperature in the dense focus stage. Since the internal inductance of the focus apparatus rises less rapidly with time at higher pressures, the current, especially the rest current I in the focus phase, will be greater at higher pressures. In cases of larger values of pl the condenser bank energy E_c is more efficiently utilized due to the longer discharge time. As pl is varied, the square of the particle density, n^2 (a measure of the neutron production efficiency), shows a clear maximum similar to that of the neutron production observed in the experiment. The predicted decrease of the ion temperature T_i implies that the neutrons are not of the thermonuclear origin. On the other hand, the course of variation of the electric field E_z near

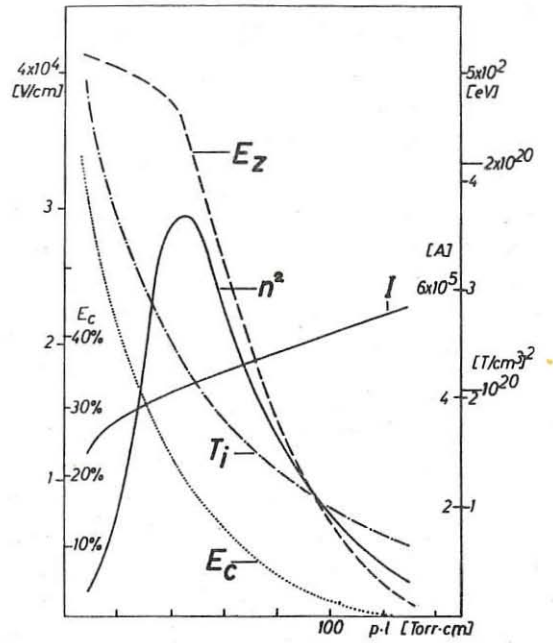


Fig. 3 Some results of MHD calculations in the dense focus phase as funtions of pl.

the axis indicates that non--adiabatic acceleration mechanisms proposed by Bernstein /4/ may be present.

Variations of other electrical circuit parameters obtained from the earlier "snow-plough" theory /5/ were confirmed by the present MHD calculations. Especially, one can show that the external inductance L_o should not be smaller than 10 nH, because then the higher current in the early stage is damped out too strongly by the variable inductance L_1 of the focus machine and the magnetically stored energy is not large enough to draw a sufficiently high current in the collaps phase.

Ref.: /1/ Rapp, H.; DPG Frühjahrstagung Berlin 1973.

/2/ Trunk, M.; IPF-73-1.

/3/ Potter, D.E.; Phys. Fluids 14/9.

/4/ Bernstein, M.J.; Phys. Fluids 13/11.

/5/ Rapp, H. and Trunk, M.; IPF-71-1.

DIFFUSION AND BEAM HEATING IN THE DENSE PLASMA FOCUS

[x] V.A.Gribkov, [x] O.N.Krokhin, [x] G.V.Sklizkov, [xx] N.V.Filippov,
[xx] T.I.Filippova

[x] P.N.Lebedev Physical Institute, Moscow, USSR

[xx] I.V.Kurchatov Institute of Atomic Energy, Moscow, USSR.

Abstract: The analysis of interferograms and obscurograms in soft X-rays of the Plasma Focus (PF) shows that the collapse of the current sheath becomes stronger due to accumulation of impurities by means of diffusion processes; and the reason for the current sheath rupture is a high level turbulence; and the electron beam heating of the plasma during "second compression" is of great importance.

1° The comparison of the processed interferograms with MHD calculations /1,2/ showed that the distance between the current sheath and shock wave was smaller than in theory and the electron density in this shock was greater than it had to be for $\beta = 4$ and the electron density distribution at the moment about 20 nsec after the first compression had "a step" (Fig. 1). The analysis of diffusion processes in the PF (the two component mixture D + 1 + 2% N or Xe) at initial stages (Enskog - Chapman method - /3/) and in the first compression phase (Grad method of 13 momentum - /4/) showed that taking into account inertia and viscosity the shock front and skin layer had been improverished by heavy impurities. But it follows from the numerical calculations

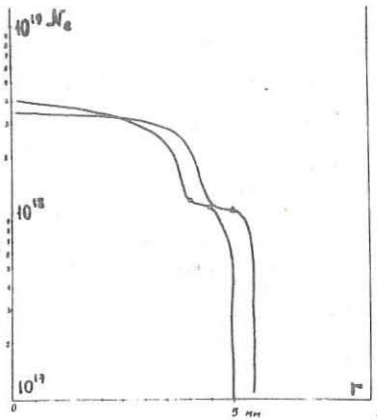


Fig. 1

/1,2/ that carrying-out of plasma due to the noncylindricity of the PF takes place just from these zones. So at the moment of the first compression we have a collapse of the "heavy shell". This idea gives a good explanation to the above-mentioned results and to other experimental facts and it also follows from interferometry.

Namely, the total plasma mass at first compression is only 1/100 of the initial mass (instead of theoretical prediction 1/20) and the velocity of the axial "shock" deduced from smearing of the interferometric fringes and the laser pulse duration appears to be of the order of $1{,}4 \cdot 10^8$ cm/sec. The last fact makes it possible to produce the neutrons by means of the collision of this axial stream with cold duterium above the PF. Besides, the small diameter of the PF in soft X-ray obscurograms in comparison with interferograms is explained now as the luminosity of the collapsing impurity ($J \sim Z^2$).

2° The interferograms of a skin layer at the initial stages of collapse showed the absence of interferometric fringes (Fig. 2) that could be explained by neither refraction and absorption nor classical light diffusion. An anomalous light diffusion due to longitudinal plasma oscillation can take place if $\frac{\lambda^t}{2} = 3.5 \cdot 10^{-5}\,\text{cm} < \lambda^e \simeq \frac{2\pi V}{\omega_{pe}} \simeq 5 \cdot 10^{-5}\,\text{cm}$ The estimation of $\frac{We}{nT}$ in our experimental case (with the critical light diffusion angle ~1°) /5/ gave us a value of the order of 0.2. By the moment of t=0 (the rupture of the current sheath,

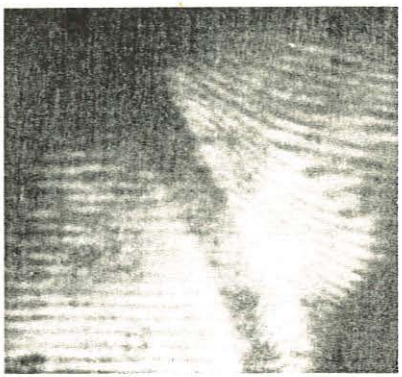


Fig. 2

30 nsec after the first compression) plasma is considered to become cool due to the expansion and luminosity of impurities and the current velocity becomes not only more than V_{Te} but more than the amplitude of oscillation of electrons in plasma oscillations ("strong turbulence"). It leads pinch to the situation when the sharp boundary of the magnetic field and plasma disappears /6/.

3° Magnetic energy is spent on the plasma carrying-out and on the electron beam creation in the circular zone near the skin layer so this beam has a tube-like structure. The neck of the PF (also with a tube-like structure /6/) serves as a "plasma cathode".

Then the electron beam is disturbed by the so-called "hose instability" and is degenerated to several filaments in mixture with the back current filaments /7/ (Fig. 3). Due to finite conductivity of the back-ground plasma first the beam is focused on the anode (hard X-ray pulse) and then into the plasma. The moment of the cessation of the hard X-rays was near the main maximum of the neutron emission. The soft X-ray obscurograms showed this tube-like electron beam near the main pinch with the maximum luminosity near its focal region (Fig. 4).



Fig. 3

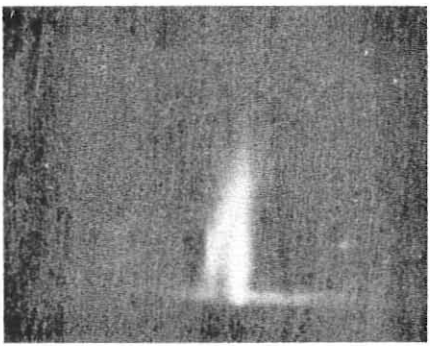


Fig. 4

It follows from the above-mentioned that the heating can take place only in a small region near the focal spot and only due to "two stream instability". An estimation of the neutron yield for this zone ($V = \pi r^2 \ell \simeq 5 \cdot 10^{-2} cm^3$, $T \simeq 10^8 °K$ /8,9,10/, $n \simeq 10^{18} cm^{-3}$, $\tau_\ell \simeq 10^{-7} sek$, $\langle \sigma v \rangle_{DD} \simeq 10^{-22} \left(\frac{T°K}{10^7} \right)^4$ /11/):

$$W \sim V \tau_{beam} \langle \sigma v \rangle_{DD} n^2 \sim 5 \cdot 10^9$$

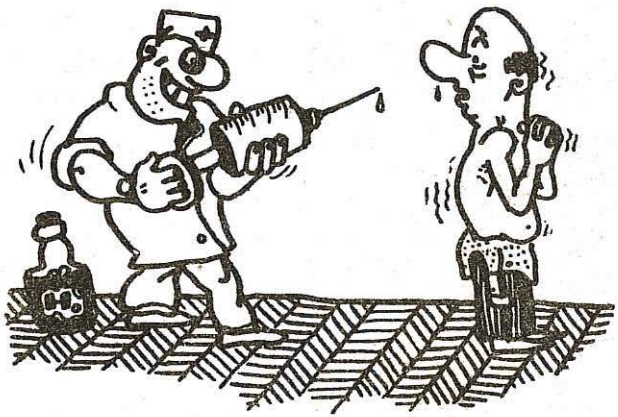
is in a good agreement with the experimental value.

Acknowledgement. We should like to thank N.G.Basov for stimulation of this work and V.S.Imshennik and V.V.Pustovalov for discussions.

Литература

/1/. В.Ф.Дьяченко, В.С.Имшенник. Сб."Вопросы теории плазмы" под ред. М.А.Леонтовича, вып.5, Атомиздат, М. (1967).
/2/. D.E.Potter. Phys.Fluids, 14, N 9, 1911 (1971).
/3/. С.П.Дьяков, ЖЭТФ, 27, 3(9), 283 (1954).
/4/. Л.Д.Цендин. ЖЭТФ, 56, 929 (1969)
В.Жданов и др. ЖЭТФ, 42, 857 (1962).
/5/. В.Н.Цытович. "Теория турбулентной плазмы", Атомиздат,М.(1971)
/6/. В.А.Грибков и др. Письма в редакцию ЖЭТФ, 15, 329 (1972).
/7/. В.А.Грибков и др. Письма в редакцию ЖЭТФ, в печати (1973).
/8/. C.Patou, A.Simonnet. Note C.E.A. N 1189, Commis. a l'Energie Atomique (1969).
/9/. H.Conrads et al. Phys.Fluids, 15, 209 (1972).
/10/. Ch.Maisonnier et al. 4th Conf. on Plasma Phys. and Contr. Nuclear Res., CN-28/D-2, Madison, USA (1971).
/11/. Л.А.Арцимович. "Управляемые термоядерные реакции", Физматгиз, М. (1961).

2.6. INJECTION



PENETRATION OF SOLID H_2 CLUSTERS IN A PLASMA

Franco Bottiglioni, Jacques Coutant and Mario Fois

ASSOCIATION EURATOM-CEA SUR LA FUSION
Département de Physique du Plasma et de la Fusion Contrôlée
Centre d'Etudes Nucléaires
Boîte Postale n° 6. 92260 FONTENAY-AUX-ROSES (FRANCE)

I. INTRODUCTION.-

Injection of accelerated cluster beams has been considered for plasma formation [1], for refuelling and heating of CTR systems [2] [3]. Trapping efficiency and penetration in a target depend on cluster dissociation and evaporation rates, dues to collisions with cluster components [4]. As a qualitative feature, the production rate of any fragment and, in particular, of atoms or protons by cluster break up, present a maximum somewhere inside the target. This feature allows a more uniform plasma production and therefore a more regular radial profile of the density than injection of atomic beams. In this paper, we present some recent experimental data, obtained in INGRA experiment [5], concerning the attenuation of accelerated cluster beams passing through a gaseous H_2 target, as well as the corresponding production of light fragments. We present also some preliminar computations on cluster evaporation, which so far has been neglected.

II. EXPERIMENTAL RESULTS.-

The outlines of INGRA apparatus are shown in Fig.1. The accelerated cluster beam is selected in mass by a magnetic analyser; then it passes through an hydrogen target. Initially charged clusters are attenuated by collisions with gas molecules, by breaking up in lighter fragments, evaporating and eventually losing their electrical charge. In this experiment only charged particles are measured. Fragments have the same velocity as the parent clusters ; therefore their energy is proportional to their mass. Magnetic mass selection of parent clusters, followed by electrostatic deflection results in a mass analysis of the fragments, which are finally detected by a scintillation counter. The exponential attenuation of the intial beam of charged clusters allow to define their total attenuation cross section as $\sigma_N = \frac{1}{n \cdot \ell} \ln(\frac{I_0}{I})$. I_0 and I are respectively the

initial and final intensity of the cluster beam and $n\ell$ is the target thickness. Measured $n\ell = 1/\sigma_N$, versus clusters atomic mass number N, are shown in Fig.2. Cluster velocities are in the range $9\ 10^5$- $2\ 10^5$ m/s, corresponding to $4\ 10^4$- $3.5\ 10^3$ eV per atom. Fig.3 shows the three lightest fragment intensity measured versus the target thickness $n\ell$. It can be seen that the higher the fragment the smaller is the target thickness corresponding to the maximum. Initial clusters have N=85 and energy 3 keV per atom. It can be seen that H_3^+, H_2^+, H^+ peaks appear respectively for $n\ell \simeq 8\ 10^{18}$, $4\ 10^{19}$, $1.5\ 10^{20}$ m^{-2}. It must be pointed out, by comparison, that an H neutral beam, passing through the same target at the same velocity, would produce the maximum of H^+ density for $n\ell \simeq 2\ 10^{19}$ m^{-2}. It seems therefore proved that initial mass decreases mainly by loosing fragments, including H_2 and H, rather than by evaporation.

III. CLUSTER EVAPORATION.-

We present now some preliminary computations on cluster evaporation rates under the impact of electrons ions and neutrals. Clusters are considered as a very dense gas, since characteristic collision times of primary particles with cluster molecules are shorter then time scale of propagation of a disturbance inside solid lattice. Primary particles are considered to interact individually with cluster molecules. Cluster evaporation, that is the sudden change into a molecular beam, occurs when the total energy got by the solid lattice in several successive collisions is greater than a stability threshold, assumed equal to $N_M W_D$. Here N_M is the molecular mass number of clusters and W_D the intermolecular binding energy, which is about 10^{-2} eV. Cluster stability is affected mainly by collisions with ions or neutrals ; in particular by elastic momentum transfer, by ionization followed by secondary electron recombination [6] and by dissociation of cluster molecules. In Fig.4 is shown the target thickness for an e-folding attenuation by evaporation of a cluster beam, in dependence on cluster mass N.

IV. CONCLUSION.-

From data shown before, it can be concluded that generally electrons contribute essentially to cluster fragmentation, by multiple ionization. On the contrary, heavy particles contribute to

evaporation at most at the same rate as to break up. Cluster interaction with gas molecules or atoms can be considered also as representative of interaction with ions, althouth in this latter case a higher rate of fragmentation should be expected due to the charge exchange reaction :

$$C^+ + H^+ \rightarrow C^{++} + H^\circ \rightarrow C_1^+ + C_2^+ + H_o \quad (C_1^+ + C_2^+ = C^{++})$$

Hence, evaporation should not be faster than fragmentation for clusters of moderate size (N < 500) injected into a plasma. This relatively slow evaporation rate can be explained by the fact that, contrary to pellets, clusters do not absorb the whole energy of primary particles impinging on them. The peaked distribution of fragments and of the atomic components, has been observed in our experiments with a gas target. The maximum of atomic components is found far beyond the thickness values corresponding to expected plateau occuring with injection of molecular or atomic hydrogen. Effects on plasma profile of this atomic source shifted into the plasma must be evaluated for each specific case, since magnetic field and the relative amount of charged and neutral fragments can affect strongly the maximum position of the atomic component.

References.-

[1] W.Henkes, Physics Letters 12, 322 (1964).

[2] M.Fois, Euratom Fusion Technology Adv. Group, EUR-4874 e, 161 (1972).

[3] J.R.Hiskes, Nuclear Fusion 12, 423 (1972).

[4] F.Bottiglioni, J.Coutant, M.Fois, IVth European Conference on Controlled Fusion and Plasma Physics, Roma (1970), 96.

[5] F.Bottiglioni, J.Coutant, M.Fois, F.Prevot, Proc. of the IVth IAEA Conference, Madison (1971), 2, 585.

[6] F.Bottiglioni, J.Coutant, M.Fois, Phys.Rev.A, 6, 1830(1972).

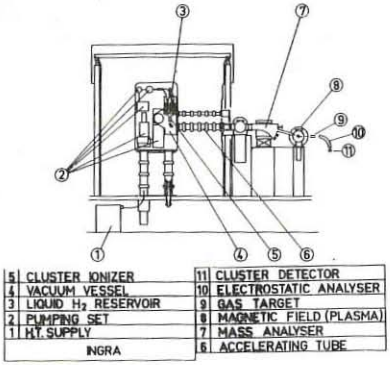


FIG.1

Fig.1 - INGRA apparatus. Schematic drawing.

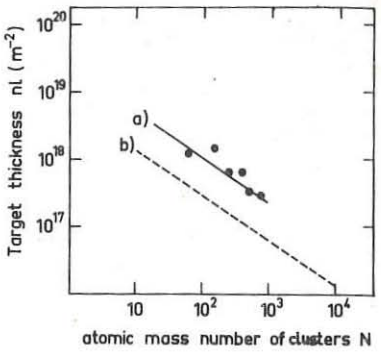


FIG.2

Fig.2 - $nl=1/\sigma_N$ versus N for charged cluster beam colliding with H_2. (a)experimental ; (b) computed with σ_N equal to the cluster geometrical cross-section

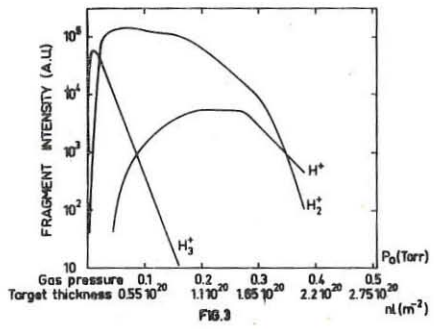


FIG.3

Fig.3 - Intensity of H_3^+, H_2^+, H^+ fragments versus nl of the H_2 target (or versus the pressure). Intensity is given by the counting rate of the scillation counter.

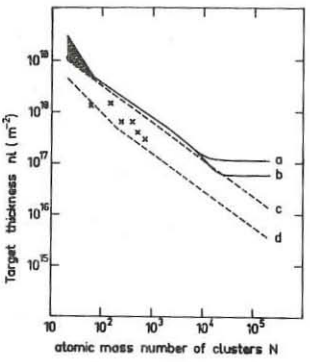


FIG.4

Fig.4 - nl versus N, for 1/e attenuation of a cluster beam :
-by evaporation - Cluster energy W_c=2 keV/atom (curve a) and 600 eV/atom (curve b).
-break up in collisions with H (curve c-Evaluated in paper/3/) and with electrons (curve d - W_E=1 keV, W_c=5 keV/atom).
Experimental points of Fig.1 are shown by crosses.

Plasma Buildup in Toroidal Reactors by Neutral Injection.

H.O. Falter, W. Henkes
Institut für Kernverfahrenstechnik, Kernforschungszentrum Karlsruhe
75 Karlsruhe, Germany

One of the more favorite methods currently in discussion for starting a fusion reactor is heating of a dense, relatively cold plasma by neutral injection. In order to penetrate to the plasma core the injected particles must have an energy of the order of 1 MeV. The efficiency for the production of neutral particles in this energy range is known to be low. To ameliorate the situation it has been proposed to heat a reactor plasma of lower density to be able to inject particles of lower energy.[1] This procedure is limited towards low plasma density n by energy losses that are not proportional to n^2, as for instance cyclotron radiation.

A different approach would be to start a fusion reactor by buildup of a high temperature, high density plasma on a tenuous trapping plasma by injection of neutral particles with an energy of the order of 10 keV.[2] The problem of penetration depth can be circumvented by producing a plasma of high density and small diameter near the magnetic axis and by adding layer after layer of high density plasma until the desired diameter is reached. This can be achieved by taking advantage of the geometrical properties of the confining field as schematicly shown by Fig. 1. A beam of neutral atoms is injected either normal (vertical injection) or tangential (parallel injection) to the magnetic axis. Particles trapped in an interval Δl of the beam trajectory inside a particular plasma layer are distributed evenly in its volume by the rotational transform. Because of the smaller volume of inside layers the plasma density will rise more rapidly near the magnetic axis than on the boundary of the plasma volume. Given sufficient injection current the density near the magnetic axis exponentiates until one or both of the two conditions occurs:

a. All of the injected beam is trapped, that is, the plasma becomes opaque with respect to the beam.
b. With rising density the gradient rises until, finally, diffusion towards the periphery limits the plasma density on the axis.

In this paper we calculate the buildup of plasma in a confinement field with the dimension of the R-85 reactor.[3] We show that under the simplified assumptions used high density plasmas can be produced in the manner described

above. We do not consider energy transfer between ions and electrons, the effect of thermonuclear reactions, or the effect of injection on plasma stabilitiy.

The major radius of the torus is taken to be 550 cm, the minor radius 125 cm, the magnetic field 10 Tesla, the rotational transform at the plasma boundary $\iota = 0.1$. We subdivide the plasma volume in layers of thickness 0.5 cm (approximately twice the gyroradius of a T^+-ion of 10 keV). For reasons of simplicity we assume a filamentary neutral beam as in Fig. 1 which is either normal (vertical injection) or tangential (parallel injection) to the magnetic axis. We treat two cases of plasma diffusion, Pfirsch-Schlüter (PS) for electrons of $kT_e = 5.4$ eV and ions of $kT_i = 10$ keV, and Galeev-Sagdeev (GS) for $kT_e = kT_i = 10$ keV. The trapping cross section used, $\sigma = 2\ 10^{-16}$ cm^2, does not include ionization by electrons. Also trapping of high energy particles by charge exchange on cold, trapped ions is not included. For comparison we also use $\sigma = 10^{-16}$ cm^2 and $\sigma = 2\ 10^{-15}$ cm^2 [4].

Fig. 3 shows density profiles for some of the cases calculated. Parameter is the time elapsed from the start of injection. In all cases the plasma density on the axis grows quickly during the initial phase of buildup. After the plasma radius exceeds about 30-50 cm the central density does not change significantly and the calculation is discontinued. The last values of the central plasma density n_{pf} are listed in the following table:

Case No.	Diff. Coeff.	σ / 10^{-16} cm^2	I/A_o	Inj. Geom.	n_{pf} / 10^{13} cm^{-2}
1	PS	1	1000	vert	0.14
2	PS	1	1000	par	2.9
3	PS	2	1000	vert	0.38
4	PS	2	1000	par	2.7
5	PS	20	1000	vert	1.8
6	GS	1	1000	par	41
7	GS	2	1000	par	28
8	GS	2	1000	vert	56
9	GS	2	100	par	19
10	GS	20	1000	vert	23
11	GS	20	1000	par	25

For all PS-cases the plasma density obtained is lower by at least one order of magnitude compared with the that of the GS-cases. The plasma density rises with the trapping cross section σ and the injected current I. For parallel injection the trapping lengths are longer, particularly near the magnetic axis, leading to a higher plasma density.

In all GS-cases the central density quickly reaches a high value because of the lower diffusion coefficient and all beam particles are being trapped when the plasma radius exceeds a few cm. Therefore the influence of σ and the injection geometry is less pronounced. It acts in the opposite sense as with PS-diffusion, that is, a high trapping cross section and parallel injection result in a lower plasma density. This can be explained by the fact that with a small cross section and vertical injection the injected particles penetrate into deeper layers. For a given density the gradient becomes smaller, or, conversely, a higher density is required to drive the diffusion current.

The dependence of the plasma radius on time is plotted in Fig. 6. In all cases, where most of the beam is beeing trapped, that is for high nr_p - values, $r \propto t^{1/2}$. For small nr_p, as in some PS-cases (e.g. case 3), the trapped fraction of the beam is $\propto r_p$ and we have $r_p \propto t$.

So far we have made no calculation with a beam of finite diameter. In the GS-cases no strong influence of the beam diameter is to be expected, as long as it is small compared with the final plasma radius.

We have shown that the filling of a reactor can be achieved in principle by vertical as well as parallel injection with a power of 1-10 MW provided some additional heating mechanism supplies energy to the electrons to insure GS-diffusion.

We are grateful to Prof. E.W. Becker for his continued interest throughout this work.

---

1) T.H. Stix, Plasma Physics 14, 367 (1971)

2) Plasma buildup in smaller, experimentell devices has been discussed by several authors, e.g.:
A.H. Futch, C.C. Damm, Plasma Physics 9, 423 (1967)
M. Fumelli, J.P. Girard, Gourdon, Eur-CEA-FC-432 (1967)
R.H. Bickerton, Drogmann, Nuclear Fusion 6, 287 (1966)

3) R. Carruthers, P.A. Davenport, J.T.D. Mitchell, CLM-R85

4) A trapping cross section of 2.8 10^{-15} cm^2 has ben reported for the Phoenix II-experiment.
E. Thompson, D.R. Sweetman, E.G. Murphy, M.J. Church Proc. of the IV europ. Conf. on Contr. Fusion and Plasma Phys. 85, (1970)

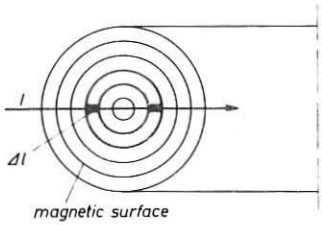


Fig. 1: Schematic of vertical Injection.

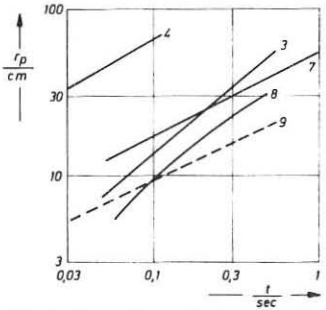


Fig. 2: Dependence of plasma radius on time. The numbers refer to cases.

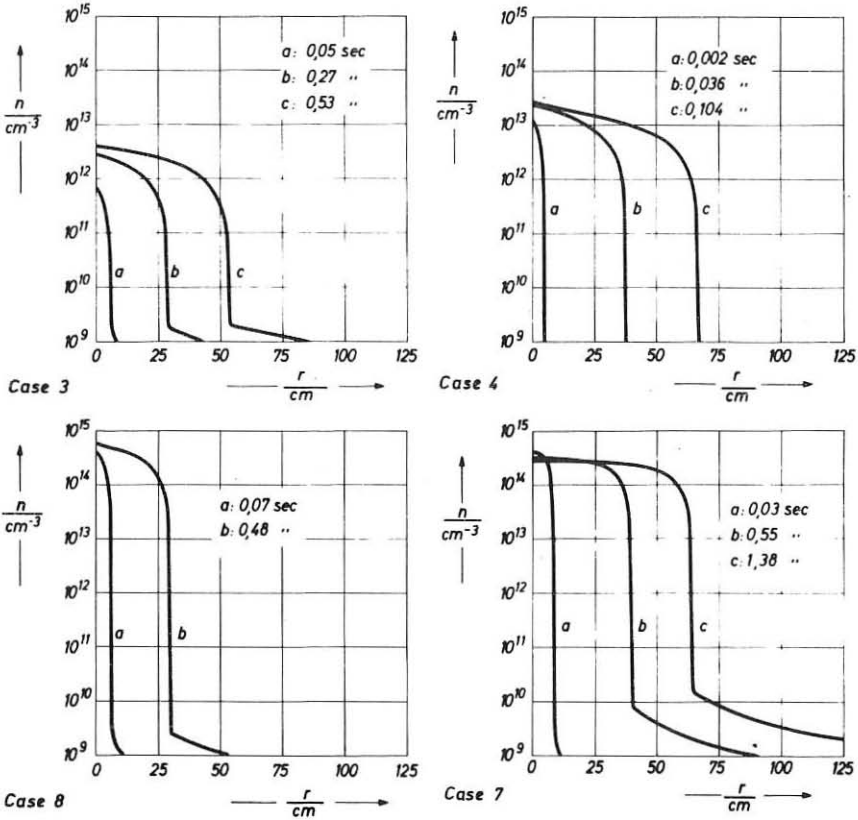


Fig. 3: Radial distribution of plasma density as function of time.

PRODUCTION OF A QUASI STEADY-STATE HIGH DENSITY MIRROR PLASMA

J.Jacquinot, C. Leloup, J.P. Poffé, M. de Prétis

ASSOCIATION EURATOM-CEA SUR LA FUSION
Département de Physique du Plasma et de la Fusion Contrôlée
Centre d'Etudes Nucléaires
Boite Postale n° 6. 92260 FONTENAY-AUX-ROSES (FRANCE)

ABSTRACT

A fast sustained thetapinch discharge as developed in the Bille en Tête experiment is envisaged as a target plasma for neutral beam injection in a mirror machine. Calculations and experimental results are presented.

I - INTRODUCTION

Encouraging results on the stability of mirror confined free decaying plasmas [1,2] at ε values relevant to reactor conditions ($\varepsilon=\omega_{pi}^2/\omega_{ci}^2 \gtrsim 10^3$) need confirmation in a quasi stationary regime. Several ways of creating the needed plasma have been suggested, all using fast neutral injection and avoiding the instability due to the monochromaticity of the beam : programmed build up [3] multi-energy and multi-angle injection [4] hot electron target plasma [5]. We examine here a fourth method based on fast neutral injection into a hot ion plasma target created by pulse technique; we will present an experimental study of the plasma production aiming at the obtention of a suitable target plasma and a numerical study of the fast neutral injection by the Fokker Planck equation. In this work the conditions are different from [3] and include the charge exchange between fast atoms and target ions ; the parameters are optimized to avoid the instability due to double-humped distribution function when injection is used also to increase the plasma mean energy.

II - EXPERIMENTAL RESULTS ON BILLE EN TETE MB

Recent operation of the device at a magnetic field level increased by a factor 2 ($B_o \simeq 4$kGs) yields, for the same value of the induced azimuthal electric field (E≃500 V/cm), the production of a

plasma with unchanged characteristics ($n_i = 5\times10^{11}$ cm^{-3}, $\langle E_i \rangle \simeq 2.5$ keV). This result is compatible with heating by current driven electron-ion instabilities, insensitive to magnetic field level and depending mainly on the value of applied electric fields. However, operation at 4 kGs level allows improvement in the shape of the confined ion distribution function f(E) : formerly truncated at ≃ 5 keV [2] it exhibits now a monotonically decreasing exponential behaviour (Fig. 1, curve a). This improvement is likely the consequence of the extension to higher energies of the domain of adiabatic confinement. The confined spectrum agrees with observations by other authors [6] made immediately after heating.

III - EVOLUTION OF PLASMA PARAMETERS DURING INJECTION

Using the J. Killeen and K. Marx's code [7] we studied the solution of the two dimensional time-dependent Fokker-Planck equations. We consider the evolution of an initial target plasma created in a magnetic mirror configuration and into which energetic neutral hydrogen atoms are injected in such a way that a quasi-static plasma density could be obtained. Effect of beam energy modulation and oblique injection are included. At the present state of calculations, the time dependence of the cross sections for ionisation and charge exchange of fast neutral is not taken into account. The model has been applied to a target plasma of $n = 5\times10^{11}$ cm^{-3} and with the experimental ion energy distribution function (Fig. 1, curve a) for a steady pressure of $H_2^\circ \simeq 2\times10^{-9}$ torr representative of the situation inside the plasma in burn out conditions. An example of the results for time evolution of n_i, $\langle E_i \rangle$, T_e, ambipolar potential ϕ and pressure anisotropy $p_\perp/p_{//}$ is represented in Fig. 2 ; cases a) and b) refer to conditions without and with injected beam respectively ; the beam energy E_b = 5 keV and the energy spread is 2.5 keV (FWHM) . Target plasma with mean energy of 5 keV, beam energy 10 keV and energy spread of 5 and 10 keV (FWHM) have also been examined. These calculations show that : i - the use of a beam energy about twice as large as the initial target plasma mean energy is acceptable. The ion distribution function can be maintained single peaked, but it is necessary to have an energy spread in the beam > 50 %. ii - In such a condition due to the fact that the charge

exchange cross section between fast neutrals and target ions is larger than the ionization cross section, the mean energy of the plasma increases up to almost the injection energy in a time shorter than τ_{ii} (0.2 to 0.5 τ_{ii} typically); the improvement in target plasma quality is rather fast and allows initial target plasma of moderate characteristics. iii - The anisotropy increase can be lowered using oblique injection. iv - The electron temperature is well inside the domain of maximum efficiency for ionization of fast neutrals.

IV - CONCLUSION

On the basis of the calculations discussed before and of the latest results in turbulent heating experiments, it seems now possible to produce and maintain a moderately dense plasma in a low magnetic field and in a relatively large volume ($n \simeq 10^{12} cm^{-3}$, 10 liters plasma volume, $\langle E_i \rangle \simeq$ 2 to 5 keV initially, $B_o \simeq$ 5 to 8 kGs in a Yin Yang magnet encompassing a volume of 1 cubic meter). To make the plasma sufficiently gas-free an axial separation between the heating zone and the target plasma is needed. Studies on a fast transfer of heated plasma through a vacuum-tight fast shutter have been undertaken. The recent improvements in beam intensity and energy modulation could provide the fast neutral beam required (E_b = 5 to 10 keV, I ≃ 6 Amps, $\Delta E/E_b \simeq 50$ %). In such a plasma the normalized density ε will be high enough (ε ≃ 360) to be well within the instability domain representative of the reactor conditions ; in particular the characteristic plasma length would be such that stability domain against all oblique modes would be accessible. The analysis of stability of a plasma representative of reactor conditions over times much larger than τ_{ii} should thus be possible.

REFERENCES

[1] F.H.Coensgen et al., Vth Eur.Conf.(Grenoble 1972) Vol.II, 71 ; D.Launois et al., ibid, Vol.I, 83.

[2] J.Jacquinot et al., Madison Conf.(IAEA Vienna 1971) Vol.II, 595.

[3] K.H.Berkner et al., ibid, Vol.II, 707.

[4] R.Dei Cas and F.Hennion, IVth Eur.Conf.(Rome 1970) 95.

[5] W.B.Ard et al., Madison Conf.(IAEA Vienna 1971)Vol.II,619.

/6/ E.K.Zavoiskii et al., Madison Conf.(IAEA Vienna 1971) Vol.II, 3 ; S.M.Hamberger et al., ibid. Vol.II, 37 ; D.S.Prono and C.B.Wharton, Plasma Physics 15,253(1973).

/7/ J.Killeen, K.D.Marx, Methods in computational Physics 9, Academic Press, New York (1970) 461.

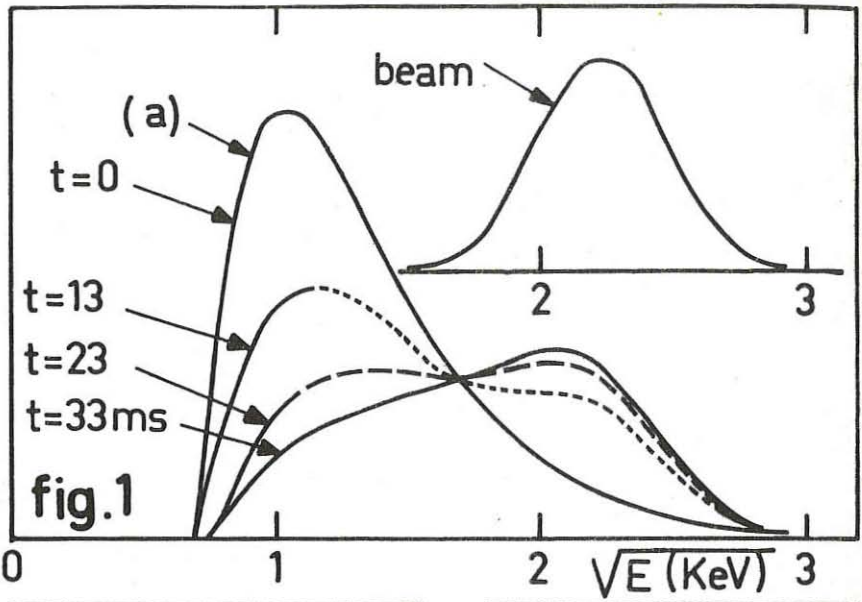


fig.1

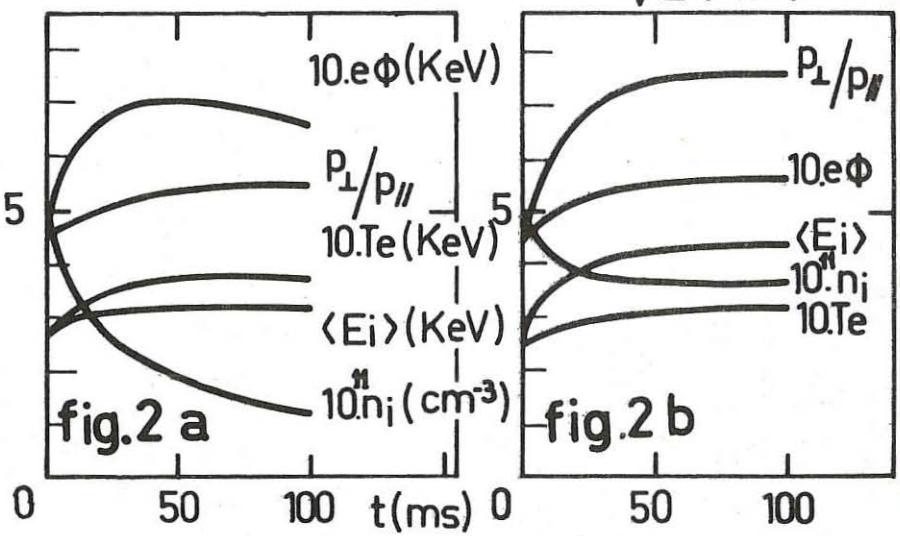


fig.2 a

fig.2 b

POLARIZATION PHENOMENA IN PLASMA INJECTED INTO A MAGNETIC TRAP

by

M.Sadowski, E.Składnik-Sadowska, K.Sudlitz, and A.D.Timofeyev[+]

Institute of Nuclear Research

Świerk k. Otwocka, Poland

Abstract: This paper reports experimental investigations of the electric polarization of a plasma stream injected into the spherical multipole /SM/ magnetic trap. Influence of small cusped regions surrounding the central minimum-B trap is also discussed.

Plasma injection is one of the most popular methods used for filling up of magnetic traps. During injection and trapping of plasma, polarization phenomena are often observed [1-3]. When a plasma stream is injected perpendicularly to the magnetic field lines, e.g. in an open-ended trap of cusp type [1] or in a closed trap of multipole type [2], polarization effects play an important role and decide practically about trapping of plasma. At plasma injection along the magnetic field lines, e.g. in the mirror trap, polarization phenomena manifest themselves less distinctly, but they are also of importance. The polarization effects are of particular importance when simultaneous injection of counter-streaming plasmas is realized, e.g. in the conventional cusp- or mirror-trap [1,3] or in the spherical multipole /SM/ configuration [4,5].

The high-order SM systems have been the subject of detailed investigations since they form true minimum-B traps having no linear loss-gaps, in contrary to the conventional cusped systems. The topology of high-order SM traps has been fully described elsewhere [5,6]. It has been shown that the SM trap in question has an effective confinement region surrounded by 30 small cusped regions which can be used for plasma injection. In the initial SM experiments [5, 7] plasma was produced by 6 coaxial guns spaced symmetrically around the spherical chamber. Since the injectors were placed close to the point cusps of the effective confinement region, the situation was analogous to that in the conventional cusp trap. Directed energy of plasmoids was partially randomized by collisions of counter-streaming plasmas [7]. The containment of plasma was however influenced by impurities and unionized gas coming from the injectors.

In order to eliminate an inflow of unionized gas the injector should be placed far from the experimental chamber. In such a system plasma has however to penetrate the magnetic field barrier of the external cusped region, and to pass through the low-field zone, and after that to pierce the actual point cusp of the effective confinement region. Such situation is shown in Fig.1, where only one symmetry plane of the SM trap is presented. The penetration of a plasma stream through the external magnetic field regions can influence polarization of plasmoids and conditions of trapping. In order to investigate this effect and to learn more about plasma trapping in the SM configuration, experimental studies on polarization phenomena have been undertaken.

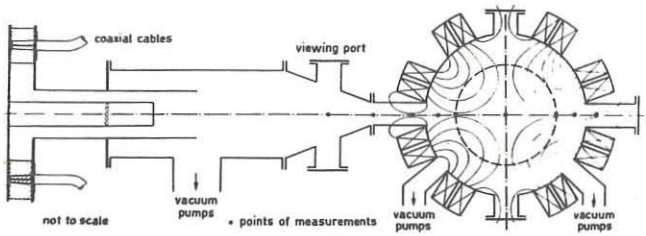


Fig.1.

In the measurements to be described, use was made of the "Kaktus" machine [6]. The experimental conditions, except for plasma injection, were practically identical as in the previous experiments with the SM trap [5,7]. In order to investigate a single plasma stream and to make possible measurements along the injection axis, only one coaxial gun was used. The outer diameter of the annular gap between the electrodes was 6.6 cm, and the inner diameter 3.3 cm. The outer electrode was 30 cm long, and the inner one was 5 cm shorter. Hydrogen was fed with the aid of an electromagnetic fast gas-valve placed within the inner electrode. To eliminate the inflow of unionized gas, the gun was situated at a distance of 80 cm from the trap's center, and equipped with an additional pumping stand. The gun was energized by a 4.6 μF, 30 kV, condenser bank. The discharge had an oscillatory character but was strongly damped. The current rose to the peak value of

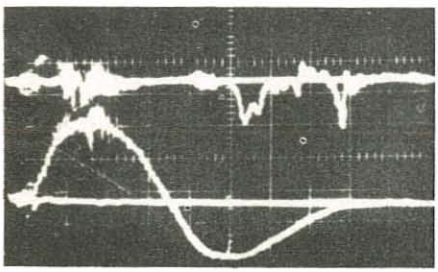


Fig.2.

about 50 kA in 2 μs. An attempt was made to operate the gun in such a way as to get clean hydrogen plasmoids of maximum density. The plasma concentration, as determined with Langmuir probes placed at a distance of 40 cm from the injector's outlet, amounted to some 10^{13} cm^{-3}, and the electron temperature - to about 8 eV. The velocity of plasmoids injected into the trap, as determined with magnetic probes, reached $5x10^6$ cm/s.

To measure axial electric field of plasma polarization, use was made of a coaxial double-probe similar to that used in the work [8]. The probe could be moved along the axis of plasma injection. A typical signal obtained with the probe placed close to the point cusp is presented in Fig.2, where the lower trace is the discharge current in the plasma gun. This oscillogram shows that under described experimental conditions there occur two distinct polarization peaks. On the basis of measurements carried out at different positions of the probe, a time shift of polarization signals /in relation to the current maximum/ has been determined. The results presented in Fig.3 show that the two polarization peaks are descended of the same plasmoid that propagates with the velocity of about $4x10^6$ cm/s. The first peak is probably connected with the plasmoid's portion in which protons prevail, and the second peak - with the portion in which other ions are in excess, as was shown by the previous measurements performed with a mass-energy analyzer [9].

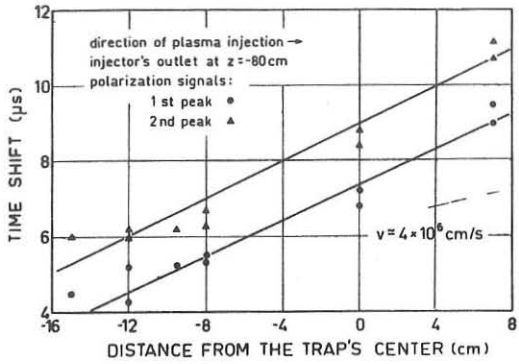


Fig.3.

The amplitudes of polarization signals have also been investigated. Because the measurements were, of necessity, taken on a shot-to-shot basis, and the system did not operate quite reproducibly, many shots have been performed and averaged in order to obtain mean experimental data. The results presented in Fig.4 show evidence of a weak dependence of axial polarization on the external magnetic field, although the decrease in polarization during plasma passing through the outer

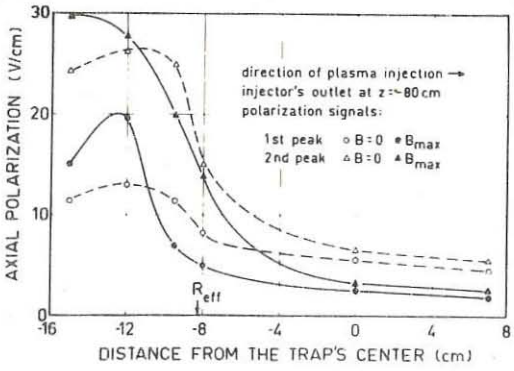


Fig.4.

cusped region is more distinct when the magnetic field is applied. It should also be noted that the amplitudes of the two polarization peaks are comparable and they behave in a similar way. The results of the experimental studies performed so far can be summarized as follows: Polarization measurements have demonstrated that a plasma stream is not trapped in the external low-field zone and can penetrate to the central confinement region of the investigated SM system. This is consistent with the results of the previous investigations [9]. On the other hand, the experimental results show that the plasma penetrating into the trap's center has remarkable polarization, and the magnetic field alone does not suffice for effective randomization. Therefore we are going to inject counter-streaming plasmas, as in the initial experiments [5,7], but with more efficient cleaning of plasma in the injection channels. To learn more about polarization phenomena in plasma injected into a magnetic field experiments have been undertaken on plasma injection through a magnetic channel with an uniform and/or weakly corrugated field. The most important question is how to utilize polarization and induction effects in order to reach effective injection and trapping. Studies on these subjects are being continued.

+ On leave from the Physico-Technical Institute, Kharkov, USSR

[1] V.G.Zykov et al., Zh. Tech. Fiz. 35, 1390 /1965/
[2] D.W.Kerst et al., Phys. Rev. Lett. 15, 396 /1965/
[3] P.F.Little et al., Plasma Phys. 12, 565 /1970/
[4] M.Sadowski, Phys. Lett. 25A, 695 /1967/; 27A, 435 /1968/
[5] M.Sadowski, Proc. 3rd European Conf./Utrecht 1969/, p.20
[6] M.Sadowski, Rev. Sci. Instrum. 40, 1545 /1969/
[7] M.Sadowski, J. Plasma Phys. 4, 1 /1970/
[8] D.V.Berezov et al., Zh. Tech. Fiz. 42, 1212 /1972/
[9] M.Sadowski et al., Proc. 5th European Conf./Grenoble 1972/, p.102

Plasma streams in inhomogeneous magnetic fields

Erik T. Karlson
Department of Plasma Physics
Royal Institute of Technology
S-100 44 Stockholm, Sweden

Abstract. The adiabatic motion of a finite plasma stream in an inhomogeneous, transverse magnetic field is studied theoretically. Some results are given also for the adiabatic motion of a finite plasma stream in a curved magnetic field.

Transverse field. The interaction of a plasma stream with a transverse magnetic field is of interest in many connections, such as the filling of magnetic bottles for fusion purposes, and separation of hydrogen plasma from impurities. Experiments have been performed by many investigators |1,2|, but no self-consistent theoretical treatment has been given. Our aim is to give such a treatment along the same lines as used previously for an infinite plasma stream |3,4|. The magnetic field is in the z-direction, and its magnitude is varying only with x. It is assumed that no quantities depend on z. The particle motion is adiabatic, and the magnetic field is not appreciably altered by the plasma currents. All ions are taken to have the same magnetic moment μ_i, and all the electrons the same magnetic moment μ_e.

From the equations of motion, we find through an expansion in m/e |3|:

$$\bar{v}_i = \frac{\bar{B}}{B^2\left|1+\frac{m_i}{eB^2}(\nabla^2\phi - B^{-1}\nabla B\cdot\nabla\phi)\right|} \times \nabla\left|\phi + \frac{\mu_i}{e}B + \frac{m_i}{2e}\left(\frac{\nabla\phi}{B}\right)^2\right| \qquad (1a)$$

for the ion velocity, whereas the electron velocity is

$$\bar{v}_e = \frac{\bar{B}}{B^2} \times \nabla\left|\phi - \frac{\mu_e}{e}B\right| \qquad (1b)$$

Using the continuity equations, and the condition of charge neutrality, we get an equation for the potential distribution

$$\nabla^2\phi - B^{-1}\frac{dB}{dx}\frac{\partial\phi}{\partial x} = 0 \qquad (2)$$

The boundary conditions are derived from the fact that the outermost trajectories for ions and electrons must (nearly) coincide. Thus

$$\phi + \frac{\mu_i}{e}B + \frac{m_i}{2e}\left(\frac{\nabla\phi}{B}\right)^2 = \text{const. on boundaries} \qquad (3a)$$

and

$$\phi - \frac{\mu_e}{e}B = \text{const. on boundaries} \qquad (3b)$$

Of course, the boundaries are not known until the solution is found, and thus it is not a trivial problem to solve Eq. (2) with the boundary conditions (3). However, if the width of the stream L_y is much smaller than the characteristic length L_x for the change in B, the problem can be solved by an expansion in $\varepsilon = (L_y/L_x)^2$. Taking the length units in the x- and y-directions as L_x, and L_y, respectively, and expanding

$$\phi(x,y) = \phi_o(x,y) + \varepsilon\phi_1(x,y) + \ldots$$

we find from the lowest order equations

$$\phi_o(x,y) = \phi_{oo}(x) - \frac{E_o L_y}{B_o}B(x)\left|1-\lambda\left(\frac{B}{B_o}-1\right)\right|^{1/2}y = \phi_{oo}(x) - f(x)y$$

Here B_o is the initial magnetic field, E_o is the initial electric field, and $\lambda = \dfrac{2(\mu_i+\mu_e)B_o^3}{m_i E_o^2}$ is the initial ratio between thermal energy and the energy in the ordered motion. The function $\phi_{oo}(x)$ is not determined by the lowest order equation. However, to next order we get a differential equation for ϕ_{oo}:

$$\phi''_{oo} - \left(\frac{B'}{B}+\frac{f'}{f}\right)\phi'_{oo} + \left|\left(\frac{f'}{f}\right)^2 - \frac{f''}{f} + \frac{B'f'}{Bf}\right|\left(\phi_{oo} - \frac{\mu_e}{e}(B-B_o)\right) = 0 \qquad (4)$$

and solving this, we get the potential distribution, and thus the behaviour of the stream is determined. Obviously, this depends strongly on the value of $\lambda(\frac{B_{max}}{B_o}-1)$ > 1, the stream is stopped completely). There is also another parameter, determining the behaviour of the stream, namely $\kappa=\frac{\mu_e B_o}{eE_o L_y}$. This is illustrated in Figs. 1 and 2, where we for the magnetic field

$$B(x) = \frac{B_o}{2} |n+1+(n-1)\tanh x|, \quad n=10$$

and for $\lambda=0.05$ give the shape of the stream, and the potential distribution, for two different values of κ, $\kappa=0.1$ (Fig. 1) and $\kappa=1$ (Fig. 2). We see that there is a contraction of the stream, in fact, the width is inversely proportional to $B|1-\lambda(B/B_o-1)|^{1/2}$. The equipotentials show that the electrons pass into regions with higher electrostatic potential. The potential change along the stream is in Fig. 1 of the same order as the potential difference across the stream, and there is a weak deflection of the stream, in the direction of the gradient drift for the ions. In Fig. 2,

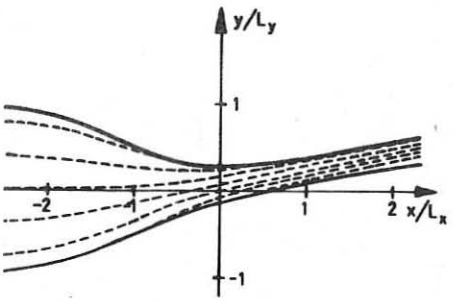


Fig. 1. The shape of the stream, and the equipotentials for $\lambda=0.05$, $\kappa=0.1$.

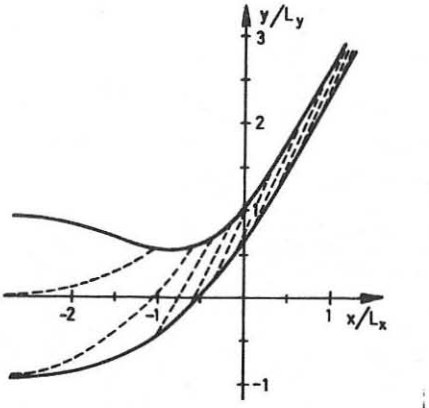


Fig. 2. The shape of the stream, and the equipotentials for $\lambda=0.05$, $\kappa=1$.

the deflection of the stream is much stronger, and the change in potential along the stream is much larger than the potential difference across the stream.

Curved field. The behaviour of a finite plasma stream in a curved magnetic field is studied by Lindberg and Kristoferson [5,6]. The plasma stream is injected along a longitudinal magnetic field into a region of curved magnetic field. The stream becomes deflected in the direction opposite to that in which the field is curved, and this deflection takes part also in the region of straight field. When entering the curved field, the stream contracts to a flat slab, with a sharp boundary on one side. We have started a theoretical treatment of such a situation, using a method similar to the one described above. Here, however, the existence of a longitudinal electric field is very important. For a 'simple' velocity distribution i.e. one where no particles move backwards, it is shown that in a curved field, a solution exists under certain conditions. A feature of this solution is that in parts of the stream the electron velocity is much higher than the ion velocity, and thus the situation is two-stream unstable. The instability leads to trapping of electrons, and it can be shown that there are stationary solutions with trapped particles, which give agreement with the results of the experiment.

References

1. Baker, D.A., and J.E. Hammel, Phys. Fluids 8, 713 (1965)
2. Demidenko, I.I., N.S. Lomino, V.O. Padalka, B.O. Saponov, and K.D. Sinelnikov, J. Nucl. Energy, C, Plasma Phys. 8, 433 (1966).
3. Karlson, E.T., Phys. Fluids 5, 476 (1962)
4. Karlson, E.T., Phys. Fluids 6, 708 (1963)
5. Lindberg, L., and L. Kristoferson, Cosmic Electrodyn. 2, 305 (1971)
6. Lindberg, L., and L. Kristoferson, Electron and Plasma Physics Res. Rep. TRITA-EPP-72-32 (1972).

PHYSICS OF TARGET PLASMAS IN MINIMUM-B GEOMETRIES*

W. B. Ard, R. J. Colchin, E. C. Crume, J. L. Dunlap
G. R. Haste, N. H. Lazar, and J. F. Lyon

Oak Ridge National Laboratory
Oak Ridge, Tennessee, U.S.A.

Abstract

Experiments with microwave-heated, hot-electron target plasmas in magnetic well geometry are described. Losses associated with (1) non-adiabaticity of energetic electrons and (2) instability resulting from high plasma anisotropy are identified. These result in the observed large radial density gradient.

This work with microwave-heated, hot-electron plasma is motivated by the expectation that such plasma can be developed to provide efficient targets for accumulation of a hot-ion plasma by energetic neutral injection. The intended application requires that the hot-electron plasma be established at low neutral gas density. These plasmas are unstable to flute modes at low pressure in simple magnetic mirror traps, and for this reason we have investigated properties of the plasma in magnetic well geometry.

We report experiments performed in the IMP facility, where superconducting mirror and quadrupole windings provide a variety of field configurations. The microwave sources have frequencies of 36 and 55 GHz. These are CW, each with a nominal power rating of 1 kW. The power at 36 GHz is used for resonant heating (resonant B = 12.5 kG) and that at 55 GHz for upper off-resonant heating. Our approach is to establish the plasma in a high mode cavity by application of the microwave power. Neutral density within the cavity is elevated above that of a surrounding vacuum chamber by a hydrogen gas leak. Plasma parameters are studied as a function of magnetic field configuration, H_2^o density within the cavity, and microwave power levels. Principal diagnostics include ionization current flow out along field lines, free-free bremsstrahlung, diamagnetic pickup coils for total stored $W_\perp$, faster coils for monitoring rapid changes in $W_\perp$, injected fast H^o beam, and calorimeters placed to measure plasma power to the walls.

Figure 1 shows a field configuration typical of those used in most of the experiments, which have involved resonant heating on closed magnetic surfaces. Indicated are the cavity outline, contours of constant $|B|$ (labeled by the ratio $|B|/B_o$), and field lines. Note that the contours with labels 1.1, 1.25, and 1.4 are the contours for the heating resonanace with B_o = 11.5, 10.0, and 9.0 kG, respectively.

*Research sponsored by the U.S. Atomic Energy Commission under contract with the Union Carbide Corporation.

Approximate radial profiles of $\int n_e d\ell$ can be obtained from the ionization current measurements. Examples are shown in Fig. 2 for the field configuration of Fig. 1. The experimental parameters ($n_0 = 10^{11}$ cm^{-3}, resonant power = 300 watts, off-resonant power = 500 watts) are near optimum for plasma generated on such closed magnetic contours.

In the region near the z axis, the measurements yield hot-electron line densities $\int n_e d\ell \approx 5 \times 10^{12}$ cm^{-2}, where the line length between resonant contours on axis is $\sim$ 12 cm in the case B_0 = 10 kG. This density figure is confirmed by measurements of trapping out of a fast H^0 beam, and is also consistent with measurements of the total stored energy ($\approx$ 10-15 J), mean hot-electron energy (500-700 keV), and estimates of mean plasma volume (100 cm^3) based on the radial profiles. The expected distribution of plasma along the central field line suggests peak densities of $n_e = 1 \times 10^{12}$ cm^{-3}, so the highest ratio of plasma density to ambient neutral density (n_e/n_0) is about 10.

The radial profiles indicate a non-uniform filling of the available magnetic volume (that is, the volume within the |B| contour for resonance). Possible explanations are that either the microwave power is not absorbed as efficiently at the larger radii, or the confinement of hot electrons is not as good in those regions. Since calorimetric measurments of power carried to the wall by the plasma show equal power density to be deposited in the plasma on and off axis, poor confinement is indicated.

Two mechanisms have been identified which can account for more rapid loss of energetic plasma in the outer regions: (a) non-adiabaticity of energetic electrons and (b) mirror instability caused by high anisotropy. Estimates of the effects of non-adiabaticity, based on the criterion that $1/\Omega^2 \, d\Omega/dt < C$, show electrons of energy greater than 4 MeV to be poorly confined even near the axis. The perpendicular field gradient increases with radius, and so confinement is expected to be poorer at larger radii. Anisotropy of confined plasma, and hence the possibility of loss due to mirror instability, also increases with radius in these magnetic fields. The |B| surface for resonant heating is also that for reflection of particles, so the mirroring field value does not vary with radius. However, the minimum field along flux lines increases with radius, and as a consequence the mirror ratio for confined particles approaches unity at the radial edge of the well. Plasma confined there is highly anisotropic and can become mirror unstable even at low β.

Evidence for non-adiabaticity is given in Fig. 3, which shows the electron distribution derived from bremsstrahlung data as a function of time in the plasma decay. The collimated line-of-sight was through the B_0 field point and was essentially in the median plane. The high energy cut-off for the steady state distribution is in good agreement with the calculated adiabatic limit for this central region. The most energetic electrons are observed to decay most rapidly in direct contradiction to the expected $\sim E^{3/2}$ dependence of lifetime. This rapid decay is presently interpreted as arising from classical scattering of these electrons into loss cones which are considerably larger for energetic electrons than for those of low energy. This "anomalous" loss cone arises from loss of adiabaticity of the very energetic particles as their parallel energy increases by scattering.

Signals which provide evidence for mirror instability (that is, a compression of the plasma configuration followed by a loss of stored energy) are observed with fast response magnetic pickup coils. Measurements of the power drain associated with these changes in stored energy indicate that the direct losses from this instability are much too low to effect the overall power balance. Although indirect effects on confinement (as, for example, electric fields leading to radial drift) are much more difficult to assess, our present feeling is that non-adiabaticity is the more dominant cause of poor confinement at larger radii.

The experiments detailed above dealt with plasma created by resonantly heating on a closed $|B|$ contour. We have also examined plasma in field configurations with less deep wells and the resonant contour an open one moved back into the coil throats. Only resonant power was available in such configurations. With this arrangement, the field lines linking the heating contours pass only through the central portion of the magnetic well. Stable plasma is formed with density comparable to that described above at significantly lower microwave power levels, with significantly higher n_e/n_o, more uniform radial profiles, and negligible power to a calorimeter just outside the column defined by the heating resonances. These observations reinforce our conclusion that plasma formed by resonance on closed magnetic contours exhibits poor confinement near the radial edges of the well. Further, since heating with the microwave fields did not cause drift of particles across surfaces of constant $J = \int p_z d\ell$ even with low $\partial J/\partial r$, the observations demonstrate that shallow magnetic well geometries can provide good confinement of these plasmas.

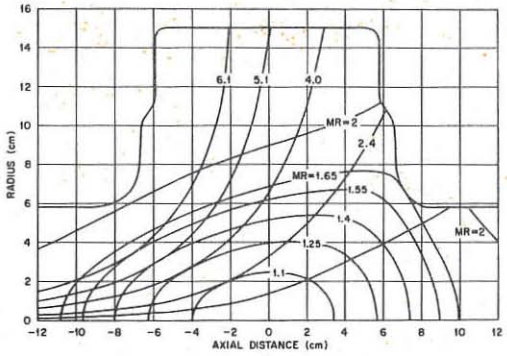


Figure 1

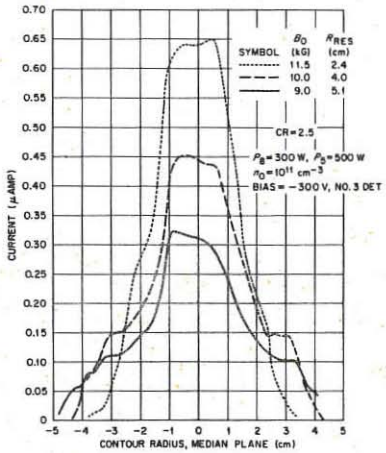


Figure 2

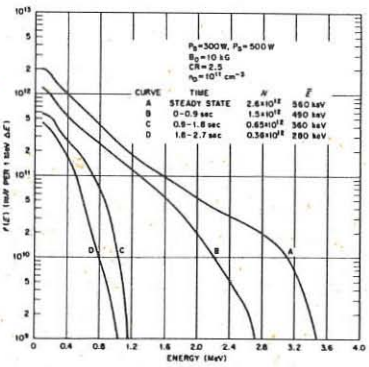
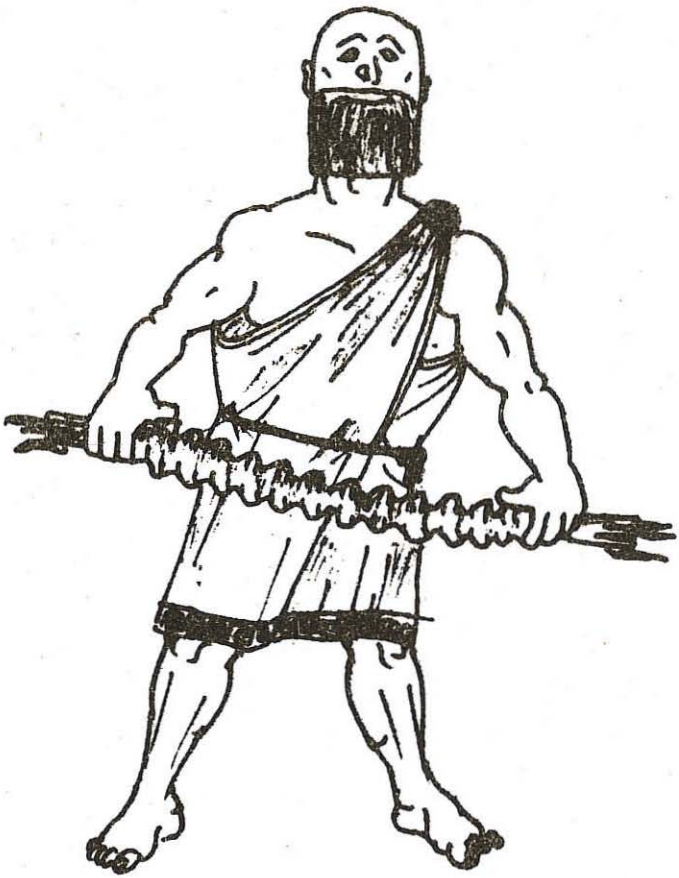


Figure 3

2.7. DENSE PLASMAS



ON HIGH-BETA PLASMA CONFINEMENT IN A POLOIDAL MAGNETIC FIELD

B. Lehnert, T. Hellsten and R. Raggi
ROYAL INSTITUTE OF TECHNOLOGY, S-10044 Stockholm 70, SWEDEN

Abstract. Equivalenta beta values as high as about 0.25 have been obtained in a fully ionized rotating plasma. The plasma boundary region is sharply defined and separated from the walls of a surrounding vessel, in a way consistent with a stable quasi-stationary state.

1. Introduction. Investigations on dense rotating plasmas are not merely limited to a special class of crossed-field gas discharges, but provide means for the study of important problems of general interest. The centrifugal force due to the rotation thus becomes equivalent to the large thermal pressure of more dilute and hot plasmas, at least in respect to some fundamental equilibrium and stability problems of high-beta systems [1]. This report extends earlier experiments [2] to higher densities and beta values, as well as to a further analysis of the plasma boundary region.

2. Experimental Arrangement. The experiments have been performed with device FI outlined in Fig.1 [2]. Two condenser banks are connected consecutively between the anode rings and the cathode plate to produce a fully ionized rotating hydrogen plasma in the magnetic field $\underline{B}$ within the shaded region of Fig. 1. The plasma which is surrounded by a neutral gas blanket of atom density n_{no} has the midplane ion density n_o in a quasi-steady state. It is separated from the blanket by a partially ionized boundary region of thickness x_b in the midplane (the "x_b-layer") [1]. The electrode voltage ϕ_{12}, which is nearly equal to the integral of $v_\varphi B$ in the range $r_{01}^* \leq r \leq r_{02}^*$ of the midplane, is recorded by means of a voltage divider. The azimuthal current density j_φ, which produces the force balancing the centrifugal pressure due to the rotational velocity v_φ, yields a total azimuthal current J_φ as measured by a Rogowski coil surrounding the plasma. Finally, the plasma boundary region is investigated by means of several types of single and double probes placed in the midplane and being movable in the radial direction. The probe signals are recorded by an oscilloscope connected across a resistance R_p forming part of the probe circuit.

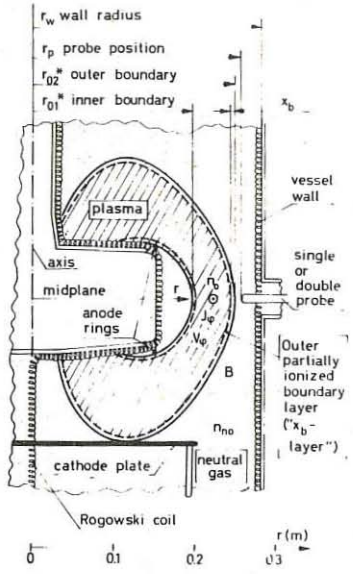


Fig. 1

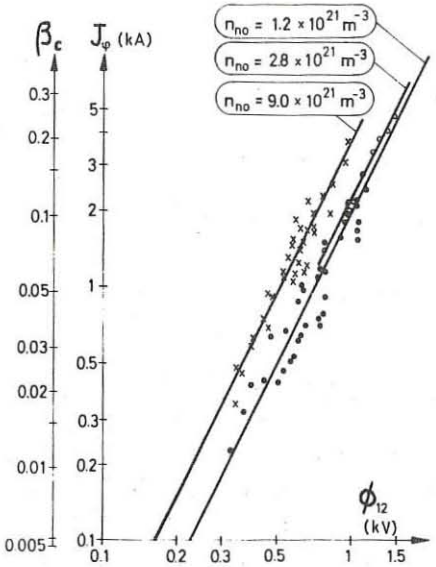


Fig. 2

3. Results and Discussion. All measurements have been made at a mean magnetic field strength $\langle B_o \rangle \simeq 0.41\ Vs/m^2$ in the midplane, and with the cathode plate at a distance $z_c = 0.17$ m from the same plane.

3.1. Rogowski Coil Measurements. At a power input smaller than a burnout power of the order of 3 MW [1,2], no measurable signal could be detected by the Rogowski coil. On the other hand, when exceeding the burnout power, large Rogowski signals $J_\varphi = \text{const.} \phi_{12}^2$ were observed, as shown by the sets of points in Fig.2 obtained at the neutral filling densities $n_{no} = 1.2 \times 10^{21} m^{-3}$, $2.8 \times 10^{21} m^{-3}$ and $9.0 \times 10^{21} m^{-3}$, with the associated densities of the fully ionized plasma ranging from about $n_o = 3 \times 10^{21}$ to $9 \times 10^{21} m^{-3}$. Both the slope of the corresponding lines in Fig.2 and their mutual separation distances agree with the theoretical model of a fully ionized quasi-stationary plasma which is surrounded by a neutral gas blanket [1]. The beta-value being equivalent to the centrifugal force becomes [3]

$$\beta_c \simeq 4\mu_o m_i \langle n_o \rangle \phi_{12}^2 f_\phi / \langle B_o^4 \rangle (r_{02}^{*2} - r_{01}^{*2}) \simeq 2\mu_o J_\varphi f_J / \langle B_o \rangle L_{II} \qquad (1)$$

where < > stands for a mean value formation in the midplane, μ_o is

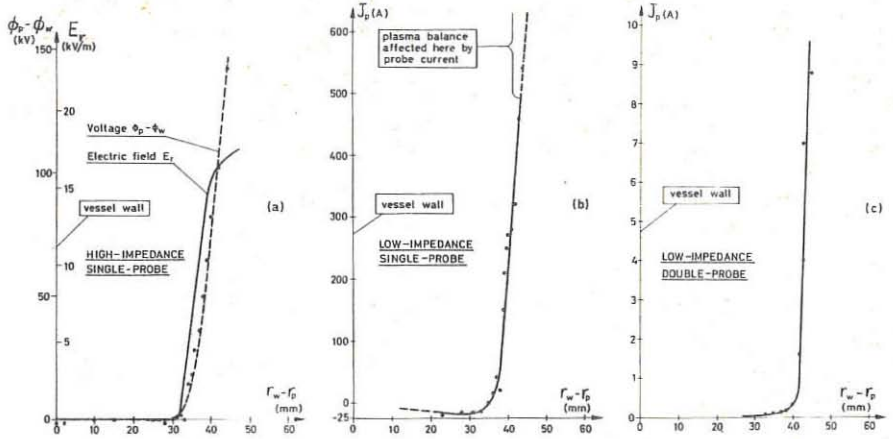


Fig. 3

the permeability, m_i the ion mass, r^*_{01} and r^*_{02} are the boundary positions in Fig.1, f_ϕ and F_J are dimensionless factors close to unity, and $L_{||}$ is the effective extension length of the plasma body along $\underline{B}$. From Fig.2 is seen that beta values have been reached being as high as about $\beta_c=0.25$.

3.2. Probe Measuremsets. The recorded probe signals become functions of the plasma particle density and energy, as well as of the electromotive forces produced in the probe circuit by the plasma and/or by externally applied voltage sources. Three types of probe measurements have been performed at $J_\varphi=4.2$ kA (Figs. 3a,b,c):

(i) Recordings by a high-impedance single-probe connected to the vessel wall through a resistance $R_p=5.6$ kΩ map the midplane distributions of the electrical potential and the radial electric field E_r (Fig. 3a). The dots refer to the difference between the local probe potential ϕ_p and the potential ϕ_w measured in the wall-near region. Figs. 1 and 3a show that the boundary conditions due to the present geometry result in a region with nearly zero electric field in the spacing between the vessel wall and the plasma, having the thickness of about 30 mm. This is to be expected because the rotational velocity $v_\varphi \simeq E_r/B$ has to become small in regions containing

noticeable amounts of neutral gas, and because such regions should extend from the gas blanket almost up to the inner edge of the x_b-layer.

(ii) A low-impedance single-probe with R_p=0.05 Ω records appreciable probe currents J_p when approaching the fully ionized plasma body in the radial direction (Fig.3b). When r_w-r_p exceeds about 45 mm, the recordings become uncertain since the probe begins to affect the plasma balance noticeably. Thus, Fig.3b shows that in the region r_w-$r_p \gtrsim$40 mm there must be both a fully ionized plasma of considerable density and a strong voltage source due to a non-zero electric field E_r. Further, in the region $0 \leq r_w - r_p \lesssim 35$ mm there are small negative signals J_p which can be explained by a negative floating potential.

(iii) With a low-impedance floating double-probe having R_p=0.05 Ω connected in series with an external dc source of voltage ϕ_p=12 V, steeply increasing currents J_p are obtained when approaching the plasma body (Fig.3c). The currents depend only on the density and energy of the plasma particles as well as on the externally applied voltage, i.e. they are not driven by the radial electric field. Thus, the increase in J_p shows that the plasma density and energy are much smaller in the wall-near region $0 \leq r_w - r_p \lesssim 40$ mm than in the interior of the plasma body.

(iv) All the probe measurements of Figs. 3a,b,c clearly show that the fully ionized plasma is separated from the vessel wall. However, the detailed spatial structure of the plasma boundary layer, as well as the induced magnetic field pattern, depend on β_c and the applied power input in a complicated manner which cannot be discussed here. It should only be added that radial displacements $\Delta r_{02} \simeq 0.01$ m have been observed as functions of J_φ for curves similar to those of Figs. 3a,b,c, roughly in agreement with the theoretically predicted "centrifugal expansion" value [3]

$$\Delta r_{02}/r_{02}^{*} \simeq \mu_o J_\varphi F/2\langle B_o \rangle L_{II} \qquad (2)$$

where $F \simeq 1$ is a dimensionless function of the distribution of j_φ.

[1] B. Lehnert, Nuclear Fusion 11(1971)485 and 8(1968)173.
[2] J. Bergström, S. Holmberg and B. Lehnert, Plasma Physics and Controlled Nuclear Fusion Research, IAEA, Vienna I(1966)341.
[3] B. Lehnert, Roy.Inst. of Technology, Stockholm, TRITA-EPP--72-28(1972).

THE DYNAMICS OF COOLING OF A DENSE WALL-CONFINED PLASMA

P.Z.Chebotaev, D.D.Ryutov, M.D.Spector, G.E.Vekstein

Institute of Nuclear Physics, Novosibirsk, USSR

The dynamics of heating and cooling of a dense wall-confined plasma is considered. The plasma containment time in this system is determined by means of numerical solution of hydrodynamic transport equations. The characteristic features of plasma nonmagnetic confinement are revealed, such as formation of a cold near-wall layer, plasma flow, great changes of density and magnetic field.

In traditional systems for confinement of plasmas with density $n\sim(10^{13}-10^{14})cm^{-3}$ the basic problem is to ensure a reliable isolation of plasma from container walls. This is possible, of course, only if $\beta\equiv 16\pi nT/H^2\leq 1$ (so called magnetic confinement). When passing to plasmas with $n\sim(10^{17}-10^{18})cm^{-3}$ and $T\sim 10^4 eV$, a magnetic confinement needs very strong magnetic fields of megagauss range, their creation being rather complicated problem. Therefore, the consideration of a possibility of dense plasma confinement by container walls seems to be important, because in this method magnetic field is necessary only for suppression of the transverse heat conduction, this can be attained at rather moderate magnetic fields, such that $\beta \gg 1$. The corresponding possibility has been noted by Sakharov /1/ and since that time has been mentioned by various authors.

The characteristic feature of the problem of high β plasma confinement by walls is that the plasma pressure is almost homogeneous over cross section, so that the condition $n\sim T^{-1}$ is valid. Thus, the region of a very high density should appear near walls. While cooling, the layers, adjoining this region, are being compressed, and the flow to walls arises in the volume of plasma. The presence of the

cold boundary layer results in the increase of the bremsstrahlung from plasma. Indeed, the radiation power per unit volume of plasma Q_{rad} is proportional to $n^2\sqrt{T}$, and provided $n \omega T^{-1}$, Q_{rad} increases as $T^{-3/2}$ towards boundary, that in principle can cause sharp growth of the bremsstrahlung role in comparision with the case of magnetic confinement. The stated circumstances (very wide range of density and temperature change over cross section, presence of plasma flow towards walls, uncertainty of bremsstrahlung intensity) make it difficult to estimate analitically the dense plasma containment time. Therefore, in the present article the problem of dense plasma cooling is solved numerically.

The plasma layer is considered, restricted by fixed perfectly conducting planes $x = \pm L$, their temperature is assumed to be constant. Magnetic field is parallel to walls. The power (per unit volume) of external heating sources is given by the formula:

$$Q(x,t) = W \cdot \frac{\exp[1-(x/L)^2]-1}{e-1} \cdot \frac{t \exp(-t/\Delta t)}{(\Delta t)^2}$$

(such dependence may simulate, for instance, plasma heating by a relativistic electron beam). Thermonuclear sources of heat are not included in the problem, because at present time, to our opinion, calculation of such model experiments is of interest, in which the maximum temperature is several times lower, than thermonuclear one.

Variables x, t, n, T, H, v are made dimensionless in accordance with:

$$x \to \frac{x}{L}, \quad t \to \frac{t\, 3L^2 e H_0 n_0}{cW}, \quad n \to \frac{n}{n_0}, \quad T \to \frac{T \cdot 3n_0}{W}$$

$$H \to \frac{H}{H_0}, \quad v \to v \frac{cW}{3L e H_0 n_0}$$

where n_0 and H_0 are initial values of density and magnetic field. Plasma transport equations across magnetic field /2/ are written in dimensionless variables as follows:

$$\varepsilon n \frac{dW}{dt} = -\frac{\partial}{\partial x}\left(nT + \frac{H^2}{\beta_0}\right) \qquad (1) \qquad \frac{dn}{dt} + n\frac{\partial v}{\partial x} = 0 \qquad (2)$$

$$\frac{d}{dt}\left(\frac{H}{n}\right) = \frac{4}{\beta_0 n}\frac{\partial}{\partial x}\left(\delta_0 \frac{H}{n}\frac{\partial H}{\partial x}\right) + \frac{1}{n}\frac{\partial}{\partial x}\left(\delta_1 \frac{\partial T}{\partial x}\right) \qquad (3)$$

$$n\frac{dT}{dt} - \frac{2}{3}T\frac{dn}{dt} = \frac{\partial}{\partial x}\left[\frac{nT}{H}\delta_2\frac{\partial T}{\partial x}\right] + \frac{4}{3\beta_0}\frac{\partial}{\partial x}\left(\delta_1 T\frac{\partial H}{\partial x}\right) + \frac{4}{3\beta_0}\frac{\partial H}{\partial x}\left[\frac{4\delta_0}{\beta_0 n}H\frac{\partial H}{\partial x} + \right.$$

$$\left. + \delta_1\frac{\partial T}{\partial x}\right] + \frac{t\exp(-t/\Delta t)}{(\Delta t)^2}\cdot\frac{\exp(1-x^2)-1}{e-1} - \alpha n^2\sqrt{T}\,\frac{(T-\gamma)^2}{\gamma^2+(T-\gamma)^2}$$

$$\beta_0 = \frac{16\pi W}{3H_0^2}, \quad \alpha = \frac{3L^2 e H_0 n_0}{cW\tau_{rad}}, \quad \varepsilon = \frac{c^2 WM}{6L^2 e^2 H_0^2 n_0}$$

Parameter ε characterizes the plasma inertia (in cases ofpractical importance $\varepsilon << 1$), and parameter α is equal to the ratio of Bohm's containment time to radiational cooling time. Quantity $\gamma << 1$is the dimensionless wall temperature. The factor $(T-\gamma)^2/[\gamma^2+(T-\gamma)^2]$ in the last term of the right hand of the equation (4) is introduced to take into account that plasma can not get cold down to temperature lower, than that of the wall. Parameter δ_0 is equal to $\frac{\nu_e}{\omega H_e}$ (ν_e is electron scattering frequency), and quantities δ_1 and δ_2 are proportional to the thermoforce and the heat conductivity. Their dependence on δ_0 is interpolated by the next formulas (see ref.[2]):

$$\delta_1 = \frac{3\delta_0}{2+4\delta_0^2}, \quad \delta_2 = \delta_0\left(\frac{1}{0{,}6+\delta_0^2} + \frac{1}{3\cdot 10^{-2}+37{,}5\,\delta_0^2}\right)$$

(in δ_2 the ion heat conductivity for deuterium plasma is also taken into account).

Owing to its symmetry the system (1-4) should be solved only in the interval $0 \le x \le 1$ with the following boundary conditions:

$$V_{x=0} = V_{x=1} = 0, \quad T_{|x=1} = \gamma, \quad \frac{\partial T}{\partial x}\Big|_{x=0} = \frac{\partial H}{\partial x}\Big|_{x=0} = 0$$

$$\left(\frac{4\delta_0}{\beta_0}H\frac{\partial H}{\partial x} + \delta_1 n\frac{\partial T}{\partial x}\right)\Big|_{x=1} = 0$$

As long as the plasma transport coefficients seem to be about of Bohm's, just this case is examined, which yields, roughly speaking, the lower estimate of containment time. In our designations it cor-

responds to $\delta_0=1$. Other parameters of the problem are chosen the following: $\varepsilon = 10^{-4}$; $\alpha = 10^{-1}$; $\Delta t = 0{,}3$; $\gamma = 10^{-3}$; (farther decrease of γ does not affect the nature of processes in the hot plasma region).

The basic results of the computation are illustrated by Fig. (1-3) and by the Table; the plasma containment time is rather well estimated by the Bohm's formula $\tau = \frac{l^2}{\mathcal{D}_B}$; $(\mathcal{D}_B = cT/eH)$ (inspite of the features of dense high β plasma, mentioned above).

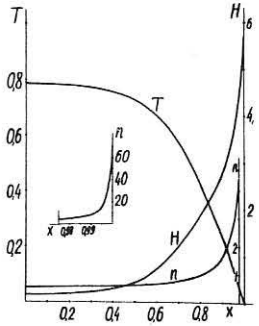


Fig.1. Profiles of n,T,H in the centre (x = 0) at the moment, when $T = T_{max}$ ($\beta_0 = 10^2$).

β_0	T_{max}	n_m	$\tau_{1/2}$
10^{-1}	0,698	0,58	1,6
1	0,706	0,58	1,7
10^2	0,79	0,54	1,7
10^3	0,75	0,43	2

T_{max} - maximum temperature at x = 0,
n_m - density at x = 0, when $T = T_{max}$
$\tau_{1/2}$ - cooling time from T_{max} to $\frac{1}{2} T_{max}$

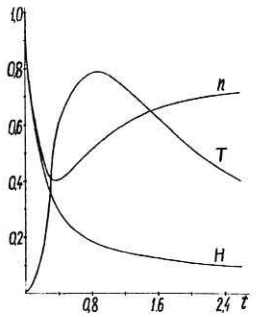


Fig.2. Time dependence of n,T,H at x = 0 ($\beta_0 = 10^2$).

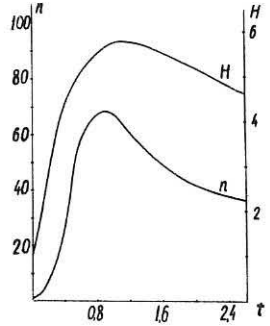


Fig.3. Time dependence of n and H at x = 1 ($\beta_0 = 10^2$).

References.

1. Sakharov A.D. In "Plasma Physics and Controlled Nuclear Fusion Research", V.1, p.29, M., 1958.
2. Braginskii S.I. In "Plasma Theory", V.1, p.183, M., 1963.

NONSTATIONARY EXPERIMENTS ON PLASMA CONFINEMENT IN MULTIPLE-MIRROR TRAP

V.V.Danilov, E.P.Kruglyakov, E.V. Shun'ko
Institute of Nuclear Physics, Novosibirsk, USSR

Abstract. A transient decay of alkaline plasma in multiple-mirror trap after abrupt cut-off of plasma flux was studied. The experimental results were found to be in a good agreement with existing theory of plasma confinement in multiple-mirror systems.

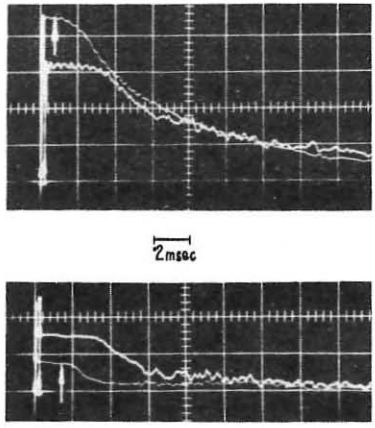


Fig.1
Time behaviour of plasma density at system outlet (n_L) and at the distance of 9 cells from last probe (n_9). Arrows indicate the moment of cut-off. Nonmarked oscilloscope traces are records of n_L.
a) Corrugated field: steady-state density ratio $n_9/n_L=2,3$.
b) Homogeneous field: $n_9^*/n_L^*=1$.
Values for homogeneous field are marked with *).

It was shown /1/ that longitudinal plasma confinement in the case $\lambda < L$ (λ-Coulomb mean free path, L - device length) may be essentially improved if a multiple-mirror trap is used. The theory /1/ was confirmed in experiments with steady-state plasma flux /2,3/. Experiments with abrupt cut-off of plasma flux enable to get additional data for comparison with theory. In described experiments 13 mirror cells of 16 cm length each were used. Maximum value of the magnetic field was 5400 Oe and mirror ratio was 1,83. Plasma was produced by contact ionization of cesium vapor on hot tangsten plate mounted on one of the device ends.

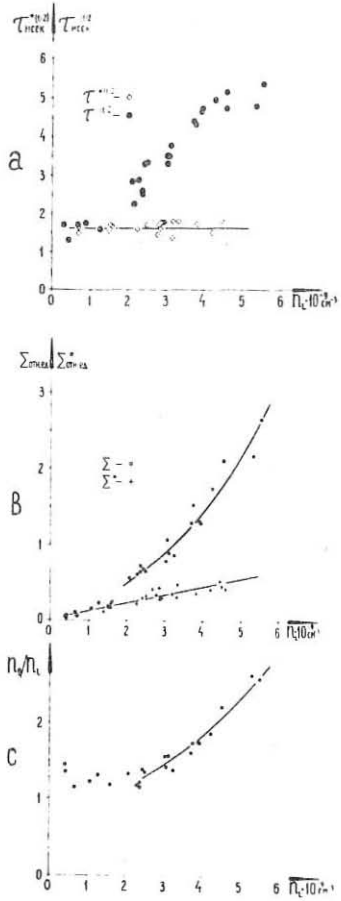


Fig.2

a) $\tau^{(1/2)}$ as a function of n_L in the last mirror cell.
b) the total number of particles in the axial magnetic tube, $\Sigma = \Sigma(n_L)$.
c) the treatment of the stationary parts of oscillograms. Density ratio n_e/n_L as a function of n_L

Measurement methods and the more detailed description of the device is presented in /4/. Oscillograms characterizing the time behaviour of plasma density in multiple-mirror (a) and homogeneous(b) magnetic configurations are given in Fig.1. Oscillograms treatment results obtained for several values of plasma density at the outlet of the device are given in Fig.2.

Plasma confinement may be characterized (Fig.2) by time $\tau^{(1/2)}$ during which concentration is decreased twice (the time is read from the moment when plasma flux is interrupted near ionizer). $\tau^{(1/2)}$ increase with density shows an improvement of the plasma confinement effectiveness with the ion mean free path λ decreasing.

Graphical integration of oscillograms enables to find value $\Sigma_{exp} = \int_{t_0}^{\infty} n_L(t)dt$ where t_0 is a moment when plasma flux is interrupted. With the absence of radial losses this value is proportional to the number of particles in a magnetic tube on the system axis (since plasma density n_L is proportional to the plasma flux at the device outlet).

In accordance with theory [1] the steady-state distribution of plasma density along the axis at $1 < \lambda < L$ must be as follows: $n(z) = n_L \cdot \exp(A \frac{z}{\lambda_L}) = n_L \cdot \exp[B(T_i) \cdot z \cdot n_L]$. Here z is the distance from the device outlet, $A \sim 1$. As it is seen from Fig.3 the density stationary destribution in the trap is really close to that predicted by the theory.

Using formula given above and carrying out integration along the whole length of the trap $L = N \cdot l$ one can calculate the number of particles stored in the same magnetic tube before the flux interruption $\Sigma_{theor} = C(T_i)\{ \exp[B(T_i) N \cdot l \cdot n_L] - 1 \}$.

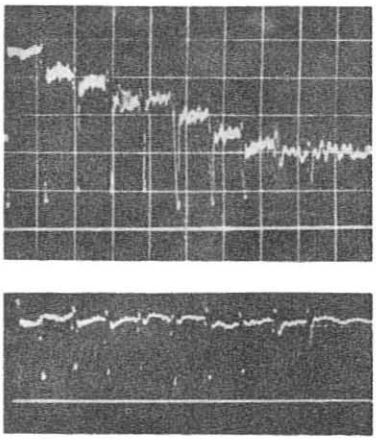


Fig.3
Stationary distribution of densities on the device axis in corrugated (a) and homogeneous (b) magnetic fields. The total mirror cell number is 14. Probes are fixed in the following mirror cells: №№ 3,4,5,6,7,8,9, 11,13,14. Ionizer is monted in cell №1.

Dependence $\Sigma_{theor}(n_L)$ is shown in Fig.2b (the solid curve) as the result of experimental points treatment with the least squares method. In the same Figure oscillograms treatment results are shown for homogeneous magnetic field to compare plasma confinement effects in corrugated and homogeneous fields.

Oscillograms treatment results for the stationary values of density just before the flux interruption are given in Fig.2c. Solid curve is an exponent drawn through the experimental points with the least squares method.

It is interesting to note

that in the region of low densities ($n_L < 2 \cdot 10^9 cm^{-3}$) where the collisionless plasma flowing is realized there is no density gradient along the device length and for this density region $\tau^{(1/2)} \approx \tau^{*(1/2)}$ as it is seen in Fig.2a.

Ion temperature value T_i found from the exponential power of the curve shown in Fig.2c (T_i = 0,46 eV) is in a good agreement with value calculated from data given in Fig.2b (T_i = 0,45 eV).

At transition from homogeneous to multiple-mirror magnetic field the confinement time $\tau^{(1/2)}$ increase more than 3 times was observed.

Experimental data obtained are in agreement with the theory of plasma confinement in a multiple-mirror trap not only qualitatively but to considerable extent quantitatively.

Authors are indebted to G.I.Budker and D.D.Ryutov for the encouragement and helpful discussions and to V.V.Mirnov for the interest to the work.

REFERENCES

1. Г.И.Будкер, В.В.Мирнов, Д.Д.Рютов. Письма в ЖЭТФ, 14, 320, (1971).
2. B.Grant Logan, I.G.Brown, M.A.Lieberman and A.J.Lichtenberg. Phys.Rev.Letters, 29, 1435, (1972).
3. Г.И.Будкер, В.В.Данилов, Э.П.Кругляков, Д.Д.Рютов, Е.В.Шунько. Письма в ЖЭТФ, 17, 117, (1973).
4. Г.И.Будкер, В.В.Данилов, Э.П.Кругляков, Д.Д.Рютов, Е.В.Шунько. ЖЭТФ (в печати).

NEUTRON PRODUCTION IN HIGH ENERGY-DENSITY EXPLODED-WIRE Z-PINCH PLASMAS

D. Mosher, L. S. Levine, S. J. Stephanakis, I. M. Vitkovitsky, and F. Young
Naval Research Laboratory, Washington, D. C. 20375 USA

ABSTRACT

A high power pulse generator has been used to produce hot, dense plasmas from the explosion of fine deuterated polyethylene fibers. Neutron yields from the plasma exceed 10^{11} when CD_2 coated electrodes are employed.

Recent experiments employing high power pulse generators to create high energy-density plasmas have used either exploded CD_2 fibers[1] or CD_2-bearing electrodes and targets[2] to produce D-D neutron yields of order 10^{10}. In the work presented here, we examine the effect of coating the electrodes with CD_2 in order to enhance the neutron yield and to elucidate the relevant neutron producing mechanisms in exploded fiber Z-pinch plasmas. Yields of D-D neutrons in excess of 10^{11} were produced routinely by this technique. We show that the bulk of these were produced by the interaction of plasma produced at the cathode with the exploded wire Z-pinch. Measurements are consistent with these neutrons having been produced by thermal fusion.

Natural and fully deuterated polyethylene fibers ranging in diameter from 1×10^{-3} to 1×10^{-2}cm were mounted in vacuo between the output electrodes of the Gamble II generator[3]. Electrodes were prepared by melting approximately 0.5 mm thick coatings of CD_2 on their surfaces. Typical current driven by the generator was 1.2 MA with peak voltages of about 0.6 MV across the plasma. The power pulses were about 5×10^{-8}sec in duration. Neutron yield and isotropy of emission were measured by delayed activation of Ag, Pb, and Rh; neutron energy measurements were made by determining the time of flight across a 15 m path[4]. The properties of neutron producing exploded fiber plasmas in the absence of CD_2 bearing electrodes have already been reported[1,4].

Table 1 summarizes the neutron yield measurements from exploded fiber plasmas incorporating CD_2 coated electrodes. Fibers labeled CH_2 contain the natural .015% abundance of deuterium. An open space in the Table, indicates an uncoated electrode. Scatter in neutron yields of about a factor of three are due primarily to variations in fiber diameter of about 25%.

TABLE 1

NEUTRON YIELD MEASUREMENTS FOR 2.5×10^{-3}cm DIAMETER FIBERS

	A	B	C	D	E	F
ANODE	-	CD_2	CD_2	-	-	-
FIBER	CD_2	CD_2	CD_2	CD_2	CH_2	CH_2
CATHODE	-	CD_2	-	CD_2	CD_2	-
YIELD	10^{10}	10^{11}	10^{10}	10^{11}	10^{10}	10^{9}

Columns A through D demonstrate that the neutron yield can be enhanced by an order of magnitude by coating the steel cathode with CD_2. Comparison of columns D and E show that the increased yield is not due primarily to high energy deuterons from the exploded fiber plasma entering the CD_2 cathode coating. If this were the case, the disparity would be more than an order of magnitude. On the other hand, since these two yields are different, the higher yields with deuterated cathode must depend on the presence of deuterium in the Z-pinch plasma channel. It is therefore believed that the enhanced neutron yield arises from the interaction of plasma produced at the cathode with the exploded CD_2 fiber Z-pinch. The yield associated with the configuration of column E is believed to be due to the cathode plasma alone.

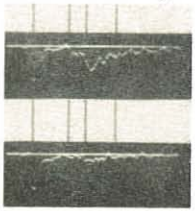
Figure 1 shows neutron time of flight oscilloscope traces for the configurations described by columns D and E. The leading edge of the large neutron pulse is delayed with respect to the X-ray pulse by a time consistent with the time of flight of 2.45 MeV D-D fusion neutrons. The measured neutron energy, however, has an uncertainty of about 300 keV if it is assumed that neutrons can be created at any time during which X-radiation is emitted. Also shown are a few neutrons with energies significantly higher than 2.5 MeV, indicating the existence of deuterons with energies of the order of 1-3 MeV*. The broad tail of the neutron pulse is associated with scattering within the time of flight detector.

*Higher energy neutrons are most likely created in the body of the Z-pinch plasma since they have been observed in similar quantities when uncoated electrodes are used with CD_2 fibers of small diameter ($\leq 2.5 \times 10^{-3}$cm). Of the order of 100Amperes of $\geq$1 MeV deuterons are required in the plasma channel to produce observed yields of higher energy neutrons[4]. Neutron yields of about 10^7 with energies of the order of 10 MeV have been recorded by time of flight traces.

Lack of certainty in neutron energy allows for the possibility that thermonuclear-like neutrons were produced by deuterons accelerated to 100-300 keV energies in the Z-pinch plasma. An upper limit on the yield of such neutrons can be determined by assuming that the maximum current of ions which can flow in the plasma is down from the electron current by the square root of their mass ratio. This scaling is consistent with ions accelerated towards the cathode by the applied electric field. Maximum deuteron current obtained in this fashion is about 1×10^4A. Neutron yields associated with these currents are less than 1×10^{10} and are therefore inadequate to account for the high yields observed. If collective processes stimulated by microinstabilities created the 10^5A current of deuterons required to account for the observed yields, enhanced neutron production would be expected when the anode was coated with CD_2. This was not observed.

FIGURE I

NEUTRON TIME-OF-FLIGHT TRACES
CD_2 ON STEEL CATHODE



Neutron isotropy measurements performed on the high yield configuration shots support the assumption of the thermonuclear origin of the bulk of neutrons since emission is isotropic to within the 10% accuracy of our measurements.

REFERENCES

1. S. J. Stephanakis, L. S. Levine, D. Mosher, I. M. Vitkovitsky, and F. Young, Phys. Rev. Letters 29, 568 (1972).
2. B. Freeman, et al., Bull. Am. Phys. Soc. 17, 1030 (1972).
3. L. S. Levine and I. M. Vitkovitsky, IEEE Trans. Nucl. Sci. 18, 225 (1971).
4. F. Young, S. J. Stephanakis, I. M. Vitkovitsky, and D. Mosher, IEEE Trans. Nucl. Sci. 20, 439 (1973).

Kiel experiments of electrically exploded liquids containing deuterium

U. Fischer, H. Jäger, and W. Lochte-Holtgreven

At Kiel we have exploded capillaries filled with saturated solutions of lithium dissolved in heavy ammonia. This solution contains about 70 atomic percent deuterium and has metallic conductivity, comparable to that of mercury. If high current pulses are sent through the capillaries the phenomena resemble to the explosive evaporation of thin wires, well known from the blowing of fuses. Discharging a condenser bank through the capillary, we observe the emission of neutrons. In case of identical experiments but using ordinary ammonia instead of heavy ammonia, no neutrons could be detected.

During the first stages of evaporation the resistance of the liquid raises sharply to several kilohms. In case simple condenser discharges are used, the charge potential should be as high as possible for to obtain high energy input during the initial time interval of heating. The inductivity of the circuit needs not to be extremely low.

In our experiments the capacity was 5 μF and the maximum charge potential 200 kV. The ringing frequency of the circuit was 4 to 6 μsec depending on the dimensions of the discharge vessels. The later, made from aluminum had cylindrical shapes containing the capillary at the axis. Glass capillaries of 3 to 7 cm in length and 0,3 to 0,8 mm inner diameter were used. To prevent sliding discharges along the surface of the capillary the filling pressure of the vessel was increased to about 15 atm (N_2). The neutrons were detected from 6 scintillation counters

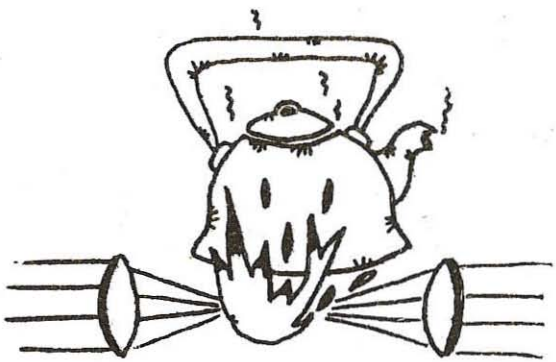
arranged in a circle around the discharge vessel.

The duration of neutron emission is relatively short. The bursts lasted for 10 to 50 nsec and occured right at the begin, i.e. about 50 to 100 nsec after start of the ignition. Preliminary calibration showed 10^5 neutrons in the burst when the capacitor was charged to 100 kV. The number of neutrons is increased with higher charge potentials. Occasionally single neutrons could be observed at later times, when the capillary is destroyed and a spark discharge through the evaporated liquid of decreased density takes place. These neutrons seem to be stray neutrons from the metallic parts of the installation. No X-ray emission could be detected.

At the time of neutron emission the density within the capillary is at least 10^{22} particles per cm^3. The pressure is highly increased because of the heating and is counteracted by the pinch-forces and the inertia of the capillary. Taking into account all data available, pressures of about 10^5 atm have been estimated for regions near the axis.

The origin of the neutrons is not clear. The energy dissipated in the liquid when the neutrons appear is not sufficient, to heat the total volume of the capillary to fusion temperatures. On the other hand, in view of the densities mentioned above accelerations of deuterium particles by electrical fields sufficient for production of the neutrons appear to be improbable. Up to the time of neutron emission and even later, instabilities could not be observed using optical and X-ray pulse techniques. It seems possible that shock waves play an important part in the production of locally restricted small areas of extremely high density and temperature suited for production of neutrons in the plasma.

3.1. LASERS IN FUSION



Sixth European Conference on Controlled Fusion and Plasma Physics
Moscow, USSR. 30 July - 3 August 1973.

X-RAY SPECTROSCOPY OF THE ION POPULATION IN THE PLASMA PRODUCED AT THE SURFACE OF A PLANE MASSIVE TARGET BY INTENSE LASER IRRADIATION.

M Galanti† N J Peacock

UKAEA Culham Laboratory, Abingdon, Berkshire, England.

†ESRO Research Fellow.

ABSTRACT.

Plasma produced at the surface of a $(CH_2)_n$ target irradiated by a 1.06 μm Nd laser with flux density up to 10^{12} Watts/cm^2 has been the subject of quantitative X-ray spectroscopic measurements. Electron temperatures up to 200 eV, and a mean electron density of 4.10^{20} cm^{-3} within 100 μm from the target surface, have been measured from the spectral intensity of the recombination continuum into C^{6+} and C^{5+} ions.

INTRODUCTION. The temperature and density of a plasma produced by focusing an intense laser beam onto a plane thick target are rapidly varying functions of the distance from the target. The ions in the hot region exist for less than a nano-second. Within a few tens of microns from the target surface the plasma density drops by more than an order of magnitude. In order to obtain quantitative information on the structure of the plasma layer close to the target surface we carried out absolute intensity spectroscopic measurements in a region a few tens of microns from the target surface. The plasma electron temperature and density are measured by the continuum emission using an intensity calibrated X-ray grazing incidence spectrograph. Ratios of ion populations are measured and compared with ratios calculated on a steady state model using the measured plasma electron temperature and density. A consistent value of the product of the ion inertial confinement time and density, $n\tau$, is thus derived. The experiment has been performed with flux densities ranging from 10^{11}-10^{12} watts/cm^2 and is being extended into the region 10^{12}-10^{14} watts/cm^2.

The measurement of the electron temperature from the spectral shape of the continuum as recorded by an intensity calibrated X-ray spectrograph is likely to be more accurate than that derived using absorber foils, the latter technique sometimes giving a range of values dependent on the absorber foil thickness [1].

EXPERIMENTAL APPARATUS. The high powered Nd laser used gives a peak power of 4 Gigawatt with a 4 nanosecond pulse width produced by operating the oscillator stage in a pulse transmission mode. In the present experiment a f/3 10 cm lens is used giving a focus spot size of 300 μm. A f/5 two element lens system has also been used giving a focus spot less than 100 μm. The focus size is determined

from X-ray pinhole pictures. The laser beam is focused in vacuum onto a massive target 5 mm from the horizontal entrance slit of a 2-metre grazing incidence spectrograph intensity calibrated over the range 5 Å-45 Å [2]. The radiation from the plasma transmitted by the horizontal slit, is stopped down by a 100 μm vertical slit placed half way between the entrance slit and the pole of the grating. This enables the spectrum to be space resolved orthogonal to the dispersion. X-ray pinhole pictures with a 50 μm resolution have been taken to give an overall picture of the plasma.

TEMPERATURE AND DENSITY MEASUREMENT. The plasma region within 100 μm from the irradiated $(CH_2)_n$ target surface is characterized by an intense continuum due to free-bound recombination into C^{6+} and C^{5+} ions. The free-bound continuum frequency and temperature dependence is [3].

$$\frac{d\,E_{f,b}}{d\nu} = C\,\frac{N_e\,N_{z+1}\,Z^4\,e^{-(h\nu-X_z)/k\,T_e}}{(k\,T_e)^{3/2}}$$

where C is a constant and X_z is the ionization potential of the ion of charge Z. The fall off in the C^{6+} and C^{5+} free bound continuum (Fig.1) is in good agreement

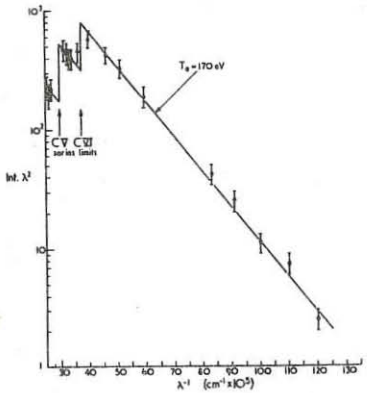


Fig.1

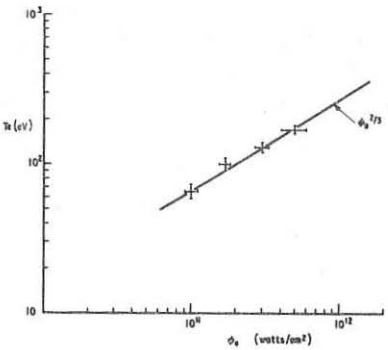


Fig.2

with a thermal energy electron distribution. The spectral range of the free bound continuum and thus the temperature, increases with increasing laser flux. Fig.2 illustrates this experimental dependence.

$$T_e\ (eV) = 2.9\ (\pm\ 0.4)\ 10^{-6}\ \phi^{2/3}(Watts/cm^2)\ .$$

The absolute level of the continuum gives the electron density. The average density within a layer 100 μm from the target measured in this way is

$$N_e = 4.0\ (\pm\ 3.0)\ 10^{20}/cm^3\ .$$

From the limited number of lines of the Lyman series that can be resolved from the continuum, within 10 microns from the target surface, the density is estimated to be greater than $10^{21} cm^{-3}$ [4].

ION CONFINEMENT TIME. The ratio of the relative free bound continuum of C^{6+} and C^{5+} ions gives the ratio $R = N_C 6+/N_C 5+$ of the ion population. This ratio (fig.3) has been compared with the value, R_s, given by a steady state model. The value of $n\tau$ can be derived from:

$$\frac{R}{R_S} = \left(1 - e^{-\frac{n\tau}{(nt)_s}}\right)$$

where $(nt)_s$ corresponds to the steady state. The experimental dependence of $n\tau$ on the temperature is shown in fig.4.

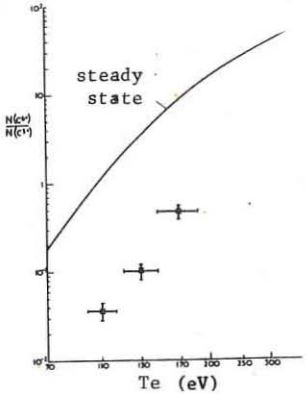


Fig.3

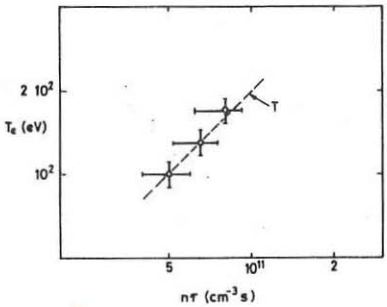


Fig.4

Fig.5 shows the satellite lines of CV that appear within 100 μm from the target surface, $1s^2\ 2s\ ^2S - 1s\ 2p\ (^1P)\ 2s\ ^2P^o$, $1s^2\ 2p\ ^2P - 1s\ 2p^2\ ^2D$ and $1s^2\ 2p\ ^2P - 1s\ 2p^2\ ^2P^e$. The first two lines are due to dielectronic recombination into the He-like ions. The third line is due to direct ionization from the ground state of the Li-like ions [5]. The intensity ratio of the last line to the other two gives therefore the relative ion population N_{He}/N_{Li}. The comparison of this experimental ratio with that calculated on the steady state model gives, for T_e = 170 eV,

$$n\tau \sim 5.10^{10} cm^{-3} \text{ sec} .$$

This is in reasonable agreement with the values obtained from the ratio $N_C 6+/N_C 5+$.

CONCLUSIONS. Analysis of the results indicates:

1. The region within 100 μm from a $(CH_2)_n$ target irradiated by an intense laser beam is characterised by an intense continuum due to recombination into C^{6+}

and C^{5+} ions. The mean electron density in this region is $4.0\ (\pm\ 3)\ .\ 10^{20}\ cm^{-3}$.

2. The dependence $T_e \propto \phi^{2/3}$ in the regime 10^{11}-10^{12} Watts/cm^2 is in agreement with a time independent model for the energy absorption mechanism [6].
3. It is deduced from the shape of the continuum spectra that the electron energy distribution is Maxwellian.
4. The inertial confinement time of the ions, obtained from the measurement of $n\tau$ and the density, is a few hundreds of picoseconds and is a linear function of the temperature.
5. The laser energy is absorbed at very high densities between 10^{20}-10^{21} cm^{-3} within a few tens of microns from the target surface.

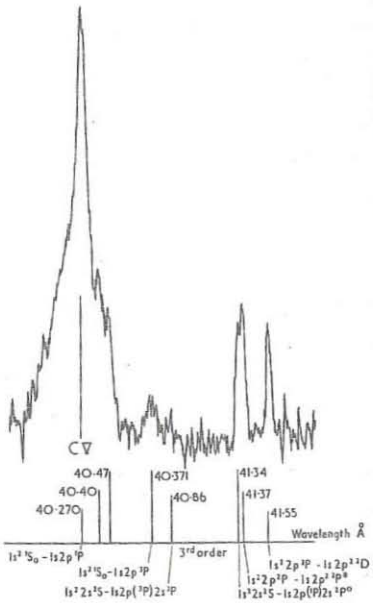


Fig. 5

REFERENCES.

[1] Büchl, K. et al (1971) Plasma Physics and Controlled Nuclear Fusion Research IAEA Vienna pp. 645-655.

[2] Hobby, M.G. and Peacock, N.J. (1972) paper submitted to Journal of Physics E.

[3] Stratton, T.F. (1965) Plasma Diagnostic Techniques, Chapter 8 Acc. Press. N. York, London.

[4] Plasma Diagnostics (1968) pp. 110-113. North Holland Publishing Company Amsterdam.

[5] Gabriel, A.H. (1972) Paper presented at 3rd Symp. on X-ray and U.V. Spectroscopy of Lab. and Astr. plasmas.

[6] Bobin, J.L. et al (1971) IAEA-CN-28/D-12 pp. 657-671.

Sixth European Conference on Controlled Fusion and Plasma Physics
Moscow, USSR. 30 July - 3 August 1973

THE EFFECT OF THE ELECTRON FREE-STREAMING LIMIT ON LASER COMPRESSION

D E T F Ashby and J P Christiansen

UKAEA Culham Laboratory, Abingdon, Berkshire, England.

INTRODUCTION. The possibility of imploding deuterium/tritium pellets to high densities and initiating thermonuclear burning by irradiation from high-powered lasers has been described recently by several authors and is supported by computer calculations, e.g. [1] and [2]. This method of achieving thermonuclear burn conditions depends critically upon the conduction of heat from the outer tenuous plasma, where the laser energy is absorbed, to a dense inner shell. It has been pointed out [3,4,5] that the required energy flux may exceed the limit set by electron free-streaming, thus invalidating the computer calculations. This paper describes preliminary computations on the effect of limiting the heat flux to that set by the free-streaming limit.

THE COMPUTER MODEL. A one-dimensional two-fluid Lagrangian code named MEDUSA has been used. The basic physics used in the model is as follows:

1. Hydrodynamics with shocks treated by artificial viscosity.
2. The ion and electron fluids are treated as perfect gases. At present the effect of degeneracy has been allowed for by choosing a start temperature such that the total fluid pressure corresponds approximately to the pressure of a fully degenerate electron gas; because a degenerate electron gas obeys the adiabatic law $pv^{5/3}$ = constant, the hydrodynamic behaviour of the fluid is approximately correct.
3. Laser light absorption by inverse bremsstrahlung up to the critical density where the remaining energy is deposited, thus simulating anomalous absorption.
4. Radiation by bremsstrahlung. The normal formula is modified so that radiated power $\sim n(T_e - T_a)^{\frac{1}{2}}$ where $T_a = (n/n_o)^{2/3} T_o$. Thus if the fluid is compressed adiabatically there is no radiation.
5. Classical thermal conduction by both ions and electrons and classical energy exchange between electrons and ions.
6. Thermonuclear reactions including burn-up of material. The neutrons escape while the energy in charged reaction products is deposited locally.

COMPARISON WITH THE RESULTS OF CLARKE ET AL [2]. At present MEDUSA contains less physics than the code used by Clarke et al [2]. The main omissions are degeneracy effects and reabsorption of bremsstrahlung. To ensure that this incomplete

model adequately describes laser fusion, comparisons have been made between results from the two codes (see Figs.1 and 2). In the three cases compared the laser power varied as $P_o(1-t/t_o)^{-2}$. P_o, t_o and laser energy were optimized to give the maximum thermonuclear output with 10 micron radiation and involved some 50 computer runs. The values of t_o used were 15, 20 and 23 nanosec. for 14, 60 and 250 μ gm respectively.

THE EFFECT OF FREE-STREAMING. The heat flux due to thermal conduction is $F_1 = \kappa\, dT/dx$. If the maximum heat flux possible due to the limit set by free-streaming is $F_2 = \alpha\, 1/4\, n \bar{c} k T_e$, where α is a constant, then a reasonable empirical heat flux to use in the computations is $F = F_1/(1+F_1/F_2)$; thus at low fluxes $F \to F_1$ and at high fluxes $F \to F_2$. The third figure shows the effect on thermonuclear yield of varying α. It should be noted that the three cases were optimized with $\alpha = \infty$; no attempt has yet been made to re-optimize the laser pulse for the different values of α. The reason for the decreased yields when $\alpha \neq \infty$ is illustrated in Figure 4 where the compressional force acting on the dense core is plotted against laser power for the 60 μ gm case. The compressional force is obtained from the fluid pressure p at the radius of the ablation layer which divides dense material moving inwards from tenuous material moving outwards. The decrease in the compressional force arises because the outer corona heats up and reduces the efficiency of momentum production as the free-streaming limitation tends to reduce the heat flux inwards.

CONCLUSIONS. The results presented, obtained with a simplified physical model, suggest that with 10μ radiation the thermonuclear yield is drastically reduced when the free-streaming factor $\alpha \lesssim 1$. Some improvement can be expected when the shape of the laser pulse is re-optimized for $\alpha \neq \infty$. However it is unlikely that $\alpha = 1$ is physically possible; the papers by Morse and Nielson [4] and Bickerton [5] suggest that α could be of order 10^{-1} or less.

Acknowledgment. The authors wish to thank Dr K V Roberts for advice and assistance in designing the computer code and for helpful discussions.

References

[1] Nuckolls,J., Wood,L., Thiessen,A. and Zimmerman,G. Nature 239, 139 (1972).

[2] Clarke,J.S., Fisher,H.N. and Mason,R.J. Phys.Rev.Lett. 30, No.3, 89 (1973).

[3] Salzman,H. Phys.Rev.Lett. 41A, No.4, 363 (1972).

[4] Morse,R.L. and Nielson,C.W. LA-4896-MS (1972).

[5] Bickerton,R.J. "Thermal Conduction Limitations in Laser Fusion" submitted to Nuclear Fusion.

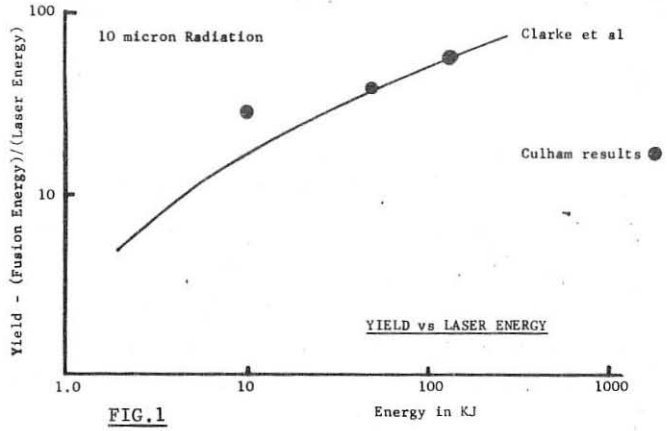

100
10
10 micron Radiation
Clarke et al
Culham results
Yield - (Fusion Energy)/(Laser Energy)
YIELD vs LASER ENERGY
1.0
10
100
1000
Energy in KJ

FIG.1

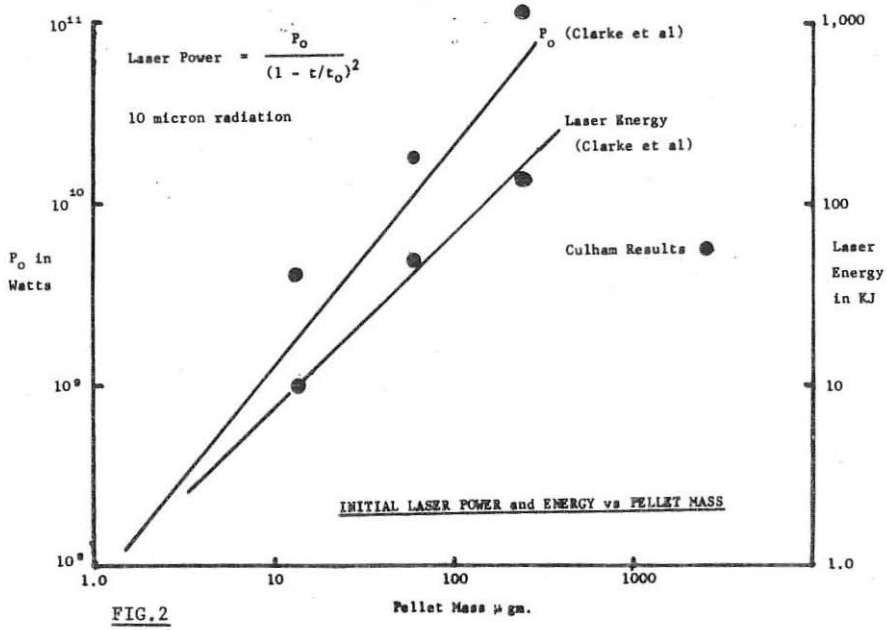

10^{11}
10^{10}
10^{9}
10^{8}
Laser Power = $\frac{P_o}{(1 - t/t_o)^2}$
10 micron radiation
P_o (Clarke et al)
Laser Energy
(Clarke et al)
Culham Results
P_o in
Watts
1,000
100
10
1.0
Laser
Energy
in KJ
INITIAL LASER POWER and ENERGY vs PELLET MASS
1.0
10
100
1000
Pellet Mass μ gm.

FIG.2

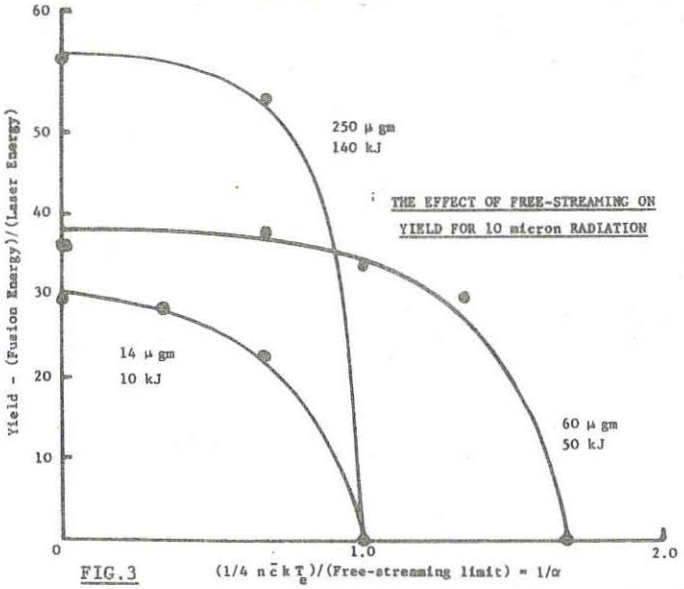

Yield - (Fusion Energy)/(Laser Energy)
60
50
40
30
20
10
0
1.0
2.0
250 μ gm
140 kJ
14 μ gm
10 kJ
60 μ gm
50 kJ
THE EFFECT OF FREE-STREAMING ON
YIELD FOR 10 micron RADIATION
(1/4 n c̄ k T_e)/(Free-streaming limit) = 1/α

FIG.3

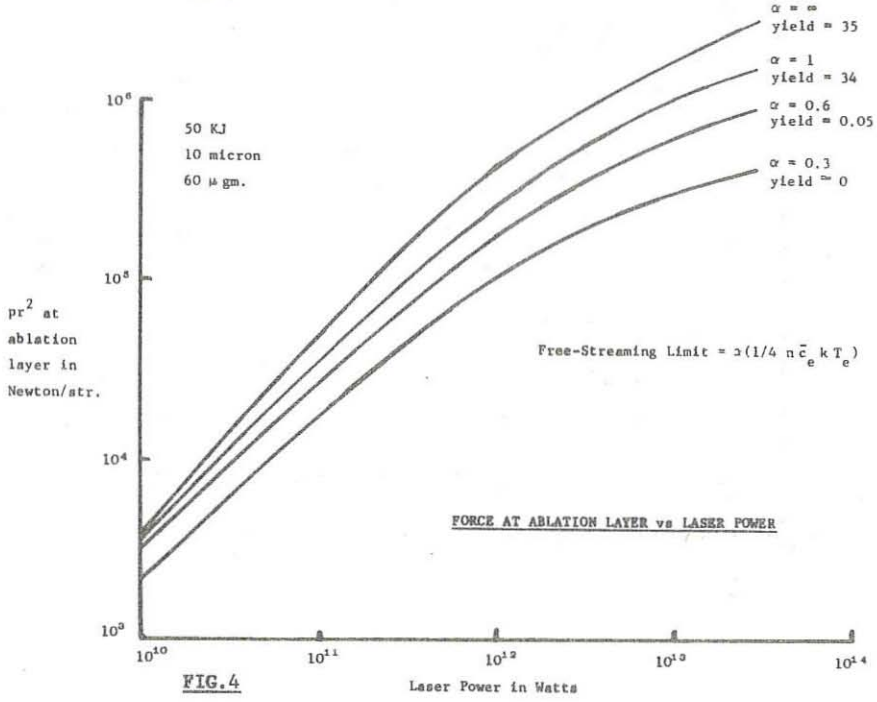

α = ∞
yield = 35
α = 1
yield = 34
α = 0.6
yield = 0.05
α = 0.3
yield ≃ 0
50 KJ
10 micron
60 μ gm.
pr² at
ablation
layer in
Newton/str.
10⁶
10⁵
10⁴
10³
Free-Streaming Limit = ↄ(1/4 n c̄_e k T_e)
FORCE AT ABLATION LAYER vs LASER POWER
10¹⁰
10¹¹
10¹²
10¹³
10¹⁴
Laser Power in Watts

FIG.4

Investigation of the fast electrons in a laser produced plasma by X-ray measurements.

by K. Eidmann, R. Sigel
Max-Planck-Institut für Plasmaphysik, Euratom Associated,
Garching bei München, W. Germany

Abstract: Measurements of the X-ray emission from a Nd-laser-produced deuterium plasma show the following results: 1) an enhanced emission of energetic X-rays indicating an excess of fast electrons in the tail of the electron distribution function, 2) run away electrons, which leave the plasma and produce X-rays at the wall of the target chamber and 3) isotropic X-ray emission from the target indicating that the energetic tail of the electron velocity distribution function is essentially isotropic.

It has been reported earlier that laser produced deuterium plasmas show an enhanced X-ray emission at high photon energies /1/. Recently Godwin et al. /2/ measured a weak polarization of X-rays ($h\gamma \gtrsim 10$ keV) emitted from a polystyrene target irradiated with a subnanosecond laser pulse. Here we report on similar experiments made in our laboratory under somewhat different conditions.

A Nd-glass-laser with pulse energies of up to 50 J and a pulse length of 5 ns was focussed onto sticks of solid deuterium. With an f = 7.5 cm lens the measured focal spot diameter is 20 µm, the intensity in the focal spot is $3 \cdot 10^{14}$ W/cm^2 at 20 J laser energy.

To measure the bremsstrahlung, scintillation X-ray detectors covered with Be and Al foils of different thicknesses were used. A typical result is shown in Fig. 1, in which the measured X-ray signal is plotted against the cut off energy E_c of the foils. It was found that fast electrons can leave the plasma and produce X-rays at the wall of the target chamber. To discriminate the radiation of the target from that of the wall the viewing solid angle of the detectors was restricted to $\Delta\Omega \approx 2 \cdot 10^{-3}$ by a lead shielding. Curve 1 was measured without shielding, curve 2 with shielding. In the case of curve 2 the radiation from the wall is eliminated, the X-ray intensity here decreases by a factor 3 ... 10 in the whole energy range under observation. To confirm whether sufficient shield-

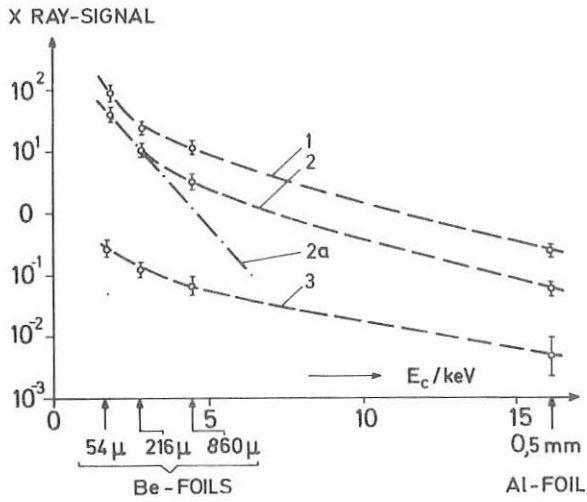


Fig. 1

ing is reached in the case of curve 2, the detectors with the lead shielding were readjusted, so that only the X-ray radiation from the small area of the wall limited by the lead shielding could be detected. The X-ray signals now obtained (curve 3) are indeed small in comparison with curve 2.

From the results of Fig. 1 we can conclude: Curve 2 represents the bremsstrahlung from the target. Since the measured points for electrons with a maxwellian distribution should be on a straight line (curve 2a is calculated for kT_e = 600 eV and fits the measured points of the thinnest foils), the typical excess of hard X-rays and hence of fast electrons in the plasma is evident from this curve. - Curve 3, the X-ray spectrum from the wall, indicates that the wall is bombarded by fast electrons with energies up to at least 16 keV. The total energy carried by these run away electrons can be estimated to be of the order of 10^{-4} ... 10^{-3}J.

If the velocity distribution of the electrons in the plasma would be anisotropic, this could lead to an anisotropic X-ray emission from the plasma. For a completely directed electron velocity distribution $f(v) \propto \exp\left(-\frac{m}{2}v^2/kT^{(\rightarrow)}\right)$ the angular dependence of the emitted bremsstrahlung was calculated using the nonrelativistic theory of Sommerfeld /3/. The result is shown in Fig. 2. Here ϑ' is the angle between the electron velocity and the X-ray observer. From Fig. 2 it is evident that a large intensity anisotropy as well as a strong polarization of the emitted X-rays could be expected, if the fast electrons would be completely directed.

The measurement of the angular dependence of the X-ray intensity is shown in Fig. 3. The signal of a detector looking un-

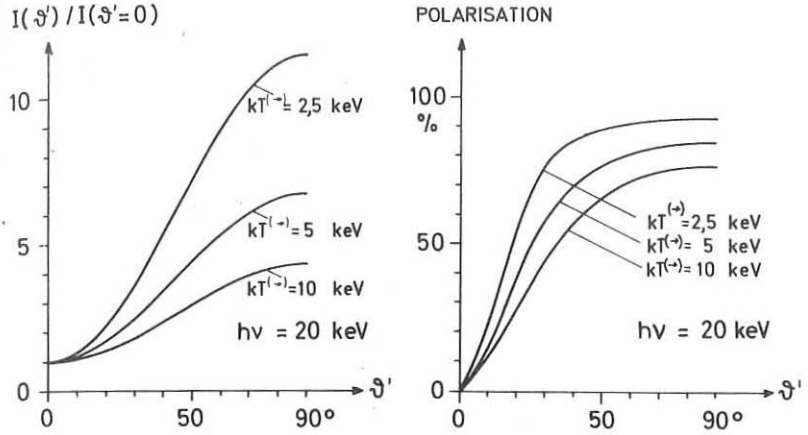


Fig. 2

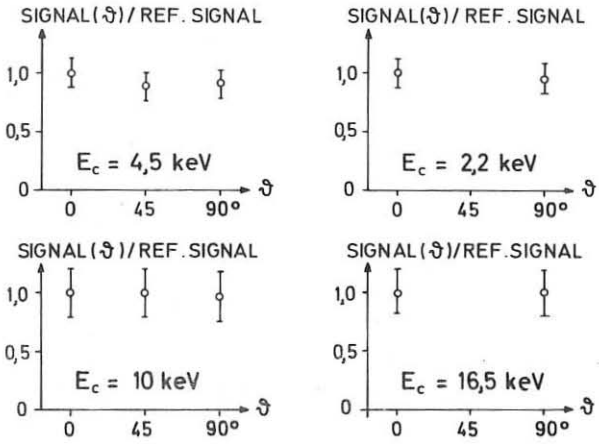


Fig. 3

der different angles ϑ to the laser axis was measured together with a reference signal from a detector, which was always in a fixed position. The measured points of Fig. 3 represent mean values of 20 ... 30 shots. The $\vec{E}$-vector of the incident laser light was always in the plane, in which the detector was moved. The measurements show clearly an isotropic X-ray emission indicating an isotropic high energy tail of the electrons up to energies of at least 16.5 keV. This result was obtained for an f = 7.5 cm ($\varnothing \approx 3 \cdot 10^{14} W/cm^2$) lens as well as for an f = 60 cm ($\varnothing \approx 5 \cdot 10^{12} W/cm^2$) lens. Since the weak X-ray anisotropy observed in /2/ has been measured with much shorter, thus more intense laser pulses, the results of these two experiments are not necessarily in contradiction.

As the electron mean free path is some mm for 10 keV electrons at the critical density, the fastest electrons observed in this experiment are mainly collisionless. Therefore the velocities of the energetic electrons should represent to a certain degree the direction of the accelerating fields. Thus, from the X-ray measurements we conclude that the accelerating fields are essentially isotropic.

From our recent observations of collimated laser light backscattering /4/ we expect that electromagnetic backscatter instabilities /5/ take place in our plasma. In this case the fast electrons should be accelerated preferentially parallel to the laser axis, whereas in the case of electrostatic instabilities /6/ or resonance absorption /7/ they should be accelerated mainly parallel to the $\vec{E}$-vector of the incident light or parallel to the density gradient in the critical layer respectively. However, the experimental observation of isotropic X-ray emission within the measuring accuracy of this experiment does not allow to attribute the origin of the observed fast electrons to one of the above-mentioned absorption mechanisms.

References

/1/ R. Sigel et al., Quantovaya Elektronika, 2 (1972) 37
/2/ R.P. Godwin, J.F. Kephart, G.H. McCall, Bull. APS (1972) 971
/3/ A. Sommerfeld, Ann. d. Phys. 11 (1931) 257
/4/ K. Eidmann. R. Sigel, Report IPP IV/46 (1972)
/5/ D.W. Forslund, J.M. Kindel, E.L. Lindman, Preprint, LASL 1972, LA-UR-73-207
/6/ W.L. Kruer, J.M. Dawson, Phys. Fluids 15 (1972) 446
/7/ J.P. Freidberg et al., Phys. Rev. Lett. 28 (1972) 795

FUSION ENERGY PRODUCTION IN A SPHERICAL, LASER-HEATED DT-PLASMA

JUKKA LAAKSONEN, JORMA VIRTAMO AND PEKKA JAUHO
TECHNICAL RESEARCH CENTRE OF FINLAND, HELSINKI, FINLAND

ABSTRACT. The breakeven condition in a laser-heated DT-pellet, initially at solid density, is determined taking into account the finite duration of the energy equilibration between electrons and ions, the fusion energy feedback and radiation losses. The input energy required turns out to be of the order of 10^9 J.

INTRODUCTION. One way for attaining thermonuclear conditions is to heat a dense target very rapidly with a laser pulse. Using this approach, one must be content with the confinement resulting from the plasma's inertia. The feasibility of such a method for producing net energy has previously been investigated e.g. by Johnson and Hall [1] and by Hora and Pfirsch [2]. The purpose of this paper is to more carefully examine the condition for the breakeven point. We will show that the previous estimates for the input energy required to bring the system to the breakeven point are much too optimistic in the case of plasma of solid density - the concept of increasing the plasma density by laser compression will not be considered here. The point is that in the earlier works the ions are assumed to have been initially heated to fusion temperatures, whereas, in a real situation, energy from the external source is first delivered to the electrons, and the ions are only gradually heated by electron-ion collisions. As it turns out, the thermalization is too slow, compared with the expansion. Aside from the finite thermalization time, we shall also take into account radiation losses and feedback of the fusion energy into the plasma. In addition, the optimal length of the laser pulse is studied.

THEORY. Consider a homogenous plasma sphere of solid density, composed of an equal number of D and T particles. The source feeds energy to the electron component of the plasma, and the energy is assumed to be absorbed uniformly. Ions will be heated by means of electron-ion collisions, and at the same time that the sphere expands, fusion energy is generated. A fraction of the fusion power is fed back into the plasma through the slowing down of α-particles. At the temperatures of interest most of this fusion power is taken up by the electrons. Near the breakeven point the burn-up is so small that its influence on the composition of the plasma can be neglected.

The dynamics of the plasma sphere is described by the simple similarity model first formulated by Basov and Krokhin [3] and by Dawson [4]. In this model it is assumed that the hydrodynamic profile of the sphere is fixed. The radius R is determined by the equation of motion:

$$\frac{d^2R}{dt^2} = \frac{1}{\bar{M}} 4\pi R^2 (p_e + p_i), \qquad (1)$$

where the effective mass $\bar{M}$ takes a value $\frac{3}{5}M$, and M is the real mass, provided that the density and temperature profiles are uniform and that the velocity profile is linear. We assume that the plasma components obey the ideal gas law, whence the partial pressures p_s (s=i,e), in terms of respective densities n_s and temperatures T_s, are given by

$$p_s = n_s k T_s . \qquad (2)$$

The temperatures can be solved from the energy equation, which for the electrons reads

$$N_e \frac{d}{dt}(\tfrac{3}{2}kT_e) = -4\pi R^2 \dot{R} p_e - \tfrac{3}{2}N_e \frac{kT_e - kT_i}{\tau} + Q_e + Q_f - Q_l . \qquad (3)$$

Here N_s (s=i,e) is the total number of s-particles, and the terms on the rhs describe, respectively, (a) the power lost by the electrons through the expansion, (b) the power transferred to the ions, where τ is the thermalization time, (c) the power absorbed from the laser beam, (d) the fraction of the fusion power fed back into the plasma, and (e) the radiation loss power. Hereafter, term (c) is referred to as "the laser pulse" for brevity. Correspondingly, the ion temperature is determined by

$$N_i \frac{d}{dt}(\tfrac{3}{2}kT_i) = -4\pi R^2 \dot{R} p_i + \tfrac{3}{2}N_e \frac{kT_e - kT_i}{\tau} . \qquad (4)$$

For the therminalization time, τ, and the bremsstrahlung emission rate we utilize the well-known formulas (cf.,e.g. Eqs. 8 and 10 in ref. [4]).

While the plasma sphere expands, as described by equations (1) through (4), fusion power is generated at the rate

$$P_f = \tfrac{1}{4}N_i n_i \langle\sigma v\rangle E_f , \qquad (5)$$

where E_f is the energy liberated in one fusion reaction, 17.6 MeV, and $\langle\sigma v\rangle$ is the rate coefficient of the reaction. For the Maxwell averaged reaction rate coefficient, we use the functional form

$$\langle\sigma v\rangle = a\Theta_i^{-3/2} e^{-b\Theta_i^{-c}} \quad \text{cm}^3/\text{ns}, \qquad (6)$$

where $\Theta_i = kT_i/\text{keV}$. When the parameters a, b and c are chosen to fit to the data given by Greene [5] they take values

Θi	a	b	c
0...10	4.620×10^{-18}	27.62	0.293
10...25	1.201×10^{-20}	25.68	0.500
25...60	6.492×10^{-21}	27.44	0.560

The energy E_f is shared between a neutron, 14.1 MeV, and an α-particle, 3.5 MeV. Since the mean free path of neutrons at the densities considered is of the order of 20 cm, the assumption that they escape without being slowed down is justified. On the other hand, the α-particles deposit a finite fraction, k, of their energy, E_α, into the plasma. Thus, the power fed back into the plasma is $Q_f = k(E_\alpha/E_f)P$ assuming that the energy deposition of the α-particle occurs instantaneously. At the temperatures of interest, the α-particle energy is mainly absorbed by the electrons. The coefficient, k, is then a function of R, n_e and T_e. We have derived an approximation for k by (a) utilizing the expression for slowing-down rate per unit length, as given by Boulegue et al. [6], (b) integrating this over the path length, L, of the α-particle in the plasma, and, finally, (c) averaging over the distribution of L among the α-particles, emitted uniformly and isotropically in a sphere of radius R, namely $p(L) = (3/4)(1-(L/2R)^2)$.

RESULTS. First, we investigated the fusion gain of the pellet as a function of both its initial radius and the energy of the laser pulse. In this study, the laser energy is assumed to be delivered instantaneously. Two cases are considered as follows: (a) laser energy is delivered to the electrons, and (b) laser energy is evenly distributed among the electrons and ions. The results obtained by the Runge-Kutta integration of the differential equations are shown in fig. 1. The solid curves correspond to the former, more realistic case; the dotted curves refer to the latter case. The curves have a maximum with respect to the pulse energy. This is quite reasonable, since no fusion reactions occur when input energies are too small, and conversely, when input energies are excessive, fusion rates begin to saturate, and the increased expansion velocity causes a reduction in the gain. Our curves for small pellets (R_o<1cm) in the case (b) above agree closely with those of ref. [1], in spite of the fact that there both energy feedback and radiation losses were disregarded. The effect of these two factors can be roughly described by a slight shift of each curve along the input energy axis. Radiation losses shift the curves in the direction of greater input energies, whereas, less input energy is required when the energy feedback is included. The effects are small since the characteristic time of energy leakage by bremsstrahlung is much larger than the confinement time, and on the other hand, the mean free path of an α-particle is larger than the radii of the spheres under consideration. Yet there is an essential difference between case (a) and case (b). The reason for this is that thermalization time is too long for the ions to be heated to fusion temperatures before the plasma is blown out. The importance of this effect decreases as the size and the confinement time of the sphere increase. However, in the neighbourhood of the breakeven-point the effect is quite significant. Consequently, our calculations predict that the breakeven energy is increased to approximately 2×10^9J.

Secondly, we investigated the effect of the length of the laser pulse on the gain. Fig. 2 illustrates the maximum gain, acquired by optimal pulse energy, as a function of the pulse length. The size of

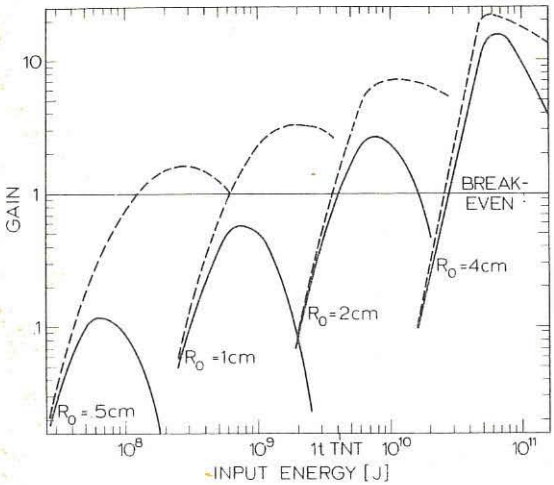


Fig. 1. The fusion gain as a function of the laser energy input for different sizes of spherical DT-particles. The heating is assumed to be instantaneous.

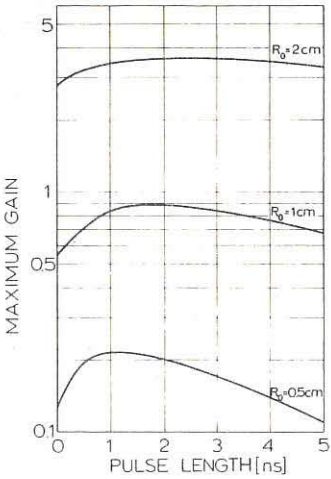


Fig. 2. The effect of the pulse length on the maximum gain attained by optimal pulse energy.

the sphere is a parameter. Each curve has a maximum, showing that there is no advantage in shortening the laser pulse beyond a certain limit. Again, this is physically reasonable since shortening the pulse much over the therminalization time does not appreciably accelerate the heating of ions, but merely leads to a more rapid expansion. The maxima, however, are not very prominent, and the gains do not differ much from the case where the pulse length is set to zero. Thus, the breakeven energy given above cannot be reduced more than by a factor of two by properly choosing the pulse length.

In conclusion, a practical pulsed fusion reactor based on the laser induced fusion seems not to be technically feasible unless the DT-pellet can be compressed to lower the breakeven energy.

REFERENCES.

1. Johnson, R.R., Hall, R.B., J.Appl.Phys. 42(1971), 1035.
2. Hora, H., Pfirsch, D., In Laser Interaction and Related Plasma Phenomena, Vol. 2, Schwartz, H., Hora, H., Eds., (Plenum Press, New York 1972), 515.
3. Basov, N.G., Krokhin, O.N., in Proceedings of the Conference on Quantum Electronics, Paris, 1963.
4. Dawson, J.M., Phys.Fluids 7(1964), 981.
5. Greene, S.L.Jr., Lawrence Radiation Laboratory, Rep. UCRL-70522 (1967).
6. Boulegue, G., Chanson, P., Combe, R., Felix, M., Strasman, P., Second U.N. International Conference on the Peaceful Uses of Atomic Energy, Band 31 (1958), 242.

VARIATION OF THE TEMPERATURE OF LASER-PRODUCED PLASMAS WITH LASER PULSE AND TARGET PARAMETERS

B. M. Klein, C. M. Dozier, D. J. Nagel and R. R. Whitlock
Naval Research Laboratory, Washington, D. C. 20375, U. S. A.

ABSTRACT

It is shown how x-ray spectral data may be used to deduce the electron temperature of laser-produced plasmas. Results for Al plasmas are discussed.

X-ray spectra from laser-produced plasmas have proven very useful in understanding some of the basic properties of plasmas formed by irradiating targets with high-powered laser radiation [1]. In this paper we will describe some of the analysis techniques that we use, and the conclusions we have drawn with respect to the laser-plasma experiments at the Naval Research Laboratory (NRL).

Our experiments have used the NRL high-powered Nd:glass laser which has been described in detail elsewhere [2]. This laser, operating at wavelengths of 1.06 μm or 0.53 μm, is focused onto slab targets with a focal spot diameter of ~ 50 μm. Pulse lengths of both 0.9 and 0.25 nanoseconds have been used, and the pulse energy content has varied from below 1 to about 5 joules on target. The laser irradiances have therefore been $\gtrsim 10^{14}$ watts/cm^2. Most of the spectral measurements have been made with Bragg flat-crystal spectrographs, with the x-ray spectra recorded on film. In addition, some high resolution measurements have been made with a grazing incidence grating spectrograph [3]. Spectra from many different elements and compounds have been measured, but for the purposes of illustration we will consider aluminum data obtained with crystal spectrographs as an example in this paper.

Figure 1 shows an Al spectrum for a laser pulse of 1.85 joules and 0.25 ns at 1.06 μm. The x-ray energy range shown is $\sim$ 1.5 to 2.2 keV. The lines are from the K-series of Al which come from transitions for which an electron in a p-shell drops into a (1s) hole. In the laser-plasma experiments, the leading edge of the laser pulse forms an aluminum plasma into which the bulk of the laser energy is absorbed. This causes a rapid heating of the initial plasma and the formation of highly ionized states of Al. As can be seen in figure 1, most of the x-radiation comes from these highly stripped atoms. For instance, those lines labeled by 'He' are K-lines from Al atoms with all but two electrons stripped-off. The He-like line at 1.598 keV corresponds to an initial state of (1s 2p) and a final state of ($1s^2$). Other He-like K lines are from configurations ($1s\,np \rightarrow 1s^2$), and extend out to the series limit of 2.086 keV above which a free-to-bound

continuum is evident. Similarly, the H-like lines are from configurations with all but one electron removed. These lines extend from 1.73 to 2.30 keV. On the low energy side of many of the stronger lines are low intensity satellite lines. The satellites to the He-like lines are Li-like lines which are distinguished from the parent lines by the initial and final states having a single extra passive electron present. The initial states for these transitions are populated by dielectronic recombination onto the parent ionization state [4]. In the energy range shown in figure 1, there is no measurable Bremsstrahlung continuum radiation.

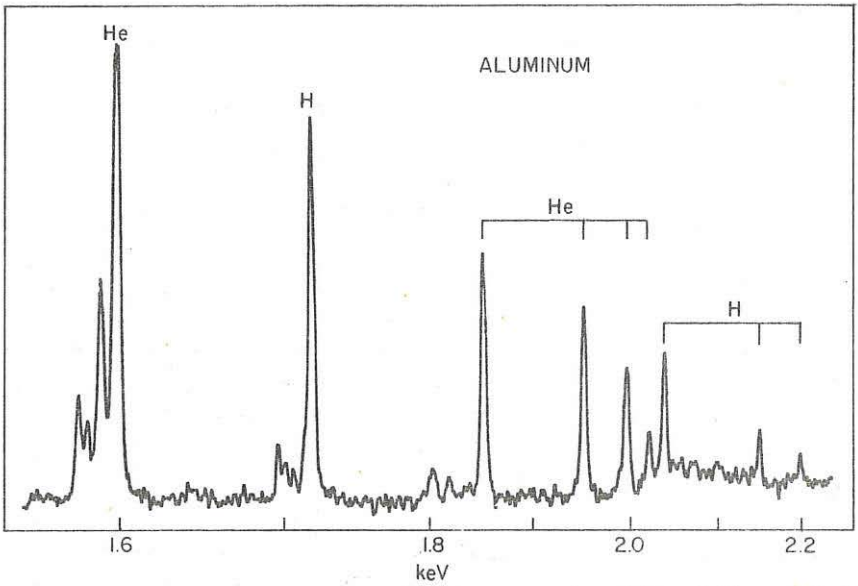


Figure 1. Al x-ray spectrum from the plasma produced by a 1.06 μm, 0.25 ns, 1.8 J laser pulse.

The most striking thing about the Al spectrum in figure 1 is that almost all of the line radiation we observe is from He and H-like atoms. Lines from less highly ionized atoms are extremely weak. This is typical of all of our spectral results: the line radiation is confined predominantly to a relatively narrow spectral range and comes from a few ionization stages of the atom in question.

It is evident that the laser heats the plasma very rapidly to some maximum temperature determined by the target material, the laser pulse time and energy content. To this maximum temperature (T) there corresponds a population of stripped atoms from which the x-radiation is emitted. These x-rays can cor-

respond to K, L, or M lines depending on the target material and T. Time resolved x-ray measurements indeed verify that the x-rays are emitted very fast; in times of the order of the laser pulse time. With these qualitative conclusions as a guide, we have used the measured x-ray spectra to infer the electron plasma temperature. To do this, we have assumed the plasma to be in coronal equilibrium [5] with a Maxwellian distribution of electron speeds and an electron temperature T. In this approximation, the ratio of the total intensity of any two x-ray lines is a function of T only but different for each specific material. Our approach is to make a theoretical calculation of the intensity ratio of two lines as a function of T, and then use the experimental intensity ratio to determine the coronal equilibrium electron plasma temperature. Although the coronal model undoubtedly does not hold in detail for the transient plasmas we produce, the temperatures we determine provide at least a semiquantitative and physically appealing picture of the plasma conditions corresponding to the x-ray emission that we observe.

For Al we have chosen to ratio the lowest energy H and He-like lines. These lines have the greatest intensity in each spectral series, and the relevant Gaunt factors [6] and oscillator strengths [7] needed in the theoretical calculation are readily available in the literature. The theoretical results are shown in figure 2.

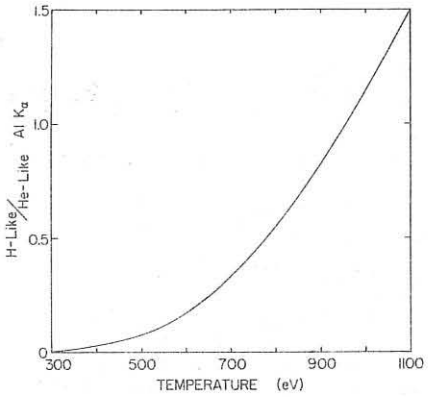


Figure 2. Ratio of total intensity in H and He-like Al (2p → 1s) K x-ray lines versus electron plasma temperature.

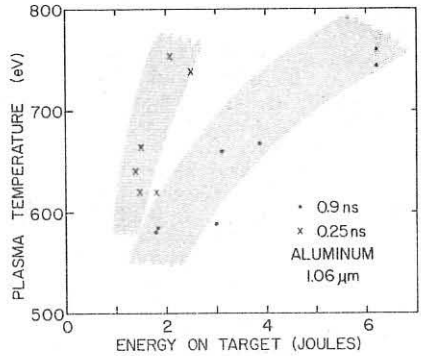


Figure 3. Electron plasma temperature versus laser energy on Al targets for 0.25 and 0.9 ns laser pulses.

In figure 3 we have plotted the temperature versus energy on target for 1.06 μm laser light incident on Al targets for two different laser pulse times. As might be expected, the shorter pulses heat the plasma to a hotter temperature for a given laser energy. The 0.25 ns points form a curve which rises very sharply as the energy on target is increased. Of course, the steep rise will not continue ad infinitum, and we are extending our short pulse measurements to higher powers where the curve is expected to flatten out. The shaded region represents an estimate of the uncertainty in the experimental data.

Plasma temperatures have been obtained for Al for cases where we have varied the laser wavelength (1.06 and 0.53 μm) and alloyed the targets (50% Al-50% Ni). Our results to date indicate that the plasma temperature, as we have defined it, is approximately independent of the target material. This seems reasonable, as the heating is largely due to inverse Bremsstrahlung absorption by the electrons at the critical density; and these critical density electrons do not maintain any signature of their parent atoms.

We expect that our methods will be useful as a plasma diagnostic tool in TNF experiments where the low-Z target materials may be doped with higher Z material to improve the heating [8].

This work was sponsored by the Atomic Energy Commission and the Defense Nuclear Agency.

REFERENCES

1. See paper by D. J. Nagel, et al., this conference.
2. J. M. McMahon and J. L. Emmett, Record of 11th Symposium on Electron, Ion, and Laser Beam Technology, p. 269 (R. F. M. Thornley, ed., San Francisco Press, Inc., 1971).
3. U. Feldman, G. A. Doschek, D. J. Nagel, W. E. Behring and Leonard Cohen, Astrophysical Journal, to be published.
4. For a recent review of the various approximations see: R. C. Elton, Atomic Processes, in Methods of Experimental Physics 9A, 115 (H. R. Griem, ed., Academic Press, New York, 1970).
5. A. H. Gabriel and T. M. Paget, J. Phys. B5, 673 (1971).
6. R. W. Mewe, Solar Physics 22, 459 (1972).
7. W. L. Wiese, M. W. Smith and B. M. Miles, Atomic Transition Probabilities, National Bureau of Standards, NSRDS-NBS 22, Vol. II (1969).
8. S. D. Zakharov, O. N. Krohkin, P. G. Kryukov and E. L. Tyurin, Kvantovaya Elektronika 1, 102 (1971) [Engl. Trans., Sov. J. of Quant. Elect. 1, 196 (1971)].

X-RAY AND UV EMISSION OF LASER-PRODUCED PLASMAS

D. J. Nagel, O. C. Barr, P. G. Burkhalter, G. A. Doschek, C. M. Dozier, U. Feldman, B. M. Klein, J. H. McCrary, J. M. McMahon, R. R. Whitlock
Naval Research Laboratory, Washington, D. C. 20375, U. S. A.

ABSTRACT

K, L, and M x-ray spectra and UV spectra emitted by laser-produced plasmas indicate which ionization stages exist in the plasmas. Data on the total intensity, duration and size of the x-ray source were also obtained.

INTRODUCTION

Plasmas produced by focussing subnanosecond laser pulses with power about 1 GW or greater on solid targets emit intense x-ray and UV radiation [1, 2, 3, 4]. Such plasmas, which are primarily of interest as sources of thermonuclear fusion power [5, 6], are also unique radiation sources. This paper describes spectroscopy and other experiments performed for two reasons: (a) to determine the emission characteristics of this unusual source of x-ray and UV radiation, and (b) to understand the heating of laser-produced plasmas. Here we discuss measurements with targets of $Z > 10$. These are relevant to the fusion problem since high-Z doping of DT targets has been suggested to improve heating [7]. We will present data on emission from low-Z targets in later papers.

EXPERIMENTAL

The laser system consisted of a mode-locked Nd:YAlG oscillator; a Pockels' cell gate which switched out a single pulse with an energy of a few mJ; two Nd:YAlG preamplifiers; three Nd:glass amplifiers and a second Pockels' cell gate which was usedfor isolation. The pulse duration was controlled by Fabry-Perot etalons in the oscillator cavity to be either 0.25 ns or 0.9 ns. This system, the development of which was described earlier [8], is shown schematically in figure 1. Back reflection limited the energy on target to about 5 J.

The laser pulse was focussed to a ~ 50 μm diameter on slab targets with a 74 cm focal length lens. Hence, power densities in the present work approached 10^{15} watts/cm^2.

Crystal and grazing-incidence-grating spectrographs were both used to obtain spectra from over 2000 eV to below 40 eV. The slitless crystal spectrographs were extremely simple, flat-KAP-crystal devices which were useful down to about 800 eV, the cutoff of the Be foils used to protect the Kodak No Screen film from light. The 3 m grating spectrograph was that used for earlier investigations of solar and vacuum spark spectra [9]. It has a 1200 line/mm gold replica grating (88° incidence angle) which yields data on Kodak 101 plates below about 2000 eV. Good spectra can be obtained with both crystal and grating instruments in a single shot, although 3 shots were usually made to obtain UV spectra.

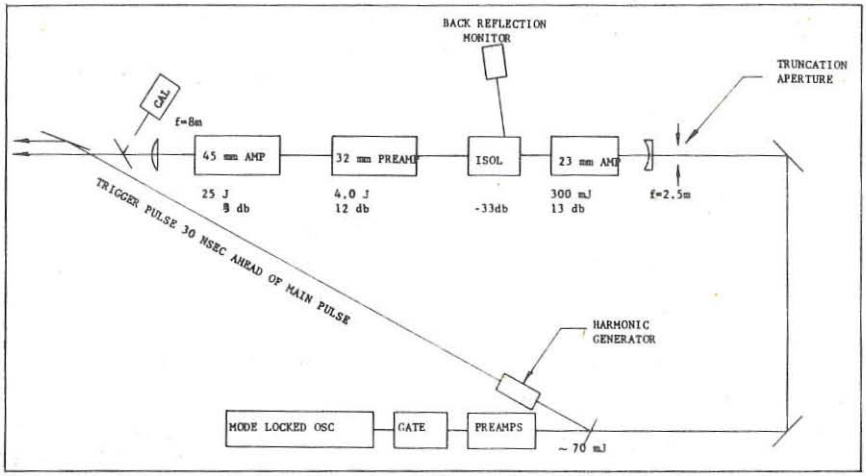


Figure 1. Schematic of high-power, Nd:glass laser system.

Crude temporal and spatial information was obtained by the use of a pyroelectric detector and pinhole photographs. Time-integrated intensities are being measured with ionization chambers [10], thermopiles, and dosimeters.

RESULTS

K, L, and M x-ray spectra have been obtained from a wide variety of elements using the crystal spectrographs, as shown in figure 2 [11]. K spectra from elements between Na and S consist primarily of Rydberg series lines from H- and He-like ions, with some satellite lines [12]. L spectra, which were obtained from elements in the range Ti to Br, are similar to earlier laboratory and solar observations [13, 14]. M Spectra of Ba and several rare earth elements obtained in this work have not been measured before, as far as we know.

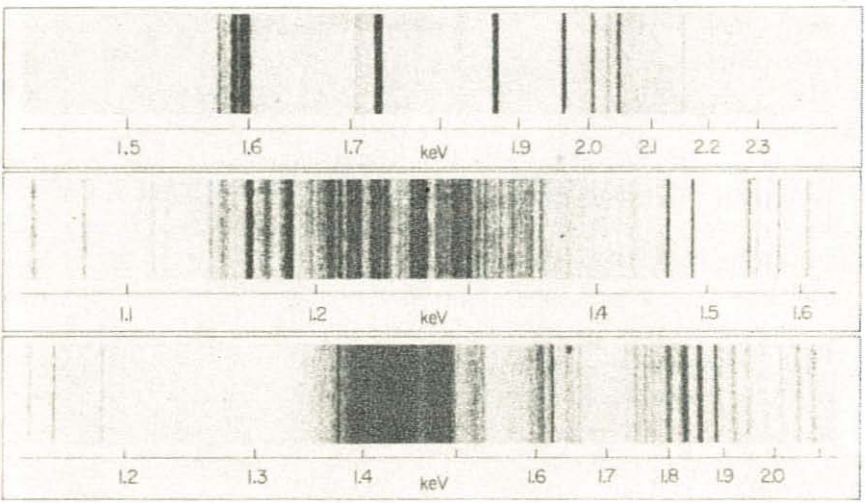


Figure 2. Al K (top), Zn L (center) and Gd M (bottom) x-ray spectra.

Iron spectra obtained with the grating spectrograph for the target at or near focus of the laser pulse are shown in figure 3. Lines from higher ionization stages are more intense in the spectrum emitted by the hotter plasma produced at focus, compared to emission from the colder plasmas produced by lower power densities which were obtained by slightly defocussing the laser pulse. This ability to vary the emission, and the purity of the spectra, have permitted identification of Fe XVIII and XIX lines near 100 A which were previously observed but unclassified in solar spectra.

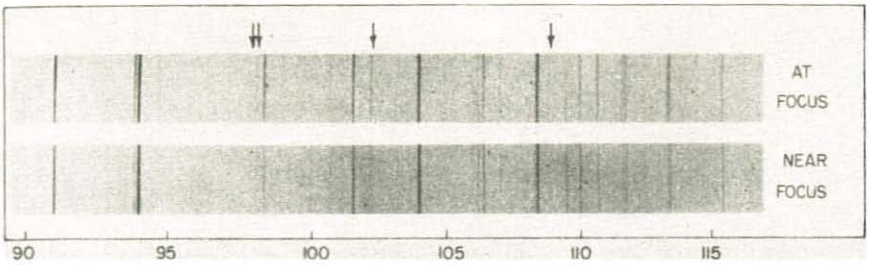


Figure 3. UV spectra from Fe plasmas. Arrows indicate lines from higher ionization stages.

The total x-ray intensity in Al K and Ni L lines has been obtained using the known values for reflectivity of KAP crystals [16], sensitivity of Kodak No Screen film [17] and absorption in the Be windows. Preliminary estimates of the ratio of x-ray-line-energy to laser-pulse-energy are $< 1\%$ for Al K lines and $\sim 5\%$ for Ni L lines. These values are based on two assumptions, isotropic emission and no reciprocity loss in film, both of which are being checked by use of active and thermoluminescent detectors.

A limit on the x-ray emission time was obtained by use of a pyroelectric detector which yielded an x-ray pulse width of < 2 ns for a laser pulse of 0.9 ns [18]. It is likely that the x-ray and laser pulse widths are nearly equal. X-ray pinhole pictures have shown the source to be about 100 μ in size [19].

DISCUSSION

The present results indicate that a laser-produced plasma is a source of soft x-rays which is uniquely intense, fast and small. The K, L, and M spectra shown in figure 2 are emitted by elements which have lost about 10, 20 or 35 electrons, respectively, in being stripped down to the K, L or M shell. The plasmas and ionization stages produced in this work are of some interest in relation to potential x-ray lasers, since most schemes for the production of a high-photon-energy laser involve a laser-produced plasma [20].

The profiles of long wavelength lines from high ionization stages are being examined for information on the ion temperature and the magnetic field [21] in the hottest part of the plasma. Theoretical study and numerical simulation of laser-produced plasmas are also being done in this laboratory [22].

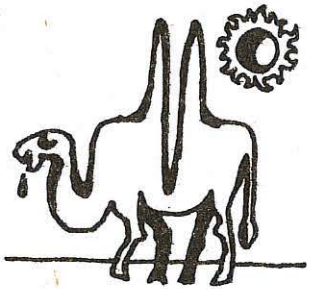
ACKNOWLEDGEMENTS

This work was sponsored by the Atomic Energy Commission and the Defense Nuclear Agency. We appreciate discussions with L. S. Birks and J. A. Stamper, and operation of the laser by T. deRieux and L. Scott.

REFERENCES

1. Ye. V. Aglitskiy, et al., Brief Comm. in Phys. (Russian), No. 12, 36 (1971).
2. P. J. Mallozzi, et al., Fundamental and Applied Laser Physics, (Proc. of Esfahan Symposium), A. Javan and M. S. Feld, ed., Wiley, New York, 1972.
3. S. W. Mead, et al., Appl. Optics 11, 345 (1972).
4. D. J. Nagel, et al., Bull. Am. Phys. Soc. 17, 972 (1972).
5. J. Knuckolls, et al., Nature (London) 239, 139 (1972).
6. J. S. Clarke, et al., Phys. Rev. Ltrs. 30, 89 (1973).
7. S. D. Zakharov, et al., Kvantovaya Elektronika 1, 120 (1971) [Engl. Trans., Sov. J. of Quant. Elect. 1, 196 (1971)].
8. J. M. McMahon and J. L. Emmett, Record of 11th Symposium on Electron, Ion, and Laser Beam Technology, R. F. M. Thornley, ed., San Francisco Press, Inc., 1971, p. 269.
9. W. E. Behring, et al., Astrophys. J. 175, 493 (1972).
10. J. H. McCrary, et al., in Appl. of Low Energy X- and γ-Ray Sources, C. A. Ziegler, ed., Gordon and Breach, Inc., New York (1971) p. 409.
11. D. J. Nagel, et al., to be published.
12. B. M. Klein, et al., elsewhere this conference.
13. M. Swartz, et al., J. Phys. B. 4, 1747 (1971).
14. G. A. Doschek, Space Science Reviews 13, 765 (1972).
15. U. Feldman, et al., sub. to Astrophys. J. (Letters).
16. P. G. Burkhalter, et al., to be published.
17. J. V. Gilfrich, et al., to be published.
18. D. J. Nagel, to be published.
19. J. Holzrichter, et al., to be published.
20. A. V. Vinogradov, et al., Proc. of Int. Conf. on Inner Shell Ionization Phenonenon and Future Applications, R. W. Fink, ed., U. S. At. En. Comm. (1973) p. 2364.
21. J. A. Stamper, et al., Phys. Rev. Ltrs. 26, 17 (1971).
22. D. Tidman, N. Winsor, J. Davis and K. Whitney, to be published.

3.2. NONLINEAR PHENOMENA



INVESTIGATION OF THE MECHANISM OF PLASMA TURBELENT HEATING.

L.P.Zakatov, D.M.Zlotnikov, Yu.G.Kalinin,
A.S.Kingsep, A.G.Plakhov and V.A.Skoryupin.

I.V.Kurchatov Institute of Atomic Energy
Moscow, USSR

I. At the Madison conference the results on plasma turbulent heating investigations were reported [1], which proved that anomalous resistance was due to the development of the ion acoustic instability in plasma with a current. However according to the theory [2,3] the ion acoustic instability cannot prevent electron "runaway" and, as a result, the resistance should decrease after the electron temperature increases by several times. At the same conference this disagreement between the theory and experiment was explained by L.I.Rudakov[4]. He found that the quasilinear relaxation due to the ifluence of ion acoustic noises while heating in the external electric field which was parallel to the external magnetic field resulted in a formation of leaps on the electron distribution function which excited electron cyclotron instability. This specific instability can prevent the "runaway".

II. We report some new experimental data indicating that in the turbulent heating electron cyclotron oscillations do occur with a polarization corresponding to the theoretical predictions[4]. These experiments were carring out on the NPK-2 installation[1].

In the first measurement run plasma noises were detected by means of a double Langmuir probe connected with a waveguide. The probe signal was devided into two by means of double T-bridge.

There was an unresonant detector on the E-side of the bridge and the resonator with low Q tuned on the $\lambda = 3$ cm on the other side. The ratio of readings of the resonant and nonresonant detectors was plotted as a function of the magnetic field. In spite of great spread of the experimental data, one can dearly see a maximum in Fig.1 a in the noise distibution corresponding to $\omega_{res} = \frac{eH}{mc}$. The measurements were carried out in $0,2\,\mu$sec after the current onset in typical regimes described in /1/. The noise intensity increased with the charge voltage and the increase in the initial plasma concentration from $4\ 10^{+12}$ to $2\ 10^{13}\,cm^{-3}$ led to the spreading of the maximum and to its displacement in the direction of the higher magnetic fields.

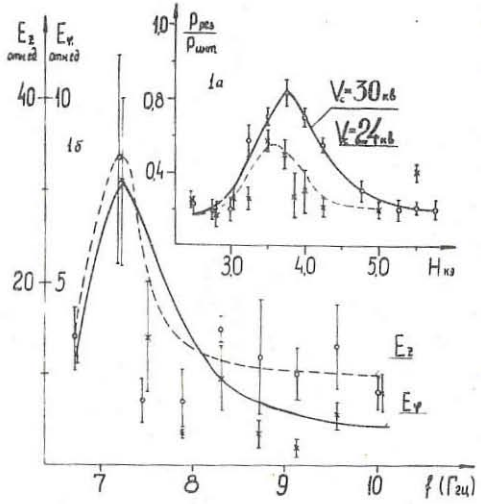


Fig.1

In the other measurements run the anysotropy of oscillations was investigated. The probe was placed to receive E_φ or E components of the cyclotron modes. The spectrum of oscillations was analysed by means of a Fabry-Perot interferometer.

The normalised intensity of the oscillations of two polarization depending of the frequency is given in Fig.1b (h=3koe, n=

$(5 - 10)\ 10^{12} cm^{-3}$).

Such an anysotropy is in agreement with the theoretical predictions. It is distinguishing feature of this type of electron cyclotron instability. (There may exist other types e.g. those due to the plasma inhomogenity when the fluit modes are unstable).

III. The experiment on the investigation of the turbulent plasma by means of an external electron beam was made on the PN-2 installation described in Ref. /5/. The electron beam with the current of 10a was injected into the cold plasma ($n \simeq 2\ 10^{12} cm^{-3}$) along the magnetic field. The injection duration was 130 μs and beam energy was of the order of 20kev. The voltage on the electrodes and the discharge current were of the order of 5 - 7kv and 1ka, respectively. In the center of each electrode there was a hole for beam injection and analysis.

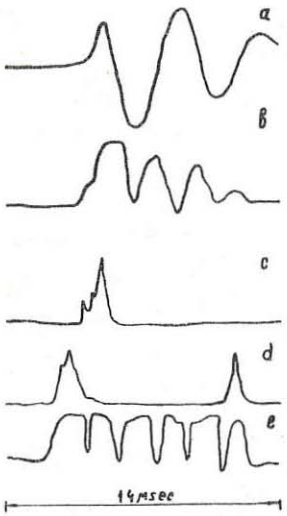


Fig. 2.

In Figs. 2a and 2b the currents of the discharge and of the beam are shown, respectively. It can be seen that the beam current decreases till zero in some stages of the discharge. Observing the h.f. radiation from two different points on the length of the installation (Figs. 2c and 2d) we succeeded in revealing a correlation of radiation flares and beam current breakes (Fig. 2c) and found that they were of a local type. Detecting the x-rays from a solid target placed outside the beam one can observe the scattered electrons of the beam

simultaniously with the beam current breakes (Figs. 3a and 3b). The oscillograms 3c and 3d obtained by simultaneous detection of the x-rays from two targets placed on different sides of the beam at a distance of the order of the beam diameter from the system axis demonstrate the scattering effect.

The data obtained in section III can be interpretated as beam electron scattering in the regions of localization of Langmuir oscillations which are excited in some stages of turbulent discharge evolution.

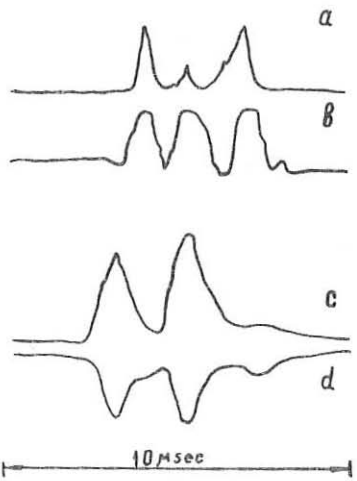


Fig.3.

References.

1. E.K.Zavoisky et al. IV IAEA Fusion Conference proceedings Volume II, p.3. Vien, 1971.

2. L.I.Rudakov, L.V.Korablyov. JETP 50, 220 (1966).

3. G.E.Vekstein, D.D.Kyutov, R.Z.Sagdeev. JETP, 60, 2142 (1971).

4. L.I.Rudakov. IV IAEA Fusion Comference proceedings Volume II, p.235. Vien, 1971.

4. L.P.Zakatov, A.G.Plakhov, D.D.Ryutov, V.V.Shapkin JETP, 54, 1088 (1968).

of about $\pi/4$.

We base the calculation on the modified quasi-linear theory due to Dupree[6]. The equation for the space averaged distribution functions is

$$\frac{\partial f_j}{\partial t} + \frac{\underline{E}e}{m_j} \cdot \frac{\partial f_j}{\partial \underline{v}} = \frac{\partial}{\partial v_\alpha} D_{j\alpha\beta} \frac{\partial f_j}{\partial v_\beta} \tag{1}$$

where

$$D_{j\alpha\beta} = \frac{8\pi^2 e^2}{m_j^2} \sum_{\underline{k}} \frac{k_\alpha k_\beta}{k^2} W_{\underline{k}} R_{j\underline{k}} , \tag{2}$$

$W_{\underline{k}}$ being the electrostatic energy in the mode $\underline{k}$. The function $R_{j\underline{k}}$ is a broadened resonance function replacing the more usual $\delta(\underline{k}.\underline{v} - \omega_{\underline{k}})$ and we take it to have the Gaussian form

$$R_{j\underline{k}} (\underline{k}.\underline{v} - \omega_{\underline{k}}, kw_{j\underline{k}}) = \frac{1}{\sqrt{2\pi}\, kw_{j\underline{k}}} \exp - \frac{(\underline{k}.\underline{v} - \omega_{\underline{k}})^2}{2k^2 w_{j\underline{k}}^2} \tag{3}$$

where $w_{j\underline{k}}$ measures the width of the resonance. We generalise Dupree's approximation for this width and obtain for the present case

$$w_{j\underline{k}} = (D_j/3k)^{\frac{1}{3}} \text{ where } D_j = \frac{k_\alpha k_\beta}{k^2} D^o_{j\alpha\beta} , \tag{4}$$

$D^o_{j\alpha\beta}$ being the value of $D_{j\alpha\beta}$ for $\underline{k}.\underline{v} - \omega_{\underline{k}} = 0$.

The corresponding non-linear growth rate is given by

$$\gamma_{\underline{k}} = \sum_j \gamma_{j\underline{k}} \text{ with } \gamma_{j\underline{k}} = \frac{\pi \omega_{pj}^2}{k^2 n} \left(\frac{d\epsilon}{d\omega}\right)^{-1}_{\underline{k}} \int \underline{k}. \frac{\partial f_j}{\partial \underline{v}} R_{j\underline{k}}\, d\underline{v} , \tag{5}$$

ϵ being the dielectric function for ion waves.

Using equation (1) for the electrons together with the marginal stability condition $\gamma_{e\underline{k}} = - \gamma_{i\underline{k}}$ we obtain

$$\frac{d\langle \underline{v}_e \rangle}{dt} + \frac{\underline{E}e}{m_e} = \frac{2}{nm_e} \sum_{\underline{k}} \underline{k}\, \gamma_{i\underline{k}} W_{\underline{k}} \left(\frac{d\epsilon}{d\omega}\right)_{\underline{k}} \tag{6}$$

Taking Maxwellian distribution functions and using equations (3) and (5) we find

$$\gamma_{j\underline{k}} (v_{Tj}^2, w_{j\underline{k}}^2) = \gamma_{j\underline{k}} (v_{Tj}^2 + w_{j\underline{k}}^2, 0).$$

Thus the non-linear growth term is simply equal to the corresponding linear growth term for a higher effective temperature determined by the level of turbulence.

In order to determine $w_{j\underline{k}}$ in terms of the level of turbulence we use equations (2) and (4) to obtain

$$w_{j\underline{k}} = \left[\frac{4\sqrt{2}\, \pi^{3/2} e^2}{3 m_j^2} \frac{k_\alpha k_\beta}{k^3} \sum_{\underline{k}} \frac{k_\alpha k_\beta}{k^3} \frac{W_{\underline{k}}}{w_{j\underline{k}}} \right]^{\frac{1}{3}}$$

By using the features of the spectrum described above we obtain a characteristic value w_j of $w_{j\underline{k}}$ given by

$$\frac{w_j}{c_s} = \left(\frac{m_i}{m_j}\right)^{\frac{1}{2}} \left(\frac{\sqrt{2\pi}}{3} \frac{W}{nm_e v_{Te}^2}\right)^{\frac{1}{4}} \tag{7}$$

where W is the total electrostatic energy.

We define an effective collision frequency ν by putting the left hand side of equation (6) equal to νv_d, where v_d is the electron-ion relative drift velocity. Then, substituting for W from equation (7) we have

$$\frac{\nu\, v_d}{\omega_{pe}\, v_{Te}} = 3 \frac{(w_i/c_s)^4}{(T_i/T_e + (w_i/c_s)^2)^{3/2}} \exp - \tfrac{1}{2} \left(\frac{T_i}{T_e} + \left(\frac{w_i}{c_s}\right)^2\right)^{-1} \tag{8}$$

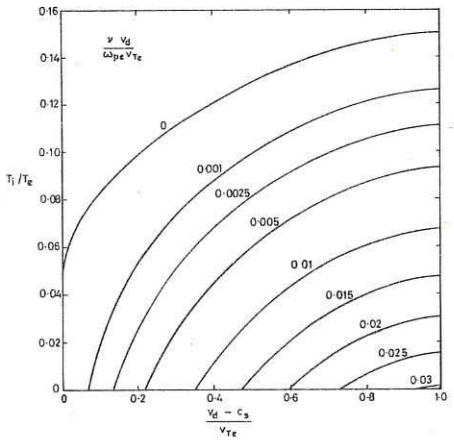
To obtain w_i we use the non-linear marginal stability condition for ion-sound waves which, together with the result $w_e = (m_i/m_e)^{\frac{1}{2}} w_i$ from equation (8), gives

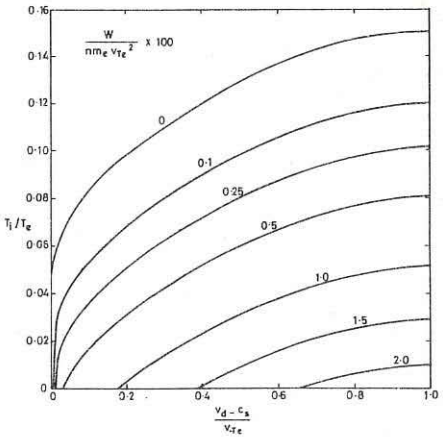
$$\left(\frac{1 + (w_i/c_s)^2}{T_i/T_e + (w_i/c_s)^2}\right)^{3/2} \exp - \tfrac{1}{2}\left(\frac{T_i}{T_e} + \left(\frac{w_i}{c_s}\right)^2\right)^{-1} = \frac{v_d - c_s}{v_{Te}} \exp - \frac{(v_d - c_s)^2}{2v_{Te}^2(1 + (w_i/c_s)^2}} \tag{9}$$

Equations (8) and (9) now give the required collision frequency

$$\nu = \nu(T_i/T_e,\ v_d)$$

and the results are plotted in the following figures.





The figures give the effective collision frequency ν by means of contours of constant $\nu v_d/\omega_{pe} v_{Te}$, and the electrostatic energy of the turbulence by contours of constant $W/n m_e v_{Te}^2$, expressed as a percentage.

References

[1] R.Z. Sagdeev, Congress on Appl. Maths. New York, 1965.

[2] T.H. Dupree, Phys. Rev. Letts. 25, 789 (1970).

[3] V.N. Tsytovich, Plasma Physics 13, 741 (1971).

[4] D. Biskamp and K. Chodura, Phys. Rev. Letts. 27, 1553 (1971).

[5] A. Sykes and J.A. Wesson, 5th European Conf. on Contr. Fusion and Plasma Physics, Grenoble 1972, p.170.

[6] T.H. Dupree, Phys. Fluids, 9, 1773 (1966).

Anomalous Resistivity and Stabilization of Ion Sound Instability.

D. Biskamp, R. Chodura, C.T. Dum

Max-Planck-Institut für Plasmaphysik, 8046 Garching bei München, Federal Republic of Germany

Abstract: The stabilization mechanism of the ion acoustic instability is investigated by computer simulation. For a wide range of initial parameters and either constant current or constant ratio of current to electron thermal velocity stabilization occurs by formation of a high energy ion tail.

There appears to be general agreement that the ion acoustic instability is responsible for anomalous resistivity in turbulent heating and shock experiments. In order to determine the macroscopic effects of the instability it is then essential to know the maximum attainable effective collision frequency and the length of time over which the instability can be maintained (heating time). Numerous stabilizing mechanisms have been proposed, involving quasilinear or nonlinear effects on either the electrons or ions. We have done extensive studies in order to provide a test for these basic theoretical predictions. The two dimensional code has been described previously [1].

Computer simulation and experiments show that the instability grows to a maximum fluctuation level which depends relatively little on the initial conditions and the mass ratio, $W/nT_e = 10^{-3}$ to 10^{-2}. Generally however, no quasisteady state $\gamma=\gamma_e+\gamma_i+\gamma_N \approx 0$ develops but saturation is followed by a decay of the spectrum, i.e. quenching of the instability at drift velocities which exceed several times the sound speed c_s.

From Fig. 1 it is seen that in the decay process the ratio between the collision frequency and W/nT_e remains remarkably constant and close to the value expected from quasilinear theory. We have chosen the case of a current perpendicular to a weak magnetic field $\frac{\omega_e}{\Omega_e} >> 1$ in order to prevent the formation of an electron runaway tail, which would greatly complicate the situation. From laboratory experiments ($j \,||\, B$) it is generally believed that no substantial runaway tail is formed.

We conclude that the electron wave interaction can be described at least qualitatively by quasilinear theory and that no substantial nonlinear modification γ_e takes place. The current excites a broad spectrum (in k and

the angle to the current direction) of waves so that it is not possible for γ_e to vanish simultaneously for all waves. The distribution $f_e(|v_\perp|)$ flattens however, which leads to an increase in the effective electron temperature $\left[T_e^{eff} = \left\langle \frac{1}{mv^2} \right\rangle^{-1}\right]$ and a reduction of the growth rate. For a 2 D flat top distribution the effective temperature is increased by a factor of 2 and the growth rate reduced by $(2\pi)^{1/2}$ as compared to a Maxwellian of the same energy $T_e = \langle mv^2 \rangle$.
(In the 3D case the figures are $5/3$ and $(10/\pi)^{1/2}$ resp.)
Theories of stabilization which rely on modification of the electron wave interaction thus cannot explain our observations and we must turn to the ion-wave interaction.
The bulk of the ion distribution cannot interact linearly with the waves and our experiments show that it is accelerated at a rate which is close to free acceleration. The bulk is heated relatively little. At the same time a high energy ion tail is formed (Fig.2) as is also observed in laboratory experiments.
According to Bekhstein and Sagdeev [2], the instability goes over into a selfsimilar state $\gamma = \gamma_e + \gamma_i \simeq 0$, $\delta \simeq \frac{c_s}{u} \simeq \left(\frac{m}{M}\right)^{1/4} T_e \sim T_2$ where δ is the fraction of resonant particles, T_2 is the tail temperature and u is the drift velocity. In our simulation studies we have kept either u or u/v_e, $v_e^2 = T_e/m_e$ constant in time. For fixed $u/v_{eo} = 1$ and the mass ratios 100, 400 and 1600 we find that the instability is quenched at $v_e/u = 2{,}13$; 3 and 4 - 4,5 (extrap.) respectively, i.e. v_e/u scales as $(M/m)^{1/4}$. The estimated Landau damping on the ion tail is sufficient to explain stabilization. Stabilization occurs in much the same way if v_e/u is kept constant e.g. $v_e/u = 1{,}64$ for $M/m = 100$. From conservation of energy it follows that with increasing u/v_e a smaller and smaller fraction of the thermal energy is given to the ions, $\frac{\delta T_2}{T_e} < \frac{c_s}{u}$. Stabilization by formation of an ion tail thus becomes increasingly more difficult. Optimizing γ_i under the constraints of energy and momentum conservation we find that stabilization is always possible for constant u, but for u/v_e constant there is a limit u/v_e max which depends on $(M/m)^{1/4}$. Beyond this limit it appears possible that a quasisteady state can be maintained by nonlinear effects. However for not too large mass ratios ($\frac{M}{m} \lesssim 1836$), $u/v_e\,\mathrm{max} = O(1)$ which is outside the ion acoustic regime discussed here. Nevertheless we see a tendency towards a plateau in W/nT_e at large u/v_e. A quasisteady state which is usually assumed in theoretical investigations, thus is only possible if the formation of the

ion tail is prevented, e.g. by collisions. The spectrum is peaked at $k\lambda_D \gtrsim 1$ which also indicates that it is determined by quasilinear rather than nonlinear effects such as nonlinear Landau damping.
Heating of the ion bulk and the increase in the number of resonant particles must be connected with nonlinear effects [3]. This is evidenced by the threshold like increase in the ion energy near the maximum of W/nT_e. $W/nT_{e\ max}$ agrees very well with a simple trapping estimate.

References:

[1] D.Biskamp and R.Chodura, Plasma Physics and Controlled Nuclear Fusion Research 1971, Vol.II, p.265, Vienna 1971

[2] G.E. Bekhstein and R.Z.Sagdeev, JETP Letters 11, 194, 1970

[3] E.K.Zavoiskii and L.I.Rudakov, Soviet Atomic Energy 23, 1171, 1967

Figure captions

Fig. 1

Field energy $\frac{W}{nmu^2}$, relative field energy $\frac{W}{nT_e}$ and effective collision frequency $\frac{\nu_{eff}}{\omega_e}$ over relative field energy for a 2D run with $\frac{M}{m} = 400, \frac{\omega_e}{\Omega_e} = 25$ $\frac{u}{v_{eo}} = 1$, $\frac{T_{eo}}{T_{io}} = 50$.

Fig. 2

Ion distribution in current direction for a 2D run, $\frac{M}{m} = 400$, $\frac{\omega_e}{\Omega_e} = 25$ $\frac{u}{v_{eo}} = 1$ $\frac{T_{eo}}{T_{io}} = 50$.

"This work was performed under the terms of the agreement on association between the Max-Planck-Institut für Plasmaphysik and EURATOM".

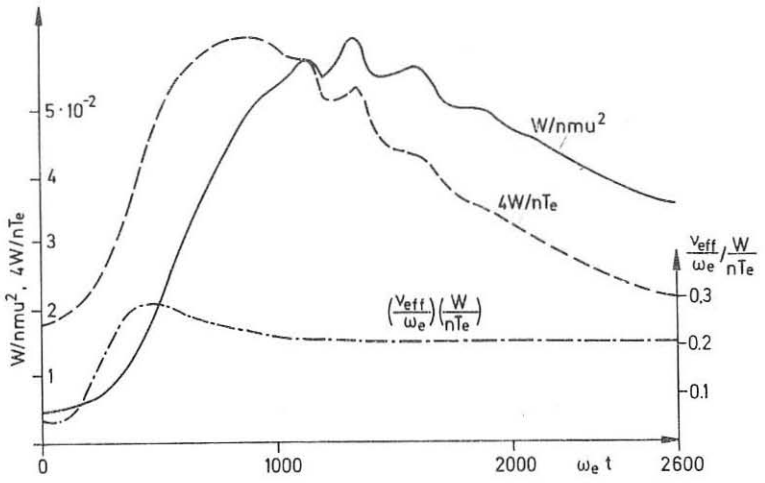

W/nmu²
4W/nTe
$\frac{v_{eff}}{\omega_e}\frac{W}{nT_e}$
$\left(\frac{v_{eff}}{\omega_e}\right)\left(\frac{W}{nT_e}\right)$
W/nmu², 4W/nTe
$5\cdot10^{-2}$
4
3
2
1
0.3
0.2
0.1
0
1000
2000
$\omega_e t$
2600

Fig. 1

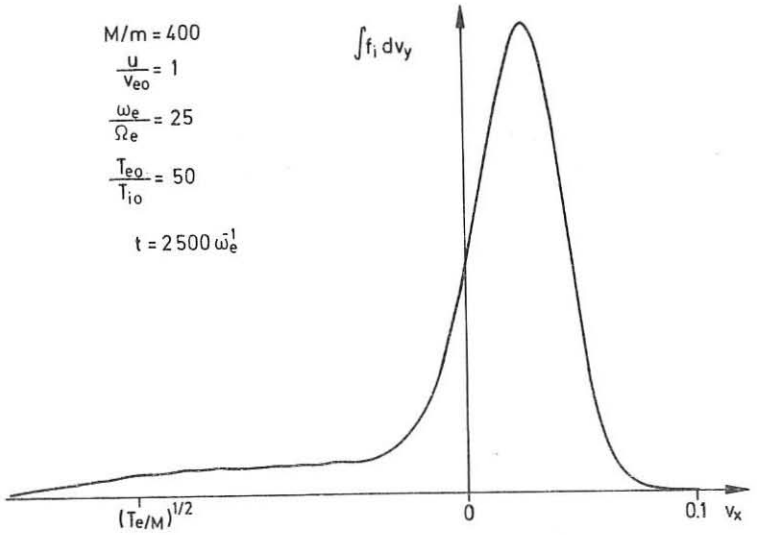

M/m = 400
$\frac{u}{v_{eo}} = 1$
$\frac{\omega_e}{\Omega_e} = 25$
$\frac{T_{eo}}{T_{io}} = 50$
$t = 2500\,\omega_e^{-1}$
$\int f_i\, dv_y$
$(T_e/M)^{1/2}$
0
0.1
v_x

Fig. 2

THE SPATIAL EVOLUTION OF THE ELECTRON ENERGY DISTRIBUTION UNDER INFLUENCE OF A LARGE AMPLITUDE PLASMA WAVE

by

E.P. Barbian

Euratom-FOM Association Contract

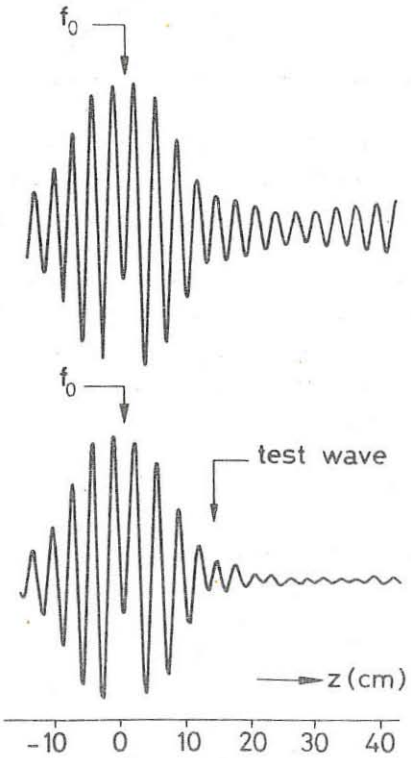
FOM-Instituut voor Atoom- en Molecuulfysica, Kruislaan 407, Amsterdam/Wgm.

Abstract: Trapping of electrons in a large amplitude wave trough is experimentally investigated. The spatial evolution of the trapped particle hump within the electron energy distribution is shown to be correlated with the oscillation of the wave amplitude. Conversely the result of detrapping by a second wave is likewise demonstrated.

Introduction: A monochromatic electron plasma wave with large amplitude is propagated through a warm collisionless plasma. The main body of the electron distribution is Maxwellian and essentially supports the wave. Within an interaction region $\Delta V=\frac{1}{2}m\Delta v^2=2q\Delta\phi$ the wave with the amplitude $\Delta\phi$ can trap electrons on both sides of the resonant electron velocity which is equal to the phase velocity $v_{po}=\omega_o/k_o$ of the wave. With a suitable choice of the experimental condition the phase velocity of this wave is several times the thermal velocity and most of the resonant electrons travel slower than the wave when trapping starts.

The amplitude of the wave is initially Landau damped but shows then under the influence of the coherent oscillation of the electrons [bounce frequency $\omega_B=(qE_ok_o/m)^{\frac{1}{2}}$, where E_o and k_o are the wave field and wavenumber of the propagating wave] an oscillatory character. This picture was initially predicted by O'Neil [1] and Al'tshul and Karpman [2] and observed by Wharton et al. [3]. Computer simulations done by Kruer and Dawson [4] show the development of a hump on the tail of the originally Maxwellian distribution and the authors discussed the spatial development both of the electron distribution and the wave amplitude in connection with the dominating trapping process. By coupling with the bounce motion of trapped electrons, sideband waves (near to the frequency of the main wave) start to exponentiate over several orders of magnitude as had been demonstrated both in experiments [3,6] and computer simulations [5]. The amplitude of especially the first lower sideband may become comparable to that of the main wave and will on its turn then influence the energy distribution.

Experiment: A quiescent plasma is produced in a single-ended potassium Q-machine (length: 90 cm; diameter hot plate 2.5 cm; B=2200 Gauss; $n=1 \times 10^7$ cm^{-3}; density decrease along the plasma column: < 3%). The main wave is excited by a probe placed slightly out of axis. A movable probe is used for detection together with PSD. A calibrated energy analyzer with high resolution is placed behind a hole (1 mm diameter) in the floating end plate. The analyzer together with the end plate is movable along the axis. The measured quantities are averaged in time. Special care was taken to minimize the influence of probes (shadow effects) on the observations. The reduction of length of the plasma column when the end-plate is moved between the distances 90 cm and 45 cm from the hot plate causes no change in density (deviation < 3%). This point was also checked by the interferometer plot in the region between probe emitter and hot plate. Other instabilities than the involved trapped particle instability are not important in the experimental parameter region. The excitation is kept below a level where decay processes become observable.



Results: The aim of the current investigation is to demonstrate the correlation between the spatial dependence of the amplitude of the large plasma wave and the spatial variation of the electron energy distribution. For this purpose it is important to keep a coherent movement of the trapped particles at least over one trapping period. Due to the small density gradient in the present experiment three oscillation periods ($\approx$ 50 wavelengths) could be observed along the plasma column. Contributions to a randomization of phases come still from the variation in wave amplitude and from the sinusoidal shape of the wave trough.

Fig.1 - Interferometer plots with f_0=19 MHz ($\omega_0=0.95\ \omega_p$)
a) upper curve: single-wave excitation;
b) lower curve: test wave ($f=f_0$) added in contraphase at z=14 cm.

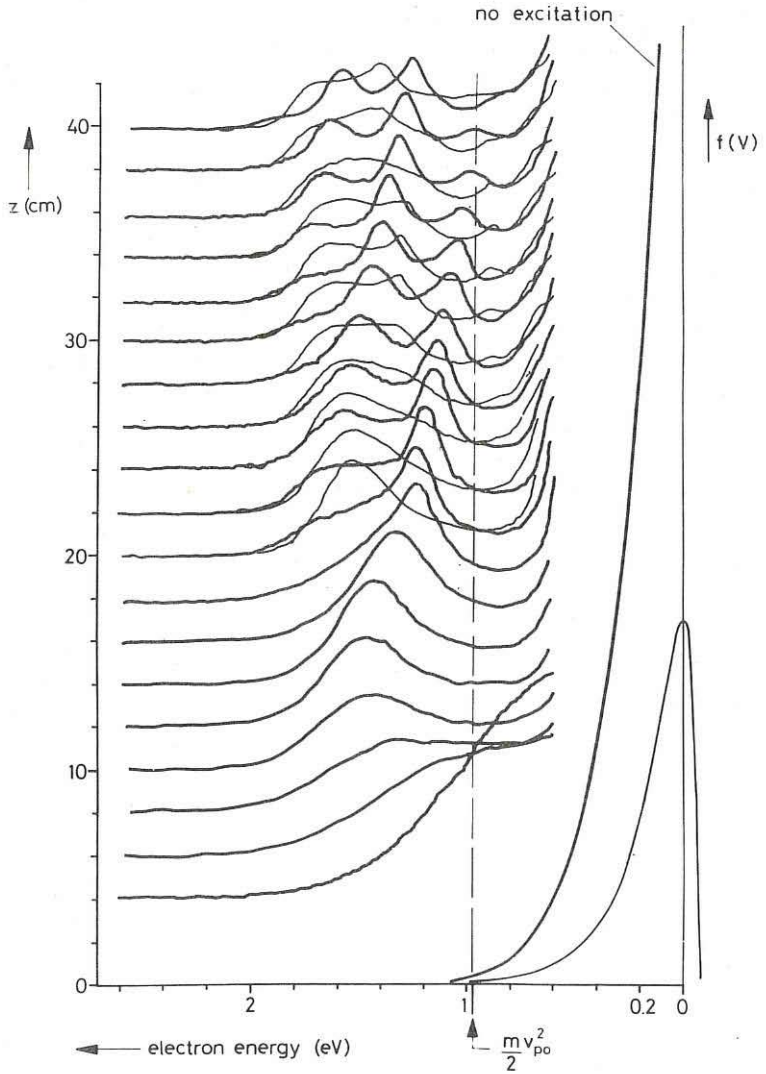


Fig.2 - Spatial dependence of the energy distribution f(V). The large amplitude wave is excited at z=0 and acts at $V=\frac{1}{2}mv_{po}^2$ on the Maxwellian distribution
Strong lines: single wave excitation.
Fine lines: test wave added (compare Fig.1, lower curve).

Excitation at the center of the plasma column was preferred for the situation shown in the diagrams. In Fig.1 we observe an initial damping near the emitter

and a partial recovering of the wave amplitude after about 10 wavelengths. A similar picture can be obtained by diode registration. We deduce from Fig.1 that the interaction width $1/2\ m\Delta v^2$ is strongly reduced already after several wavelengths to a value related to that of the residual bouncing wave.

Fig. 2 shows in steps of 2 cm the spatial evolution of the electron energy distribution which is Maxwellian when no excitation takes place (in the diagram the measured Maxwellian is given at sensitivity ratios of 1:1 and 1:4 compared to that of the humped distribution). Overlooking the diagram Fig.2 we can deduce the following properties:

1) Starting from the region near to the emitter a hump is formed on the upper energy side of the interaction line $\frac{1}{2}mv_{po}^2$ (electron energy = phase velocity v_{po}). 2) This hump consists of initially trapped electrons. But after few wave periods most of these electrons are already untrapped. 3) The residual wave (compare with Fig.1) interacts on the further run only with the lower energy part of the hump (according to Fig.1 the regrowth of the wave starts at about z=20 cm). 4) The phase velocity of the recovering wave becomes situated on a "positive slope" of the hump containing trapped electrons and this hump moves towards lower energies (20 cm $\leq$ z $\leq$ 38 cm). 5) Additional humps on the high energy side develop indicating trapping of other groups of particles. The growth of these humps is tentatively ascribed to the action of the exponentially growing first and second lower sideband of the trapped particle instability.

A complementary experiment was carried out to confirm the observations discussed sub 3) and 4). A testwave (Fig.1) is applied at z=14 in contraphase to the local wave. As shown in Fig.2 (fine lines) this results in a destruction of the trapped particle peak. The electrons are accelerated and removed from the previous interaction region (0.1 eV to both sides of $\frac{1}{2}mv_{po}^2$). In agreement with this observation the amplitude of the main wave is reduced to a small level (Fig.1, lower curve) and and the regrowth of the wave amplitude is suppressed.

A similar result was also demonstrated in a computer simulation experiment by Rosen et al. [7].

REFERENCES

[1] T.M. O'Neil, Phys.Fluids 8, 2255 (1965).
[2] L.M. Al'tshul and V.J. Karpman, Zh.Eksp.Teor.Fiz. 49, 515 (1965).
[3] C.B. Wharton, J.H. Malmberg and T.M. O'Neil, Phys.Fluids 11, 1761 (1968).
[4] W.L. Kruer and J.M. Dawson, Phys.Fluids 13, 2747 (1970).
[5] J. Denavit and W.L. Kruer, Phys.Fluids 14, 1782 (1971).
[6] R.N. Franklin, S.M. Hamberger, H. Ikezi, G. Lampis, G.J. Smith, CLM-report P 296 (1972).
[7] B. Rosen, G. Schmitt and W.L. Kruer, Phys.Fluids 15, 2001 (1972).

Computation of ion-acoustic wave excitation and its anomalous effects for double-sided laser-plasma interaction

H. Wilhelmsson and K. Östberg
Institute for Electromagnetic Field Theory,
Chalmers University of Technology,
Göteborg, Sweden

Abstract

Computer results based on a self-consistent nonlinear analysis are given for the (one-dimensional) problem of laser interaction with a plasma layer. The effects of ion-acoustic wave excitation are studied assuming that the plasma is exposed to incident radiation from two oppositely directed laser beams.

Introduction

Anomalous effects, such as nonlinear reflection due to nonlinear interaction of radiation with excitations in the plasma medium may play an essential rôle for the problem of plasma heating by laser [1,2]. In a recent report [2] the effects of ion-acoustic waves, excited by laser radiation, on the nonlinear reflection and absorption was studied in a one-dimensional case considering an inhomogeneous plasma layer. For laser powers exceeding a certain threshold value an appreciable nonlinear reflection was found even when the plasma layer was linearly transparent. A nonlinear absorption that amounted to a few percent was also caused by the presence of the ion-acoustic waves, excited during the process. The plasma medium was assumed to be exposed by continuous laser radiation from one side only and the frequency spreads $\Delta\omega$ of the transverse waves in the medium were considered much larger than the characteristic nonlinear growth rates γ^{NL} ($\gamma^{NL} < \Delta\omega$).

The purpose of the present report is to extend the previous study [2] to the situation where the inhomogeneous plasma layer is exposed to radiation by two laser beams incident from opposite directions. We then have a situation, that is symmetric with regard to the center of the plasma slab, provided the two laser

beams have the same power. For this situation it is not possible to determine uniquely to what extent the radiation emerging out from the plasma in opposite directions consists of light from one laser beam that has been reflected by the medium or of transmitted light from the other beam. However, it should be of interest to investigate the excitation of ion-acoustic waves and the nonlinear absorption caused by them for the double-sided excitation by incident radiation and, furthermore, to compare the results with those of single-sided exposure.

Basic equations

Let us introduce the notations

$$I_o = \frac{i_o(x)}{i_o(-\infty)} \quad ; \quad I_1 = \frac{i_1(x)}{i_o(-\infty)} \quad ; \quad W_+ = \frac{W^+_{2\omega_o v_s/c}}{i_o(-\infty)} \quad ; \quad W_- = \frac{W^-_{2\omega_o v_s/c}}{i_o(-\infty)} \ ,$$

where ω_o is the frequency of the incident laser light and v_s the ion sound velocity. I_o and I_1 are normalized quantities referring to laser intensity for incident and reflected light and $W^{\pm}_{\omega}$ is the energy density in the frequency interval $\Delta\omega$ of ion sound waves propagating in the positive and negative x-directions respectively. The basic set of nonlinear equations for a random phase situation then becomes [2]

$$\frac{dI_o}{d\xi} = \pm\, \alpha\, \frac{v_s}{c}\, [-8 I_o I_1\, \frac{v_s}{c} \mp (I_o - I_1)(W_+ + W_-)] \qquad (8a, b)$$

$$\frac{dW_{\pm}}{d\xi} = \mp\, W_{\pm} \pm \alpha [2 I_o I_1 \pm W_{\pm}(I_o - I_1)] \mp W_{\pm} \sqrt{\alpha\, \frac{W_{\pm}}{W^*}} \qquad (8c, d)$$

where

$$\xi = \frac{x_o \omega}{c\sqrt{2\pi\, m_e/m_i}} \quad ; \quad \alpha = \frac{\pi\, \omega_{pe}^4\, i_o(-\infty)}{4 n T \omega_o^3 \sqrt{2\pi\, m_e/m_i}} \quad \text{and } W > \alpha W^* \text{ corresponds}$$

to a critical ion sound intensity, where interaction between ion sound waves becomes essential [2]. For double-sided excitation the meaning of the notations in (8a-d) are extended to relate to the symmetry of the problem (cf. Fig. 3).

Computations

Eqs. (1a-1d) were solved numerically assuming incident laser radiation from two opposite sides of the plasma slab. The boundary

conditions thus are

$$I_o(-\xi_o) = I_1(+\xi_o) = 1 \ ;$$

$$W_+(-\xi_o) = W_-(+\xi_o) = 0.01$$

The density profile α we take in the form

$$\alpha = \alpha_o/2(1 + \cos \pi \xi/1000) \ ; \ |\xi| < 1000 \ ; \ \alpha = 0 \ ; \ |\xi| > 1000$$

The remaining parameters are taken $W^* = 10$ and $v_s/c = 10^{-3}$.

For the sake of comparison Figs. 1 and 2 show the results of single-sided excitation, where the laser power in Fig. 2 is twice the power in Fig. 1, and equal to the total power of the two incident laser beams of Fig. 3, which shows the results for double-sided excitation.

Discussion

From the diagrams we notice the interesting result that the nonlinear absorption, caused by the ion-acoustic waves, is appreciably enhanced by the splitting of the incident laser radiation into two oppositely directed beams. This is a consequence of the fact that the symmetry leads to a more thorough excitation of ion-acoustic waves propagating in both directions of the plasma layer. The key point here is that in the symmetrically excited medium radiation from one side interacts with radiation that is caused by incident laser radiation from the other side and not only with the reflected laser radiation which for one-sided excitation may be extremely weak in the central parts of the plasma layer.

Acknowledgement

We extend our gratitute to professors V.N. Tsytovich and L. Stenflo for stimulating discussions and comments.
Support from the Swedish Board for Technical Development is gratefully acknowledged.

References

1. Rosenbluth, M.N., Fifth Eur. Conf. on Contr. Fusion and Plasma Phys., Grenoble (1972).
2. Tsytovich, V.N., Stenflo, L., Wilhelmsson, H., Gustavsson, H.-G. and Östberg, K., Physica Scripta (Sweden), 7, 241 (1973).

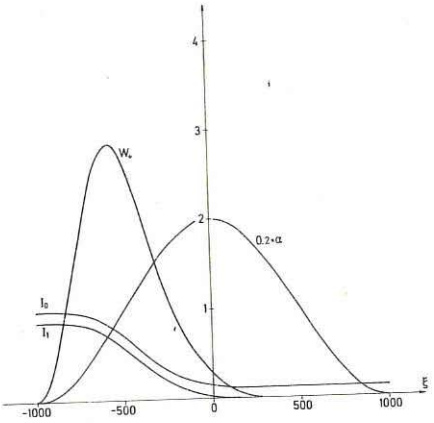


Fig. 1. The laser light is incident only from the left hand side on the plasma slab. The parameter α_o, which is a measure of the intensity of the incident radiation is equal to 10. The intensity W_- of the backward ion-acoustic wave is neglected. The nonlinear absorption amounts to 1.6% of the incident laser power.

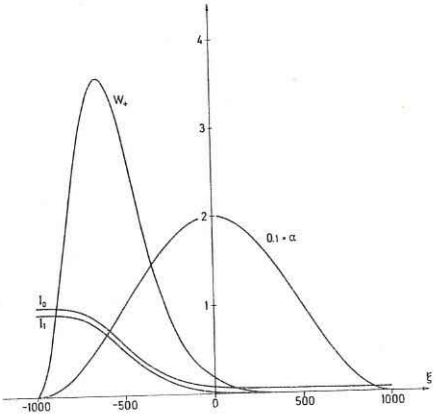


Fig. 2. The effect of doubled laser intensity, i.e. $\alpha_o = 20$, for the situation otherwise corresponding to the previous Fig. 1. The nonlinear absorption amounts to 2.4% of the incident laser power.

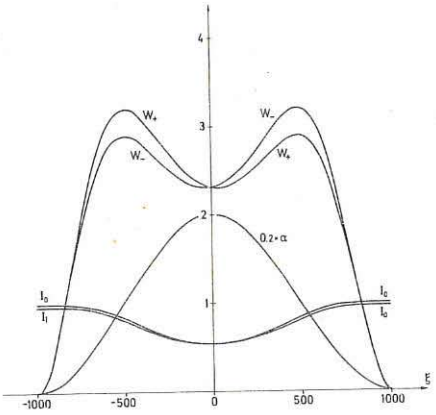


Fig. 3. The laser light is incident on the plasma slab from two opposite sides simultaneously. The power of each laser beam is equal to the one in Fig. 1, i.e. $\alpha_o = 10$. The nonlinear absorption amounts to 8.1% of the total power (sum of the two incident laser beam powers).

INVESTIGATION OF NONSTATIONARY SELF-FOCUSING OF ELECTROMAGNETIC WAVES IN PLASMA

V.A.Isaev, V.N.Kruglov, A.G.Litvak, B.K.Poluakhtov

Radiophysical Research Institute, Gorki, USSR

Experimental results of the thermal self-focus- of a beam of millimeter electromagnetic waves (ew) in plasma are given. The main attention is concentrated upon the nonstationary stage of the effect.

The self-focusing is one of the nonlinear effects determining the dynamics of electromagnetic waves in plasma and may be revealed under absolutely different conditions. For example, the self-focusing effects must have an essential influence upon a physical picture and efficiency of collisionless heating in a laser plasma and experiments on microwave plasma heating in toroidal devices.

The first attempts to investigate experimentally the wave self-focusing in plasma were made in [1,2]. The present paper deals with the results of experiments made for studying the dynamics of the effects more in detail.

The experimental conditions are similar to those reported in paper [1]. A cylindrical vacuum chamber (100 cm long, 30 cm diameter) evacuated to a pressure 0.2 torr was filled with a plasma the maximum density of which was $N_e \sim 10^{14} cm^{-3}$. As a plasma source serves a pulsed coaxial injector. After the end of the source operation the plasma decay sets in with the characteristic time $\tau \sim 1$ msec. By this time the density of plasma in the chamber has been homogeneous and the temperatures of electron and ion components have become equal. When the density reached $\sim 2.10^{13} cm^{-3}$, a pulse of electromagnetic radiation with 400 sec duration was delievered to a plasma by a horn antenna with a correcting lens. A MCR-type generator was used to produce microwave oscillations. The power was about 15 kw at the wavelength $\lambda_0 = 5$ mm.

In the course of the experiment we measured the distribu-

tion of the density of microwave energy at different power levels in the beam cross-section at z = 24 cm from the lens. For this purpose a scanned receiving device was employed which consisted of five rectangular waveguides (I.8 x 3.6 mm) situated in a horizontal plane. An absorber making the total absorption coefficient ~ 30 db was placed before the system of the receiving waveguides. This permitted to exclude the distortion of the beam inside the chamber by the receiving system. Distri-

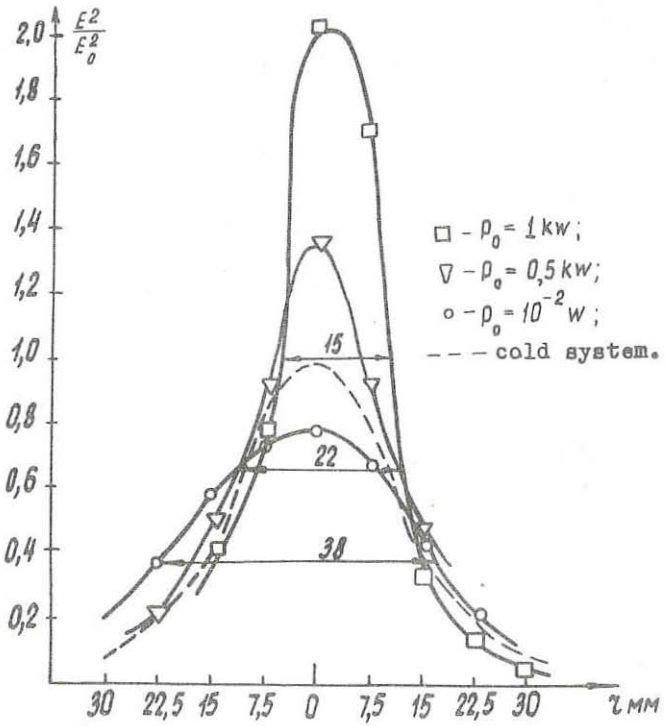


Fig I

The distribution of the energy density in a beam of electromagnetic waves passed through a plasma layer to the depth z =24 cm; N_e = 0.5 (E_0^2 ~ is the energy density on the beam axis in a cold system).

butions of the density of energy $E^2(\tau)/E_0^2$ at different incident powers (E_0 is the field amplitude on the beam axis in the absence of plasma) are shown in Fig I. The curves are plotted for one and the same moment of time and obtained using averaged results of a number (~ I0) of measurements. It follows from this figure that the distribution of $E^2(\tau)/E_0^2$ in a beam depends essentially on the power. In particular when P_0 =0.5;I.0 kw the energy density in the near-axis region greatly increases (almost two times) and the effective beamwidth is narrowed.

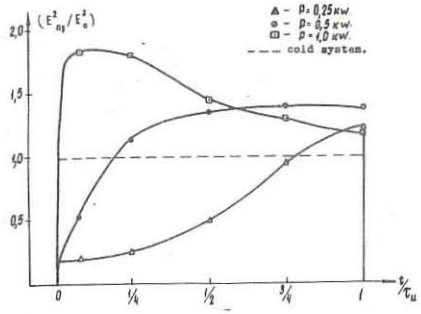


Fig 2. An averaged oscillogram of a signal passed through a plasma at different powers (in the near-axis region).

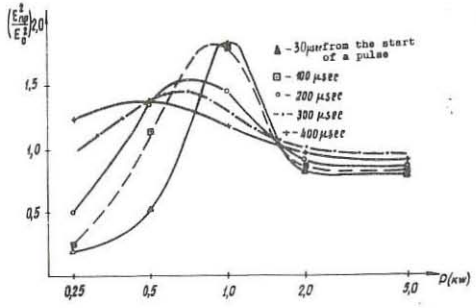


Fig 3. The normed energy density on the beam axis in the cross section $\bar{z}$ = 24 cm at different moments of time as a function of the incident power.

The behaviour of the time dependence of the observed effects illustrates pulse oscillograms taken from the beam axis at different powers (Fig 2). Based upon these oscillograms, the power dependence of $E^2(\tau=0)/E_0^2$ was built for different moments of time (Fig 3). It is seen from Figs 2,3 that as P_0 increases, the moment of appearance of a maximum value of $E^2(0)$ in the plane of receiving waveguides moves towards the start of a pulse.

The results indicate that in this experiment we observed the nonstationary self-focusing of a wave beam.The obtained experimental data are in satisfactory agreement with the theoretical estimation and may be ac-

counted for by the concept of "a moving focus"[4] (i.e. at the nonstationary self-focusing a focal plane moves from ∞ to $Z_f < Z = 24$ cm).

Indeed as is followed from the elementary theory[3], in plasma with the parameters $N_m = 10^{16}$ cm^{-3}, $N_e = 2.10^{13}$ cm^{-3}, $T_e = T_i = T_m = 3.10^{3}$°K for the ew beam with the half-width $a = 1.5$ cm the principal effect of self-action is the thermal self-focusing. In the stationary case the critical power of the beam self-focusing with $Z_f = 24$ cm is about 3 w. However since the characteristic time of the nonlinearity relaxation (the time of a redistribution of the density of charged particles in the field) $T_r = 4a^2 \nu_{im} M_i / 2T$ considerably exceeds the pulse duration $T_r / T_p = 10$ there appears possible only the nonstationary case of the type of a moving focus which is characterized by an essentially value of the critical power.

The nonlinear saturation effects occurring at $P_0 \geq 1$ kw are also essential in the experiment made. They seem to be responsible for the absence of a marked increase of the field amplitude at $P_0 > 2$ kw. Note here that at a strong nonlinearity saturation a degree of the field self-focusing in the nonstationary regime may be considerably higher than that under the stationary conditions. This feature is well supported by numerical estimations of the stationary self-focusing made by the computer.

The authors express their gratitude to Dr.B.G.Eremin for useful discussion.

References

1. B.G.Eremin, A.G.Litvak. JETP Letters, 13, 603 (1971).
2. B.G.Eremin, A.G.Litvak, B.K.Poluyakhtov, Izv.VUZov Radiofizika, 15, p.1132 (1972).
3. A.G.Litvak. Phenomena in Ionized Gases, Contributed papers, p.409 Vienna, 1967.
4. V.N.Lugovoy, A.M.Prokhorov, JETP Letters, 7, 153 (1968).

Spatial Growth Properties of Parametric and Backscattering Plasma Instabilities

by

Burton D. Fried and George Schmidt†, University of California, Los Angeles

and

Roy W. Gould, California Institute of Technology, Pasadena

ABSTRACT: Simple general arguments are used to show that for instabilities resulting from the coupling of two weakly damped linear modes with oppositely directed group velocities, such as the various parametric instabilities, there exists a range of coupling strengths (pump power in the parametric case) for which the instability is convective; above this range the system is absolutely unstable. The ratio of absolute and convective instability thresholds is large whenever the damping lengths of the linear uncoupled modes have very disparate values.

The possible use of parametric instabilities for plasma heating [1][2] depends in an essential way on the mechanism and level of saturation for these instabilities. Similar considerations apply to the stimulated Raman and Brillouin backscattering of radiation from an underdense region of the plasma [3]. If an instability is absolute (exponential temporal growth at all locations in a given region) saturation can arise only from nonlinear effects. However, a convective instability may saturate due to a combination of spatial convection out of the unstable region plus nonlinear phenomena, and in some cases the former may be the dominant effect. We show here that when damping effects are neglected, the decay waves are either stable or absolutely unstable, but when damping is included there are two thresholds, P_c and P_a for the incident power P, with stability for $P < P_c$; convective instability for $P_c < P < P_a$; and absolute instability for $P_a < P$. In addition to the decay type instabilities, there are also purely growing modes (the oscillating two stream instability [4] in the parametric problem, filamentation in the backscattering problem) which have no domain of convective growth, i.e., they are always either stable or absolutely unstable.

The dispersion relation [4] for the parametric instability of a long wavelength electromagnetic "pump" wave for $\omega \ll \omega_{pi}$ can be written

$$\varepsilon_e(\underline{k},\omega-\omega_o)\varepsilon_e(\underline{k},\omega+\omega_o)\varepsilon(\underline{k},\omega) = -(\rho^2/4)\varepsilon_e(\underline{k},\omega)[\varepsilon_e(\underline{k},\omega-\omega_o) + \varepsilon_e(\underline{k},\omega+\omega_o)] \qquad (1)$$

where $\varepsilon_e = 1 + \chi_e$, $\varepsilon = 1 + \chi_i + \chi_e$, and χ_i, χ_e are the conventional linear suscep-

tibilities for ions and electrons. Typically, $\omega \sim kc_s$ and $\omega_o \sim \omega_p$, and $\rho = (keE_o/m\omega_o^2)$ is a small parameter equal to 2π times the electron excursion distance in pump field, divided by the wavelength. The dispersion equation for backscattering [3] is of a similar form. The small ($\rho^2 << 1$) right hand side provides a coupling between the modes whose dispersion relations are $\varepsilon_e(\underline{k},\omega\pm\omega_o) = 0$ and $\varepsilon(k,\omega) = 1 + \chi_i + \chi_e = 0$. These modes, illustrated in Figure 1, are the ion acoustic modes, $\omega = \pm kc_s(1 + k^2\lambda_D^2)^{-1/2}$, and the pump-shifted Bohm-Gross modes $\omega = \pm(\omega_o - \omega_k)$ with $\omega_k = \omega_p(1 + 3k^2\lambda_D^2)^{1/2}$.

There are 10 intersections for which <u>two</u> of the dispersion relations are satisfied simultaneously (neglecting damping). Our approximation consists of considering the coupling of just <u>two</u> modes, near one of these intersections, and ignoring the effects of others. This approach can be applied to any <u>pair</u> of modes, so long as ρ is small enough. We write Eq. (1) as $\varepsilon_1(k,\omega)\varepsilon_2(k,\omega) = A$, and expand about a point $(\bar{k}\ \bar{\omega})$ at which the real parts of ε_1 and ε_2 vanish, i.e., $k = \bar{k} + \delta k$ and $\omega = \bar{\omega} + \delta\omega$

$$(\delta\omega - V_1\delta k + i\gamma_1)(\delta\omega - V_2\delta k + i\gamma_2) = -B \equiv A(\partial\varepsilon_1'/\partial\omega)^{-1}(\partial\varepsilon_2'/\partial\omega)^{-1} \qquad (2)$$

where the $V_\alpha = -(\partial\varepsilon_\alpha'/\partial k)/(\partial\varepsilon_\alpha'/\partial\omega)$ are group velocities, and the $\gamma_\alpha = \varepsilon_\alpha''/(\partial\varepsilon_\alpha'/\partial\omega)$ are the damping decrements for the two uncoupled modes, and the terms in A have been simply evaluated at $(\bar{k}\ \bar{\omega})$. This form is quite general, applying to the weak coupling of any two modes. $A > 0$ gives instability (complex $\delta\omega$ for real δk) and occurs only if one mode has positive energy and the other negative energy. For intersections of type b in Fig. 1 corresponding to modes with <u>oppositely</u> directed group velocities, $V_1 > 0$, $V_2 < 0$, the solution of (2) for real k is $2\delta\omega = \Omega_1 + \Omega_2 \pm [(\Omega_1 + \Omega_2)^2 - 4\Omega_1\Omega_2 - 4B]^{1/2}$ where $\Omega_\alpha = V_\alpha\delta k - i\gamma_\alpha$ are the incremental frequencies for the uncoupled modes. It follows that when these modes have no damping ($\gamma_1 = \gamma_2 = 0$) there is instability ($Im\omega > 0$ for real k) when $B > (V_1 - V_2)^2(\delta k)^2/4$. At the coupling point, $k = \bar{k}(\delta k = 0)$, the threshold is actually zero: any $B > 0$ causes instability. With damping, there is a non-zero threshold even at $\delta k = 0$, the condition for instability at $k = \bar{k}$ being $B > B_c = \gamma_1\gamma_2$. Since B, like A, is proportional to pump power for instability. For the decay and oscillating two stream instabilities (intersections of type a and b, respectively) the threshold coincides with the usual Nishikawa result [4]. We shall see that this is a threshold for <u>convective</u> instability. To determine the absolute/convective nature of the instability, we simply solve for δk,

$$2\delta k = \kappa_1 + \kappa_2 \pm [(\kappa_1 - \kappa_2)^2 - 4B/V_1V_2]^{1/2} \qquad (3)$$

where $\kappa_\alpha = (\delta\omega + i\gamma_\alpha)/V_\alpha$ are the incremental wave numbers of the uncoupled modes. A necessary condition for an absolute instability is the existence of a saddle point in $\omega(k)$, i.e., the coalescence of the two roots [5]. For $V_1V_2 < 0$, this occurs when $\kappa_1 - \kappa_2 = \pm 2i(B/|V_1V_2|)^{1/2}$. This condition is also sufficient; since the two roots are on opposite sides of the real k axis for $Im\delta\omega \to \infty$, the coalescing roots come from different halves of the k plane, as required [5]. At the saddle point, $\delta\omega_s = i[\pm 2(BV_1|V_2|)^{1/2} - \gamma_1|V_2| - \gamma_2V_1]/(V_1 + |V_2|)$. In absence of damping, there will always be a saddle point in the upper half plane for $B > 0$, hence an absolute instability. With damping, however, $Im\delta\omega_s < 0$ and there is no absolute instability unless

$$B > B_a = (\gamma_1|V_2| + \gamma_2V_1)^2/4V_1|V_2| \qquad (4)$$

By the Schwarz inequality, $B_c/B_a = 4L_1L_2/(L_1+L_2)^2 \leq 1$ where $L_\alpha = |V_\alpha/\gamma_\alpha|$ are the damping lengths. Thus when damping is included there exists a region of convective instability for $B_c < B < B_a$ and B_a, with stability for $B < B_c$ and absolute instability for $B > B_a$. Since B is proportional to pump power, and the convective regime is realtively large, when L_1/L_2 is either very large or very small. On the other hand, for an intersection like b where $L_1 = L_2$ (which here corresponds to the oscillating two stream instability) there is no convective regime. In general any purely growing instability ($\omega = i\gamma$) will be absolute.

We mention two further consequences of (3):

1. For $B < B_c$, both of the roots (3) represent spatially damped waves; at $B = B_c$ it is the wave with the largest damping length L_α originally, which goes convectively unstable. This is illustrated in Fig. 2, which shows the map of the real $\delta\omega$ axis in the complex δk plane for a given set of V_α, γ_α and various values of B.

2. At the absolute instability threshold, $B = B_a$, $Im\ k = (L_2 - L_1)/L_1L_2$ so the coalescence of roots occurs in the lower half of the k plane if $L_2 < L_1$ (cf. Fig. 2). As shown by Briggs [5], it follows that the absolutely unstable mode will propagate in the positive x direction, i.e., in the V_1 direction. If, instead, $L_2 > L_1$, then it propagates in the V_2 direction.

This research was supported in part by the U.S. Atomic Energy Commission and in part by the Office of Naval Research.

†Permanent address: Stevens Institute of Technology

References

[1] A. Y. Wong and R. J. Taylor, Phys. Rev. Lett. 27, 644 (1971); H. C. Carlson, J. Geophys. Res. 77, 1242 (1972).

[2] R. P. H. Chang, M. Porkolab and B. Grek, Phys. Rev. Lett. 28, 206 (1972).

[3] M. N. Rosenbluth and R. Z. Sagdeev, Comments on Plasma Physics and Controlled Fusion 1, 129 (1972).

[4] K. Nishikawa, J. Phys. Soc. Japan 24, 1152 (1968).

[5] R. Briggs, Electron Stream Interactions, MIT Press.

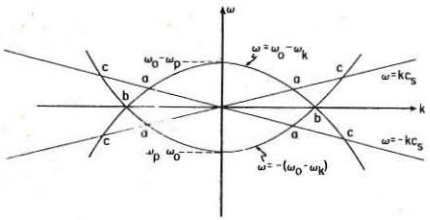


Figure 1. The uncoupled linear modes, $\omega = \pm kc_s$ (ion acoustic waves) and $\omega = \pm(\omega_0 - \omega_k)$ (Langmuir waves)

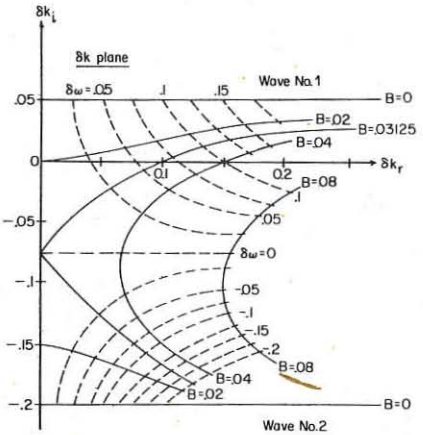
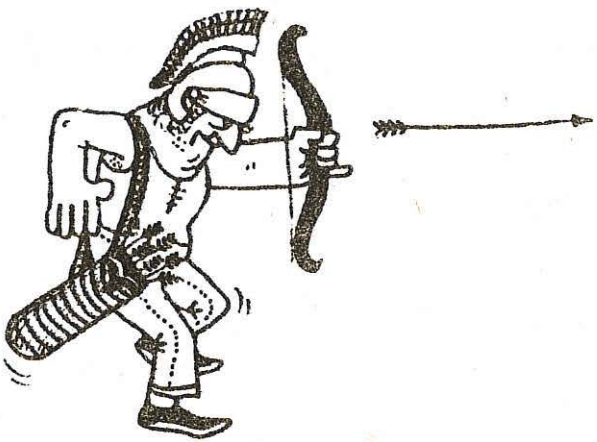


Figure 2. Map of the real $\delta\omega$ axis in the δk plane for Eq.(3) with $V_1 = 1$, $V_2 = -2$, $\gamma_1 = .05$, $\gamma_2 = 0.4$. For these values, $L_1 = 20$, $L_2 = 50$, $B_c = .02$ and $B_a = .03125$.

3.3. RELATIVISTIC ELECTRON BEAMS



HIGH CURRENT DENSITY ELECTRON BEAM APPLICATION TO FUSION STUDIES*

Gerold Yonas, James W. Poukey, John R. Freeman, Kenneth R. Prestwich,
Alan J. Toepfer, Milton J. Clauser, Everet H. Beckner
Sandia Laboratories, Albuquerque, New Mexico 87115

ABSTRACT

Mechanisms are considered for electron beam focusing and absorption in solid targets with emphasis on applications to spherically driven, super-compression of D-T pellets. With recent developments in beam concentration and in pulse power technology, the principal unanswered question is the requirement for efficient coupling of the high current density beam to the target.

Introduction

Initiation of pulsed fusion using intense electron beams was first proposed separately by F. Winterberg and E. K. Zavoisky in 1968. Although this problem has been considered in greater detail since then by workers in the U.S.S.R. and U.S.A., serious interest has only recently been aroused as a result of the following:

1. Experimental demonstrations of successful beam focusing methods to current densities of $\sim 10^7$ A/cm^2.
2. Numerical studies of ablation driven compression.
3. Developments in pulse power technology.

This paper considers some aspects of electron beam behavior which are of concern to pellet fusion concepts. We address questions of focusing beams to achieve the necessary power densities, shaping and guiding the beams to achieve symmetric energy delivery, and efficient absorption in the target.

Fusion Requirements

Earliest proposed approaches to initiation of fusion reactions in solid targets involved rapid heating of bare D-T spheres directly. Needed power densities have been estimated to range between 10^{16} and 10^{17} W/cm^2 with breakeven estimated to occur at 10^7 J. As pointed out by several authors, the inertial confinement time for a smaller pellet can be increased by surrounding the fuel with a high density material or by confining the fuel magnetically, thus resulting in a lower energy requirement. For instance, Babykin and Starykh[1] estimate an ignition energy of 5×10^5 J for a tamped cylindrical pellet, but still requiring a power density of 10^{16} W/cm^2. More recently, Nuckolls et al.[2] have proposed employing laser driven spherical ablation of the outer shell of a pellet to achieve up to 10^4 compression with breakeven energies reduced to as low as 10^3 J. In order to achieve this degree of compression, Clarke et al.[3] predict that a carefully tailored laser pulse shape with a peak power density of 10^{15} W/cm^2 is sufficient to produce a yield of 58 kJ with an input energy of ~ 5 kJ.

Although one can optimistically expect electron beam power densities in the future in the range of 10^{14} - 10^{15} W/cm^2, larger values are probably unlikely. If we are, therefore, to employ the super-compression technique, we must, of necessity, consider scaling up the pellet size and pulse duration from the similar laser approach.

*This work was supported by the U.S. Atomic Energy Commission.

If we do this, we find breakeven energies of roughly 1 MJ with energy deposition times of ~ 10 ns are possible using pellets of a few mm diameter with one of the most crucial parameters in such a calculation being the deposition length. The penalty one must pay in total energy delivered is compensated by the fact that techniques presently exist for fabricating pulsed relativistic electron accelerators in the 10^{13} watt range with energies up to 3 MJ and operating with efficiencies approaching 50%.[4] If we are to consider the application of electron beams, we must first address the questions of beam focusing, spherical loading, and absorption in the pellet. As we shall see, the uncompensated self field of the beam will play a vital role in providing solutions to these problems.

Beam Focusing

Prior to recent emphasis on focusing intense electron beams in diodes, propagating beams have been concentrated to current densities of only 10^5 A/cm^2 or less, with the major limitation on compression being the beam heating due to extraction from the diode and subsequent transport. On the other hand, it is known that high ν/γ vacuum diodes self pinch when the current exceeds a critical value. In this way, current densities $\gtrsim 10^6$ A/cm^2 are achieved, but with limited reproducibility. Additionally, this diode pinch forms late in the pulse with a radial collapse velocity of ~ 0.1 cm/ns. Recent numerical experiments with a 2-D particle code that solves the high ν/γ diode problem for the first time[5] show that the degree of final beam compression is limited because of space-charge effects. As charge is concentrated, equipotential surfaces are distorted, resulting in electron loss to the anode before these electrons can approach the diode axis.

Introduction of plasma on the axis of such diodes leads to substantial improvements. Experiments have shown that even with a relatively low current beam diverging from a pointed cathode, a tight pinch occurs when the diode becomes filled with plasma from the electrodes.[6] In order to employ such a high impedance geometry for fusion, beams in the tens of MeV range would be needed further complicating the problem of energy absorption. In order to obtain both highly pinched beams as well as low impedance diodes, we have used a resistive current carrying plasma near the axis of a large diameter diode to provide beam focusing and space charge neutralization.[7]

The concept is shown schematically in Fig. 1. In some applications, the plasma near the diode axis has been produced by stretching a 0.5 mil W wire from a depression in the cathode surface to the anode. Other plasma injection techniques have shown similar results. Typically we find that the current emitted by the large area cathode is reduced by the magnetic field of the current-carrying plasma, but that the resultant beam is focused to a radius of a few mm or less. With such diodes, current densities of ~ 5 x 10^6 A/cm^2 have been demonstrated with diode impedances as low as three ohms.

Additional 2-D particle code calculations have been carried out by Poukey[8] to illustrate the role of the plasma region. He has found that the longitudinal electric field in the resistive plasma combined with the self-magnetic field of the beam result in the formation of a "super pinch" within the plasma. He showed that a self-pinched, high ν/γ beam will be incident on the anode with current densities of ~ 10^7 A/cm^2. Since these calculations show that current neutralization is not necessary to achieve a consistent equilibrium, it is possible to consider self-field effects in beam deposition and target confinement. In particular, we note that the large spread in angles

of a high ν/γ beam should allow uniform spherical irradiation with only two beams incident on a pellet from opposite sides.

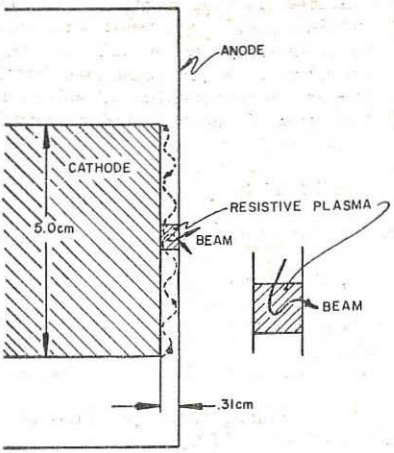


FIGURE I
Beam Focusing Using Current-Carrying Plasma in Diodes

Energy Deposition

The fusion concept considered here involves electron deposition in a relatively cold, dense, outer region of a pellet. Before appreciable expansion of this heated outer layer can occur, deposition will be governed by classical two-body collisions and augmented by self-field effects. Collisional damping of two-stream instabilities[9] in the high-density region and nonlinear saturation of instabilities in the low density blowoff region[10] make these instability effects unimportant.

If current neutralization is incomplete inside the solid, and collisional effects are negligible, then based on a single particle model, we expect that the beam will be magnetically stopped with only the Alfven limiting current able to propagate beyond a Larmor radius. The importance of such self-field effects will depend on the material properties as well as current density. In cases where the electron Larmor radius is much smaller than the classical deposition length, range shortening by as much as an order of magnitude is possible. In other cases, scattering will dominate, also shortening the region of energy deposition. By relying on such range shortening mechanisms, considerably higher kinetic energy beams can be used simplifying the problems of accelerator design. Since it is difficult to predict the actual degree of range shortening, experiments using the existing tightly focused beams will be required before a definitive evaluation of any electron beam fusion concept is possible.

Conclusion

Recent developments in numerical and experimental studies of electron beam focusing in high ν/γ diodes with plasmas on axis suggest that electron beam power densities $\geq 10^{14}$ W/cm^2 range are achievable. Such beams when employed to compress spherical pellets to many times solid density may be able to achieve fusion breakeven with extensions of present day technology. Major questions involve scaling of focusing techniques to higher voltages, demonstration of spherically symmetric loading and efficient absorption of tightly pinched beams in solid targets.

REFERENCES

1. M. V. Babykin and V. V. Starykh, Sov. Phys. Tech. Phys. 16, 1273 (1972).
2. J. Nuckolls et al., Nature 239, 139 (1972).
3. J. S. Clarke et al., Phys. Rev. Letters 30, 89 (1972).
4. B. Bernstein and I. Smith, Bull. Am. Phys. Soc., 18, 194, (1973).
5. J. W. Poukey, J. R. Freeman and G. Yonas, 12th Symposium on Electron Ion and Laser Beam Technology Symposium, Boston (1973).
6. L. P. Bradley and G. W. Kuswa, Phys. Rev. Letters, 29, 1441 (1972).
7. G. Yonas, J. W. Poukey, K. R. Prestwich, and J. R. Freeman, Phys. Rev. Letters, 30, 164, (1973).
8. J. W. Poukey, Sandia Laboratory Report, 1973, (to be published).
9. H. E. Singhaus, Phys. Fluids, 7, 1534, (1964).
10. A. J. Toepfer and J. W. Poukey, Phys. Letters A, 42A, 383, (1973).

ON INITIATING THE IMPULSE NUCLEAR FUSION REACTION BY MEANS OF DT-MIXTURE COMPRESSING BY THE SHELL HEATED WITH A STRONG RELATIVISTIC ELECTRON BEAM

L.I.Rudakov
I.V.Kurchatov Institute of Atomic Energy
Moscow, USSR

A.A.Samarsky
Institute of Applied Mathematics
Academie of Sciences USSR

In a substance with a great Z electrons having energies about 3-5 Mev have free path length of the order of 1 mm. Therefore if the spherical shell of thickness 0,2-0,3 mm and 3-4 mm in diameter filled in by the gaseous DT-mixture is irradiated by a high-current electron beam it can be heated quickly and oonverted into a plasma. Coulomb energy losses of the fast electrons in the substances are strictly proportional to the charge of its atoms, i.e. every electron both in shell and in DT-mixture obtains approximately the same energy. Therefore the internal layer of the shell substance should fly to the center of the sphere and compress and heat DT-mixture ionized and heated by the beam.

The DT-mixture spherical compression by the plasma of the heavy shell was computed using two-components gas dynamics equations with allowance for electron viscosity and heat conductivity but not taking into account the radiation. To involve the ionization processes in a heavy shell effective values γ and Z were used: γ_{eff}= 1,2, Z_{eff}=50. For the estimation of the fusion reaction intensity the α-particle energy was calculated over the total volume of the DT-mixture. However the influence of this energy on the dynamics wasn't taken into account. In the table the initial parameters and results of some variants of the calculation are given in which one can see

the influence of energy E_o put into the shell and of the heating time τ (the time dependence of the heating was $E=E_o\frac{t}{\tau}$ with $t<\tau$) and also of the shell mass and thickness δ and DT-mixture mass on the values of the density and final temperature T_e^* and T_i^* of the DT-mixture and on the fusion energy output in α-particles E_f.

One can see from this table that τ may be delayed till the shell collapse time t^* so as $T(t^*)$ does not change appreciably. This is very important because the rise in the power is the most complicated problem in the beam producing technique. In the variants given above for $E_o \geqslant 3\cdot10^6$ j the heat losses due to the electron heat conductivity out of DT-mixture are significant, which manifests itself in a weak rather than linear dependence $T^*(E_o)$ (see var. 3,4) E_f and T^* increase rapidly in the decrease of the shell mass (see var. 5,6) and more slowly in the decrease in the DT-mixture density (see var. 5,8,9). It is advantageous also to take a thin shell (var. 5,7).

The compression dynamics for variant 5 is shown in Fig.1. From the very beginning ($t < 3\cdot10^{-9}$ sec.) the internal layers of the heated shell which expands almost isothermically fly to the center with an supersonic velocity, $V\simeq 3C_s$. The effect of the spherical density cumulation is masked by the effect of the density decrease due to the expansion into a vacuum.

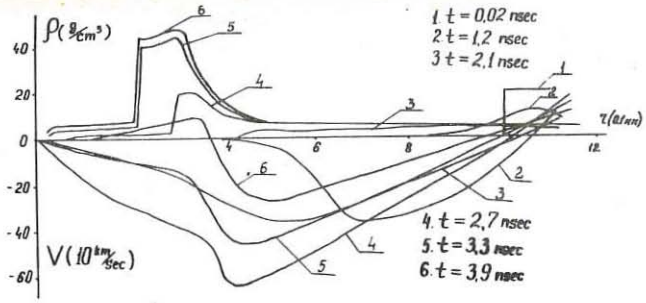
The hydrogen is compressed adiabatically. Its pressure increases rapidly according to the law $p=p_o\left(\frac{R_o}{R}\right)^5$ where R_o and $R(t)$ are the initial DT-mixture radius and the radius at present time. Thus at some radius R_f defined from the condition $p \geq \rho_{sh}\cdot v^2$

supersonic stream stops suddenly and a strong shock wave is formated ($t > 3 \cdot 10^{-9}$ sec.). During the time of the shell substance influx a dense and hot hydrogen nucleus exists where the fusion reaction proceeds.

In the best calculated variants (5,8) the internal energy E_{in} of DT-mixture turns out to be of the order of 2 ÷ 2,5% of the total energy stored in the shell. This low efficiency of the heating is accounted for on one hand by the high ionization energy losses (till 70%) in a heavy substance and on the other hand by the fact that only thin layer of the shell compresses the DT-mixture. Generally speaking, these losses in heating efficiency may be reduced provided that gas dynamics is organized properly. But even in the above mentioned variants the total energy in α-particles is comparable with internal DT-mixture energy thanks to almost 100-times compression of the mixture and to the long duration of compressed state. If the fuel heating by α-particles were taken into account the fuel temperature would increase, the reaction velocity would rise sharply, the share of combustion and fusion energy output would be greater too.

In our calculation the radiation losses from the shell haven't been taken into account at all. According to the estimations the equilibrium radiation power becomes comparable with the power of shell heating at a temperature higher than 500 eV or higher than 2 kV in "successful" variants. How dangerous are such losses the correct calculations with allowance for the radiation heat conductivity will show.

Thus for heating the DT-mixture up to a temperature higher than 5 kV and for impulse nuclear fusion initiation it is sufficient to dissipate $(1 \div 3) \cdot 10^6$ j in the shell 3÷4 mm in diameter during the time of $(3 \div 5) \cdot 10^{-9}$ sec.



№	E_0 10^{-6} j	ρ_{oDt} g/cm³	ρ_{osh} g/cm³	R_o mm	δ	10^{-9} sec	t^* 10^{-9} sec	$\frac{T_e^*}{T_i^*}$ kev	$\rho(t^*)$ g/cm³	$E_{in}(t^*)$ x 10^{-4} j	Ef x 10^{-4} j
1	4.2	0.03	20	2	0.27	1.25	12.5	$\frac{2.6}{2.6}$	0.93	2.8	0.4
2	4.0	0.03	20	2	0.27	10	20,0	$\frac{2.2}{2.2}$	0.92	2.4	0.15
3	3.3	0.025	20	1	0.2	1	7.5	$\frac{3.9}{4.0}$	2.2	4.6	2.3
4	9.9	0.025	20	1	0.2	1	3.2	$\frac{7.1}{8.3}$	3.2	7.5	33
5	3.2	0.025	20	1	0.1	1	3.2	$\frac{6.2}{7.6}$	1.3	7.5	8.8
6	3.4	0.025	20	1	0.36	1	6.3	$\frac{2.6}{2.6}$	1.4	2.8	0.3
7	3.2	0.025	20	1	0.65	1	3.8	$\frac{3.1}{3.6}$	0.2	3.8	0.24
8	3.2	0.05	20	1	0.1	1	3.1	$\frac{5.3}{5.9}$	1.1	12	8
9	3.2	0.0125	20	1	0.1	1	3.1	$\frac{6.6}{9.8}$	1.8	4.4	7

THE EFFECT OF MAGNETIC FIELD ON THE INTERACTION BETWEEN A RELATIVISTIC ELECTRON BEAM AND PLASMA

B.N.Breizman

Institute of Nuclear Physics, Novosibirsk, USSR

The role of helicons in the process of relaxation of the relativistic electron beam is investigated. The conditions are found, under which helicons rather than Langmuir oscillations are responsible for the relaxation. The relaxation length is estimated for the problem of stationary injection of the beam into plasma.

To estimate the efficiency of plasma heating by a relativistic electron beam it is necessary to investigate the collective processes connected with the beam instability. This problem has been solved /1/ for the case of the stationary injection of the beam into isothermal plasma without any magnetic field. Under such conditions the beam interacts only with Langmuir oscillations. The density of their energy is limited due to induced scattering of the oscillations by plasma ions. If so, the relaxation length is

$$l = \frac{c}{\omega_p}\frac{n}{n'}\left(\frac{E}{mc^2}\right)^3\left(\frac{mc^2}{T}\right)^2\frac{m}{M} \qquad (1)$$

Here n' and n represent beam and plasma concentrations respectively, T - plasma temperature, E - the energy of beam electrons.

It is pointed out in this paper, that if magnetic field exists in plasma, then the other mechanism of the relaxation is possible, which under proper conditions is more effective than the generation of Langmuir oscillations. The origin of this mechanism is the beam instability with respect to the generation of helicons. It appears already at $\beta \equiv 8\pi nT/H^2 \geqslant 1$, when the field practically does not

affect neither the dispersion of Langmuir oscillations, nor the magnitude of the matrix element of the scattering of these oscillations by ions.

For excitation of helicons by the beam the resonance condition $\omega - K_z V_z - n\omega_H \frac{mc^2}{E} = 0$ must be held. Since the phase velocity of helicons is much less than the velocity of light, the resonance is possible only at $n \neq 0$. If so, in an elementary act of interaction the wave with energy ω is radiated, the change of transverse energy of a beam electron being $\frac{mc^2}{E}\omega_H \gg \omega$. Therefore, relaxation results mainly in the increase of the beam angle spread and only in small energy losses (relative energy loss is proportional to $\frac{\omega}{\omega_H}\frac{E}{mc^2}$).

It follows from the analysis of the instability increment γ that a beam with angle spread $\Delta\theta$ excites most effectively the oscillations with $K_z \sim \frac{\omega_H}{c}\frac{mc^2}{E}$; $K_z \leq K_\perp \leq K_z/\Delta\theta$, the characteristic value of γ being given by

$$\gamma \sim \omega_H \frac{n'}{n}\frac{mc^2}{E}\frac{1}{\Delta\theta^2} \qquad (2)$$

At $\omega_p \gg \omega_H$ this quantity is small compared to that for Langmuir oscillations. Nevertheless, if the energy density of Langmuir oscillations is restricted by nonlinear processes, it is the excitation of helicons that turns out to be the mechanism of beam - plasma interaction. In the following we shall consider this very situation.

First, we shall give the estimates for the relaxation length and the final energy density assuming the nonlinear wave - wave interaction to be negligible. In this case the relaxation length is $l_o \sim V_{gr}/\gamma$ (V_{gr} - the oscillation group velocity). At the distance l_o from the plasma boundary the level of oscillations becomes

much greater than the thermal one and the beam angle spread increases up to $\Delta\theta \sim 1$. Substituting the value of the characteristic wave vector of beam excited oscillations into the expression for l_o and assuming $\Delta\theta \sim 1$, one gets:

$$l_o \sim \frac{c}{\omega_p} \frac{n}{n'} \frac{\omega_H}{\omega_p} \qquad (3)$$

The energy of oscillations is determined from the momentum flux conservation law. Taking into account, that there are no oscillations at the plasma boundary, and at $z = l_o$ the momentum fluxes of oscillations and beam electrons are of the same order of magnitude because of the considerable beam electrons scattering, one gets: $V_{gr} \frac{k_z}{\omega} W \sim n' E$. This leads to

$$W \sim n' E \qquad (4)$$

The estimate (3) can be easily extended to that situation in which nonlinear wave - wave interaction is essential, and therefore the energy of oscillations interacting with a beam can not be estimated by formula (4). In order to do it one should note, that as it comes from the quasilinear equation for beam electrons, the relaxation length is inversely proportional to the oscillation energy density W . Therefore in the nonlinear regime of the relaxation one gets:

$$l_{NL} \sim l_o n' E / W \qquad (5)$$

Here the energy density W must be determined from the fact, that the inverse time of the nonlinear interaction of helicons is of the order of instability growth rate γ .

It follows from the estimates of matrix elements of nonlinear processes with beam excited helicons that the process responsible for the limitation of oscillation amplitude is the decay process

$$\omega(\vec{k}) = \omega(\vec{k}_1) + \omega(\vec{k}_2) \quad ; \quad \vec{k} = \vec{k}_1 + \vec{k}_2$$

(here $\omega(\vec{k}) = \omega_H |\vec{k}| |k_z| c^2/\omega_p^2$). For this process $\gamma_{NL} \sim \omega W/H^2$. Substituting into formula (5) the value of W, determined from the equation $\gamma_{NL} \sim \gamma$, one gets the following expression for the length of relaxation

$$l_{NL} \sim \frac{c}{\omega_p} \frac{n}{n'} \frac{\omega_H}{\omega_p} \sim l_0 \qquad (6)$$

The values l_{NL} and l_0 are of the same order of magnitude. This means that for the beam excited helicons nonlinear processes are considerably less essential than those for Langmuir oscillations.

Comparing formulae (1) and (6) one finds, that for

$$\beta^2 < \left(\frac{\omega_p}{\omega_H}\right)^5 \left(\frac{E}{mc^2}\right)^3 \frac{m}{M} \qquad (7)$$

inequality $l_{NL} < l$ is held. Thus at $\beta \geq 1$ inequality (7) gives the condition under which namely the excitation of helicons is decisive for the relaxation of a beam.

Strictly speaking, the obtained formulae are valid only for the beams having large enough radii ($R \gg l_0$), since otherwise, the waves leave too fast the region of the interaction with a beam, propagating in the radial direction. However under real conditions this restriction seems to be not very essential. The reason is that because of the radial inhomogeneity of both plasma concentration and magnetic field the plasma coulumn may become a waveguide. Then the oscillations will be trapped, the qualitative pattern of the relaxation being the same as in the case of the wide beam.

The author is grateful to D.D.Ryutov for useful discussions.

Reference:

1. B.N.Breizman, D.D.Ryutov, P.Z.Chebotaev. JETP, 62, 1409 (1972).

INVESTIGATION of PLASMA HEATING by a RELATIVISTIC ELECTRON BEAM

Yu.I.Abrashitov, V.S.Koydan, V.V.Konyuchov, V.M.Lagunov, V.N.Lukyanov, K.I.Mekler

Institute of Nuclear Physics, Novosibirsk, USSR

The heating of a hydrogen plasma by a high-current relativistic electron beam was investigated for plasma in a strong magnetic field. This work is a continuation of experiments /1/.

Schematic of apparatus was given in /1/. The electron beam with an initial energy of 1 MeV, current ~ 5 kA and ~ 70 nsec duration was produced with a pulsed electron accelerator. A beam was injected into plasma chamber through 0,05 mm thick titanium foil. The beam diameter was 2 cm at the entrance into a plasma. The fieldemission diode and the plasma chamber were placed in quasistationary mirror magnetic field with the mirror ratio equal to 1,7. The distance between mirrors was 230 cm. Maximum value of the magnetic field in homogeneous region achieved 15 kOe. The main part of the vacuum chamber was the glass tube of 11 cm diameter. Initial plasma with density up to 10^{14} cm^{-3} was produced by a pulsed Penning-type discharge, Diameter of plasma column being of 8 ÷ 9 cm. The entrance and exit foils of 6 cm diameter situated in magnetic mirrors were used as cathodes. The 8 cm diameter ring in the midplane of the vacuum chamber was used as anode of this discharge. The exit electrode receiving an electron beam was connected with the accelerator by the return current conductors placed symmetrically around the glass tube. The fieldemission cathode voltage was controlled with a capacitive divider. The cathode diode current and the total current in plasma were measured by Rogov-

INVESTIGATION of PLASMA HEATING by a RELATIVISTIC ELECTRON BEAM

Yu.I.Abrashitov, V.S.Koydan, V.V.Konyuchov, V.M.Lagunov, V.N.Lukyanov, K.I.Mekler

Institute of Nuclear Physics, Novosibirsk, USSR

The heating of a hydrogen plasma by a high-current relativistic electron beam was investigated for plasma in a strong magnetic field. This work is a continuation of experiments [1].

Schematic of apparatus was given in [1]. The electron beam with an initial energy of 1 MeV, current ~ 5 kA and ~ 70 nsec duration was produced with a pulsed electron accelerator. A beam was injected into plasma chamber through 0,05 mm thick titanium foil. The beam diameter was 2 cm at the entrance into a plasma. The fieldemission diode and the plasma chamber were placed in quasistationary mirror magnetic field with the mirror ratio equal to 1,7. The distance between mirrors was 230 cm. Maximum value of the magnetic field in homogeneous region achieved 15 kOe. The main part of the vacuum chamber was the glass tube of 11 cm diameter. Initial plasma with density up to 10^{14} cm^{-3} was produced by a pulsed Penning-type discharge, Diameter of plasma column being of 8 ÷ 9 cm. The entrance and exit foils of 6 cm diameter situated in magnetic mirrors were used as cathodes. The 8 cm diameter ring in the midplane of the vacuum chamber was used as anode of this discharge. The exit electrode receiving an electron beam was connected with the accelerator by the return current conductors placed symmetrically around the glass tube. The fieldemission cathode voltage was controlled with a capacitive divider. The cathode diode current and the total current in plasma were measured by Rogov-

sky coils. The beam current at the exit from plasma was recorded by means of a shunt. The total energy of a beam behind the exit foil was measured with graphite calorimeter of 6 cm diameter. To visualise the cross-section shape of a beam in certain experiments thin polymer plates were placed behind the exit foil. Passing through the plates the beam made them darkened. This darkening enabled to qualitatively fix changing of the beam configuration depending on plasma density and the magnetic field. The plasma density was determined by microwave methods with λ =3, 1.3, 0.8 and 0.4 cm The transversal plasma pressure was measured by four diamagnetic loops located at 35, 90, 140, 190 cm from the entrance foil.

The experiments showed that when the beam passed through the vacuum, then diamagnetic loops recorded signals with 15 ÷ 30 nsec risetime and duration approximately equal to that of the beam. These signals are the diamagnetism of the beam. If the beam passed through plasma then the signals increased 5 ÷ 7 times in amplitude and their durations raised up to some microseconds. The energy value per plasma column unit length ($nT_{\perp}S$) in dependence on the initial plasma density is shown in Fig. 1. The smooth rise of plasma pressure is observed up to density of $\sim 5 \cdot 10^{13} cm^{-3}$. Note that the density value inthe maximum of diamagnetism is nearly two orders of magnitude greater than that in paper [2].

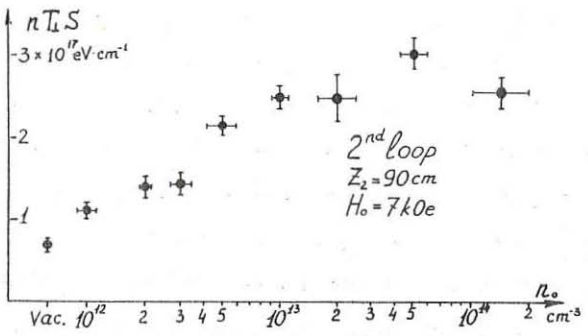


Fig. 1

The comparison of diamagnetic signals from several loops showed that as a rule the largest signal was observed from the first loop (Z_1 = 35 cm). At the last loop (Z_4 = 190 cm) diamagnetic signal is approximately 2 ÷ 3 times less. Apparently this fact shows that observed diamagnetism is due not to the trapped electrons of the beam but to plasma heating. As it is seen in Fig. 1 the maximum diamagnetism value is $nT_\perp S \simeq 3.10^{17}$ eV.cm^{-1}. If one assumes that the heating takes place only in the plasma column region through which the beam passes ($S \simeq 7$ cm^{-2}), then the energy accumulated in the unit volume is $nT_\perp \simeq 4{,}5.10^{16}$ eV.cm^{-3}. For density $n \simeq 5.10^{13}$ cm^{-3} it corresponds to plasma heating up to $T_\perp \sim 1$ keV. Estimated with diamagnetic measurements the value of energy stored in the full plasma column after electron beam passing is of 10÷15% of the total beam energy.

The dependence of transversal plasma pressure on external magnetic field H_0 was studied in the experiments and shown in Fig.2. The field H_0 was changed in the range 3kOe ≤ H_0 ≤ 15 kOe. For the fixed density the plasma pressure increases when magnetic field changes from 3 to 10 kOe. Plasma pressure in the range 10 kOe ≤ ≤ H_0 ≤ 15 kOe doesn't change.

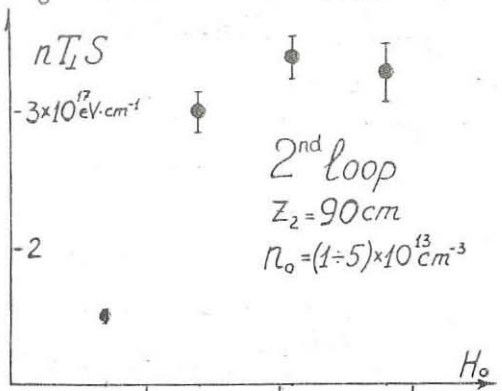


Fig. 2

With the aid of the polymer plates it was observed that the beam passing through the vacuum (p = 10^{-6} Torr) at the exit of device had symmetrical form (~2,5 cm in diameter) at it is seen in Fig. 3a. If the beam passed through plasma it might be

significantly deflected and simultaneously broadened (generally speaking, irregularly both in radial and azimuthal directions).The beam broadening and its deflecting were especially large for density values $10^{12} \div 10^{13}$ cm^{-3} (Fig. 3b). In this regime some part of beam can be "eaten" by the vacuum chamber walls. In this case the exit calorimeter will record large energy losses (up to 50÷70 %). Such a behaviour of beam can be responsible to some extent both for the value of energy losses observed before and for their dependence on plasma density /1,2/. For large densities ($n > 10^{13}$cm^{-3}) broadening of the beam was small.

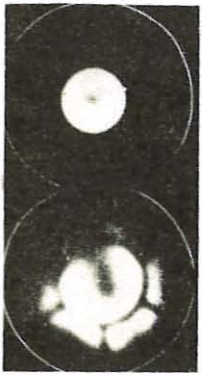


Fig. 3

The experiments on measurement of total current in plasma in the beam presence showed that for plasma density $n \sim 10^{14}$cm^{-3} the beam current was completely neutralized by return current. If $n \sim 10^{12}$cm^{-3}, the neutralization of a beam current practically disappeared.

After the beam passing through partly ionized plasma an additional ionization of neutrals was observed within ~ 500 nsec. Such an ionization could be produced by plasma electrons heated to temperature ~ 1 keV. This value is in satisfactory agreement with temperature $T_\perp$ obtained in diamagnetic measurements.

The authors sincerely thank G.I.Budker, D.D.Ryutov,E.P.Kruglyakov for the interest to this work, O.P.Sobolev,G.I.Shuljenko for their assistance.

R E F E R E N C E S

/1/ V.S.Koydan et al. 5th Europ.Conf. on Control.Fusion and Plasma Physics. Grenoble, V. 1, p. 161, 1972.

/2/ A.T.Altyntsev et al. Plasma Physics and Controlled Nuclear Fusion Research, IAEA, Vienna, V. 2,p. 309, 1971.

PLASMA HEATING BY INTENSE RELATIVISTIC ELECTRON BEAMS

W. F. Dove, K. A. Gerber, G. C. Goldenbaum,
D. A. Hammer, C. A. Kapetanakos and B. G. Logan
Naval Research Laboratory, Washington, D. C. 20375 USA

ABSTRACT - The heating of magnetically confined plasma in the density range 10^{11} - 10^{15} cm^{-3} by intense relativistic electron beams is discussed. The presence of strong collective interactions is evidenced by coupling efficiency being much higher than "classical" mechanisms predict. The self field effects of the $\nu/\gamma > 1$ beams are evident for the lower plasma densities.

INTRODUCTION - The availability of intense relativistic electron beams having power in excess of 10^{12} watts and energies of many kilojoules has aroused great interest in their use for heating large volumes of plasma to temperatures applicable to thermonuclear fusion. How well intense beams will couple their energy into a plasma is of great importance to their ultimate utility in fusion applications. In particular, coupling via classical coulomb interaction between beam and plasma is not strong enough, and it is necessary that a collective process take place in order to decrease the energy coupling length by several orders of magnitude. Experiments reported so far [1-3] have been performed using beams in which the self fields, even if not neutralized by the plasma, are not sufficiently strong to dominate the beam-plasma system. These experiments have found that significant turbulent energy loss occurs over a fairly narrow beam-plasma density ratio centered around ~ 0.1. The beam intensity parameter ν/γ was no higher than ~ 0.1 for any of these experiments, where ν is the number of electrons per classical electron radius of beam length (2.83×10^{-15} m) and γ is the electron total energy in rest mass units (511 keV). In the experiments reported here, beams having ν/γ in the range 1-2 are injected axially into magnetically confined plasmas in the density range $n_p = 10^{11}$ - 10^{15} cm^{-3}. Since the beam densities are $n_b \sim 10^{12}$, at the lowest plasma densities beam self fields should play an important role in the beam-plasma interaction. A regime in which a strong two stream electrostatic instability is expected to exist, occurs when $(n_b/n_p)^{\frac{1}{3}} \gamma \sim 1$. Finally, if an ion acoustic mode, which requires $\nu/\gamma > 1$ for any significant plasma heating [4], were to be operative, it would occur at the higher plasma densities. However, throughout the plasma density range tested, it appears that the electron-electron two stream instability is the main interaction mechanism.

The two experiments reported here differ as follows: In the SOL experiments, the beam is injected into a magnetic mirror confined 10^{11} - 10^{14} cm^{-3} density plasma. In the TRITON experiments, the plasma (10^{14} - 10^{15} cm^{-3}) is contained in a long, uniform magnetic field to separate the effects of a non-uniform magnetic field from the beam-plasma interaction.

SOL EXPERIMENT - A schematic of the experiment is shown in Fig. 1. The 5 cm outside diameter, 0.6 cm thick annular electron beam is emitted from a carbon cathode that is immersed in a uniform magnetic field. The beam, after passing through the 2.5 X 10^{-3} cm thick titanium foil anode, enters the 60 cm long drift region which contains air at ~ 700 mTorr pressure. A 1.2 X 10^{-3} cm thick titanium foil separates this drift region from the 40 cm long, 14 cm diameter magnetic mirror region (mirror ratio 1.8:1) containing the plasma. This plasma is produced by a Z-discharge and has a temperature of approximately 1 eV and a peak density of 3 X 10^{14} cm^{-3}. As a result of the various losses the plasma density decays to 10^{11} cm^{-3} in about 1 msec. When the desired plasma density is reached the electron beam is injected into the plasma.

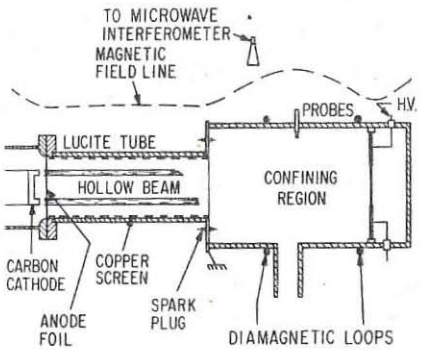


Figure 1

The energy content of the plasma (= $n_p kT$, where n_p is the plasma density and T is the sum of ion and electron plasma temperatures) after beam injection is measured using diamagnetic loops and a piezoelectric probe. Figure 2 (solid curve) shows the variation of $n_p kT$ with plasma density. The curve is peaked when the plasma density is comparable with the beam density n_b. The maximum observed value of $n_p kT$ is approximately 10^{17} eV - cm^{-3}, corresponding to a coupling energy efficiency from the beam into the plasma of about 25%. The rapid drop of $n_p kT$ for n_p less than n_b is attributed to poor propagation of the electron beam. The results for $n_p \geq 5 \times 10^{11}$ are consistent with computer calculations of the saturation of the electron-electron two-stream electrostatic

instability [5]. The dashed curve in Fig. 2 shows the beam energy reaching a calorimeter placed just outside the far mirror. At $n_p \simeq n_b \simeq 5 \times 10^{11}$ cm^{-3} only 1/10 of the available beam energy passes through the far mirror. Thus, the calorimetry always gives beam energy loss much greater than required to explain the observed plasma heating. It is also found that $n_p kT$ is independent of externally applied magnetic field provided that $B > 2.5$ kG.

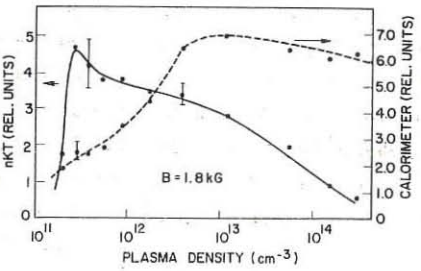


Figure 2

Furthermore, for $B \leq 2$ kG the plasma return current oscillates with frequency of $\geq 10^8$ sec^{-1} when $n_p \leq n_b$. These oscillations, and the above mentioned sharp drop in coupling efficiency at low plasma density, appear to be manifestations of the beam self fields for the $\nu/\gamma > 1$ beam.

Preliminary data indicate that x-rays of energy greater than 10 keV are emitted for several microseconds from the confining region over a large range of magnetic field. Experiments are in progress to determine the origin and spectrum of these x-rays.

TRITON EXPERIMENT - The TRITON experiment is designed to study the beam plasma interaction with a minimum of complications due to plasma confinement. The target plasma is produced in a low energy theta pinch that is 4 m long by 15 cm diameter. The beam is transported an additional 1 m from the accelerator to the theta pinch by a magnetic guide field that extends from the cathode to the theta pinch and is matched in amplitude (5 kG) to the peak theta pinch field. For the experiments reported here no mirror regions exist in the theta pinch so that the beam makes only one pass through the plasma and is stopped in a carbon calorimeter. The beam plasma interaction is studied by an assortment of diagnostic techniques including optical line emission spectroscopy, x-ray emission spectroscopy, and Thomson scattering of ruby laser radiation. We report here on the results obtained for one set of initial parameters. A 1.0 MeV, 50 kA, 70 nsec, 5 cm diameter beam of electrons is injected into a helium plasma whose electron

density and temperature in the theta pinch is determined to be $\sim 7 \times 10^{14}$ cm^{-3} and ~ 7 eV. X-ray emission is observed 4 m from the accelerator with a dual channel plastic scintillator and photomultiplier combination which is collimated to view at right angles to the beam trajectory. Metal filters were used to observe various wavelength regimes of the emitted spectrum. The total x-ray pulse lasts for about 100 nsec and contains two shorter duration pulses which contain peak photon energies of 200 keV and 250 keV respectively. A longer duration lower energy ($\lesssim$ 50 keV) spectrum also exists. The geometry and sensitivity of the light scattering apparatus enable us to observe the radial distribution of electron velocities from zero to about twice the electron thermal speed. Approximately 99% of the electrons fall within this range. For times up to two microseconds after the beam passage no change is seen in this part of the electron velocity distribution. Many collisions occur in this time so the results may be taken to imply that no changes in the speed distribution occurs out to energies at least four times the thermal energy. Finally, the calorimeter records less than 20% of the initial beam energy.

For our parameters, $(n_b/n_p)^{\frac{1}{3}} \gamma \approx 0.3$. Consequently, the electron-electron two stream instability is expected to be strongly excited. We interpret our results to mean that the relativistic beam strongly interacts with the less than 1% of the plasma electrons on the Maxwellian tail of the initial plasma distribution function, resulting in a class of electrons with average energy $\approx$ 200 keV and total energy content of the same order of magnitude as the initial beam. These results are consistent with the computer simulation and theory of Thode and Sudan [6] in which the high energy electron tails are overpopulated and the electrons gain about 25% of the beam energy through the parametric decay of the beam excited electron plasma wave energy to lower phase velocity waves.

1. A. T. Altyntsev, et. al., Plasma Physics and Controlled Nuclear Fusion Research, Vol 2, (IAEA, Vienna, 1971) p. 309.
2. V. S. Koydan, et. al., Proc. Fifth European Conference on Controlled Fusion and Plasma Physics, 1972, Vol 1, p. 161.
3. D. R. Smith, Phys. Letters 42A, 211 (1972).
4. R. V. Lovelace and R. N. Sudan, Phys. Rev. Letters 27, 1256 (1971).
5. A. J. Toepfer and J. W. Poukey, Phys. Letters 42A, 383 (1973).
6. L. E. Thode and R. N. Sudan, Phys. Rev. Letters 30, 732 (1973).

PLASMA HEATING WITH A RELATIVISTIC ELECTRON BEAM

P. Korn, F. Sandel and C. Wharton

Cornell University, Ithaca, N.Y., U. S. A.

ABSTRACT

Significant plasma heating due to the interaction of an intense relativistic electron beam with a plasma column has been observed in a new experiment. The threshold for the onset of heating and the dependence of total perpendicular energy on beam current are similar to the cases for direct turbulent heating in the same plasma geometry.

1. Description of the Experiment

The experiment geometry is sketched in Fig. 1. The portion to the right of the electron gun cathode is the original THM turbulent heating apparatus, whose performance is well known[1,2].

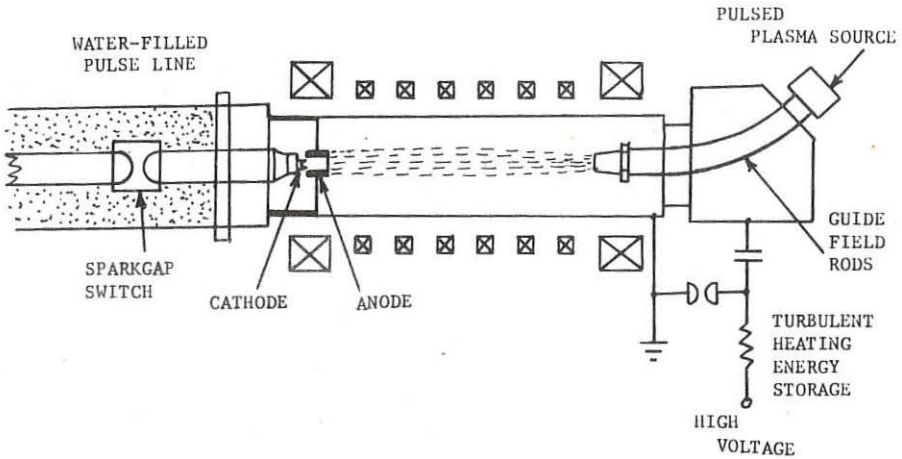


Fig. 1 Cornell THM installation modified to permit plasma heating by an intense relativistic electron beam. The chamber diameter is 40 cm; distance between electrodes is 180 cm.

All the diagnostic instruments and the same plasma conditions before heating have been retained, permitting a direct comparison between conventional turbulent heating and heating with the electron beam. A hydrogen plasma column having a density of 3 to 6×10^{13} cm^{-3} and a diameter of 5 cm is supported by a magnetic mirror field of 2000 to 5000 gauss (central) in a vacuum of 3 to 5×10^{-6} torr. The absence of background gas around the plasma column is important to the performance of the beam-plasma interaction.

The electron beam has an energy of 500 keV at a current of up to 83,000 amperes (6 Ω water-filled energy storage line) and a pulse duration of 60 nsec. The maximum energy in the beam is thus 2500 joules, which is somewhat more than that available for direct turbulent heating.

Two types of diode structures were used, one with a 2.54×10^{-3} cm thick titanium anode foil, and one without. The plasma heating indicated by the diamagnetic loop was similar for both configurations as long as plasma was allowed to enter the anode region. The main disadvantage of the foil anode was that the foil ruptured after 5 to 20 firings requiring that the experiment be opened for anode replacement. That procedure caused delays and unavoidable vacuum contamination leading us to adopt the foil-less diode for most experiments. The beam diameter was matched to that of the plasma column, with the diode immersed in the magnetic field at the peak of the mirror.

2. Diode and Beam Characteristics

The foil-less diode impedance was found to depend on several features, but was most sensitive to the presence of magnetized plasma in the anode region. Without magnetized plasma (to neutralize spacecharge) the impedance was high, and very little current could be extracted. The current that was extracted did not propagate very far in the vacuum magnetic field.

Without magnetic field the impedance was low due to direct electron transit to the anode ring, followed by "gap closure" from metal vapors filling the anode-cathode space. Considerable anode and cathode erosion occurred unless the proper geometry and conditions were found. With plasma present, in a strong magnetic field ($B \geq 6000$ gauss), a brass tubular anode and a carbon ring (sharp-edged) cathode were useful for ~500 firings.

In one experiment the cathode emitting surface was annular, but the beam filled in to a solid cross section within ~20 cm in the plasma column, as evidenced by damage patterns on a slender plastic rod inserted in the plasma column.

Foil-anode diodes have been discussed by numerous authors in a wide variety of configurations. Our experiments did not show any new effects except that the presence of plasma against the outside of the foil seemed to lengthen its lifetime before rupture, presumably by diverting some of the return current.

3. Plasma Heating

For direct turbulent heating we found that the onset-threshold was at a plasma current of ~8000 amperes.[1] The same value of threshold was found for the relativistic electron beam current in these preliminary experiments. This evidence suggests the possibility that the reverse current induced by passage of the primary beam through the plasma is responsible for the heating,[3] since other mechanisms would not have the same threshold. Fig. 2 shows the sudden onset of heating and the steep dependence of total perpendicular energy $W_\perp$ on current.

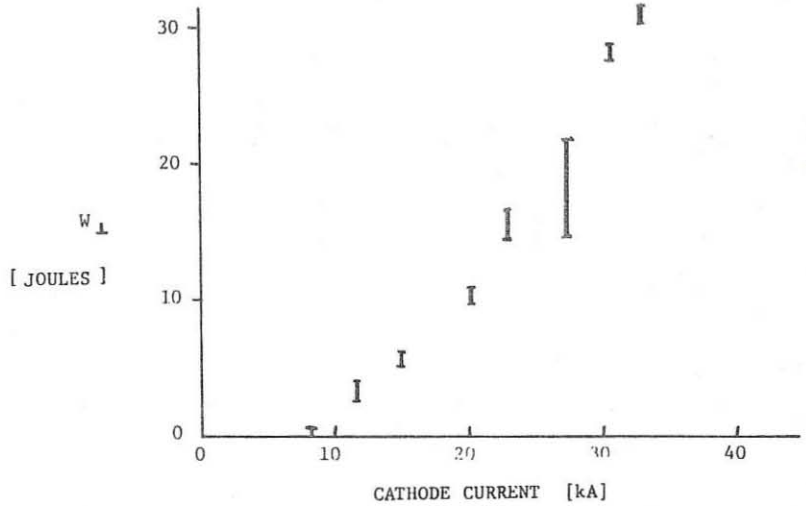


Fig. 2 Dependence of total perpendicular energy $W_\perp$ on diode current. Carbon cathode and 0.0025 cm Ti.foil anode used in diode. Magnetic field 3000 gauss at the diode.

$W_\perp$ was obtained with a diamagnetic loop. The values shown were read just after the heating pulse, before the decay due to confinement losses. The time-dependence of the diamagnetic signal was very similar to that for direct turbulent heating. At the end of heating the maximum $W_\perp$ was about 30 joules, corresponding to an energy of $\geq$5 keV per electron-ion pair. A rapid drop, with τ ~ 6 μsec, was followed by a slower decay with τ ~ 50 to 100 μsec. We associate the initial decay with loss of electron energy (e.g. by thermal conductivity to electrodes) and the slower decay with loss of energetic ions by scattering and charge exchange. The decay time of the electron density, as read by a 4 mm λ microwave interferometer, is longer than either of the above. There is the possibility that the long decay was

due to trapping of primary beam electrons, but we have no evidence that this is the case.

Because we held the diode voltage pulse constant at ~500 kv, the various currents were obtained by changing the diode impedance (mis-matching). No evidence of heating saturation is seen in this figure.

4. Ion Energy Spectrum

Ion heating has been observed with a 4-channel energy analyzer for fast neutral hydrogen atoms arising from charge exchange. We have insufficient data at this time to draw valid conclusions regarding the spectral shape, the average energy or the isotropy, but it is clear that there are hot ions present after heating, and thus at least a portion of the diamagnetic signal is undoubtedly due to ion heating. In experiments to date this heating occurs near the diode region, since the beam does not propagate the full length of the plasma column. That result is not unreasonable in the modest magnetic fields employed.

References

1. Robertson, S., P. Korn and C. Wharton "Parametric Study of Turbulent Heating." (Dec. 1972) Submitted to IEEE Soc. of Nuclear and Plasma Sciences for publication in Transactions.

2. Wharton, C. et al. Proc. 4th Intl. Conf. on Plasma Physics and Controlled Nuclear Fusion Research, Madison, Wisc., U.S.A., 1971; Vol. II p. 25 (1971).

3. Lovelace, R. and R. Sudan "Plasma Heating by High Current Relativistic Electron Beams." Phys. Rev. Letters 27 (19), 1256 (1971).

This work was supported in part by the U. S. Atomic Energy Commission and the Office of Naval Research.

ENERGY SPECTRUM MEASUREMENT OF RELATIVISTIC ELECTRONS IN EXPERIMENTS ON INTERACTION OF HIGH-CURRENT BEAM WITH PLASMA

T.S.Gosteva, L.V.Dubovoi, G.R.Zablotskaya,
B.A.Ivanov, V.I.Chernobrovin

D.V.Efremov Scientific Research Institute
of Electrophysical Apparatus,
Leningrad

A B S T R A C T

The present paper is concerned with the experimental investigation of distribution processes of an intense beam of 50 kA relativistic electrons in neutral gases. Conditions of plasma formation in this case are determined and an energy spectrum of accelerated electrons is measured.

In the experiments a 50 kA relativistic electron beam with bunch energy of about 1 kj, and pulse duration of 20 ns was used [1] . Accelerated electrons came into a 0.5 m metal drift chamber of 12 cm diameter through a 50 μ - titanium foil. The drift space is free from external electric and magnetic fields. The experiments were made in the chamber pressure range of 0.02-60 torr, working gases were air, hydrogen and argon.

In the experiments time dependence of full current pulse form in the air pressure range of 0.04-0.4 torr in the chamber was found. The oscillograms of Fig.1 show that the current pulse shortens with increasing gas density, which is especially discernable at the pressure of $\sim$ 0,35 torr.

Fig.2 gives the dependence of the electron bunch energy registered by a calorimeter at a distance of 18 cm (1) and 45 cm (2) from the anode foil.

The highest value of the bunch energy of about 700j is registered in the experiments at the pressure of $\sim$ 0.3 mm Hg at 18 cm from the anode foil.

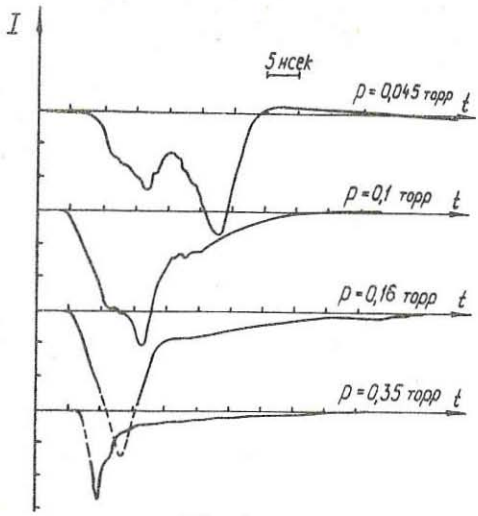


Fig.1

The presented measurement results are indicative of the strong effect of the electron beam gas focusing at pressures exceeding 0.2 mm Hg.

The difference between the beam energy at the beginning and the end of the chamber (more than 100j) may arise from the insufficient gas focusing of the beam. Another reason of the observed effect may be energy losses of the electron beam associated with the formation of plasma and the subsequent generation of the return current by an induced electric field.

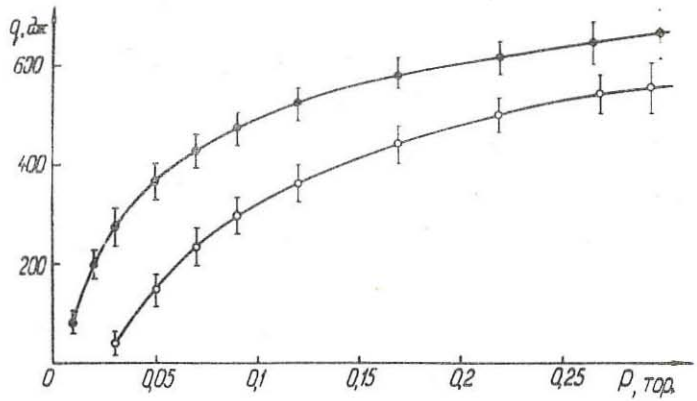


Fig.2

The energy losses of the electron bunch may also be caused by the excitation of plasma-beam instabilities in the chamber arising from the interaction between the beam and the plasma

formed by it.

To determine the energy spectrum of the accelerated electrons a magnetic analyzer, calibrated by a monoenergetic electron beam, was used.

Fig.3 shows energy distribution functions of the primary beam electrons obtained in the experiments at the gas pressures of 0.04, 0.065 and 0.2 torr in the chamber.

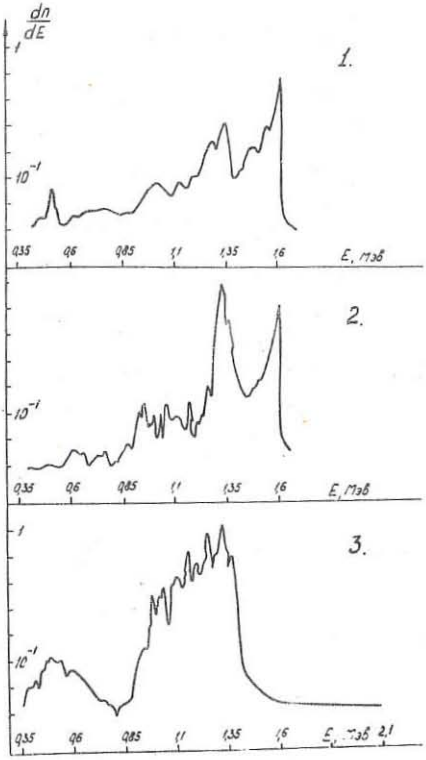


Fig.3

As seen from Fig.6-1 at small values of gas pressure the largest peak of the beam intensity corresponds to the bounary energy of 1.5-1.6 MeV. There is another peak with the smaller intensity of 1,3 MeV - particles. The peak amplitude with the smaller energy increases as the pressure in the chamber increases.

In the pressure range of 0.2-1 torr the spectrum has a diffused character and tends to form a "plateau", in this case the maximum of the spectrum intensity is noticeably shifted to the side of smaller energies (about 1.3 MeV). It is interesting to note that in this pressure range a group of high-temperature electrons with an energy up to 2 MeV appears, which exceeds the

boundary energy of the beam spectrum in other pressure ranges.

It should be noted that in the energy range of 0.01-1 torr a periodic structure begins to show itself in the spectrum. This may point to the presence of the beam-plasma instabilities in the experiments.

Fig.4 gives the dependence of energy E_m, corresponding to the maximum intensity of the spectrum, on the density of gas at charging voltages of 3.6Mv (1), 3.18 Mv (2) and 2.9 Mv (3) in the forming line. As seen, under conditions of best focussing the appreciable decrease of value E_m takes place (20%). This value is in agreement with the above results of calorimetric measurements.

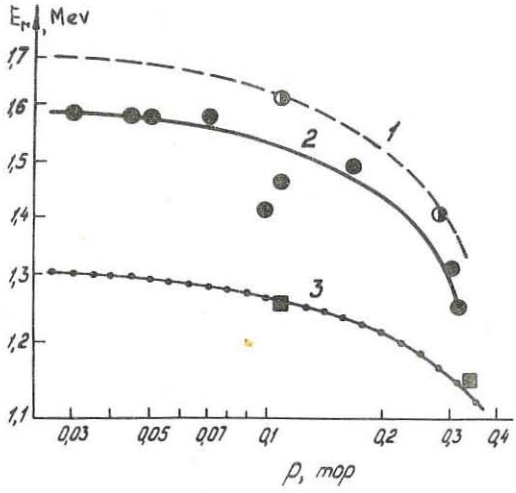


Fig.4

The mentioned effect points to the fact that the reason of the observed losses is the consumption of the beam energy on the formation of plasma and the generation of return current.

R e f e r e n c e s

1. T.S.Gosteva, G.R.Zablotskaya, B.A.Ivanov, V.I.Chernobrovin. Distribution of relativistic electron beam with current of about 50 kA. Symposium on collective acceleration. Dubna,1972. Preprint of JINR. Dubna, 1972, pp.125-128.

Injection of Relativistic Electron Beams with Arbitrary Radial Profiles into Warm Plasmas with Collisions.

G.Küppers, A.Salat and H.K.Wimmel
Max-Planck-Institut für Plasmaphysik, Garching bei München,
Federal Republic of Germany

Introduction: Injection of an electron beam into a plasma induces a reverse electron current, which strongly reduces the beam's azimuthal magnetic field. Beam currents well above the Alfvén current may be transported in this way. Most calculations on injection theory have been done with a radial step function profile of the beam /1/,/2/,/3/,/4/, /5/.

Calculations without collisions /6/ show a strong dependence of the B-field on the radial beam profile. The purpose of this paper is to show the effect of collisions and finite plasma pressure on charge and current screening for an arbitrary beam profile. Furthermore, we have numerically evaluated several criteria for beam propagation.

The model: As usual we assume a rigid, parallel, cold electron beam with small density compared with the plasma density. The plasma is of infinite extent and the ions are infinitely heavy. We start with the following system of equations: the Maxwell equations, the equation of motion of the plasma electrons

$$n_e m_e \frac{d\underline{v}_e}{dt} = - en_e(\underline{E} + \frac{1}{c}(\underline{v}_e \times \underline{B})) - \nabla(n_e T_e) - \nu n_e m_e \underline{v}_e,$$

the equation of continuity for the plasma electrons and an adiabatic law $n_e T_e^{\alpha} = \text{const}$.

After linearizing this system with $v_e^o = 0$ and $T_e^o = \text{const}$ and after Fourier transforming each quantity, and with the ansatz for the beam current

$$j_z(\underline{r},t) = \begin{cases} j_z(r_\perp)(1-e^{-\tilde{t}/\tau}) & \tilde{t} > 0 \\ 0 & \tilde{t} < 0 \end{cases} \quad \tilde{t} = t - \frac{z}{c}$$

where a cylindrical coordinate system is introduced by $\underline{r} = (r_\perp\cos\phi, r_\perp\sin\phi, z)$, $\underline{k} = (k_\perp\cos\theta, k_\perp\sin\theta, k_z)$, in which the beam propagates in the z-direction

with the speed of light c, we get for the magnetic field

$$B(k_\perp,\tilde{t})=4\pi i k_\perp \cos(\theta-\phi) j_z(k_\perp)\left\{\frac{1}{k_\perp^2}-\frac{1-\nu\tau}{k_\perp^2(1-\nu\tau)+a^2}\,e^{-\tilde{t}/\tau}-\right.$$

$$\left.-\frac{a^2}{k_\perp^2}\,\frac{1}{k_\perp^2(1-\nu\tau)+a^2}\,e^{-\frac{k_\perp^2\nu\tilde{t}}{k_\perp^2+a^2}}\right\}$$

$a = \omega_p/c.$

Results: The B-field shows a diffusion-like behaviour if $\nu\tilde{t} >> 1$. This means that for times $\tilde{t} >> t_D$, $\nu t_D = (r_1 a)^2$, the return current inside the beam with radius r_1 has diffused out of the beam and screening inside the beam is lost. In contrast, the charge density is not affected by collisions in such a way. Plasma oscillations, which are induced in the beam front, are damped out by collisions for $\nu\tilde{t} >> 1$. In constrast to the space charge, the magnetic field is independent of the plasma temperature. In the cold plasma limit the space charge ρ completely disappears in the steady beam phase $t >> \tau$. In the build-up phase ρ is non-zero owing to the inertia of the plasma electrons. For a warm plasma, space charge may exist even in the steady beam phase.

For weak collisions, $\nu\tilde{t} << 1$, there is a strong dependence of the B-field on the beam profile /6/. In the following, we only consider $\nu\tilde{t} >> 1$ and $\tilde{t} >> \tau$ because for $\tilde{t} << \tau$ the results are only slightly modified. The B-field can be written

$$B(r,\tilde{t}) = \frac{4\pi}{c}\,\frac{1}{r}\left[\int_0^r dr' r' j_z(r') e^{-(r-r')^2\rho^2/4}\right.$$

$$\left.-\frac{\rho^2}{2\pi}\int_0^\infty dr' r' j_z(r') \int_{|r-r'|}^{r+r'} dr'' r'' e^{-r''^2\rho^2/4} \arccos\frac{r'^2+r''^2-r^2}{2r'r''}\right]$$

$\rho^2 = a^2/\nu\tilde{t}$. This shows that the normalized B depends only on the two variables r/r_1 and q, $q^2 = r_1^2\,\rho^2/4$, if the beam profile is disregarded. For large radii the B-field decays more strongly than r^{-1}. This proves that the total net current remains zero, i.e. the total reverse current remains constant. This is possible because additional return currents are induced outside the beam and the average radius of the return current

grows proportionally to $(\nu\tilde{t})^{1/2}$. The return current inside the beam is only a fraction of order $r_1^2\rho^2\nu(\nu\tilde{t})^{-1}$ of the beam current.

The criteria: A numerical evaluation of several criteria relevant to beam propagation in plasmas is done for beam currents greater than the Alfvén current, and the effect of the beam profile is demonstrated by comparing a step function and a parabolic profile. The B-field grows because of diffusion until at some critical time $\tilde{t}_c$ it is strong enough to modify or destroy the propagation of the beam. In figures 1 and 2 several critical times are plotted, which we discuss in the following.

a) The "Alfvén time" t_A: At $\tilde{t} = t_A$ the gyroradius R_e of the beam electrons has become equal to the radial width of the B-field region δr.

b) The "virial time" t_p: For $\tilde{t} > t_p$ the magnetic pressure is larger than the maximum possible transverse beam pressure $p_{max}=nm_ec^2\gamma$, $\tilde{t} > t_p$ leads to catastrophic pinching, while for $t_p > \tilde{t} > t_A$ propagation is still possible, in principle, if the beam manages to change to a new self-consistent structure.

c) The diffusion time t_D.

d) The "heating time" t_H corresponds to a critical length $L_H = ct_H$ after which the beam has lost all its kinetic energy by dissipation of the return current /8/.

From the graphs in figures 1 and 2 we get the results: The Alfvén time t_A is well below the diffusion time t_D as soon as the beam current is appreciably larger than the Alfvén current. From this, large differences between the parabolic and the step function profile might be expected. This, however, does not occur. The t_A never disagree by more than a factor of two, the reason for this being as follows. The step function profile indeed needs less time to reach a certain magnetic field level; additional time is used, however, to quench the gyroradius to the small value δr of the B-region, typical of this profile.

For very large beam currents the violation of the Alfvén criterion for a step function profile would not be taken too seriously since it occurs in a very thin sheath only. Figure 1 shows that in this case t_p is not too far off, any way. For the parabolic profile in figure 2 t_p is consistently somewhat higher than for the sharp profile. The difference never exceeds a factor of three. For small beam currents t_p runs into t_D, which indicates that catastrophic pinching no longer occurs. The criteria that have been used are based on simplifications, so that factors of the order one should

be allowed for all critical times.

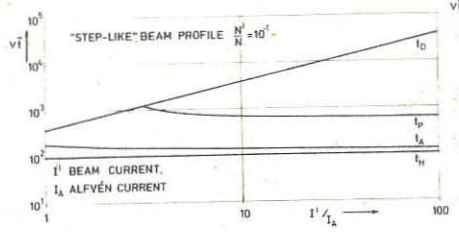


Fig. 1

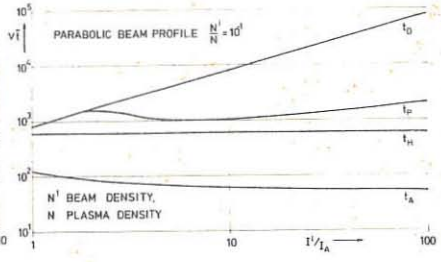


Fig.2

References:

/1/ COX Jr., J.L., BENNETT W.H., 1970, Phys.Fluids 13, 182

/2/ HAMMER, D.A., ROSTOKER, N., 1970, Phys.Fluids 13, 1831

/3/ ROSINSKII, S.E., RUKHADZE, A.A., 1972, Sov.Phys.Techn.Phys.16, 1989

/4/ RUKHADZE, A.A., RUKHLIN, V.G., 1972, Sov.Phys.JETP 34, 93

/5/ ROSINSKII, S.E., RUKHADZE, A.A., RUKHLIN, V.G.,EPELBAUM Ya.G., 1972, Sov.Phys.-Tech.Phys.17, 737

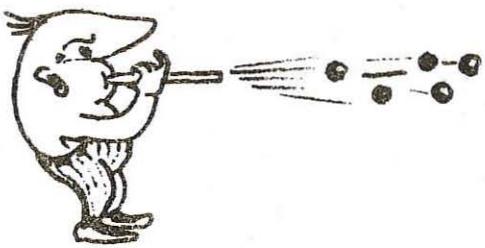
/6/ KÜPPERS, G., SALAT, A., WIMMEL, H.K., 1973 Plasma Physics 15, 429

/7/ KÜPPERS, G.,SALAT, A., WIMMEL, H.K., to be published

/8/ LOVELACE, R.V., SUDAN, R.N., 1971 Phys.Rev.Letters 27, 1256

"This work was performed under the terms of the agreement on association between the Max-Planck-Institut für Plasmaphysik and EURATOM".

3.4. BEAM-PLASMA INTERACTIONS



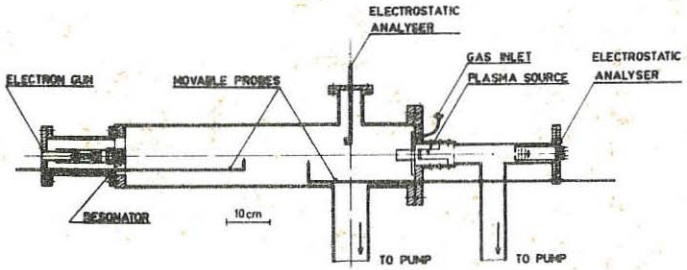
FUNDAMENTAL AND SATELLITE WAVES GENERATION IN MODULATED BEAM-PLASMA SYSTEMS

P. Šunka

Institute of Plasma Physics, Czechoslovak Academy of Sciences
Nademlýnská 600, Prague 9, Czechoslovakia

1. INTRODUCTION

We have studied experimentally the nonlinear interaction of an initially cold weakly modulated electron beam (beam current $I_b \leq 6mA$ voltage $U_b = 4kV$, diameter 5 mm) with magnetized ($B_0 = 360G$) argon plasma (initial electron temperature $T_e \approx 5eV$, diameter 8 mm) produced by an external source. The scheme of the experimental facility is drawn in Fig. 1.



The beam has been modulated at one and a half of the electron cyclotron frequency ($f_M = 1535$ MHz). The plasma density n_p ensuring the largest spatial growth of the beam-excited wave near the injector has then been adjusted. (With our currents, the unmodulated beam passed through the system without any remarkable relaxation). Under the experimental conditions only the Čerenkov type of interaction ($\omega \approx k_{\parallel} V_b$) of the beam with the upper branch of electron plasma oscillations ($max(\omega_p^2, \omega_B^2) < \omega^2 < (\omega_p^2 + \omega_B^2)$) has been observed. All measurements have been performed slowly i.e. point by point during many injection pulses.

2. EVOLUTION OF THE FREQUENCY SPECTRUM ALONG THE SYSTEM

At a low modulation level and low beam densities solely the fundamental wave having the frequency of modulation f_M and spatially growing amplitude (in the beam direction) is excited in the whole interaction region. By increasing either the modulation power input or the beam current the amplitude of this wave reaches its first maximum at some distance z_1 from the injector and beyond this maximum decreases again. The value of z_1 is proportional to the beam voltage and inversely proportional to the beam current and modulation power input. If $z_1 < L/2$ a second maximum of the fundamental wave

amplitude has been observed Fig. 2h ($L = 65$ cm is the length of our interaction region).

The frequency spectrum is very narrow ($\Delta f \leq$ 3MHz) Fig. 2a and the wave amplitude grows almost exponentially near the injector ($z \leq z_{1/2}$). Approaching the first maximum of the r.f. field, the spectrum of the basic wave becomes broader and simultaneously its higher harmonics and satellite waves at frequencies $f_s \approx f_M \pm 70$ MHz (Fig. 2b) are well detectable. Beyond this maximum the satellite waves (occurring in the form of short irregular bursts -- similarly as the spontaneously excited oscillation) are strongly excited. Although the "blue" satellite starts its rapid growth sooner (Fig. 2c), the red satellite becomes dominantly excited beyond the second maximum of the basic wave amplitude (Figs. 2g, i). The spectrum of "red" satellites is then relatively broad at the end of the system (Figs. 2e, f) and its maximum shifts towards the lower frequencies. The peaks corresponding to the fundamental wave have been limitted in (Figs. 2a - f).

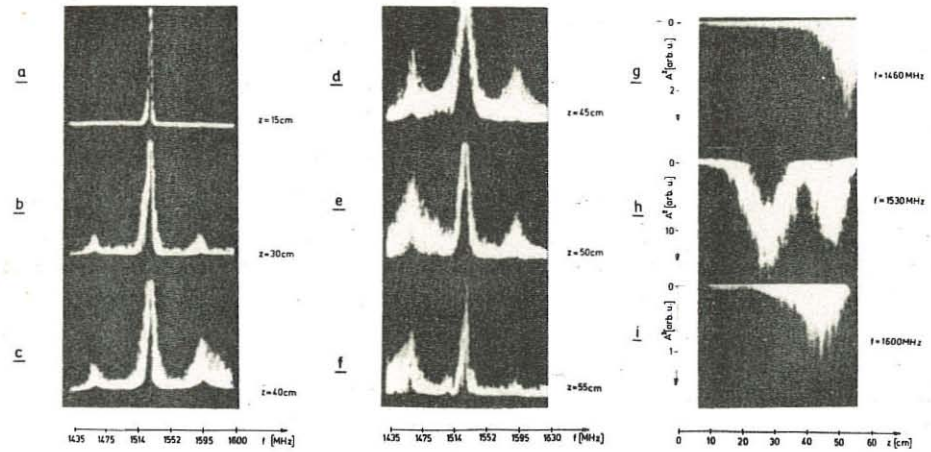


Fig. 2 Evolution of the frequency spectrum and of the wave-amplitudes along the system

The measured phase velocity of the second harmonic corresponds precisely to that of the fundamental wave ($v_{ph} \approx 0{,}92\, v_b$). On the other hand all observed satellite waves have lower phase velocities ($v_{phs} \approx 0{,}8\, v_b$). The observed behaviour of the fundamental wave is in a good agreement with the numerical calculations of the nonlinear interaction of a weakly modulated beam with a stationary monochromatic wave.

3. NONLINEAR WAVES EXCITATION BY A BEAM MODULATED AT TWO FREQUENCIES

To regularize the occurence of the satellite waves and to get under control their role in the process of beam relaxation we have modulated the beam at two frequencies $f_{M1} < f_{M2}$ simultaneously. The modulation power input, comparable at both frequencies, has been chosen too low for each of these waves to excite the satellites separately. So far as $\Delta f = |f_{M1} - f_{M2}| \neq |f_M - f_s|$ the beam relaxation has been the same as in the case of a single frequency modulation. If, however, Δf becomes comparable with the frequency difference between the fundamental wave and its nearest satellite ($\Delta f \approx |f_M - f_s|$), the situation is quite different. Both waves (having the same phase velocities) reach their maximum of amplitude at the same place inside the system and decrease then again. The absolute value of the amplitude of otther wave is suppressed by the presence of the other one. Beyond their maxima, new waves with frequencies $f_n = f_{M1} - n\,\Delta f$ are excited ($n = -1; +2, +3 \ldots$).

As a rule beyond the maximum of amplitude of the n-th satellite the strong excitation of the (n+1)-th has been observed. Thus for larger Z the maximum of the amplitude shifts towards lower frequencies. Although the spectrum retains the structure of narrow peaks, its envelope develops similarly as the "red" satellite-waves spectrum excited by a beam modulated at a single frequency Figs. 3a, b. (The behaviour of the "blue" satellite is somewhat obscure. Its detailed study has not been performed, since its amplitude remains relatively low. Moreover, no remarkable role of this wave in the beam relaxation process has been observed).

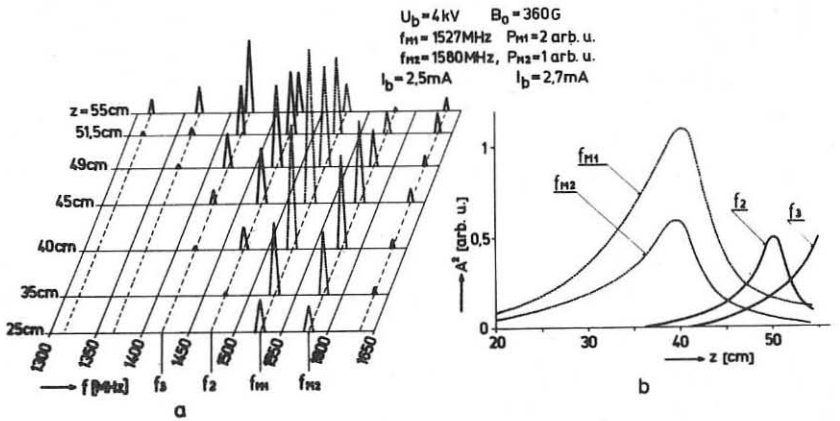


Fig. 3 Frequency spectrum (a) and the wave-amplitudes (b) excited by a beam modulated at two frequencies.

It seems plausible that the mechanism of new waves generation remains almost the same in both cases. The comparison of the measured beam relaxation and of the phase velocities of the satellite waves has provided further strong arguments in favour of this statement.

In Fig. 4 typical beam distribution functions are plotted, corresponding to the following three different conditions:

(a) one of the modulation frequencies has been switched off

(b) the beam is modulated at both frequencies simultaneously

(c) the beam is modulated at a single frequency, the modulation power input and the beam current have, however, been increased, to ensure the spontaneous excitation of satellite waves.

The curves (b), (c) are close to each other. They differ from the curve (a) mainly in the lower energy part. In the cases (b), (c) the beam is more relaxed and electrons with significantly lower energy are present. The measured phase velocities of the satellite waves (absent in the case (a)) have also been plotted in the Figs. 4b,c, to demonstrate that these waves should be excited by the slower beam electrons. This results in further deceleration of the beam and in the broadening of its distribution function.

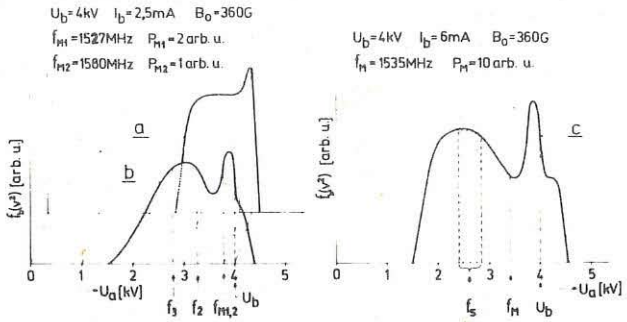


Fig. 4 Beam distribution functions for: (a) single fundamental wave (b) frequency spectrum as in Fig. 3c (c) frequency spectrum as in Fig. 2f

The amplitude of satellite waves grows up to high levels at very short distances. This is possible only if strong nonlinearities of the beam particles motion (their bunching, trapping and decelerating in the fundamental wave) provide sufficiently high initial perturbations which may be resonantly amplified by the decelerated beam particles. The modulation at two appropriate frequencies enhances predominantly the level of the initial perturbation, the mechanism of its further amplification remaining almost the same.

ACKNOWLEDGEMENT: The author is grateful to Dr K. Jungwirth for stimulating discussions and useful comments on the manuscript.

MEASUREMENTS OF PHASE- AND GROUP VELOCITY OF THE ELECTRON CYCLOTRON INSTABILITY IN A BEAM-PLASMA EXPERIMENT

J.A.C. Cabral and M.E.F. Silva

Centro de Estudos de Electrónica - Comissão de Estudos de Energia Nuclear - Instituto Superior Técnico - LISBOA - Portugal

ABSTRACT - We measured both the phase and the group velocity of the cyclotron instability. These measurements were performed with a sampling oscilloscope. We verified that the phase velocity is about 70 % of the beam velocity, and that the group velocity is of the order of the thermal velocity of the plasma electrons.

INTRODUCTION - Our beam-plasma experiment has been briefly described in another publication also submitted to this Conference (1). There we proved that the amplitude statistics of the cyclotron bursts does not qualitatively change with z. This fact suggested that the field structure of the cyclotron instability should travel along the interaction chamber. Therefore, under those conditions, it would be possible to detect the motion of the bursts. This should also lead to the determination of their group velocity. With all generality, we could, à priori, have three possibilities for the group velocity: a- it is negative due to the anomalous dispersion of the plasma alone (absolute instability); b- it is positive and of the order of the beam velocity, as suggested by the study of the linear dispersion diagrams (2); c- it is positive but of the order of the thermal velocity of the plasma electrons, which are known to support the oscillations by their coherent motion.

EXPERIMENTAL DETAILS - The measurements were performed under conditions similar to those of our other paper (1):- A fixed probe receives the signals from the plasma that are directly used to trigger a sampling scope. This one is only triggered by the highest bursts. The signals received by the axially movable probe are fed into the vertical input of the sampling scope, after being delayed of 90-300 ns, depending on the time scale used in the scope. It was verified that the passage of the movable probe through the region where the fixed probe was placed, did not affect the signals taken out by the latter one. Therefore we can trust the triggering process. The measurements of the group velocity were based upon displacements of the bursts in time, obtained from sampling analysis made at different values of z, with the scope always

triggered by the fixed probe. The scope has two auxiliary outputs, permitting the use of an X-Y recorder for improvement of the resolution of the measurements.

EXPERIMENTAL RESULTS - Figure 1 presents an example of a measurement of the instability group velocity. The fixed probe was placed at z=53.5 cm. In this figure we plotted, as a function of time, referred to the trigger moment, the electric field of the cyclotron bursts, for different values of z. In this figure we clearly can see the displacement of the bursts towards larger values of time when we move the probe to larger values of z. Therefore the group velocity is positive. Knowing the increase given to z (Δz) and the associated value of the displacement of the burst in time (Δt) the group velocity is simply $v_g \cong \Delta z/\Delta t$. From figure 1 we determined $v_g = 3.33 \times 10^8$ cm s^{-1}. Therefore the group velocity is of the order of the thermal velocity of the plasma electrons ($T_e \cong 8$ eV). In figure 2 we did a similar measurement but now in a much shorter time scale. From this figure it is clear that the phase of the wave changes coherently in time as well as in space. Again knowing Δz and Δt we determine, now, the value of the wave phase velocity $v_{ph} = 1.64 \times 10^9$ cm s^{-1}. In figure 2 a dot identifies the displacement in time of the same maximum of the field. Figure 3 shows the spatial variation of the electric field of the bursts. The sampling scope works now with a fixed delay after triggering τ, that we vary in steps of 20 ns, to obtain the five instantaneous pictures of the bursts in space. The X-Y recorder plots now the instability electric field against z, for a certain instant of time. From this figure we see that the bursts, opposite to the measurements presented in (3) and (4), have a rather long coherence length, perhaps due to the low value of the frequency (we only see 5 wavelengths). Finally to observe in a good way the growth of the bursts towards the collector side of the experiment, we made sampling measurements (figure 4) of these bursts, at different values of z, but now with the scope triggered by the sampled bursts themselves. As we see the bursts become much better defined in time and the growth process becomes much more evident than in figure 1, where it was hidden by the loss of coherence between the signals of the two probes.

CONCLUSIONS - From the presented set of measurements we can conclude that the electron cyclotron bursts are originated near the electron gun and that they afterwards travel along the experimental chamber, gaining energy from the beam, and that they finally must be absorbed near the

collector, as there is no evidence for a coherently reflected burst, in figure 4. The group velocity is found to be of the order of the thermal velocity of the plasma electrons. Concerning the phase velocity, there is good agreement between the measured value and the theoretical one. Indeed, the cyclotron instability (Cerenkov effect) is excited by the beam slow space charge wave. Therefore we should have $v_{ph}=v_b \cdot f_{ex}/(f_{ex}+f_{pb})$ (5), where f_{ex} is the excited frequency and f_{pb} is the plasma frequency of the beam. As in our case f_{ex} = 225 MHz and f_{pb} is of the order of 100 MHz, the phase velocity was expected to be about 70 % of the beam velocity, as it was experimentally observed. From figures 3 and 4 we can see the temporal coherence of the bursts (5) (6), is much better than their spatial coherence (3) (4). Indeed, we can not clearly observe, in figure 3, the displacement of the bursts in space. Finally we stress that these measurements suggest that the shape of the electron cyclotron bursts does not correspond to a saturation in time of the instability electric field. On the contrary, we believe that this shape represents the response of our beam-plasma system, at a fixed point z_o, to the excitation and propagation of a convective instability.

REFERENCES -

(1)-Cabral,J.A.;Silva,M.E.F.;-"6th Europ. Conference Controlled Fusion and Plasma Physics", Moscow, 1973.

(2)-Cabral,J.A.;Hopman,H.J.; Insinger,F.G.;Ott,W.- "Plasma Physics and Controlled Nuclear Fusion Research", IAEA, Vienna, 749,1969

(3)-Van Wakeren,J.H.A.; Hopman,H.J.-"10th Int. Conf. Phenomena in Ionized Gases", Oxford, 1971.

(4)-Yaremenko,Yu.G.; Deev,V.M.;Eremin,S.M.;Kharchenko,I.F. - Soviet Phys. - Technical Phys., 14, 1158,1970.

(5)-Cabral,J.A.; Hopman,H.J.-Plasma Physics 12, 759, 1970.

(6)-Hopman,H.J.; Jurgens,B.;Van Wakeren, J.H.A.- "5th Europ. Conf. Controlled Fusion and Plasma Physics" - Grenoble, 152,1972.

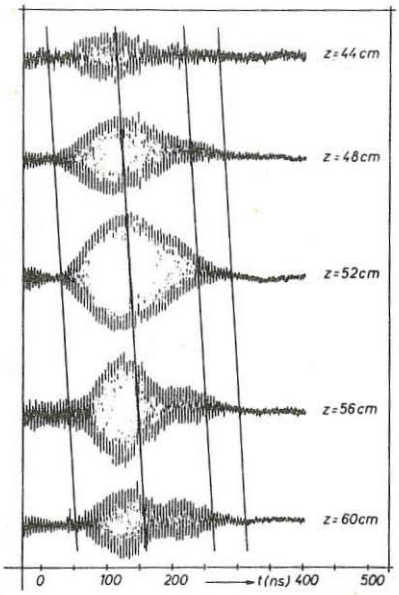


Figure 1

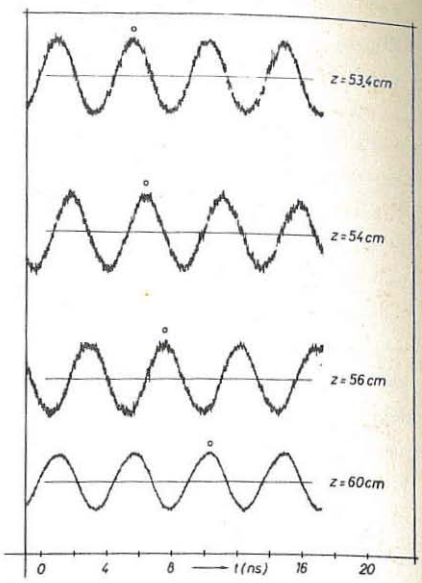


Figure 2

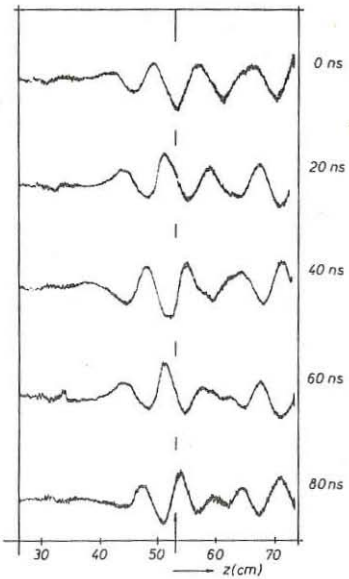


Figure 3

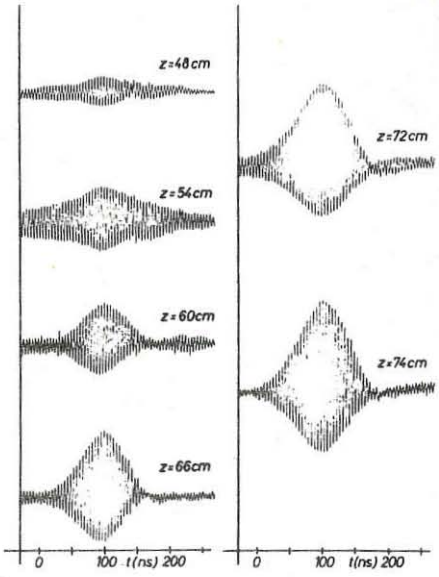


Figure 4

STATISTICAL ANALYSIS OF THE HIGH-FREQUENCY BURSTS OF A BEAM-PLASMA EXPERIMENT

J.A.C. Cabral and M.E.F. Silva
Centro de Estudos de Electrónica - Comissão de Estudos de Energia Nuclear - Instituto Superior Técnico - LISBOA - Portugal

ABSTRACT - In this paper we experimentally determine the probability that an electron cyclotron burst has to attain a certain amplitude. These measurements suggest that the complete field structure of the cyclotron instability travels along the experimental chamber.

1.- INTRODUCTION - Our beam-plasma experiment has been described in a former publication (1). It consists of a cylindrical interaction chamber ($\emptyset$ = 8 cm) with a length of 75 cm. This chamber is filled with Helium at a pressure of 4.2×10^{-4} Torr. The axial magnetic field is homogeneous and has the value of 0.0060 Wb m^{-2}. An electron gun continuously injects a beam of 1500 eV with a current of 17 mA. The injection is parallel to the magnetic field. The beam is collected on the external wall of an electrostatic energy analyser. In this paper we intend to study the statistical behaviour of the high-frequency bursts originated by the beam, while crossing its own created plasma. For this purpose we chose a state of the beam-plasma system that was characterized by a simple spectrum of oscillations. Under the above given conditions, the beam energy spread, when leaving the plasma, is small, 1400 to 1600 eV. The excited spectrum is, for every position of the axially movable probe, z, constituted by a strong and narrow electron cyclotron peak (50 dB above noise level) with a central frequency of 225 MHz. Besides this peak we also observed the weak excitation of the 2nd, 3rd and 4th harmonics of the fundamental instability. As is well known, the bursts of radiation vary widely in amplitude. The typical duration of these bursts is 300 ns.

2.- EXPERIMENTAL DETAILS - The statistical analysis of the amplitude of the electron cyclotron bursts is made in the following manner: A pin probe receives the rf signals from the plasma. These signals are then fed into a very fast (1.2 GHz) detector. In this way we obtain a succession of fast pulses with an amplitude proportional to the instantaneous power of the bursts. These pulses are then amplified of 40 dB, further sent through a calibrated attenuator, and finally they actuate an electronic counter. The triggering level of the counter is set for maximum

sensitivity. With the attenuator set at zero dB, we measure a certain frequency of occurrence of the bursts (about $2 \times 10^6\ s^{-1}$). As we increase the attenuation, in steps of 2dB, the number of pulses which are able to trigger the counter decreases. So, we obtain an integral curve, representing the number of pulses occurring per second, with an amplitude at least a certain number N of dB above that of the minimum trigger pulse. From this curve it is now easy to obtain the relative probability for an individual burst to attain an amplitude E. The use of the square law detector introduces a relation of the form $A \sim E^2$, where E is the amplitude of the real bursts and A the one of the derived pulses, which drive the counter. From the integral curve f=f (logA), we determine, for every A, the value of the decrease in frequency $-\Delta f$, corresponding to an increase of 2dB on log A. As we know, the probability for a burst to have an amplitude E will be proportional to $-\delta f/\delta E$. In order to determine, approximately, this quantity, we start from the knowledge of $\Delta f/\Delta \log A$, proportional to $-\Delta f(A)$, as $\Delta \log A = Cte$. Therefore $-\Delta f/\Delta A$ is proportional to $\Delta f(A)/A$. As $A \sim E^2$, we then simply obtain:

$$(1) \qquad p(E) = -\frac{\delta f}{\delta E} \cong -\frac{\Delta f}{\Delta E} \cong -\frac{\Delta f(A)}{\frac{1}{A^2}}$$

3.- EXPERIMENTAL RESULTS - We began this study by measuring, with a bolometer, the spatial variation of the total time integrated radiated power received by the probe (figure 1, X-Y recorder curves). As we see, the power increases towards the collector side of the experiment. On this figure it is also plotted (crosses) the z-variation of the maximum power of the individual bursts. This one is determined by measuring the minimum number of dB of attenuation needed to have a zero count in the electronic counter. Next we determined, with the exposed method, the variation with z of the amplitude statistics of the electron cyclotron bursts. With formula (1) we calculated, for six different values of z, the probabilities p(E), plotted on figure 2 as a function of E (or A), measured in dB above the reference level of the counter. Further we verified that, at a fixed point in the interaction chamber, $p(E, z_o)$ is practically independent of the length of the experiment, provided that the collector is not too close to the fixed probe.

4.- INTERPRETATION OF THE RESULTS - In a recent publication (2), Jungwirth et. al. also measured the probability p(A). They assume that

the bursts have their origin on space charge fluctuations with a Gaussian character. According to them p(E) should be

$$p(E) \sim e^{-E^2/\langle E^2 \rangle} \sim e^{-A/\langle A \rangle} \quad (2)$$

To test this hypothesis, we plotted the values of p(E) as a function of A/A_{ref}, (figure 3), with A_{ref} being the power corresponding to the reference level of the counter. Therefore, we arrived to the conclusion that, also in our case, the probability p(E) is Gaussian. However the "mean electric energy" $\langle E^2 \rangle$ is an increasing function of z. This result suggests that the plasma temperature should also increase towards the collector. The Gaussian amplitude statistics found for the electron cyclotron bursts, can be closely related to the observation of a Maxwellian transverse velocity distribution function for the beam electrons (3). Returning to figure 2, we can see that the six curves p(E) can almost be obtained from each other, by a simple shift sidewards. This means that, from one point to another, the complete distribution of the rf bursts grows of the same ammount of dB, independently of the amplitude of the individual bursts. This fact strongly suggests that the cyclotron bursts travel along the experimental chamber. These measurements also indicate that spatial saturation is not yet reached. We now believe that, on these conditions, the total structure of rf fields travels away from the gun, increasing in amplitude, and that it is later absorbed near the collector. The reason for this is that every burst, once reflected, shall have indeed negative values for the phase velocity but still a positive value for the group velocity, due to anomalous dispersion of the cyclotron branch of the dispersion diagram. In figure 1, we also plotted in arbitrary units, (dots) the six values of the "mean electric energy", obtained from figure 3. The qualitative agreement existing among the z-variations of:a- the total radiated power, b- the maximum power of the individual bursts and c- the "mean electric energy" of the amplitude distributions, gives a good support to the existence of a travelling structure of rf fields, possessing the important property of conserving its amplitude statistics (as observed on figure 2). Therefore, the conservation of the amplitude statistics along z, is sufficient to introduce a direct relationship between the growth of the individual bursts and the increase on the radiated power, or equivalently, on the "mean electric energy" of the distribution of amplitudes.

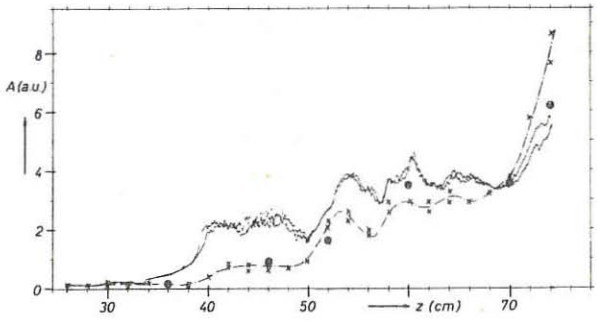


Figure 1

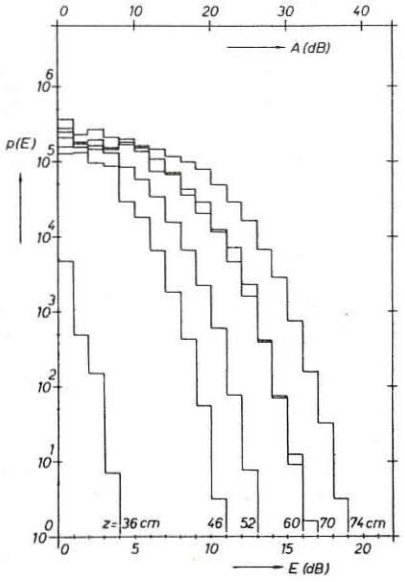


Figure 2

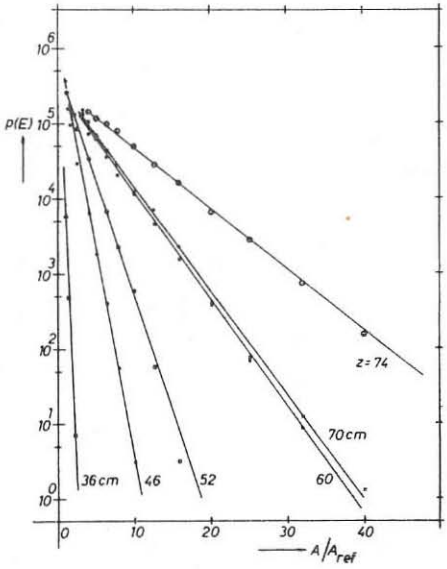


Figure 3

5.-REFERENCES

(1)- Hopman,H.J.;Matitti;Kistemaker,J.-Plasma Phys. 10,1051,1968.

(2)- Jungwirth,K.;Piffl, V; Ullschmied,J.- Plasma Phys. 14,339,1972

(3)- Cabral,J.A.;Hopman,H.J.;Van Wakeren,J.H.A.-"4th Europ. Conf. on Controlled Fusion and Plasma Physics" - Rome, 69,1970.

MECHANISM OF STOCHASTIC OSCILLATION EXCITATION AT DEVELOPMENT OF BEAM INSTABILITY IN PLASMA

V.A.Lavrovsky, I.F.Kharchenko, E.G.Shustin

Institute of Radioengineering & Electronics of the Academy of Sciences, USSR

A relation between a structure of high frequency oscillations excited at beam-plasma instability development and a form of instantaneous distribution function of beam electrons on the interaction region terminal is analyzed. Statistical relations of oscillation phase behavour are found out. Stochastisation of oscillations is shown to occur due to trapped particle instability.

It was shown[1] that interaction which takes place in a beam-plasma discharge is a single-mode one in spite of the fact that the averaged characteristics point to stochastic character of the interaction. The true form of the electron velocity distribution function (DF) agrees with the conclusions of the nonlinear single-mode interaction theory[2,3], and HF - field excited due to interaction development is chaotic sequence of quasiharmonic inclusions separated by phase abrupt changes.

In this paper on the basis of the methods proposed in[1] the connection of HF field characteristics with electron velocity DF shape, and the mechanism of intensive HF fields excitation in a beam-plasma instability are analyzed.

The experiment was performed with a beam-plasma discharge at continuous injection of an electron beam of energy of 1 keV and current 20-40 mA into hydrogen contained in a glass tube of 40 cm in length and 2 cm in diameter. A longitudinal magnetic field was of 0,2 Tl.

HF field records were performed with high-speed oscilloscope without transformations of the signal by radio circuits. High-

speed measurements of DF were carried out synchronously with HF field registrations. Time intervals of DF and HF field registration were both about 10^{-7} sec. Different stages of the discharge were tracked by increasing plasma density that corresponds to growth of γ or t in the theoretical models given in.[2,3]

DF at different stages and HF field oscillograms corresponding to these DF are shown in Fig.1. DF without plasma has a bell-shaped form (Fig 1a) with energy scatter of about 40 eV. When plasma density exceeds a threshold of discharge emerging, spreading of DF and excitation of HF oscillations occur but HF amplitude at the initial stage of instability is not sufficient for high-speed oscilloscope recording. Fig.1b corresponds to the begining of a nonlinear stage of interaction. DF has a form of a curve with many peaks with full energy scatter of order of 10^2eV and HF field is close to sinusoidal one. As the plasma density increases spreading occurs further, while a form of a curve with many peaks remains. HF field increases and takes a form of AM oscillation that corresponds to sidebands arising in its spectrum. With subsequent spreading of DF oscillation spectrum expands so that they take a form of a random process.

These results agree with ideas about changing of oscillation structure developed in nonlinear theory.[4-6]
Registration of quasi-sinusoidal oscillations confirms the conclusion about monochromatisation of oscillations to the starting of nonlinear stage of instability development. Modulation depth increasing and spectrum expanding can be recognized as a result of development of instability due to electrons trapped by the field of quasi-sinusoidal wave. From the theory sideband spectrum width is determined as $\Delta f \sim \left(\frac{e}{m} kE\right)^{1/2}$. Field intensity E can be estimated from relative losses of beam energy spending for HF oscillation excitation ($\eta = P/P_0$). Then

$$\Delta f \sim \left(\frac{e}{m} \frac{\omega_p^2}{V_0^2} \sqrt{2R\eta P_0}\right)^{1/2} \qquad (1)$$

Here R - is coupling resistance of plasma waveguide, P_0 - is the power of an unperturbed electron beam. In Fig.2 the curve $\Delta f(\sqrt{\eta})$ is plotted and values of spectrum width computed by Fourier expansion of oscillograms are marked. Discrepancy of theoretical and experimental curves at initial interval is explained by the fact

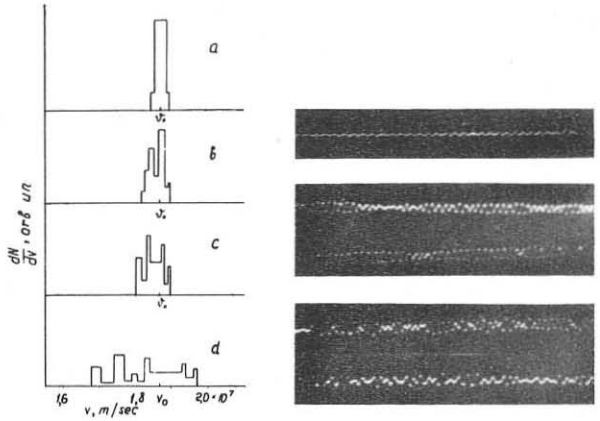


Fig.1.

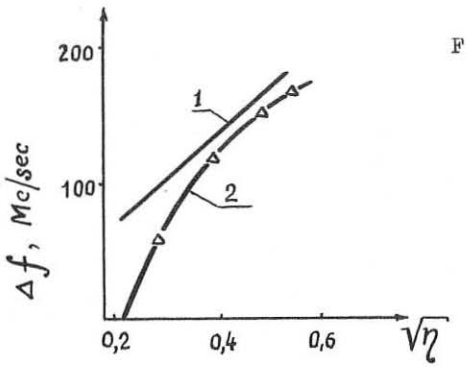


Fig.2. 1 is the theoretical curve of

2 is experimantal samples.

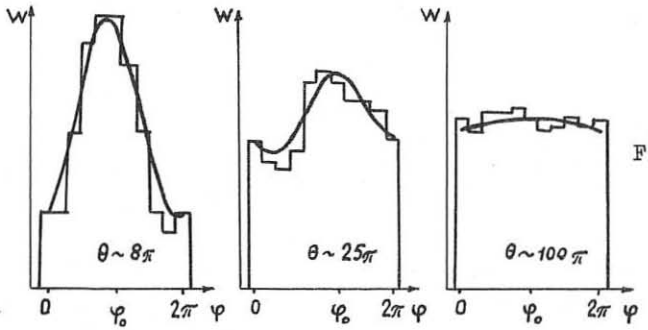


Fig.3.

that expression (1) gives the upper estimation showing sidebands frequency range only.

Ideas about stochastisation of monochromatic wave due to sideband excitation are confirmed by statistical relations of signal phase behavour.

Temporal behavour of phases was investigated over several hundreds oscillograms representing a set of patterns of HF field at the same regime. All the oscillograms were artificially phased at initial time t_0. It is found that outphasing process with time have a character of diffusion.

Phase distributions at chosen times are of Gaussian curves. That is proved by Fig.3 which represents experimental diagrams of the distributions and calculated curves

$$W(\varphi)=\frac{1}{\sqrt{4\pi D\theta}}\exp\left(-\varphi^2/4D\theta\right) \qquad (2)$$

which are curled up to interval $(0,2\pi)$. Here w is the probability density of φ, $\theta=\omega(t-t_0)$ is the normalized time, D is the phase diffusion rate.

As it follows from nonlinear wave theory[7] the observed phase distribution proves that chaotisation of the wave occurs as a result of random phase jumps of initially sinusoidal oscillation.

Thus the results presented here show that oscillations observed at two-stream instability development in plasma arise from quasi-monochromatic waves excited due to hydrodynamic instability. At a well-developed stage of the instability this wave is randomised on account of trapped particle instability resulting in excitation of sidebands in its spectrum.

References:

1. V.A.Lavrovsky,E.G.Shustin,I.F.Kharchenko. ZhETF Pis.Red. 15, 84, 1972; 16, 602, 1972.
2. B.B.Kadomtsev,O.P.Pogutse.Phys.Rev.Lets.25, 1155,1970.
3. O'Neil. Phys.Fluids, 8, 2255, 1965.
4. W.Drummond at al, Phys.Fluids, 13, 2422, 1970.
5. V.D.Shapiro, V.I.Shevchenko. Zh.Eksp.Teor.Fiz. 60,1023,1971.
6. N.I.Bud'ko,V.I.Karpman,D.R.Shklar. Zh.Eksp.Teor.Fiz. 61, 1463, 1971.
7. S.M.Rytov. Vvedenie v statistich.radiofiz."Nauka",M,1966.

TRANSFORMATION OF THE ELECTRON BEAM VELOCITIES DISTRIBUTION FUNCTION AT THE INTERACTION OF MODULATED ELECTRON BEAM WITH PLASMA.

A.I.Rogashkova, M.B.Tseitlin, V.A.Lavrovskiy, I.F.Kharchenko.

Institute of Radio Engineering & Electronics
Academy of Sciences of the USSR. USSR,Moscow.

The interaction of the velocity-modulated electron beam with longitudinal waves in plasma in the nonlinear regime has been investigated. The phase trajectories of an electron beam, the electron velocity distribution function, the field amplitudes of a spatial charge, and the electron velocities in the phase at different stages of interaction have been determined.

The development of beam instability is firstly defined by a change of the beam parameters while the plasma oscillations are excited. Analysis of these instabilities are usually carried in time dependence /1/. It makes difficult and even excludes sometimes their experimental investigations if the instabilities are convective. Besides that the electron beam-plasma interaction are usually investigated on frequency $\omega \approx \omega_p$ /2/.

In this paper the problem of space non-linear evolution of the wave generated in plasma by the modulated electron beam is solved. It allows the theory and experiment to compare more full and sequencely.

The velocity modulated electron beam is injected axially into a plasma waveguide of radius "a". The initial conditions for this model: $\xi = \frac{\omega}{v_0} z = 0$, $v = v_0 (1 + \alpha \cos \omega t)$; v-is the electron beam velocity, v_0-is the averaged beam velocity, α - is the depth of modulation. It is supposed the modulating signal amplitude considerably excesses the fluctuation one; $\frac{v_T}{v_0} \ll \frac{|\varepsilon_z|}{\frac{\omega_{pb}}{\omega_p} + |\varepsilon_z|}$;

$$\frac{\omega_{pb}^2}{\omega_p^2 |\varepsilon_z|} \left| \frac{i_n}{I_0} \right| \ll 1$$

(i_n- is the amplitude of n^{th} time current harmonic, I_0-is the beam current). In this case it is possible to neglect the plasma

nonlinearity and to investigate the beam-plasma interaction in the broad frequency range $0 < \frac{\omega}{\omega_p} < 1 + \frac{v_T}{v_0}$. In an experiment the oscillation are usually observed in that range.
The system of nonlinear equations, including the force equation and field expression, received in /3/ has been integrated by a computer. It permited to receive the information about the space evolution of the instability.

In Fig 1 the electron motion on phase plane is represented, coordinating with amplitude change of the first time field harmonic. The system parameters are $\alpha = 0{,}1$; $\frac{\omega_p^2}{\omega^2} = 1{,}6$; $\frac{\omega_{pe}^2}{\omega} = 0{,}01$. The points in Fig.1 represent the series of beam electrons on the phase plane ($\frac{v}{v_0}$, $\xi - \omega t$).
The turning of these points on the angle $\sim \frac{\pi}{2}$ (position 1-2) is accompanied by the exponential growth of field amplitude and the corresponding deformation of separatrise, dividing the particles on trapping and flying ones. The trapping particles groop in macroparticles (they are pointed by the touchs in Fig.1).

The further electrons motion resembles the oppositphase oscillations of macroparticles, which originate the space oscillations of field amplitude. The period of the oscillations is $2\pi\sqrt{\frac{mv_0^2}{e\varphi}}$ φ - of the amplitude of field potential. The maximum field amplitudes are approaches at the space coincidence of macroparticles (position 2-4); the minimum are done at the approachment of macroparticles in a velocity space. Almost all beam electrons participate in formation of the first focus. Then the macroparticles are spread in a phase space in result of the velocity difference. The density of the following focus and the corresponding maximum field amplitude are decrease due to transformation of the some trapping particles into a flying ones (compare the positions 2 and 4).

If there is the electron motion picture on the phase plane we can observe the evolution of the electron velocity distribution function (D.F.) (Fig.2). Unlike /1,2,4/ where it is shown one macroparticle forms in result of the field effect, in the present case transfromation of the D.F. along the beam path is connected with formation of two macroparticles and their motion. The D.F. has two hump with more or less expressed maximum due to the sinusoidal initial modulation at the first stage of interaction. In the field maxima the D.F. also has the two hump as the macroparticles are sepa-

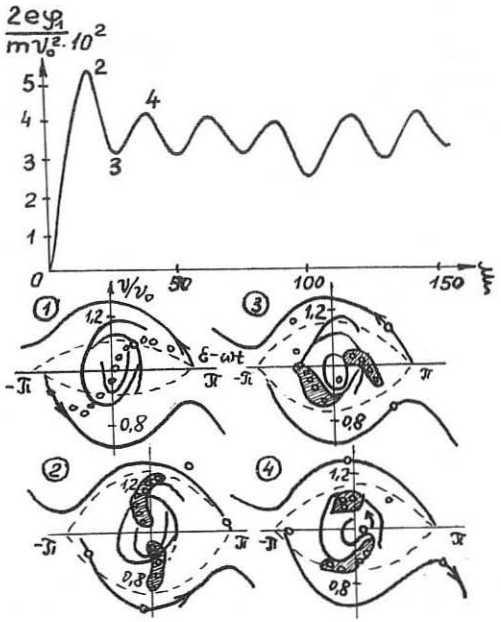


Fig.1. Unbroken line - the phase trajectories, the pointer indicate the direction of the electron motion; broken line - separatrise.

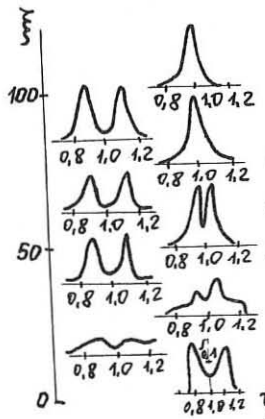


Fig.2. The DF at the beam entrance in plasma and in the field extremum points.

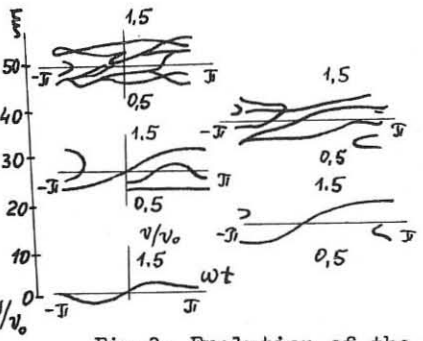


Fig.3. Evolution of the beam electron velocity wave v.s.distance.

rated in the velocities space. In the field minima the macroparticles reapproach gradually in velocities space and the two humps merge in one. In Fig. 3 the evolution of velocity wave versus distance is given. It is opportunity to observe the electron motion turbulisation process at the beam-plasma interaction. The initial sinusoidal velocity-wave "overturns" in the region of the first field maximum. Further the beam is turbulent one, so as in any fixed point the velocity v.s. time is the multivalued function. This phenomenon has observed experimentally /5/.

Thus the theoretical analysis, based on the numerical integration of the self-consistent equations permits to describe in detail the nonlinear stage of the beam relaxation and to make clear the effects connected with macroparticles formation that is the space field amplitude oscillations and D.F. evolutions, correlated with those.

References:

1. V.D.Shapiro, V.I.Shevchenko. JETP, 60, 1023 (1973).
2. V.D.Shapiro, V.I.Shevchenko. Nuclear Synthesis,12,N1 (1972).
3. A.I.Rogashkova, M.B.Tseitlin, I.F.Harchenko, JTP, N 1, (1973).
4. B.B.Kadomtsev, O.P.Pogutse. Internat. Centre for Theoretical Physics. Report N 1 C 170/45 Triest.
5. V.P.Kovalenko, M.D.Cabovich. Ukrain Phys.Journ., 15, 1894 (1970).

ON DECAY INSTABILITY OF LANGMUIR AND ION-SOUND OSCILLATIONS IN PLASMA-BEAM SYSTEM

N.G.Matsiborko, I.N.Onishchenko, V.N.Oraevsky, V.D.Shapiro, V.I.Shevchenko

Physical-Technical Institute, Acad. of Sci. of Ukr.SSR, Kharkov, U S S R

One of the main mechanisms of plasma-heating by an electron beam is connected with decay instability of Langmuir oscillations discovered in [1] . At this instability, Langmuir oscillations, excited by a beam, are transformed into slow ion-sound ones, absorbded in plasma. For the determination of the efficiency of such heating mechanism, it is necessary to make a non-linear theory of decay instability in plasma-beam system. The results of the solution of the correspondent problem are given in the report, which were obtained by means of partial simulation of the process on computer [2,3].

The decay instability of monochromatic wave is taken into consideration, which is excited when the "cold" electron beam injected into plasma. Langmuir wave is excited in this case with maximum increment in plasma, with wave number $K_{1z} \simeq \frac{\omega_p}{V_0}$ and frequency ω_1 , found from relation: $\varepsilon_p(\omega_1, K_1) = 1 - \frac{\omega_p^2}{\omega_1^2}\left(1 + \frac{v_{g1}}{V_0}\right) = 0$ $v_{g1} = \frac{3K_{1z}T}{m\omega_p}$ - group velocity of Langmuir wave, T - electron plasma temperature, $\omega_p = \sqrt{\frac{4\pi e^2 n_0}{m}}$ - Langmuir frequency. This wave is unstable relating to the decay into ion-sound and Langmuir satellit, with frequencies $\omega_s = K_s\sqrt{\frac{T}{m_i}}$, $\omega_2 = \omega_1 - \omega_s$ and wave vectors K_s , K_2, found from decay conditions:

$$\vec{K}_s = \vec{K}_1 - \vec{K}_2 \quad , \quad \frac{3}{2}(\vec{K}_1 - \vec{K}_2)\lambda_{De} = \sqrt{\frac{m_e}{m_i}} \; |\vec{K}_1 - \vec{K}_2| \qquad (1)$$

$\lambda_{De} = \frac{1}{\omega_p}\sqrt{\frac{T}{m}}$ - Debye radius.

At $K_{sz}K_{2z} > 0$ the stationar amplitude amplification of these waves takes place with increment

$$\varkappa_d = \frac{\omega_p}{\sqrt{v_0 v_{g2}}} \sqrt{\frac{E_1^2}{32\pi n_0 T}\cos\theta} \simeq \frac{1}{4\lambda_{De}} \sqrt{\frac{E_1^2}{16\pi n_0 T}\frac{K_s}{K_{2z}}\cos\theta} \qquad (2)$$

θ - the angle between $\vec{K}_2$ and beam direction (axis Z). E_1 - electric field amplitude of the fundamental wave. At maximum values of E_1 corresponding to the trapping of the beam particles by the wave, $E_1 \sim \sqrt{n_1 m v_0^2 \left(\frac{n_1 v_0}{n_0 v_g}\right)^{1/3}\frac{v_0}{v_g}}$, amplification coefficient for decay instability $\varkappa_d \simeq \varkappa_e \sqrt{\Lambda}$, $\varkappa_e$ - amplification coefficient of the fundamental wave by the beam, n_1 - beam density, v_0 - its velocity, $\left(\frac{n_1 v_0}{n_0 v_g}\right)^{1/3} \ll 1$, parameter $\Lambda = \frac{1}{\delta}\frac{m v_0^2}{T}\left(\frac{n_1 v_0}{n_0 v_g}\right)^{2/3}\frac{v_0}{v_g}$. At $\Lambda \gtrsim 1$ decay instability influences considerably on the relaxation process of electron beam. Having supposed the condition to be fulfilled $\Delta k_z \simeq |K_{1z} - K_{2z}| \gg \frac{\omega_p}{v_0}\left(\frac{n_1 v_0}{n_0 v_g}\right)^{1/3}$ we find that only fundamental wave is in the resonance with beam particles:

$$E_1(t, z) = E_1(z)\cos\left[-\omega_1\left(t - \frac{z}{v_0}\right) + \alpha_1(z)\right]$$

In this case the equations, dealing with wave excitation by the beam and the decay into Langmuir satellit

$$E_2(t, \vec{z}) = E_2(z)\cos\left(\vec{K}_2\vec{z} - \omega_2 t + \alpha_2(z)\right)$$

and into ion-sound wave:

$$E_s(t, \vec{z}) = A_s\cos\left(\vec{K}_s\vec{z} - \omega_s t\right) - B_s\sin\left(\vec{K}_s\vec{z} - \omega_s t\right)$$

in dimensionless variables:

$$\epsilon_{1,2} = E_{1,2}\Big/\sqrt{4\pi n_1 m v_0^2\left(\frac{n_1 v_0^4}{n_0 v_g^4}\right)^{1/3}}\,; \quad \xi = \frac{\omega_p z}{v_0}\left(\frac{n_1 v_0}{n_0 v_g}\right)^{1/3}$$

$$\tau = -\frac{\omega_1}{2\pi}\left(t - \frac{z}{v_0}\right); \quad \nu = 2\pi\frac{d\tau}{d\xi}\,; \quad a_s, b_s = \frac{4(A_s, B_s)\frac{K_1^2}{K_s^2}}{\left(\frac{n_1 v_0}{n_0 v_g}\right)^{1/3}\sqrt{4\pi n_1 m v_0^2\left(\frac{n_1 v_0}{n_0 v_g}\right)^{1/3}}} \qquad (3)$$

have the form:

$$\epsilon_1\frac{d\alpha_1}{d\xi} = \Lambda\epsilon_2\left(b_s\cos(\alpha_1 - \alpha_2) - a_s\sin(\alpha_1 - \alpha_2)\right) - \int_{-1/2}^{1/2} d\tau(0)\sin(2\pi\tau + \alpha_1)$$

$$\frac{d\epsilon_1}{d\xi} = \Lambda\epsilon_2\left(a_s\cos(\alpha_1 - \alpha_2) + b_s\sin(\alpha_1 - \alpha_2)\right) - \int_{-1/2}^{1/2} d\tau(0)\cos(2\pi\tau + \alpha_1)$$

$$\epsilon_2 \frac{d\alpha_2}{d\varsigma} = \Lambda \epsilon_1 \left(\beta_s \cos(\alpha_1 - \alpha_2) - \alpha_s \sin(\alpha_1 - \alpha_2)\right); \quad \frac{d\epsilon_2}{d\varsigma} = \Lambda \epsilon_1 \left(\beta_s \sin(\alpha_1 - \alpha_2) + \alpha_s \cos(\alpha_1 - \alpha_2)\right)$$

$$\frac{d\alpha_s}{d\varsigma} = -\epsilon_1 \epsilon_2 \cos(\alpha_1 - \alpha_2); \quad \frac{d\beta_s}{d\varsigma} = -\epsilon_1 \epsilon_2 \sin(\alpha_1 - \alpha_2)$$

$$\frac{d\nu}{d\varsigma} = -\epsilon \sin(2\pi\tau + \alpha_1); \quad \frac{d\tau}{d\varsigma} = \frac{\nu}{2\pi} \qquad (4)$$

In the first part of the equations for $\epsilon_1(\varsigma), \alpha_1(\varsigma)$ the first terms define the amplitude and phase variation for the decay instability and correspond to the account of small non-linearity at oscillations of plasma particles, the second terms in these equations describe interaction between the wave and resonance beam particles, integration in these terms is performed over the time of beam particles incoming into plasma $0 < t(0) < \frac{2\pi}{\omega_1}$; the dependence $\tau(\varsigma, \tau(0))$ is determined by integration of beam particle motion equations. Taking into consideration the angle dependence of decay increment in (2) we limit ourselves with consideration of the oscillation with $\theta \ll 1$. At $\delta = \frac{V_0}{V_{Te}} \mu^{1/2} > 1$ decay conditions (1) in taken case $K_{2z} K_{sz} > 0$ are fulfilled for onedimensional spectrum $\theta = 0$; if $\delta \ll 1$ equation system (3) is suitable at $\left(\frac{n_1 V_0}{n_0 V_g}\right)^{1/6} < \theta < \frac{2}{\sqrt{\ln \frac{E_{max}}{E(0)}}}$, in this case $K_s = K_1 \theta$, $|\vec{K}_1 - \vec{K}_2| = K_1 \theta \delta$

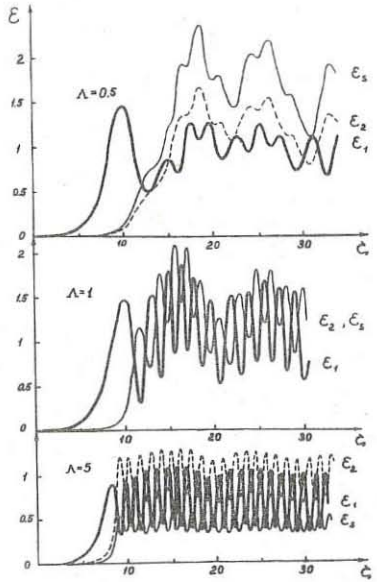
The system of the equations (4) was integrated by means of computer for various parameter values Λ for a set of 100 beam particles. Decay instability becomes essential at $\Lambda > 0.1$. The curves of the functions $\epsilon_1(\varsigma), \epsilon_2(\varsigma), \epsilon_s = \sqrt{\alpha_s^2 + \beta_s^2}$ for $\Lambda = 0.5, 3, 5$ are given in the figure I. Reversible energy transfer at the decay between fundamental wave and satellite [5] leads to the modulation $\epsilon_1(\varsigma)$ and correspondently $\epsilon_2(\varsigma), \epsilon_s(\varsigma)$ with a period, defined by a decay amplification coefficient $\varkappa_d$: $\varsigma_1 = \frac{1}{\sqrt{\Lambda}}$, then the slower changing with period $\varsigma_2 \sim \delta$ is connected with phase oscillations of beam particles trapped into a potential well and

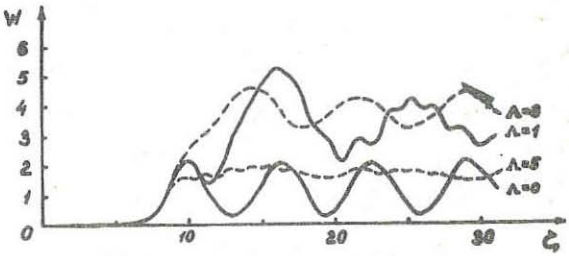
also occurs at $\Lambda=0$. The regions of phase trajectories of these particles on which they are moving in the decelerating field phase, correspond to negative energy of the fundamental wave.

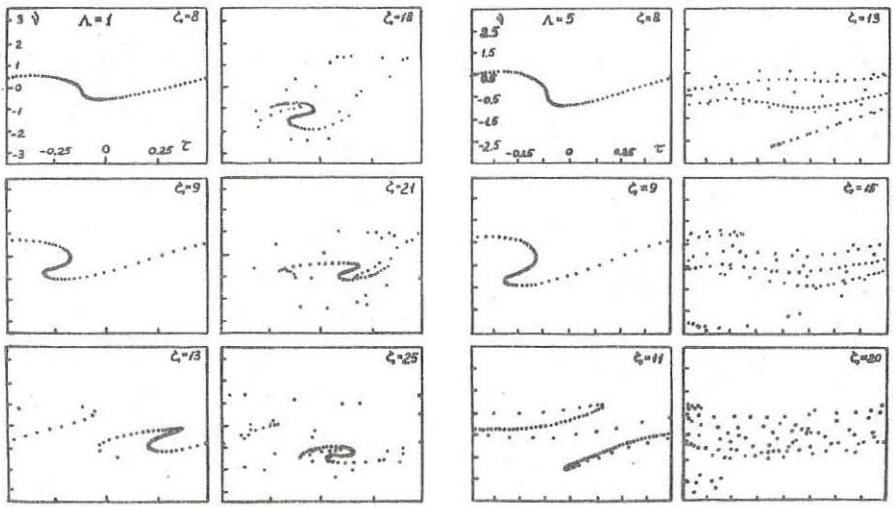
In this case the development of the decay instability leads to the amplification and the more effective taking-off energy from the beam of trapped particles. Fig. 2 - the dependence of the total energy oscillation $\epsilon_1^2+\epsilon_2^2$ over ς for various Λ ; for $\Lambda \leq \Lambda_{kp} \approx 4$ the energy taken from the beam increases approximately 3 times in comparison with a case of absence of decay instability. Dynamics of beam phase plane for $\Lambda=1$, $\Lambda=5$ is shown in the fig. 3,4. In the first case $\Lambda < \Lambda_{kp}$ and the particles are bunched so well as at $\Lambda=0$. This bunch causes phase oscillations in a potential well of the wave. At $\Lambda > \Lambda_{kp}$ stochastic instability of the trapped particles caused by a periodic amplitude changeness of a fundamental wave at the decay becomes significant. In the result of instability the "mixing" of the trapped particles takes place on phase plane, the decay in these conditions does not lead to a considerable increase of energy, taken from the beam. In conclusion we notice, that the obtained results confirm the experimental results on the opportunity of the effective beam energy transformation into energy of ion-sound oscillations due to the mechanism of decay instability: under such a mechanism energy of ion-sound oscillations $W_s = \left(\frac{n_1 v_0}{n_0 v_\varphi}\right)^{2/3} W_L$, W_L - energy of Langmuir oscillations, excited by the beam.

1. V.N.Oraevsky, R.Z.Sagdeev, JTPh, 32, 291 (1962).
2. I.N.Onishchenko, A.R.Linetsky, N.G.Matsiborko, V.D.Shapiro, V.I.Shevchenko, JTPh Letters, 12, 407 (1970).
3. Th.O'Neil, J.H.Malmberg, J.H.Winfrey, Phys. Fluids, 14, 1204 (1971).
4. V.D.Shapiro, V.I.Shevchenko, Nucl.Fus., 12, 133 (1972).

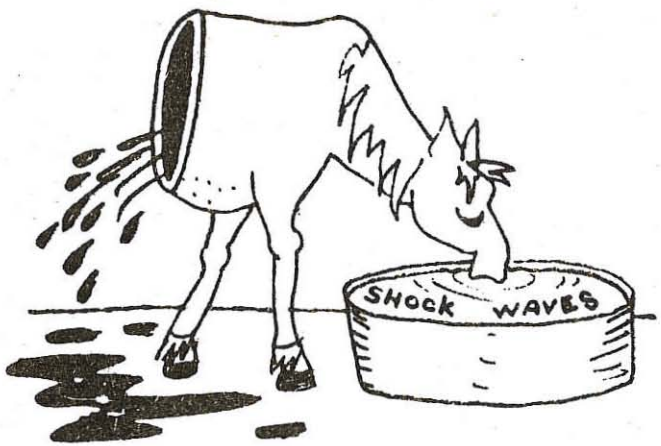
5. Blombergen, N., Non-linear Optics, Benjamin, USA (1956).
6. B.B.Kadomtsev, A.B.Mikhajlovsky, A.V.Timofeev, JTPh, 47, 2266 (1964).
7. G.M.Zaslavsky, Uspekhi Fizicheskikh Nauk, 107, 4 (1972).
8. O.F.Kovpik, E.A.Kornilov, JTPh, 43, 3 (1973).







3.5. RF AND SHOCK HEATING



DIFFERENT THEORETICAL CHARACTERISTICS OF RF HEATING OF HOT ELECTRON-ION TOROIDAL PLASMAS.

A.M. MESSIAEN*, R. KOCH*, P.E. VANDENPLAS, R.R. WEYNANTS**

Laboratoire de Physique des Plasmas+ *- Laboratorium voor Plasmafysica*+

Ecole Royale Militaire - Koninklijke Militaire School ; 1040 Brussels, Belgium.

Abstract. *A toroidal plasma column excited by a set of external coils is described by hot fluid theory. The plasma boundary is allowed to vibrate and collisional, "turbulent" and collisionless damping considered. Coil loading by the plasma and the external wall is computed from* $\omega \ll \omega_{ci}$ *up to* $\omega \gg \omega_{LH}$.

INTRODUCTION. New bounded plasma resonances of a hot plasma have been predicted in the magneto-ion domain [1]. A comprehensive fluid theory [2] of *rf* absorption by a uniform hot ion-electron plasma cylinder was presented and the role of the boundedness of the plasma with respect to the coupling to an external field emphasized. This field is an arbitrary $e^{-i\omega t}$ electromagnetic wave periodic (real $k_{//}$) along the *z*-axis (r, θ, z cylindrical coordinates). Such a wave can be represented as the sum of transverse electric (*TE*) and transverse magnetic (*TM*) cylindrical waves characterized by an $e^{i(n\theta+k_{//}z)}$ dependence. The plasma was described by the linearized fluid equations using scalar pressures to introduce T_e and T_i. The boundary conditions at $r = a$ (a : radius of the plasma) were the continuity of E_z, E_θ, H_z, H_θ and the normal perturbed conduction current densities $J_{re} = J_{ri} = o$. Afterwards plasma inhomogeneity [3] and helical excitation [4] were considered. Comparison of the spectrum of predicted bounded plasma resonances with the results of a small scale experiment proved successful [5]. The same basic model is now applied to the problem of coupling a *rf* field from a set of coils to a toroidal plasma but moving plasma boundaries consistent with the magnetic confinement and appropriate values of effective collision frequencies ν_e and ν_i are considered for TTMP, ICR and LHR. The coil loading due to plasma heating and losses in the external wall is computed in a broad frequency domain (from $\omega \ll \omega_{ci}$ up to $\omega \gg \omega_{pi}$; $\omega_{p\alpha}$, $\omega_{c\alpha}$: plasma and cyclotron frequencies with $\alpha = e, i$).

THEORETICAL MODEL. (i) Excitation. We consider the cylindrical approximation of a toroidal plasma excited by a set of helical coils placed around the torus (fig. 1). The applied field (i.e. in absence of plasma) is first computed. Each coil is approximated by a tape helix [4][6] which defines a surface current distribution $\bar{K}$ at $r = b$. This current is expanded in cylindrical harmonics $\bar{K} = \frac{I}{2\pi b} \sum_n \sum_k A_{nk} e^{i(n\theta+kz/R+\beta_o z)} (\bar{1}_z + tg\ \psi\ \bar{1}_\theta)$ (I : current ; $\beta_o = k_o/cos\ \psi$; k_o vacuum wavenumber ; $k_{//} = k/R$ axial wavenumber with $k = o, \pm 1, \pm 2, \ldots$;

$tg\ \psi = 2\pi b/p$; p : pitch of the helix). The spatial period is the torus length $2\pi R$ or an integral fraction of it if the coils are distributed and fed periodically. In order to satisfy current continuity, one must take into account the radial current feeders. These define a volume current distribution in the region $b < r < d$ (e.g., for one coil of length L its expression is $\bar{J}(r, \theta) = \frac{I}{r}$ [$\delta(\theta - \frac{2\pi L}{p})\ \delta\ (z - L)e^{i\beta_o L} - \delta\ (\theta)\ \delta\ (z)$] $\bar{1}_r$). For $r < b$, the fields are the solutions, bounded on the axis, of Maxwell's equations ; for $b < r < d$, they are the solution satisfying E_z and $E_\theta = o$ at $r = d$ and these fields are matched at $r = b$ by $curl_s \bar{E} = o$ and $curl_s \bar{H} = \bar{K}$. Each A_{nk} excites the sum of a *TE* and a *TM* wave but, as shown in [4], a pure *TE* or pure *TM* excitation is possible when $\beta_o L \ll 1$ if the coil is excited by a standing wave at respectively current or voltage antinode. (ii) Plasma description. The plasma (uniform and submitted to an uniform axial magnetic field $\bar{B}_o$) is described in the introduction. The losses are introduced by effective ν_α for which two frequency domains are considered : a) $\omega < \omega_{ci}$ and $|k_{//} V_e|$ ($V_\alpha^2 = KT_\alpha/m_\alpha$): the values of ν_α take into account Cerenkov absorption by electrons and ions and ion cyclotron damping around $\omega = \omega_{ci}$. The ν_α obtained by comparing appropriate tensor elements of the fluid and kinetic permittivities are : $\nu_e/\omega = \sqrt{\pi/2}\ (|k_{//} V_e|/\omega + \omega^3/|k_{//} V_e|^3) e^{-\omega^2/2(k_{//} V_e)^2}$; $\nu_i = \sqrt{\pi/2}[(|k_{//} V_i|/\omega + \omega^3/|k_{//} V_i|^3)\ e^{-\omega^2/2(k_{//} V_i)^2} + (|k_{//} V_i|/\omega) e^{-(\omega - \omega_{ci})^2/2(k_{//} V_i)^2}]$. b) $\omega > \omega_{ci}$ and $|k_{//} V_e|$. For that case experiments indicate that the losses mostly have a nonlinear character due to excitation of ion electrostatic waves by parametric decay [7] . The effective ν_α depends on the excitation level and corresponding turbulence spectrum. We therefore consider ν_α as a parameter in this domain. (iii) Boundary conditions. At $r \tilde{=} a$ we match the field induced into the plasma to the external applied and scattered fields. The boundary conditions with a vibrating boundary (consistent with the magnetic confinement) are obtained from the equations of energy and momentum conservation [8] and from Maxwell's eqs.(assuming $\partial/\partial t \equiv - \bar{u}_b . \nabla$; $\bar{u}_b$: boundary velocity). The boundary conditions are : continuity of E_z and H_θ ; $H_{zext}(1 + \beta/4) = H_{zpl}(1 - \beta/4) + p/<B_o>$; $E_{\theta ext}(1 - \beta/4) = E_{\theta pl}(1 + \beta/4)$; $\bar{u}_{be} = \bar{u}_{bi} = \bar{1}_r <E_\theta>/<B_o>$ (< > : mean value at boundary, p : perturbed total pressure, β : $2\mu_o NK\ (T_e + T_i)/<B_o>^2$).

RESULTS. Coil loading due to the plasma, R'_{Ip} and to the outer wall, R'_{IW}, is computed versus ω($R'_I = R_I/|A_{nk}|^2$; $R_I = \frac{2}{I^2} d\ P_{abs}/dz$; P_{abs} : absorbed power) for typical parameters (here Wega machine). At low ω, Fig 2 shows a first absorption zone near $|k_{//} V_i|$ and $|k_{//} V_S|$. It corresponds to TTMP of the ions and P_{abs} agrees with standard values but is much less than that obtained in [2] where the different boundary condition led to strong absorption by peripheral electrons.

(Note that if $T_i \ll T_e$, this zone splits into two, one near $|k_{//} V_i|$

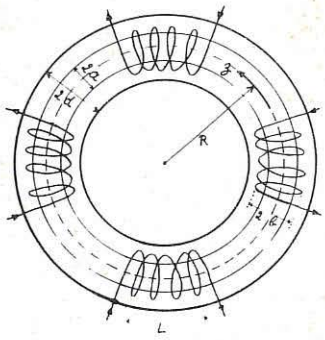


Fig 1. Plasma torus with shell and coils.

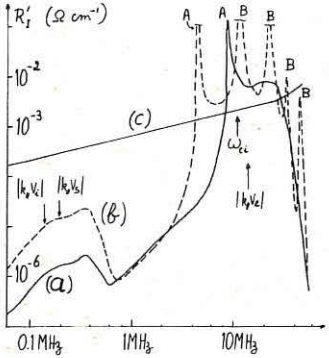


Fig 2. a) R'_{Ip} versus ω with collisionless damping; b) same as (a) except $N = 10^{14}$ cm^{-3}; c) R'_{IW} corresponding to (a).

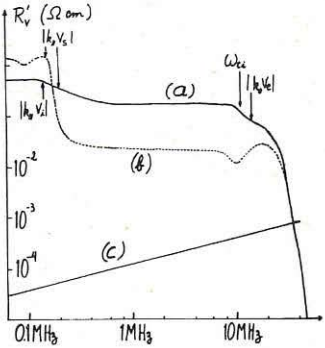
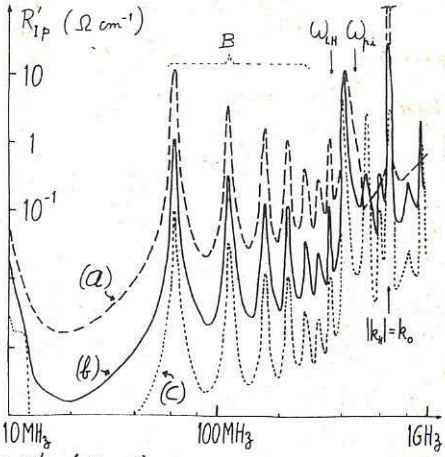


Fig 4. a) R'_{Vp} versus ω with collisionless damping; b) same as (a) but $T_i = 10^5$K; c) R'_{VW} corresponding to (a).



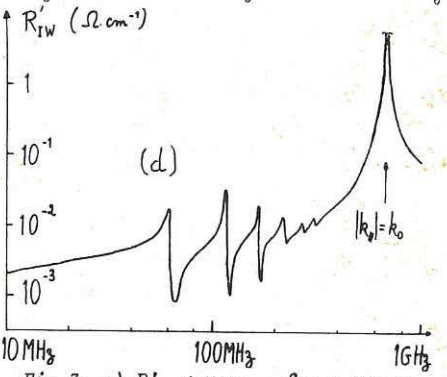


Fig 3. a) R'_{Ip} versus ω for $\nu_e = \nu_i = 10^6$Hz; b) id. except $\nu_e = \nu_i = 10^5$Hz; c) id. except $\nu_e = \nu_i = 10^4$Hz; d) R'_{IW} corresponding to (b).

Parameters common to Figs 2, 3, 4 (except otherwise stated) : a = 10cm; b = 14.5cm; d = 19cm; Deuterium ; n = o; $k_{\parallel} = 0.14$cm^{-1}; $T_e = T_i = 10^6$K; $B_o = 15$kG; $N = 10^{13}$cm^{-3}; p = 6.3cm; conductivity of outer wall : $3 \times 10^4 (\Omega cm)^{-1}$.

and an electron one near $|k_{\parallel}V_S|$). An electron absorption region starts with a resonance (labelled *A* on Fig 2) near $\omega = |k_{\parallel}V_A|$ (if $\omega >> k_{\parallel}V_A$; V_A : Alfvèn velocity) or $\omega = \omega_{ci}$ (if $\omega_{ci} << k_{\parallel}V_A$) and ends when $\omega > |k_{\parallel}V_e|$ (no more electron Cerenkov absorption). More or less pronounced ion cyclotron absorption appears near ω_{ci} . Furthermore magnetoacoustic bounded plasma resonances (eigenvalues of ω/V_A ; labelled *B* on Figs 2 and 3) lead to absorption peaks. Fig 2b shows an interesting case for heating : coincidence of $k_{\parallel}V_e$, ω_{ci} and first *B* resonance. Fig 3 shows a typical spectrum of *B* resonances extending up to $\omega \sim \omega_{LH}$. At $|k_{\parallel}|=k_o$ appears the first of a resonance series of the coaxial type (standing wave between plasma and outer wall). These may be interesting for efficient coupling of *rf* energy near ω_{LH}. Fig 4 gives typical curves for pure *TM* excitation (R_V is the real part of the impedance between coil and ground [4]). This excitation has a more favorable R_p/R_W but requires high values of electric field for heating.

REFERENCES.

[1] P. VANDENPLAS, A. MESSIAEN, J. MONFORT, J. PAPIER, Phys.Rev.Letters, 22, 1243 (1969); Plasma Phys., 12, 391 (1970).

[2] A. MESSIAEN, P. VANDENPLAS, Nuclear Fusion, 11, 556(1971); Plasma Phys. (June 1973).

[3] D. DUBOIS, A. MESSIAEN, P. VANDENPLAS, Proc.Vth Eur.Conf.Fusion, Grenoble, vol. 1, 114 (1972).

[4] A. MESSIAEN, D. DUBOIS, P. VANDENPLAS, Proc. Vth Eur.Conf.Fusion, Grenoble, vol. 1, 115 (1972).

[5] J. JUSSERAND, A. MESSIAEN, R. WEYNANTS, to be published in Plasma Phys.(1973).

[6] L. STARK, J. Appl. Phys., 25, 1155 (1954).

[7] V. VDOVIN et al., JETP Letters 14, 149(1971); W. HOOKE, S. BARNABEI, Phys.Rev. Letters 29, 1218(1972); T. CHU, S. BARNABEI, W. HOOKE, R. MOTLEY, paper V8, Int. Congress waves & instab., Innsbruck (1973).

[8] F. ARUMI, M. OAKES, Phys. Fluids, 15, 837 (1972).

+ Association "Euratom-Etat belge" - Associatie "Euratom - Belgische Staat".

* Chercheur I.I.S.N.

** Aangesteld navorser N.F.W.O.

THE ABSORPTION OF INTENSE ELECTROMAGNETIC WAVES BY DENSE COLLISIONLESS PLASMA.

Yu.Ja.Brodskii,S.V.Golubev,V.L.Gol'tsman.A.G.Litvak

Radiophysical Research Institute,Gorkii,USSR.

It is experimentally discovered that the anomalous absorption of microwave energy leads to the bleaching of "transcritical" plasma.Threshold field values obtained and the characteristic time of dissipation are in good agreement with the assumption on the hydrodynamic instability occurence.

In paper /I/ the passage of an intense electromagnetic wave through opaque (at the small power level) plasma with the concentration above critical was observed. Since in /I/ a weakly ionized plasma was used with a small free length path of electrons it was possible to explaine the experimental data by the assumption that redistribution of the plasma density in the field occured due to ordinary ohmic heating. At the same time the problem of the role of the parametric instability processes remains unclear although the requirements for its development have been satisfied in the experiment. The present paper is devoted to the investigation of this problem.

For the experiment to be fulfilled the set up given in /I/ was modernized (Fig I). The high-frequency discharge was produced inside the evacuated chamber (80cm diameter, 200cm long) with the help of two-turn inductor (40cm diameter) being an element of the oscillating circuit of HF generator which works in the continuous regime of oscillation at the frequency of 5.2MHz with the maximum power 60 kw.

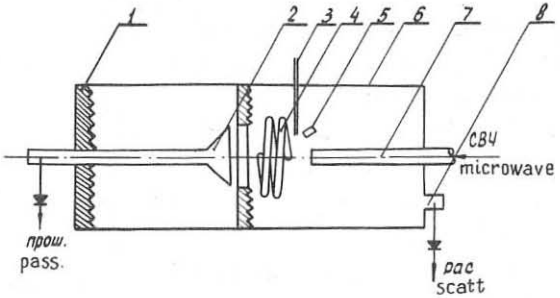


Fig I. Experimental set up. I.Absorber,2.Receiving horn,3.Double probe 4.Inductor,5.Multigrid probe,6.Chamber, 7.Radiatoring waveguide,8.Receiver of scattered signal.

...e distribution of concentration of the plasma developed ... inhomogeneous both over the radius and the axis of the chamber. Concentration dependence on the co-ordinates is given in Fig 2. Electron temperature and the value of the maximum concentration depend on the pressure in the chamber and on the power of HF energy applied. When the pressure $p_m \approx 10^{-3} \div 10^{-4}$ torr the case of plasma with rare collisions is realized, i.e. the free length path of electrons exceeds the characteristic scale of plasma layer that excludes the possibility of observation of ohmic heating effects. In this case the concentration in the centre of the layer reached the value of $N_0 \approx 3.10^{11} cm^{-3}$ and the temperature of electrons was T_e = 20 ev. The microwave pulse of S range (λ =10cm) with the duration τ_i =12.5 msec and the power up to 300 kw was radiated from the open end of a circular waveguide situated at the distance of 20 cm from the inductor. Two absorbing diaphragms were placed in the chamber to eliminate effects of echo and microwave signal rounds the plasma layer. The receiving horn was located between diaphragms also at the distance of 20 cm from the inductor. Temperature and concentration measurements were carried out by the cylindric and multigrid probes. Besides, concentration was measured over the cut off of a weak microwave signal passing through the same tract that the power pulse did. The frequency of the signal sweeps in the range 2.8 ÷ 4.0 GHz for the time t = 5 msec. Experiments made show that at the plasma concentration $N_e^s \approx (1 \div 2)N_c$ $N_e \approx (1 \div 2)\ 10^{11} cm^{-3}$ beginning with the value of the incident pulse power P_{inc} =10 kw the form of pulse reflected from plasma

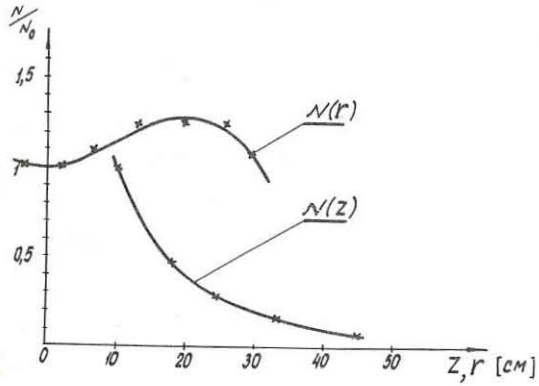


Fig 2. Radial and longitudinal distribution of plasma density.

essentially changes (Fig 3c). At the further power increase the reflected pulse becomes more regular and one may easily separate sections of the reflected wave decrease and saturation. The characteristic time of relaxation τ_{reb} depends on the plasma concentration and the pulse power. As seen from the given oscillograms this time markedly decreases with the power increase.

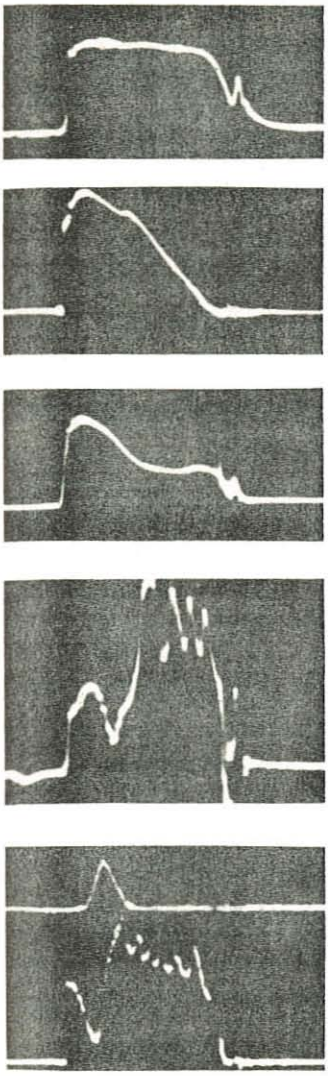


Fig.3. Oscillograms of reflected (a-e) and transmitted (f) pulses.

Unfortunately the detail investigation of the dependence of the wave reflection coefficient on the power were not carried out due to the effects of breakdown occured in the radiating waveguide (see oscillograms 3 d,e). However in cases when the time of breakdown development τ_{br} exceeds τ_{reb} it was determined that the coefficient of the wave reflection from plasma considerably decreased. For example, at $P_{inc} \approx 50$ kw it accounts for one third of the reflection coefficient of the weak signal. With the increase of plasma concentration the time τ_{br} decreased and was compared to τ_{reb}. In this case the stationary part in the oscillogram of the reflected pulse vanished (Fig 3 d,e) and the value of the reflection coefficient directly before the breakdown became characteristic. It was estimated that at $P_{inc} \approx 50$kw and $N_e = 2N_{cr}$ the reflection coefficient may decrease by almost

one order of magnitude. The further power increase leads to the earlier breakdown and beginning from $P_{inc} \geq$ I50 kw the breakdown occurs on the leading front of the pulse. At P_i = 50 kw the passage of the microwave signal through "opaque" plasma was regularly observed at the appearance of the minimum in the reflected pulse (Fig 3 e). As measurements show simultaneously with the decrease of the reflected wave the noticeable decrease of the scattered signal takes place (Fig 4).

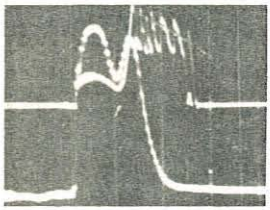


Fig 4. Oscillograms of reflected(I) and scattered(2) pulses.

The results obtained testify to the fact that at the incidence of the power e.m. wave on the opaque plasma with rare collisions there primary occurs effects of the anomalous absorption which apparently associated with the development of parametric instability of plasma oscillations in the vicinity of the reflection point of a plasma wave /2/. Really, at P_{inc} =I0 kw the electric field intensity greatly exceeds the threshold fields for all types of parametric instability (the decay t → l+S, the kinetic and hydrodynamic induced scattering of particles t → t). Already at the power P_{inc} =I0kw the relation $E^2/8\pi NT_e \approx 10^{-2}$.+) The effects of e.m. wave passing through opaque plasma (self-trapping) may be associated with this instability leading to the accumulation of plasma oscillations and to the further plasma redistribution in the nonlinear satnding plasma waves. In favour of this conclusion testify the results of papars /4,5/ where the nonlinear transparence collisionless "transcritical" plasma also was observed.

In conclusion the authors are grateful to B.G.Eremin for the useful discussions.

References.

I.Yu.Ja Brodskii,B.G.Eremin,A.G.Litvak,Yu.A.Sakhonchik.JETP Lett. 13,163 (I971).
2.B.P.Silin,UFN,108,625 (I972).
3.A.G.Litvak,V.Yu.Trachtengerts,JETP,60,I702 (I972).
4.G.M.Batanov,V.A.Silin,JETP Letters,I4,445 (I97I).
5.V.A.Silin,JETP Letters 16,I53 (I972).

+) Here the hydrodynamic stage of induced scattering takes place /3/. Its increment exceeds the value $\gamma \approx (m/M)^{1/2} K_p v_{T_e} \approx 10^{-7}$ sec^{-1} ($K_p = 0{,}2 \frac{\omega_{pe}}{v_{T_e}}$ is ions plasma frequency).

INVESTIGATION OF THE MAGNETOSONIC PLASMA HEATING IN THE TOKAMAK.

V.L.Vdovin, O.A.Zinov'ev, A.A.Ivanov, T.A.Kosinova, M.F.Krotov, Ya.R.Rakhimbabaev, V.D.Rusanov, N.V.Shapotkovskii.

I.V.Kurchatov Institute of Atomic Energy
Moscow, USSR

It is known that the efficiency of the Joule heating in the Tokamak drops with increasing temperature. This stimulates an intensive search for new plasma heating methods. The heating by means of h.f. electromagnetic fields, in particular by magnetosonic (m.s.) waves, seems to be one of the simplest acceptable methods. In Refs. /1,2/ the possibility for plasma heating in the Tokamaks by the excitation of magnetosonic oscillations has been experimentally shown. In the present work this effect is investigated in more detail.

A small "ТМ-1-ВЧ " Tokamak as described in Refs. /1,2/ was used in the experiment. The plasma was heated by means of a high-frequency generator (f=21 m.c. and 36 m.c.) connected with the plasma by a narrow loop. The loop was inserted into the liner and isolated with quartz from the plasma (in some experiments the isolation was lacking).

The experiments with hydrogen and deuteron plasma were carried out using the semisinusoidal current pulse of 3 msec duration and amplitude 10kA; the plasma column diameter was about 12 cm.

Fig.1 shows the trend of the amplitude of the high frequency signal from the receiving loop embracing the plasma column and located diametrically relative to the coupling loop of the generator. The generator frequency was 21 m.c. In two upper curves differing in the values of the strength of the magnetic field H_o the double

excitation of the main radial magnetosonic oscillation mode is clearly seen. Two symmetric (relative to n_{max}) resonances are due to the excitation of modes with m=1 (at a low density).

Fig.2 shows the plasma heating effect while applying the high frequency pulse duration of 400 μsec. One can readily see the increase in $n(T_e+T_i)$ as well as the increase of $T=T_e+T_i$ due to magnetosonic wave. The mean temperature T_e+T_i was then doubled. The average density of the plasma at the moment of the pulse swithching was about $10^{13}cm^{-3}$; 40kw active power was received by the plasma from the generator, which corresponded to the heating performance coefficient of 40 per cent.

To determine the ion

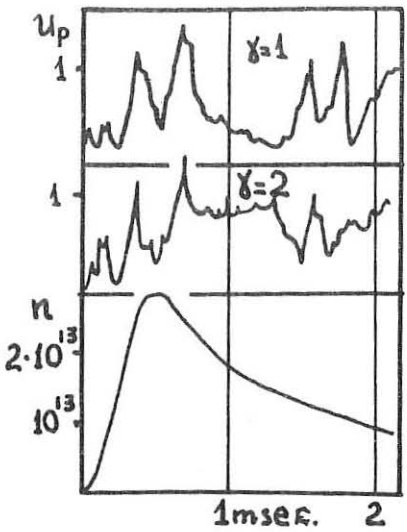


Fig.1. Excitation of magnetosonic waves in the Tokamak plasma. The upper curve is the signal from the probe at H_o=14 ke f=21 m.c. The second curve from the top is the signal from the probe at H_o=12ke f=21m.c.

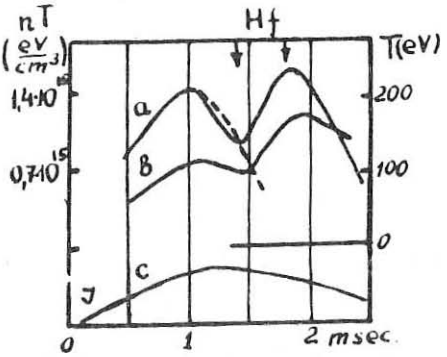


Fig.2. "a" is the time dependence $n(T_e+T_i)$: solid line in magnetosonic heating; dashed line-without high-frequency heating, "b" is the time dependence of T_e+T_i; "c" is the oscillogram of the current in the plasma.

temperature the halfwidth of the extrinsic line C III (λ =4647A) was measured. In the excitation of magnetosonic oscillations the ion temperature increased and could be equal to or even higher than T_e, which correspondeds to the increase in T_i by several times.

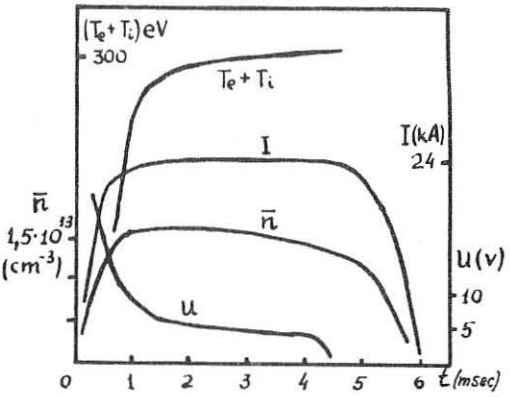


Fig.3. U is the perimeter voltage, is the concentration averaged over the diameter.

After modernization of the ohmic heating system the investigations were continued with the discharge in helium. Improvement in the parameters was reached by forming a trapezoidal current pulse I with a duration of 6 msec and amplitude up to 30ka. At the current of 24ka and magnetic field of 14ke the energy content of $n(T_e+T_i)$ amounted to $3.5\ 10^{15}\ \frac{ev}{cm^3}$. The main characteristics of the helium discharge are shown in Fig.3.

After attenuation of the high-frequency preionization pulse the same generator (f=36mc) excited magnetosonic waves in the plasma to heat the ion component. The line He II λ =4686A was chosen as the temperature indicator. Fig.4 shows the additional heating of helium ions. The high-frequency power introduced did not exceed 20kw.

It should be noted that no negative effect of high frequency power on the stability or life time of particles or energy in the

plasma was observed either in hydrogen or helium plasma. On the contrary, an increase in both parameters was observed the magnetosonic waves having been excited in the plasma column.

The experimental value of the plasma quality is close to 10 in the order of magnitude, which may be accounted for by the decay of the initial magnetosonic wave to the "electrosonic" $\omega \sim k V_{Ti}$ and drift $\omega_* \simeq k \frac{c T_i}{eH} \frac{\Delta n}{n}$ This must provide a low threshold of the noise generation and quality factor $Q \simeq 10$ [4].

Thus an effective heating of the ionic plasma by magnetosonic waves in the Tokamak is shown.

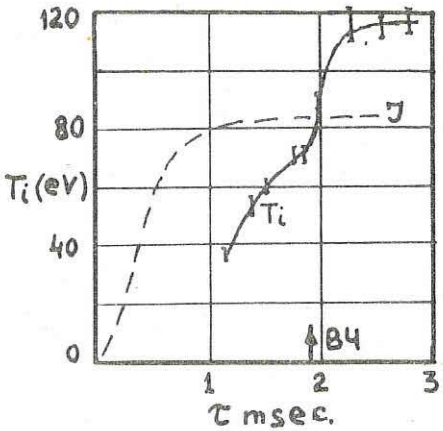


Fig.4. The additional heating of helium ions by the high-frequency pulse.
T_i is the temperature of single-ionized atoms.

R e f e r e n c e s.

1. V.L.Vdovin, O.A.Zinov'ev, A.A.Ivanov, L.L.Kozorovitskii, V.V.Parail, Ya.R.Rakhimbabaev, V.D.Rusanov. J.E.T.P., Pisma, 14, 228 (1971).

2. V.L.Vdovin, O.O.Zinov'ev, A.A.Ivanov. L.L.Kozorovitskii, M.F.Krotov, V.V.Parail, Ya.R.Rakhimbabaev, V.D.Rusanov, N.V.Shapotkovskii. J.E.T.P., Pisma, 17, 4 (1973).

3. Yu.A.Galushkin, V.I.Gerviso, V.I.Kogan. Proceedings of the Conference in Medison, June 17-23, 1971; IAEA-CN-28/F-6, vol.II, p.407.

4. A.A.Ivanov, V.V.Parail. J.E.T.P., 62, 932 (1972).

RESONANCE EXCITATION OF LARGE-AMPLITUDE OSCILLATIONS IN A NON-UNIFORM PLASMA NEAR ION CYCLOTRON RESONANCE

L.I.Grigor'eva, B.I.Smerdov, S.A.Sapogov, V.V.Chechkin.

Physical-Technical Institute, Ukrainian Academy of Sciences, Kharkov, U.S.S.R.

Resonance excitation of large-amplitude oscillations near ion gyrofrequency ω_{Hi} has been studied in a radially non-uniform plasma cylinder. A resonance layer have been found in which a sharp increase of the amplitude of the alternating field takes place.

In the present paper a possibility is investigated of excitation of e.m. oscillations with $\omega \sim \omega_{Hi}$ in a plasma with strong radial non-uniformity. The amplitude of these oscillations should be large enough for the current velocity across the d.c. magnetic field $\vec{U} = \vec{U}_i - \vec{U}_e$ to exceed some critical value $\sim \left[(T_e + T_i)/m_i\right]^{1/2}$. This is known to result in excitation of high-frequency small scale plasma instabilities which in turn result in turbulent heating of the plasma [1,2].

Recently an efficient heating of a plasma by fast magnetosonic ($\omega \gg \omega_{Hi}$) and ion cyclotron ($\omega \lesssim \omega_{Hi}$) waves of large amplitude was observed in [1-4].

The experiments described below were carried on a plasma produced by a pulsed high-current straight discharge in hydrogen at $\sim 10^{-3}$ Torr. The inner diameter of the quartz discharge tube was 6.2 cm, distance between the electrodes 88 cm. The plasma was placed in a quasy-constant magnetic field H. The oscillations in the plasma were excited by a 8-section Stix coil with axial period $2\pi/k_{\parallel} = 20$ cm. This coil served as an inductance of

RESONANCE EXCITATION OF LARGE-AMPLITUDE OSCILLATIONS IN A NON-UNIFORM PLASMA NEAR ION CYCLOTRON RESONANCE

L.I.Grigor'eva, B.I.Smerdov, S.A.Sapogov, V.V.Chechkin.

Physical-Technical Institute, Ukrainian Academy of Sciences, Kharkov, U.S.S.R.

Resonance excitation of large-amplitude oscillations near ion gyrofrequency ω_{Hi} has been studied in a radially non-uniform plasma cylinder. A resonance layer have been found in which a sharp increase of the amplitude of the alternating field takes place.

In the present paper a possibility is investigated of excitation of e.m. oscillations with $\omega \sim \omega_{Hi}$ in a plasma with strong radial non-uniformity. The amplitude of these oscillations should be large enough for the current velocity across the d.c. magnetic field $\vec{U} = \vec{U}_i - \vec{U}_e$ to exceed some critical value $\sim \left[(T_e + T_i)/m_i\right]^{1/2}$. This is known to result in excitation of high-frequency small scale plasma instabilities which in turn result in turbulent heating of the plasma [1,2].

Recently an efficient heating of a plasma by fast magnetosonic ($\omega \gg \omega_{Hi}$) and ion cyclotron ($\omega \lesssim \omega_{Hi}$) waves of large amplitude was observed in [1-4].

The experiments described below were carried on a plasma produced by a pulsed high-current straight discharge in hydrogen at $\sim 10^{-3}$ Torr. The inner diameter of the quartz discharge tube was 6.2 cm, distance between the electrodes 88 cm. The plasma was placed in a quasy-constant magnetic field H. The oscillations in the plasma were excited by a 8-section Stix coil with axial period $2\pi/K_{\parallel} = 20$ cm. This coil served as an inductance of

a shock-excited circuit with natural frequency 6.6 Mc/sec and stored energy ~ 7 J.

At the moment of turning on the HF field (~ 10 μsec after discharge current is stopped) the radial distribution of plasma density $n(r)$ estimated from microwave measurements is shown in Fig.3a. The HF energy going into the plasma vs H (in per cent to the energy stored in the circuit) is presented by a two humped resonance curve (Fig.1), the value of α in the maxima attains 65%. The measurements of the alternating longitudinal magnetic field H_z on the axis performed with the aid of a magnetic probe show that HF field in the plasma is a superposition of two oscillations with parallel wavelengths being close to $2\pi/k_{\parallel}$ and frequencies depending on H. This dependence is shown in Fig.2 (the lines a,b,c mark ω_{Hi} and the positions of the absorbtion maxima, respectively). The graph presented here is similar to a graph representing the variation of natural frequencies of two coupled oscillating systems vs detuning. This dependence is well-

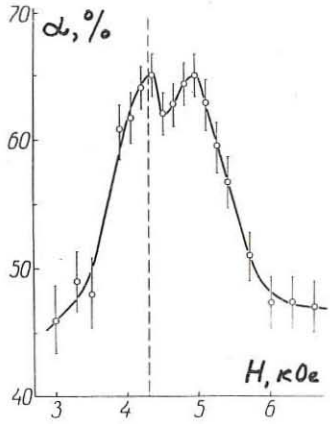


Fig.1

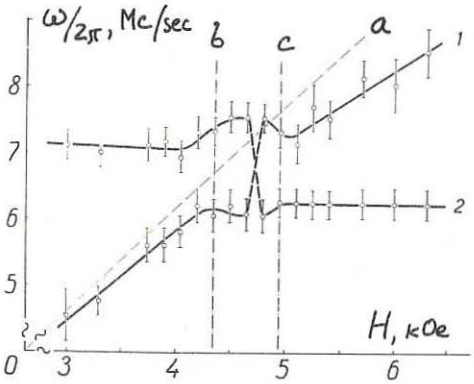


Fig.2

known in radiophysics, the only difference is that in the case considered the coupling between the plasma and the circuit increases when H changes in the coupling resonance region. The maxima of HF energy transferred from the circuit into the plasma take place in the vicinity of those values of H where the frequency difference between branches 1 and 2 is minimum. To find out the nature of the oscillations excited in the plasma the measurements were made of radial distribution of the azimuthal alternating magnetic field $H_\varphi(r)$ (Fig.3b, $|H_\varphi|$ is plotted on the vertical axis) and phase shift $\Delta\theta(r)$ between H_φ and H_r (Fig.3c) in a cross-section between two adjacent sections of the exciting coil at $H \approx$ 4.7 kOe. The vertical dashed line in Fig.3 marks the position of the wall of the discharge tube. It follows from Fig.3b that H_φ sharply increases in the vicinity of $r_0 = 1{,}5$ cm. At the same point $\Delta\theta$ experiences a 180°-jump (Fig.3c). At $r > r_0$ the sense of polarization of the oscillations corresponds to ion cyclotron wave while at $r < r_0$ it corresponds to fast magnetosonic wave.

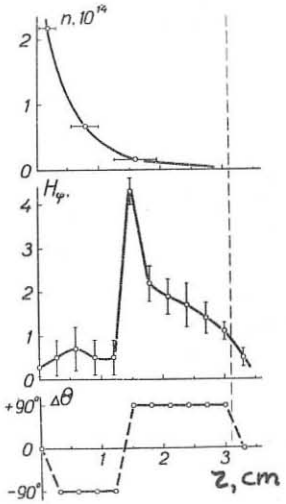


Fig.3

The data presented here is the evidence of a resonance layer in the plasma in which $n_\parallel = \frac{k_\parallel c}{\omega} \approx \varepsilon_1$, $\varepsilon_1 \approx \omega_{pi}^2/(\omega_{Hi}^2 - \omega^2)$ is a dielectric tenzor component [5-7]. In the resonance layer H_φ reaches 500 Oe. The corresponding current velocity $U_r \approx k_\parallel c H_\varphi / 4\pi n(r_0) e \approx 4 \cdot 10^7$ cm/sec considerably exceeds pre-

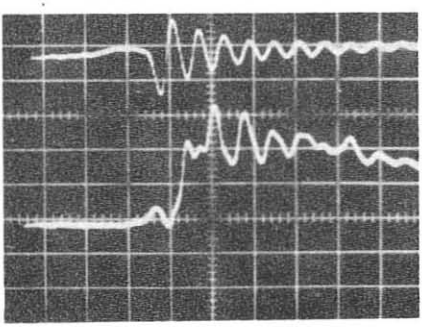


Fig.4

sumable ion thermal velocity before turning on HF field ($<10^7$ cm/μsec). Therefore turbulent heating of the plasma is possible in the resonance layer region.

In the experiments reported here a fast (for a time $\sim 2\pi/\omega$) heating of the plasma after HF field was turned on really took place. This is confirmed by Fig.4 where oscillograms of the current in the exciting coil (top trace, 0.25 μsec/div) and the diamagnetic signal (bottom trace) are presented. At a maximum of HF energy absorbtion the increase of plasma perpendicular pressure averaged over discharge tube cross-section was $7 \cdot 10^{15}$ ev/cm^3. We believe that this increase is caused at least partially by plasma heating in the resonance layer having been found in the presented work.

References

1. L.I.Grigor'eva, V.L.Sizonenko, B.I.Smerdov, K.N.Stepanov, and V.V.Chechkin. Zh.Eksp.Teor.Fiz. 60, 605 (1971) Sov.Phys.-JETP 33, 329 (1971).

2. L.I.Grigor'eva, A.V.Longinov, A.I.Pyatak, V.L.Sizonenko, B.I.Smerdov, K.N.Stepanov, V.V.Chechkin. Plasma Physics and Controlled Nuclear Fusion Research 1971, vol.III, IAEA, Vienna, 1971, p.573.

3. L.V.Dubovoi and V.P.Fedyakov. Zh.Eksp.Teor.Fiz. 53, 689 (1967) Sov.Phys.- JETP 26, 433 (1968).

4. A.Jiyoshi, J.Fujita, S.Sakakibara, N.Inoue, C.Leloup, Kakuyugo Kenkyu 25, 61 (1971); J.Phys.Soc.Japan 31, 315 (1971).

5. T.H.Stix. Phys.Fluids 3, 19 (1960); The Theory of Plasma Waves. McGrow-Hill Book Co. NY (1962).

6. V.V.Dolgopolov and K.N.Stepanov. Nucl.Fusion 5, 276 (1965).

7. V.V.Dolgopolov and K.N.Stepanov. Zh.Tekh.Fiz. 36, 1003 (1966).

LINEAR DISCHARGE TURBULENT HEATING EXPERIMENT

Ion Heating and Oscillations with Frequencies near f_{pi}

K. Adati, R. Sugihara, T. Uyama* and K. Watanabe*

Institute of Plasma Physics, Nagoya University, Nagoya, JAPAN
*Research Inst. for Atomic Energy, Osaka City Univ., Osaka, JAPAN

ABSTRACT The temporal variation of the intensity of oscillations around the ion plasma frequency f_{pi} has been compared with that of the Doppler broadening of He II 4686 Å line. It is found that the ion heating is not observed during excitation of oscillations of high intensity, but rather during that of low intensity.

In turbulent heating experiments it has been confirmed that the ion heating is almost always accompanied with an anomalously high resistivity or appearance of a hump in the profile of the temporal variation of applied axial heating voltage.[1] The hump is observed when the heating voltage is higher than a critical value or when the initial plasma density is lower than a critical value. In order to clarify the mechanism of the ion heating in a linear turbulent-heating experiment, an experiment has been carried out in a condition that an applied heating voltage is a little higher than the threshold voltage. If the heating voltage is much higher than the critical value, the resultant ion temperature reaches very high value but the plasma behavior becomes very complex. In our experimental condition the resultant ion temperature is rather low but the plasma behavior is simple and clear, so that the phenomena concerned may be analysed clearly.

The experiment has been carried out in the BSG II device,[2,3] a gas of helium being used. A plasma is produced by a theta-pinch discharge, the gas being introduced through a fast-acting valve, and the plasma expands into a chamber 50 cm in diameter and 400 cm in length, where a longitudinal and uniform magnetic field of 2 kG is applied. A pair of hollow electrodes, with a distance of 100 cm, are set coaxial to the axis of the chamber and their apertures (6 cm in diameter) limit the diameter of the plasma before heating. The plasma density and temperature between the electrodes are fairly uniform along the axis and have values of $1 \sim 2 \times 10^{13}\,cm^{-3}$

and 2 eV, respectively, before the heating voltage is applied. The density and temperature before heating are derived from data of diamagnetic loops, a pulse-biased Langmuir probe, and Laser light scattering.

The power of heating discharge is supplied from a capacitor of 1.1 μF with a charging voltage of 36 kV. The measurement of oscillations in the region near f_{pi} is made by means of a coaxial floating probe, which consists of a Micro Coax solid-jacketed coaxial cable, 3.6 mm - 2.2 mm in diameter. The cable is cut at an angle to expose the conductors, and the beveled part is 5.0 mm in length. An Echelle monochromator with twelve channels of photo-electric detectors is used to obtain the temporal change of the ion line profiles.

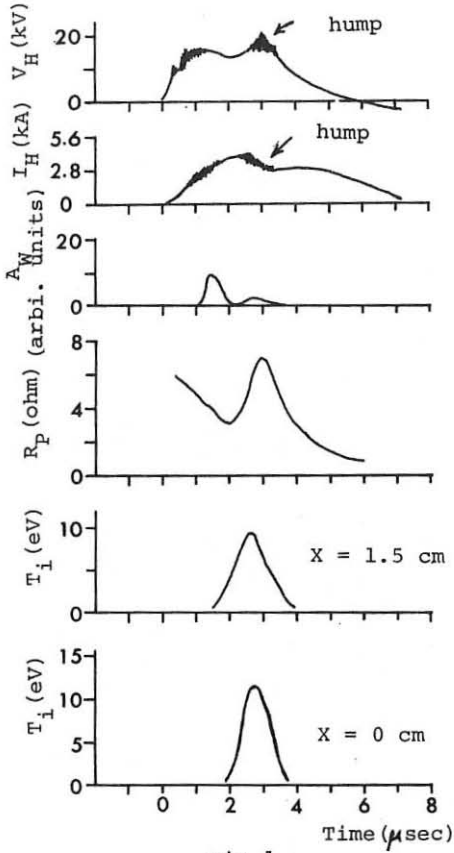


Fig.1.

Simultaneous measurement of the ion energy and oscillation intensities has been made and the result is shown in Fig.1, where V_H is the voltage between the electrodes, I_H the heating current through the plasma, A_w the amplitude of the oscillations with frequencies between 25 MHz and 2 GHz, R_p the phenomenological resistance between the electrodes, and T_i the ion temperature. The x value is a distance between the plasma axis and a chord in the plasma cross-section, along which the profiles of He II 4686 Å line are measured. It is found that the ions are heated only during the voltage (resistive) hump, while the intense oscillations are excited not only during the hump but also before the onset of the hump. Under these experimental conditions, the oscillations are excited, then decay, and finally reoccur combined with ion heating and the resistive

"hump". The intensity of the oscillations is much higher in the first stage before the hump than that in the ion heating stage. Radial dependence of the duration of oscillations is presented in Fig.2, where the dotted line (1) shows the onset time of the first excitation, the line(2) is the disappearance time of it, and the lines (3) and (4) are the onset time and the disappearance time of the second excitation. The intensity of the first excitation is always higher than that of the second excitation in every radial position. Therefore, our experiment does not necessarily agree with the usual arguments that the ion heating is made through absorption of the energy of oscillation with frequencies near f_{pi}. At least types of oscillations which are effective to ion heating are very restricted. Or in more extreme arguments the heating might not be related with oscillations with frequencies near f_{pi} but with the other type of oscillations or instabilities. The same conclusion has been experimentally shown by observation of the simultaneous heating of He ions and test-particle Ar ions by authors.[3] The dotted line (1) in Fig.2 means that the onset time of the oscillations is succesively delayed, and the delay corresponds probably to the skin effect of the pulsed heating current. The disappearance of oscillations between the lines (2) and (3), and the re-onset of oscillations throughout the plasma column is not interpreted completely now, but may be understood in terms of the drift velosity of the electrons. If the heating voltage is increased a little, the disappearance of oscillations between the lines (2) and (3) is not observed, and the relation between the line broadening and the intensity of oscillations does not change. Fig.3 shows the power spectra of oscillations observed at a radius, r = 1.5 cm. Fig.3 (1) shows the spectrum at the time shown by the line

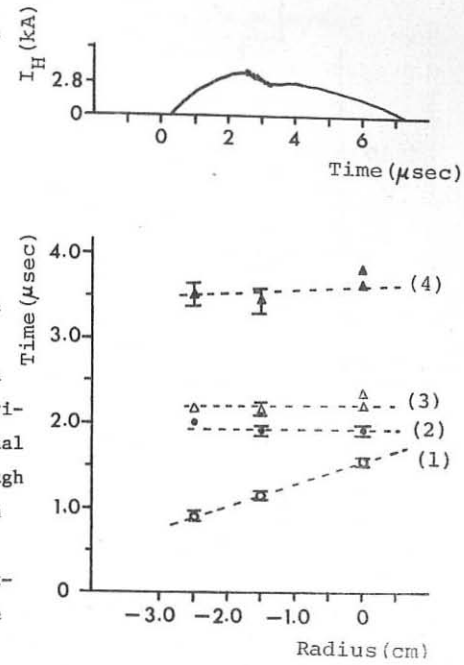


Fig.2

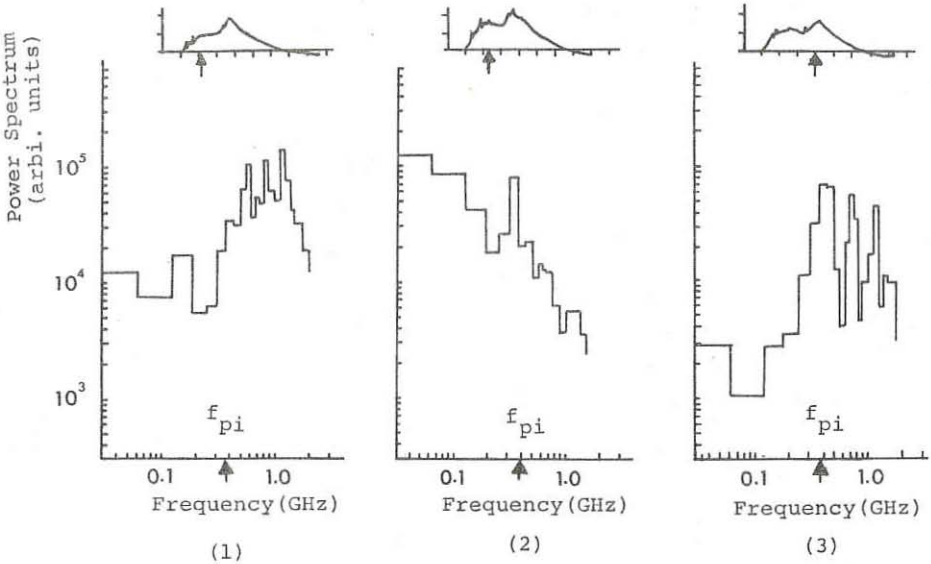


Fig.3

(1) of Fig.2. The observing times of the spectra, Fig.s.3 (2) and 3 (3), correspond to that of the lines (2) and (3) of Fig.2, respectively. The power spectra of the first excitation is very similar to that of the second excitation in Fig.2.

This work was carried out under the cooperative research program at the Institute of Plasma Physics, Nagoya University.

References

1) T. Kawabe, J. Iannucci and H. Eubank, Phys. Rev. Letters, 25, 642 (1970)

2) T. Uchida et al., Nucl. Fusion 9, 259 (1969)

3) K. Adati, T. Kawabe, T. Oda, Y. Takezaki, T. Yokota, T. Uyama and Watanabe, Phys. Rev. Letters, 29, 1223 (1972)

RF TURBULENCE HEATING IN TOROIDAL MACHINE

S.Corti, G.Lisitano, G.Pacher, H.Renner, H.Ringler, E.Würsching
Max-Planck-Institut für Plasmaphysik,Euratom-Association,
D-8046 Garching

Abstract - RF wave-launching structures (L-Coils) have been excited in a Stellarator. The characteristics of the discharge are presented. They cannot be explained by known wave-plasma interactions except by RF turbulence heating.

In a recent paper /1/ a RF system used in the Stellarator W IIb for gas preionization has been briefly mentioned. The relevance of this system to RF heating will be reported in the following.
As shown in Fig. 3 of Ref./1/, three L coils were incorporated in the W IIb.The internal diameter of this coil, Fig. 2, is 14 cm;the length is 7 cm.The coils are made of pure stainless steel,i.e. they include no ceramic components and can thus be subjected to RF, ohmic heating (OH) or any other discharges. So far only two coils have been put into operation and each of these is fed with a pulsed power of 400 W in the S Band(Δt=2 ms; f = 2.4 GHz). With this total RF power of 800 W it was possible to produce an hydrogen plasma with a high degree of ionization.Typical discharge parameters are:$p_{oH_2} \approx 5\times10^{-5}$ torr, $B \approx 10$ kG, $N_e \approx 5\times10^{12}$ cm^{-3}, $T_e \approx 10$ eV, $T_i \approx 5$ eV.
The following are some features of this RF discharge in the Stellarator WIIb:

1) Reproducibility of the OH discharge

By simultaneous input of the RF power and the OH pulse voltage it was possible to obtain completely reproducible OH discharges down to a neutral gas pressure of 3×10^{-5}torr. Without induced OH voltage, an ignition plasma of a few times 10^{11}cm^{-3} is required to initiate the RF discharge. This is probably due to the relatively low RF power ($p_{RF} \approx 800$ W) in a 100 liter vacuum vessel. The RF power density of 8 mW/cm^3 is not sufficient for a self-starting discharge. Experience with linear machines of same i.d., has shown that preionization is unnecessary at higher RF power ($\approx$2 kW)./2/

2) Possible improvement in efficiency of the OH discharge

With the OH main discharge (OH II), plasma density numbers of $N_e \approx 5 \times 10^{12}$ cm^{-3} and electron temperatures of $T_e \approx 100$ eV were obtained in the W IIb. The OH input power in the plasma is 5 to 15kW. Air-cored transformers (like that of OH II) usually have a low efficiency, and so with these discharge parameters a primary pulse power of approx.10 MW at a pulse length of 5 ms is required.

Owing to the enhanced conductivity of the RF-preionized plasma it is very probable that the efficiency of the OH air cored transformer could be improved by increasing the applied RF power to the L coils. The three L coils in the W IIb can be loaded with a total pulse power of $p_{RF} \approx 3 \times 5$ kW which may be sufficient for a measurable improvement of the efficiency of the main OH discharge which is now $\eta \approx 1.5 \times 10^{-3}$.

3) Maintenance of the plasma confinement times

At a high RF power level most of the RF energy is converted into plasma turbulence, and the design of the L coil is such as to maintain plasma confinement in fusion-orientated experiments.The RF power used hitherto in the W IIb is perhaps too small to allow a final pronouncement on this property of the L coil. The influence of RF heating on the plasma confinement time in the W IIb may be better studied by increasing the RF power to a few times 10 kW.

From available data on RF heating in the W IIb (RF discharges in the low gas pressure range $p_{OH_2} \approx 2 \times 10^{-5}$ torr) it can be concluded qualitatively that the plasma confinement times are maintained. Elsewhere, with other heating systems (such as microwave horn antennas, ohmic heating, Stix coils, etc.), the plasma has been lost in this low-pressure region because of pump-out effects.

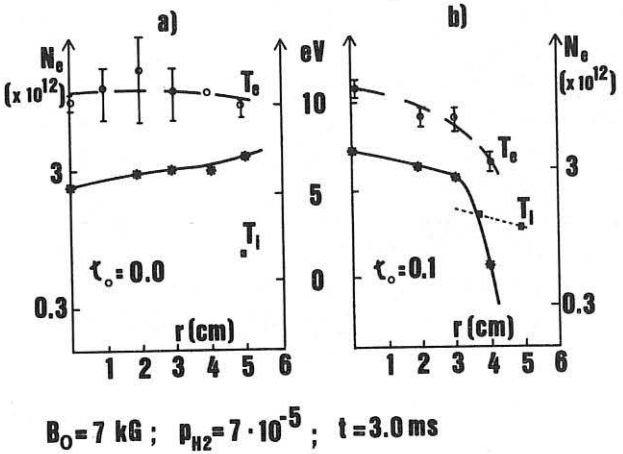
4) X-ray yield

As already mentioned above, this RF heating system cannot be explained by any known method of wave-plasma interaction, except by that of RF turbulence heating /2/. The electron and ion energy distribution can therefore be expected to contain high-energy electrons and ions. This may probably explain the yield of X-ray by the RF heating. This X-ray yield is however controllable by reducing the duration of the RF pulse /3/ and in some discharge conditions is less than that with the OH discharge alone. A more exact analysis of

the energy distribution would clarify the question of RF turbulence heating or coherent electron energy growth rate. Unfortunately, the method of X-ray measurements used up to date in W IIb cannot yield sufficient informations on the distribution of the electron energy.

5) Preionization in Tokamaks.

Another property of the RF plasma produced with the L coils was the maintainance of a RF discharge, even at $\iota = 0$, i.e. the stellarator W IIb was operated without exciting the helical windings. This proves the possibility of RF preionization in Tokamak operation which is equivalent to the condition $\iota = 0$ in the stellarator W IIb. No X-ray yield was observed with $\iota = 0$. No OH discharge at $\iota = 0$ is possible without the use of the RF power. Figure 1 shows the electron density and temperature radial profiles at $\iota = 0$ and $\iota = 0.1$. At $\iota = 0$ the RF discharge fills the vacuum tube with hydrogen plasma of $N_e \approx 3 \times 10^{12}$ cm^{-3} and $T_e \approx 10$ eV, which is quite sufficient for initiating a Tokamak discharge at $p_{OH_2} \approx 10^{-5}$ to 10^{-4} torr.



$B_o = 7$ kG ; $p_{H_2} = 7 \cdot 10^{-5}$; $t = 3.0$ ms

Fig. 1 Plasma density and electron temperature radial profiles for a) $\iota = 0$ and b) $\iota = 0.1$

6) RF ion heating

Finally, the problem of RF turbulence ion heating should be mentioned. In the W IIb an ion temperature of about 4 eV was measured at the plasma boundary. The size of the ion probe did not allow the ion temperature further inside the plasma core to be measured. At the

site of the ion temperature measurements, i.e.at the plasma boundary, an electron temperature of 7 eV was measured. As can be seen from Fig. 1b, the electron temperature rises to $T_e \approx 10$ eV in the centre of the plasma core. If the same temperature profile is assumed for electrons and ions, an ion temperature of $T_i \approx 6$ eV can be expected in the centre of the plasma.

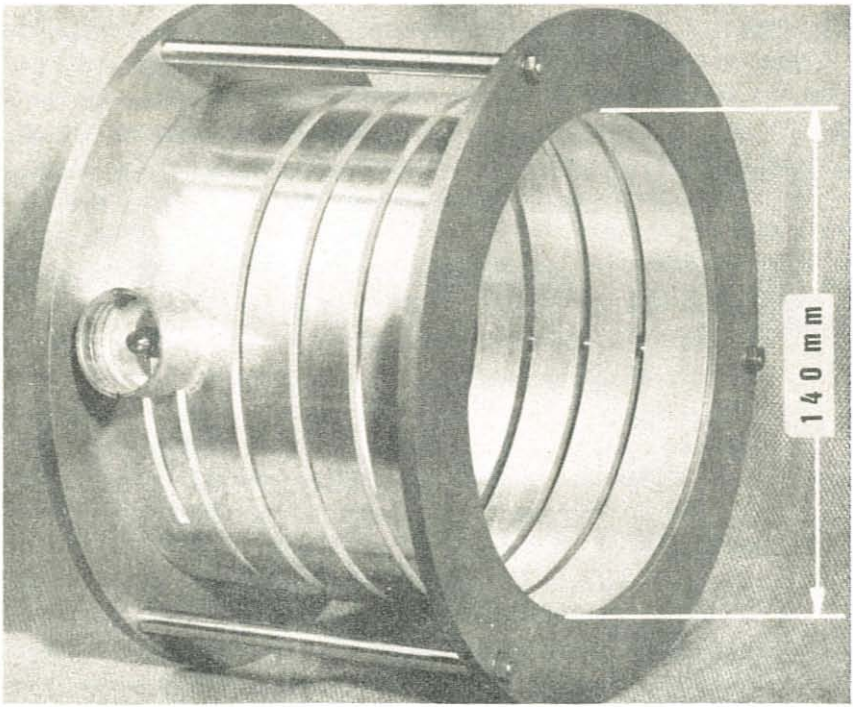


Fig. 2 - L coil of pure stainless steel with no ceramic components. Excitation frequency: 5×10^8 to 10^{10} Hz. Pulse input power limit: 5 kW.

References

/1/ G.Grieger, Third Int.Symp.on Toroidal Plasma Confinement, Garching, 26-30 March 1973,paper D3-1.

/2/ G.Lisitano, S.Corti,M.Bergbauer,A.Capitanio,A.van Heumen, A.Reiter and E.Rossetti. Annual Report IPP-1972(Abt.E-3)

/3/ S.Corti,G.Lisitano,G.Pacher,H.Renner,H.Ringler,E.Würsching, Bulletin of the American Phys.Society 17,1038, 1972.

PROPAGATION OF "SWITCH-ON" SHOCK IN A MAGNETIZED COLLISIONLESS PLASMA

T. El-Khalafawy, M. El-Nicklawy, M. El-Gwaily,
A. Beshara, V. Demnchenko[+)] and N.I. Rudnev[+)]

Atomic Energy Authority, Cairo, A.R.E.

Abstract. The results of the experimental investigations of the parameters and structure of a shock wave propagating along a static magnetic field are discussed. It is also shown that the wave observed represents a "switch-on" shock the structure of which is determined by the mechanism of the energy "collisionless" dissipation.

1. Introduction. At the present time the problem of the propagation of a shock wave (SW) along the magnetic field in a highly ionized plasma is a subject of intensive experimental and theoretical researches [1-4]. Until now there is not a single opinion what concerns the physical mechanism which leads to the establishment of the SW front, however.

2. Experimental Set-Up. The experiments were carried out in a cylindrical glass chamber 80 cm long and 4 cm diameter. The bias magnetic field B_{oz} remains essentially constant throughout the period of the discharge. The result presented here refer to a fixed value of B_{oz} = 1.5 kG. The SW is produced by a coaxial plasma source with a short central electrode. The main radial discharge is produced due to the application of the electric field 15 kV/cm between the central short electrode (ℓ = 1 cm) and the outer annular electrode (d = 3 cm). The discharge current reaches its maximum value ~ 140 kA during the time ~ 1 usec and remains practically constants for 3 usec. The chamber is filled with the working gas (in our case hydrogen under pressure ~ 10^{-3}Torr) through the opening in the central electrode. The radial current sheath moves axially under the $J_r \times B_\theta$ force and under certain conditions it degenerates to a shock wave.

3. Results and Discussion. The main experimental results are presented in Figs. (1)and(2). In the oscillograms of the axial magnetic field (Fig.1-a) and the diamagnetic signals (Fig. 2-a,b) one can see a distinct fracture which separates the zones of the piston and SW. This oscillograms one can make a conclusion that the shock front is established at the distance of

(10 to 15 cm) from the source. Its width remains constant for distances of nearly to cm. The SW velocity estimated from the oscillograms of the diamagnetic signal is 2.10^7cm/sec.

The principal feature of the signals obtained is the presence of the radial and azimuthal components of the magnetic field Fig. (1-b,c), which is characteristic of "Switch-On" shocks. The amplitudes of the magnetic fields B_r and B_0 are (0.4÷0.5) of the value of the bias magnetic field. The fact that the front velocity is close to the Alfvén velocity $V_A \approx 1.8.10^7$ cm/sec confirms once again the fact that the wave observed is of a "Switch-On" type. The estimated value of the Mach number $M=V_f/V_A = 1.1<M_{cr}=2$, where M_{cr} is the critical Mach number above which a "Switch-On" shock can not exist.

The presence of an oscillating "tail" ahead of the SW is another feature observed in out experiment. It is characteristic of the propagation of "Switch-On" shocks. Such oscillations which have a nature of a "precursor" were observed before by Robson and Sheffield [5]. In our experiment the presence of the "precursor" oscillations is clearly seen in the oscillograms of B_r, B_0 Fig. (1-b,c), of the diamagnetic signals Fig. (2-a,b), (lower traces) and in the oscillogram of the E_0 (lower trace in Fig. (2-c)). The characteristic frequency of these oscillations is $\sim 2.10^7 sec^{-1}$ and it coincides with frequency of the "whistler" oscillations.

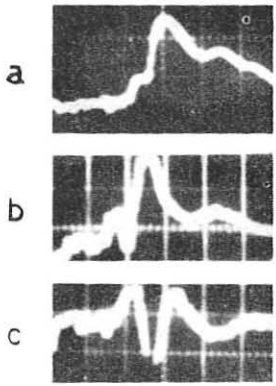


Fig. 1. Oscillograms of magnetic fields.
a) B_z, b) B_0, c) B_r.
($P_0=5.10^{-3}$Torr, scanning time is 1 usec/div).

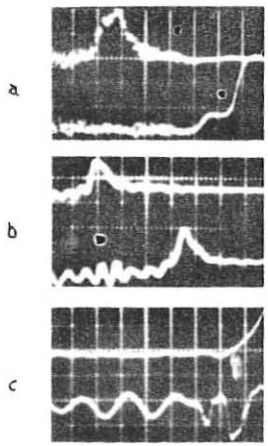


Fig. 2. Oscillograms of diamagnetic signals and the electric and magnetic fields. a,b) diamagnetic signal. c) E_0 (lower trace) and B_z (upper trace); $P_0=5.10^{-3}$Torr; 0.5 usec/div.

In order to investigate the structure of SW we shall take advantage of the model of a "Switch-On" shock, worked out in detail in paper [6]. According to this paper the structure of the shock front in the forepart represents damped periodic oscillations:

$$|B|^2 \equiv \left(B_\theta^2 + B_z^2\right) \sim \exp i\left[\frac{x}{\delta}\left(1 + i\frac{\nu_{eff}}{\omega_{ce}}\right)\right], \quad \delta \equiv \frac{c}{\omega_{pi}} \cdot \frac{2B_{0z}\sqrt{B_{0z}^2 + B_{0z}^2}}{B_{0z}^2}, \quad (1)$$

where ν_{eff} is the effective frequency of the electron-ion collisions, which determines the energy dissipation process at the SW front; B_{0z} is the value of B_θ behind the SW front.

Thus, in the forepart of the SW there are magnetic field oscillations with a frequency of an order $\omega \sim \omega_{ci} \sim 10^8 s^{-1}$ and with a wavelength of an order $\frac{c}{\omega_{pi}}$. The damping factor $\varkappa_{eff} = (\nu_{eff}/\omega_{ce})$ and the total width of the transition region $\Delta = (c/\omega_{pi})(\omega_{ce}/\nu_{eff})$.

From the damping factor measured in the forepart of the SW one can determine the value of the collision frequency. As it is easily seen in the oscillograms presented, the value of $\varkappa_{eff}$ under experimental conditions is within (1/3 to 1/5), which corresponds to the value $\nu_{eff} = 3.5.10^{10} sec^{-1}$. At the same time the binary (Coulomb) collision frequency in the case under consideration ($n \sim 5.10^{13} cm^{-3}$, $T_e \sim 1$ eV), $\nu_{ei} = 1.3.10^9 sec^{-1}$. So fast damping of the oscillations in the forepart of the SW can not be caused by the dissipation of the energy due to Coulomb collisions. Therefore, the anomalous plasma conductivity which leads to the establishment of the SW front is caused by some machnism of the energy "collisionless" dissipation. Without any doubt the development of h.f. small scale instability at the SW front is the cause which leads to the establishment of the "collisionless" shock front. So, it is necessary to measure experimentally the frequency, the wavelength, the electric field intensity, plasma temperature, etc., an order to identify exactly the mode of the unstable oscillations.

Acknowlegement. The authors are obliged to Prof. Dr. A. Kamal for useful discussion.

References

[1] D. Tidman and N. Krall, Shock Waves in Collisionless Plasmas, Wiley & Sons, New York, 1971.

[2] R. Kh. Kurtmullaev, V.L. Masalov, et al., Sov. Phys. JETP, 33, 216, 1971.

[3] J.W.M. Paul, C.C. Daughney, et al., IV IAEA Conference, III, 251, 1971.

[4] J.C. Woods, J. Plasma Phys., 6, 615, 1971.

[5] A.E. Robson and J. Sheffield, III IAEA Conference, I, 119, 1969.

[6] V.I. Karpman, Sov. Phys., Tech. Phys., 8, 715, 1964.

+) On leave from the Atomic Energy State Committee, USSR.

3.6. AGAIN ABOUT RF AND SHOCK HEATING



EXPERIMENTS ON MAGNETOACOUSTIC EIGENOSCILLATIONS IN A PLASMA CONFINED IN A PURELY POLOIDAL MAGNETIC FIELD

M. Bureš, E. Tennfors and B. Thorstensen
Royal Institute of Technology, S-100 44 Stockholm 70, Sweden

Abstract: Oscillations are excited at the lowest magnetoacoustic resonance of a plasma confined in an internal ring device. The eigenfrequency and the velocity of propagation through the plasma are observed to vary with heating power and velocity of rotation. The dependence of ion mass agrees with the theory for Alfvén waves.

1. Introduction. In the internal ring devices FIIA and FIVB a dense fully ionized rotating plasma is created by crossed fields. To enable magnetic shielding of the supports for the internal ring the rotation must be stopped and the viscous shear heating replaced by some other method. In a number of earlier experiments with FIIA and FIV the lowest magnetoacoustic resonance has been used for this purpose [1,2,3]. The aim with the present work is to examine this resonance with respect to heating, in particular the problems connected with ranging resonance frequency during the transition from rotating to non-rotating plasma and temperature dependence of the frequency. Another application of the eigenoscillations is to use them for diagnostics as discussed elsewhere [4,5,6].

2. Experimental arrangement. The experiments have been made in the internal ring devices FIIA [1] and FIVB, a modified version of FIV [3]. The devices differ only in the supports for the internal ring, which are unimportant provided the plasma is rotating. The particle density is $10^{21} m^{-3}$ and the mean magnetic field strength in the mid-plane of the device is 0.33 Vsec/m^2. The filling gas is hydrogen or deuterium with an initial pressure of 30×10^{-3} mmHg.

The eigenoscillations are excited by a current pulse in two parallel single-turn coils encircling the plasma close to the wall and to the mid-plane.

In part of the experiments HF-power is fed into the plasma by two coils coupled anti-parallel to reduce the coupling between the

heating circuits and the eigenoscillation circuits. The generator frequency is chosen as high as possible (2.8 MHz) to separate it from the eigenfrequency. Thus it is not tuned to any known resonance, but for deuterium the frequency is in the ion cyclotron frequency region.

3. Experiments. The radial current J_r and the voltage ϕ_{12} across the plasma associated with the rotation are shown in Fig.1 as functions of time for a D-plasma without HF-heating. The voltage decreases to a level below which the power is too low to sustain a fully ionized plasma. Then a transition to a lowly ionized state takes place and the voltage rises to the level of the now almost unloaded condenser bank. The picture becomes essentially the same for hydrogen. If HF-heating is applied, the transition moves to later times and disappears if the HF power is high enough to sustain the plasma without rotation.

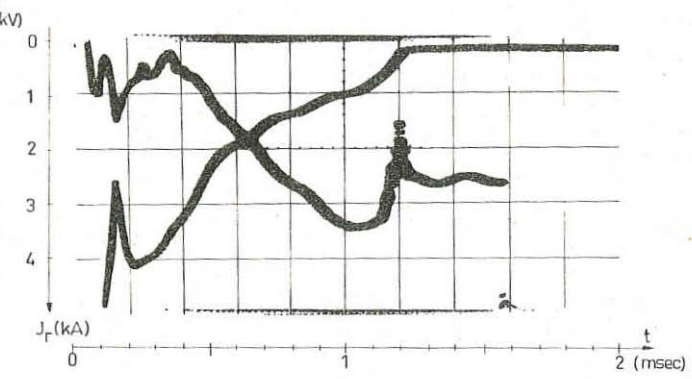


Fig.1. Radial current J_r and voltage ϕ_{12} for rotating deuterium plasma in FIVB.

Eigenoscillations are excited at different times t_p and observed by a Rogowski coil measuring the total azimuthal current J_ϕ and locally by small picup coils outside the plasma at various positions along the field lines. The time-integrated signal from a picup located ≈ 0.1 m along the field lines from the midplane is shown in Fig.2 together with the current pulse for rotating D-plasma. In the fully ionized state we get regular eigenoscillations starting about 0.5 μsec after the exciting pulse. At 1150 μsec a much smaller signal comes without delay but still with some small oscillations. At later times the picup signal just follows the original pulse. In

the fully ionized state the resonance frequency agrees with theoretical values obtained for a homogeneous cylindrical shell [6]. The delay time Δt of the picup signal has the order of magnitude expected for a perturbation propagating through the plasma with the Alfvén velocity $v_A = 8/\sqrt{\mu_o nm}$. Picup coils at other positions show that the initial perturbation is not restricted to the mid-plane. Therefore further investigation is needed to understand the excitation process and the coupling between the plasma and the generator coils.

The delay time varies in the same way as the time period of the eigenoscillations with the velocity of rotation. Thus the variation can be interpreted as a change of density with velocity of rotation. The spatial density distribution is influenced by the balance between the centrifugal force and the thermal pressure. If the balance is suddenly changed by switching off HF-heating, a transient increase in delay is observed in agreement to calculations of the centrifugal compression made by Bonnevier [7]. Fig. 3 shows how the eigenfrequency varies during the discharge. First the density decreases due to reduced centrifugal force and later due to diffusion and recombination. When HF-heating is applied, the frequency becomes constant until the d.c. supply voltage of the generator drops. This value differs from the frequency used in the earlier heating experiments [1,2,3]. The frequency choice in those

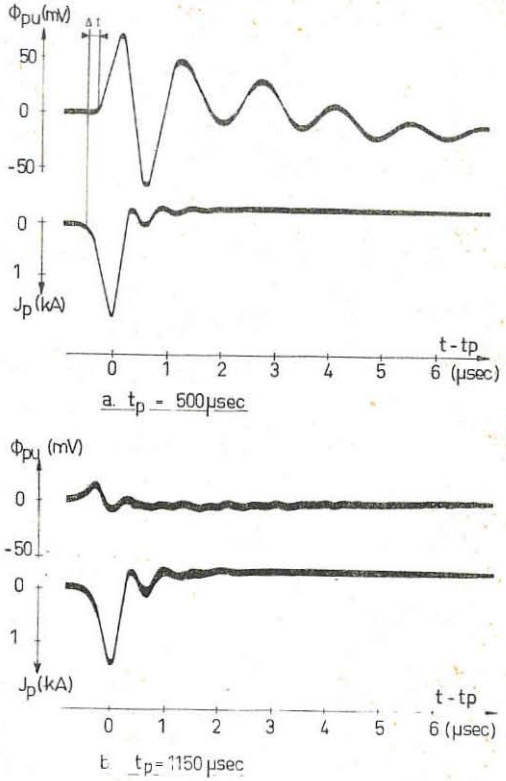


Fig.2. Picup signal for highly and lowly ionized states.

experiments was based essentially on an experimental optimization from a rotating to a non-rotating plasma at a relatively low power and temperature level. Since the frequency depends on the temperature profile at low temperatures [6], the tuning to a low temperature plasma has the result that the plasma goes out of resonance when the temperature rises. An increase in generator power then results in a corresponding decrease in coupling to the plasma.

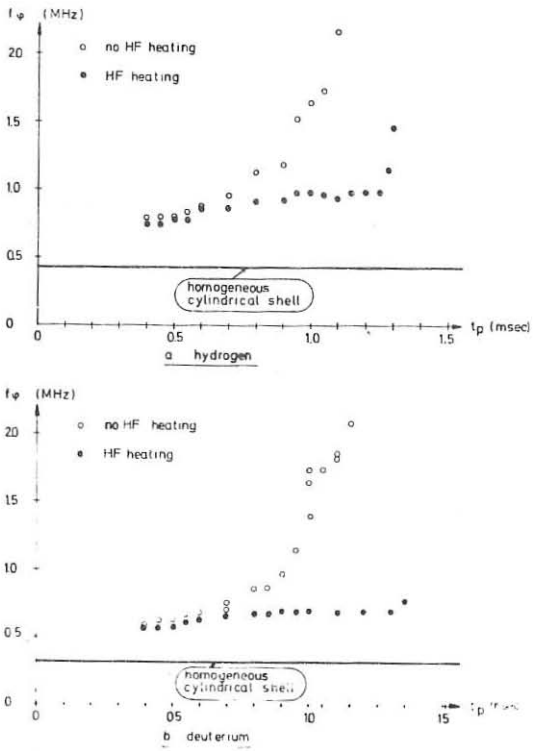


Fig.3. Resonance frequency variation during various discharges.

4. Conclusions. Magnetoacoustic resonance heating can probably be improved by a more careful choice of frequency. Higher modes including the one used in this work and the excitation process needs further examination.

This work has been supported by the Swedish Atomic Research Council and the Bank of Sweden Tercentenary Fund.

References.

[1] B.Lehnert,J.Bergström,S.Holmberg and E.Tennfors,Electron and Plasma Physics,Roy.Inst.of Techn.Rep.69-34(1969).
[2] B.Lehnert,J.Bergström,M.Bureš and E.Tennfors,Fourth Europ.Conf. on Contr.Fusion and Plasma Physics,C.N.E.N.,p.102,Rome(1970).
[3] B.Lehnert,J.Bergström,M.Bureš,E.Tennfors and B.Wilner,Plasma Phys.and Contr.Nucl.Fusion Research,vol.I,p.59,IAEA,Vienna(1970).
[4] B.Lehnert,Plasma Physics,10(1968)p.281.
[5] B.Lehnert,Electron and Plasma Phys.,Roy.Inst.of Techn., Rep.67-26(1967).
[6] M.Bureš and E.Tennfors,Roy.Inst.of Techn.,Stockholm, TRITA-EPP-72-84(1972).
[7] B.Bonnevier,private communication(1972)

NUMERICAL SIMULATION OF HIGH-FREQUENCY HEATING OF PLASMA

Yu.S.Sigov and Yu.V.Khodirev

Institute of Applied Mathematics, Academy of Sciences
Moscow, USSR

In one-dimensional computer experiments the kinetic phenomena in rarefied plasma driven by a large electric field oscillating at nearly the electron plasma frequency (case 1) and the twice electron plasma frequency (case 2) are investigated. Strong parametric instabilities [1,2] and anomalous absorption of hf driver field energy are observed.

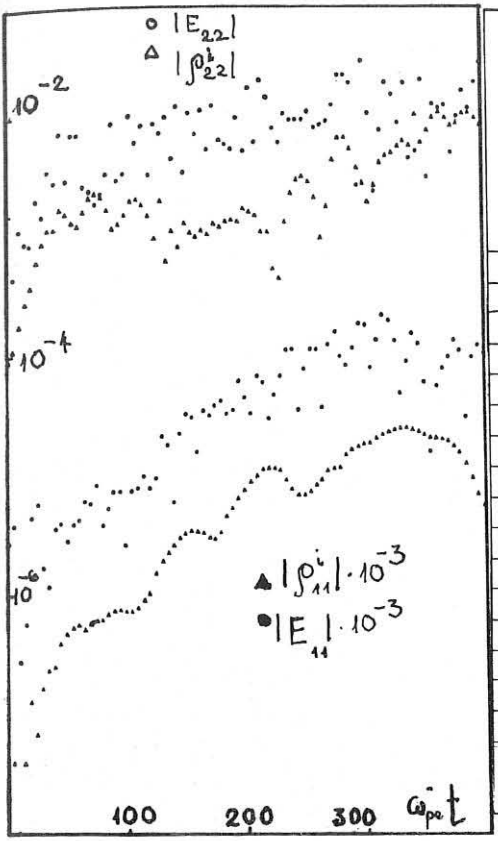
1. The statement of a problem corresponds to a widely used discrete model of self-consistent behavior of Vlasov plasma driven by an external field [3,4]. We used some version of Cloud-in-Cell method [5] and "area weighting" technique and generally handled 50 electrons and 50 ions per initial Debye length D_{eo} in a 300 D_{eo} periodic system with an ion-electron mass ratio of 100.

The initial space uniform Maxwellian distribution of velocities has been specified by "stiring" of a number of beams during two ion plasma periods before a moment t=0. A driver field for $t \geq 0$ is taken in a form $E_o \cos(\omega_o t - k_o x)$. An analytical approach to a similar problem may be found in [6-8].

In our set of runs we used the following values of parameters:

$E_o/(4\pi n T_{eo})^{1/2} = 0.2 \div 1$, $\omega_o/\omega_{pe} = 0.95 \div 1.05$ (1) or $2.05 \div 2.4$ (2), $k_o = 0$ (1) or $1/12 \div 1/2$ (2).

2. The case (1), $\omega_o \simeq \omega_{pe}$, gives a possibility, particularly for $T_{eo}/T_{io}=1$, to investigate in details main features of nonlinear mechanism of hf plasma heating by development of instability wich may be treated as a decay of driver wave ($k_o=0$) accompanied by arising of longitudinal Langmuir and ion acoustic waves. The typical pictures are presented in figures 1-4 where $\omega_o=1.05$, $E_o/(4\pi n T_{eo})^{1/2}=1$, $T_{eo}/T_{io}=1$.



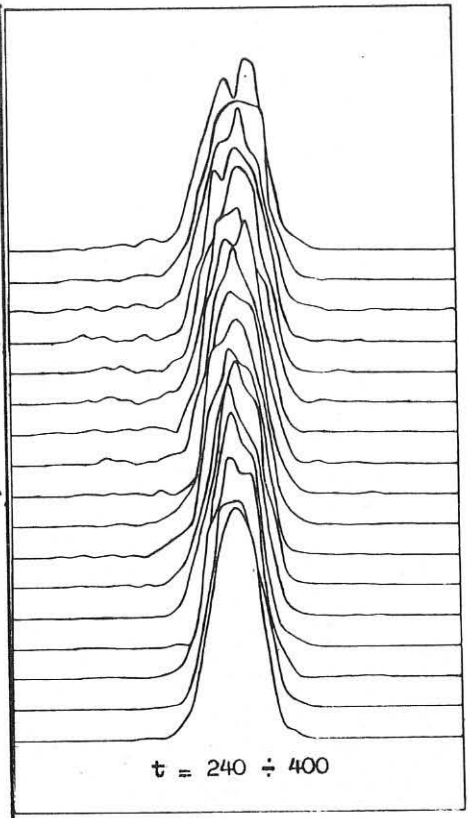


Fig.2 Fourier coefficients $|\rho_n^i|, |E_n|$ for n= 11,22 depending on time, $2\pi n/L=k$, $L = 300\ D_{eo}$

Fig.3 Time evolution of electron distribution function $\langle f_e \rangle$

$$\langle f_e \rangle = \int_{-L/2}^{+L/2} f_e(v,x)\,dx$$

an appearance of non-Maxwellian electrons in the distribution function (fig. 1,3).

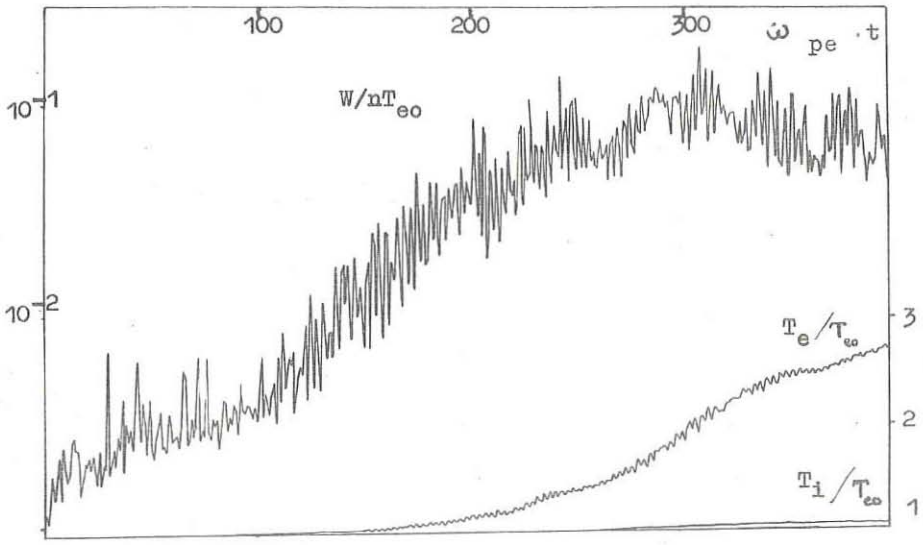


Fig.4 Electrostatic energy density W and electron and ion temperatures $T_{e,i}$ depending on time, $T = m\{\int v^2 f\, dv - (\int vf\, dv)^2\}$.

3. The case $\omega_o \approx 2\omega_{pe}$, $k_o \neq 0$ may be considered as a rough one-dimensional analogy of situation /8/. The results of computation are in qualitative agreement with a theory of the two plasmons' decay and illustrate a possibility of plasma heating near the doubled plasma frequency. The ratio of the wave saturation energy to the electron temperature for differnt values of E_o was in the limits of $(1\div6)10^{-2}$.

Authors are grateful to R.Z.Sagdeev and A.A.Ivanov for useful discussions.

R e f e r e n c e s

1. Oraevskii and R.Z.Sagdeev. Zh.Techn.Fiz., 32, 1291 (1962)
2. V.P.Silin. Zh.Exp.Teor.Fiz., 48, 1679 (1965)
3. Yu.S.Sigov,K.V.Khodataev,Yu.V.Khodirev. Dokl.Ak.Nauk,207,75(1972)
4. W.L.Kruer,J.M.Dawson. Phys.Fluids,15,446 (1972)
5. C.K.Birdsall,D.Fuss. J.Comput.Phys.,3,494 (1969)
6. V.V.Pustovalov,V.P.Silin.Zh.Exp.Teor.Fiz.,59,2215 (1970)
7. E.Valeo,C.Oberman,F.W.Perkins.Phys.Rev.Letters,28,340 (1972)
8. A.A.Galeev,V.N.Oraevsky,R.Z.Sagdeev.Pisma ZhETF,16,194 (1972)
9. B.B.Kadomtsev.Voprosy Teorii Plasmy,4, Atomizdat, 1963
10. R.Z.Sagdeev,A.A.Galeev. Nonlinear Plasma Theory, N.-Y.,1969
11. K.Nishikawa.J.Phys.Soc.Japan,24,916,1152 (1968)

PLASMA HEATING AND DAMPING OF THE FAST WAVE NEAR THE SECOND HARMONIC OF THE ION CYCLOTRON FREQUENCY.*

by

R. Dollinger, M. Kristiansen, M. O. Hagler
Department of Electrical Engineering, Texas Tech University
Lubbock, Texas 79409 USA

J. Beraström**
Royal Institute of Technology, Department of Plasma Physics,
S-10044 Stockholm 70, Sweden

Abstract: Wave damping and plasma heating has been observed for the fast (right-hand polarized) wave near the second harmonic of the ion cyclotron frequency (Ω_i) in a dense plasma ($\gtrsim 10^{20}$ m^{-3}). The wave was launched with a 60% field modulation and damped in a magnetic beach where $\omega \to 2\Omega_i$.

We report further measurements[1-2] on the predicted damping of the fast wave at $\omega = 2\Omega_i$. The hydrogen plasma was prepared by an axial discharge of 10 kA at filling pressures of 5-10 mtorr, resulting in more than 50% ionization and a temperature of a few eV. The 80 cm long pyrex discharge tube has an i.d. of 10 cm. The magnetic field, B_o, has 150% mirrors and a 10% magnetic beach adjacent to one mirror. The magnetic field is measured with 1% absolute and 0.01% relative accuracy. The waves are launched by discharging a specially designed high energy capacitor into a one turn coil around the plasma tube. The circuit rings at 5 MHz with a Q of about 20. A movable pyrex tube (10 mm) allows magnetic probe ($\dot{b}_z$) measurements along the axis.

Figure 1 shows the normalized magnetic field B_o vs z, the distance from the wave launcher. It also shows the vacuum and wave magnetic fields ($\dot{b}_z$) vs z for two different values (B_1 and B_2) of B_o. We have chosen B_1 and B_2 so that the second harmonic occurs at $z \simeq 10$ cm and $z \simeq 15$ cm, respectively.

Near the wave launcher, where the wave amplitude is $\simeq 60\%$ of B_o, we see essentially only the vacuum near-field of the launcher. Further away, the wave propagates in the plasma with an amplitude higher than the vacuum field. The wave

propagates with collisional damping until the point in the beach at which $\omega \approx 2\Omega_i$ where it appears to damp drastically. The damping length is longer for B_1 than for B_2 because the beach is flatter at z = 11 cm than at 15 cm. Some of the wave appears to be transmitted beyond the point where $\omega = 2\Omega_i$ for the B_2 case. The apparent damping is extraordinarily strong in both cases and one must suspect that a large fraction of the power is reflected. Because of the short rf pulse, the dispersive nature of the plasma, and the collisional damping it is very difficult to measure standing wave ratios. The probe is fixed at z = 10 cm (Fig. 2A) and at z = 15 cm (Fig. 2B) and B_0 varied. The wave propagates with no damping except when $\omega \approx 2\Omega_i$ between the top of the beach and the probe position. The cutoff is very sharp for $\omega \approx 2\Omega_i$ at the beginning of the beach because the wave is then damped before it can reach the probe. By increasing the magnetic field, the probe signal increases back to its original value as the point of damping approaches the location of the probe. The minimum in Fig. 2B is less than in Fig. 2A because the probe is 5 cm further down the beach. This is also why the signal in Fig. 2B reappears at a larger value of B_0 than in Fig. 2A.

Figure 3 shows the unintegrated signal amplitude from a diamagnetic loop located at z = 15 cm. Figures 2 and 3 show a good correlation between damping and heating. The actual amount of heating is not known at this time but the results show that all the energy is not reflected from the resonance point.

*This work was supported in part by the U.S. Atomic Energy Commission and the National Science Foundation.

**Visiting Scientist.

[1] J. E. Cato, N. Kristiansen, M. O. Hagler, and C. M. Watson-Munro, Proc. 5th European Conf. Cont. Fusion and Plasma Physics, Grenoble, France, Aug. 21-25, 1972, p. 117.

[2] J. E. Cato, N. Kristiansen, M. O. Hagler, and C. M. Watson-Munro, Phys. Lett. 40A, 151 (1972).

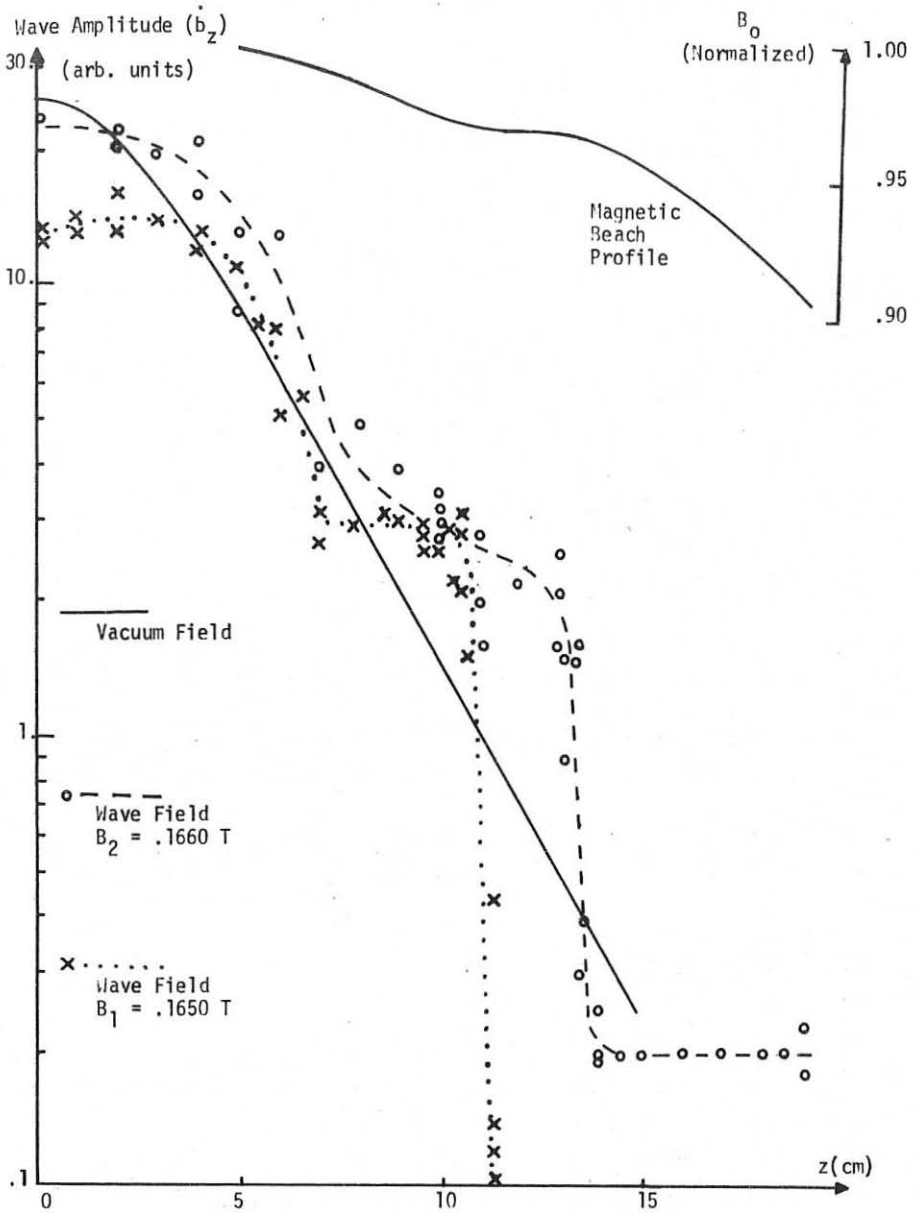


Fig. 1: Wave Amplitude and Magnetic Beach Profile vs Distance From Wave Launcher.

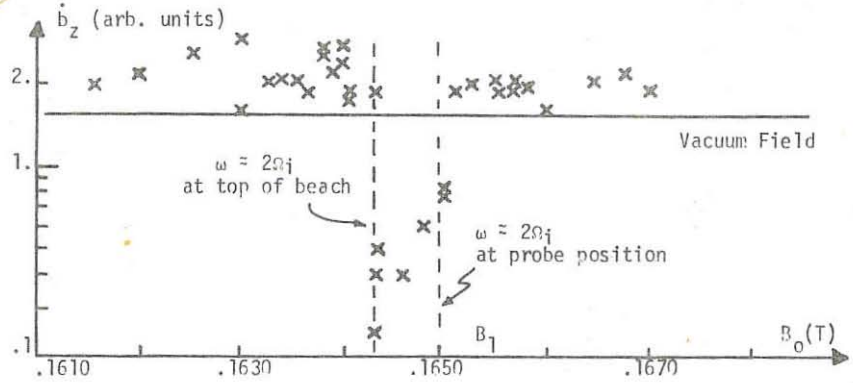


Fig. 2A: Wave Signal vs B_0 at z = 10 cm.

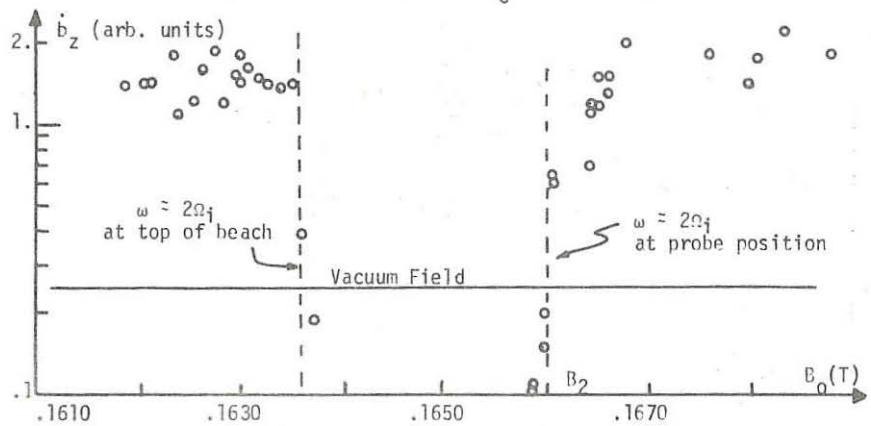


Fig. 2B: Wave Signal vs B_0 at z = 15 cm.

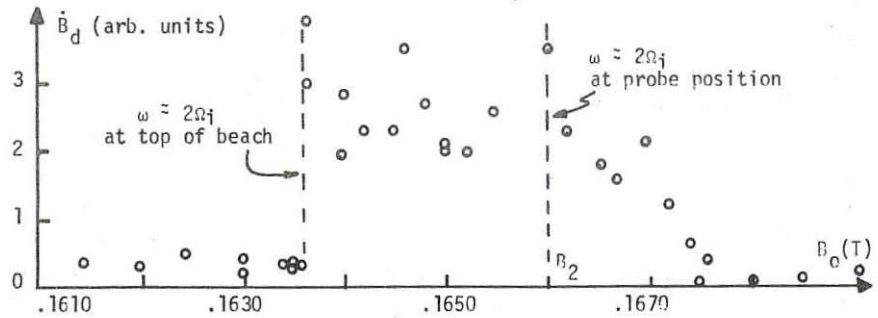


Fig. 3: Diamagnetic Loop at z = 15 cm.

LOCALISATION OF ELECTROMAGNETIC WAVE ABSORPTION PROCESSES IN A PLASMA OF TOROIDAL DISCHARGE

V.E.Golant, M.M.Larionov, L.S.Levin, L.P.Pakhomov, K.A.Podushnikova, V.V.Rozhdestvensky, G.A.Serebreny

A.F.Ioffe Physico-Technical Institute, Leningrad, USSR

In Tokamak FT-I device efficiency and localisation of microwave power absorption in a plasma were studied. For this purpose a method of light intensity measurements was applied. Gyroresonance absorption at 2^{nd} harmonics of electron cyclotron frequency and absorption due to electromagnetic wave transformation into the plasma wave in upper hybrid resonance conditions were observed.

In FT-I Tokamak the absorption of microwaves in a plasma is studied, in order to realise a high-frequency heating of plasma electrons. FT-I device has the discharge chamber major radius of 62 cm, limiter radius of I7 cm and magnetic field to 9 kG. Absorption of microwave power is studied by a method of light intensity measurements /I/. In relatively small discharge current conditions, when a plasma is not completely ionized, the optical emission of neutral atoms and ions is the main mechanism of energy losses. In this case the electron temperature is "frozen" at the level of some eV. Optical emission of a plasma is proportional to the power absorbed in it. Study of light emission allows to measure the power absorbed and to observe the plasma regions where this absorption takes place.

The experimental arrangement is shown in Fig.I. The discharge is ignited in hydrogen gas by the pressure about 0.2 mtorr. Discharge currents were I-5 kA. In this conditions the plasma remains partially ionized, the electron temperature is "frozen" at the level of about 4 eV and the electron density varies depending on discharge current from $I.IO^{I2}$ to $7.IO^{I2}$ cm^{-3}. The data on n_e and T_e are obtained using microwave interferometry and plasma conductivity measurements. The visible light emission of a plasma is detected by photomultipliers. There are wide field PM (I) and two collimated ones (2) and (3). Microwave power is radiated into the discharge chamber by a horn antenna (4). Microwave generator (5) operates in 200 μsec.

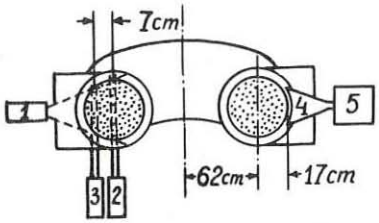


Fig. 1

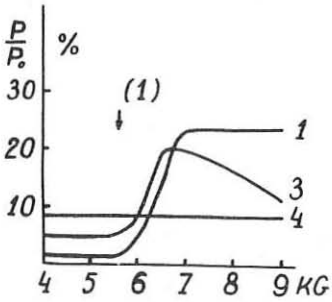


Fig. 2

pulses and provides the power of I2 and 50 kW in frequency bands of 22 and 30 GHz respectively. Radiation losses restrict the energy life time at the level about 20 μsec, therefore the processes under consideration are quasistationary.

The flash of light emission is observed during microwave power pulse, superimposed on the light signal of joule heating. The intensity of this flash depends on the power absorbed in a plasma. Thus, we can study the efficiency of absorption processes. In /2/ the efficiency dependence on magnetic field and plasma density is presented. The results of measurements in 22 GHz waveband are shown in Fig.2. The power absorbed was measured using the signal of wide-field P.M. By weaker magnetic fields the efficiency is small and is determined by electron collision frequency. When the magnetic field reaches some value, fast increase of absorption to 25% of generator power is observed. By this value, if the toroidal magnetic field inhomogeneity is taken into consideration, the electron cyclotron resonance conditions appear inside a plasma volume. This field is shown by an arrow in Fig.2.

Collimated light-detectors enable us to observe the spatial distribution of light emission. In Fig.3 signals of P.M.s (2) and (3) are plotted against the magnetic field value in the center of discharge chamber. Microwave generator frequency is 30 GHz. The sharp peak of signal is seen in the narrow region of magnetic fields, where the condition $H = \frac{1}{2} H_{ce}$ is fulfilled in the plasma volume viewing by P.M. The difference in resonance regions for (2) and (3) is due to the field toroidal inhomogeneity. Thus, the absorption near the 2nd harmonics of electron gyrofrequency takes place in the narrow plasma

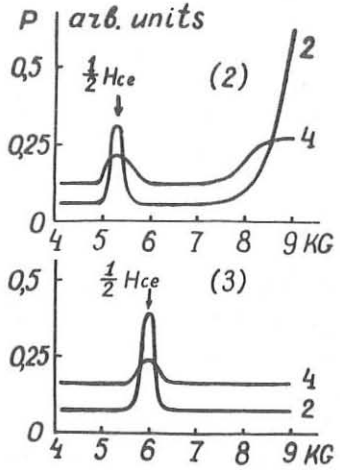


Fig. 3

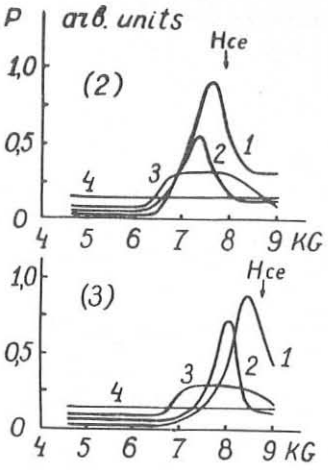


Fig. 4

layer, thickness of which does not exceed 4 cm. The efficiency of this mechanism of absorption is not too high.

In Fig.4 are shown the same signals as in Fig.3, but microwave generator frequency is 22 GHz. In this case it is possible to reach the cyclotron resonance field in the plasma region viewing by P.M. This field is pointed by an arrow. Curves I,2,3,4 are for plasma densities (I; I.6; 3; 4.5).10^{12} cm^{-3} respectively. The flash of light emission near $H = H_{ce}$ is more intense than by $H = \frac{1}{2} H_{ce}$. The position of absorption zone near $H = H_{ce}$ depends on plasma density. It moves towards the weaker magnetic field when density increases. At the same time the size of absorption peak decreases and when density reaches $4.5.10^{12}$ cm^{-3}, the dependence on magnetic field vanishes.

In experimental conditions described some absorption mechanisms are important. Collisional non-resonance absorption manifests itself in all magnetic field range, but its efficiency is small. Besides, gyroresonance absorption and electromagnetic wave transformation into the plasma wave are of interest. Gyroresonance absorption [3] is caused either by collisions, or by thermal movement of electrons. Non-collisional absorption is important when $\nu/\omega_{ce} \ll v_{Te}/c$, where ν - collision frequency, ω_{ce} - gyrofrequency, v_{Te} - thermal velosity of electrons. In our conditions $\nu/\omega_{ce} \leq 10^{-4}$, $v_{Te}/c \cong 4.10^{-3}$. Thus, non-collisional case is realized. The efficiency for arbitrary direc-

tion of wave propagation is proportional to $(v_{Te}/c)^2$ for $\omega=\omega_{ce}$ and $\omega=2\omega_{ce}$. In our conditions it does not exceed 5% of generator power, if we take into account repeated reflections inside the discharge chamber. This value corresponds to the effect, observed at 2nd harmonics.

Absorption by electromagnetic wave linear transformation into the plasma wave in a toroidal magnetic trap conditions is considered in [4]. Transformation occurs in plasma region where upper hybrid resonance condition is fulfilled: $\omega_p^2+\omega_{ce}^2=\omega^2$. The plasma wave arising is absorbed then in a volume between an upper hybrid and an electron cyclotron resonance surfaces. Efficiency of this process is high and does not depend on electron collision frequency. But it is essential for this process that the upper hybrid resonance surface should be "accessible" for electromagnetic wave. This is the case when a maximum value of magnetic field in a plasma exceeds the electron cyclotron one. The nature of absorption in 22 GHz range corresponds to these theoretical predictions. The level of absorbed power becomes high when magnetic field in a plasma reaches the cyclotron value (Fig.2). The location of zone, where electromagnetic wave energy is thermalized, depends on plasma density but always lies between upper hybrid and electron cyclotron resonance surfaces (Fig.4).

The experiment shows a strong dependence of absorption on plasma density. Only by smaller densities, when $\omega_p^2 \leq \frac{1}{2}\omega^2$, the dependence on magnetic field is sharp. We may suppose that in a dense plasma the energy absorption zone moves to the plasma boundary and all the energy absorbed in it is lost at the wall of discharge chamber.

References

1. M.M.Larionov, L.S.Levin. A paper submitted at XI Conf. on Phenomena in Ionized Gases, Prague 1973.
2. V.E.Golant et al. Proc. of 3 Intern. Symposium on Toroidal Plasma Confinement, Garching, 1973, E-5.
3. V.L.Ginsburg. Electromagnetic wave propagation in a plasma. "Nauka", Moscow, 1967.
4. V.E.Golant, A.D.Piliya. Uspekhi Fiz. Nauk, 104, 413 (1971).

PROPAGATION OF TORSIONAL ALFVÉN-WAVES IN INHOMOGENEOUS AXISYMMETRIC MAGNETIC FIELDS

G.Müller, E.Räuchle, and P.G.Schüller

Institut für Plasmaforschung
Universität Stuttgart, West-Germany

Abstract: The propagation of torsional Alfvén-waves in axially symmetric, inhomogeneous magnetic fields is investigated. Field inhomogeneities cause partial reflection and trapping of the waves.

This paper concerns the axial propagation of torsional Alfvén-waves in a cylindrical plasma immersed in various types of axially symmetric magnetic fields. Propagation into (i) magnetic "cliff", (ii) magnetic "beach", and (iii) axially periodic structure ("bumpy" field) is studied.

Experiment: The plasma is formed by a pulsed electric discharge between two electrodes in a cylindrical tube of 1 m length. The initial hydrogen gas pressure is in the range of 0.1 Torr. A homogeneous stationary magnetic field up to 4 kG, in which the plasma is immersed, can be distorted by additional field coils. The plasma possesses a low value of β, an electron density of 2.10^{15} cm^{-3}, and an electron temperature of several eV. Torsional Alfvén-waves are launched from one electrode by a single-pulse generator. The azimuthal component, b_φ, of the wave

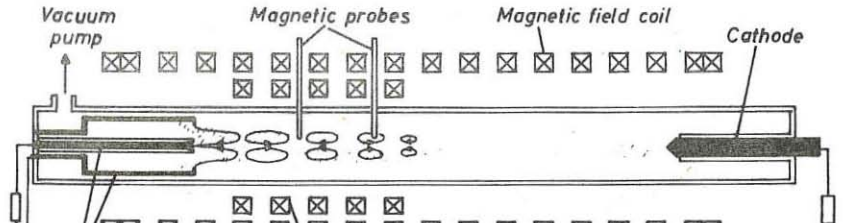


Fig.1 Schematic diagram of the experimental device

magnetic field is detected by magnetic probes. The transient signals are Fourier-analyzed in amplitude and phase. By this method the frequency behaviour as well as the radial and axial wave profiles have been analyzed for the three types of axially symmetric inhomogeneities of the magnetic field. The experimental set-up is shown in Fig. 1.

Results: In the case of a homogeneous magnetic field, the wave behaves like $J_1(\varkappa r)\, e^{ikz}\, e^{-\gamma z}$, i.e. the wave propagates as a cylindrical axisymmetric m=0 wave, which is damped mainly due to the ion-neutral collisions and resistivity. For axially inhomogeneous magnetic fields both phase and amplitude of the measured wave fields deviate from the $e^{ikz}\, e^{-\gamma z}$ variation because of partially reflected waves from the transition regions of the magnetic field. In the following figures the wave amplitude is shown for different frequencies as a function of axial distance from the exciting electrode at a fixed radius of 0.8 cm, the location of the maximum of the lowest radial mode.

Fig. 2, 3, and 4 show the results for "cliff", "beach", and "bumpy" geometries. The "cliff" geometry with a mirror ratio 1:2.8 shows only relatively weak reflection at high frequencies. The "beach" geometry, however, causes strong reflection at high field ratios, whereas no reflection was observed at lower ratios in agreement with /1/. The "bumpy" structure which can be regarded as successive cliffs and beaches produces wave trapping which is especial in the case where the half

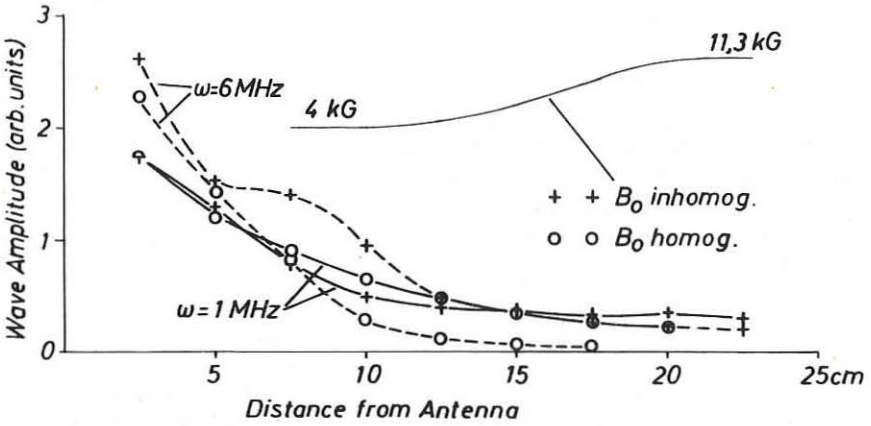


Fig. 2 Measured b_φ-component of torsional Alfvén-wave propagating in a homogeneous magnetic field and into a magnetic "cliff" as a function of distance

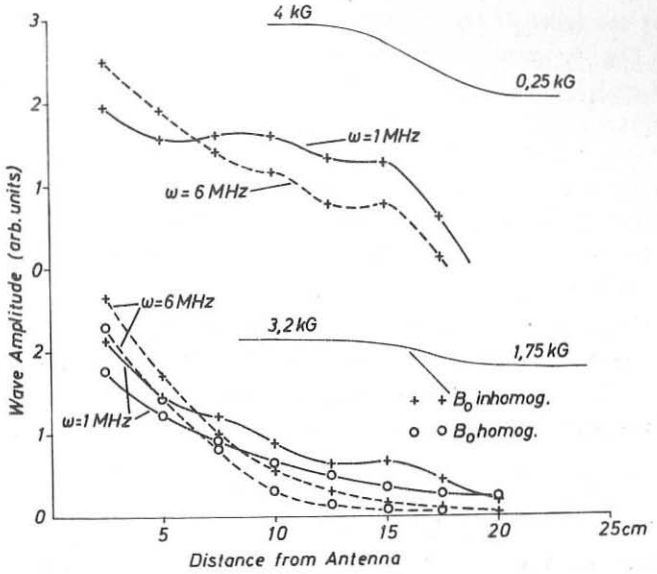


Fig. 3 Measured b_φ-component of torsional Alfvén-wave propagating in a homogeneous magnetic field and into magnetic "beaches" with different strengths as a function of distance

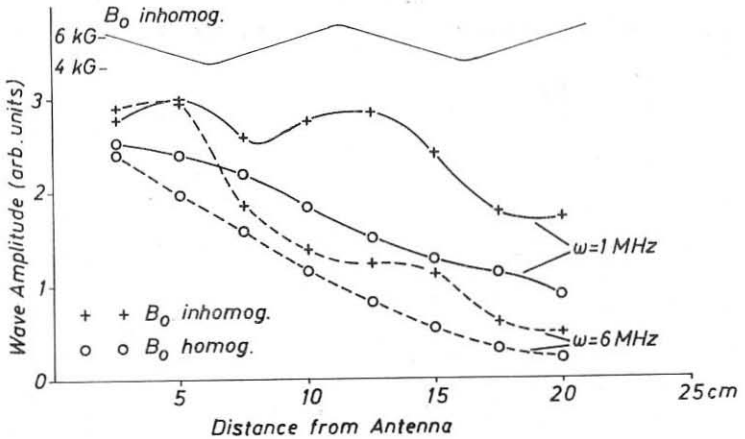


Fig. 4 Measured b_φ-component of torsional Alfvén-wave propagating in a homogeneous magnetic field and into a "bumpy" magnetic field as a function of distance

wavelength is of the order of the modulation length of the "bumpy" field. This is clearly seen in Fig. 4, where for the frequency ω = 1 MHz the half of the wavelength ($\frac{\lambda}{2} \simeq 10$ cm) is equal to the modulation length, whereas for ω = 6 MHz the half wavelength is $\simeq$ 6 cm.

Theory: The investigated phenomena can be described by MHD equations which account for the inhomogeneity of the stationary magnetic field. A WKB solution is not applicable because the wavelength is of the order of the characteristic length of the inhomogeneity.
A systematic analysis on the basis of curved coordinates was done in /2/ and /3/. In the present work the two dimensional wave equation was reduced by radial integration with Ritz-Galerkin method to an one dimensional equation for the b_φ - component of the wave magnetic field:

$$\frac{d^2}{dz^2} \tilde{b}_\varphi + a_1(z) \frac{d}{dz} \tilde{b}_\varphi + a_2(z) \tilde{b}_\varphi = 0 \ ,$$

where the functions $a_1(z)$ and $a_2(z)$ are solutions of the radial integration.

References:

/1/ Lehane, J.A., Paoloni, F.J., Plasma Phys. 12 (1970) 823.

/2/ Winterberg, F., Z. Naturf. 18a (1963) 545.

/3/ Gajewski, R., Winterberg, F., Ann. Phys. 32 (1965) 348.

SHOCK HEATING IN TOROIDAL SYSTEMS WITH ELONGATED CROSS-SECTION

A.G.Es'kov, R.Kh.Kurtmullaev, A.I.Malyutin, V.N.Semenov, A.L.Chernyakov

Kurchatov Institute of Atomic Energy

Moscow, USSR

This work consideres some possible ways of widening the range of shock plasma heating in an elongated toroidal configuration up to $nT \sim 10^{18} \div 10^{19}$ ev/cm^3 at $T \sim 1 \div 10$ kev including a method of controlled magnetic fluxes reconnection for the formation of a powerful shock piston.

1. A toroidal configuration with the elongated cross-section displays important specific advantages; a) there improve time relations between ℓ / V_A and rise time of the field, b) at the longitudinal plasma compression by the poloidal field H_φ magnetic energy does not increase as it does in θ- and Z-pinches, but falls inversely with the compression coefficient k providing, thus, high efficiency of the device (up to 0.6 at $\beta_\varphi \sim 1$).

II. Diffusion and trapping of the toroidal field into plasma, which take place before the shock heating phase, greatly decrease the possibility of high-β obtaining. Let us consider the following consequence of the processes.

The initial plasma being previously produced in the chamber is transversely compressed by a rapidly rising poloidal field to some relatively small dimension of b, and as a result an axially non-equilibrium configuration is formed. If up to this moment the toroidal field H_θ sufficient for the final state stabilization is applied, and it has

diffused into the plasma, then it could be assumed, that the freezed flux is being captured and conserved at the shock heating stage. The transition to the equilibrium final state occurs in shock-like manner, and apparantly is accompanied by increasing the plasma layer thickness. Simple calculations show this increase almost compensates the length reduction, thus the plasma volume insignificantly changes. Therefore, the toroidal component both inside and outside the plasma is slightly sensitive to compression. As a consequence the final plasma pressure turns out to be almost equal to the poloidal field pressure $kH_\varphi^2/8\pi$, where H_φ is the initial value of the field. Taking this fact into consideration it is easy to obtain the expression for $\beta = \frac{k}{k+(H_\theta/H_\varphi)^2}$. The exact solution of the problem is given in Fig.1, where x=b/a characterizes the degree of the initial transverse compression.

At the appropriate semiaxes ratio of the elongated plasma layer cross section in the final state of the order of 3÷4 it is possible to obtain the necessary q-value (q > 1) if $H_\theta/H_\varphi \simeq q\sqrt{k}\frac{\pi r}{\ell} \simeq 3 \div 4$, and this gives $\beta \simeq 0{,}1$-$0{,}2$.

III. β-increasing thus is a non-trivial problem. A certain success here appeares to be achieved, if to introduce an independent programmed change of the components H_θ and H_φ. In addition to apparent possibility of the q-value varying, such functional field separation permits to force the poloidal field at the shock compression phase and to apply the main stabilizing field H_θ at the confinement phase. Now for stability of the initial configuration it is sufficient to have $H_\theta/H_\varphi \sim 1$, and at an admissible value of $x \simeq 0{,}2$ we can obtain $\beta \simeq 0.7$.

Thus, reaching of the finite value of H_θ is expedient after heating when rising toroidal field due to adiabatic compression cannot essentially change β. The principle necessity of the adiabatic phase re-

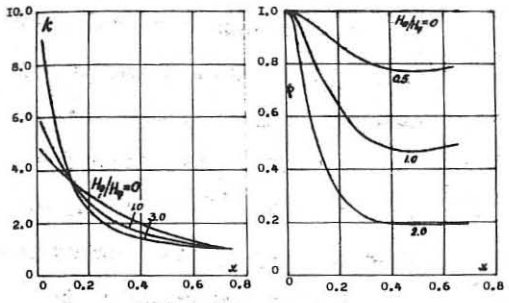


Fig.1.

quires more detailed consederation of this process.

IV. Of the two possible directions of adiabatic compression the most attractive is a transverse one. In this case the components H_θ and H_φ change in the necessary direction, and l=const; as a result $q=\frac{H_\theta}{H_\varphi}\frac{\ell}{\pi r}$ rapidly increases. On the contrary, at longitudinal compression l decreases, H_φ =const, and q changes very slowly.

The transverse adiabatic compression is provided by the system, in which shock heating and confining are spatially separated. Due to disconnected fluxes the main fraction of the poloidal field energy turns out to be in shock sections, and its large part dissipates in plasma at longitudinal contraction. The same fluxes fix l in adiabatic phase, and because of this the compression takes place in the transverse direction (Fig.2a). Fig.2s presents time behavior of the fields H_θ and H_φ in two points of the chamber. Computes calculations carried out for this configuration in asumption of a small skin thickness ($\delta \ll \ell$), showed that such process allows to enlarge q up to $\gtrsim 2$. In doing so it is necessary for the value of the unconnected poloidal fluxes to be sufficiently

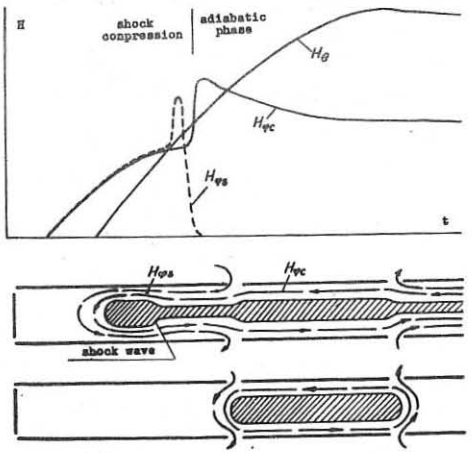


Fig.2.

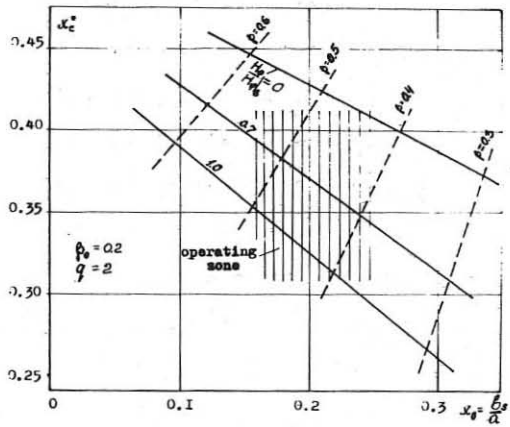


Fig.3.

large, in other words, the plasma layer thickness in the middle part $x_c = \frac{\delta_c}{a}$ before the shock wave must exceed some critical value of x_c^*. The dependence of x_c^* on $x_s = \frac{\delta_s}{a}$ and H_θ/H_φ is shown in Fig.3, where constant -β levels are shown dotted.

It should be said that above-mentioned values of β are characteristic of the shock heating only. The inclusion of extra heating in the skin must lead to β increasing.

V. The system considered opens up an interesting possibility of using the pecularity of a piston formed of contracting lines of force in oder to control the shock wave start. Fig.4a,b shows two controlling schemes. On the first one (a) current in operating coil produces the field, which breaks piston lines of force. In the second case (b) the contraction is prevented by broadening the end-part of the plasma layer. The key energy transfer into plasma occurs after rising the poloidal field by means of current change in operating coils.

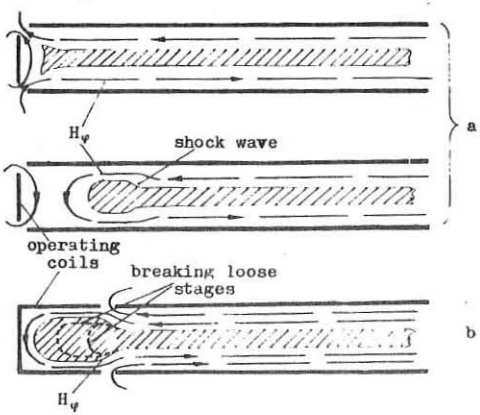


Fig.4.

It is apparent, that feasibility of such controlling is an alternative of modern complicated sharpening technique and it gives a great promise for using shock heating in small-size ebergy-consuming systems.

EXPERIMENTS ON PRODUCING THE PLASMA OF HIGH-β BY LONGITUDINAL SHOCK WAVES

A.G.Es'kov, O.A.Zolotovsky, R.Kh.Kurtmullaev, Ya.N.Lauhin, A.J.Malyutin, A.J.Markin, V.N.Semenov

Kurchatov Institute of Atomic Energy, Moscow, USSR

In the work presented here the authors investigate plasma heating and motion under the action of a piston formed of elongated poloidal magnetic lines of force. First of all possibilities of reaching large values of nT, β, T were of interest, these being among urgent problems in the programme on toroidal plasma devices. The system was simultaneously examined as an induction injector of a hot plasma for the scheme of a θ-pinch with liner. Finally, the plasma and magnetic field behaviour at the controlled lines of force reconnection is of interest for astrophysical applications.

The scheme of a desired structure formation and plasma dynamics is given in Fig.1. In wide cylindrical tube void (D=16 cm, l=70 cm) an initial plasma ($n_o = 10^{14} \div 2 \cdot 10^{15}$ cm^{-3}) with a longitudinal stationary freezed-in field (Ho = 0÷5 kG) is produced. On the plasma cylinder surface a field of the opposite sign ($H_\sim$ = 0÷11 kG) is rapidly excited with the aid of the

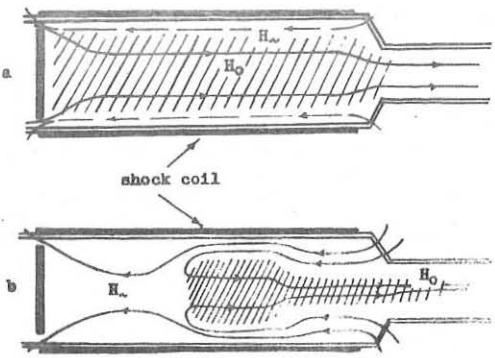


Fig.1.

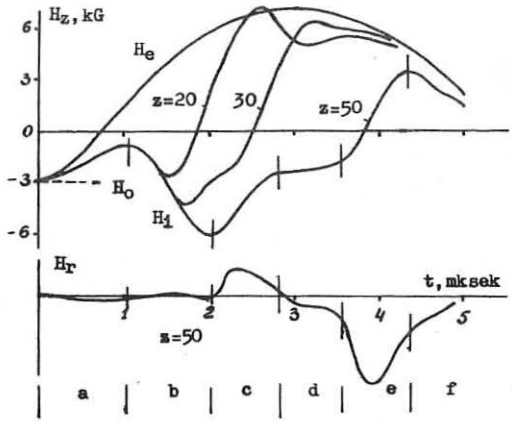


Fig.2.

cylindrical shock coil. Owing to the metal disc located on the butt-end of the device fluxes of fields H_o and $H_\sim$ are displaced into the narrow gap between the shock coil and the disk. Thereby the process of coupling is removed from the bulk of the plasma and therefore is not associated with its parameters.

Determination of the field structure wasperformed by probes measuring components H_z and H_r inside and outside the plasma. Kinetic pressure and the plasma column radius were estimated from these fields relation. Fig.2 shows oscillograms of the axial component H_e outside the plasma (near the wall), the component H_i in the plasma (on the axis r=o at distances z=20,30,50 cm from the end) and the radial component Hr (r=5cm at z=50 cm).

In the initial phase (a) probes indicate synchronous changing of the magnetic field on the axis, that corresponds to radial movement of the plasma column with freezed-in field according to the external pressure changing $H_e^2/8\pi$. During the interval (b) the reconnection of the internal and external fluxes takes place on the plasma cylinder butt-end, and as a result the probe signal behaviour essentially changes. Fig.2 points to the fact, that the longitudinal movement of plasma butt-end arises (the successive field change at various points), which is accompanied by the plasma column expansion (c) with the expansion front running away with the velocity

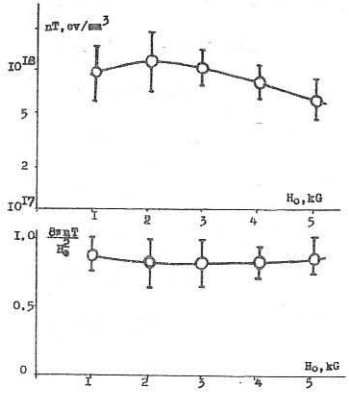


Fig.3.

$u \simeq (4 \div 7) \cdot 10^7$ cm/sec (a longitudinal wave). On the last curve (z=50 cm), the wave front is followed by a plateu (disturbed state, the interval d) then the component H_z reduces to zero (piston) and changes the sign (e). H_z changing is accompanied by the Hr burst with the sign being correspondent to the turn of the line of force to the wall at first (front) and after that to the axis (piston). Behind the piston magnetic pressures on the axis and near the wall are equalized (f), this points at the effective longitudinal raking out of the hot plasma.

Plasma pressure in the longitudinal wave (Fig.3) exceeds by a factor of 10 the value which had been obtained behind the front of the transverse shock wave with the same capacitor technique /1,2/. This gain is apparently due to increasing of the characteristic length l and piston efficiency enhancing, because the magnetic energy now does not accumulate in a vacuum cavity during the contraction process, but releases into the plasma.

The plasma flow behaviour at the right end of the shock chamber is essentially defined by the magnetic field strength H^* at the entrance to the small tube. At $H^* < H$ the magnetic collapse in the shock cavity causes the plasma jet outflow to the small tube (injection regime) In case $H^* > H$ the shock cavity is locked and the quasiequilibrium state here appears. Basic parameters of this process and the final state ($\beta = 0.6 \div 0.9$, the constriction coefficient $l_0/l = 3 \div 5$, diamagnetic expansion $r/r_0 \approx 1.5$) are in rather

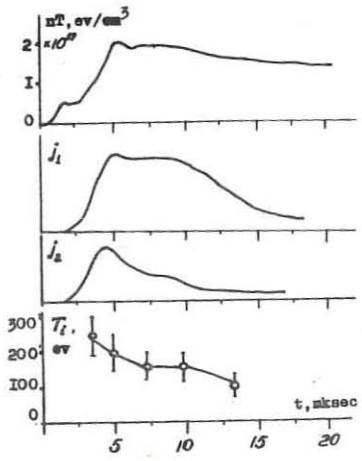


Fig.4.

good agreement with the model assuming the conservation of the total energy and the magnetic flux in the plasma.

In the injection regime parameters of the plasma jet flowing to the small volume were measured with the aid of internal and external diamagnetic probes (nT, $V_{\parallel}$), 9 - channel electrostatic neutrals charge exchange analyzer of the ion energy spectrum, and a microwave circuit (n, $V_{\parallel}$). Typical signal oscillograms from the probe (nT) and two channels of the analyzer are plotted in Fig.4 (J_1 for E=400 ev, J_2 for E=800 ev). The last curve represents the transverse ion temperature.

These results were obtained when the bank energy constituted a quarter of a nominal operation value. Under optimal conditions pressure in the jet reaches 10^{18} ev/cm^3.

It might be well to point out the sufficient homogeneity of jet parameters and a possibility of controlling its diameter by the magnetic field strength in a small tube. Thus experimental data demonstrate the plasma heating and acceleration efficiency with the aid of the poloidal field and a possibility of reaching extreme plasma parameters in the scheme described.

References

1. R.Kh.Kurtmullaev et al. Zh.Tekh. Fiz.XL, 1044, (1970).
2. M.Keilhacker et al. Z.Physik 223, 385-396, (1969).

CO_2 LASER BEAM ABSORPTION BY A PLASMA NEAR PLASMA FREQUENCY

E. FABRE, C. STENZ, J. MAIGNAN

Ecole Polytechnique, Laboratoire de Physique des Milieux Ionisés, Paris, France.

Equipe de Recherche Associée au C.N.R.S.

Abstract : We study the interaction of CO_2 laser with a dense plasma near plasma frequency. The absorption of laser light corresponds,for flux below 10^{10} W/cm^2,to inverse Bremstrahlung.

We have studied by experiment the interaction of an intense electromagnetic wave with a dense plasma for which plasma frequency ω_p is near the wave frequency ω_ℓ, in order to observe the anomalous absorption [1] or the backscattering [2] of the wave due to parametric instabilities, when the power flux into the plasma is sufficiently high. The experiment is the following : we irradiate transversaly with the output beam of a TEA CO_2 laser (Fig. 1) a cylindricaly shaped target plasma.

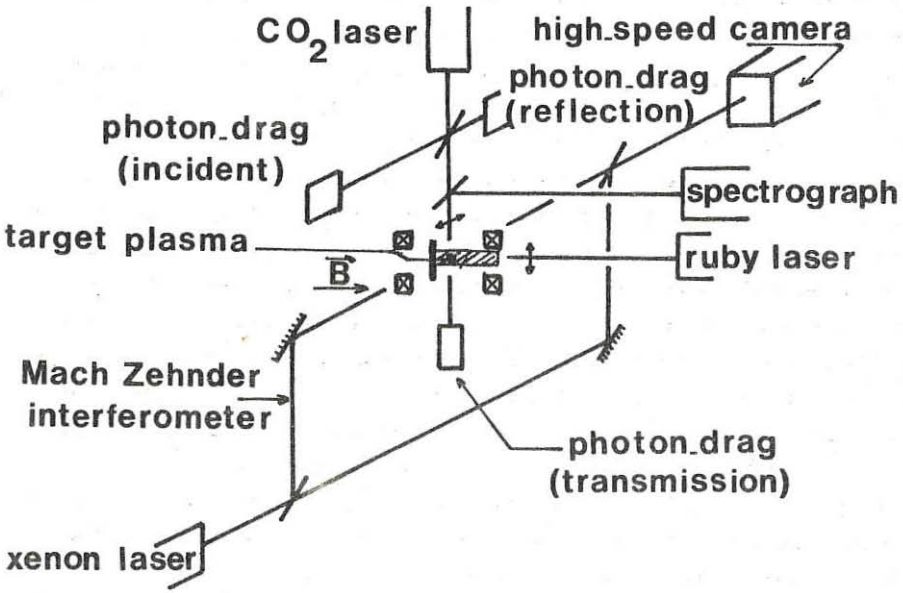


Figure 1

The target plasma is obtained in confining in a 65 kilogauss magnetic field a plasma created by ruby laser irradiatior of polyethylene foil [3]. The plasma diameter is 2.3 mm and its length increasing linearly with time is 1.5 cm, 100 ns after plasma production.

We have measured by Mach-Zenhder interferometry the electronic number density distribution in the plasma along the axis of the CO_2 laser. The maximum value reached in the middle of the target plasma is 9.10^{18} e/cm^{-3} $\pm$ 10^{18}. The electronic temperature of the plasma obtained by spectroscopy is 9 eV $\pm$ 2 and is an average value. The laser beam focussed into the plasma is obtained from a TEA CO_2 laser of the Lumonics Company and the maximum power density in the focal spot is 2 - 4.10^{10} W/cm^2. Photon drag detectors are used to monitor the incident CO_2 laser pulse and to determine the fraction of the beam transmitted or reflected.

Our experimental results show an intense absorption of the CO_2 laser beam by the plasma and no evidence of sigrificant reflection which could be superior to the background light coming from reflection by the windows or the lens of the system. The figure 2 gives the experimental points which correspond to the measured absorption coefficient of the plasma as a function of power density in the focal spot. Below a flux of the order of 10^{10} W/cm^2 the absorption coefficient decreases when the flux increases. This is in rather good agreement with what one could expect when taking account of plasma heating due to inverse Bremstrahlung absorption, because when the flux is increased, the plasma temperature T_e also increases and then the absorption coefficient which varies a $T_e^{-3/2}$ should diminish. The solid curve on figure 2 gives the result of a theoretical prediction of the absorption coefficient obtained on a simple basis, for a self consistent calculation where plasma heating by the incident laser is considered and density variation by plasma expansion or additional ionisation is neglected. Agreement between experimental points and calculation is better for a maximum electronic number density lower than the measured one, because the high value of 9.10^{18} e cm^{-3} is found only in a fraction of the focal spot of the CO_2 laser and for the absorption we have to consider an average value of the electronic density over the entire area of the focus of the beam.

First experiments for a flux higher than 10^{10} W/cm^2 show an unexpectively high absorption coefficient. We have obtained for 4.10^{10} W/cm^2 60 percent of absorption instead

of the 15 percent that we would expect from inverse Bremstrahlung. This could be interpreted as evidence for anomalous absorption which occurs for a part of the CO_2 laser beam in the center of the focal spot where the power density can be somewhat higher than 4.10^{10} W/cm^2 which is only an average value over the entire focal spot. A flux of 10^{11} W/cm^2 which is in the range of the expected value for the occurance of parametric decay instabilities, could be obtained in this experiment. We have computed the increase of plasma temperature due to inverse Bremstrahlung absorption. The temperature reaches 100 eV for 10^{11} W/cm^2. This value should reduce collisional effects and permit the onset of parametric decay instabilities which can explain our large value of absorption coefficient for higher flux.

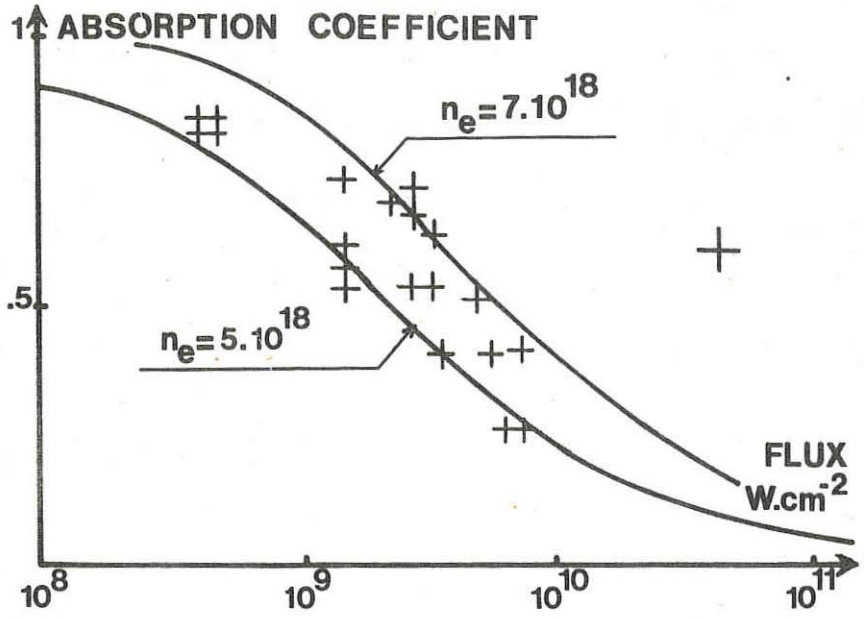


Figure 2

In conclusion, our experiment has shown the CO_2 laser beam absorption by a dense plasma near ω_p, and for high flux above 10^{10} W/cm^2 the possibility of anomalous absorption due to parametric instability. Thomson scattering experiments are in progress to confirm this, and also experiment with higher power density up to 10^{12} W/cm^2.

REFERENCES

1 R. Gehker, O.U. Sizukhim, Zh. Exp. Teo Fys., 9 - 408 (1969) (JETP Letter, 9, 243 (1969).

P.K. Kaw, E. Valeo and J.M. Dawson, Phys. Rev. Lett., 25, 430 (1970).

2 M.N. Rosenbluth, Phys. Rev. Lett., 29, 565 (1972).

3 E. Fabre, C. Stenz, J. Maignan, Bulletin A.P.S., 1001 Nov. (1972).

3.7. THEORETICAL ASPECTS



STRUCTURE OF A BOUNDARY LAYER SEPARATING A FIELD FREE PLASMA FROM A VACUUM MAGNETIC FIELD

R. Gruber, E.S. Weibel
Centre de Recherches en Physique des Plasmas
Lausanne . Switzerland

Abstract

Self consistent solution of Vlasov's equations describing a plane boundary layer without shear are given.The currents within the layer are due to free and trapped electrons.The ion current is neglected since $m_e << m_i$. The free electrons and the ions are assumed maxwellian at infinity. Field and density profiles are computed for E(x), B(x), $n_e(x)$, $n_i(x)$ and j(x) for different numbers of trapped electrons.

Introduction

The structure of boundary layers separating a field free plasma from a vacuum magnetic field has been examined previously [1-11]. The earliest work used certain singular particle distributions which allowed the existence of solutions without trapped particles [1,2,3,4]. Imposing maxwellian distributions at infinity, a unique solution exists without trapped particles as long as $m_e = m_i$ [5,6,7]. Laval and Pellat [7] were the first to correctly demonstrate, that for $m_e \neq m_i$ the distribution functions must be continuous on the boundary separating free and trapped particles, if the distributions at infinity are maxwellian. Paskievici et al [11] concluded earlier that no boundary exists without trapped particles.Morse [9] has given a solution evolving from initial confinement by a wall, by switching on adiabatically a B field. Many more particles are trapped in this process than are necessary for the existence of a sheath.

In the present work we assume $m_i >> m_e$, maxwellian distributions at $x = +\infty$ and a one-parameter family of trapped electron distributions allowing us to examine numerically the structure of the layer as a function of the number of trapped electrons.

The computation of boundary profiles presents a peculiar difficulty which is due to the fact that two very different lengths appear in the problem:the Debye length $\delta = \sqrt{T/en(+\infty)}$ and the electron larmor radius $R = \sqrt{m_e T}/eB(-\infty)$. Poisson's equation for the electric potential is numerically unstable over distances larger than

$\delta \ll R$, so that the boundary profiles cannot be obtained by direct integration. This is certainly the reason why no satisfactory profiles taking account of charge separation have so far been published. Some authors have attempted to turn the problem by assuming charge neutrality: $n_e = n_i$. This assumption is only correct as long as the local Debye length $\delta(x)$ is much smaller than the local electron larmor radius. It breaks down as one approaches the vacuum side of the sheath and gives an incorrect asymptotic behaviour [10]. In fact, since the ions are essentially confined to the sheath by the electrostatic field, the relative charge separation becomes large on the vacuum side.

Method of Solution

We overcome the difficulty by expressing the problem in a variational form which we solve by a finite element method. The constants of motion are the energy $H = \frac{1}{2m}\left[p_x^2 + (p_y - qA)^2\right] + q\,\phi$ and the momentum p_y ($m = m_e$, $q = -e$ for electrons, $m = m_i$, $q = e$ for ions). $A(x)$ and $\phi(x)$ are the magnetic and electric potentials: $B_z = A'$, $E_x = -\phi'$. A and ϕ are assumed monotonic and increasing. One must distinguish free particles which can reach $x = \infty$ from trapped particles where x coordinate remains finite. The boundary in phase space separating free and trapped electrons is given by $H = \frac{1}{2m} p_y^2$. Any distribution of the form $f(H, p_y)$ satisfies Vlasov's equation. Assuming such distributions one can express the current and the charge density in the sheath

$$\varsigma = q\int F(H,p_y)\,dp_x\,dp_y$$

$$j = \frac{q}{m}\int F(H,p_y)(p_y - qA)\,dp_x\,dp_y$$

as well as the kinetic pressure

$$\Pi = \frac{1}{m}\int F(H,p_y)\,p_x^2\,dp_x\,dp_y$$

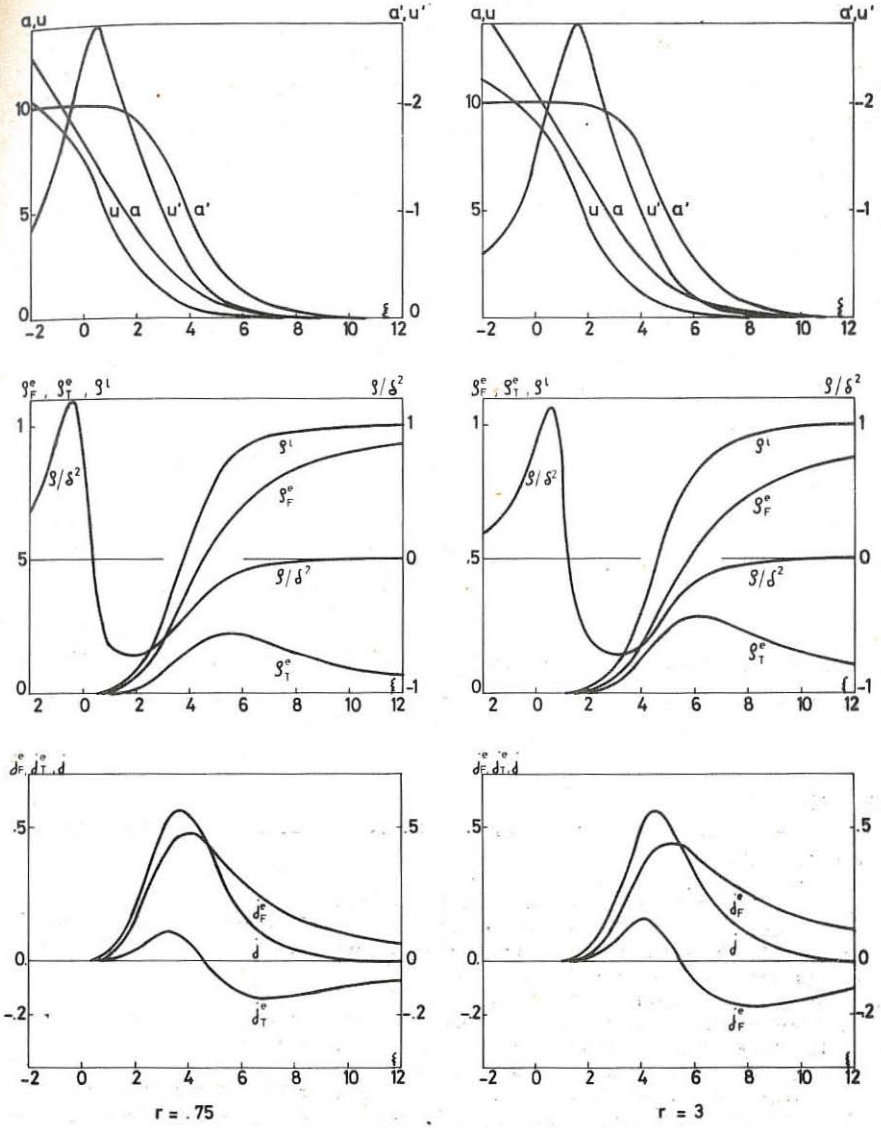
One notes that $\partial\Pi/\partial\phi = -\varsigma$ and $\partial\Pi/\partial A = j$. The potentials satisfy $\Sigma j + A'' = 0$, $\Sigma\varsigma + \phi'' = 0$. Hence the pressure balance equation

$$\Sigma\Pi + \frac{1}{2}(A')^2 - \frac{1}{2}(\phi)^2 = \text{const.}$$

The potentials are also the solution which makes stationary the integral

$$\int\left(\Sigma\Pi - \frac{1}{2}(A')^2 + \frac{1}{2}(\phi')^2\right)dx$$

This variational problem is solved by a finite element method. We introduce the following dimensionless variables $F = (n_0/mT)\varphi$, $H = T\eta$, $p_x = \sqrt{mT}\,\xi$, $p_y = \sqrt{mT}\,\alpha$, $\phi = (T_e/e)u$, $A = (\sqrt{m_e T_e}/e)a$, $x = \sqrt{m_e/e^2 n_0}\,\xi$, we choose the following distributions



Figs: Potential, field, density and current profiles for $\delta = 10^{-2}$ and r = .75 resp. r = 3.

ions $\quad \varphi = e^{-h_i}/\pi$

free electrons $\quad \varphi = e^{-h_e}/\pi$

trapped electrons $\quad \varphi = \exp\left(-\frac{\alpha^2}{2} + \frac{1}{r}\left(h_e - \frac{\alpha^2}{2}\right)\right)/\pi$

where r is a free parameter regulating the abondance of trapped electrons. The variational problem takes now the form

$$\text{variation of } \int \left[P(a,u) - \frac{1}{2}(a')^2 + \frac{\delta^2}{2}(u')\right] dx = 0$$

where $P = P_i + P_f + P_t$

$$P_i = e^{-u}$$

$$P_f = (2\pi)^{-1/2} e^{u} \int_0^\infty \xi^2 e^{-\xi^2/2} (1 - \phi(z_F))\, d\xi \quad , \quad z_F = (-\xi^2 + 2u + a^2)/2a$$

$$P_t = (2\pi)^{-1/2} e^{u} \int_0^\infty e^{G} \xi^2 (1 + \phi(z_T))\, d\xi \quad , \quad z_T = (-\xi^2 + 2u - (1 + 2/r)a^2)/2a$$

$$\phi(x) = \sqrt{\frac{2}{\pi}} \int_0^x e^{-x^2/2}\, dx \quad , \quad G = (\xi^2 + a^2(1 + 1/r) - 2u)/2r - u$$

δ is the ratio of the thermal velocity of the electrons to the speed of light, or the ratio of the Debye length in the plasma to the electron larmor radius. Solutions for two values of the parameter r, for $\delta = 10^{-2}$ and $\varphi'(-\infty) = 0$, (no electric field at infinity) are given. The sheath is some 6 electron larmor radii wide. It appears that the magnetic field profile is much narrower than the region over which currents flow since trapped and free currents cancel over part of the sheaths, Figs.

References

1) M.N. Rosenbluth, Magnetohydrodynamics, Landshoff ed, Stanford University Press, Calif. 1957
2) E.S. Weibel, Phys. Fluids 2, 52 (1959)
3) A.I. Morozov, L.S. Solovev, JETP 13, 927 (1961)
4) K. Husimi, N. Yajima (Nagoya University, Japan), T. Tsuzuki (Osaka University, Japan), On the structure of a fresh plasma surface.
5) A. Sestero, Phys. Fluids 8, 739 (1965)
6) H. Grad, Phys. Fluids 4, 1366 (1961)
7) G. Schmidt, D. Finkelstein, Phys. Rev. 126, 1611 (1962)
8) G. Laval, R. Pellat, Journal de Mécanique 2, 67 (1963)
9) R.L. Morse, Phys. Fluids 8, 308 (1965)
10) A. Sestero, Phys. Fluids 7, 44 (1964) el static problem (transition $n \neq 0$)
11) W. Paskievici, A. Sestero, H. Weitzner, Report NYO 9193 (1962) Courant Instr. Math. Sci., New York Univ.

THE MOTION OF CHARGED PARTICLES IN A MIRROR MACHINE IN THE PRESENCE OF THE CYCLOTRON OSCILLATIONS

A.V.TIMOFEEV

I.V.Kurchatov Institute of Atomic Energy

Moscow, USSR

A b s t r a c t . The chaotic motion condition of charged particles in a mirror machines in the presence of cyclotron oscillations has been determined. It has been found that the particles losses from mirror machines under the influence of cyclotron oscillations with small wave lengths can be very small.

The development of the cyclotron instability in mirror machines often leads to the regular oscillations with a fixed frequency ω and the wave vector $\vec{k}$, often additional losses of the particles turning out to be very small. The losses question is discussed in this work.

The motion of the charged particle in such oscillations is described by the Hamiltonian, see for instance /I/:

$$H(\mu,\theta) = \mu\left(\omega_i(z(t)) - \frac{\omega}{n}\right) + e\varphi\, J_n(a_\mu)\cos n\theta$$

Here μ - is the magnetic moment, $\theta = \alpha - \frac{\omega}{n}t$, α - is the angle of the cyclotron rotation, $\omega_i(z) = \omega_{i0}\left(1 + z^2/L^2\right)$ - cyclotron frequency, axis $0z$ is directed along the magnetic field, the dependence of z on the time is connected with the ion's motion on the mirror machine, $\omega = n\omega_{i0}$ - this condition provides the maximum of the resonance cyclotron interaction, φ is the amplitude of the electric potential's oscillation, $J_n(a_\mu)$ - is the Bessel's function with the index-n and the argument $a_\mu = k r_i$, $r_i = \left(2\mu/m_i\omega_i\right)^{1/2}$, $\vec{k} \perp \vec{H}$, usually $k \gg r_i^{-1}$.

For the oscillations of sufficiently large amplitude $\frac{e\varphi}{\mu\omega_i} \gg a_\mu^{-1/2}\left(\frac{r_i}{L}\right)^{2/3}$ the ω_i - dependancy on the time can be taken into account parametrically. Figs / 1-3/ give notion of the motion's

character by the various ratios between $\delta\omega_n = \omega_i - \omega/n$ and $\omega_{\mu n} = n\,\frac{e\varphi}{\mu}\left(\frac{a_\mu}{2\pi}\right)^{1/2}$ The situation with $\delta\omega_n = 0$ was considered earlier in /2/. In the figs it is designated $\phi_\theta = n\theta$, $\phi_\mu = a_\mu - \frac{n\pi}{2} - \frac{\pi}{4}$. From these figs it follows, that μ can be changed under the influence of oscillations by the quantity, not exceeding $\mu\,\frac{2\pi}{a_\mu}$. The particles with the closed trajectories are captured by the wave, while their average rotation frequency is equal to $\frac{\omega}{n}$, but not to the cyclotron frequency. The captured particles possess the adiabatic invariant $J = \oint \mu\, d\theta$ for the uncaptured particles, correspondingly, $J = \int_0^{2\pi} \mu\, d\theta$ /1/. The resonance between oscillations in mirror machine (frequency ω_B) can destroy the invariant. Using the general theory, developed in /3/ and in other works, we find the destructive condition $\frac{\omega_{iz}}{\omega_B}\,a_\mu^{-2} \gg 1$, here $\omega_B = 2\omega_{io}\frac{r_i}{L}$, $\frac{\omega_{iz}}{\omega_i} \sim e^{-\frac{\omega_{\mu n}}{\omega_B}}$, $\omega_{\mu n} \gg \omega_B$. This result is just for the simplest case of the motion near the elliptic point in the figs I,2. In the stochastic regime the ion's distribution diffuses with the diffusion's coefficient, which approximately is equal to $D \approx a_\mu^{-1}\,\mu^2\,\omega_{iz}^{3/2}\,\omega_B^{-1/2}$.

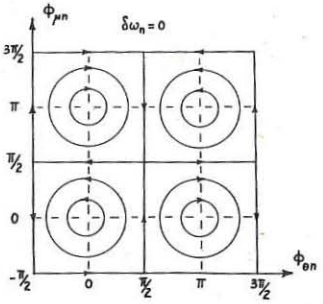


Fig.I

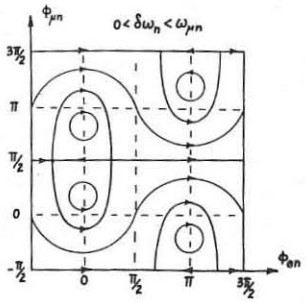


Fig.2

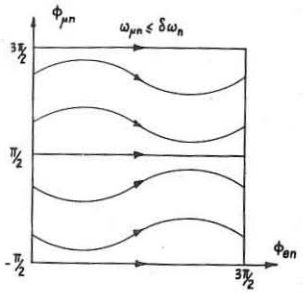


Fig. 3

At the moderate magnitude of the electric field $a_\mu^{-1/2}\left(\frac{\tau_i}{L}\right)^{2/3} \gg \frac{e\varphi}{\mu\omega_i} \gg a_\mu^{1/2}\left(\frac{\tau_i}{L}\right)^{5/3}$ we can suppose, that the ion's magnetic moment is not changed by the motion on the magnetic mirror, and only at the resonance point it experiences the sharp and uncorrelated jumps / 5-7/. In this case the diffusion's coefficient is equal to $\mathcal{D} \approx a_\mu^{-1}\left(\frac{L}{\tau_i}\right)^{1/3}\frac{e\varphi}{\omega_i}$. It turns into zero by the critical values of the μ_{nm}, determined by the condition $J_n(a_\mu) = 0$. Therefore the maximum variation of the magnetic moment $\delta\mu$, just as in the case of the large field is equal to $\mu\,\frac{2\pi}{a_\mu}$ $\left(\delta V_\perp \approx \pi\,\frac{\omega_i}{k}\right)$. It is easy to understand, that on the $v_\perp, v_\parallel$ plane the region of the ion's retention in the magnetic mirror will have stepped appearance. In fig. 4 it is shaded, the projection of the loss cone is depicted by the straight line $V_{\perp nm} = \left(\frac{2\omega_i}{m_i}\mu_{nm}\right)^{1/2}$. It is obvious, that the short wave oscillations with $k \gg \tau_i^{-1}$ weakly influence the retention of the ions in the magnetic mirror, as under their influence the loss cone broadens averagely by the small value $\delta\psi \approx (k\tau_i)^{-1} \ll 1$

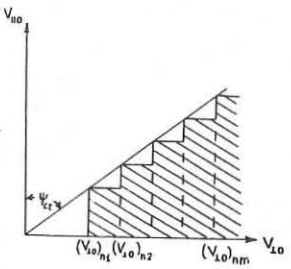


Fig. 4

These results are applied to the uncollisioned plasma. Under collisions action the ions can overcome the zones near the critical values μ, where the diffusion coefficient turns into zero. If the collision's frequency is sufficiently great $\nu \gg \omega_B\, k^{-4}(\tau_i L)^{-2}$, the ions are weakly delayed in these regions, and for the diffusion's coefficient the above cited expression can be used. By the small collision frequency the diffusion coefficient is

equal $\mathcal{D} \approx a_\mu^{-1} \left(\frac{e\varphi}{\mu\omega_i}\right)^{-2} \left(\frac{r_i}{L}\right)^{10/3} \mu m_i \omega_i \nu K^{-2}$

Finally in the small electric field $\frac{e\varphi}{\mu\omega_i} \ll a_\mu^{1/2} \left(\frac{r_i}{L}\right)^{5/3}$ the ion's motion under the cyclotron oscillation's action becomes deterministic. In this case the maximum variation of the magnetic momentum does not exceed $\mu \left(\frac{e\varphi}{\mu\omega_i}\right)^{1/2} \left(\frac{r_i}{L}\right)^{1/6} a_\mu^{-1/4}$.

REFERENCES

1. R.E. Aamodt, Phys. Rev. Lett., 27, 135 (1971).
2. R.E. Aamodt, S.E. Bodner, Phys. Fluids, 12, 1471 (1969).
3. Б.В. Чириков, Ат. энергия, 6, 630 (1959).
4. Г.М. Заславский, Б.В. Чириков, УФН, 105 , 3 (1971).
5. A.K.Nekrasov, Nucl. Fusion, 10,387 (1970).
6. F. Jaeger, A.J.Lichtenberg, M.A.Lieberman, Plasma Phys., 14,(1972).
7. M.N. Rosenbluth, Phys.Rev.Lett., 29,406 (1972).

COMPUTER SIMULATION OF RF PLASMA CONFINEMENT*

J. L. Shohet
University of Wisconsin
Madison, Wisconsin, U.S.A.

Albert J. Hatch
Argonne National Laboratory
Argonne, Illinois, U.S.A.

ABSTRACT: The particle-in-cell method of computer simulation has been used to demonstrate rf confinement of low-density plasmas and to verify the Φ quasipotential-well theory of rf confinement. Computations have been made for a 2-dimensional central cross section of the quadrupole electric mode in a cubical resonant cavity.

Radiofrequency confinement of low-density plasmas (density n less than the cutoff density n_c) is conveniently described [1, 2] in terms of a period-averaged quasipotential function $\Phi = q^2E^2 / 4m\omega^2$ which is derived by use of an adiabatic oscillation-center approximation. [3] Here q and m are the charge and mass of a plasma particle and E and ω are the local amplitude and radian frequency of the confining field. An effective drift force $\mathcal{F} = -\nabla\Phi$ causes the oscillating particle to move slowly in the direction of decreasing electric field and to acquire a component of drift energy. For the collisionless case, the conservation of energy requires that the sum of the quasipotential energy Φ plus the drift energy T remain constant. Rf confinement occurs only in field configurations that exhibit a Φ quasipotential well. Such fields are of the generic type of electric quadrupole and higher order electric multipoles. [4] The Φ wells are characterized by a central nodal point where $\Phi = 0$ and by a rim defined as the locus of all points at which $\Phi = \Phi_R$, where Φ_R is the lowest point along the crest of the potential barrier (usually a saddle point) on the Φ surface surrounding the nodal point.

The purpose of this paper is to describe computer simulation of the behavior of single charged particles and of multiple-particle plasmas in rf-confinement fields.

All computations were made for the field in the xy midplane of the TE_{111} electric quadrupole mode of a cubical cavity. This field and its associated Φ potential well are shown in Fig. 1. The field components are

$$E_x = E_0 \cos(\pi x/L)\sin(\pi y/L)\sin\omega t, \quad (1)$$

$$E_y = -E_0 \sin(\pi x/L)\cos(\pi y L)\sin\omega t, \quad (2)$$

$$B_z = -(E_0/\sqrt{3}c)\cos(\pi x/L)\cos(\pi y/L)\cos\omega t, \quad (3)$$

where L is the cavity dimension.

The motion of a charged particle in the xy plane is determined by a finite-difference solution of the equations of motion

$$m(dV_x/dt) = q(E_x + V_y B_z), \quad (4)$$

$$m(dV_y/dt) = q(E_y - V_x B_z), \quad (5)$$

where V_x and V_y are the components of the velocity $\vec{V}$.

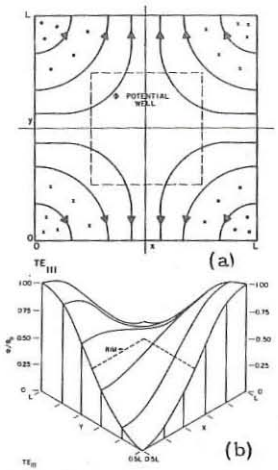


Fig. 1. TE_{111} mode. (a) Field. (b) Φ potential.

The typical single-particle trajectory shown in Fig. 2 was computed for an electron launched with zero drift speed ("quiet start") inside the rim of the Φ well. The Lissajous-like trajectory represents computations for 100 periods of the rf field (36 time steps per period) and clearly indicates confinement.

Multiple-particle plasmas were simulated by the particle-in-cell method.[5] A large number (10,000) of simulation particles (5×10^7 real particles) of both species (electron and ion) were launched with zero drift velocity in a uniformly-distributed array of initial positions. Motions of simulation particles were computed by the same finite-difference time-step method used in the single-particle case. However, the local electric field used in the computations was the vector sum of the applied rf field evaluated at the location of each simulation particle and the self-consistent quasistatic field produced by the particles themselves. The latter was obtained by solving Poisson's equation for the entire array of particles at each time step by means of the Buneman algorithm.[6] A particle striking a wall is specularly reflected from it with an arbitrary reflection coefficient. The

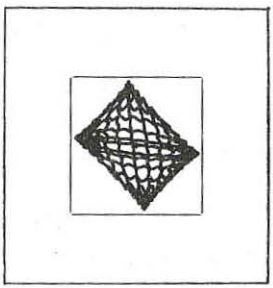


Fig. 2. Single-particle trajectory in Φ well.

parameters used for the computations were

$L = 63$ m	$\lambda_D = 3.4$ m	$E_0 = 2000$ V/m
$T_e = 26$ eV	$\Delta x = \Delta y = 2.03$ m	$f = \omega/2\pi = 4.125$ MHz
$T_i = 5.3$ eV	$N\lambda_D = 29$	$\Phi_e = 132$ eV
$m_i / m_e = 5$	$\eta = 5 \times 10^7$	$\Phi_i = 26.4$ eV
	$N = 10\,000$	

Here Δx and Δy are the Poisson mesh spacings, T_e and T_i are the electron and ion temperatures, λ_D is the electron Debye length, N_{λ_D} is the number of simulation particles in a Debye square, η is the number of real particles per simulation particle, N is the number of simulation particles, and Φ and Φ_i are the potential well depths for electrons and ions, respectively.

The establishment of the equilibrium confinement condition is portrayed in Fig. 3. Both electrons and ions (not shown) are concentrated inside the well whose rim is indicated by the dashed square. The occurrence of maximum density in the vicinity of the central nodal point is consistent with the experimental observation of maximum luminosity in the same region in an rf confined plasma.[7] The kinetic energy of the particles oscillates at twice the frequency of the rf field, but does not grow in time. Note that particles are also concentrated in the corners of the cavity. However, this is not rf confinement, since two sides of these regions are material (the walls of the cavity).

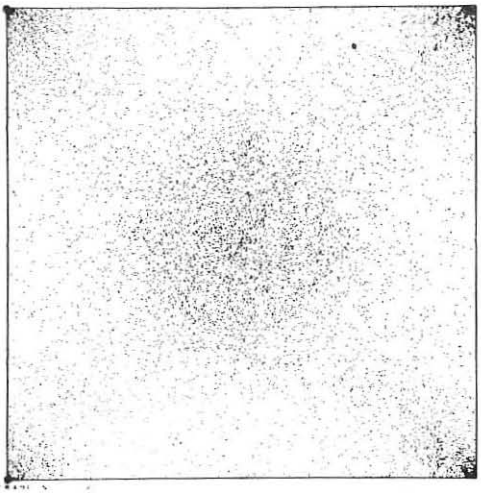


Fig. 3. Simulation electrons in Φ well at 2500^{th} time step.

The populations of simulation ions and electrons inside the potential well are shown in Fig. 4. Both populations increase from the original value of 2500 (uniform distribution) and level out at about 3600—3800. The number of electrons inside the well oscillates at

roughly the electron plasma frequency and the ions oscillate at roughly the corresponding ion plasma frequency.

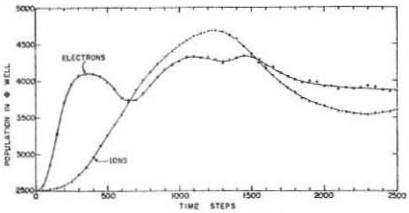


Fig. 4. Populations in Φ well.

REFERENCES

*Work supported by the National Science Foundation and the U.S. Atomic Energy Commission.

[1] A. V. Gapanov and M. A. Miller, Zh. Eksp. Teor. Fiz. 34, 242 (1958) [English transl.: Sov. Phys. — JETP 1, 168 (1958)].

[2] H. Motz and C. J. H. Watson, Adv. Electronics Electron Phys. 23, 153 (1967).

[3] G. Schmidt, Physics of High Temperature Plasmas; An Introduction (Academic Press, Inc., New York, 1966), pp. 47 - 50.

[4] A. J. Hatch, M. Hasan, and W. E. Smith, Proc. 2ème Colloque International sur l'Interaction des Champs H. F. associés à un Champ Magnétique Statique avec un Plasma, Saclay, 1968 (l'Institut National des Sciences et Techniques Nucléaires, Saclay, 1968), Vol. 3, p. 949.

[5] R. L. Morse and C. W. Nielson, Phys. Fluids 12, 2418 (1969).

[6] O. Buneman, Stanford University Institute for Plasma Research, Report No. 294 (1969).

[7] C. F. Shelby and A. J. Hatch, Phys. Rev. Letters 29, 834 (1972).

ABSORPTION OF ALFVEN WAVES IN A PLASMA CYLINDER WITH DISTRIBUTED CURRENT.

Z. Jankovich*)
Institute Nuclear Research Sversk, Poland

A b s t r a c t. Resonant absorption of Alfven waves by a current-carrying plasma is considered in connection with plasma heating in tokamak-type systems.

Let a uniform magnetic field B_{oz} and equilibrium current $j_{oz}(r)$ be given for an equilibrium cylindrical plasma column. Let magnetic field oscillations with the radial component $b_r = b_r(a)\exp(-i\omega t + i[m\varphi + k_z z])$ be excited on the plasma boundary at r=a. If the plasma is considered to be perfectly conducting and incompressible then to determine the radial component b_r of the magnetic field (in Eq.(1), the function F(r) is proportional b_r: $F(r) \sim b(r)$ following equation can be derived from the linearized systems of one fluid hydromagnetic equations /1/ after performing Fourier tranformation over Z, φ corrdinates and time

$$F_{rr}'' + K_\perp^2(r) F = 0, \qquad (1)$$

where $K_\perp^2(r)$ is the function of r, wave parameters ω, m, k_z and equilibrium values of B_{or}, $\rho_o(r)$, $j_{oz}(r)$. The proper form of $K_\perp^2(r)$ is not given here since the resultant expression is very cumbersome. For given m, K_z the oscillation frequency ω is selected so that it should be equal to the local Alfven frequency in the plasma $\omega^2 = (\vec{K}\vec{B})^2/4\pi\rho_o = \omega_A^2$ at certain $r=r_o$. For $r \to r_o$, $K_\perp^2 \to \infty$. It should be noted that as ω, K_z, m vary r_o displaces over the plasma radius. It is known that in the vicinity of the point where the refractive index is infinite the waves are absorbed effectively /2/ and various methods of plasma heating are based on this fact /3/. For a wave to be absorbed effectively and internal plasma layers to be heated it is

---

*) The work was carried out at the Moscow State University.

necessary that r_0 should be deep in the plasma, and $K_1^2(r)$ remain positive in the range from the plasma boundary to the point r_0. The estimates show that when the current j_{0z} and plasma density ρ_0 are distributed parabolically over the plasma radius it is possible to select such m, ω, K_z for typical tokamak plasma parameters that the penetrability barrier should be absent at $r_0 \leq r \leq a$ and the Kruskal and Suydem stability criteria should be fulfiled. The approximate solution of Eq.(1) for slowly varying $K_1^2(r)$ can be given in the form

$$F = [K_1^2(r)]^{-1/2}\left(A\exp\left[i\int^r K_1(r)dr\right] + B\exp\left[-i\int^r K_1(r)dr\right]\right) \qquad (2)$$

For an incident wave the constant B is given and determined from the continuity condition for B_r on the boundary at r=a. Near the resonance Eq.(1) takes the form

$$F_{\mathcal{J}\mathcal{J}} + K_1^2(\mathcal{J})F = 0, \qquad K_1^2(\mathcal{J}) \approx \lambda/\mathcal{J} + \alpha^2/\mathcal{J}^2. \qquad (3)$$

Here $\mathcal{J}$ is the dimensionless distance from the point r_0.

$$\alpha^2 = \frac{K_z^2 B_r^2}{4\pi^2}\Big|_{r=r_0}, \quad \lambda = \frac{B_\varphi K_z^2 r}{\pi^2 \Omega}\left(B_\varphi' + \frac{B_\varphi}{r}\right)\Big|_{r=r_0}, \quad \pi^2 = m^2\left(B_\varphi' - \frac{B_\varphi}{r}\right)^2_{r=r_0}.$$

$\Omega \ll 1$.

Solution for b_r

$$b_r = a\,H_{id}^{(1)}(2\sqrt{\lambda\mathcal{J}}) + b\,H_{id}^{(2)}(2\sqrt{\lambda\mathcal{J}}). \qquad (4)$$

$H_{id}^{(1)(2)}$ are the Hankel functions.

Using the asymptotic behavior of $H_{id}^{(1)(2)}$ (1), (2) and substituting for $\mathcal{J}$ in (2) one can "sew" Eqs. (2) and (4). The point $\mathcal{J} = 0$ is the branch point for (4). However, taking into account finite conductivity $\mathcal{J} - i\delta$ $(\delta \ll 1)$ should be substituted for $\mathcal{J}$, this indicates a way to turn the beginning of the coordinates. By turning the point J=0 below we obtain a=R=0. As is seen the reflected wave is absent. If one estimates the dissipation energy power

$$Q = \frac{1}{\sigma}\int_0^a 2\pi |\vec{j}|^2 r\,dr \qquad (5)$$

it appears that the integral in (5) diverges. This shows that the energy release is not zero. To determine Q one should take into account the finite plasma electrical conductivity. Then it is not difficult to write the following equation instead of (3)

$$\eta^2 b_r^{(VI)} + 2\eta\mathcal{J} b_r^{(IV)} + 3\eta b_r^{(III)} + b_r^{(II)}(\mathcal{J}^2 + \eta\lambda) + b_r^{(I)}\mathcal{J} + b_r(\lambda\mathcal{J} + \alpha^2) = 0. \qquad (6)$$

In this case

$$\eta = i\Omega/2R_m, \quad R_m = \frac{4\pi\sigma\omega r_0^2}{c^2}, \quad \mathrm{Re}\,\eta = 0, \quad |\eta| \ll 1.$$

To obtain an accurate equation (6), $\mathcal{J}$ should be substituted for $\mathcal{J} - \eta K_{\parallel}^2$ where $K_{\parallel}^2 = m^2 + k_z^2 r_0^2$.

Using the contour Laplace transrormation in Eq.(6) one can determine (see, for example, /4/ expressions for b_r at $\eta \to 0$. This solution is found to satisfy the required damping conditions at infinity. This solution on the positive part of the real axis takes the from (4), while on the negative part of the real axis, the solution involves Exp. (4) and an additional term describing local Alfven oscillations $a)$ $\mathcal{J}>0$, $b_2 = -2i\sqrt{\pi}\, ch\frac{\pi\alpha}{2}(\lambda\mathcal{J})^{-1/4} exp(-2i\sqrt{\lambda\mathcal{J}} + i\pi/4)$

$b)$ $\mathcal{J}<0$, $b_2 = -2i\sqrt{\pi}\, ch\frac{\pi\alpha}{2}(\lambda|\mathcal{J}|)^{-1/4} exp(-2\sqrt{\lambda|\mathcal{J}|} + i\pi/2) -$

$- e^{-i3\pi/8}|\eta/\mathcal{J}^3|^{1/4} exp(\sqrt{2}/3(i-1)|\frac{\mathcal{J}^3}{2}|^{1/2}\left[f(\alpha,\mathcal{J},\eta,\lambda) + e^{-\frac{3}{4}\pi\alpha/4} f^*(\alpha,\mathcal{J},\eta,\lambda)\right]$

$$f(\alpha,\mathcal{J},\eta,\lambda) = \lambda^{i\alpha/2}\frac{\Gamma(i\alpha/2-1)}{\Gamma^2(i\alpha-1)} exp\left(\frac{i\alpha}{2}\ln|\eta/\mathcal{J}| + \frac{3\pi\alpha}{8}\right) \qquad (7)$$

where $f^*(\alpha,\mathcal{J},\eta,\lambda)$ is the value complex conjugated with $f(\alpha,\mathcal{J},\eta,\lambda)$

The term represents the wave propagating along the negative axis from point J=0 towards increasing $|J|$. This is a damping wave. Solution (7) is not valid for $|\mathcal{J}| < |\eta|^{1/3}$. When $|J| < |\eta|^{1/3}$ this term is related with J and η is through $S=J/\eta^{1/3}$ Therefore,

$$Q \sim \frac{1}{\sigma|\eta|}\int_0^\infty d\alpha\left(\frac{d^2b_2}{ds^2}\right)\left(\frac{d^2b_2}{ds^2}\right)^* \qquad (8)$$

Since $|\eta| \sim 1/\sigma$, Q is independent of σ due to the resonance. Therefore, there is no reflected wave, and Q is independent of σ

A perturbation in the form of a Alfven wave when it is near the resonance gives rise to local oscillations of the magnetic field. These Ohmically damped local waves propagate along an equilibrium field $\vec{B}_0$, they rapidly oscillate and their amplitude decreases as they remove from the resonance surface $r=r_0$. The given perturbation propagating from the plasma boundary near the resonance becomes "dissipative". Near the resonance point, the amplitude of axial and azimuthal current components increase rapidly. As a result, a peculiar skin-layer arises. A characteristic dimension at which "sewing" of solutions takes place allow determination of the order of this layer width.

$$\Delta r \sim r_0\left(R_m\frac{d\ln\omega_A(r)}{d\ln r}\right)^{-1/3}_{r=r_0} \qquad (9)$$

The absence of a reflected wave as well as formation of an anomalous internal skin layer in which the oscillations damp show that the energy should be intensively absorbed near the resonance point.

It should be pointed out that when the energy is absorbed completely Q should not depend on the other plasma parameters, in particular, on the characteristic nonuniformity of the magnetic field as α well. Unfortunately, this complicated problem cannot be accurately solved analytically. Nevertheless, the above analysis shows that plasma can be heated under the condition of the resonance described, and the phenomenon of resonance absorption of the wave in a plasma with distributed current is of interest for plasma heating experiments in the tokamak-type systems as well as for experiments on plasma confinement by the travelling wave field. The presence of the resonance point stabilizes perturbations excited randomly in plasma /5/.

Acknowledgement. The author expresses his deep gratitude to Dr.E.P.Velikhov for his interest to the work.

References:

1. В.Д. Шафранов - "Физ. плазмы и проблема управ. термоядерного синтеза" т.IУ Москва (I958)

2. T.H.Stix - "The theory of plasma waves".

3. А.В. Лонгинов, К.Н. Степанов - препринт АН УССР и Физ.-Тех. Инст. Харьков (I972)

4. W.Wasow - Ann. of Math. 58 222 /1953/.

5. А.В. Тимофеев - УФН т.I02 в.2 (I970).

STABILIZATION OF VOLUME FLUTE MODES IN MIRROR MACHINES BY THE ELECTRODE FEEDBACK SYSTEM

V.V.Arsenin

I.V.Kurchatov Institute of Atomic Energy
Moscow, USSR

A b s t r a c t.

Volume flute oscillations of a finite plasma cylinder are investigated. It is shown that the instability can be suppressed by the feedback system which controles the perturbation field outside the magnetic mirrors.

The experiments on rarefied plasmas performed for last years [1-3] demonstrated a possibility of feedback suppression of the flute instability in mirror machines. A feedback system establishes special boundary conditions for the perturbation field outside the side surface of the plasma cylinder. The stabilization occured for large-scale surface waves. Volume flute modes (which oscillate in the r-direction) are unsensitive to boundary conditions on the cylindrical surface. Therefore these modes are not to be stabilized by side electrodes. In this paper we show that it is possible to stabilize volume modes controlling the perturbation field outside the magnetic mirrors. It is necessary to suppress only a finite number of large-scale modes (the short waves are stabilized by the finite Larmor radius effect). Therefore the hydromagnetic stability without the "minimum-B" can be achived when the plasma is surrounded by a finite number of the electrodes with controlled potentials.

For the sake of brevity, we use a plane slab model. The plasma of a concentration n(x) occupies the region $0 \leq x \leq a$, $|z| \leq \ell$. The magnetic field $\vec{B} \parallel z$ is uniform ($\beta \ll$

$\ll 1$). There is a "gravitational" force $m_i g$ in x-direction. It gives rise to the ion drift $v_y = \frac{g}{\omega_{Bi}}$, where ω_{Bi} is the ion cyclotron frequency. This force imitates a magnetic field inhomogeneity distabilization effect in mirror machines. Let us consider stability of this plasma against perturbations $A(x,z)\exp(iK_y y - i\omega t)$. The modes of interest can be described quasiclassically $A \sim \exp(iK_x x)$, $K_x \gtrsim \frac{1}{a}$.

Let us consider the most interesting case of a dense plasma $\omega_{oe} \gg \frac{c}{a}$, $\omega_{oi} \gg \omega_{Bi}$ (ω_{oe}, ω_{oi} denote electron and ion Langmuir frequencies respectively) and suppose, for the sake of simplicity, that the electrons are "cold": $\frac{v_{Te}}{\omega}\frac{\partial}{\partial z} \ll 1$. The electric field inside the plasma satisfies the equations /4/

$$\frac{\partial^2}{\partial z^2}E_y + \frac{\omega^2}{c^2}\left(1 + \frac{K_y^2}{K_\perp^2}\frac{g\varkappa}{\omega^2}\right)\varepsilon E_y = 0, \qquad (1)$$

$$E_x = \frac{K_x}{K_y}E_y, \qquad (2)$$

$$E_z = -\frac{i}{K_y}\frac{K_\perp^2 c^2}{\omega^2}\frac{\partial E_y}{\partial z} \qquad (3)$$

where $\varepsilon = \frac{\omega_{oi}^2}{\omega_{Bi}^2}$, $K_\perp^2 = K_x^2 + K_y^2$, $\varkappa = -\frac{1}{n}\frac{dn}{dx}$ $(\varkappa > 0)$. In vacuum regions ($b < |z| < d$) the electric field has a potential $\vec{E} = -\nabla\varphi$. Two boundary conditions at the plasma butt-end (both the tangential electric field and the normal component of the induction $(1 - \frac{\omega_{oe}^2}{\omega^2})E_z$ are continuous) give the following dispersion equation for the symmetric ($E_y(Z) = E_y(-Z)$) oscillations:

$$\frac{K_\perp^2 c^2}{\omega^2}\lambda\, tg\,\lambda b = \frac{1}{\varphi}\frac{\partial\varphi}{\partial z}\Big|_{z=b+0} \qquad (4)$$

where $\lambda^2 = \frac{\omega^2}{c^2}\left(1 + \frac{K_y^2}{K_\perp^2}\frac{g\varkappa}{\omega^2}\right)\varepsilon$. For the flute-like perturbations ($|\lambda|b \ll 1$) this equation simplifies to

$$\varepsilon\left(K_\perp^2 + K_y^2\frac{g\varkappa}{\omega^2}\right) = \frac{1}{b}\frac{\partial \ln\varphi}{\partial z}\Big|_{z=b+0}. \qquad (5)$$

The value of $\frac{\partial \ln\varphi}{\partial z}\Big|_{z=b+0}$ depends on the boundary conditions for φ at the vacuum region boundaries $z = \pm d$.

If there are metallic surfaces at $z = \pm d$

$$\varphi|_{z=\pm d} = 0 \qquad (6)$$

we have $\left.\frac{\partial \ln \varphi}{\partial z}\right|_{z=b+0} = -\kappa_\perp \operatorname{cth} \kappa_\perp (d-b)$. Taking into account $\varepsilon \gg 1$ we find (for the typical case $k_\perp(d-b) \gtrsim 1$, $k_\perp b \gtrsim 1$) the instability $\omega^2 = -\frac{\kappa_y^2}{\kappa_\perp^2} g\varkappa$.

We'll show that this instability can be suppressed by a feedback system which establishes the boundary conditions different from the condition (6). We suppose that there is a set of electrodes at the planes $z = \pm d$ and the potential distribution is

$$\varphi(x, y, \pm d) = \Delta(\kappa_x, \kappa_y, \omega) \cdot \varphi(x, y, \pm b) \qquad (7)$$

where $|\Delta| \gg \operatorname{ch} k_\perp (d-b)$. Eq. (5) becomes

$$\varepsilon\left(\kappa_\perp^2 + \kappa_y^2 \frac{g\varkappa}{\omega^2}\right) = \frac{\kappa_\perp \Delta}{b \operatorname{sh} \kappa_\perp (d-b)} . \qquad (8)$$

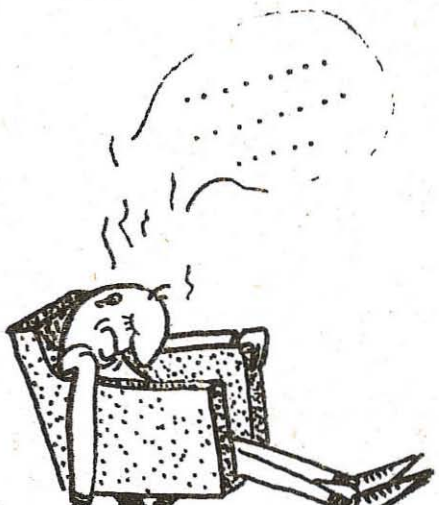
Let us consider for instance $\Delta = \frac{\kappa_y \Delta_0}{\omega}$ where Δ_0 is a real constant. (Such a condition can be realized if the electric field E_y measured at the plasma butt-end is integrated, amplified and the resulting signal is put to the suitable electrode.) In this case Eq. (8) becomes quadratic. The perturbation is stable if

$$|\Delta_0| > 2\varepsilon b \sqrt{g\varkappa}\, \operatorname{sh} \kappa_\perp (d-b). \qquad (9)$$

References

1. V.V.Arsenin, V.A.Zhiltsov, V.A.Chuyanov. Plasma Physics and Controlled Nuclear Fusion Research, IAEA, Vienna, 1969, vol.II, 515.
2. M.J.Church, V.A.Chuyanov, E.G.Murphy, M.Petravic, D.R.Sweetman, E.Thompson. III European Conference on Controlled Fusion and Plasma Physics, Utrecht, June 1969. Contributions, p.12.
3. V.A.Chuyanov, E.G.Murphy. JETP Letters, 13, 553 (1971).
4. A.B.Mikhailovskii. Plasma Physics Problems, vol.3, p.141. Gosatomizdat, 1963.

3.8. STABILITY (THEORY)



SIXTH EUROPEAN CONFERENCE ON CONTROLLED FUSION AND PLASMA PHYSICS (MOSCOW USSR)
(1973)

LOW FREQUENCY STABILITY THEORY OF AXISYMMETRIC TOROIDAL PLASMAS

J.W. Connor and R.J. Hastie,
UKAEA Research Group, Culham Laboratory, Abingdon, Berkshire, England

1. Introduction

The kinetic theory of low frequency electrostatic modes of short transverse wavelength and long parallel wavelength ($k_\perp a_i \sim 1$, $k_\parallel a_i \sim \epsilon$ where a_i is the ion larmor radius, and ϵ labels the small parameter a_i/L where L is a typical equilibrium scale length) is well understood for plasmas confined by magnetic fields which have closed lines of force. Difficulties arise, however, when the equivalent analysis is attempted for configurations in which the magnetic field lines form surfaces, and magnetic field shear is present, i.e. for the investigation of flute instabilities, drift waves and short wavelength trapped particle modes in Stellarators, Tokamaks or Levitrons.

In this paper we consider axisymmetric toroidal geometry and for simplicity consider vacuum magnetic fields. The problems encountered by previous treatments are essentially caused by the conflict between the periodicity constraints implied by the toroidal geometry and the $k_\parallel a_i \sim \epsilon$ condition, in strongly sheared magnetic fields. A resolution of this conflict is proposed and a consistent solution of the Vlasov-Poisson equations is obtained.

2. (a) The Equilibrium

The equilibrium to be considered is that of a low β plasma in an axisymmetric vacuum magnetic field, having toroidal and poloidal components given by

$$\underset{\sim}{B}_T = I/R \, \hat{\underset{\sim}{e}}_\theta \tag{1}$$

$$\underset{\sim}{B}_p = \nabla\chi = \nabla\psi \times \nabla\theta \tag{2}$$

where (ψ, χ, θ) form an orthogonal set of coordinates, ψ being the poloidal magnetic flux, θ the angle about the axis of symmetry, while R is the distance to that axis and I is a constant.

We denote the rotational transform by ι where $\iota = \frac{1}{q}$ and

$$q = \oint \nu d\chi \quad \text{with} \quad \nu = B_T/RB_p^2$$

(b) The Perturbation

Previous analysis [1,2,6,7] has taken the general form

$$\Phi = \Phi_o(\psi, \chi) e^{i \frac{\ell}{\epsilon} [\theta - \int^{\chi} \nu d\chi] + i \frac{S(\psi)}{\epsilon}} \tag{3}$$

(where ϵ is included to label the large terms) for the perturbed

electrostatic potential, since the phase factor is strictly constant along a field line and $k_{\parallel} a_i \sim \epsilon$ is thus assured. However periodicity of $\Phi(\chi)$ requires that

$$\Phi_o(\chi + \chi_o) e^{i \frac{\ell}{\epsilon} \oint \nu d\chi} - \Phi_o(\chi) = 0 \tag{4}$$

and hence after differentiation with respect to ψ and substitution

$$\left[\frac{1}{\Phi_o} \frac{\partial}{\partial \psi} \Phi_o \right] + i \frac{\ell}{\epsilon} \frac{\partial q}{\partial \psi} = 0 \tag{5}$$

where $[A] \equiv A(\chi + \chi_o) - A(\chi)$ is the jump in $A(\chi)$ and $\chi_o \equiv \oint d\chi$. Since Φ_o varies on the equilibrium scale, the periodicity condition (5) can only be satisfied if $\partial q / \partial \psi \sim \epsilon$. To avoid this restriction we shall take a slightly different form for the potential Φ , given by

$$\Phi = \Phi_o(\psi, \chi) e^{i \frac{\ell}{\epsilon} [\theta - \int^{\chi} (\nu + G) d\chi] + i \frac{S(\psi)}{\epsilon}} \tag{6}$$

where $G = G(\psi, \chi)$ is an arbitrary function which must meet the constraints imposed by periodicity: namely, taking $\Phi_o(\chi)$ periodic to remove the necessity for jump conditions, we require

$$\frac{\ell}{\epsilon} \oint (\nu + G) d\chi = 2\pi m \tag{7}$$

and consequently

$$\frac{\partial}{\partial \psi} \oint (\nu + G) d\chi = 0 \tag{8}$$

both of which conditions play an important role in the following analysis.

Having ensured periodicity we return to the small $k_{\parallel} a_i$ condition to determine what further constraints must be imposed on $G(\psi, \chi)$. Taking $k_{\parallel} \sim (\underset{\sim}{B} . \nabla \Phi)/(\Phi B)$ it follows that

$$k_{\parallel} \sim - \frac{\ell}{\epsilon} \frac{B^2 p}{B} G(\psi, \chi) \tag{9}$$

and we must take

$$G(\psi_o, \chi) = \epsilon G_o(\chi) \tag{10}$$

and consider modes localised around $\psi = \psi_o$.

Turning now to the form of the perturbed distribution function

$$\delta f = f e^{i \frac{\ell}{\epsilon} [\theta - \int^{\chi} (\nu + G) d\chi] + i \frac{S(\psi)}{\epsilon}} \tag{11}$$

it follows from equation (9) that although the longitudinal wavelength of the modes is long, $k_{\parallel}$ is nevertheless a rapidly varying function of ψ , so that since f will be found to be a functional of $k_{\parallel}$ we must take

$$f = f\left(\frac{\psi}{\epsilon}, \chi, \mu, \kappa, \varphi, \sigma\right) \tag{12}$$

Physically this rapid variation of $k_{\parallel}(\psi)$ means that there will be

finite larmor radius, and finite banana width averaging effects on $k_{\parallel}$ as well as on $k_{\perp}$.

(c) Solution for f

Substituting the forms (6) and (11) for Φ and δf into the linearised Vlasov equation and expanding f in powers of ϵ, the solution for f_o is obtained by following the averaging procedure of Hastie and Taylor[3] or Rutherford and Frieman[4]. The analysis is complicated by the rapid variation of f as a function of ψ, but an explicit solution for f_o can nevertheless be obtained.

(d) Applications

Taking F_o to be the Maxwellian distribution

$$F_{oj} = n(\psi)\left(\frac{m_j}{2\pi T_j}\right)^{3/2} e^{-m_j \frac{\kappa}{T_j}} \qquad (13)$$

we make one of two fundamental approximations corresponding to $\frac{\omega}{\omega_b} \gg 1$ and $\frac{\omega}{\omega_b} \ll 1$, where ω_b is the bounce frequency. For $\frac{\omega}{\omega_b} \gg 1$, and provided that $\Phi_o(\chi)$ is not strongly localised in χ [i.e. not within a range of order $\left(\frac{\omega_b}{\omega}\right)$], the charge density ρ for species j reduces to

$$\rho_j \simeq -\frac{e_j^2 n}{T_j}\frac{\omega_*}{\omega}\Phi_o - \frac{e_j^2 n}{T_j}\left(1-\frac{\omega_*}{\omega}\right)\left\{b + \frac{T_j}{e_j}\frac{\ell B_p^2}{\omega}\left[\frac{B^2}{B_p^2}\frac{\partial}{\partial\psi}\left(\frac{1}{B^2}\right) - RB_T\frac{\partial}{\partial\chi}\left(\frac{1}{B^2}\right)\int^{\chi}(\nu'+G')\right]\right.$$
$$\left. + \frac{T_j}{e_j}\frac{B_p^2}{\omega}RB_T S'\frac{\partial}{\partial\chi}\left(\frac{1}{B^2}\right) + \frac{T_j}{m_j\omega^2}B_p^2\left[\frac{\partial}{\partial\chi} - i\ell(G_o+xG')\right]\frac{B_p^2}{B^2}\left[\frac{\partial}{\partial\chi} - i\ell(G_o+xG')\right]\right\}\Phi_o \qquad (14)$$

where $\omega_* = \frac{T_j}{e_j}\ell\frac{n'}{n}$, $b = \left(\frac{T_j}{m_j\omega_c^2}\right)\left\{(RB_p)^2\left[S' - \ell\int^{\chi}(\nu'+G')\right]^2 + \left(\frac{\ell B}{RB_p}\right)^2\right\}$

$\omega_c = \frac{e_j B}{m_j}$, the prime denotes differentiation with respect to ψ and $x = \frac{(\psi-\psi_o)}{\epsilon}$.

In addition to the $\frac{\omega_b}{\omega} \ll 1$ approximation we have assumed

$$k_{\perp} a_j \ll 1 \; ; \quad \frac{k_{\perp} v_d}{\omega} \ll 1 \; ; \quad \frac{k_{\parallel} v_{\parallel}}{\omega} \ll 1 \; .$$

This expression for $\rho_j\left(\frac{\omega}{\omega_b} > 1\right)$ differs from that normally encountered in the appearance of the arbitrary phase function G and its derivative G'. One consequence of the appearance of G' in equation (14) is that the effective curvature for flute modes in the $\omega > \omega_{be}$ regime, found by Rutherford et al. [1] to be V**, becomes functionally dependent on G', and takes the value V** only for one particular choice of G'. The

particular choice of G' which gives rise to V^{**} is in fact the one which minimises the shear stabilising term subject to the constraint (8). In the $\omega < \omega_b$ regime a complicated expression for ρ_j is obtained containing finite banana width averaging of $k_{\parallel}$ and $k_{\perp}$. The geodesic drifts average to zero in this limit so that the analogue of the $\int(\nu' + G')$ term in (14) is absent. In the $\omega < \omega_{bi}$ regime the effective curvature for flute modes is found to be V^{++} (as in (1)), but the origin of the passing particle correction V'' now emerges as an F.L.R. averaging of $k_{\parallel} v_{\parallel}$ over a transit. In the intermediate frequency range $\omega_{bi} < \omega < \omega_{be}$, the arbitrary function G' appears in the ion geodesic drift term and for appropriately chosen G' contributes an additional destabilising term. The flute modes are readily stabilised by weak shear but the foregoing observations suggest that the charge separation caused by geodesic drifts might drive a trapped particle instability. In the intermediate frequency range the analysis of the trapped electron drift instability [5 - 7] is modified by the coupling of the phase G' to the ion geodesic drift. For this mode we obtain an equation similar to that found by Adam, Laval and Pellat [6, 7] but with their aperiodic coefficients replaced by periodic coefficients depending on the arbitrary phase function G'. The new terms do not themselves cause instability but must modify the frequency and eigenfunction and consequently the growth rate.

3. Conclusion

A rigorous treatment of electrostatic instabilities of short transverse wavelength in strongly sheared axisymmetric toroidal systems has been developed. This resolves the conflict between the double periodicity implicit in toroidal geometry and the $k_{\parallel} a_i \sim O(\epsilon)$ property of flute and trapped particle modes, and drift waves. Preliminary investigation indicates the possible importance of the geodesic drifts for trapped particle modes in the intermediate frequency ($\omega_{bi} < \omega < \omega_{be}$) regime.

REFERENCES

[1] P. Rutherford, M. Rosenbluth, W. Horton, E. Frieman and B. Coppi, in Plasma Physics and Controlled Nuclear Fusion Research (Proc. 3rd. Int. Conf. Novosibirsk, 1968), 1, IAEA, Vienna (1969) 367.
[2] E. Jamin, Thesis, Princeton University (1971).
[3] J.B. Taylor and R.J. Hastie (1968) Plasma Physics 10, 479.
[4] P.H. Rutherford and E.A. Frieman (1968) Phys. Fluids 11, 569.
[5] B.B. Kadomtsev and O.P. Pogutse, Dokl. Akad. Nauk. SSSR 186 (1969), 553.
[6] J.C. Adam, G. Laval and R. Pellat, in Plasma Physics and Controlled Nuclear Fusion Research (Proc. 4th. Int. Conf., Madison, 1971) 2, IAEA, Vienna (1971) 539.
[7] J.C. Adam, G. Laval and R. Pellat (1973) Nuclear Fusion 13, 47.

THE INFLUENCE OF HIGH-FREQUENCY ELECTROSTATIC OSCILLATIONS ON THE LOW-FREQUENCY PLASMA INSTABILITY

V. Kopecký

Institute of Plasma Physics
Nademlýnská 600, Prague 9, Czechoslovakia

Abstract. The influence of the principal mode of h.f. electrostatic oscillations on the flute instability of an inhomogeneous plasma is studied. Instability conditions in a collisional as well as collisionless plasma are obtained and it is demonstrated that in certain circumstances the beam-excited h.f. oscillations can stabilize the flute instability.

In experiments on beam-plasma interaction, predominantly the oscillations corresponding to the so-called lower branch of electrostatic waves with frequencies $\Omega < \omega_{pe}$ are excited, if the plasma density is not too high ($\omega_{pe} < \omega_{ce}$, ω_{pe} is the electron plasma frequency, ω_{ce} is the electron cyclotron frequency). In the direction transverse to the magnetic field, these oscillations constitute the principal mode, i.e. their transverse wave-length is comparable to the transverse dimension of the plasma. These oscillations have a sufficiently regular character, occur on the frequency in the form of bursts lasting several reciprocal increments and their amplitude reaches about several hundred Volts/cm [1]. The question therefore arises, how such intense high-frequency oscillations influence the plasma stability with respect to low-frequency disturbances.

With the h.f. field inhomogeneity the high-frequency forces are connected [2] which cause the electrons to drift across the magnetic field and can therefore lead to low-frequency instability in dependence on the drift direction [3, 4]. We shall discuss the stability conditions with respect to the simplest disturbances having the wave-vector perpendicular to the magnetic field in a simple plasma model which simulates to a certain extent the situation in beam-plasma experiments.

Consider a cold plasma which is inhomogeneous in the y direction in a magnetic field $\vec{H} \parallel \vec{z}$. We shall assume that in this plasma a travelling electrostatic wave with frequency $\Omega < \omega_{pe\,max}$ is excited which is a principal mode in the y-direction, is independent of the x-coordinate and its amplitude is independent of the z-coordinate. We shall restrict ourselves to the study of the instability of electrostatic flute oscillations ($k_z = 0$) with frequency $\omega \ll \omega_{ci}$ (ω_{ci} is the ion cyclotron frequen-

cy). Then the effect of the h.f. wave can be described by means of averaged h.f. forces and the influence of the h.f. field on the ions can be neglected. For the averaged motion of the electrons and ions we shall therefore use the MHD equations in the form

$$\frac{\partial n_{e,i}}{\partial t} + div\left(n_{e,i}\vec{v}_{e,i}\right) = 0 , \tag{1}$$

$$\frac{e}{m}\left(\nabla\varphi - \frac{1}{c}\left[\vec{v}_e\vec{H}\right]\right) + \frac{1}{m}\vec{F} = \frac{\vec{v}_e}{\tau_e} , \tag{2}$$

$$\frac{\partial\vec{v}_i}{\partial t} + \left(\vec{v}_i\nabla\right)\vec{v}_i = \frac{e}{M}\left(-\nabla\varphi + \frac{1}{c}\left[\vec{v}_i\vec{H}\right]\right) - \frac{\vec{v}_i}{\tau_i} , \tag{3}$$

where τ_e , τ_i are the mean time intervals between the collisions of the electrons or the ions, respectively, with the neutrals. In Eq. (2) we have neglected the electron inertia, which is justified in the frequency-range in question. The averaged high-frequency force $\vec{F}$ is equal [2]:

$$\vec{F} = -\frac{1}{8\pi}\nabla\left\{\frac{1}{n}\left(\delta_{\alpha\beta} - \varepsilon_{\alpha\beta}\right)\left\langle\tilde{E}_\beta\tilde{E}_\alpha\right\rangle\right\} . \tag{4}$$

$\hat{\varepsilon} = \varepsilon_{\alpha\beta}$ is the cold plasma dielectric tensor and the symbol $\langle\ldots\rangle$ denotes the averaging not only over the h.f. field period, but also over the stochastic ensemble of h.f. oscillation bursts. The frequency Ω , the wave-vector K_z and the h.f. field gradients can thus be interpreted as some mean quantities.

For the h.f. field $\vec{\tilde{E}} = -\nabla\phi\left(\phi = \phi_0(y)\ exp\left\{-i\Omega t + iK_z z\right\}\right)$ we shall use the equation

$$div\left(\hat{\varepsilon}\vec{\tilde{E}}\right) = 0. \tag{5}$$

In a steady state, the electrons are acted upon by an averaged h.f. force (4), (5)

$$F_{oy} = -\frac{e^2}{2m\Omega^2}\frac{d\phi_o}{dy}\frac{\left(\omega_{ce}^2 + 2\omega_{pe}^2 - 2\Omega^2\right)K_z^2\phi_o + \frac{\Omega^2}{\omega_{ce}^2 - \Omega^2}\frac{d\omega_{pe}^2}{dy}\frac{d\phi_o}{dy}}{\omega_{ce}^2 + \omega_{pe}^2 - \Omega^2} \tag{6}$$

If we restrict ourselves to the case $\omega_{pe\ max}^2 < \omega_{ce}^2/2$, then $F_{oy} > 0$ everywhere, on condition that ω_{pe}^2 and ϕ_o are smooth functions with one maximum at $y = 0$. For the perturbation of the h.f. force we obtain, again using Eqs. (4) and (5), the expression

(7) $$\vec{F}_1 = \frac{\nabla n_{e1}}{n_o} Q = -\frac{\nabla n_{e1}}{n_o} \frac{e^2\phi_o^2}{2m\Omega^2} \frac{\omega_{pe}^2}{\Omega^2} \frac{K_z^4 \frac{\omega_{ce}^2(\omega_{ce}^2-\Omega^2)}{\omega_{ce}^2+\omega_{pe}^2-\Omega^2} + \frac{k_y^2\lambda^2\Omega^4}{\omega_{ce}^2-\Omega^2}}{(k_x^2+k_y^2)(\omega_{ce}^2+\omega_{pe}^2-\Omega^2)},$$

where $\lambda^{-1} = (d\ln\phi_o/dy)^{-1}$ is the characteristic dimension of the h.f. field inhomogeneity.

On condition that in the steady state no transverse electric current flows through the plasma, we obtain from the linearized equations (1)–(3), using the Poisson equation and Eqs. (6), (7), in the WKB approximation ($k_y \gg \varkappa = d\ln n_o/dy$) the following dispersion relation

(8) $$(k_x^2+k_y^2)\left(1+\frac{\omega_{pi}^2}{\omega_{ci}^2}\right) = \frac{\omega_{pi}^2}{\omega_{ci}} \left\{ \frac{\varkappa k_x - i(k_x^2+k_y^2)/\omega_{ci}\tau_i}{\omega + \alpha k_x v_{xo} + \alpha k_y v_{xo}/\omega_{ci}\tau_i} - \right.$$
$$\left. - \frac{\varkappa k_x + i(k_x^2+k_y^2)/\omega_{ce}\tau_e}{\omega - k_x v_{xo} + k_y v_{xo}/\omega_{ce}\tau_e - Q[\varkappa k_x + i(k_x^2+k_y^2)/\omega_{ce}\tau_e]/m\omega_{ce}} \right\}.$$

Here $v_{xo} = -F_{oy}/m\omega_{ce}$ and $\alpha = m\tau_i/M\tau_e$ is a parameter which is usually much smaller than one. We shall discuss two extreme case, namely A) the frequency $\omega \ll 1/\tau_i$, B) $\omega \gg 1/\tau_e$ i.e., a collisionless plasma, $\tau_e \to \infty$, $\tau_i \to \infty$. In the first case we obtain from Eq. (8) the condition for the onset of a drift-dissipative instability in the form

(9) $$\lambda\varkappa k_x^2 (k_x^2+k_y^2)\left[(\omega_{ce}^2+2\omega_{pe}^2-2\Omega^2)K_z^2 + \frac{\Omega^2\omega_{pe}^2}{\omega_{ce}^2-\Omega^2}\lambda\varkappa\right] >$$
$$> \left[\varkappa^2 k_x^2 + \frac{(k_x^2+k_y^2)^2}{\omega_{ce}\tau_e\omega_{ci}\tau_i}\right] \frac{\omega_{pe}^2}{\Omega^2}\left[K_z^4 \frac{\omega_{ce}^2(\omega_{ce}^2-\Omega^2)}{\omega_{ce}^2+\omega_{pe}^2-\Omega^2} + k_y^2\lambda^2\frac{\Omega^4}{\omega_{ce}^2-\Omega^2}\right]$$

The region of instability determined by Eq. (9) is schematically shown in Fig. 1, where

$$k_{xkrA}^2 \simeq \frac{\varkappa}{\lambda}\frac{\omega_{pe}^2}{\Omega^2}\frac{K_z^4\omega_{ce}^2(\omega_{ce}^2-\Omega^2)}{(\omega_{ce}^2+\omega_{pe}^2-\Omega^2)\left[(\omega_{ce}^2+2\omega_{pe}^2-2\Omega^2)K_z^2 + \frac{\Omega^2\omega_{ce}^2\lambda\varkappa}{\omega_{ce}^2-\Omega^2}\right]}$$

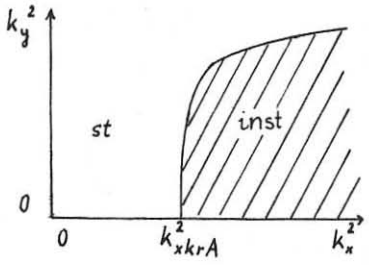


Fig. 1

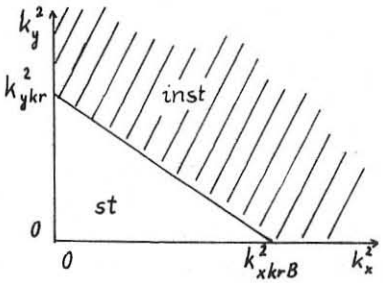


Fig. 2

In the second case, that of a collisionless plasma, we obtain from Eq. (8) the instability condition in the form

$$k_y^2 K_z^2 \frac{\lambda}{\varkappa} \frac{\omega_{ce}^2 + 2\omega_{pe}^2 - 2\Omega^2}{\Omega^2} > K_z^4 \frac{\omega_{ce}^2 \omega_{pe}^2 (\omega_{ce}^2 - \Omega^2)}{\Omega^4(\omega_{ce}^2 + \omega_{pe}^2 - \Omega^2)} -$$

(10)

$$-k_x^2 \left\{ \frac{\lambda^2 \omega_{pe}^2}{\omega_{ce}^2 - \Omega^2} + \frac{\lambda}{\varkappa} K_z^2 \frac{\omega_{ce}^2 + 2\omega_{pe}^2 - 2\Omega^2}{\Omega^2} \right\}.$$

This condition determines the region of unstable k_x and k_y which is schematically depicted in Fig. 2. Here

$$k_{xkrB}^2 = \frac{K_z^4 \omega_{ce}^2 \omega_{pe}^2 (\omega_{ce}^2 - \Omega^2)/\Omega^4(\omega_{ce}^2 + \omega_{pe}^2 - \Omega^2)}{\frac{\lambda^2 \omega_{pe}^2}{\omega_{ce}^2 - \Omega^2} + \frac{\lambda}{\varkappa} K_z^2 \frac{\omega_{ce}^2 + 2\omega_{pe}^2 - 2\Omega^2}{\Omega^2}}$$

(11)

$$k_{ykrB}^2 = K_z^2 \frac{\varkappa}{\lambda} \frac{\omega_{ce}^2 \omega_{pe}^2 (\omega_{ce}^2 - \Omega^2)}{(\omega_{ce}^2 + \omega_{pe}^2 - \Omega^2)\Omega^2(\omega_{ce}^2 + 2\omega_{pe}^2 - 2\Omega^2)}.$$

If the values k_{xkr} and k_{ykr} are much larger that $\varkappa$, it is obvious that a stability region for long wave-length oscillations exists. For this to occur it is necessary, on condition that the coefficients involving characteristic frequencies are of the order of unity, that $K_z \gg \varkappa$, i.e. waves with the frequency sufficiently close to $\omega_{pe\ max}$ must be excited. Thus, in this case, the h.f. field can stabilize the gravitational instability. When an effective gravitational field ($g_y = T_i/MR$, T_i is the ion temperature and R is the radius of curvature of the magnetic lines of force) is introduced into Eq. (3), the stability condition in a collisionless plasma is obtained in the form

(12) $$e^2\phi_0^2 > 2 \frac{k_x^2 + k_y^2}{K_z^2} \frac{1}{\varkappa R} \frac{T_i m v_{fr}^2}{1 - \Omega^2/\omega_{ce}^2}.$$

Here we have assumed that $K_z \simeq \omega_{pe}/v_{fr}$, v_{fr} denoting the electron beam velocity. Thus, at not too high ion temperature, the long wave-length flute oscillations can be stabilized.

References:

[1] K. Jungwirth et al.: Plasma Phys. 15 (1973) in press

[2] L.P. Pitaevskii: Zh. Eksp. Teor. Fiz. 39 (1960), 1450

[3] V. Kopecký: Plasma Phys. 10 (1968), 609

[4] R.A. Demirkhanov et al.: Physica 47 (1970), 610

CANONICAL METHOD FOR CALCULATION OF ELECTROSTATIC PLASMA WAVES AND ENERGY-MOMENTUM CONSERVATION LAWS

J. Lacina

Institute of Plasma Physics, Czech. Academy of Sciences

Prague - Czechoslovakia

Abstract: Using a method of canonical variables a set of equation for the nonlinear evolution of wave amplitudes and of macroscopic quantities is derived for a collisionless plasma; this set of equations is suitable for numerical computor calculations of plasma waves and instabilities. It is shown that the equation for the complex wave amplitudes is equivalent to the energy-momentum conservation laws.

I. The starting equations are as follows

$$\frac{\partial f_\alpha}{\partial t} + \{f_\alpha, \mathcal{H}\} = 0, \qquad \mathcal{H} = \mathcal{H}_0 + e_\alpha \sum_m U_{0m}(t) e^{i\vec{k}_m \vec{x}}, \qquad \{\} = \text{Poisson bracket} \tag{1}$$

$$\mathcal{H}_0 = \frac{1}{2m}\left[\vec{p} - \frac{e}{c}\vec{A}\right]^2 + {}^{(e)}U(\vec{x}), \qquad \nabla^2 U = -4\pi \sum_\alpha e_\alpha \int f_\alpha \, d^3\vec{p};$$

here $\vec{A}(\vec{x})$, ${}^{(e)}U(\vec{x})$ define an arbitrary magnetic and scalar field. The initial non-equilibrium state of a plasma is given by initial particle distributions $f_\alpha(\vec{p}, \vec{x}; 0)$. The only restriction for these distributions is that they are to be periodic in the $\vec{x}$ space.

The time evolution of the wave amplitudes is given by the particle trajectories in the following way:

$$U_{0m}(t) = \frac{4\pi}{k_m^2 V} \sum_\alpha e_\alpha \int \exp\left[-i\vec{k}_m \vec{x}_\alpha(\vec{p}_0, \vec{x}_0; t)\right] f_\alpha(\vec{p}_0, \vec{x}_0; 0)\, d\phi_0 \tag{2}$$

$$V = \int d^3\vec{x}, \qquad \int\int d^3\vec{p}_0 \, d^3\vec{x}_0 \equiv \int d\phi_0$$

where the particle motion is given by canonical equations (3):

$$\vec{x}_\alpha(\vec{p}_0, \vec{x}_0; t), \qquad \vec{p}_\alpha(\vec{p}_0, \vec{x}_0; t), \qquad \dot{\vec{x}} = \frac{\partial \mathcal{H}_0}{\partial \vec{p}},$$

$$\vec{x}_\alpha(\vec{p}_0, \vec{x}_0; 0) = \vec{x}_0, \qquad \vec{p}_\alpha(\vec{p}_0, \vec{x}_0; 0) = \vec{p}_0, \qquad \dot{\vec{p}} = -\frac{\partial \mathcal{H}}{\partial \vec{x}}. \tag{3}$$

To obtain the amplitude equation (2) we have multiplied the Poisson equation of the set (1) by the orthogonal function $e^{-i\vec{k}\vec{x}}$ and have integrated over $\vec{x}$. Moreover, on the right-hand side of the Poisson equation we have transformed the canonical variables $\vec{x}$, $\vec{p}$ by means of the canonical transformation (3). As we may see from Eqs. (3), $\vec{x}_0$, $\vec{p}_0$ are particle initial values of $\vec{x}$, $\vec{p}$.

The set of Eqs. (2),(3) is suitable for a numerical solution by means of computors. As we can see, we only need to calculate the particle trajectories and the amplitudes from relatively simple Eqs. (2),(3). The distribution functions enter into the calculation only through the initial distributions; we need not calculate their time evolution. The derived Eqs. (2),(3), and also the equations for macroscopic quantities (8)-(10) admit to solve the particle trajectories in arbitrary useful canonical variables. For the magnetoactive plasma the canonical guiding center variables proves to be very convenient [1].

This method appears as a hybrid method between the particle simulation method (e.g. [2]) and the direct Vlasov's solutions (e.g. [3]).

II. The equivalency of the amplitude equation (2) to the energy-momentum conservation laws. Let us write Eq. (2) in the form

$$W_{Em}(t) + U^*_{on}(t) \sum_\alpha e_\alpha \int exp\left[-i\vec{k}_m \vec{x}_\alpha(t)\right] f_\alpha \, d\phi_0 = 0 \tag{4}$$

where

$$W_{E_m} \equiv \frac{1}{8\pi}\int\left[|E_m|^2 + |E^*_m|^2\right] d^3\vec{x} = \frac{k_m^2 |U_{om}|^2}{4\pi} \cdot V, \qquad W_E^{TOTAL} = \frac{1}{2}\sum_m W_{Em}$$

The expression W_{Em} determines the electric field energy of the m-th mode. Now, for the particle energy it holds

$$H^{(\alpha)}(t) = \int f_\alpha \mathcal{H}_0(\vec{p}_0, \vec{x}_0; t)\, d\phi_0, \qquad \dot{H}^{(\alpha)} = \int f_\alpha \{\mathcal{H}_0, e_\alpha U\}\, d\phi_0 = \sum_m \frac{1}{2}\dot{H}^{(\alpha)}_{on}$$

$$\dot{H}^{(\alpha)}_{on} = i e_\alpha \langle \vec{k}_m \dot{\vec{x}}_\alpha U^*_\alpha \rangle + c.c., \qquad \langle S \rangle \equiv \int f_\alpha(\vec{p}_0, \vec{x}_0; 0)\, S\, d\phi_0 \tag{5}$$

As follows from (5), $\dot{H}^{(\alpha)}_{on}$ is a change of the energy of α-particles due to the interaction with the m-th mode. Finally, for the time derivative of Eq. (4) we get

$$\dot{W}_{Em} + \sum_\alpha \dot{H}^{(\alpha)}_{on} = 0. \tag{6}$$

Hence, as follows from (6), the real part of Eq. (4) determines the energy conservation of the m-th mode.

For the kinetic momentum of α-particles it holds

$$\vec{\Pi}^{(\alpha)}(t) = m_\alpha \int f_\alpha \dot{\vec{x}}_\alpha(t)\, d\phi_0, \qquad \dot{\vec{\Pi}}^{(\alpha)} = {}^{(e)}\dot{\vec{\Pi}}^{(\alpha)} + {}^{(s)}\dot{\vec{\Pi}}^{(\alpha)}, \qquad {}^{(e)}\dot{\vec{\Pi}}^{(\alpha)} = m_\alpha \int f_\alpha \{\dot{\vec{x}}_\alpha, \mathcal{H}_0\}\, d\phi_0,$$

$${}^{(s)}\dot{\vec{\Pi}}^{(\alpha)} = m_\alpha \int f_\alpha \{\dot{\vec{x}}_\alpha, e_\alpha U\}\, d\phi_0 = \frac{1}{2}\sum_m {}^{(s)}\dot{\vec{\Pi}}^{(\alpha)}_{on}, \qquad {}^{(s)}\dot{\vec{\Pi}}^{(\alpha)}_{on} = i e_\alpha \langle \vec{k}_m U^*_m \rangle + c.c. \tag{7}$$

According to (7) the imaginary part of Eq. (4) expresses the conservation of particle momentum of the m-th mode; $\sum_{\alpha}^{(s)} \vec{\Pi}_{on}^{(\alpha)} = 0$. Note, that the total momentum is not conserved due to the external fields, in accordance with (7).

III. The space-time evolution of macroscopic quantities is determined by this method in the following way.

The particle density:

$$(8)\quad N^{(\alpha)}(\vec{x},t) = \int f_\alpha d^3\vec{p} = \sum_m N_m^{(\alpha)}(t) e^{i\vec{k}_m\vec{x}}, \qquad N_m^{(\alpha)} = \frac{1}{V}\int f_\alpha e^{-i\vec{k}_m\vec{x}_\alpha(t)} d\phi_0$$

The particle momentum:

$$(9)\quad \vec{\Pi}^{(\alpha)}(\vec{x},t) = m_\alpha \int f_\alpha \vec{v} d^3\vec{p} = \sum_m \vec{\Pi}_m^{(\alpha)}(t) e^{i\vec{k}_m\vec{x}}, \qquad \vec{\Pi}_m^{(\alpha)} = \frac{m_\alpha}{V}\int \dot{\vec{x}}_\alpha(t) e^{-i\vec{k}_m\vec{x}_\alpha(t)} f_\alpha d\phi_0$$

The particle energy:

$$(10)\quad H^{(\alpha)}(\vec{x},t) = \int \mathcal{H}_0 f_\alpha d^3\vec{p} = \sum_m H_m^{(\alpha)}(t) e^{i\vec{k}_m\vec{x}}, \qquad H_m^{(\alpha)} = \frac{1}{V}\int \mathcal{H}_0 e^{-i\vec{k}_m\vec{x}_\alpha(t)} f_\alpha d\phi_0$$

One can easily verify that the continuity equation and the energy-momentum balance equations are satisfied if the set of Eqs. (2),(3) is satisfied.

IV. Let us apply now this method to the linear stage of waves and instabilities in a magnetoactive plasma. The magnetic field is supposed to be uniform and in the z-direction: $\vec{B} = (0,0,B_0)$. The uniform electric field is given by the scalar potential: $^{(e)}U = -E_0 \cdot y$. We assume the electrostatic wave in the form $U = U_0 \exp i[k_x x + k_z z - \omega t]$, where

$$k_x = \frac{2\pi}{L_x} n_2, \quad k_z = \frac{2\pi}{L_z} n_3, \quad n_2, n_3 = 0, \pm 1, \pm 2, \ldots; \quad \omega = \omega_0 + i\mu.$$

The perturbed linear motion may be solved very easily using the canonical guiding center variables [1]. Substituting this motion into (2) (or (4)) and taking into account only linear terms of U_0 (or quadratic in Eq. (4)) we obtain (asymptotically in time) the energy-momentum conservation equation in the form of the known dispersion equation:

$$W_E\left[1 + \sum_\alpha \varepsilon^{(\alpha)}\right] = 0, \qquad W_E = \frac{k^2|U_0|^2}{4\pi} e^{2\mu t}$$

$$(11)\quad \varepsilon^{(\alpha)} = -2\frac{(2\pi)^4}{k^2 V}\sum_\alpha e_\alpha^2 N_\alpha \iint dP_1 dP_2 \int_C dP_3 \sum_{m_1} n_k \frac{\partial E_\alpha}{\partial P_k}\cdot\frac{J_{m_1}^2}{n_e\nu_e - \omega}$$

Here $f_{0\alpha} = N_\alpha \cdot E_\alpha(P_k)$ is a stationary particle distribution, $E_1 = \nu_1 P_1$,

$$Y = -\frac{2\pi}{m\nu_1 L_x}\cdot P_2, \quad p_z = \frac{2\pi}{L_z}P_3, \quad \nu_1 = \frac{eB_0}{m_c}, \quad \nu_2 = \frac{2\pi}{L_x}\cdot\frac{cE_0}{B_0}, \quad \nu_3 = \frac{2\pi}{L_z}\frac{p_z}{m};$$

Y is the guiding center position in y-direction; C denotes the Landau contour of integration. Hence, the dispersion equation has the following physical interpretation. The real part of it is the energy conservation equation expressed in the inertial system of the wave:

$$(12) \quad W_E \cdot Re\left[1+\sum_\alpha \varepsilon^{(\alpha)}\right] = 0, \qquad W_E \cdot Re\left[\varepsilon^{(\alpha)}\right] = {}^{(w)}H_0^{(\alpha)},$$

where ${}^{(w)}H_0^{(\alpha)}$ determines the perturbation energy of α-particles in the wave system. The imaginary part of the dispersion equation is the momentum conservation equation:

$$(13) \quad W_E\, J_m\left[\sum_\alpha \varepsilon^{(\alpha)}\right] = 0, \qquad \frac{\vec{k}}{\mu} W_E \cdot J_m\left[\varepsilon^{(\alpha)}\right] = \vec{\Pi}_0^{(\alpha)};$$

$\vec{\Pi}_0^{(\alpha)}$ determines the perturbation momentum of α-particles. The perturbation energy of α-particles in an inertial system L (e.g. laboratory system), where the wave frequency possesses a value $\omega_0 \neq 0$, is given as follows:

$$(14) \quad {}^{(L)}H_0^{(\alpha)} = {}^{(w)}H_0^{(\alpha)} + \frac{\omega_0}{k_z}\cdot\Pi_{0z}^{(\alpha)} = -W_E \cdot 2\frac{(2\pi)^4}{k^2 V} e_\alpha^2 N_\alpha \int_C d^3P_i \sum_{m_1} \frac{n_k n_e \nu_k \frac{\partial F_\alpha}{\partial I_e} J_{m_1}^2}{\mu^2 + (n_s\nu_s - \omega_0)^2}$$

Let us note here, that the contribution from the integration around poles (in the case of a damped wave) expresses the contribution from the perturbation particle streaming to the particle energy and momentum [4].

In the limit $\mu \ll \omega_0$, one may as usually, divide the particle contributions in Eqs. (11) – (14) into resonant and non-resonant parts and thus one obtains the energy and momentum of plasmons (waves) and of resonant particles.

V. The nonlinear solution of the set of Eqs. (2) – (10) is prepared for computor calculations. An investigation of beam-plasma interaction, including higher modes, is in progress,

References:

[1] Lacina J., Czech. J. Phys. B 23 (1973), 306.

[2] Morse R.L. and Nielson C.W., Phys. Fluids 12 (1969), 2418.

[3] Knorr G., Z. Naturforsch. 18a (1963), 1304.

[4] Lacina J., Plasma Physics 14 (1972), 605.

CONVECTIVE ION SOUND MODES AND ANOMALOUS SKIN EFFECT

F. Santini (*)

Laboratori Gas Ionizzati (Associazione EURATOM-CNEN)
C.P. 65 - 00044 Frascati, Rome, Italy.

ABSTRACT

The excitation of convective ion sound modes in a sheared magnetic field is investigated. Their energy convection is proposed as a possible mechanism for the observed anomalous skin effect in Tokamak discharges and compared with other mechanisms of transport.

The rapid disappearance of a temperature peak in the skin layer observed at the early stages of a Tokamak discharge / 1 / indicates that, among other effects, an anomalous transport of energy should be present. Drift modes excited by the temperature gradient may contribute to this transport / 2 /. Here an excitation of convective ion sound modes is proposed as an efficient mechanism for the energy transport. Indeed the solution of the dispersion equation for the latter modes within a radial region where the skin current is present, show an energy convection toward the periphery of this region which can exceed the collisional transport and also the convection connected with drift waves / 3 /.

We consider a plane slabe model where the electron drift velocity U_e is larger than the sound velocity $V_s = (T_e/m_i)^{\frac{1}{2}}$ with T_e larger than the ion temperature T_i. The characteristic parallel wave lengths are assumed to satisfy the inequality $K_\parallel V_s > \omega_*$ and $K_\parallel U_e > \omega_T$, where ω_* and ω_T are the drift frequencies connected with the characteristic length of the density gradient r_n and that of the electron temperature gradient r_T respectively. The magnetic field is assumed to be expressed by $\vec{B} = B_0(\vec{e}_z + \vec{e}_y x/L_s)$, L_s being the characteristic shear length, and the current to flow mainly along the z direction. The point x = 0 is taken to correspond to the maximum of T_e within the skin layer while their x-variations are neglected in a region sufficiently close to the center x = 0. The dispersion equation is derived from the charge neutrality and Vlasov equations for low frequency modes / 4 / of the form $\phi = \tilde{\phi}(x) \exp(-i\omega t + i k_y y + i k_z z)$ with $\omega < \Omega_i$, the ion gyrofrequency, and $K_\parallel = K_z + K_y x / L_s$, and reads

$$\left(1-\frac{k_\parallel^2 V_s^2}{\omega^2}-\rho_i^2\frac{d^2}{dx^2}+i\sqrt{\pi}\;\frac{\omega-k_\parallel u_e}{|k_\parallel|\,V_{the}}\right)\tilde{\phi}(x)=0 \qquad (1)$$

where $V_{the}=(2T_e/m_e)^{\frac{1}{2}}$, $\rho_i=V_s/\Omega_i$, and $(k_y\rho_i)<\rho_i d/dx<1$ has been assumed for, simplicity. Expanding ω around $\omega_o=k_z V_s$ i.e., with $\omega\simeq\omega_o+i\gamma$ we obtain the equation

$$\left(\frac{d^2}{dx^2}+\frac{x}{\delta\rho_i^2}+i\,\frac{\eta}{\rho_i^2}\right)\tilde{\phi}(x)=0 \qquad (2)$$

which is valid in the region $|x|\ll\delta\equiv L_s\omega_o^2/2V_s^2k_zk_y=L_sk_z/2k_y$. In Eq. (3) η is defined by

$$\eta=\frac{\sqrt{\pi}\,(u_e-V_s)}{V_{the}}-\frac{2\gamma}{\omega_o}\,. \qquad (3)$$

The solutions of Eq. (2) have the form of Airy functions, $\tilde{\phi}=A_i(-z)$ with $z=x(\delta\rho_i^2)^{-1/3}+i\eta(\delta/\rho_i)^{2/3}$. They satisfy the following boundary conditions: for $k_y>0$ (the case with $k_y<0$ is equivalent to changing x into $-x$) we demand that for $0\leq x\leq\Delta$ the solution shows a standing wave character while for $x>\Delta$ only a travelling wave is set up which carriers energy along the x-direction out of the localization region of width $\Delta\ll\delta$. This loss of energy at a rate $\eta\omega_o$ is compensated by the energy input from resonant coupling with electrons given by $\omega_o\sqrt{\pi}(u_e-V_s)/V_{the}$. For $x<0$ the standing solution goes to zero over a characteristic distance of the order of or smaller than Δ. In turn, this length Δ has to be smaller than the skin width and is related to the parameter η by the relation $\eta=\rho_i/(\Delta\delta)^{\frac{1}{2}}$. In fact, in the case where $\eta\leq(\rho_i/\delta)^{\frac{2}{3}}$, for $x<0$ the standing solution is damped over a distance $\simeq(\delta\rho_i^2)^{\frac{1}{3}}$, while for $x>0$ it goes to zero over a length $\Delta\simeq\rho_i^2/\delta\eta^2$, and the travelling wave appearing has the form:

$$\tilde{\varphi}(x)\propto\left[\frac{(\rho_i^2\delta)^{\frac{1}{3}}}{x}\right]^{\frac{1}{4}}\exp\left\{-i\,\frac{2}{3}\left[\frac{x}{(\rho_i^2\delta)^{\frac{1}{3}}}\right]^{\frac{3}{2}}+\eta\,\frac{(x\delta)^{\frac{1}{2}}}{\rho_i}\right\}. \qquad (4)$$

From Eq. (4) for $x>0$ one can define $k_x\equiv-x^{\frac{1}{2}}/\rho_i\delta^{\frac{1}{2}}$, showing that the travelling wave propagates inwards ($\omega/k_x<0$) in x, while it carries energy outwards since $(\omega/k_x)\partial\omega/\partial k_x=-\rho_i^2\omega^2<0$.

The power transport toward the periphery of the skin region due to convection of a spectrum of ion sound modes can be derived from energy conservation. It turns out to be given typically by

$$\dot{W}_{i.s} \simeq \int d^2k\, \omega_0 \frac{\partial \varepsilon}{\partial \omega_j} \frac{|\tilde{E}_k|^2}{8\pi} \eta\, \omega_0 \simeq$$

$$\simeq \left| \frac{e\phi}{T_e} \right|^2 n T_e \overline{(2k_\parallel k_\perp)}^{\frac{1}{2}} \lambda_{de}\, \omega_{pi} \frac{\rho_i}{(\Delta L_s)^{\frac{1}{2}}} \qquad (5)$$

where the bar indicates an average over the spectrum.

For a spectrum of drift waves, on the other hand, the convection / 2 / of energy $\dot{W}_{drift}$ is estimated to amount to $n T_e \bar{\omega}_* |e\bar{\phi}/T_e|^2 r_n / L_s$ so that

$$\frac{\dot{W}_{i.s.}}{\dot{W}_{drift}} \sim \left(\frac{L_s}{\Delta}\right)^{\frac{1}{2}} > 1 \qquad (6)$$

for comparable excitation level and magnitude of the characteristic wave lengths. A comparison with the collisional energy transfer from electrons to ions $\dot{W}_{ei} \simeq 3\nu_{ei} n T_e m_e/m_i$ (ν_{ei} being the electron-ion collision frequency), gives

$$\frac{\dot{W}_{i.s.}}{\dot{W}_{ei}} \sim \frac{\omega_{pe}}{3\nu_{ei}} \left(\frac{m_i}{m_e}\right)^{\frac{1}{2}} \overline{(2k_\parallel k_\perp)}^{\frac{1}{2}} \lambda_{de} \frac{\rho_i}{(L_s \Delta)^{\frac{1}{2}}} \left(\frac{\overline{e\phi}}{T_e}\right)^2 \qquad (7)$$

which can easily be larger than unity even for a low level of the fluctuation amplitude.

For example, if typically $\omega_{pe}/\nu_{ei} \sim 10^6$, $\overline{(2k_\parallel k_\perp)}^{\frac{1}{2}} \lambda_{de} \sim 10^{-1}$, $L_s \sim 10^2$ cm, $\Delta \sim 1$ cm $\rho_i \sim 10^{-1}$ cm, then the ratio (7) is larger than unity if $(e\bar{\phi}/T_e) > 10^{-2}$. Indeed the anomalous energy transport necessary to justify the observed behaviour of the skin effect would correspond to values of the ratio (7) somewhat larger than unity.

The author is indebted to B. Coppi and to F. Engelmann for useful discussion and suggestions.

REFERENCES AND FOOTNOTE

(x) Permanent address: FOM-Instituut voor Plasma-Fysica - Jutphaas, Netherlands

/ 1 / W. STODIEK: Proceedings of the Fifth European Conference on Controlled Fusion, Grenoble 1972, Vol. II, p. 1.
/ 2 / C.S. LIU, M.N. ROSENBLUTH and C.W. HORTON, Jr.: Phys. Rev. Letts. 29; 1498 (1972)
/ 3 / B. COPPI : Phys. Rev. Letts. 25, 851 (1970)
/ 4 / H.L. BERK and L.D. PEARLSTEIN: Phys. Rev. Letts. 23, 220 (1969).

EXCITATION OF ELECTROMAGNETIC WAVES IN PLASMA BY FUSION PRODUCTS.

T.D.Kaladze, D. G.Lominadze, K.N.Stepanov

Institute of Applied Mathematics, Tbilisi State University, Institute of Physics of Georgian Academy of Sciences, Tbilisi, Physical-Technical Institute of the Ukrainian Academy of Sciences, Kharkow, U.S.S.R.

A b s t r a c t s. The excitation of fast magnetosonic, Alfven and non-potential ion cyclotron waves by high energetic ions is studied, the ions being produced in fusion reactions. Growth rates and thresholds of excitation of these instabilities have been obtained.

I. The existence of charged fusion products in a fusion reactor plasma results in appearence of various instabilities [1-6]. In a uniform plasma excitation is possible of potential oscillations $\omega \sim 10\,\omega_{Bi}$ [2,5] and magnetosonic waves $\omega \sim \omega_{Bi}$ which propagate normally to the magnetic field [6]. The results [1-6] relate to a low pressure plasma ($\beta = 4\pi n T / B_0^2 \ll 1$).

In the present report a more general class of "thermonuclear instabilities" is considered. It has been shown that at $\beta \ll 1$ Alfven and fast magnetosonic branches of the oscillations are unstable not only at $\omega \ll \omega_{Bi}$ [3,4] but at $\omega \gtrsim \omega_{Bi}$ as well. In particular wistlers with $\omega \gg \omega_{Bi}$ can be unstable. If fusion products concentration n'_0 islarge enough whistlers can be excited in a finite pressure plasma ($\beta \sim 1$). At low concentration of fusion products in a plasma with $\beta \gtrsim 1$ Alfven magnetohydrodynamic waves are unstable. Excitation have been also considered of non-potential ion cyclotron waves and fast magnetosonic waves which propagate perpendicularly to the magnetic field in a plasma with $\beta \lesssim 1$.

2. We shall consider ion and electron temperatures T_i, T_e of the plasma much less than the energy $(1/2) m' v_0^2$ of the reaction products and neglect thermal energy spread of fusion products. Then fast magnetosonic and Alfven waves will be excited by energetic resonance ions. The frequency of these waves at $\beta \ll 1$

is obtained from

$$\mathcal{D}(\omega) = \cos^2\Theta\, N^4 - \varepsilon_1 (1+\cos^2\Theta) N^2 + \varepsilon_1^2 - \varepsilon_2^2 = 0, \quad (1)$$

Here

$$\varepsilon_1 = \sum_i \frac{\omega_{pi}^2}{\omega^2 - \omega_{Bi}^2}, \quad \varepsilon_2 = -\frac{\omega_{pe}^2}{\omega\omega_{Be}} - \sum_i \frac{\omega_{pi}^2 \omega_{Bi}}{\omega(\omega^2-\omega_{Bi}^2)}, \quad (2)$$

$N = ck/\omega$, Θ is the angle between wave vector $\vec{k}$ and magnetic field $\vec{B}_0$, $\omega_{p\alpha} = (4\pi Z_\alpha^2 e^2 n_{0\alpha}/m_\alpha)^{1/2}$. In Eq.(2) the sum is taken over various species of the ions. At $kc \gg \omega_{pi}$ Eq(1) gives the frequency of the whistlers $\omega = \omega_{Be}\cos\Theta (kc/\omega_{pe})^2$. At $kc \ll \omega_{pi}$ one finds from (1) the frequency of Alfven magnetohydrodynamic wave $\omega = k_\parallel v_A \equiv k_\parallel c\left[\sum_i (\omega_{pi}/\omega_{Bi})^2\right]^{-1/2}$. The growth rate in this case is $\gamma = \gamma_f - \gamma_e$, γ_e is damping rate due to absorption of waves by resonance electrons, γ_f is a contribution to the growth rate by fast ions.

If $\omega \sim kv_A \sim \omega_{Bi}$ one can obtain at $k_\parallel \sim k_\perp$ and $\omega \sim k_\parallel v_0$ from general dispersion formula [7] the following estimates:

$$\gamma_e \sim (m_e/m_i)(v_{Te}/v_A)\omega, \quad (3)$$

$$\gamma_f \sim (n_0'/n_0)\omega_{Bi}. \quad (4)$$

The critical value of fast ion density for the instability to appear is determined by condition $\gamma_e \sim \gamma_f$

$$n_{cr}'/n_0 \sim (m_e/m_i)(v_{Te}/v_0). \quad (5)$$

The value (5) for n_{cr}' coincides with the expression for n_{cr}' for low-frequency fast magnetosonic waves $\omega \approx kv_A \ll \omega_{Bi}$ [3]. For whistlers the value of γ_e considerably exceeds (5).

$$\gamma_e \sim (kv_{Te}/\omega_{Be})\sin^2\Theta\,\omega. \quad (6)$$

Therefore the whistlers propagating almost parallel to the magnetic field with $\Theta \sim (\omega_{Bi}/\omega)^{1/2}$ and $\omega \approx k_\parallel v_0$ are excited most readily. In this case

$$\frac{n_{cr}'}{n_0} \sim \frac{m_e}{m_i}\frac{v_{Te}}{v_0}\frac{\omega}{\omega_{Bi}} \sim \frac{v_{Te}v_0}{c^2}\frac{\omega_{pe}^2}{\omega_{Be}^2}. \quad (7)$$

In a finite pressure plasma ($\beta \gtrsim 1$) the phase velocity of the waves $\omega \sim \omega_{Bi}$ having been considered above becomes comparable with or even less then thermal ion velocity ($v_A \gtrsim v_{Ti} = (T_i/m_i)^{1/2}$). Therefore these waves are strongly absor-

bed by plasma ions and their excitation by a small group of fast ions becomes impossible. Nevertheless the absorbtion of Alfven magnetohydrodynamic waves ($\omega = k_{\parallel} v_A \ll \omega_{Bi}$) is small even at $\beta \gg 1$ [8]. The attenuation rate of these waves due to Cherenkov absorbtion by resonance ions by the order of magnitude

$$\gamma_i \sim \omega \left(\frac{\omega}{\omega_{Bi}}\right)^2 \left(\frac{v_{Ti}}{v_A}\right)^3 \exp\left(-\frac{v_A^2}{2v_{Ti}^2}\right) . \qquad (8)$$

The excitation of these oscillations takes plaae when $k_{\parallel} v_0 \sim \omega_{Bi}$, the growth rate is expressed by (4) and the critical value of fast ion density by the relation

$$n'_{cr}/n_0 \sim (v_{Ti}/v_0)^3 \exp\left(-v_A^2/2v_{Ti}^2\right) . \qquad (9)$$

In a high pressure plasma ($v_A \ll v_{Ti}$) the damping rate γ_i is v_{Ti}/v_A times smaller for $\theta \approx \theta_0 = \operatorname{arctg}\sqrt{2/3}$ [8]. For these angles the rate of decrease of n'_{cr} is the same .

When v_{Ti}/v_A becomes smaller the ion Cherenkov damping (8) rapidly decreases and becomes less than electron Cherenkov damping [7,8].

$$\gamma_e \sim (m_e/m_i)(v_{Te}/v_A)(\omega^3/\omega_{Bi}^2) . \qquad (10)$$

In this region the value of n'_{cr} is determined by [4]:

$$n'_{cr}/n_0 \sim (m_e/m_i)(v_{Te} v_A^2/v_0^3) . \qquad (11)$$

The threshold density for the instabilities considered is very low: $n'_{cr} \leq 10^{-3} n_0$ at $v_{Ti} \sim 0,1\, v_0 \sim 10^8$ cm/sec.

4. At $\theta = \pi/2$ the existence of a small group of fast ions leads to a coherrent excitation of the oscillations. When the finite Larmor radius of plasma ions is taken into account the fast magnetosonic and ion cyclotron waves become coupled (See [9,10]). These waves become unstable when their frequency $\omega(k)$ is equal or close to $n\omega'_{Bi}$, where ω'_{Bi} is fast ion gyrofrequency. In this case the natural frequencies of the oscillations are plotted against wave number in Fig.1 for a deiterium plasma with a small group of fast thritium ions.
The growth rate is

$$\gamma = \eta (n'_0/n_{0d})^{1/2} \omega_{Bd} . \qquad (12)$$

Here $\eta \sim 0,2$ at $\beta = 0.1$ and $v_{Td} = 0,1 v_0$. At $\beta \geq 1$ only the first cyclotron branch of deiterium plasma oscillations

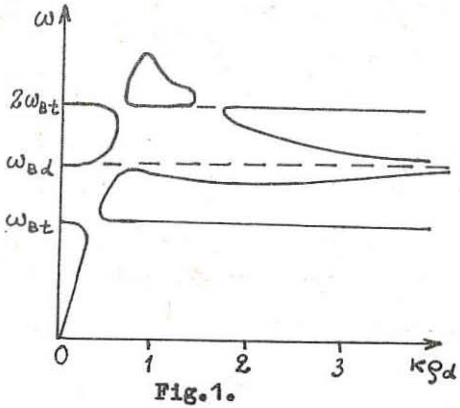


Fig.1.

($\omega(\kappa) < \omega_{Bd}$) is unstable. Fast ions of He^3 also excite cyclotron waves with $\gamma_{max}=1.35$ at $\beta=0.1$. But it should be mentioned that cyclotron oscillations are relatively easy stabilized by a shear.

REFERENCES.

1. Ya.I.Kolesnichenko, V.N.Oraevsky. Atomnaja Energija, 23, (1967) 289.
2. L.V.Korablev, JETP, 53, 1600 (1967)
3. L.V.Korablev, L.I.Rudakov, JETP 54, 818 (1968)
4. V.S.Belikov, Ya.I.Kolesnichenko, V.N.Oraevsky, JETP, 55, 2210 (1968).
5. B.S.Belikov, Ya.I.Kolesnichenko, V.N.Orayevskii. Plasma Phys. and Controlled Nucl.Fus.Res.Vienna, IAEA (1971), v.III, p.411.
6. A.B.Mikhailovskii. Voprosy teorii plasmy, vol.6, Atomizdat, 1964.
7. A.I.Akhiezer, I.A.Akhiezer, R.V.Polovin, A.G.Sitenko and K.N.Stepanov. Kollektivnye kolebaniya v plasme, Atomizdat (1964).
8. K.N.Stepanov 34, 1929 (1958).
9. A.B.Kitsenko, K.N.Stepanov Nuclear Fusion 4, 272,(1958)
10. T.D.Kaladze, D.G.Lominadze, K.N.Stepanov, Zh.Tekh.Fiz. 42, 243, (1972).

A NUMERICAL INVESTIGATION OF THE STABILITY CRITERION FOR INHOMOGENEOUS NON-MAXWELLIAN VLASOV EQUILIBRIA

by

S. Cuperman and I. Tzur

CIRES, University of Colorado and NOAA-SEL, Boulder

and Depart. of Phys. and Astron., Tel-Aviv Univ., Israel

Abstract: The existence of an instability criterion for inhomogeneous non-maxwellian Vlasov equilibria is demonstrated by the aid of numerical integration techniques.

This paper investigates numerically the possible existence of a simple instability criterion for inhomogeneous non-maxwellian Vlasov equilibria. Such a criterion has been recently suggested by Minardi (1972). To derive it, the author used a statistical mechanics of cells in an "information" space, rather than the familiar (and more general) "phase space". The cells are considered to be identifiable objects to which are ascribed random variables of the relevant observable quantities of the systems (information variables). The peculiarity of the Vlasov model is embodied from the beginning into the theory by treating the collective and individual effects as independent. As a result, the following condition for instability is found by Minardi:

$$I \equiv \frac{1}{L}\int_0^L S(\underline{x})\left[\phi(\underline{x}) - \phi_o\right] dV > 0 \qquad (1)$$

where $S(\underline{x})$ is the information variable depending on the physical system under consideration, $\phi(\underline{x})$ the corresponding potential and ϕ_o its spatial average; $\underline{x}_j$ represents the coordinates of the cell center ΔV_j.

To check Minardi's criterion (1), we have considered a simple inhomogeneous non-maxwellian Vlasov case; namely, a one-dimensional collisionless selfgravitating class of systems, including both stable and unstable equilibria, depending on one basic parameter. The similarity between this

class of systems (in which long range Coulomb forces are dominant) and plasma systems is obvious. Thus, the conclusions of this work are relevant for the plasma case.

Specifically, the systems considered consist of a "ring" of constant density in phase space bounded by two energy curves labeled ε_1 and ε_2 and known as "water-bag models". The basic parameter is $\nu = \varepsilon_1 / \varepsilon_2$.

The equilibrium conditions are determined by the stationary solutions of the Vlasov and Poisson system of equations

$$\partial f/\partial t + v\partial f/\partial x - (\partial \phi/\partial x)(\partial f/\partial v) = 0 \qquad (2)$$

$$\partial^2 \Phi/\partial x^2 = 4\pi G \int f \, dv \qquad (3)$$

Upon solving these equations for our case and substituting the results into expression (1) one obtains the results given in Fig. 1. Thus, for $\nu < 0.325$ one has stability while $\nu > 0.325$ corresponds to instability.

We considered five initial equilibrium states characterized by the initial values of the parameter ν indicated in Fig. 1. The systems where perturbed by introducing initial sinusoidal (in phase space) perturbations and were then allowed to evolve. The integration method used consists of following the boundary curves ε_1 and ε_2 enclosing the system and is described elsewhere (Cuperman et al, 1970; see also Roberts and Berk, 1967).

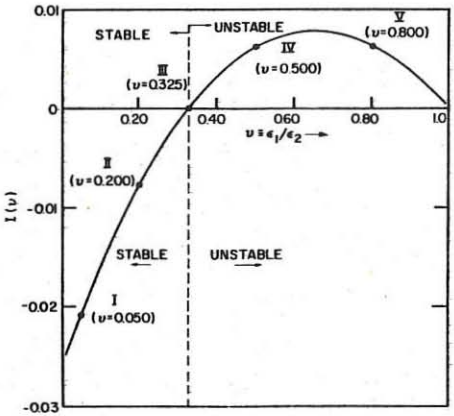


Fig. 1

Some of the results obtained are illustrated in Fig. 2 giving the states of the systems corresponding to the cases I and V at the end of the run and Fig. 3 giving the time behavior of the relative spread in the energy distribution function $F(\epsilon)$. As seen from the changes in the phase space configuration, those in the mass density $\rho(x)$ (in ordinary space) and in the energy distribution function, cases I and II appear to be stable, cases IV and V are unstable and case III (predicted to be linearly marginal unstable) becomes unstable at later times.

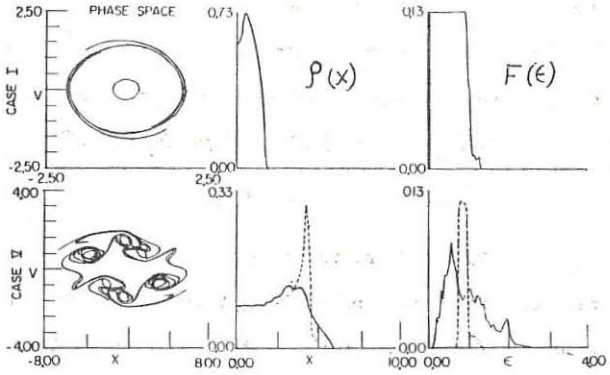


Fig. 2

We conclude that the results of our numerical integration of the time-dependent Vlasov and Poisson equations support Minardi's linear instability criterion for inhomogoneous non-maxwellian Vlasov equilibria.

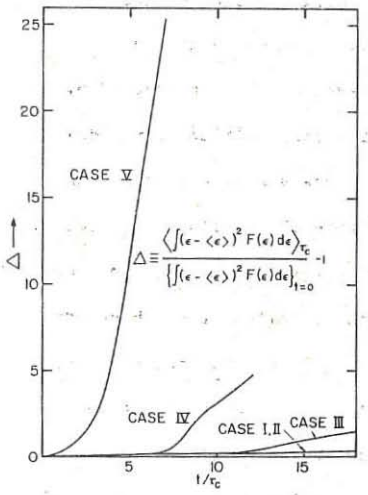


Fig. 3

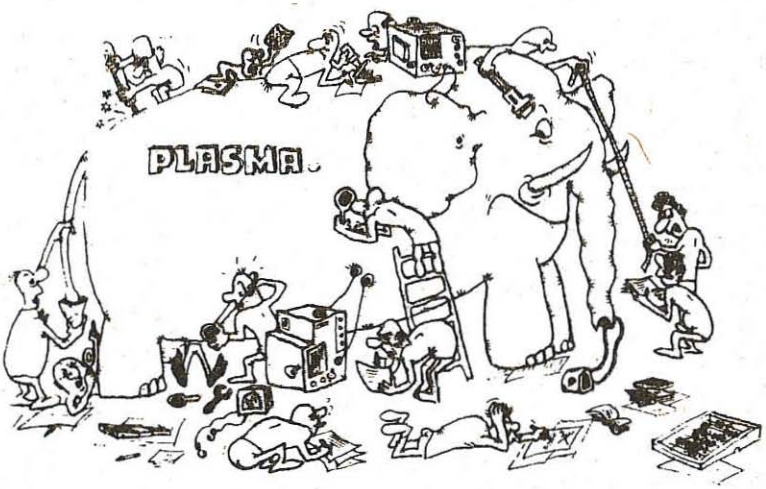
References

Cuperman, S., Harten, A. and Lecar, M., 1970 Symposium on the Gravitational N-Body Problem, p. 290; also in 1971, Ap. and Space Sci. 13, 411.

Roberts, K. V. and Berk, H. L., 1967, Phys. Fluids 10, 1595.

Minardi, E., 1972, Plasma Phys., 14, 427 and 443.

AUTHOR INDEX



A

Abrashitov Yu.I. 495
Adati K. 561
Alcock M.W. 131
Aldcroft D. 51
Alikaev V.V. 63
Andrjukhina E.D. 113
Ard W.B. 401
Arsenev Yu.I. 63
Arsenin V.V. 625
Artemenkov L.I. 153
Ashby D.E.T.F. 431
Asovsky Yu.S. 251
Astapenko G.I. 169

B

Baiborodov Yu.T. 165
Baker D.A. 293
Barbian E.P. 465
Bardet R. 247
Barnett C.F. 67
Barr O.C. 447
Bateman G. 277
Becker G. 285
Beckner E.H. 483
Bergstrom J. 583
Berry L.A. 67
Beshara A. 569
Bineau M. 221
Biskamp D. 461
Bobrovskii G.A. 63
Bodin H.A.B. 265
Bol K. 18
Boris J.P. 315
Bortnikov A.V. 165
Bottiglioni F. 381
Bradford R.E. 131
Breizman B.N. 491
Breton C. 9,183
Brevnov N.N. 165
Briand P. 247
Brodskii Yu.Ja. 549
Burcham J. 51
Bureš M. 575
Burkhalter P.G. 447
Burkhardt L.C. 293
Bush C.E. 67
Bussac J.P. 9

C

Cabral J.A.C. 521,525
Callen J.D. 67
Cano R. 195
Cannobio E. 213
Casati G. 33
Cecchi J.L. 18
Chang C.T. 349
Chebotarev P.Z. 411
Chechkin V.V. 557
Chen K. 139

Chernobrovin V.I. 507
Chernyakov A.L. 595
Chodura R. 311,461
Christiansen J.P. 431
Chu M.S. 161
Chuyanov V.A. 243
Clarke J.F. 67
Clauser M.J. 483
Cloth P. 359
Coensgen F.H. 255
Colchin R.J. 67,401
Cole H.C. 51
Connor J.W. 631
Conrads H. 359,367
Corti S. 565
Coutant J. 381
Cowlin M. 51
Crenn J.P. 9
Crow J.E. 269
Crume E.C. 401
Cummins W.F. 255
Cuperman S. 650

D

Danilov V.V. 415
Daughney C.C. 18
Daybelge U. 25
De Barbieri O. 213
Dei-Cas R. 9
Delmas M. 9
Demirkhanov R.A. 169,345
Demchenko V. 569
Deschamps P. 143
Dietz K.J. 299
Diky A.G. 105
Di Marco J.N. 293
Dippel K.H. 299
Dnestrovskii Y.N. 41
Dobrowolny M. 33
Dodo T. 121
Dollinger R. 583
Dory R.A. 67
Doschek G.A. 447
Dougar-Jabon V.D. 259
Dove W.F. 499
Dozier C.M. 443,447
Dreizin Yu.A. 147
Dubovoi L.V. 507
Düchs D.F. 29
Dum C.T. 461
Dunlap J.L. 401
Dupas L. 247
Dykhne A.M. 147

E

Eckhartt D. 325
Eidmann K. 435
El-Gwaily M. 569
El-Khalafawy T. 569
Ellis R.A., Jr. 18
El-Nicklawy M. 569
Engelhardt W. 277
Engelmann F. 329

England A.C. 67
Es'kov A.G. 595,599

F

Fabre E. 603
Falter H.D. 385
Feldman U. 447
Feneberg W. 209
Fidone I. 195
Filippov N.V. 375
Filippova T.I. 355,375
Fisher R.K. 161
Fisher U. 422
Fois M. 381
Forman P.R. 293
Forrest M.J. 363
Freeman J.R. 483
Freeman R. 131
Freidberg J.P. 87
Fried B.D. 477
Fujita J. 191
Fujiwara M. 121,125
Fünfer E. 109
Furth H.P. 18,29

G

Galanti M. 427
Gerber K.A. 499
Gibson A. 5
Ginot P. 9
Girard J.P. 337
Golant V.E. 587
Goldenbaum G.C. 499
Gollwitzer D. 367
Golovanivsky K.S. 259
Gol'tsman V.L. 549
Golubev S.V. 549
Goncharenko V.P. 251
Gorbunov E.P. 1
Gormezano C. 247
Gosteva T.S. 507
Gould R.W. 477
Gowers C.W. 265
Gravier R. 143
Green B.J. 225,229
Grelot P. 79
Gribkov V.A. 375
Grieger G. 101
Grigor'eva L.I. 557
Grossmann W. 83
Gruber O. 285
Gruber R. 609

Haas F.A. 87
Haas G. 325
Haberstich A. 293
Hacker H. 101
v. Hagenow K.U. 225,325
Hagler M.O. 583
Hammond D.P. 131
Hammer D.A. 499
Haste G.R. 401
Hastie R.J. 631
Hatch A.J. 617
Hellsten T. 407
Herold H. 285,333
Hintz E. 299
Hofmann F. 289
Hogan J.T. 67
Horton W. 95
Hosea J. 195,199
Höthker K. 299
Howell R.B. 293
Hsieh C.L. 161
Hugill J. 5,157
Huguet M. 9

I

Ignat D.W. 289
Isaev V.A. 473
Itagaki T. 319
Ivanov A.A. 553
Ivanov B.A. 507
Ivanov V.D. 355

J

Jacobsen R.A. 18
Jacquinot J. 389
Jäger H. 422
Jankovitch Z. 621
Jauho P. 439
Jensen T.H. 161
Jobes F.C. 199
Johnson L.C. 18

K

Kadomtsev B.B. 59
Kaladze T.D. 646
Kalinichenko S.S. 105
Kalinin Yu.G. 453
Kanaev B.I. 235
Kapetanakos C.A. 499
Karetkina N.V. 41
Karlson E.T. 397
Karr H.J. 293
Kaufmann M. 109,341

Kawahata K. 125
Keilhacker M. 303,307
Kelley G.G. 67
Kharchenko I.F. 529,533
Khelladi M. 337
Khodirev Yu.V. 579
Kholnov U.V. 113
Killeen J. 269
Kingsep A.S. 453
Kirov A.G. 169
Kitsunezaki A. 173
Klein B.M. 443,447
Koch R. 545
Komar E.G. 177
Konovalov I.I. 105
Konyuchov V.V. 495
Kopecky V. 635
Köppendörfer W. 341
Korn P. 503
Kornherr M. 303,307
Korten M. 14
Korzhavin V.M. 355
Kosinova T.A. 553
Koslov P.I. 153
Kostomarov D.P. 41
Koydan V.S. 495
Krause H. 273
Kristiansen M. 583
Krokhin O.N. 375
Krotov M.F. 553
Kruglov V.N. 473
Kruglyakov E.P. 415
Krupin V.A. 55
Kugler E. 14
Küppers G. 511
Kursanov Yu.V. 345
Kurtmullaev R.Kh. 595,599
Kvartskhava I.F. 281

L

Laaksonen J. 439
Lacina J. 639
Lackner K. 209
Lagunov V.M. 495
Lang J. 5
Larionov M.M. 587
Lauhin Ya.N. 599
Launois D. 9
Lavrent'ev O.A. 251
Lavrovsky V.A. 529,533
Lazar N.H. 401
Lazzaro E. 33
Lecoustey P. 9
Lehnert B. 407
Leloup C. 389
Leonov V.M. 55
Levin L.S. 587
Levine L.S. 419
Likhtenshtein V.Kh. 243
Lisitano G. 565
Litvak A.G. 473,549
Lochte-Holtgreven W. 422
Logan B.G. 499
Lominadze D.G. 646
Long J.W. 265
Lortz D. 91,135
Lotz W. 109
Lukyanov V.N. 495
Lyon J.E. 401

M

Maeda H. 173
Maignan J. 603
Maissonier Ch. 359
Malikh N.I. 169
Malyutin A.I. 595,599
Mann L.W. 293
Marcus F.B. 239
Marder B.M. 87
Maret G. 307
Markin A.I. 599
Martone M. 10
Marty D.A. 337
Maschke E.K. 205
Matsiborko N.G. 537
Mattioli M. 9
Mazzucato E. 18
McCormick K. 191
McCrary J.H. 447
McMahon J.M. 447
McNally J.R. 67
Meade D. 139
Mekler K.I. 495
Melin G. 247
Melikhov P.I. 153
Merezhkin V.G. 55
Mercier C. 75
Messiaen A.M. 545
Miyamoto K. 121,125
Mohri A. 125
Moiseeva M.P. 355
Molvik A.W. 255
Morgan P.D. 359
Mori S. 173
Moriette P. 9
Mosher D. 419
Mukhovatov V.S. 55
Muller G. 591
Murakami M. 67

N

Naboka V.A. 251
Nagel D.J. 443,447
Neidigh R.V. 67
Neuhauser J. 109
Newton A.A. 265
Nexsen W.E., Jr. 255
Niedermeyer H. 303,307
Nocentini A. 329
Noll P. 14
Norton B.A. 363

O

Ogata A. 121
Ohkawa T. 161
Okabayashi M. 139
Onishenko I.N. 537
Oraevsky V.N. 537
Orefice A. 33

Orlinskii D.V. 165
Ortolani S. 83
Östberg K. 469
Ovcharenko L.I. 251
Ovchinnikov S.S. 105

P

Pacher G. 101,565
Pakhomov L.P. 587
Pankrat'ev Yu.I. 251
Panov D.A. 243
Papoular R. 183
Paris R.B. 205
Pashnev V.K. 105
Paul J.W.M. 5,157
Pavlichenko O.S. 105
Pavlova N.L. 41
Peacock N.J. 359,363,427
Pecorella F. 359
Pergament V.I. 165
Petrov M.P. 1
Phillips J.A. 293
Plakhov A.G. 453
Plinate P. 9
Podushnikova K.A. 587
Poffe J.P. 389
Pogutse O.P. 59
Pokhmelnykh L.A. 259
Poluakhtov B.K. 473
Popov A.M. 41
Potapenko V.A. 251
Potter D.E. 217
Poukey J.W. 483
Poznyak V.I. 63
Prestwich K.R. 483
De Prétis M. 389

R

Rager I.P. 359
Raggi R. 407
Rakhimbabaev Ya.R. 553
Rapp H. 371
Räuchle E. 591
Razumova K.A. 63
Rebhan E. 135
Rebut P.H. 9
Rehker S. 117,187
Reid G.W. 157
Renaud C. 143
Renner H. 101,565
Reynolds P. 5
Ringler H. 101,565
Riviere A.C. 131
Roberts M. 67
Robinson D.C. 265,269
Robson A.E. 315
Rogashkova A.I. 533
Roife I.M. 177
Romanovskii M.K. 165
Rome J.A. 67
Ross D.W. 95
Röthlein B. 311

Rozhdestvensky V.V. 587
Ruchko L.F. 169
Rudakov L.I. 487
Rudnev N.I. 569
Rusanov V.D. 553
Rutherford P.H. 29
Ryutov D.D. 411

S

Sadowski M. 393
Saito K. 319
Salat A. 511
Samain A. 143
Samarsky A.A. 487
Samuelli M. 359
Sand F. 14
Sandel F. 503
Santini F. 643
Sapogov S.A. 557
Scherbakov A.G. 243
Schmidt G. 477
Schmidt H. 367
Schmidt J. 139
Schramm G. 109
Schüller P.G. 591
Semenov V.N. 595,599
Sen A. 37
Serebreny G.A. 587
Seredenko E.V. 177
Shanny R.A. 315
Shapiro V.D. 537
Shapotkovskii N.V. 553
Sharp W. 45
Sheffield J. 51
Shevchenko V.I. 537
Shiitna S. 319
Shimomura Y. 173
Shohet J.L. 617
Shpiegel I.S. 113
Shun'ko E.V. 415
Shustin E.G. 529
Shvets O.M. 105
Sidorkin V.A. 251
Sigel R. 435
Sigov Yu.S. 579
Silva M.E.F. 521,525
Simonen T.C. 255
Skladnik-Sadowska E. 393
Sklizkov G.V. 375
Skoryupin V.A. 453
Skripal L.P. 345
Slavny A.S. 105
Sledziewski Z. 9
Smerdov B.I. 557
Sokolov N.I. 165
Sokolov Yu.A. 63
Soldner F. 303
Spector M.D. 411
Speth E. 51
Stenz C. 603
Stepanov K.N. 646
Stepanenko I.A. 251
Stephanakis S.J. 419
Steuer K.-H. 303,307
Stodiek W. 18

Stott P.E. 5,51,157
Suchareva N.K. 355
Sudlitz K. 393
Sugihara R. 561
Šunka P. 517
Suprunenko V.A. 105
Svishev V.S. 153
Sweetman D.R. 131
Sykes A. 457

T

Tachon J. 9
Tarasenko V.F. 105
Taylor J.C. 45
Tennfors E. 575
Tessarotto M. 329
Thorstensen B. 575
Tikhanov E.K. 281
Timofeyev A.D. 393
Timofeev A.V. 613
Toepfer A.J. 483
Tolok V.T. 105
Torossian A. 9
Trunk M. 371
Tseitlin M.B. 533
Tuttle G.H. 217
Tzur I. 650

U

Us A.M. 165
Uyama T. 561

V

Vandenplas P.E. 545
Varma R.K. 37
Vasilevsky M.A. 177
Vdovin S.A. 251
Vdovin V.L. 553
Vekstein G.E. 411
Verhage A.J.L. 265
Virtamo J. 439
Vitkovitsky I.M. 419
Vlasenkov V.S. 55
Voronov G.S. 113

W

Waelbroeck F. 14
Waidmann G. 14
Watanabe K. 561
Watson C.J.H. 239
Weibel E.S. 609
Weisse J. 79

Wesson J. 457
Weynants R.R. 545
Wharton C. 503
Whitlock R.R. 443,447
Wilhelm R. 273,333
Wilhelmsson H. 469
Wimmel H.K. 511
Wing W.R. 67
Winsor N.K. 315
Wobig H. 117,187
Wuersching E. 101
Wursching E. 565

Y

Yokoyama K. 319
Yonas G. 483
Yoshikawa M. 173
Yoshikawa S. 139
Yoshimura H. 319
Young F. 419
Yushmanov E.E. 235

Z

Zablotskaya G.R. 507
Zakatov L.P. 453
Zakharov L.E. 165
Zaverjaev V.S. 1
Zehrfeld H.P. 225,229
Zharikov V.N. 169
Zhdanov V.A. 169
Zhil'tsov V.A. 243
Zhukovskii V.G. 165
Zinov'ev O.A. 553
Zlotnikov D.M. 453
Zolotovsky O.A. 599
Zukakishvili G.G. 281
Zwicker H. 273,333

Copyright © 1973

Joint Institute for Nuclear Research

Издательский отдел Объединенного института ядерных исследований.
Заказ 16336. **Тираж** 1200. **Уч.-изд.листов** 41,6.

Обложка художника Ю.И.Миронова.
Рисунки И.Максимова, В.Санникова.